Development of a Novel Polyketone Biomaterials Platform from Renewable Resources

by

Lukmanul Hakim Samada

A thesis submitted to the University of Birmingham for the degree of

Doctor of Philosophy

School of Chemistry

College of Engineering and Physical Sciences

University of Birmingham

September 2024

ABSTRACT

Commodity plastics derived from petroleum sources are inherently non-degradable or minimally degradable which inevitably leads to the formation of microplastics or nanoplastics. The adverse consequences impact on the environment and human health. Over the past few years, renewable feedstocks, such as biomass, have become an alternative to petrol-derived feedstocks, thanks to their sustainability, abundance, and being environmentally friendly. Nonetheless, the manufacturing process still needs some non-degradable additives to enhance the mechanical properties and thermal stability of the polymer materials from renewable resources.

Polyketones (PKs) are generally an important family of thermoplastics, along with polyesters, polycarbonates, polyamides, polyurethanes, polyurethanes, and polyimides, that have been developed and manufactured to fulfill the needs of modern society for high-performance materials with excellent thermomechanical properties. Recently, polyketones have gained interest for some applications related to photo-triggered materials use. PKs are generally prepared *via* chain-growth metal-mediated polymerization which usually uses carbon monoxide and transition metals. In addition to the harm of monomer and catalyst used, this strategy also limits the structural complexity and range of thermomechanical properties of the resultant polyketones.

Conventional polyketones contain polyolefin backbones and behave like polyolefin in their photodegradation. They commonly degrade into a nonselective degradation pathway which is known as Norrish pathways. Therefore, a step-growth click polymerization is employed to address these challenges by inserting renewable and sustainable building blocks in their preparation. Manipulating the pendant group or main chain of the polymers enables structurally diverse polyketones and variable thermomechanical properties, yet their degradation can be controlled through well designed photocleavable linkage. The resulting polyketones (F-C_6A and Poly(HMDA$_{10}$-*co*-EDEA$_{90}$) display comparable tensile strengths to PET and HDPE respectively (but having half of their elongation at break values) with high glass transition temperature values (amorphous behavior). In addition, they enable to degrade under controlled UV light *via* a novel photodegradation pathway.

ACKNOWLEDGEMENTS

First of all, I would like to express my deepest gratitude to Allah subhanahu wa ta'ala (SWT) for his uncountable sustenance and blessings.

I must thank my supervisor Professor Andrew Dove for his guidance and support during my PhD journey. I am grateful for the opportunity to learn how to be a good scientist and develop my soft skills. It was such an honor to be part of your amazing research group. I also should thank my sponsor – Indonesian Endowment Fund for Education (LPDP) for funding my study and living costs.

Thanks to the Dove and O'Reilly group (current and previous members) for being supportive friends. Special thanks to Dr. Joshua C. Worch for your mentorship at the beginning of my PhD study and Dr. Arianna Brandolese for your help in proofreading my thesis multiple times. Next, another special thanks to my best friends and lab buddies Dr. Neha Yadav and Dr. Maher Alraddadi for the exciting chat and meaningful support (including proofreading).

I also want to thank my lab mentor Dr. Connor Stubbs for the helpful suggestions in terms of lab work. Thanks to Dr. Steven Street, Dr. Thiago Ouriquez Machado, and Dr. Tugce Nihal Gevrek for your professional proofreading. I need to mention Gabriela Garbanova, Dr. Siriporn "Snook" Chaimueangchuen, Daniele Giannantonio, Laihui Xiao, Dr. Ana Cubillo Alvarez, Tianlai Xia, and Flore Kilens for the enjoyable chats.

I’d like to thank Dr. Daniel Smith and Julia Valvarde for helping me to overcome any lab issues. Also, thank Tessa Kintail for the administrative support. I also thank everyone who got involved in the outreach activities and open days. Those are such nice experiences.

Finally, I would like to say thanks a lot to my parents for your mental support and prayers. You really supported me to pursue the highest level of formal education, so I became more confident to study overseas. I want to make you proud of my achievements.

TABLE OF CONTENTS

LIST OF FIGURES

LIST OF EQUATIONS AND TABLES

LIST OF ABBREVIATIONS

ADMET	Acyclic Diene Metathesis
2D	2 dimensional
3D	3 dimensional
$CDCl_3$	Deuterated chloroform
CGP	Chain-growth polymerization
$CHCl_3$	Chloroform
cm	Centimeter
CuAAC	Copper-catalyzed azide-alkyne cycloaddition
d	doublet "^{1}H-NMR splitting"
Da	Dalton
$Đ_M$	Dispersity
DBU	1,8-diazabicyclo[5.4.0]undec-7-ene
DCM	Dichloromethane
DMTA	Dynamic mechanical thermal analysis
DSC	Differential Scanning Calorimetry
E	Young's modulus
EDEA	2,2'-(ethylenedioxy)bis(ethylamine)

EI-MS	Electron ionization mass spectrometry
EtOAc	Ethyl acetate
Et_2O	Diethyl ether
EA	Elemental Analysis
FDCA	2,5-furandicarboxylic acid
FT-IR	Fourier-transform infrared
GC-MS	Gas chromatography mass spectrometry
GPC	Gel Permeation Chromatography
HDI	Hexamethylene diisocyanate
HDPE	High density polyethylene
HMDA	1,6-hexanediamine/ Hexamethylenediamine
HOMO	Highest Occupied Molecular Orbital
HRMS	High-Resolution Mass Spectrometry
iPP	Isotactic polypropylene
J	Joule
kDa	Kilodalton
kPa	Kilopascals
LDPE	Low-density polyethylene
LUMO	Least Unoccupied Molecular Orbital
m	meter
$MgSO_4$	Magnesium sulfate
mm	Millimeter
M_n	The number-average molar mass

NEt_3	Triethylamine
NMR	Nuclear magnetic resonance
Pa	Pascals
PC	Polycarbonate
pH	Potential hydrogen
PCL	Polycaprolactone
PET	Polyhydroxyalkanoates
PHA	Polyethylene terephthalate
PLA	Poly(lactic acid)
PS	Polystyrene
PTA	Purified Terephthalic Acid
q	Quartet "^{1}H-NMR splitting"
RAFT	Reversible addition−fragmentation chain-transfer
S	Singlet "^{1}H-NMR splitting"
SEC	Size Exclusion Chromatography
SEM	Scanning electron microscopy
SGP	Step-growth polymerization
t	Triplet "^{1}H-NMR splitting"
T_c	Crystallization Temperature
TDI	Toluene diisocyanate
T_g	Glass Transition Temperature
TGA	Thermogravimetric analysis

THF	Tetrahydrofuran
T_m	Melting Transition Temperature
U_T	Toughness
UTS	Ultimate tensile strength
UV	Ultraviolet
δ	Chemical shift
ΔH_c	Enthalpy of crystallization
ΔH_m	Enthalpy of melting
ε	Elongation
ε_b	Elongation at break
μ	Viscosity
σ	Uniaxial stress

LIST OF LESS COMMON NOMENCLATURE

Name	Generic Structure
Weinreb amide	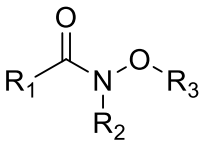
Ynone	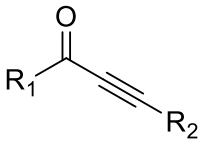
β-diketone (enol form)	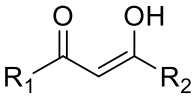
β-diketone (keto form)	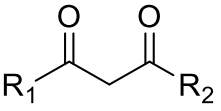
α-diketone	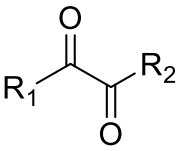
Enamine	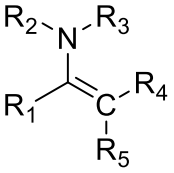
2,5-furandicarboxylic acid	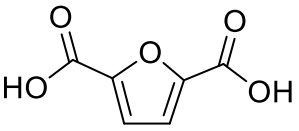
Allenolate	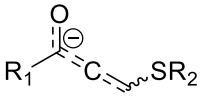
Thiyl	
Thiolate	

DECLARATION OF AUTHORSHIP

This thesis is submitted to the University of Birmingham in support of my application for the degree of Doctor of Philosophy. The material contained in this thesis has not been submitted in any previous application for any degree at any institution.

Parts of this thesis are displayed in a format suitable for publication in peer-reviewed journals, as outlined in the University of Birmingham alternative thesis format guidelines. The work presented in this thesis (including data generated and data analysis, materials characterization, writing, and figure design) was performed by myself, except for co-author contributions which are outlined below and before each chapter.

Chapter 2 - Manuscript Prepared: Lukmanul Hakim Samada, Maher Alraddadi, Joshua C. Worch, Arianna Brandolese, Andrew P. Dove, Versatile Synthesis of Bio-based Photodegradable Polyketones with Controllable Thermomechanical Properties, *Manuscript Prepared.*

Dr. Maher Alraddadi (University of Birmingham; Royal Commission for Yanbu Colleges & Institutes) synthesized a few small molecules and guided mechanical testing. Dr Joshua C. Worch (University of Birmingham; Virginia Tech) provided technical and synthetic guidance. Dr. Arianna Brandolese provided editing of the manuscript. Prof. Andrew P. Dove (University of Birmingham) supervised in addition to providing guidance and editing the manuscript.

Chapter 3 - Manuscript Prepared: Lukmanul Hakim Samada, Neha Yadav, Joshua C. Worch, Arianna Brandolese, Andrew P. Dove, Spontaneous Amino-yne Click Polymerization to Generate Photodegradable Bio-Derived Polyketones with Tunable Thermomechanical Properties, *Manuscript Prepared.*

Dr. Neha Yadav (University of Birmingham) synthesized the precursor and imaged microcapsules using SEM. Dr. Joshua C. Worch (University of Birmingham; Virginia Tech) provided technical and synthetic guidance and editing of this manuscript. Dr. Arianna Brandolese (University of Birmingham) provided editing of the manuscript. Prof. Andrew P. Dove (University of Birmingham) supervised in addition to providing guidance and editing the manuscript.

Chapter 4 - Manuscript Prepared: Lukmanul Hakim Samada, Joshua C. Worch, Arianna Brandolese, Andrew P. Dove, Tuning Thermomechanical Properties of Photodegradable Copolyketones *via* Spontaneous Amino-yne "Click" Copolymerization, *Manuscript Prepared.*

Dr Joshua C. Worch (University of Birmingham; Virginia Tech) provided technical and synthetic guidance and editing of this manuscript. Arianna Brandolese (University of Birmingham) provided editing of the manuscript. Prof. Andrew P. Dove (University of Birmingham) supervised in addition to providing guidance and editing the manuscript.

CHAPTER 1: INTRODUCTION

1.1 Structure-property relationships in polymers

Over the last few decades, polymeric materials have been commercially developed and manufactured to fulfill the primary needs of modern society, such as bags, cups, food packaging, utensils, medical devices, automotive parts, and so forth. However, some issues have emerged during their widespread application. The detrimental effects on the ecosystem resulting from their inherently non-biodegradable polyolefin composition have become a general limitation.

To address these issues, there has been significant research into the development of degradable and sustainable polymers, such as poly(lactic acid) (PLA), polyhydroxyalkanoates (PHA), and starch. These commodity bioplastics have been highly utilized as they are cheap, biodegradable, and biocompatible. They were investigated and designed based on their structure-property relationship towards their thermal stability, mechanical strength, processability, recyclability, degradability, biocompatibility, morphology, and thermodynamic behavior.

The relationship between the structure of polymeric materials and their properties can be elucidated through various fundamental factors at the molecular level. This includes their molecular architecture, chain length, branching, and monomer unit nature.

1.1.1 Molecular architecture

Based on their chain architecture, there are three categories of polymer in general. They are linear, branched, and cross-linked polymers (Figure 1.1). For instance, polyethylene, polystyrene, polyamides, and PVC are examples of linear polymers. Branching polymers are frequently illustrated by low-density polyethylene (LDPE). Epoxy resins, adhesives, vulcanized rubber, polyester fiberglass, and polyurethanes utilized as coatings are examples of cross-linked polymers.

The intrinsic viscosity of most linear polymers is dependent on their molecular weight, which is associated with chain entanglements. This chain entanglement will affect the chain mobility and flexibility of the polymers. This relationship was described as frictional free volume which is a parameter of the glass transition temperature (T_g).[1,2] Unlike linear polymers, the intrinsic viscosity of hyperbranched polymers and hydrodynamic dimension are lower than their linear polymer counterparts, and display a maximum intrinsic viscosity in their dendrimer analogues system. The branching enables a reduction in the hydrodynamic volume due to molecular perturbation of chain conformation. A high degree of branching with a short branch length related to the steric hindrance prevents the chain entanglement formation. The high degree of branching leads to a very compact structure and increased segment density whereas a sparse structure results from a low degree of branching. This will affect the polymer behavior both in solution and in melt.[3,4]

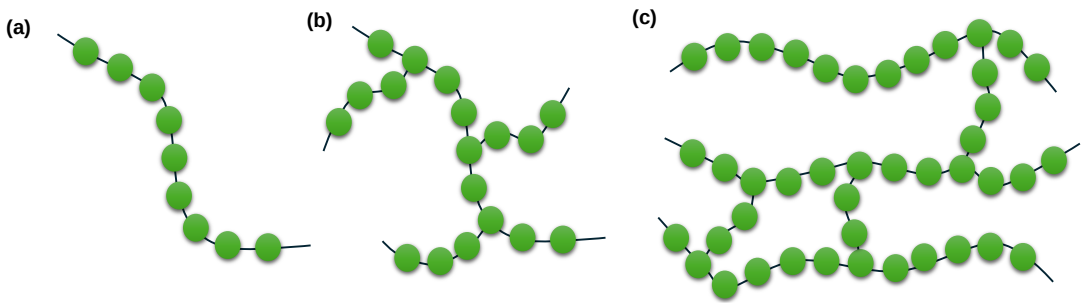

Figure 1.1 Illustration motif of (a) linear polymer, (b) branched polymer, (c) cross-linked polymer

Other molecular features that contribute to the change of glass transition (T_g) temperature are crosslinker functionality and the crosslinker molecular weight Furthermore, backbone stiffness is another parameter that is affected by a change of chemical architecture, such as from an aliphatic to an aromatic backbone. Incorporating reversible covalent cross-links into covalent network polymers enhances the mechanical performance of the polymer materials. This system can generate polymers with reprocessibility, malleability, and self-healing behaviour.[5,6]

1.1.2 Chain length

A close relationship between the viscosity and chain length of the polymer was simply determined by their molecular weight. The molecular weight plays a vital role in thermomechanical and rheological properties as well as viscoelastic behavior. In the case of diethylene adipate, the density increase with chain length is also a result of a decrease in free volume, rather than an excess volume of the end-groups.[7–9] A high molecular weight polymer will lead to a greater chain entanglement that affects the polymer's toughness and processibility. Disentangling the polymer without raising the moulding temperature can significantly reduce the viscosity of polymer melts, leading to enhanced fluidity,

reduced flaws, and increased quality. In addition, reducing entanglement can facilitate the process of crystallization and the development of appropriate shapes, hence enhancing the overall mechanical strength of the end products.[10] The discontinuous nature of the distribution in which macromolecules exist in discreate fractions "i" containing N_i molecules of molar mass M_i is typically used to define molar mass averages.

$$\bar{M}_n = \sum_{\square}^{\square} X_i \, M_i \;\rightarrow\; \bar{M}_n = \frac{\sum_{\square}^{\square} N_i \, M_i}{\sum_{\square}^{\square} N_i}$$

Equation 1.1 The number-average molar mass ($\bar{M}_n$) defined as the sum of the products of the molar mass of each fraction multiplied by its mole fraction

$$\bar{M}_w = \sum_{\square}^{\square} w_i \, M_i \rightarrow \bar{M}_w = \frac{\sum_{\square}^{\square} N_i \, {M_i}^2}{\sum_{\square}^{\square} N_i \, M_i}$$

Equation 1.2 The weight-average molar mass ($\bar{M}_w$) defined as the sum of the products of the molar mass of each fraction multiplied by its weight fraction

$$\bar{M}_z = \frac{\sum_{\square}^{\square} N_i \, {M_i}^3}{\sum_{\square}^{\square} N_i \, {M_i}^2} = \frac{\sum_{\square}^{\square} w_i \, {M_i}^2}{\sum_{\square}^{\square} w_i \, M_i}$$

Equation 1.3 Z-average molar mass ($\bar{M}_Z$) defined as the higher molar mass averages than $\bar{M}_w$

1.1.3 Monomer unit nature

Apart from their bio-renewability, natural products are preferred as an alternative to fossil fuel-based polymers due to the diversity of their structure and stereochemistry. This means that they can potentially generate novel reactions or methods that lead to unpredictable properties. Carbohydrates are among the most

abundant bio-based building blocks in nature that are intensively used for monomer synthesis. They offer a wide variety of chemical structures and stereochemistry, for example, cellulose, starch, and glycogen. These polysaccharides can be converted into monosaccharide units, including unsaturated carboxylic acid, polyols, and furan derivatives which are subsequently able to be manipulated to become functional monomers. This strategy is powerful to mimic the structure of natural product-based polymers with enhanced physicochemical properties.[11,12]

1.1.4 Copolymerization

Copolymerization can be defined as a simultaneous polymerization that involves two or more types of monomers. In general, the copolymerization strategy also contributes to the improvement of physicochemical properties of the materials. The resulting polymers could be classified into random copolymer, graft copolymer, and block copolymer. These different architectures provide distinct phase segregation behavior and transition temperatures. Moreover, the copolymers' architecture greatly influences the surface energy, thermal transitions, and mechanical performance of the material. This demonstrates that the ability to modify the arrangement of monomers in the structure is an effective method for adjusting the physical and mechanical properties of these polymers.[13] Several methods have been employed to modify and expand the glass transition behavior of polymers. These methods involve plasticization (*e.g*. plasticizer addition), incorporation of fillers (*e.g*. nanofiber, carbon black insertion), and the synthesis of polymers with nanoheterogeneous morphology, such as interpenetrating polymer networks or gradient blends. In nanoheterogeneous multicomponent polymers, the presence

of significant interfacial regions allows for a wide variety of glass transition temperature (T_g) responses. For example, polystyrene-block-polybutadiene-block-polystyrene (SBS) triblock copolymers offer a wide spectrum of service temperatures due to the widely separated glass transition temperature T_g of the constituent phases.[14,15]

1.2 Step-Growth Polymerizations

In general, polymerization can be classified into two categories: step-growth polymerization (SGP) and chain-growth polymerization (CGP). In step-growth polymerizations, the chain propagates progressively through reactions between the functional chain-terminal groups of the monomer, oligomers, and ultimately polymers. The reaction can occur between monomers, dimers, trimers, *etc.* at any given moment that is initiated with one or more multifunctional monomer(s), resulting in the formation of larger macromolecules with high molecular weight (there is no need for external radical initiator for the initiation step).[16]

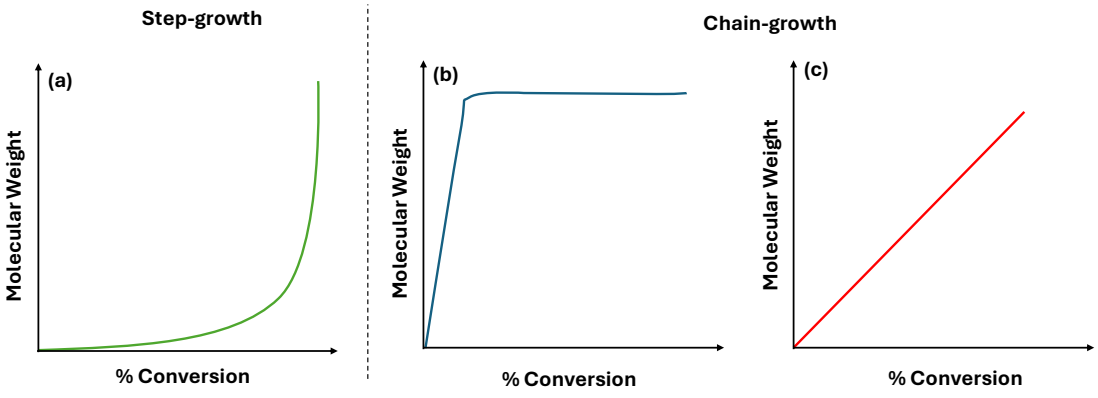

Figure 1.2 Molecular weight dependence on extent of conversion in different polymerization mechanisms a) step-growth polymerization b) chain growth polymerization and c) living chain-growth polymerization.

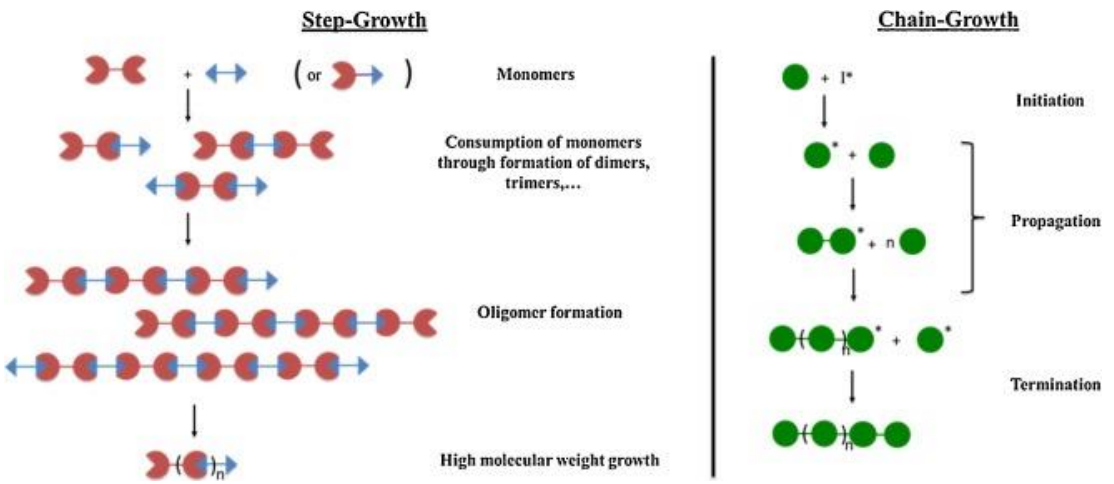

Figure 1.3 Illustration of difference scheme between (a) step-growth polymerization; (b) chain growth polymerization. Reproduced with permission from Ref. 16. Copyright 2018 Elsevier Ltd.

Beginning with the formation of dimers from monomers, the mechanism of growth in step-growth polymerisations gradually expands to trimers and tetramers until high molecular weights are achieved (Figure 1.2a and 1.3a). In the chain growth polymerisation process, an initiation phase results in the formation of a reactive intermediate, such as a radical, anion, cation, or metallocene. The reactive centre is transferred to the end of the chain through a propagation phase, where it reacts with a monomer, typically alkene derivatives. Monomers are successively added to increase their molecular weight until the reactive centre is consumed by termination (Figure 1.2b and 1.3b). Living chain growth polymerization is a viable alternative to chain growth polymerization, in which the molecular weight increases linearly through the conversion process (Figure 1.2c).

Typically, there are two categories of step-growth polymerization reactions, including polyadditions and polycondensations reaction. Polycondensation reactions, such as the synthesis of polyesters, polyamides, and polyketones, and

so forth involve the release of small molecules (such as water and methanol) as by-products. The typical step-growth polymerizations with polyaddition reaction commonly include the synthesis of polyurea, and polyurethanes, where the monomers undergo a reaction with no release of a small molecule. Nevertheless, specific experimental requirements must be met to attain clearly specified compositions and predicted molecular weights of the polymer materials produced using step-growth polymerization. For the manufacture of polymers with high molecular weight, it is crucial to have monomer functionality equal to two, functional group stoichiometry equal to one, high reaction conversions, no side reactions, and rapid removal of side products.[17,18]

The step-growth polymerization process relies on a well-established theory of classic kinetics (Carothers-Flory theory). This theory states that in order to generate high molecular weight polymers in linear fashion, a precise balance of bifunctional monomers is necessary. The reactivity of all reactive groups is assumed to be equal, with the oligomer and polymer terminal groups determined by the molar ratio between monomers. However, even a slight stoichiometry imbalance of the monomers, caused by physical loss of monomers and not perfect monomer synthesis, can lead to a drastic decrease in the number-average degree of polymerization.[19,20] The molar mass of polymers prepared by step polymerization can be predicted using a straightforward analytical method that Carothers developed. He recognized that the number-average degree of polymerization in relation to monomer units is represented by the following relation:

$$\bar{x}_n = \frac{N_0}{N}$$

Equation 1.4 The average number of polymerization degrees in relation to monomer units

N_0 = the initial number of molecules present, N = the remaining number of molecules after a time *t* of polymerization

$$p = \frac{N_0 - N}{N_0} \quad \rightarrow \quad \frac{N_0}{N} = \frac{1}{1-p}$$

Equation 1.5 For each pairwise reaction between functional groups, the total number of molecules decreases by one.

$p = \frac{\text{Reacted number of functional groups}}{\text{Initial number of functional groups present}}$ [Time-dependent extent of reaction p]

$$\bar{x}_n = \frac{1}{1-p}$$

Equation 1.6 Carothers equation, which is the combination of equation 1.4 and 1.5

In general, SGP can be categorized into two specific strategies: AB_n homopolymerization and $A_m + B_n$ copolymerization. In step-growth polymerization, it is difficult to control the molecular weight with a low dispersity of the polymers as the monomers and oligomeric intermediates have bonded to each other unselectively. Therefore, chain-growth polymerization has been employed to tune the molecular weight and the molecular weight distribution. The reaction is started by the reaction between a monomer and a radical initiator or anion, cation, and metallocene. Additional monomers then react with the propagating site of the growing polymer chain (polymeric active site) to form longer polymers, eventually

resulting in termination of the active site.[21] The polymer chain typically grows stepwise at a time. Meanwhile, in the living chain-growth polymerization, the polymerization proceeds without termination or disproportionation. The molecular weight of the polymer can be controlled through the initiator to monomer feed ratio.[22,23] Some reports revealed that step-growth polymerizations can be converted into chain-growth polymerization by increasing the reactivity of the polymer end group relative to the monomer.[24]

1.2.1 Homopolymer Synthesis

An illustration of step-growth homopolymerization can be seen in the Nylon 6,6 synthesis through the self-condensation of an amino acid. The crystalline polymer Nylon 6,6 is composed of oleophilic hydrocarbon chains that are connected by hydrophilic functional amide groups (Figure 1.4).

$$i H_2N–R–COOH \xrightarrow{\square} H–[NH\text{-}R\text{-}CO]_i–OH + (i - 1)H_2O \qquad (1)$$

The reaction can be written as

$$(AB)i + (AB)j \xrightarrow{Ki,j} (AB)i+j + H_2O \qquad (2)$$

The molecules H_2N and COOH represent the functional groups of an amino and carboxyl group, respectively.[25] *Ki,j* refers to the rate constant of effective polymerization, which is influenced by the lengths *i* and *j* of the two chains participating in the reaction, particularly when diffusion restrictions are present. In the case of an irreversible polymerization, the presence of a condensate unit (such as H_2O in the case of Nylon polymer) does not impact the polymer chains distribution.[26]

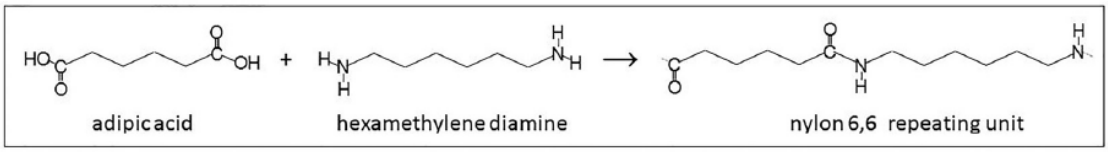

Figure 1.4 Synthesis scheme of nylon 6,6. Reproduced under Creative Commons Attribution License from *PLoS ONE*, 2016, **11**, 7. Ref. 25.

Furthermore, another class of polymers that are polymerized via step-growth homopolymerization are polyesters. This method allows for the facile integration of various monomers into the polyester backbone due to the convenient availability of diols and acids with diverse structures derived from both renewable and non-renewable feedstocks. Although there has been notable advancement, step-growth polymerization reactions still face numerous intrinsic challenges. The conventional method of polycondensation of unactivated diacids/diesters and diols is a reversible reaction that requires the constant elimination of the by-products (water or alcohol) in order to enhance the progress of the reaction. Condensation polymerization allows for the attainment of increased molecular weight through a process of high conversion. These requirements include extended reaction time, elevated temperatures, and the need for a vacuum without air or intricate azeotropic distillation arrangements, all of which diminish the appeal of this approach. In addition, the breakdown of diacids at extremely high temperatures, along with the evaporation of volatile diacids and diols, would lead to undesired imbalances in the chemical proportions, resulting in the formation of lower molecular weight polymers. Substituting acids with acid chlorides can result in quicker reactions, although their elevated reactivity frequently causes unregulated polymerization. Additionally, the hydrochloric acid that is produced during the

polymerization process might trigger the reverse reaction via acid-catalyzed cleavage of the polyester backbone.[27]

Based on the conventional theory of step-growth polymerization, all functional groups involved in the polymerization process are equally reactive at any given time, regardless of the size of the molecule they are linked to. This assumption is made under the condition that no intramolecular cyclization takes place. The molecular weight distribution that is projected as a result is referred to as the "most probable" distribution, with a dispersity of 2 at high conversion. This indicates that this type of polymerization is not suitable for synthesizing polymers with a narrow polydispersity. A recent example is the hydroxyalkylation process, which involves the acid-catalyzed condensation of ketones and aldehydes with aromatic compounds.[28] Furthermore, polyurea and polyurethanes, well recognized polymers in the industrial sector, are synthesized through a step growth polymerization reaction between diisocyanates and diamines or diols. These products are utilized as coatings, foams, adhesives, and sealants. Polyurea was initially developed by Bayer *et al*. in 1937 through the chemical interaction of an aliphatic diamine and diisocyanate. Subsequently, polyurethane was fabricated through reacting an aliphatic diisocyanate with glycol. Hexamethylene diisocyanate (HDI) and toluene diisocyanate (TDI) along with the isocyanurate trimer of TDI and TDI-trimethylolpropane, are extensively utilized in the polymer field.[29]

In addition, according to the Carothers-Flory theory, a step-growth polymerization using functional monomers is able to result in the formation of high molecular weight polymers, if there is a balanced ratio of reactive groups and a significant

extent of polymerization reaction. Due to the presence of impurities in the monomers and the potential occurrence of side reactions, ensuring precise stoichiometry of the reactive groups throughout the whole polymerization process is challenging in practical applications.[30] Despite considering stoichiometry, it is challenging to attain an exceptionally high degree of polymerization reaction within a limited timeframe. As a result, the polymers produced using the conventional homogeneous step-growth polymerization have a relatively low molecular weight. In order to tackle this issue, a step-growth polymerization process has been developed that utilizes a stoichiometric imbalance to boost the reaction between two monomers. The polymerization reaction in this process is facilitated by a reactive intermediate.[31]

In order to achieve efficient polycondensation processes that do not rely on the stoichiometric balance and allow for precise control over the molecular weights of polymers, Zou and co-workers have lately shifted their focus to Friedel−Crafts (F−C) reactions since this type of reaction does not require a precise feed control of acids used. These reactions facilitate the formation of carbon−carbon bonds and enable the incorporation of aryl units into the polymer structure. Specifically, the powerful acid has been used to catalyze reactions between ketones that are electron poor and aromatic compounds that are electron-rich.[32] These reactions have been employed to generate linear polymers, branched polymers, and dendrimers. For all of these reactions, it is vital to carefully choose arene monomers as nucleophiles in order to obtain a high level of regioselectivity and to generate polymers with well-defined structures. Aldehydes are not commonly utilized in F−C polycondensations for polymer preparation, unlike ketone

monomers. However, an exception is the reaction between formaldehyde and phenol, which produces phenol formaldehyde resin. Nevertheless, this reaction lacks regioselectivity and frequently yields a cross-linked polymer (Scheme 1.1).[33,34]

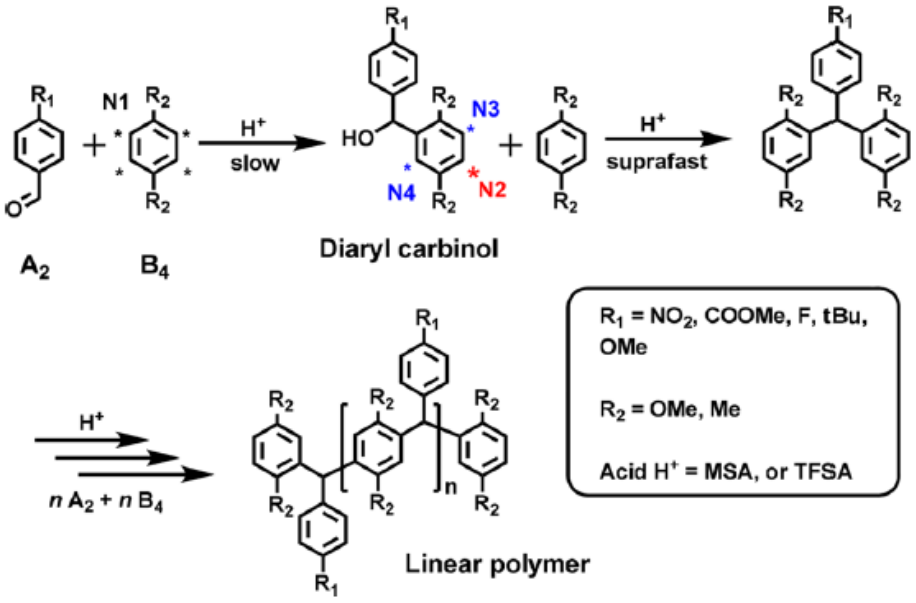

Scheme 1.1 Synthesis of Linear Polymers Using Acid- Catalyzed F−C Polycondensation of A2 + B4 Monomers. Reproduced with permission from Ref. 33. Copyright 2018 American Chemical Society.

1.2.2 Copolymer Synthesis

Palladium catalysts can be used in conjunction with insertion copolymerization to fabricate linear polyketones. It is important to highlight that this technique is by far the most dependable for creating alternating polyketones. Nevertheless, this method still has issues with methyl branching and homopolyolefin production. Controlling the microstructure is therefore still a crucial requirement for the synthesis of aliphatic polyketones. The introduction of metathesis polymerization has helped to somewhat address the aforementioned difficulty.[35] Zeng *et al*. have effectively synthesized aliphatic polyketones through sequential cross-metathesis

polymerization (CMP) and thiol-Michael chemistry. Initially, the bio-based monomer was synthesized in two stages using the natural product derivative 10-undecenal as the starting material. In order to produce polyketones with a high molecular weight, the CMP condition was optimized (Scheme 1.2).

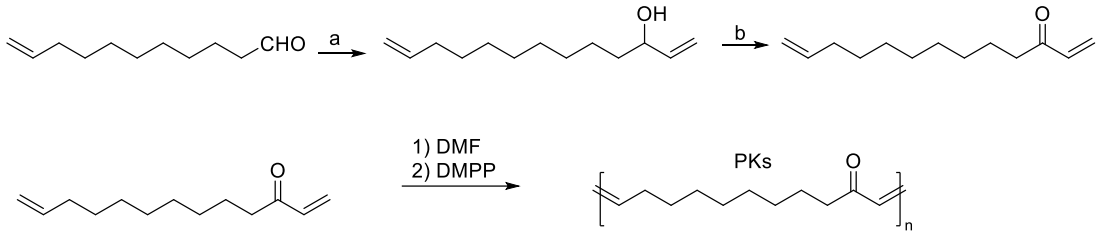

(a) 1.5 equiv. vinylmagnesium bromide (1 mol L 1 in THF), dry THF, 20 °C – 0 °C, 1 h; (b) 1.2 equiv. IBX (0.8 mol L 1 in DMSO), THF, r.t., 2 h.

Scheme 1.2 Preparation of unsaturated polyketones *via* cross-metathesis polymerization

In recent years, other considerable efforts have been devoted to developing biodegradable copolymers. This has led to notable advancements in understanding the cleavage patterns and mechanisms of aliphatic polyesters, with a specific focus on poly(lactic acid) (PLA) and its copolymers. Lactic acid-based copolymers have demonstrated promise as viable alternatives for applications in biomedicine, in particular as scaffolds utilized in tissue engineering.[36]

Nevertheless, the inherent characteristics of PLA homopolymers are inadequate for numerous technical uses without alterations. Consequently, there is a significant demand for renewable and biodegradable constituents that can enhance the polymer with advanced features. The synthesis method used was step-growth polymerization in the melt phase, as this is a commercially viable technology due to its straightforward procedure. Therefore, it was demonstrated that step-growth polymerization is a straightforward and easily manageable

technique for manufacturing sophisticated polymers based on lactic acid building blocks. Alternatively, PLA copolymers have been developed, but they need high temperature reactions in production. These products would be well-suited for packaging applications, owing to their enhanced glass transition temperature (T_g) and excellent thermal stability.[37]

Polyketones that are commercially accessible are random copolymers that are typically manufactured with a ketone-to-methylene ratio of less than 5 per 1000 units. The attraction in these materials stems from their increased sensitivity to ultraviolet (UV) light, which enables the production of photodegradable plastics. Precisely specified polyketones were initially synthesized by Acyclic Diene Metathesis (ADMET) step-growth polymerization, resulting in the incorporation of a ketone group per 19th methylene unit (equivalent to 52 ketones per 1000 methylene units).[38]

Typically, an alternating copolymer, namely a γ-polyketone, is produced *via* insertion copolymerizations. Cationic Pd(II) diphosphine catalysts were discovered to be exceptionally compatible. The insolubility of γ-polyketones in the most common solvents and their high melting temperatures (>250 °C), at which point polymer degradation becomes a significant concern, restrict their processability. In order to tackle this concern, polyketones devoid of defects are preferable. An established method for fabricating model polyethylenes that are functionalized or branched involves the copolymerization of suitably functionalized or branched α,ω-dienes with nonfunctionalized α,ω-dienes *via* acyclic diene metathesis (ADMET). Mecking and co-workers found that polyketones derived from ADMET can serve

as model polyketones devoid of defects (Figure 1.5).[39,40]

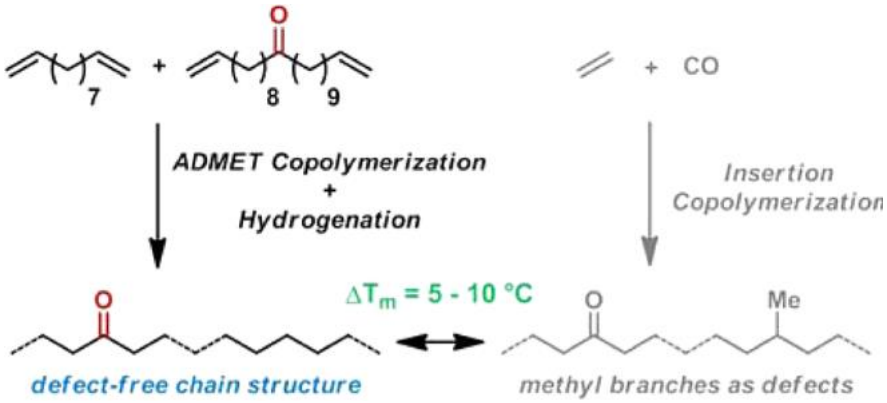

Figure 1.5 Preparation of long-spaced polyketones from ADMET copolymerization. Reproduced with permission from Ref. 39. Copyright 2021 American Chemical Society.

In addition, another strategy to synthesis especially linear and graft copolymers is Reversible addition−fragmentation chain-transfer (RAFT) step-growth polymerization. Approaching the synthesis of intricate architectures with ease, RAFT step-growth polymerization offers novel opportunities by synergistically combining the user-friendly nature and high functional group tolerance of conventional RAFT polymerization with the versatility of conventional step-growth (in the design of backbones). By leveraging the backbone's adaptability to integrate biodegradability, one could have foreseen the extensive use of these RAFT step-growth polymerization-produced linear and graft copolymers in materials science, including drug delivery.[41]

Subsequently, an emerging step-growth polymerization strategy is devised to fabricate hyperbranched star copolymers in a novel manner while preserving the characteristic of a one-pot polymerization process. Prior research has frequently utilized the step-growth polymerization as a two-step procedure, which consists of the initial synthesis of hyperbranched polymers consisting of different monomers

at their terminus.[42]

The utilization of hyperbranched star copolymers in metal catalysis, drug loading, and the incorporation of boron into ceramics has been the subject of numerous studies, all of which involve a two-step synthesis process. However, particularly for the C_1 macromonomer, the conventional two-step synthesis strategy is characterized by a lengthy synthesis time and intricate post-processing. As a result of the difficulty in determining the terminal group content of hyperbranched polymers, excessive addition and subsequent removal of C_1 monomers are required to produce hyperbranched star copolymers with a unimodal molecular weight distribution. Determining precise theoretical knowledge pertaining to one-pot step growth polymerization is thus essential for the synthesis and application of hyperbranched star copolymers. Bang *et al*. have effectively performed a one-pot one-batch synthesis of $A_m+B_n+C_1$ hyperbranched star copolymers with a multimodal molecular weight distribution. A rigorous mathematical derivation is conducted to determine the number ratio of monomeric structural units (N_A/N_B) in order to disclose the cyclic defect of intramolecular cyclisation solely through proton nuclear magnetic resonance (^{1}H NMR) spectroscopy. Hyperbranched star poly(vinyl ether ester)s (mPEG-hb-PVEEs) amphiphiles ($A_2+B_3+C_1$) synthesized through one-pot one-batch polymerization (Scheme 1.3).[41,43]

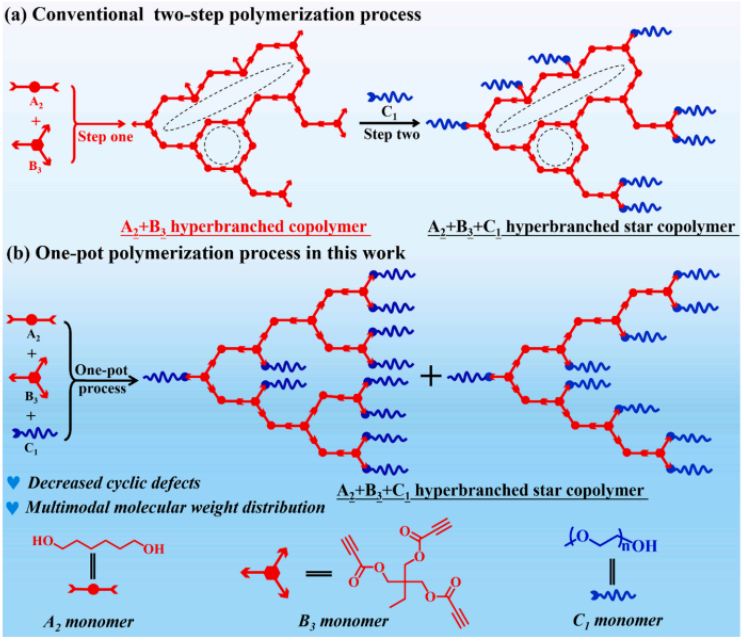

Scheme 1.3 (a) The traditional two-step polymerization method employed to produce hyperbranched star copolymers A_2+B_3+C_1. (b) One-pot polymerization method for hyperbranched star copolymers A_2+B_3+C_1 with multimodal molecular weight distribution and reduced cyclic defects. Reproduced with permission from Ref. 41. Copyright 2021 American Chemical Society.

1.3 Click reaction for polymer synthesis

The click reaction is distinguished by several noteworthy qualities, such as its exceptional efficiency, regioselectivity, atom economy, and resistance to functional groups. The click reaction has rapidly gained extensive usage across a wide range of fields, most notably in the domain of bioconjugation due to its simplicity, selectivity, and biorthogonality (Figure 1.6). Additionally, the utility of click reactions has been investigated in the field of polymer research. While considerable research has been dedicated to understanding how post-polymerization click reactions can be utilized to modify and functionalize preformed polymers, an even greater amount of effort has been invested in developing the click reaction as a novel polymerization technique. An endeavor was undertaken in the 1960s to

produce terephthalic acids *via* the cycloaddition of azido alkynes; however, the system fails to satisfy the requirements established by Sharpless for a click reaction, which precludes its classification as a click polymerization.[44] Since 2002, when Sharpless and Meldal discovered copper-catalyzed azide-alkyne cycloaddition (CuAAC) (Scheme 1.4), justify the research on click polymerization has been conducted. Click polymerization has been validated as a viable synthetic method for producing functional, regio-regular, and processable Purified Terephthalic Acid (PTAs).[45,46]

Figure 1.6 Simple illustration of a "click" reaction

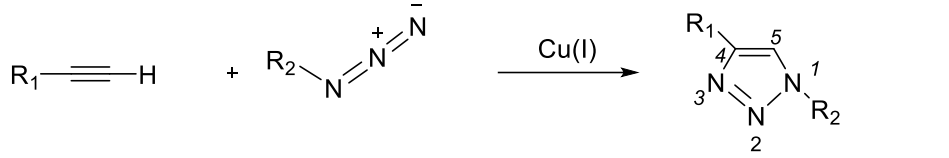

Terminal Alkyne Aliphatic Azide 1,4-disubtituted 1,2,3-triazole

Scheme 1.4 Cu(I)-Catalyzed Azide−Alkyne Cycloaddition (CuAAC)

A vast array of reactions that have demonstrated their efficacy and adaptability as chemist's companions are included in click chemistry. Because of the inherent simplicity and efficacy, this category of reaction is highly versatile. With minimal synthetic work-up, click reactions are distinguished by their selectivity, ease of experimental setup, suitability in both aqueous and aerobic environments, tolerance to a wide range of functional groups, and ability to produce quantitative results. The Cu^{I}-catalyzed azide–alkyne cycloaddition, the Diels–Alder

cycloaddition, the thiol–ene reaction, and the azide–nitrile cycloaddition are all examples of reactions that manifest these characteristics. Recent literature on click chemistry is predominated by the Cu^{I}-catalyzed azide–alkyne cycloaddition.[46] The process of synthesizing and modifying polymeric materials can be significantly facilitated by these straightforward and robust reactions. A wide range of materials have been synthesized using click reactions, including terminal and pendant functional polymers, (multi)block copolymers and micelles, complex architectures such as star, brush, graft, hyperbranched, and dendritic polymers, gels and networks, and polymers conjugated to nanomaterials.[47]

As a result, numerous long-standing challenges in polymer science are resolved by means of this reaction. These challenges include (a) inadequate functionalization efficacy with numerous conventional methods, particularly when multiple functional groups are involved; (b) difficulties in purification resulting from the frequent formation of partially functionalized mixtures; (c) incomplete reaction at interfaces and surfaces; and (d) the harsh reaction conditions inherent in conventional methods. The primary advantage is that the click reaction combines exceptionally well with numerous controlled polymerization reactions that have been developed over the last few decades. This permits an almost limitless exploration of novel functionalized polymeric architectures that were previously unobtainable through the conventional polymerization methods. Polymer chemistry is now on a par with small-molecule organic chemistry with regard to molecular addressability, structural integrity, and functional broadness, owing largely to the development of azide/alkyne click chemistry.[48]

In polymer chemistry, thiol-X reactions, which deduce the reactions of thiols with alkenes, alkynes, bromo compounds, epoxides, or specific fluoro compounds have been embraced as a means to obtain effective, dependable, and robust procedures. Fused materials, polymer architectures, and nanoparticles coated with polymers are among the numerous applications of these reactions that involve fabrication and functionalization. In polymer science, click strategies are not restricted to the aforementioned prevalent reactions in polymer chemistry. The synthesis and modification of macromolecular architectures have also been accomplished *via* a collection of additional reactions, such as sulphur(VI) fluoride exchange reactions and oxime-based carbonyls. Evidently, the concept of click chemistry is a continuous chemical phenomenon that unceasingly proposes novel chemical reactions; as a result, the application of these reactions in polymer science appears promising.[49]

The concept of modular, straightforward, and economical synthesis of molecules with varied structures and functions has also captivated polysaccharide chemists; this notion has made a substantial contribution to the progress of this domain. "Click" reactions not only circumvent the aforementioned constraints associated with traditional synthetic routes, but also enable the swift synthesis of molecules possessing a wide range of functional appendages. There have been several frequently employed "click" reactions in the field of polysaccharide chemistry. These reactions include the oxime click reaction, the renowned azide–alkyne Huisgen cycloaddition, the Diels–Alder reaction, and the thiol–ene and thiol–Michael reactions. In the past decade, numerous novel reactions that fulfil the requirements of click chemistry have been discovered.[50]

1.3.1 Thiol-yne “click” polymerization

In recent years, there has been significant interest in the application of Michael-addition of thiols to maleimides for polymer functionalization. This is primarily due to the favorable reaction conditions, which include catalyst-free reactions, high reaction yields, and selectivity. Consequently, this versatile chemistry has emerged as a crucial technique in the field of material engineering.[51] An alkyne undergoes a sequential anti-Markovnikov addition reaction with two thiols under UV irradiation during the thiol–yne reaction, which is very similar to the thiol–ene reaction.[52] Because two functional moieties can be introduced into the same site along the peptide chain, the thiol–yne reaction is a complementary over the thiol–ene reaction. In addition, The Dondoni group effectively produced peptide–protein conjugates containing both fluorophore and glucose at the same site using the thiol–yne reaction. This demonstrates that by meticulously regulating the reactant ratio and reaction time, it is possible to distinguish the two functional moieties introduced *via* the thiol–yne reaction.[53]

Through the Cu(I)-catalyzed alkyne-azide reaction, it was demonstrated that alkynes, which are generally stable until given the chance to react, are ideal substrates for a vast array of material applications, as they are comparatively simple to synthesize in a variety of structural configurations. Given this premise, it is crucial to consider how easily one chemistry can be applied to additional categories of extremely efficient reactions. It is noteworthy that an examination of the scholarly works spanning the 1940s to the 1960s reveals a conspicuous alignment between specific radical-mediated "thiol-yne" reactions with the

presence of organobase catalysts, and the characteristics commonly linked to exceptionally effective thiol-ene chemistry. Consequently, one might hypothesize that thiol-yne reactions offer a unique prospect for the advancement of thiol-ene reactions' chemistry, thereby granting access to an extensive array of novel materials and properties. As a result, numerous researchers have examined "thiol-yne" reactions as a chemical framework for the synthesis of materials applicable to network film formation, polymer functionalization for regulating solution properties in water, and the fabrication of novel highly functional chemical species. Furthermore, in order to explore additional potential applications, the thiol-yne reaction has been expanded to encompass hydrogels.[54,55]

According to the nucleophilicity of the catalyst species, these base-catalyzed processes are believed to take place through two principal pathways, which occasionally compete in the same reaction. In order to deprotonate the thiol, strongly basic amines can either attack the electron-deficient alkyne as a nucleophile to form an allene enolate, or they can function as a Brønsted-Lowry base (Figure 1.7).

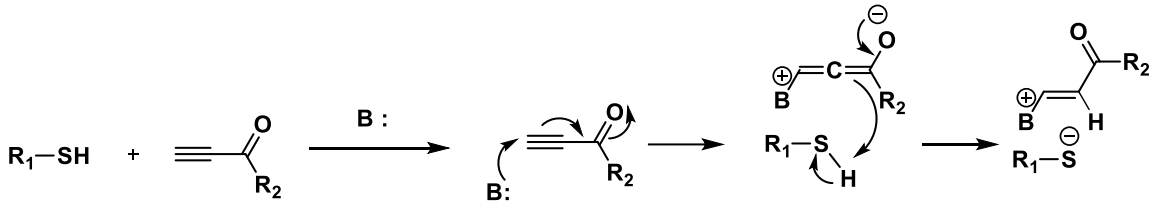

Figure 1.7 Organocatalyzed thiol-yne reaction mechanism following a nucleophilic initiated pathway

In Figure 1.8, each yne moiety reacts initially with a single thiol to produce vinyl sulfide. Subsequently, the vinyl sulfide reacts with a second thiol to produce the 1,2-disubstituted adduct. In comparison to more conventional thiol-ene reactions, this two-step reaction, which is in many ways akin to the sequential reactions of a primary amine and subsequently the secondary amine with an epoxy, considerably increases the maximum possible crosslink density and degree of substitution in these polymers.[54]

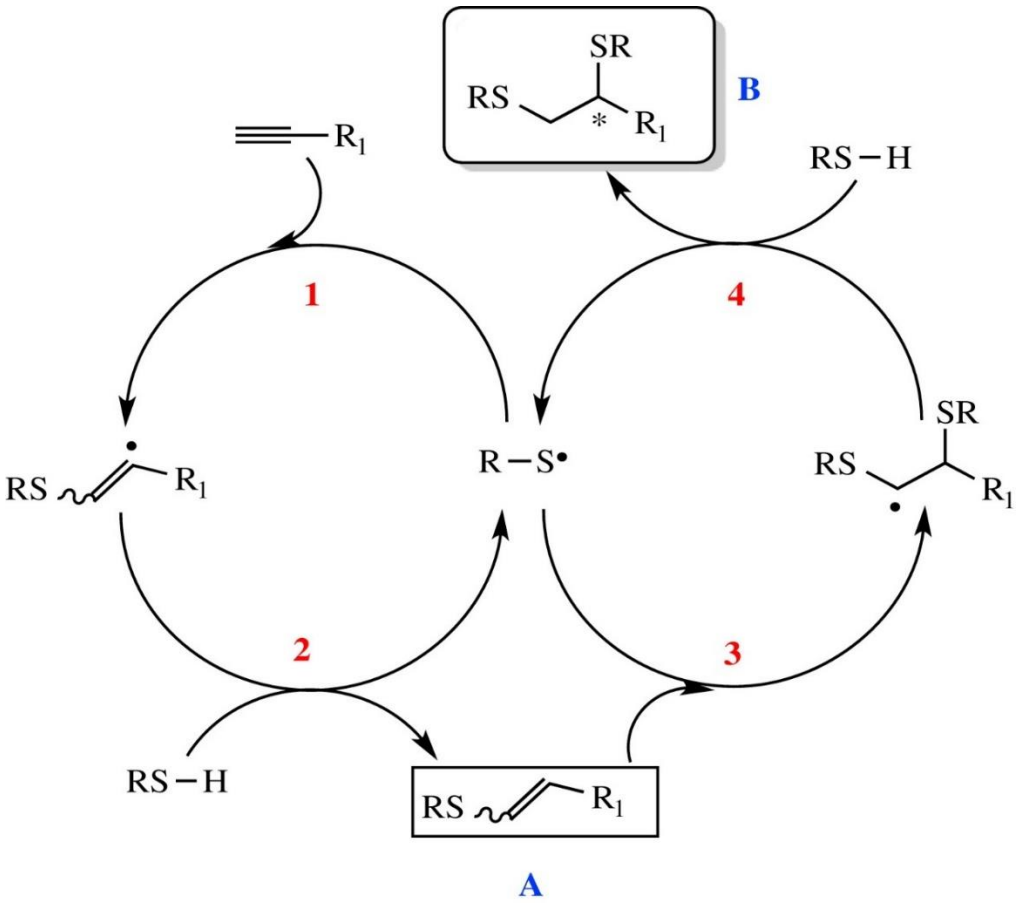

Figure 1.8 Reaction mechanism for addition of thiols to alkyne. Reproduced with permission from Ref. 54. Copyright 2014 Elsevier Ltd.

Research on "thio-click" polymerizations, particularly thiol−yne click polymerization, is still in its nascent phase, whereas the azide−alkyne click polymerization has generated substantial reports. Additional research is required to develop novel catalyst systems, including transition-metal complexes, photon, heat, and organic base systems, in addition to novel reaction types and functionalities of the resulting polymers *via* polyaddition reaction.[56] Subsequent to extensive research focusing on relative reactivity, controllability, and specificity, thiol-click polymerization reactions have been refined for the production of porous polymer monoliths, films, and gels. The aforementioned studies provide evidence that thiol-click polymerization reactions are characterized by high rate of conversation, simplicity, and resistance to oxygen inhibition. Furthermore, the resultant films exhibit network structures that are relatively uniform.[57]

1.3.2 Spontaneous amino-yne “click” polymerization

Various types of click polymerizations have been developed thus far, including those catalyzed by transition metals, organobases, metals, and spontaneous alkynes. Among these, the transition metal-catalyzed alkyne-based click polymerization has gained significant recognition. Unfortunately, it is difficult to entirely eliminate the metallic residues present in polymeric products, which would result in cytotoxicity and a decline in the products' electrooptical performance when utilized. In order to address this challenge, researchers have devised synthetic monomers or activated monomer-based spontaneous click polymerizations that do not involve the use of metals.[58]

The example of well-known spontaneous amino-yne click polymerization is synthesis of regio- and stereospecific poly(β-aminoacrylate)s with high M_w and

yields developed by Tang's group (Figure 1.9). They conducted the reaction between activated propiolates and aliphatic amines at very mild reaction condition with no use of external catalyst (Figure 1.10). This strategy enables the provision of an efficient and robust way to generate functional polymers with simple reaction and no further purification needed. This reaction is called polyhydroamination which is biocompatible to prepare functional polymeric materials for cell imaging.[59] Recently, Tang and co-workers also employed imine monomers to react with electron deficient-propiolates resulting good thermal stability and diverse features of polymers by tailoring the solvent and water content. This method is the known as imine-yne click polymerization.[60]

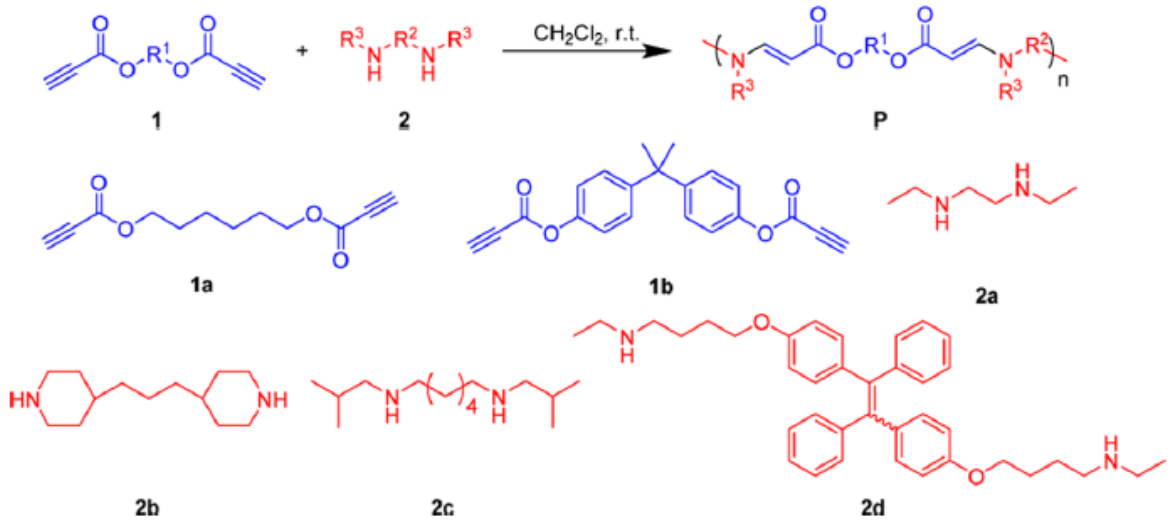

Figure 1.9 Poly(β-aminoacrylate)s were synthesized via spontaneous click polymerization of dipropiolates and diamines. Reproduced with permission from Ref. 59. Copyright 2017 American Chemical Society.

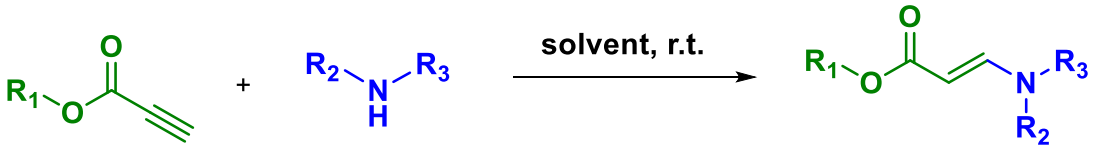

Figure 1.10 Illustration scheme of spontaneous amino–yne click reaction

Furthermore, this polymerization technique is not only useful to prepare linear polymers, but also hydrogels and networks. Amino-yne polymerization proceeds at room temperature in a short period of time with high yields. In addition, there is the potential to employ the amino-yne reaction in the synthesis of covalent adaptive networks (CAN) due to the reversible enamine bond. A high affinity of amine groups enables it to attack the activated alkyne monomer rapidly without using any external stimuli and additive (Scheme 1.5).[61]

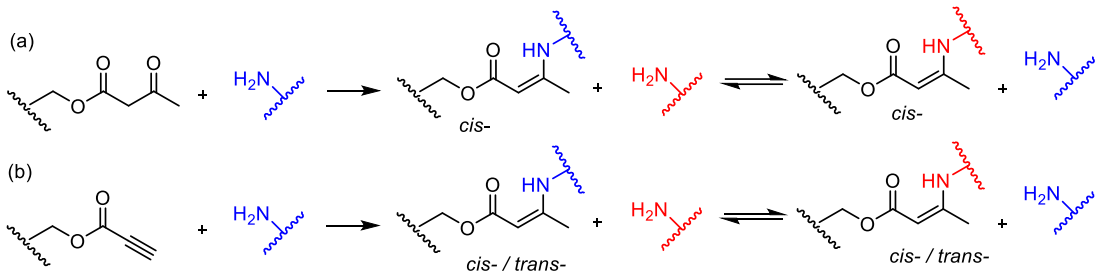

Scheme 1.5 Formation of dynamic enamine-one structure *via* (a) amine-acetoacetate condensation and (b) amino-yne "click" reaction.

Enamine bonds, which are acidic stimuli-sensitive to preserve the equilibrium between amine and enamine plus aldehyde groups, were formed during the amino-yne click reaction. As an outcome, the hydrogels that were obtained underwent reversible sol−gel transitions induced by pH. As a result, there is potential for tissue engineering and additional biomedical applications involving stimuli-responsive and biodegradable hydrogels produced *via* spontaneous amino-yne click reaction.[62]

Zhang's group utilized the amino-yne click reaction to produce metallecycle-crosslinked supramolecular polymers designed for application as adhesive materials, thereby demonstrating that the reaction is an efficient method for

synthesizing functional supramolecular polymers. In addition to enhanced mechanical strength and durability, supramolecular polymers crosslinked with metallacycle demonstrated elastomer characteristics.[63] Moreover, it shows a facile approach to synthesize nitrogen-containing polymers. Considering their simplicity, high efficiency, and mild reaction conditions, they offer a new kind of click polymerization that is an alternative to thiol-yne and azide-alkyne click polymerizations that do not require external triggers or additives, such as metal catalysts or organobase catalysts.[64,65] This process is applicable to most organic solvents and organic molecules. It also gains access to the adaptable fabrication of three-dimensional (3D) structures. Additionally, it facilitates parallel synthesis and large-scale production.[66]

1.4 Thermomechanical properties of polymer materials

Understanding the correlation between the structure at the atomic or molecular level and the fundamental physical and chemical macroscopic properties is essential for enhancing the performance and properties of a polymeric material. Despite significant advancements in understanding the correlation between the macroscopic properties and chemical constituents of polymer chains, the predictive capability of these concepts is constrained by the vast array of molecular architectures and chemical constituents that contribute to the viscoelastic properties.[67]

Based on their thermal and mechanical properties, the polymers can be categorized into thermoplastics, thermosets, and elastomers (Figure 1.11). Thermoplastics frequently comprise acrylic, polyester, polypropylene, polystyrene,

nylon, and Teflon. Polyurethane, epoxy, silicone, and phenolic are all examples of thermoset plastics and polymers. Natural and synthetic rubbers are both classified as elastomers.

Notably, thermoplastics have garnered more interest from many scientists compared to thermosets due to their cheaper processability, efficient production, and recyclability.[68] The characteristic feature of thermosets is the presence of crosslinked polymeric chains and a crosslink density dependence. However, this leads to brittleness and constrains their applications. To handle this challenge, the researchers developed a strategy by blending the fragile thermosets with tougher polymer materials.[69] Furthermore, research on elastomer has significantly increased due to their excellent thermomechanical properties. Some current reports revealed that modification of chemical architectures and composition can improve their biocompatibility, processability, and resistance. Nevertheless, their degradability issue is still a concern to date, especially regarding their cytotoxicity and degradation rate.[70]

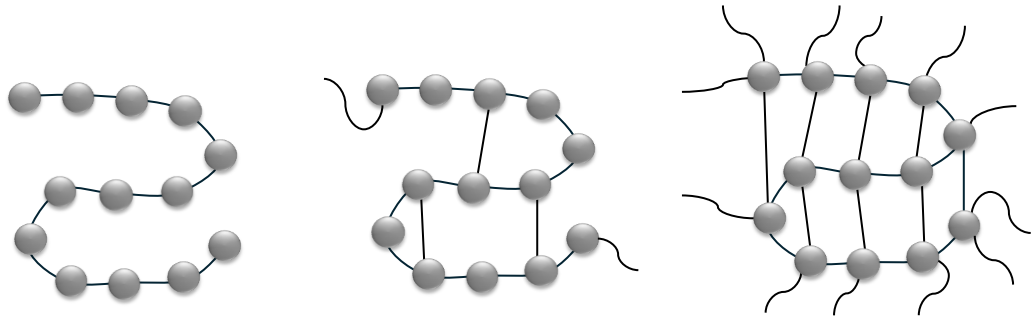

Figure 1.11 Schematical image of the structure of thermoplastics, elastomers and thermosets

Thermoplastics can be defined as polymeric substances that undergo phase

changes from a liquid state upon heating to a solid state upon cooling. Subjected to heat, they are capable of undergoing repeated shaping and softening without experiencing any alteration in their intrinsic characteristics.[71,72] In contrast to thermosets, which employ chemical cross-linking, thermoplastics comprise polymer chains that interact *via* noncovalent intermolecular forces. Typically, thermosets are cured and shaped, employed as binders, and are less recyclable.[73] Random state (amorphous) and ordered state (crystalline) are the two possible configurations of these polymeric structures. Excellent impact resistance, chemical resistance, processibility, and recyclability are several advantageous characteristics of thermoplastic polymers. Thermoplastic polymers have a diverse range of practical applications due to their unique characteristics.[74,75] Furthermore, an elastomer endures significant deformation when subjected to force, but rapidly returns to its initial shape and dimensions when the external force is removed. In addition, specific liquids induce self-healing and volumetric expansion in elastomers.[76]

Thermoplastics are generally categorized into commodity plastics and high-performance thermoplastics. Commodity plastics include polyethylene, polystyrene, polypropylene, *etc*. Meanwhile, high performance thermoplastics include polyamide, polyurethane, polyketone, polycarbonate, and so forth.[77] Due to the degradability issue of commercial plastics derived from petroleum sources, there has been a large increase in the manufacturing of biodegradable plastics such as polylactic acid and starch. Although these polymers are biodegradable and safe for the environment, they have poor mechanical performance. This means they are often embedded with plasticizer which is a non-degradable

additive and harmful to environment.[78]

Other approaches to overcome this challenge are to modify chemically the starch, incorporating other biodegradable polymers or inserting fibers and nano-filler compounds. In addition, these methods are able to generate environmentally friendly plastics with preserved mechanical performance and thermal stability.[79] This common strategy to chemically manipulate starch or starch derivatives into thermoplastic materials is *via* the esterification method.[80]

1.4.1 Thermal Properties

Generally, there are some structural factors that affect the thermal properties of polymer materials, such as chain length or molecular weight, chain branch, monomer ratio within copolymers. The glass transition temperatures, moisture contents, and temperatures at which the polymers degrade with weight loss were all obtained through thermal analysis.[81] Poly(lactic acid) (PLA) has shown a similarity in mechanical properties like commercial plastics, such as polyethylene terephthalate (PET), polycarbonate (PC), and polystyrene (PS). However, they have poor thermal properties in which they exhibited a low T_g of 60^o C. To address this challenge, researchers have modified the stereochemistry of the polymers and incorporated other polymers as well as performing other preparation techniques.[82] Furthermore, polycaprolactone (PCL) is another example of a commercially available biodegradable plastic which has both a low T_g (-50 ^{o}C) and T_m (60 ^{o}C). However, generally this drawback was overcome by blending it with PLA to enhance their thermal and mechanical performance. The other emerging weaknesses of both polymers is that PLA is very slowly degraded in the marine water and PLA is manufactured *via* petrochemical process.[83,84]

As reported, the thermal stability of polymer materials is the most significant obstacle for recycling. PLA degradation is significantly facilitated by the existence of moisture (leading to hydrolysis), active chain end groups, lactic acid residues, metal catalysts, and other impurities. An undesirable decrease in molecular weight and weight loss ensues between temperatures of 180 ^{o}C and 220 ^{o}C. Chain extenders are demonstrated to be an effective method for preventing the deterioration of PLA by modifying the material to produce branched and long structures. In general, chain extenders are readily accessible, thermally stable, and polyfunctional.[85]

To investigate the thermal degradation and stability of polymer materials, a multitude of methodologies have been implemented. Differential scanning calorimetry (DSC), thermogravimetric analysis (TGA), dynamic mechanical thermal analysis (DMTA), fourier-transform infrared spectroscopy (FTIR), scanning electron microscopy (SEM), and high-resolution pyrolysis-gas chromatography are a few of these methods.[86]

The temperature at which the writhing thermal motions of an amorphous polymeric system terminate is denoted by the glass transition temperature (T_g). Polymer chains cannot undergo long-range convolutional readjustments below T_g, which results in the material becoming rigid. A leathery state results from thermal processes occurring above the glass transition temperature.[87] Apart from that, the melting temperature (T_m) is another essential factor that affects the thermodynamics and mechanical performance of polymer materials which predicts

the desired properties of the final polymer products. Unlike amorphous polymers, crystalline polymers exhibit a T_m owing to their ordered state. These thermal properties are significantly affected by various factors, including chemical architectures and composition, chain length, crosslinking density, thermal history, intermolecular forces, morphology, heating and cooling rate. Therefore, complex factors influencing the polymer materials and composites lead to unpredictable value of T_g and T_m.[88,89] In addition, crystallization temperatures (T_c) denote the exothermic peaks that occur during the melt-solid transition. The nucleation effect causes crystal growth, which causes the crystallization temperature to fluctuate as the temperature rises.[90,91]

An endothermic reaction is depicted as a negative thermal event, whereas an exothermic reaction is plotted as a positive thermal event in DSC measurements. Figure 1.12 illustrates a typical DSC curve for a crystalline polymer. The polymer material initially undergoes a glass transition at temperature T_g and subsequently crystallizes at temperature T_c in an exothermic process. The sample undergoes an endothermic climax at temperature T_m and commences to melt as the temperature rises.

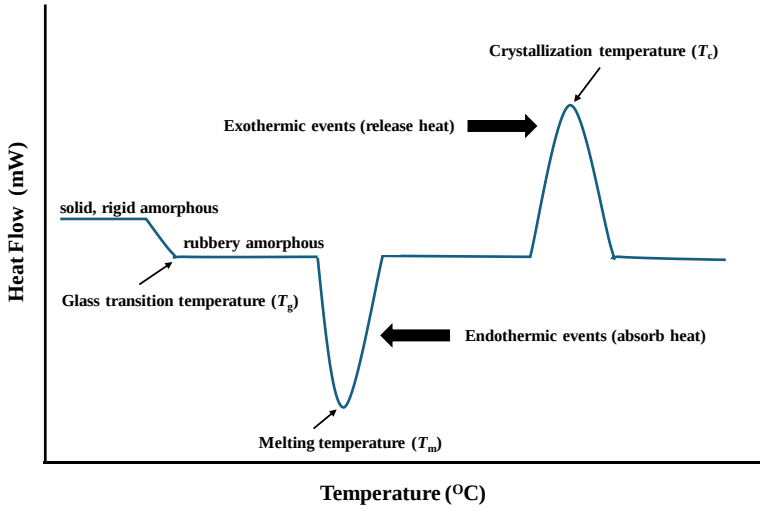

Figure 1.12 Illustration of different thermal events in a typical DSC curve

To analyze the thermal stability of polymeric materials and composites, TGA is a favorable method to use. Both degradation analysis and decomposition mode upon heating under an inert atmosphere are becoming key methods on this system and are essential in process optimization. The mechanism of degradation can be understood through the kinetics of the decomposition process. However, some factors must be considered to get into the absolute feature of the materials, such as the mass of sample, compactability of sample, rate of heating, and gas environment used.[92]

The temperature or time-dependent mass change of a sample is quantified by TGA in a controlled atmosphere, as well as the rate of change. As well as their compositional properties, the measurements are primarily employed to ascertain the thermal and/or oxidative stabilities of materials. The technique is capable of analyzing materials that demonstrate either mass loss or gain as a result of decomposition, oxidation, or the loss of volatiles (such as moisture). Polymeric materials, such as thermoplastics, thermosets, elastomers, composites, and fibres,

are particularly advantageously examined under this methodology (Figure 1.13).

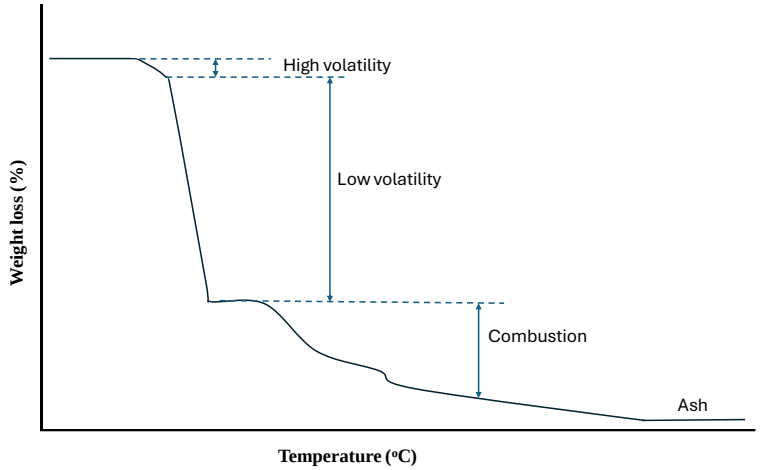

Figure 1.13 Typical thermogram for a polymer

Current research reveals that thermal stability can effectively be enhanced by incorporating the polymer materials with nanofillers.[90,93] The thermal degradation temperature and thermal decomposition rate are two key indicators of whether a material is thermally stable or not, and TGA evaluates the material's weight loss while maintaining a regulated environment and temperature. This nanofillers incorporation method has been applied to investigate the effects of loading and nanoparticles on the thermal stability of the nanocomposites through TGA analysis.[94,95]

1.4.2 Mechanical Properties

Mechanical properties of the polymer materials frequently refer to their stress-strain relationships (Figure 1.14a). Mechanical strength is determined by the average molecular weight (M_n), and higher molecular weights offer advantageous characteristics such as enhanced strain-to-break resistance, impact resistance, abrasion resistance, and so forth. The elastic portion of the mechanical properties, modulus, and yield stress are determined by the secondary bonds of the polymer

in its glassy state. On the other hand, the primary bonds within the network have the potential to induce the essential delocalization of local strain, which contributes to the material's durability.[96]

Mechanical properties play a vital role in numerous applications of polymer materials and composites. In general, there are various external factors that affect their mechanical performance, including strain rate, temperature, and pressure. Besides, internal factors also have significant affect which are related to the microstructure and composition of the materials. The majority of polymers depend on the strain rate that endows a wide range of elastic moduli, yield strengths, and post-yield behaviors (Figure 1.14b). In addition, the temperature and strain rate are responsible for changing the polymers intrinsic behavior, whereby the polymer can transform from elastic to brittle to a ductile plastic.[97] Furthermore, numerous elastomeric polymers are capable of recovering substantial deformations. In the case of hyperelastic materials, it may be necessary to conduct experimental measurements under significant strain in order to analyze the strain hardening.[98]

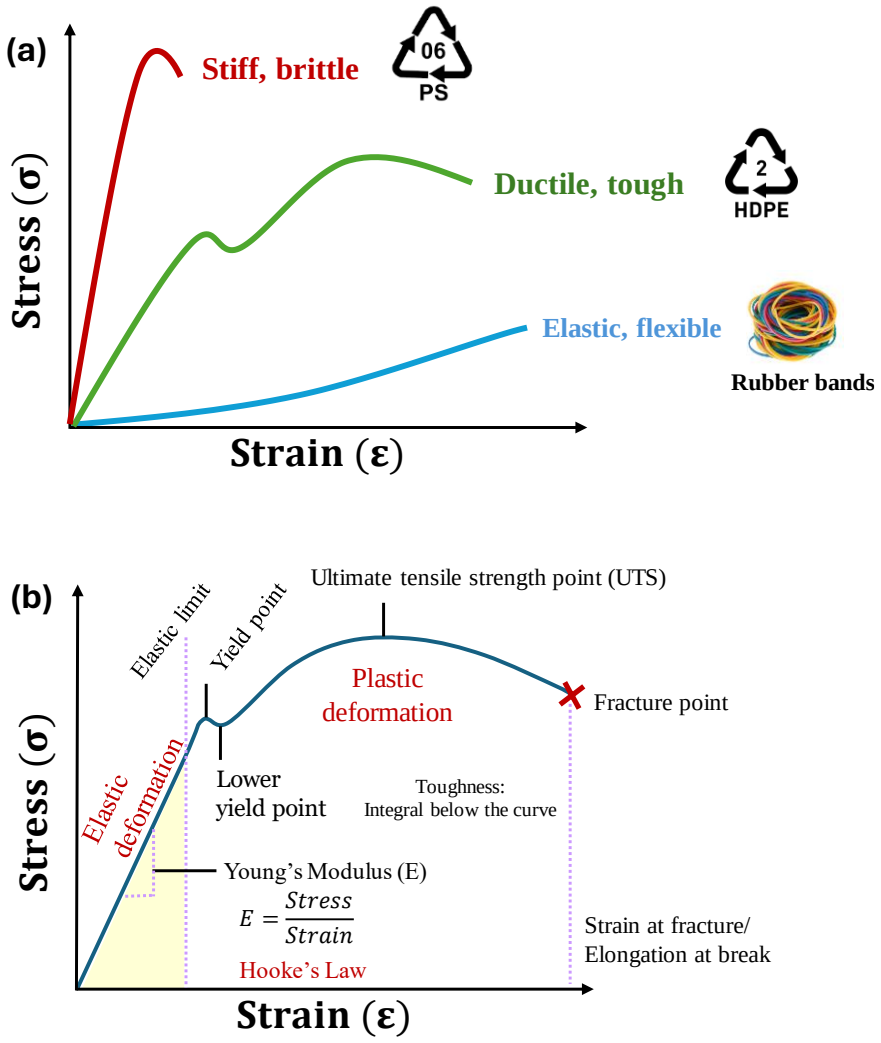

Figure 1.14 (a) Tensile curves of polymer materials, (b) Typical stress-strain curve Scheme

In addition to improve the thermal stability of the materials, fillers and fibers may enhance their mechanical performances, such as elongation at break, stiffness, toughness, tensile modulus, tensile strength, and so forth. The loading composition of fillers or fibers mainly contributes to the material performance.[99,100] The interest of many current researches leads to renewable and degradable feedstocks to achieve a circular economy and reduce the adverse environmental impacts. However, poor mechanical strength becomes a major issue to tackle.

Therefore, many scientists attempted to improve the mechanical performance of biodegradable materials by manipulating or modifying the chemical structures, architectures, compositions and stereochemistry. These polymer materials are expected to replace petroleum-based polymers. The synthesized polymers could be in different forms, such as thermoplastics, thermosets, elastomers, or even vitrimers (sub-class of the dynamic covalent networks). Lignin, soybeans, castor oil, and glucose are a few examples of bio-based feedstocks that can be introduced to generate biodegradable and sustainable polymers[101,102] Physio-mechanical properties of the currently accessible degradable polymers are extremely diverse. Copolymers and blends of the presently available materials cover the entire spectrum of strength and ductility, from extremely brittle and strong substances like high molecular weight L-PLA to extremely soft and feeble substances like poly(trimethylene carbonate) (PTMC).[103]

In addition, most reports show the use of crosslinkers or blended crosslinkers becomes a promising method to address the mechanical strength limit of creating new plastic materials. The final products demonstrated comparable mechanical performance to conventional plastics. This strategy seems to be effective to manipulate the flexibility and stiffness of the polymer materials by adjusting the rigidity modulus. Furthermore, the amount and ratio of crosslinker facilitates the adjustment of mechanical properties. However, the degree of crosslinking is not easy to control so it will significantly influence the mechanical properties of the polymers through simple crosslinker replacement. To enhance the physical performance, an introduction of a new kind of chemical bond through crosslinking the functional monomer to the pre-polymer is frequently conducted, and

consequently this acquires network polymer materials.[104]

Meanwhile, in graft copolymers like comb and bottlebrush polymers, entanglement formation and backbone and side chain conformations greatly impact their mechanical properties. The primary purpose of incorporating side chains onto comb polymers was to regulate the rheological features of their melt and solutions, with a particular emphasis on strain hardening and extensional viscosity in response to extensional deformations. On the other hand, bottlebrushes were originally intended to regulate the shear and extensional modulus of polymers, among other elastic properties, they accomplish this by independently adjusting the grafting density and the DP of the side chain.[105]

1.5 Photodegradable Polymers

Photodegradable polymers have currently gained attention as they only need light as a trigger to degrade to a lower molecular weight that possibly ends up as smaller fragments or molecules as well as losing their original performance (gradual embrittlement). The photodegradable linkages can be designed in the polymer backbones, side groups, and junction points.[106] These linkages can undergo cleavage *via* chain scissions through free radical reactions.[107] Apart from chain scission, the other main reactions that could occur are chain crosslinking and oxidative degradation (discoloration). The mechanism of solid-state (film) photolysis is significantly influenced by the mobility and bimolecular recombination of free radicals within the polymer matrix. Free hydrogen radicals diffuse extremely readily through the polymer matrix. They either combine in pairs or remove

hydrogen atoms from the polymer molecule. Hydrogen can be extracted from the immediate environment or formed through combinations with polymer radicals or hydrogen radicals.[108]

Polymers can be distinctly sensitive to the photolysis process. It depends on several micro-environmental effects, such as their chemical structures including inserted photosensitive chromophore groups, defect structures, embedded additives and their transformation product, as well as their morphology. Particular polymer matrix, environmental stress severity, material geometry, and failure criterion selection influence the time dependences of the initiation of degradation and the rate of change development. In terms of photostability test of polymers, accelerating the rate of degradation is possible to employ through the application of increased irradiance intensity, which stimulates photosensitization and photolysis to a greater degree than what occurs during natural weathering, and by favoring processes with a higher activation energy.[109] The lamp's specific attributes are detailed in Table 1.[110]

Table 1
Lamp type and its output according to standard methods.

Lamp	Output		Standard method
Open and enclosed flame carbon-arc light	Significant levels of short wavelength UV (<260 nm)	Window glass filter to simulate filtered sunlight UV filter transmits shorter wavelength and accelerates test	ISO4892-4 ASTM G152 (open arc) ASTM G153 (enclosed arc)
Fluorescent ultraviolet light	UVA-340 Emission peak at 343 nm and <1% below 300 nm	8 h UV/60 °C[a]- 4 h condensation/50 °C[a] I = 0.76e0.89 W m^{-2} 8 h UV/60 °C[a] - 0.25 h water spray - 3.75 h condensation/ 50 °C[a] I = 0.76e1.55 W m^{-2} 8 h UV/70 °C[a] - 4 h condensation 50 °C[a]	ISO 4892-3 ASTM G154
	UVB-313 Emission peak at 313 nm and >10% below 300 nm	I = 1.55 W m^{-2} 8 h UV at 70 °C[a] - 4 h condensation at 50 °C[a] I = 0.48e0.49 W m^{-2} 4 h UV at 60 °C[a] - 4 h condensation at 50 °C[a] I = 0.71 W m^{-2}	
	UVA-351 Emission peak at 351 nm and <1% below 310 nm	20 h UV at 80 °C[a] - 4 h condensation at 50 °C[a] I = 0.62 W m^{-2} 24 h UV/50 °C[a] I = 0.76 W m^{-2}	
Xenon-arc light	Emission > 270 nm		ISO 4892-2; ASTM G155

[a] Black panel temperature, I = irradiance.

The manufacturer of plastics incorporated stabilizer agents, including (a) light screeners, (b) UV absorbers, (c) excited state quenchers, (d) peroxide decomposers, and (e) radical scavengers, to reduce or prevent adverse environmental conditions—such as heat, light, and air—from causing damage to polymer materials for specific applications.[111] The initiation of weathering degradation in polymer materials by ultraviolet (UV) light has been widely recognized. The initial mechanistic investigations on this subject concentrated on ketone polymers. The inclusion of photolabile groups in the polymer backbone is critical for facilitating polymer photodegradation on demand.[112] The majority of conventional photodegradable plastics undergo incomplete or uncontrolled degradation which follows either Norrish type I or type II pathways (Figure 1.15). For instance, Poly(L-lactic acid) (PLLA), a biodegradable aliphatic polyester with carbonyl groups in its backbone, undergoes Norrish type II photo cleavage primarily at the main chain. On the other hand, Poly(D,L-lactic acid) (PDLLA) can undergo both Norrish type I and II[113,114]

1.5.1 Sustainability and Degradability of Polymers

In most cases, the disposal of synthetic polymers in landfills is the result of their non-degradability or inadequate biodegradability. The environmental impact of polymer building blocks and polymer-based products disposal is substantial. There are ongoing endeavors to develop post-use polymers that are biodegradable or readily recyclable.[115] To mitigate the adverse effects of non-degradable plastics derived from fossil fuels, the development of bio-based polymers such as starch, cellulose, pectin, chitosan, gelatin, casein, polyhydroxybutyrate and polyhydroxyvalerate is very important. In addition to improved biodegradability, physicochemical and thermomechanical properties are of key importance in polymer materials design and innovation and are expected to be comparable to commodity plastics.[116]

Therefore, it is ideal for forthcoming iterations of environmentally favorable polymer materials to possess the qualities of sustainability, recyclability, and economic viability. Polymers that can be degraded back into their monomer or into smaller valuable molecules that can be used to synthesize new materials are exceedingly desirable in this context.[117] Plastic materials that are biodegradable, biocompatible, environmentally benign, and produce minimal or no toxicity during degradation are must be developed. By virtue of their environmentally sustainable characteristics, biodegradable plastics have emerged as a decent alternative to conventional plastics and a resolution to this issue.[118]

Bioplastics can be either solely bio-based and biodegradable or meet both criteria. Bio-based plastics are derived fully or partially from renewable feedstocks,

meanwhile biodegradable plastics are degraded by microorganisms into natural fragments, such as carbon dioxide, water, methane, humic matter, biomass, and other natural compounds. Biodegradable and biobased plastics include PLA (polylactic acid), PHA (polyhydroxyalkanoates), bio-PBS(polybutylene succinate), and other bioderived plastics made up of natural products or biomass. Examples of bio-based plastics are bio-based poly (amides) (bio-PP), poly (ethylene) (bio-PE), and poly (ethylene terephthalate) (bio-PET) which they are bio-based but non-degradable. Lastly, biodegradable plastics involve poly (caprolactone) (PCL), poly (butylene adipate terephthalate) (PBAT), and poly (vinyl alcohol) (PVA) which they are derived from fossil fuel, but degradable.[119,120]

In contrast, the plastics derived from petrochemicals commonly have a high molecular weight and remarkable thermomechanical properties; however, they are not degradable in nature and are harmful for the environment as producing microplastics with a size less than 5 mm brings a toxicological effect to the ecosystem. In general, plastics undergo different degradation process such as biodegradation, photodegradation, hydrolytic degradation, and thermo-oxidative degradation.[121,122] These processes have an impact on all types of plastics and are the main contributor to the formation of microplastics. Plastics that are specifically engineered to break down through oxidation or hydrolysis processes are referred to as oxo-degradable and hydro-degradable plastics, respectively. Severe ecological, economic, and cosmetic repercussions are among the environmental issues raised by microplastics in the marine environment, which also affects humans and marine organisms on a global scale.[123,124]

Photodegradable plastics are the part of oxo-degradable plastics category where the oxidation process was triggered by UV light to enable the polymer to break down into small fragments that are easily dispersed. Hydro-degradable plastics can be decomposed into smaller particles by water uptake. The process primarily involves the scission of the main chains or side chains and not mineralized.[125,126] Both oxo-degradable plastics and hydro-degradable plastics that dominate the market are made up of petrochemical feedstocks and end up with microplastics or nanoplastics in their degradation, therefore the awareness to overcome this pollution has significantly increased by promoting sustainability using natural biomass resources. The resultant polymers mainly degraded into non-toxic products, and structural modifications were mostly conducted to improve their high thermomechanical performance, but still maintain the desired degradation rate in nature. Numerous types of bioplastics have been successfully synthesized or even commercialized in the market, such as polyesters, polyurethanes, polyketones, polyimides, polyamides, polycarbonates, and others.

1.5.2 Photodegradation Pathways

Photodegradable plastics have many advantages in real life. The current major applications of this kind of plastic are in agriculture called “plasticulture”. This farming method prevents weed growth, thus lowering the need for herbicides. Other applications include the use of “green plastics” which are beneficial as packaging materials, bin bags, plastic kitchenware, photolithography, and medical items. In general, photodegradable plastics can be designed by incorporating chromophore functional groups in the polymer backbone like carbonyl groups or

blending with additives to initiate the photodegradation reaction, in radical auto-oxidation reactions for instance.[127]

Auto-oxidation is a free radical chain reaction where the process begins with initiation by a free radical initiator. This step forms alkyl radicals which then react with oxygen to result in a peroxy radical. By abstracting a hydrogen atom from another molecule, this peroxy radical can produce hydroperoxide and an additional alkyl radical. The process of chain reaction propagation is initiated when the latter molecule removes a hydrogen atom from another molecule. The process accelerates automatically due to the instability of the initial products, hydroperoxides, which generate additional free radicals that can enter the chain. The process is terminated or inhibited, respectively, when two free radicals undergo a chemical reaction that results in their neutralization or arrest by an antioxidant-type substance. These photochemical reactions generally occur on photocleavable C-C bonds adjacent to aldehydes or ketones group within the polymer chain which are referred to as Norrish reactions.[128–130]

Norrish pathways were first investigated by Norrish and Bamford. There are two types of this photochemical reaction, including Norrish type I and Norrish type II (Figure 1.15). The initial step of the Norrish I reaction involves the cleavage of the C–O and –CH_2– bonds, resulting in the elimination of C–O. The initial step of the reaction involves the formation of OH groups through the bonding of C–O and –CH_2– in a photochemical process which is known as the Norrish II reaction.[131] In numerous investigations, such as chemical synthesis and photoinitiated polymerization, this Norrish photochemistry has been utilized extensively. In the

Earth's atmosphere, it is also crucial for the photolysis of volatile carbonyl compounds like acetone.[132] Common polyketones that have been synthesized by Guillet and Mecking group employing CO as a monomer and metal catalyst. This sort of polyketones has polyolefin-like backbones that underwent typical Norrish pathway. Moreover, they also generated microplastics, many degradation products (non-selective products), and toxicity issues (Figure 1.15).

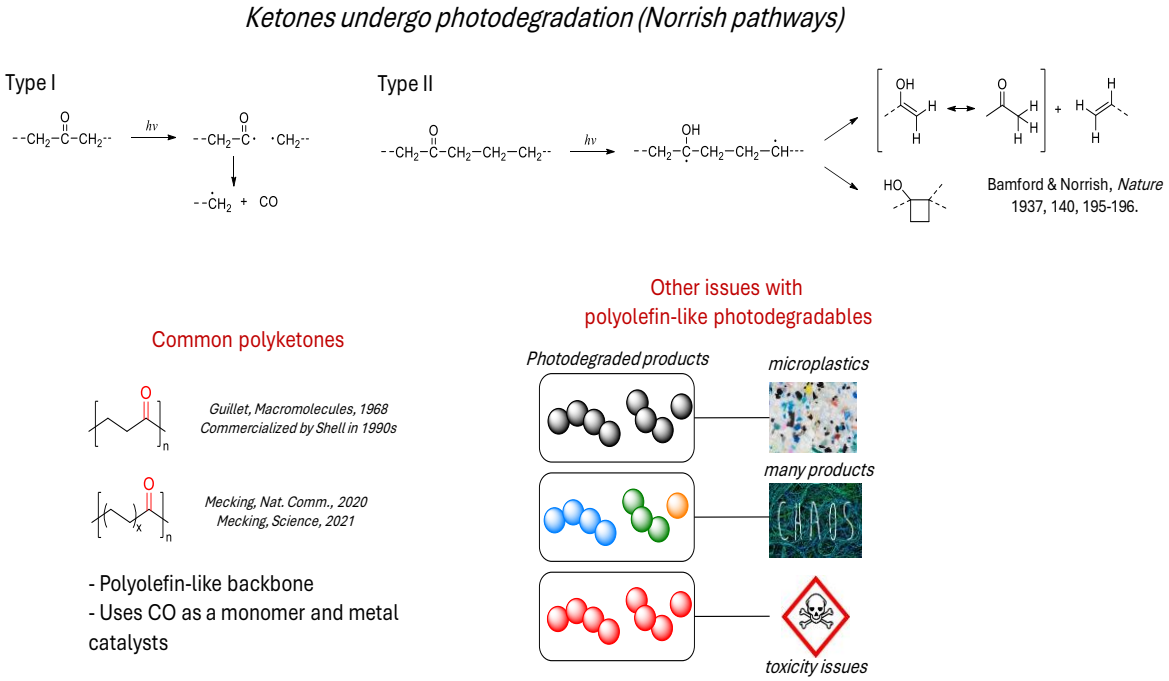

Figure 1.15 Photodegradation scheme of conventional polyketones with polyolefin backbones; common examples of polyketones; and other issues emerge from photodegradation of conventional polyketones

To understand how this reaction takes place, the concept of HOMO (Highest Occupied Molecular Orbital) and LUMO (Least Unoccupied Molecular Orbital) energy levels needs to be considered. The band gap of the HOMO and LUMO must be relatively low to reduce the activation energy necessary for photochemical excitation (Figure 1.16). Therefore, it is essential to construct the photodegradable or photocleavable linkage with a low HOMO-LUMO gap.[133,134] Ketones and

aldehydes exhibit a lower HOMO and LUMO band gap compared to other carbonyl compounds counterparts, such as esters, amides and acid halides. Hence, ketones and aldehydes proceed with photochemical reactions, yet their counterparts do not participate in this reaction.[135]

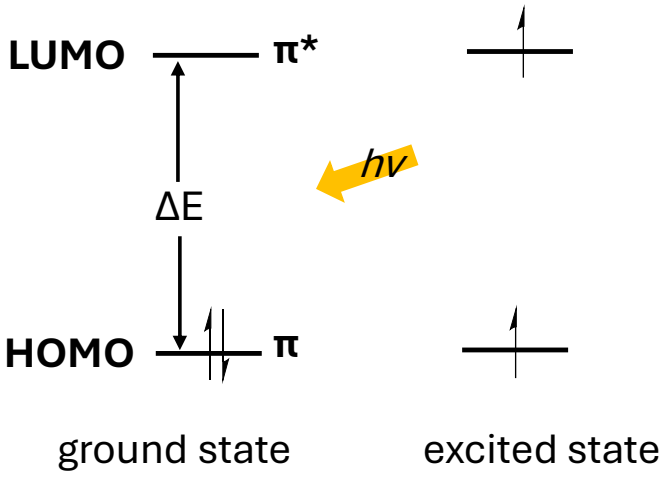

Figure 1.16 HOMO and LUMO energy level diagram of photochemical reaction

1.6 Microencapsulation techniques and its applications

Polymeric matrices can be used to encapsulate or entrap bioactive compounds or organic substances to protect them from environmental factors, such as oxygen, water, light, pressure, or heat as well as to control the release time and rate. This technique is called encapsulation and can generate either micro-size particles (microcapsules) or nano-size particles (nanocapsules). Polymeric matrices used in the encapsulation methods somehow referred to shell, wall, or coating where it is supposed to be insoluble and unreactive to the encapsulated active compounds (core materials).[136] The capsule wall materials ideally have some properties, such as being inert to active ingredients, the capability to create thin films, being taste and odor free, of moderate viscosity, soluble in solvent or aqueous media, and

cost-effective. Therefore, various physical properties of this capsule wall can be achieved, including brittle, flexible, thin, and hard. These properties will participate into the capacity to facilitate the controlled release of the active core under certain conditions at particular site.[137]

Encapsulation of active solid, gaseous, or liquid components that commonly result microparticles with diameter within the range of 1 to 1000 μm per unit usually referred to microencapsulation.[138] In addition to impeding undesirable odors and tastes, microencapsulation facilitates transport and handling and serves as a barrier to regulate solubility, bioavailability, and release. Mostly microencapsulation techniques only encapsulate one single bioactive compound, however a recent report demonstrated a successfully encapsulation of two different bioactive compounds which is termed co-microencapsulation.[139,140]

Some bioactive products that gained attention from food researchers and industries include flavoring agents, pigments, dyes, lipids, essential oils, antioxidants, probiotic microorganisms, and vitamins are among the numerous dietary components that are commonly encapsulated. Other different bioactive compounds are also frequently encapsulated are omega-3 and omega-6 fatty acids, vitamins, phenolic compounds, and carotenoids.[141] The microencapsulation method prolongs shelf life of the food products without impairing their physical, chemical, or functional characteristics; simplifies its implementation in the food industry; and mitigates the perception of potential off-flavors or colors originating from the encapsulated material, in addition to resolving stability issues.[142]

In order to introduce the natural bioactive compounds into the food system, it is imperative to create innovative delivery systems. This delivery system must surmount all of the constraints that are associated with the utilization of natural bioactive compounds, as previously mentioned. This delivery system can be developed by microencapsulating natural bioactive compounds or active constituents in a capsule or matrix (Figure 1.7).[143]

Besides within the food industry, microencapsulation methods are beneficial in the agricultural sector since they enable to enhance agricultural productivity. The crop production decreased significantly due to biotic and abiotic factors. Biotic factors include pathogens or pests and inefficient utilization of pesticides. Abiotic factors involve extreme weather such as heavy rain, heatwaves, and other climate change factors. Therefore, it is crucial to tackle this issue using this microencapsulation approach. The formulation materials used mostly affect the pesticide survival and effectiveness to control the pests and pathogens; for instance starch, alginate, chitin, and chitosan.[144,145]

Microencapsulation typically consists of the subsequent four stages: construction of the core and encapsulants, incorporation, and solidification.[146] The microcapsule's size and shape depend on the core materials used, encapsulated active compounds, and preparation techniques. The physicochemical properties of the core material, the composition of the wall material, and the microencapsulation technique employed can all contribute to the formation of distinct varieties of particles.[147] In general, microencapsulation technology can be classified based on their physical, chemical, and physico-chemical perspective. In

physical microencapsulation, examples of microencapsulation techniques are spray drying, air suspension, pan coating, centrifugal extrusion, and vibrational nozzle. In chemical microencapsulation, these techniques include interfacial polymerization, solvent evaporation, emulsification, in-situ and matrix polymerization. Furthermore, ionotropic gelation and coacervation are the examples of physico-chemical microencapsulation techniques.[148,149] Microcapsules commonly have 6 different types, including simple microcapsules, matrix (microspheres), irregular microcapsules, multicore microcapsules, multiwall microcapsules, and assembly of microcapsules (Figure 1.18).[147,150]

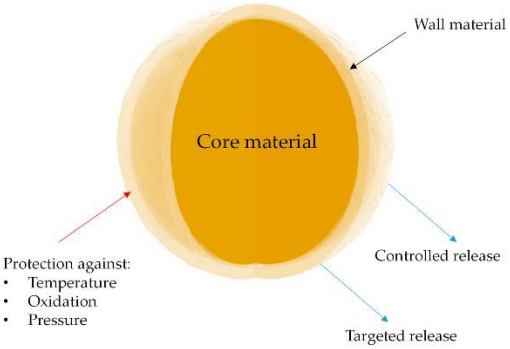

Figure 1.17 Fundamental principle of microencapsulation for bioactive compounds. Ref. 143. Copyright 2022 MDPI, Basel, Switzerland.

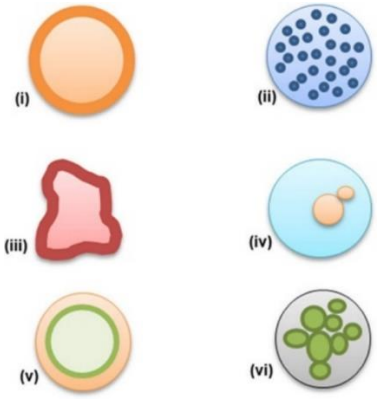

Figure 1.18 I (simple microcapsule), II (matrix or microsphere), III (irregular microcapsule), IV (multicore microcapsule), V (multiwall microcapsule), and VI (microcapsule assembly) are all distinct forms of microcapsules. Reproduced with permission from Ref. 149. Copyright 2015 Institute of Food Technologists.

The facile preparation process of interfacial polymerization has made it the most intriguing of the numerous techniques utilized in the synthesis of microcapsules.[151] This process occurs at the interface of the dispersed and continuous phases (immiscible solvents) in an emulsion system, where the two reactants are brought together (Figure 1.19). The encapsulation efficacy (EE%) is determined by dividing the total dye added by the total dye added minus the free non-entrapped dye. Polyester, polyurea, polyamide, polysulfonamide, polycarbonate, or polyurethane are among the polymeric materials utilized in this method to produce microcapsules.[152] This approach can be applied to the clickable monomers for step-growth polyaddition reaction or *via* polycondensation reaction. The click polyaddition reaction exhibits high efficiency, orthogonality, tolerance to functional groups, straightforward and very mild reaction conditions.[153]

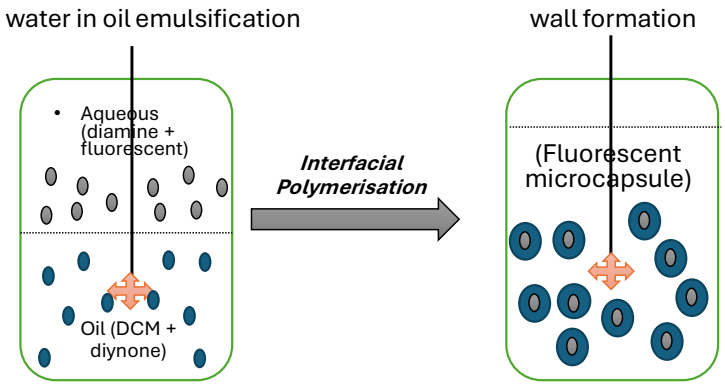

Figure 1.19 Illustration of microcapsule formation loaded with fluorescent dye *via* interfacial "click" polymerization (polyaddition reaction)

1.7. Summary

The click reaction has paved the way to manipulate the polymer structures and thermomechanical properties in ambient reaction conditions and high yield. Click polymerization has the potential to afford a variety of polymer structures with

reasonable thermomechanical performances while maintaining the desired degradability rate and controlling the degradation of products with no use of additives. Over the past few years, hydrolytically degradable polymers have been extensively explored, while photodegradable polymers remain an emerging class of materials. Among the polymers susceptible to photochemical degradation, polyketones stand out as thermoplastics capable of delivering enhanced thermomechanical performance while continuing to be fully susceptible to degradation when exposed to UV light. Therefore, these materials hold a prominent position in applications where not only performance, but also degradability on demand might be required, such as agricultural applications (*e.g*. plasticulture, light responsive microcapsules), green plastics, 3D printing, and in the biomedical field. Furthermore, polyketones are able to degrade into small molecules under UV light exposure, and do not fragment to microplastics. Therefore, these photodegradable plastics are expected to contribute to reducing the microplastic accumulation that contaminates marine and landfills.

1.8 Project aims

The aims of this thesis are to develop novel polyketones derived from renewable feedstocks by implementing the click chemistry strategy into the polymeric system as well as to investigate the photodegradable units and their photodegradation products. It was found that the thiol-yne click reaction could afford structurally diverse polyketone materials with a wide range of thermomechanical properties because of the polymer backbones modification. In addition, the photocleavable linkage was susceptible to UV light due to the by-designed ketone moiety.

Photodegradation seems to follow a more selective photodegradation pathway than conventional Norrish pathway. The model compounds synthesis was conducted to analyze the photodegradation products in depth.

Considering the ability of amines to act both as reactant and internal catalyst (no need external catalyst) as well as to form hydrogen bonds, the spontaneous amino-yne click reaction was implemented to generate polyketone materials with a better mechanical performance than the ones with thiol-yne click polymerization. It was envisioned that the synthesized polyketones have a higher tensile strength than when altering thiol-based backbones. This resulting polymer displays a comparable tensile strength to PET; however, it demonstrates a much lower elongation at break value compared to PET. The presence of amine in the polymer backbones also affected the chain cleavage that led to the different photodegradation products as obtained in the thiol-yne based polyketones. Furthermore, this amino-yne click polymerization is able to generate photo-triggered microcapsules through interfacial polyaddition reaction.

In order to improve the mechanical performance of one of the synthesized amino-yne polyketones (F-C_6A_{EG}), the click copolymerization with 1,6-hexanediamine (HMDA) was carried out. Surprisingly, a wide range of thermomechanical properties was discovered. One of the copolymers (Poly($HMDA_{10}$-*co*-$EDEA_{10}$) demonstrates a comparable tensile strength to HDPE (but owing half of its elongation at break value). It was concluded that the feed monomer ratio significantly affects the thermomechanical performances of the synthesized polyketones. In general, this typical copolymerization is effective to control over

the polymeric material properties with a simple work-up and catalyst free.

These polyketone materials enable them to be alternative photodegradable plastics to conventional ones considering their safety, renewability, and sustainability. In addition, the resultant photo-triggered microcapsules would be able to control the release of the bioactive compounds, resulting in increasing the efficacy of the encapsulated bioactive compounds. These work could be beneficial for some applications, such as crop protections and plasticultures.

1.9 References

1. Sendijarevic, I. & McHugh, A. J. Effects of molecular variables and architecture on the rheological behavior of dendritic polymers. *Macromolecules* **33**, 590–596 (2000).
2. Van Ruymbeke, E., Keunings, R., Stéphenne, V., Hagenaars, A. & Bailly, C. Evaluation of reptation models for predicting the linear viscoelastic properties of entangled linear polymers. *Macromolecules* **35**, 2689–2699 (2002).
3. Zhu, X., Zhou, Y. & Yan, D. Influence of branching architecture on polymer properties. *J. Polym. Sci. Part B Polym. Phys.* **49**, 1277–1286 (2011).
4. Ishizu, K., Tsubaki, K., Mori, A. & Uchida, S. Architecture of nanostructured polymers. *Prog. Polym. Sci.* **28**, 27–54 (2003).
5. Jin, Y., Wang, Q., Taynton, P. & Zhang, W. Dynamic covalent chemistry approaches toward macrocycles, molecular cages, and polymers. *Acc. Chem. Res.* **47**, 1575–1586 (2014).
6. Calzia, K. J. & Lesser, A. J. Correlating yield response with molecular architecture in polymer glasses. *J. Mater. Sci.* **42**, 5229–5238 (2007).
7. Flory, P. J. Viscosities of Linear Polyesters. An Exact Relationship between Viscosity and Chain Length. *J. Am. Chem. Soc.* **62**, 1057–1070 (1940).
8. Zhao, J., Nagao, S. & Zhang, Z. Thermomechanical properties dependence on chain length In bulk polyethylene: Coarse-grained molecular dynamics simulations. *J. Mater. Res.* **25**, 537–544 (2010).
9. Cicala, G., La Spina, R., Recca, A. & Sturiale, S. Influence of copolymer's end groups and molecular weights on the rheological and thermomechanical properties of blends of novel thermoplastic copolymers and epoxy resins. *J. Appl. Polym. Sci.* **101**, 250–257 (2006).
10. Kong, D. C. Yang, M. H., Zhang, X. S., Du, Z. C., Fu, Q., Gao, X. Q. and Gong, J. W. Control of Polymer Properties by Entanglement: A Review. *Macromol. Mater. Eng.* **306**, 1–20 (2021).

11. Gandini, A., Lacerda, T. M., Carvalho, A. J. F. & Trovatti, E. Progress of Polymers from Renewable Resources: Furans, Vegetable Oils, and Polysaccharides. *Chem. Rev.* **116**, 1637–1669 (2016).
12. Kristufek, S. L., Wacker, K. T., Tsao, Y. Y. T., Su, L. & Wooley, K. L. Monomer design strategies to create natural product-based polymer materials. *Nat. Prod. Rep.* **34**, 433–459 (2017).
13. Fijten, M. W. M. Kranenburg, J. M., Thijs, H. M. L., Paulus, R. M., Lankvelt, B. M. v., Hullu, J. d., Springintveld, M., Thielen. D. J. G., Tweedie, C. A., Hoogenboom, R., Vliet, K. J. V. & Schubert, U. S. Synthesis and structure-property relationships of random and block copolymers: A direct comparison for copoly(2-oxazoline)s. *Macromolecules* **40**, 5879–5886 (2007).
14. Kim, J., Mok, M. M., Sandoval, R. W., Woo, D. J. & Torkelson, J. M. Uniquely broad glass transition temperatures of gradient copolymers relative to random and block copolymers containing repulsive comonomers. *Macromolecules* **39**, 6152–6160 (2006).
15. Adhikari, R. & Michler, G. H. Influence of molecular architecture on morphology and micromechanical behavior of styrene/butadiene block copolymer systems. *Prog. Polym. Sci.* **29**, 949–986 (2004).
16. Chan, C. H., Chen, J. T., Farrell, W. S., Fellows, C. M., Keddie, D. J., Luscombe, C. K., Matson, J. B., Merna, J., Moad, G., Russell, G. T., Theato, P., Topham, P. D. & Vargas, L. S. Reconsedering terms for mechnisms of polymer growth: the "step-growth" and "chain-growth" dilemma. *Poly. .Chem*. **13**, 2262–2270 (2022).
17. Billiet, L., Fournier, D. & Du Prez, F. Step-growth polymerization and ‘click’ chemistry: The oldest polymers rejuvenated. *Polymer* **50**, 3877–3886 (2009).
18. Mizutani, M., Satoh, K. & Kamigaito, M. Metal-catalyzed simultaneous chain- and step-growth radical polymerization: Marriage of vinyl polymers and polyesters. *J. Am. Chem. Soc.* **132**, 7498–7507 (2010).
19. Gao, H. Synthesis of Linear Polymers in High Molecular Weights via Reaction-Enhanced Reactivity of Intermediates Using Friedel-Crafts Polycondensation. *ACS Omega* **6**, 4527–4533 (2021).
20. Kricheldorf, H. R., Böhme, S., Schwarz, G., Krüger, R. P. & Schulz, G. Macrocycles. 18. The role of cyclization in syntheses of poly(ether-sulfone)s. *Macromolecules* **34**, 8886–8893 (2001).
21. Bossion, A., Heifferonc, K. V., Meabe, L., Zivic, N., Taton, D., Hedrick, D. L., Long, T. E. & Sardon, H. Opportunities for organocatalysis in polymer synthesis via step-growth methods. *Prog. Polym. Sci.* **90**, 164–210 (2019).
22. Yokoyama, A. & Yokozawa, T. Converting Step-Growth to Chain-Growth Condensation Polymerization. **40**, 4093–4101 (2007).
23. Yokozawa, T. & Yokoyama, A. Chain-Growth Polycondensation: Living Polymerization Nature in Poly- condensation and Approach to Condensation Polymer Architecture. *Poly. J*. **36**, 65-83 (2004).
24. Yokozawa, T. & Ohta, Y. Transformation of Step-Growth Polymerization into Living Chain- Growth Polymerization. *Chem. Rev*. **116**, 1950–1968 (2016)
25. Ortega, R. A., Carter, E. S. & Ortega, A. E. Nylon 6,6 nonwoven fabric separates oil contaminates from oil-in-water emulsions. *PLoS One* **11**, 1–9 (2016).

26. Guzmán, J. D., Pollard, R. & Schieber, J. D. Modeling of diffusion effects on step-growth polymerizations. *Macromolecules* **38**, 188–195 (2005).
27. Biswas, S. & Das, A. A Versatile Step-Growth Polymerization Route to Functional Polyesters from an Activated Diester Monomer. *Chem. - A Eur. J.* **29**, 1-9 (2023).
28. Cruz, A. R., Hernandez, M. C. G., Guzmán-Gutiérrez, M. T., Zolotukhin, M. G., Fomine, S., Morales, S. L., Kricheldorf, H., Wilks, E. S., Cárdenas, J. & Salmón, M. Precision synthesis of narrow polydispersity, ultrahigh molecular weight linear aromatic polymers by A2 + B2 nonstoichiometric step-selective polymerization. *Macromolecules* **45**, 6774–6780 (2012).
29. Mitchell, S. M., Niradha Sachinthani, K. A., Pulukkody, R. & Pentzer, E. B. Polymerization of Cumulated Bonds: Isocyanates, Allenes, and Ketenes as Monomers. *ACS Macro Lett.* **9**, 1046–1059 (2020).
30. Tang, Q. & Zhang, K. Polymer Synthesis Based on Self-Accelerating 1,3-Dipolar Cycloaddition Click Reactions†. *Chinese J. Chem.* **39**, 3093–3100 (2021).
31. Zhang, L., Ren, X., Zhang, Y. & Zhang, K. Step-Growth Polymerization Method for Ultrahigh Molecular Weight Polymers. *ACS Macro Lett.* **8**, 948–954 (2019).
32. Hadj Mohamed, A. & Masurier, N. Recent advances in aza Friedel-Crafts reaction: strategies for achiral and stereoselective synthesis. *Org. Chem. Front.* **10**, 1847–1866 (2023).
33. Zou, L., Cao, X., Zhang, Q., Dodds, M., Guo, R. & Gao, H. Friedel-Crafts A2 + B4 Polycondensation toward Regioselective Linear Polymer with Rigid Triphenylmethane Backbone and Its Property as Gas Separation Membrane. *Macromolecules* **51**, 6580–6586 (2018).
34. Zolotukhin, M. G., Colquhoun, H. M., Sestiaa, L. G., Rueda, D. R. & Flot, D. One-pot synthesis and characterization of soluble poly(aryl ether-ketone)s having pendant carboxyl groups. *Macromolecules* **36**, 4766–4771 (2003).
35. Zeng, F. Xu, J. Xiong, Q., Qin, K. S., Xu, W. J., Wang, Y, X., Liu, Z. J., Li, Z. L. & Li, Z. C. Aliphatic polyketones via cross-metathesis polymerization : Synthesis and post-polymerization modification. *Polymer.* **185**, 121936 (2019).
36. Yang, P. B., Davidson, M. G., Edler, K. J. & Brown, S. Synthesis, Properties, and Applications of Bio-Based Cyclic Aliphatic Polyesters. *Biomacromolecules* **22**, 3649–3667 (2021).
37. Inkinen, S., Stolt, M. & So, A. Readily Controllable Step-Growth Polymerization Method for Poly (lactic acid) Copolymers Having a High Glass Transition Temperature. *Biomacro*. **11**, 1196–1201 (2010).
38. Arrington, K. J., Murray, C. B., Smith, E. C., Marand, H. & Matson, J. B. Precision Polyketones by Ring-Opening Metathesis Polymerization: E ff ects of Regular and Irregular Ketone Spacing. *Macromol*. **49**, 3655–3662 (2016)
39. Ortmann, P., Wimmer, F. P. & Mecking, S. Long-Spaced Polyketones from ADMET Copolymerizations as Ideal Models for Ethylene/CO Copolymers. *ACS Macro. Lett*. **4**, 704–707 (2015).
40. Liu, S., Yan, J., Zhang, Q. & Yan, Y. Acyclic Diene Metathesis (ADMET) as Powerful Tool for Functional Polymers with Versatile Architectures. *J. Inorg. Organomet. Polym. Mater.* **32**, 3368–3394 (2022).

41. Tanaka, J., Li, J., Clouthier, S. M. & You, W. Step-growth polymerization by the RAFT process. *Chem. Commun*. **59**, 8168–8189 (2023).
42. Ban, Q., Li, Y., Qin, Y., Zheng, Y. & Kong, J. Intramolecular cyclization in hyperbranched star copolymers via one-pot Am+Bn+C1 step-growth polymerization resulting in decreased cyclic defect. *Eur. Polym. J.* **155**, 110539 (2021).
43. Chen, H., Kong, J., Tian, W. & Fan, X. D. Intermolecular cyclization in A2 + B3 polymers via step-wise polymerization resulting in a highly branched topology: quantitative determination of cycles by combined NMR and SEC analytics. *Macromol*. **45**, 6185-6195 (2012).
44. Singh, M. S., Chowdhury, S. & Koley, S. Advances of azide-alkyne cycloaddition-click chemistry over the recent decade. *Tetrahedron* **72**, 5257–5283 (2016).
45. Castro, V., Rodríguez, H. & Albericio, F. CuAAC: An Efficient Click Chemistry Reaction on Solid Phase. *ACS Comb. Sci.* **18**, 1–14 (2016).
46. Meldal, M. & Tomøe, C. W. Cu-catalyzed azide - Alkyne cycloaddition. *Chem. Rev.* **108**, 2952–3015 (2008).
47. Golas, P. L. & Matyjaszewski, K. Marrying click chemistry with polymerization: expanding the scope of polymeric materials. *Chem. Soc. Rev.* **39**, 1338–1354 (2010).
48. Binder, W. H. & Sachsenhofer, R. 'Click' chemistry in polymer and material science: An Update. *Macromol. Rapid Commun.* **29**, 952–981 (2008).
49. Arslan, M., Acik, G. & Tasdelen, M. A. The emerging applications of click chemistry reactions in the modification of industrial polymers. *Polym. Chem.* **10**, 3806–3821 (2019).
50. Meng, X. & Edgar, K. J. 'Click' reactions in polysaccharide modification. *Prog. Polym. Sci.* **53**, 52–85 (2016).
51. Arslan, M., Gok, O., Sanyal, R. & Sanyal, A. Clickable Poly (ethylene glycol) -Based Copolymers Using Azide – Alkyne Click Polymerization. *Macromol. Chem. Phys.* **215**, 2237–2247 (2014).
52. Lowe, A. B. Thiol-yne ' click ' / coupling chemistry and recent applications in polymer and materials synthesis and modi fi cation. **55**, 5517–5549 (2014).
53. Tang, W. & Becker, M. L. 'click' reactions: A versatile toolbox for the synthesis of peptide-conjugates. *Chem. Soc. Rev.* **43**, 7013–7039 (2014).
54. Lowe, A. B., Hoyle, C. E. & Bowman, C. N. Thiol-yne click chemistry: A powerful and versatile methodology for materials synthesis. *J. Mater. Chem.* **20**, 4745–4750 (2010).
55. Van Dijk, M., Rijkers, D. T. S., Liskamp, R. M. J., Van Nostrum, C. F. & Hennink, W. E. Synthesis and applications of biomedical and pharmaceutical polymers via click chemistry methodologies. *Bioconjug. Chem.* **20**, 2001–2016 (2009).
56. Yao, B. Mei, J., Li, J., Wang, J., Wu, H., Sun, J. Z., Qin, A. and Tang, B. Z. Catalyst-free thiol-yne click polymerization: A powerful and facile tool for preparation of functional poly(vinylene sulfide)s. *Macromolecules* **47**, 1325–1333 (2014).
57. Liu, Z., Ou, J., Lin, H., Wang, H., Liu, Z., Dong, J. & Zou, H. Preparation of monolithic polymer columns with homogeneous structure via photoinitiated thiol-yne click polymerization and their application in separation of small

molecules. *Anal. Chem.* **86**, 12334–12340 (2014).
58. Chen, X. Hu, R., Qi, C., Fu, X., Wang, J., He, B., Huang, D., Qin, A. & Tang, B. Z. Ethynylsulfone-Based Spontaneous Amino-yne Click Polymerization: A Facile Tool toward Regio- and Stereoregular Dynamic Polymers. *Macromol*. **52**, 4526–4533 (2019).
59. He, B., Su, H., Bai, T., Wu, Y., Li, S., Gao, M., Hu, R., Zhao, Z., Qin, A., Ling, J. & Tang, B. Z. Spontaneous Amino-yne Click Polymerization: A Powerful Tool toward Regio- and Stereospecific Poly(β-aminoacrylate)s. *J. Am. Chem. Soc*. **139**, 5437–5443 (2017).
60. Chen, J., Xu, X., Xia, Q., Wang, J., Qin, A. & Tang, B. Z. Solvent and Water Enabled Control of Alkyne-Base Polymerization Triggered by a Spontaneous Imine-Yne Click Reaction. *Macromolecules* **57**, 1970–1978 (2024).
61. Akar, E., Luleburgaz, S., Gunay, U. S., Kumbaraci, V., Tunca, U. & Durmaz, H. Amino-yne reaction : An exquisite method for polymer-polymer conjugation and post-polymerization modification. *Eur. Polym. J.* **199**, 112470 (2023).
62. Huang, J. & Jiang, X. Injectable and Degradable pH-Responsive Hydrogels via Spontaneous Amino − Yne Click Reaction. *ACS Appl. Mater. Interfaces* 10, 361–370 (2018).
63. Chen, F., Lin, X., Li, Y., Xu, D., Qiu, H & Yin, S. Supramolecular Materials Metallacycle-crosslinked supramolecular polymers constructed by amino – YNE click reaction with enhanced mechanical properties. *Supramol. Mat*. **1**, 1–7 (2022).
64. Shi, Y., Sun, J. Z. & Qin, A. Click Polymerization : The Aurora of Polymer Synthetic Methodology. *J. Polym. Sci., Part A: Polym*. *Chem*. **55**, 616–621 (2017).
65. He, B., Zhen, S., Wu, Y., Hu, R., Zhao, Z., Qin, A. & Tang, B. Z. Cu(I)-Catalyzed amino-yne click polymerization. *Polym. Chem*. **7**, 7375-7382 (2016).
66. Li, Q., Hu, Z. & Ji, X. Hydrogel-Based Macroscopic Click Chemistry. *Angew. Chem*. **135**, 1-8 (2023).
67. Paquin, F., Rivnay, J., Salleo, A., Stingelin, N. & Silva, C. Multi-phase semicrystalline microstructures drive exciton dissociation in neat plastic semiconductors. *J. Mater. Chem. C* **3**, 10715–10722 (2015).
68. Momanyi, J., Herzog, M. & Muchiri, P. Analysis of thermomechanical properties of selected class of recycled thermoplastic materials based on their applications. *Recycling* **4**, (2019).
69. Mezzenga, R. & Månson, J. A. E. Thermo-mechanical properties of hyperbranched polymer modified epoxies. *J. Mater. Sci.* **36**, 4883–4891 (2001).
70. Li, Y., Thouas, G. A. & Chen, Q. Z. Biodegradable soft elastomers: Synthesis/properties of materials and fabrication of scaffolds. *RSC Adv.* **2**, 8229–8242 (2012).
71. Taghavi, N., Udugama, I. A., Zhuang, W. Q. & Baroutian, S. Challenges in biodegradation of non-degradable thermoplastic waste: From environmental impact to operational readiness. *Biotechnol. Adv.* **49**, (2021).
72. Minchenkov, K., Vedernikov, A., Safonov, A. & Akhatov, I. Thermoplastic pultrusion: A review. *Polymers (Basel).* **13**, 1–36 (2021).

73. Sen, S., Patil, S. & Argyropoulos, D. S. Thermal properties of lignin in copolymers, blends, and composites: a review. *Green Chem.* **17**, 4862–4887 (2015).
74. Wu, G., Xie, P., Yang, H., Dang, K., Xu, Y., Sain, M., Turng, L. S. & Yang, W. A review of thermoplastic polymer foams for functional applications. *J. Mater. Sci.* **56**, 11579–11604 (2021).
75. Parit, M. & Jiang, Z. International Journal of Biological Macromolecules Towards lignin derived thermoplastic polymers. *Int. J. Biol. Macromol.* **165**, 3180–3197 (2020).
76. Yang, L., Ou, Z. & Jiang, G. Research Progress of Elastomer Materials and Application of Elastomers in Drilling Fluid. *Polymers (Basel).* **15**, (2023).
77. Alshammari, B. A. Alsuhybani. M. S., Almushaikeh, A. M., Alotaibi, B. M., Alenad, A. M., Alqahtani, N. B. & Alharbi, A. G. Comprehensive review of the properties and modifications of carbon fiber-reinforced thermoplastic composites. *Polymers.* **13**, 1–32 (2021).
78. Surendren, A., Mohanty, A. K., Liu, Q. & Misra, M. A review of biodegradable thermoplastic starches, their blends and composites: recent developments and opportunities for single-use plastic packaging alternatives. *Green Chem.* **19**, 8606–8636 (2022).
79. Martinez Villadiego, K., Arias Tapia, M. J., Useche, J. & Escobar Macías, D. Thermoplastic Starch (TPS)/Polylactic Acid (PLA) Blending Methodologies: A Review. *J. Polym. Environ.* **30**, 75–91 (2022).
80. Ruhul Amin, M., Anannya, F. R., Mahmud, M. A. & Raian, S. Esterification of starch in search of a biodegradable thermoplastic material. *J. Polym. Res.* **27**, 1-12 (2020).
81. Gupta, S. S., Solanki, N. & Serajuddin, A. T. M. Investigation of Thermal and Viscoelastic Properties of Polymers Relevant to Hot Melt Extrusion, IV: Affinisol™ HPMC HME Polymers. *AAPS PharmSciTech* **17**, 148–157 (2016).
82. Babu, R. P., O'Connor, K. & Seeram, R. Current progress on bio-based polymers and their future trends. *Prog. Biomater.* **2**, 8 (2013).
83. Wachirahuttapong, S., Thongpin, C. & Sombatsompop, N. Effect of PCL and compatibility contents on the morphology , crystallization and mechanical properties of PLA / PCL blends. *Energ. Proced*. **89**, 198–206 (2016).
84. Wang, G., Huang, D., Ji, J., Völker, C. & Wurm, F. R. Seawater-Degradable Polymers — Fighting the Marine Plastic Pollution. **2001121**, 1–26 (2021).
85. Al-Itry, R., Lamnawar, K. & Maazouz, A. Improvement of thermal stability, rheological and mechanical properties of PLA, PBAT and their blends by reactive extrusion with functionalized epoxy. *Polym. Degrad. Stab.* **97**, 1898–1914 (2012).
86. Carrasco, F., Pagès, P., Gámez-Pérez, J., Santana, O. O. & Maspoch, M. L. Processing of poly(lactic acid): Characterization of chemical structure, thermal stability and mechanical properties. *Polym. Degrad. Stab.* **95**, 116–125 (2010).
87. Gupta, S. S., Meena, A., Parikh, T. & Serajuddin, A. T. M. Investigation of thermal and viscoelastic properties of polymers relevant to hot melt extrusion - I: Polyvinylpyrrolidone and related polymers. *J. Excipients Food Chem.* **5**, 32–45 (2014).

88. Gan, P. G., Sam, S. T., Faiq, M. & Omar, M. F. Thermal properties of nanocellulose-reinforced composites : A review. *J. App. Polym. Sci.* **137**, 48544, (2020).
89. Boublia, A., Lemaoui, T., Alyammahi, J., Darwish, A .S., Ahmad, A., Alam, M., Banat, F. & Benguerba, Y. Multitask Neural Network for Mapping the Glass Transition and Melting Temperature Space of Homo- and Co-Polyhydroxyalkanoates Using σ Profiles Molecular Inputs. *ACS Sustainable Chem. Eng*. **11**, 208–227 (2023).
90. Das, C., Tamrakar, S., Kiziltas, A. & Xie, X. Incorporation of Biochar to Improve Mechanical , Thermal and Electrical Properties of Polymer Composites. Polymers **13**, 1–32 (2021).
91. Reid, B. O., Vadlamudi, M., Mamun, A., Janani, H., Gao, H., Hu, W. & Alamo, R. G. Strong Memory Effect of Crystallization above the Equilibrium Melting Point of Random Copolymers. *Macromolecules* 46, 6485–6497 (2013).
92. Mano, J. F., Koniarova, D., Reis, R. L., Azure, C. De & Gualtar, C. De. Thermal properties of thermoplastic starch / synthetic polymer blends with potential biomedical applicability. *J. Mat. Sci.: Mat. in Med*. **14**, 127–135 (2003).
93. Tamjid, E., Najafi, P., Khalili, M. A., Shokouhnejad, N. & Karimi, M. *Discover Nano Review of sustainable , eco - friendly , and conductive polymer nanocomposites for electronic and thermal applications : current status and future prospects*. *Discover Nano* **19**, 29 (2024).
94. Din, Z. U., Marwat M. A., Ijaz, A. & Karim, M. R. A. Enhanced Thermal Stability of Polymers by Incorporating Novel Surface-Decaorated SrTiO3@Graphene Nanoplatelets. *Digit. Manuf. Technol*. **3**, 181–189 (2023).
95. You, Y., Chen, S., Yang, S., Li, L. & Wang, P. Enhanced Thermal and Dielectric Properties of Polyarylene Ether Nitrile Nanocomposites Incorporated with BN/TiO2-Based Hybrids for Flexible Dielectrics. *Polymers* **15**, 4279 (2023).
96. Meijer, H. E. H. & Govaert, L. E. Mechanical performance of polymer systems: The relation between structure and properties. *Prog. Polym. Sci.* **30**, 915–938 (2005).
97. Siviour, C. R. & Jordan, J. L. High Strain Rate Mechanics of Polymers: A Review. *J. Dyn. Behav. Mater.* **2**, 15–32 (2016).
98. Shergold, O. A., Fleck, N. A. & Radford, D. The uniaxial stress versus strain response of pig skin and silicone rubber at low and high strain rates. *Int. J. Impact Eng.* **32**, 1384–1402 (2006).
99. Cazan, C., Enesca, A. & Andronic, L. Synergic effect of tio2 filler on the mechanical properties of polymer nanocomposites. *Polymers* **13**, 1–24 (2021).
100. Taha, I. & Ziegmann, G. A comparison of mechanical properties of natural fiber filled biodegradable and polyolefin polymers. *J. Compos. Mater.* **40**, 1933–1946 (2006).
101. Moreno, A., Morsali, M. & Sipponen, M. H. Catalyst-Free Synthesis of Lignin Vitrimers with Tunable Mechanical Properties: Circular Polymers and Recoverable Adhesives. *ACS Appl. Mater. Interfaces* **13**, 57952–57961 (2021).

102. Can, E., Wool, R. P. & Küsefoglu, S. Soybean- and castor-oil-based thermosetting polymers: Mechanical properties. *J. Appl. Polym. Sci.* **102**, 1497–1504 (2006).
103. Engelberg, I. & Kohn, J. Physico-mechanical properties of degradable polymers used in medical applications: A comparative study. *Biomaterials* **12**, 292–304 (1991).
104. Yan, P., Zhao, W., Zhang, B., Jiang, L., Petcher, S., Smith, J. A., Parker, D. J., Cooper, A. I. Lei, J. & Hasell, T. Inverse Vulcanized Polymers with Shape Memory, Enhanced Mechanical Properties, and Vitrimer Behavior. *Angew. Chemie - Int. Ed.* **59**, 13371–13378 (2020).
105. Abbasi, M., Faust, L. & Wilhelm, M. Comb and Bottlebrush Polymers with Superior Rheological and Mechanical Properties. *Adv. Mater.* **31**, (2019).
106. Li, L., Deng, X. X., Li, Z. L., Du, F. S. & Li, Z. C. Multifunctional photodegradable polymers for reactive micropatterns. *Macromolecules* **47**, 4660–4667 (2014).
107. Hiraguri, Y. & Tokiwa, Y. Synthesis of photodegradable polymers having biodegradability and their biodegradations and photolysis. *Macromolecules* **30**, 3691–3693 (1997).
108. Yousif, E. & Haddad, R. Photodegradation and photostabilization of polymers, especially polystyrene: Review. *Springerplus* **2**, 1–32 (2013).
109. Pospısil, J., Pilar, J., Billingham, N. C., Marek, A., Horak, Z. & Nespurek, S. Factors affecting accelerated testing of polymer photostability. *Polym. Deg. & Stab*. **91**, 417–422 (2006).
110. González-López, M. E., Martín del Campo, A. S., Robledo-Ortíz, J. R., Arellano, M. & Pérez-Fonseca, A. A. Accelerated weathering of poly(lactic acid) and its biocomposites: A review. *Polym. Degrad. Stab.* **179**, (2020).
111. Yousif, E. & Hasan, A. Photostabilization of poly (vinyl chloride) – Still on the run. *J. Tai. Univ. for Sci*. **9**, 421–448 (2015).
112. Do, P. T., Poad, B. L. J. & Frisch, H. Programming Photodegradability into Vinylic Polymers via Radical Ring-Opening Polymerization. *Angew. Chem. Inter. Ed*. 62, 3–9 (2023).
113. Ikada, E. Photo- and Bio-degradable Polyesters Photodegradation Behaviors of Aliphatic Polyesters. *J. Photopolym. Sci. & Tech.* **10**, 265-270 (1997).
114. Wang, J. *et al.* Light-Modulated Surface Micropatterns with Multifunctional Surface Properties on Photodegradable Polymer Films. *ACS Appl. Mater. Interfaces* **9**, 37402–37410 (2017).
115. Isola, C., Sieverding, H. L., Raghunathan, R., Sibi, M. P., Webster, D. C., Sivaguru, J. & Stone, J. J. Life cycle assessment of photodegradable polymeric material derived from renewable bioresources. *J. Clean. Prod*. **142**, 2935–2944 (2017).
116. Kabir, E., Kaur, R., Lee, J., Kim, K. H. & Kwon, E. E. Prospects of biopolymer technology as an alternative option for non-degradable plastics and sustainable management of plastic wastes. *J. Clean. Prod.* **258**, 120536 (2020).
117. Guillaume, S. M. Sustainable and degradable plastics. *Nat. Chem.* **14**, 245–246 (2022).
118. Satti, S. M. & Shah, A. A. Polyester-based biodegradable plastics: an

approach towards sustainable development. *Lett. Appl. Microbiol.* **70**, 413–430 (2020).
119. Rai, P., Mehrotra, S., Priya, S., Gnansounou, E. & Sharma, S. K. Recent advances in the sustainable design and applications of biodegradable polymers. *Bioresour. Technol.* **325**, (2021).
120. Moshood, T. D. Nawanir, G., Mahmud, F., Mohamad, F., Ahmad, M. H. & Ghani, A. A. Sustainability of biodegradable plastics: New problem or solution to solve the global plastic pollution? *Curr. Res. Green Sustain. Chem.* **5**, (2022).
121. Zeenat, Elahi, A., Bukhari, D. A., Shamim, S. & Rehman, A. Plastics degradation by microbes: A sustainable approach. *J. King Saud Univ. - Sci.* **33**, 101538 (2021).
122. Fang, X., Qing, Y., Lou, Y., Gao, X., Wang, H., Wang, X., Li, Y., Qin, Y. & Sun, J. Degradable, Recyclable, Water-Resistant, and Eco-Friendly Poly(vinyl alcohol)-Based Supramolecular Plastics. *ACS Materials Lett.* **4**, 1132–1138 (2022).
123. Onyena, A. P., Uniche, D. C., Ogbolu, B. O., Rakib, M. R. J., Uddin, J. & Walker, T. R. Governance Strategies for Mitigating Microplastic Pollution in the Marine Environment: A Review. *Microplastics* **1**, 15–46 (2021).
124. Filiciotto, L. & Rothenberg, G. Biodegradable Plastics: Standards, Policies, and Impacts. *ChemSusChem* **14**, 56–72 (2021).
125. Lambert, S. & Wagner, M. Environmental performance of bio-based and biodegradable plastics: The road ahead. *Chem. Soc. Rev.* **46**, 6855–6871 (2017).
126. Rydz, J., Sikorska, W., Kyulavska, M. & Christova, D. Polyester-based (bio)degradable polymers as environmentally friendly materials for sustainable development. *Int. J. Mol. Sci.* **16**, 564–596 (2015).
127. Daglen, B. C., Tyler, D. R., Daglen, B. C. & Tyler, D. R. Green Chemistry Letters and Reviews Photodegradable plastics : end-of-life design principles Photodegradable plastics : end-of-life design principles. *Gre. Chem. Lett. & Rev*. **3**, 69–82 (2010).
128. Rosenboom, J. & Langer, R. Bioplastics for a circular economy. *Nat. Rev.: Mat*. **7**, 117-137 (2022).
129. Pascual-escudero, A., Ortiz-rojano, L., Sim, S. & Adrio, J. Aldehydes as Photoremovable Directing Groups: Synthesis of Pyrazoles by a Photocatalyzed [3+2] Cycloaddition/Norrish Type Fragmentation Sequence. *Org. Lett*. **23**, 4903–4908 (2021).
130. Ren, E., Maines, C. A. & Palmer, M. Wavelength-dependence of Norrish type I cleavage reactions in carbonyl groups of dammar resin triterpenoids and its implications for accelerated aging of organic materials. *Polym. Deg. & Stab.* **215**, 110464 (2023).
131. Chen, X., Yue, Y., Wang, Z., Sun, J. & Dong, S. Science of the Total Environment Co-existing inorganic anions influenced the Norrish I and Norrish II type photoaging mechanism of biodegradable microplastics. *Sci. Tot. Env*. **925**, 171756 (2024).
132. Kao, M., Venkatraman, R. K. & Orr-ewing, A. J. Effects of ring-strain on the ultrafast photochemistry of cyclic ketones†. *Chem. Sci.* **11**, 1991–2000 (2020).

133. Lewer, J., Huang, J., Peloquin, J. & Kostal, J. Structure − Energetics − Property Relationships Support Computational Design of Photodegradable Pesticides. *Environ. Sci. Technol*. **55**, 11713–11722 (2021).
134. Irshadeen, I. M. Walden, S. L., Wegener, M., Truong, V. X., Frisch, H. & Blinco, J. P. Action Plots in Action: In-Depth Insights into Photochemical Reactivity. *J. Am. Chem. Soc*. **143**, 21113–21126 (2021).
135. Mavroskou, A., Rieck, A. & Hopkinson, M. N. Norrish type II reactions of acyl azolium salts. *Tetrahedron* **100**, 132497 (2021).
136. Arenas-Jal, M., Suñé-Negre, J. M. & García-Montoya, E. An overview of microencapsulation in the food industry: opportunities, challenges, and innovations. *Eur. Food Res. Technol.* **246**, 1371–1382 (2020).
137. Al-Hamayda, A., Abu-Jdayil, B., Ayash, M. & Tannous, J. Advances in microencapsulation techniques using Arabic gum: A comprehensive review. *Ind. Crops Prod.* **205**, (2023).
138. Sousa, V. I., Parente, J. F., Marques, J. F., Forte, M. A. & Tavares, C. J. Microencapsulation of Essential Oils: A Review. *Polymers* **14**, 1730 (2022).
139. Calderón-Oliver, M. & Ponce-Alquicira, E. The Role of Microencapsulation in Food Application. *Molecules* **27**, 1–16 (2022).
140. Niño-Vásquez, I. A., Muñiz-Márquezb, D., Ascacio-Valdésa, J. A., Contreras-Esquivela, J. C., Aguilar, C. N., Rodríguez-Herrera, R. & Flores-Gallegos, A. C. Co-microencapsulation: a promising multi-approach technique for enhancement of functional properties. *Bioengineered* **13**, 5168–5189 (2022).
141. Choudhury, N., Meghwal, M. & Das, K. Microencapsulation: An overview on concepts, methods, properties and applications in foods. *Food Front.* **2**, 426–442 (2021).
142. Perez-Palacios, T. Ruiz-Carrascal, J., Solomando, J. C., de-la-Haba, F., Pajuelo, A. & Antequera, T. Recent Developments in the Microencapsulation of Fish Oil and Natural Extracts: Procedure, Quality Evaluation and Food Enrichment. *Foods* **11**, (2022).
143. Mehta, N., Kumar, P., Verma, A. K., Umaraw, P., Kumar, Y, Malav, O. P., Sazili, A. Q., Domínguez, R. & Lorenzo, J. M. Microencapsulation as a Noble Technique for the Application of Bioactive Compounds in the Food Industry: A Comprehensive Review. *Appl. Sci.* **12**, 1–34 (2022).
144. Saberi-Riseh, R., Moradi-Pour, M., Mohammadinejad, R. & Thakur, V. K. Biopolymers for biological control of plant pathogens: Advances in microencapsulation of beneficial microorganisms. *Polymers.* **13**, 1–23 (2021).
145. Tang, J. Tong, X., Chen, Y., Wu, Y., Zheng, Z., Kayitmazer, A. B, Ahmad, A., Ramzan, N., Yang, J., Huang, Q. & Xu, Y. Deposition and water repelling of temperature-responsive nanopesticides on leaves. *Nat. Commun.* **14**, 1–15 (2023).
146. Mehta, N., Kumar, P., Verma, A. K., Umaraw, P., Kumar, Y., Malav, O. P., Sazili, A. Q., Domínguez, R. & Lorenzo, J. M. Microencapsulation as a Noble Technique for the Application of Bioactive Compounds in the Food Industry: A Comprehensive Review. *Appl. Sci.* **12**, 1–34 (2022).
147. Xiao, Z., Liu, H., Zhao, Q., Niu, Y., Chen, Z. & Zhao, D. Application of microencapsulation technology in silk fibers. *J. Appl. Polym. Sci.* **139**, 1–17

(2022).
148. Pasha, A., Utekar, S. & Ghosh, R. Recent Advances in Microencapsulation Technology and their Applications. *Bombay Technol.* **68**, 401 (2021).
149. Balla, A., Silini, A., Cherif-Silini, H., Bouket, A. C., Alenezi, F. N. & Belbahri, L. Recent Advances in Encapsulation Techniques of Plant Growth-Promoting Microorganisms and Their Prospects in Sustainable Agriculture. *Appl. Sci.* **12**, (2022).
150. Bakry, A. M. Abbas, S., Ali, B., Majeed, H., Abouelwafa, M. Y., Mousa, A., Liang, L. Microencapsulation of Oils: A Comprehensive Review of Benefits, Techniques, and Applications. *Comp. Rev. in Food Sci. & Food Saf.* **15**, 143–182 (2016).
151. Fathi Fathabadi, H. & Javidi, M. Self-healing and corrosion performance of polyurethane coating containing polyurethane microcapsules. *J. Coatings Technol. Res.* **18**, 1365–1378 (2021).
152. Naveena, B. & Nagaraju, M. Microencapsulation techniques and its application in food industry. *Int. J. Chem. Stud.* **8**, 2560–2563 (2020).
153. Shen, Q. Advances in unusual interfacial polymerization techniques. *Polymer* **270**, 125788 (2023).

CHAPTER 2: VERSITILE SYNTHESIS OF BIO-BASED PHOTODEGRADABLE POLYKETONES WITH CONTROLLABLE THERMOMECHANICAL PROPERTIES

2.1 Manuscript and overview

Title: Versatile Synthesis of Bio-based Photodegradable Polyketones with Controllable Thermomechanical Properties

Authors: **Lukmanul H. Samada**[1], Maher A. Alraddadi[1,2], Joshua C. Worch[1,3], Arianna Brandolese[1], Andrew P. Dove[1]*

Affiliations: [1] School of Chemistry, The University of Birmingham, Edgbaston, Birmingham, B15 2TT, UK.
[2]Chemical Skills Department, Royal Commission for Yanbu Colleges & Institutes, Yanbu Industrial City, Saudi Arabia.
[3]Department of Chemistry, Virginia Tech, 24061, USA

Manuscript Prepared

Co-author contributions: Dr. Maher Alraddadi (University of Birmingham; Royal Commission for Yanbu Colleges & Institutes) synthesized a few small molecules and guided the mechanical testing. Dr Joshua C. Worch (University of Birmingham; Virginia Tech) provided technical and synthetic guidance. Dr. Arianna Brandolese (University of Birmingham) provided editing of the manuscript. Prof. Andrew P. Dove (University of Birmingham) supervised in addition to providing guidance and editing the manuscript.

Overview:

The objective of this chapter was to design photodegradable polymers *via* a thiol-Michael addition reaction in the presence of an organo-base catalyst (no use of metal

catalyst) at ambient temperature. The investigation of the effect of chain flexibility and intermolecular forces was conducted to obtain optimal thermomechanical properties of the resultant thermoplastics. The majority of photodegradable polyketones were synthesized through polycondensation which limits their structure complexity, and the polymerization reaction time was inefficient.

Our designed polymers were able to tune the thermomechanical properties through manipulation of the polymer backbones by a step-growth click polymerization. The resulting polymer can achieve high weight average molecular weights (M_w up to 138 kDa) and high yields without further purification. Differential scanning calorimetry revealed the amorphous behavior and high glass transition temperature. Additionally, thermogravimetric analysis shows outstanding thermal stability which is indicated by decomposition temperature with 5% weight loss at >260 °C. The polymer exhibits a wide range of mechanical performances as shown by its stress *vs* strain curves.

We also examine the degradation products and rate by exposing the polymer samples under controlled UV light. The photodegradation pathway looks more selective than the conventional Norrish pathways. The well-designed photodegradable linkage enables the polymers to break down *via* photooxidation in the ketone moiety resulting in polymer chain sessions. Our study highlights how the polymer chain flexibility and polymer structures can have a significant impact on their thermomechanical performance and degradability.

Versatile Synthesis of Bio-based Photodegradable Polyketones with Controllable Thermomechanical Properties

Lukmanul H. Samada[†], Maher A. Alraddadi[†,#], Joshua C. Worch[§,†], Arianna Brandolese[†], Andrew P. Dove[*,†]

[*,†]School of Chemistry, University of Birmingham, B15 2TT, UK. [#]Chemical Skills Department, Royal Commission for Yanbu Colleges & Institutes, Yanbu Industrial City, Saudi Arabia. [§]Department of Chemistry, Virginia Tech, 24061, USA.

E-mail: a.dove@bham.ac.uk

ABSTRACT: Photolytically degradable polymers have recently become an interesting material option as they are less dependent on environmental conditions than hydrolytically degradable polymers. Polymers with ketone functionality (polyketones) are intrinsically photodegradable, and they have excellent thermomechanical properties, however, the majority of the conventional polyketones are generated from non-renewable feedstocks. Here, we prepare polyketones using a renewable monomer from biobased sources, such as 2,5-furandicarboxylic acid (FDCA) derived from plant starches through a nucleophilic thiol-yne addition. This polymerization protocol between different dithiols and diynone furan-based monomers provided a range of photodegradable polyketone structures. The synthesized polyketones show excellent and variable thermomechanical performances as well as high molecular weights (M_w up to 138 kDa) and yields. In addition, photodegradation studies were conducted by irradiating these polyketones to UV light to investigate the degradation rate and the final products. These studies indicated that synthesized polyketones undergo a more selective photodegradation pathway than the conventional Norrish pathways.

INTRODUCTION

From engineering applications to consumer goods, plastics are pervasive in modern culture and are often used for packaging items.[1,2] The adverse effects of plastic waste on ecology and biodiversity prompted scientists to develop degradable polymers with a lower environmental impact by using biobased sources with photocleavable functionalities to endow them with inherent biodegradability.[3-7] Biodegradable polymers can be classified according to the origins of their manufacture, which include the extraction from biomass, synthesis from bio-based monomers into polymerizable monomers, and fabrication by microbes.[8,9] Biobased plastics (obtained from natural products or biomasses) are considered an alternative to polymers derived from petroleum sources to prevent plastic accumulation in the environment. For example, poly(lactic acid) (PLA), polyhydroxybutyrate (PHB), and polyhydroxyalkanoate (PHA) are generated from plants or microbes.[10,11] Also, these polymers are able to increase the bioavailability of bioactive compounds. In addition, they enable to manage their biodegradation and homogeneity to achieve the required therapeutic effect, particularly in sustainable drug delivery and tissue engineering.[12-14]

Biodegradable polymers are susceptible to various environmental triggers, including photodegradation, thermal deterioration, mechanical degradation, and chemical degradation.[15] Polymers that undergo photodegradation, such as polyketones, attracted attention as the majority of hydrolytically degradable polymers have poor thermal and/or mechanical properties and inefficient degradation in natural and realistic environmental conditions.[16] Improving thermomechanical performance is an ongoing challenge although progress has been made on this front.[17,18] Polyketones (PKs) are commonly known as photodegradable plastics with enhanced chemical and mechanical properties as well as photodegradability. PKs belong to the high-performance thermoplastic polymers that are mainly derived from oil sources.[19-21] They offer more excellent abrasion resistance and gas permeability compared to polyamides and polyesters, in addition to other exceptional chemical and mechanical properties. Therefore, they are typically used in packaging, water resistance, and engineering

materials, as well as different other applications considering having higher chemical resistance and impact strength than nylon.[22,23]

PKs are usually synthesized *via* a transition metal-catalyzed copolymerization of carbon monoxide and olefins.[24] Typical olefins used to prepare polyketones are ethylene, propylene, dienes, styrene, and its derivatives using complex palladium catalysts (**Figure 1a**).[25] In recent decades, free radical copolymerization strategies have been studied extensively to produce polyketones with low carbon monoxide content and reduced degree of branching.[21] However, these protocols often lead to the formation of contaminants thus reducing the applications of PKs.[26,27] Conventional PKs commonly undergo Norrish-type photodegradation pathway, which is uncontrolled and leads to multiple reaction products and/or microplastic formation from incomplete degradation.[28] Alternatively, the addition of stabilizers and photo-absorbing additives enables to enhance the flexibility, strength, and toughness of PKs as well as to improve their UV light resistance.[29-32] Conventional PKs that are commonly derived from carbon monoxide and olefins encounter sustainability and degradability challenges, therefore it is necessary to design monomers from renewable feedstocks to address these issues.[33] Chemicals derived from renewable feedstocks allow to access a diverse pool of monomers. Typically, they are comprised of numerous acid and alcohol groups or sugar-derived building blocks, such as 2,5-furandicarboxylic acid (FDCA) to afford activated alkyne. Subsequently, this alkyne monomer can be used as a building block in generating a wide range of functional polyketones by thiol-Michael addition approach (**Figure 1b**).[34-36]

Terephthalate polyesters, such as polyethylene terephthalate (PET), poly(butylene terephthalate) (PBT), and poly(propylene terephthalate) (PPT), are thermoplastic polymers with high performance and numerous applications. Still, they are not fully biodegradable, and their monomer precursors are derived from by-products of fossil fuels. As a result of its similarities in structure and performance in polymeric materials, FDCA can be a suitable sustainable substitute monomer to create polyesters,

polyurethanes, polyamides, *etc*.[37,38] The conventional approach for polymerizing FDCA is *via* direct polycondensation. However, the resulting polymer requires high-temperature reaction conditions and has a restricted shape.[39]

Step-growth polyaddition introduced "click" polymerization through Michael addition (or 1,4-conjugate addition reaction) that offers diverse structures, remarkable selectivity, enhanced yield, and proceed orthogonally (without by-product creation) under mild reaction conditions.[40-42] In recent years, the use of thiol-yne click polymerization has produced a variety of new heteroatom-dense polymer compositions with excellent thermomechanical properties.[43] This reaction occurs between thiolate anion as a strong nucleophile and alkyne (ynone) as a strong electrophile in the presence of a base catalyst, which results in an exothermic reaction.[44,45]

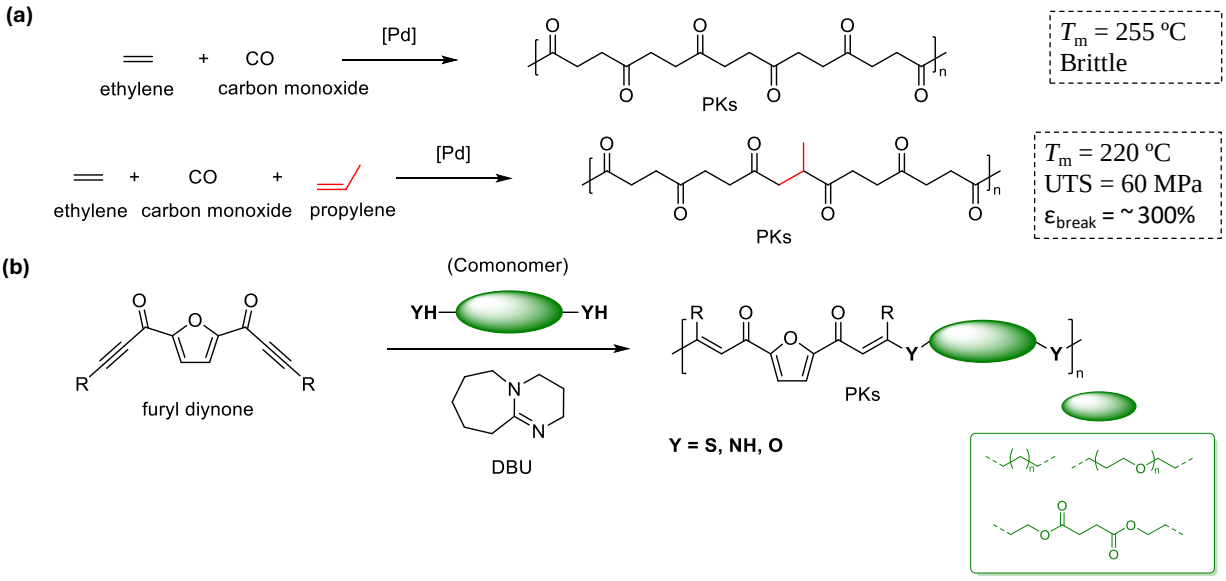

Figure 1. (a) Conventional synthesis scheme of commercial polyketones. (b) Polyketones synthesis *via* "click" polymerization from FDCA Michael acceptor.

Herein, we report the synthesis of photodegradable PKs *via* thiol-yne "click" polymerization involving diynones and dithiols as starting materials. Renewable feedstock FDCA was used to prepare furyl Weinreb amide with a one-pot reaction. This precursor was then utilized for diynone monomer synthesis under benign reaction

conditions. The monomer composition (polymer backbones) of the resultant PKs was successfully modified with respect to different chain flexibility and intermolecular force to optimize their thermomechanical properties under ambient reaction conditions producing more selective photodegradation products under controlled UV light compared to the Norrish pathways.

RESULTS AND DISCUSSION

Monomer Synthesis and Characterization

To construct linear polyketone architectures, the ketone alkyne monomer (diynone) was prepared and further reacted with commercially distilled dithiols *via* click polymerization. The diynone was synthesized from Weinreb amide using 2,5-furandicarboxylic acid (FDCA) as a building block, which is commercially available and renewably sourced from sugar[46] (**Figure 2a**). The precursor (FDCA) was converted into the Weinreb amide (obtained with 89% isolated yield after recrystallization) to prepare activated alkynes. The reaction of Weinreb amide with metalated alkynes, such as the Grignard reagent is required to yield these activated alkynes (diynone, achieved with 80% isolated yield)[48] (**Figure 2b**).

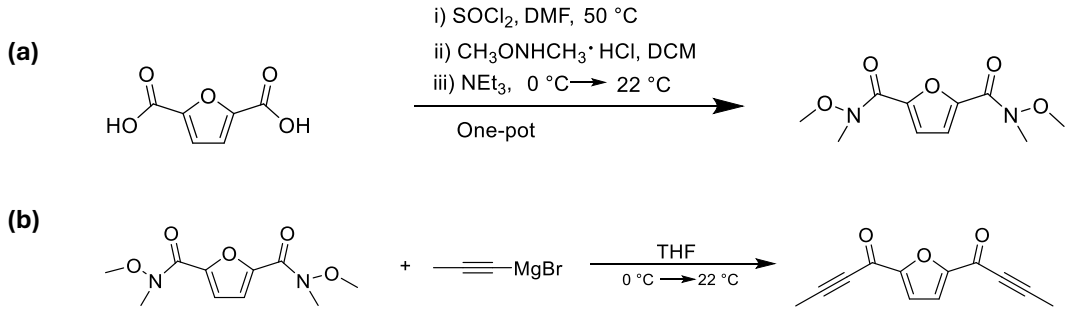

Figure 2. (a) Synthesis of furyl Weinreb amide from FDCA. (b) Synthesis of ketone alkyne monomer (diynone) from Weinreb amide.

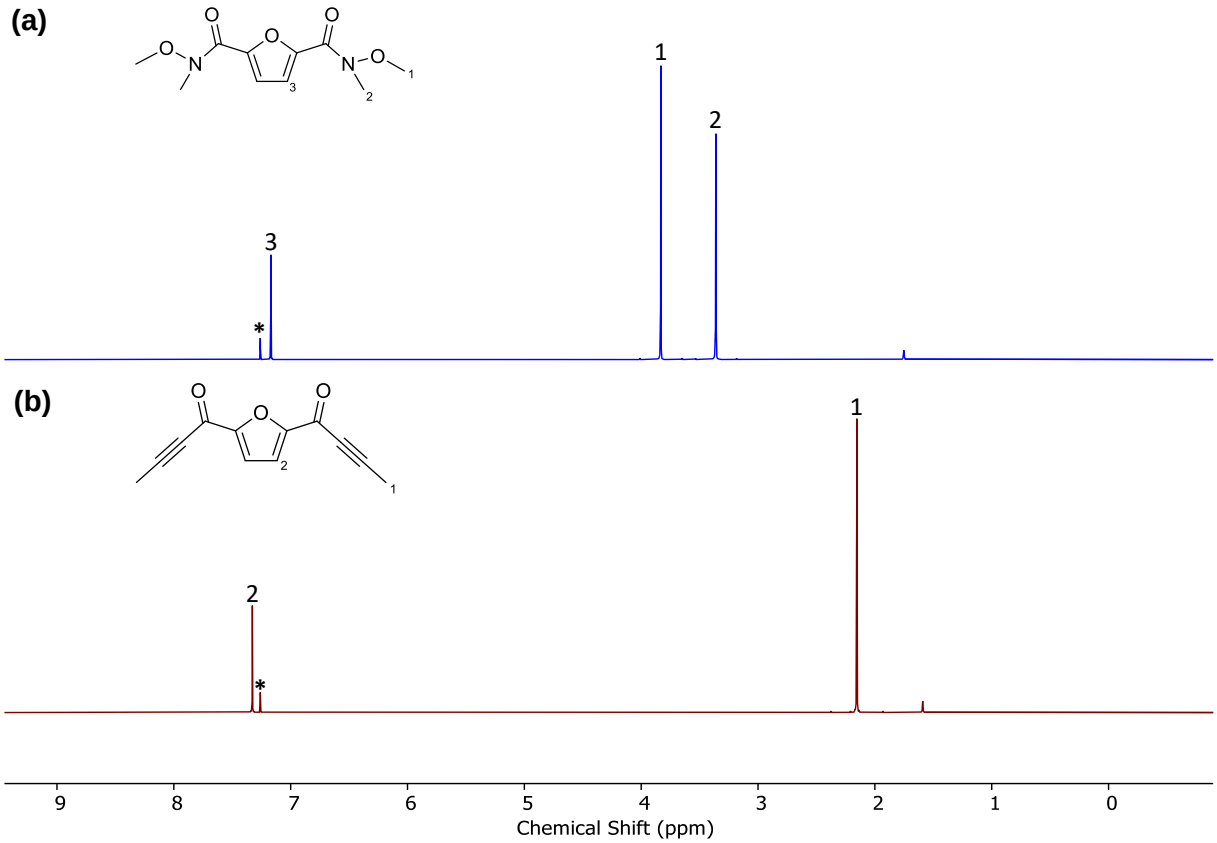

Figure 3. ^{1}H NMR spectra of (a) Furan-Weinreb amide monomer, (b) diynone monomer (400 MHz, $CDCl_3$). The solvent peaks are marked with asterisks.

The characterizing data was consistent with the proposed structures. The ^{1}H NMR spectrum of the Weinreb amide indicates the characteristic peaks at δ = 3.36 ppm, δ = 3.83 ppm, and δ = 7.17 ppm, while diynone shows new characteristic peaks at δ = 2.15 ppm and δ = 7.33 ppm (**Figure 3**). The NMR integration can be seen in the **Supplementary Figure S1 & S3**. Furthermore, Fourier Transform Infrared spectroscopy (FTIR) analysis reveals the presence of stretch N-H bond in the range of λ = 2500-3000 cm^{-1} indicating FDCA successfully converted to Weinreb amide. The stretch alkyne (C≡C) bond can be found at 2200 cm^{-1} demonstrating the formation of diynone monomer (**Figure 5b**).

Polymers Synthesis and Characterization

Step-growth polymerization is an effective method for producing a variety of polymers, including linear and crosslinked polymers.[49] Polyketones were synthesized *via* thiol-Michael addition reaction between the diynone and commercially available dithiols of different architectures (**Figure 4**). Dithiols were introduced to the alkynes monomers to synthesize polymers with high molecular weights and yields.[47] These Michael addition reactions between the various dithiols and diynone monomer were catalyzed by 1,8-diazabicyclo[5.4.0]undec-7ene (DBU) under mild reaction conditions. The butylated hydroxytoluene (BHT) was then added before precipitation to prevent crosslinking during the polymerization.

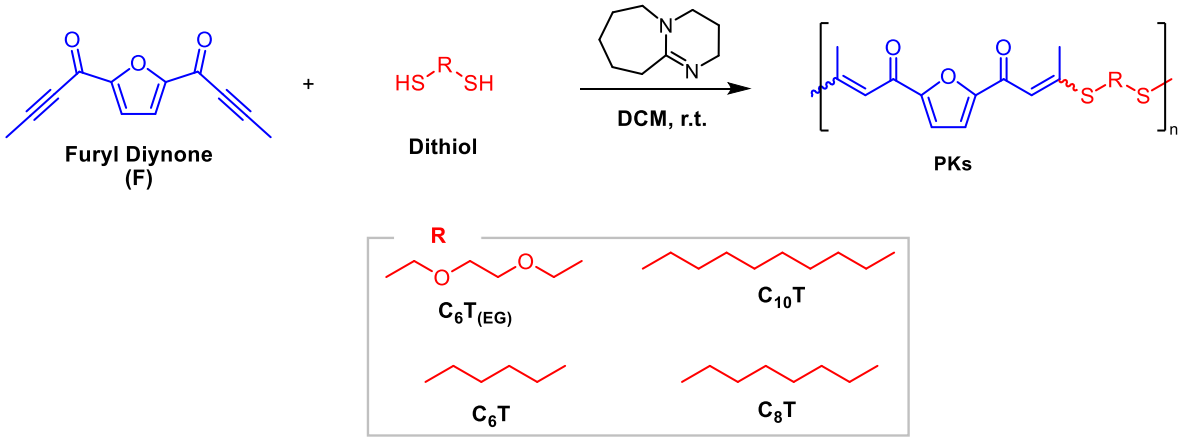

Figure 4. Base-catalyzed thiol-yne click polyaddition between furan-based diynone and various dithiol to yield substituted PKs.

Table 1. Thermomechanical properties of polyketones.

Entry	M_w[a] (kDa)	$Đ_M$[a] (M_w/M_n)	%*trans*[b]	T_g[c] (°C)	$T_{d,5\%}$[d] (°C)	E[e] (MPa)	σ_b[f] (MPa)	ε_b[g] (%)	U_T[h] ($MJ \cdot m^{-3}$)
F-C$_6$T	92	9.07	62	64	261	466 ± 40	13.3 ± 1.4	357 ± 57	40.9 ± 7.6
F-C$_6$T$_{EG}$	87	7.74	62	51	276	191 ± 9	4.6 ± 0.3	749 ± 44	25.1 ± 1.2
F-C$_8$T	101	4.10	73	58	285	427 ± 30	16.1 ± 1.4	287 ± 38	39 ± 7.1
F-C$_{10}$T	138	3.14	74	47	291	517 ± 11	35.6 ± 0.9	257 ± 21	69.7 ± 1.9

[a]M_w and $Đ_M$ were determined by size exclusion ($CHCl_3$, 0.5% NEt_3, 40 °C) analysis against poly(styrene) (PS) standards. [b]%*trans* content determined by ^1H NMR spectroscopic analysis. [c]T_g was obtained from the 2nd heating cycle. [d]$T_{d,5\%}$ was determined from the material losing 5% of mass weight. [e]Young's modulus. [f]Stress at break. [g]Strain at break. [h]Tensile toughness (n = 3). Uncertainty is presented as the standard deviation of samples.

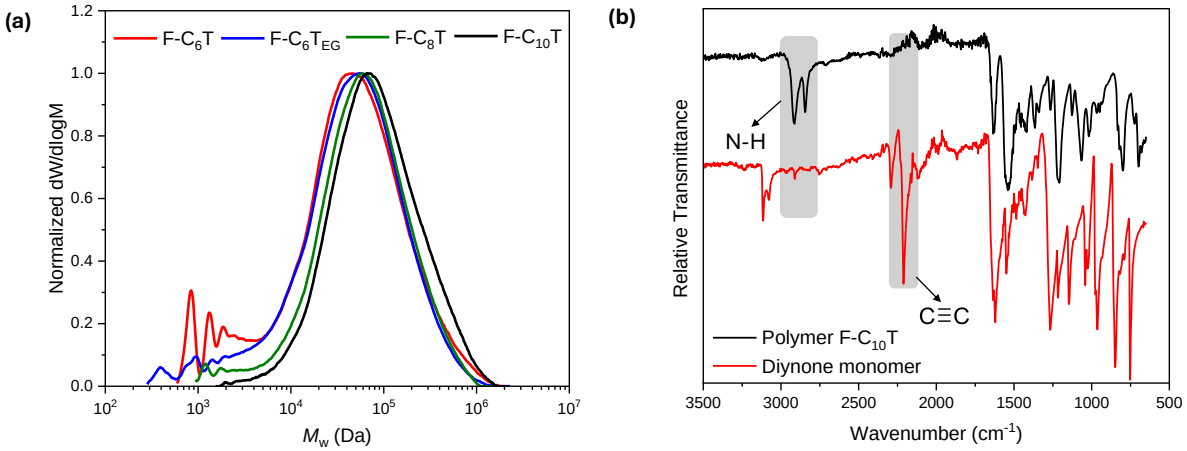

Figure 5. (a) Normalized size exclusion chromatograms of thiol-yne based PKs ($CHCl_3$, 0.5% NEt_3, 40 °C) analysis against poly(styrene) (PS) standards. (b) FT-IR spectra stacked of representative PKs and diynone monomer

The polyketone F-C_6T was synthesized *via* thiol-Michael addition reaction between the diynone and 1,6-hexanedithiol. After 2 hours of polymerization at room temperature (22 °C), a viscous polymer solution was precipitated into diethyl ether twice to purify the polymer from residues of the BHT and catalyst. The resultant polyketone (F-C_6T) shows the double bond was composed of a mixture of *trans* and *cis* isomers in the ratio of 62/38 *trans* to *cis*, respectively, as shown in ^{1}H NMR spectroscopy (**Supplementary Figures S9**). PK F-C_6T showed a weight-average molar mass (M_w) of 92 kDa with dispersity ($Đ_M$) of 9.07 measured using Size Exclusion Chromatography (SEC) (**Figure 5a**, **Table 1**). The favorable arrangement of the *trans* conformer is a consequence of the formation of the most stable enolate intermediates thus affecting the final confirmation of the double bonds within the polymer structure. As previously reported, bond rotation to the more thermodynamically stable *trans*-isomer will become more favorable as the electron-withdrawing ability increases.[48] Overall, it was assumed that the formation of an allenolate intermediate could facilitate the isomerization in reactions that employ substrates with carbonyl-containing activating groups, in order to generate products with mixed stereochemistry (as an outcome of both *syn*- and *anti*-additions).[50] Furthermore, the formation of the representative polymer F-C_6T was confirmed by the FTIR spectra analysis, as indicated by the disappearance of the stretch alkyne (C≡C)

bond at 2200 cm^{-1} which is attributed to diynone monomer (**Figure 5b**).

Mechanical and Thermal Analysis of Polyketones

The structure of the 1,6-hexanedithiol consisting of a long C-C bond suggested a stiff polymer, which was confirmed by tensile test *i.e.,* Youngs' modulus, tensile strength, and elongation. To further improve the tensile strength and elongation, the F-C_6T_{EG} was synthesized using the comonomer 2,2'-(ethylenedioxy)diethanethiol. The presence of ether bonds (C-O) in the polymer backbone could enhance the overall mechanical properties by improving the tensile elongation while maintaining a reasonable tensile strength. The tensile test shows a great improvement in the elongation compared to F-C_6T (ε = 749%), however, the tensile strength of F-C_6T_{EG} is very low (σ = 4.6 MPa). This drop in tensile strength could be attributed to both chain flexibility and the reduction in the chain packing efficiency due to the presence of ether bonds (C-O). The reduction in chain packing efficiency is shown clearly in the absence of strain-induced crystallization (in contrast to F-C_6T) (**Table 1, Figure 6a)**.

Under identical reaction conditions, the F-C_8T was synthesized using the comonomer 1,8-octanedithiol to investigate the effect of increasing the repeat unit length on the mechanical properties of the polyketones. As expected, increasing the repeat unit length of the polymer backbones could considerably improve the tensile strength (σ = 16 MPa). Furthermore, a noticeable strain induced crystallization was observed as a consequence of F-C_8T exhibiting a better chain packing efficiency than its etheric analogous, F-C_6T_{EG}.

To confirm the trend of increasing tensile strength and the molecular weight with increasing the repeat unit length of the polymer structures, the F-C_{10}T was similarly synthesized in the same reaction conditions using 1,10-decanedithiol as a comonomer with a longer carbon chain. The result agrees well with existing trends *i.e*. the tensile strength greatly increases. Furthermore, the outstanding mechanical properties of F-C_{10}T were compared to the commercial plastic PET. Overall, F-C_{10}T displayed a closer

tensile strength than other synthesized polyketones to PET. **(Figure 6b).**

The thermal testing of the synthesized polyketones films was conducted using differential scanning calorimetry (DSC) with a heating rate of 10 °C min^{-1} (0 °C – 200 °C) and thermogravimetric analysis (TGA) up to 800 °C. The DSC curves indicate that all polyketone films are amorphous, and the glass transition temperature decreases with increasing the carbon atoms present in the repeating unit. We hypothesized that the decrease in T_g with the expansion of repeat unit length is due to the increment of the entanglement between polymer chains, which creates more "free volume" between the polymer chains, and hence lowers the glass transition temperature (T_g).[51] The observed trend of enhancing Young's modulus (at very low elongation) with the extension of the chain length aligns well with the entanglement hypothesis. Furthermore, the incorporation of ether bonds in F-C_6T_{EG} decreases the T_g compared to the analogous F-C_8T, which has no ether bonds (**Figure 6c**). This result could be attributed to the presence of ether bonds which increases the chain flexibility and decreases the T_g. The TGA analysis revealed that the decomposition temperatures at 5% weight loss for all synthesized PKs were over 260 °C, indicating excellent thermal stability (**Figure 6d**).

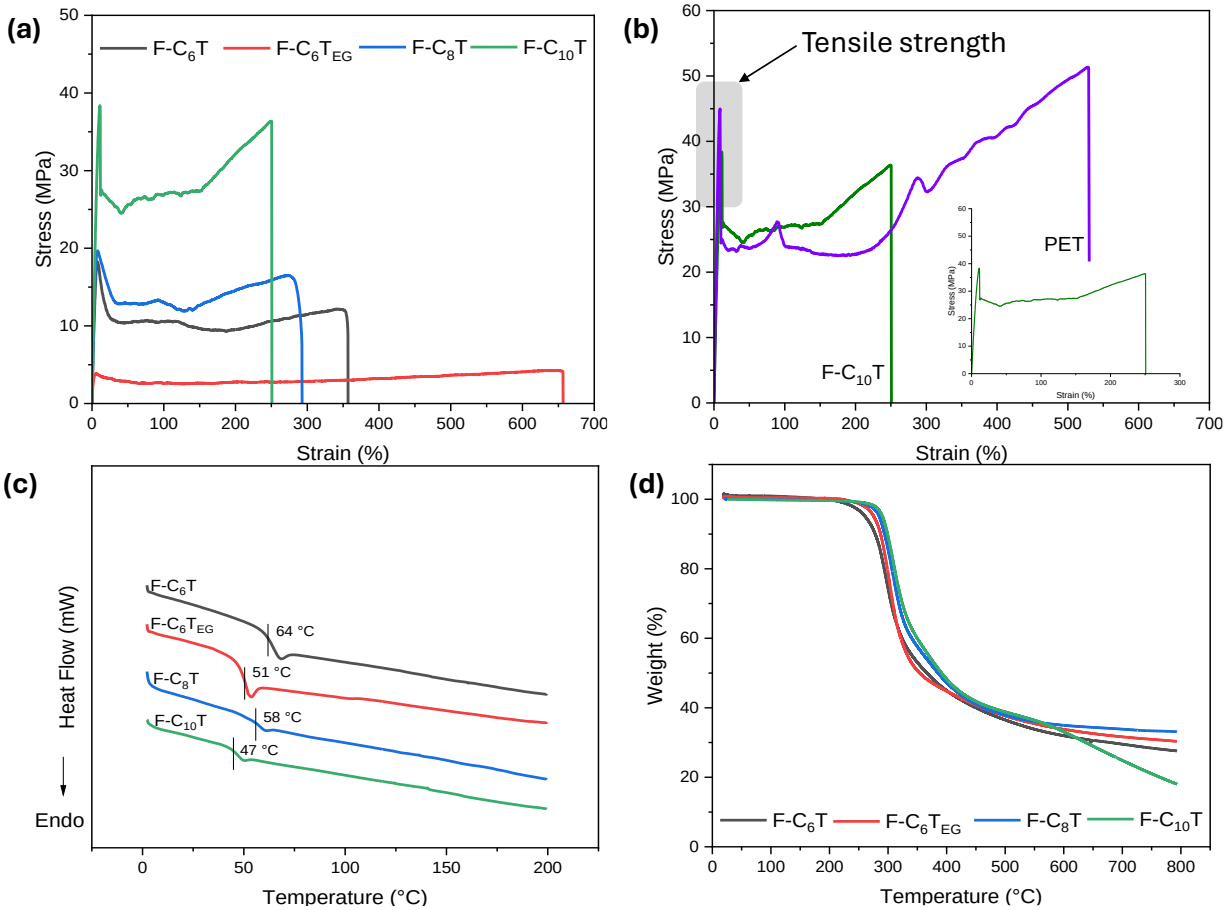

Figure 6. (a) Exemplary stress *vs* strain curves of thiol-yne based PKs tested at 10 mm min^{-1}, 22 °C. (b) Exemplary stress *vs* strain curves of F-C_{10}T and PET tested at 10 mm min^{-1}, 22 °C. (c) DSC thermograms of 2nd heating cycle were tested at 10 °C min^{-1}. The position of T_g for each polymer sample is indicated with a vertical hash mark. (d) Thermogravimetric analysis of polymers at 10 K·min^{-1}

Photodegradation Studies of Polyketones

Polyketones have photodegradable ketone moieties which lead these typical polymers to be an intriguing property to examine as they are less dependent on the environmental conditions. In addition, the furan ring is expected to contribute to the acceleration of the degradation rate due to its higher susceptibility towards the photooxidation reactions with singlet O_2 present in the atmosphere (furan moiety can in fact act as a photosensitizer)[52]. To understand the photostability of furan, Verni *at al*. reported the C-O bond in the furan ring is geometrically shorter than the C-S bond in the thiophene counterpart (heterocyclic analogues), leading to a constrained 6π-electron system and a greater HOMO energy than thiophene.[53] Thus, the furan ring in fact demonstrates a low photostability to UV irradiation. Interestingly, unlike the typical

degradation of commercial polyketones that follow the Norrish pathways[28], the photodegradation of synthesized polyketones followed a more selective pathway, with furyl β-diketone as the major product (**Figure 7).** This compound is non-toxic and environmentally friendly according to the material safety data sheet (MSDS). The proposed pathway of photodegradation is shown below. This photodegradation pathway followed by these synthesized PKs has also been previously reported. (unpublished work).

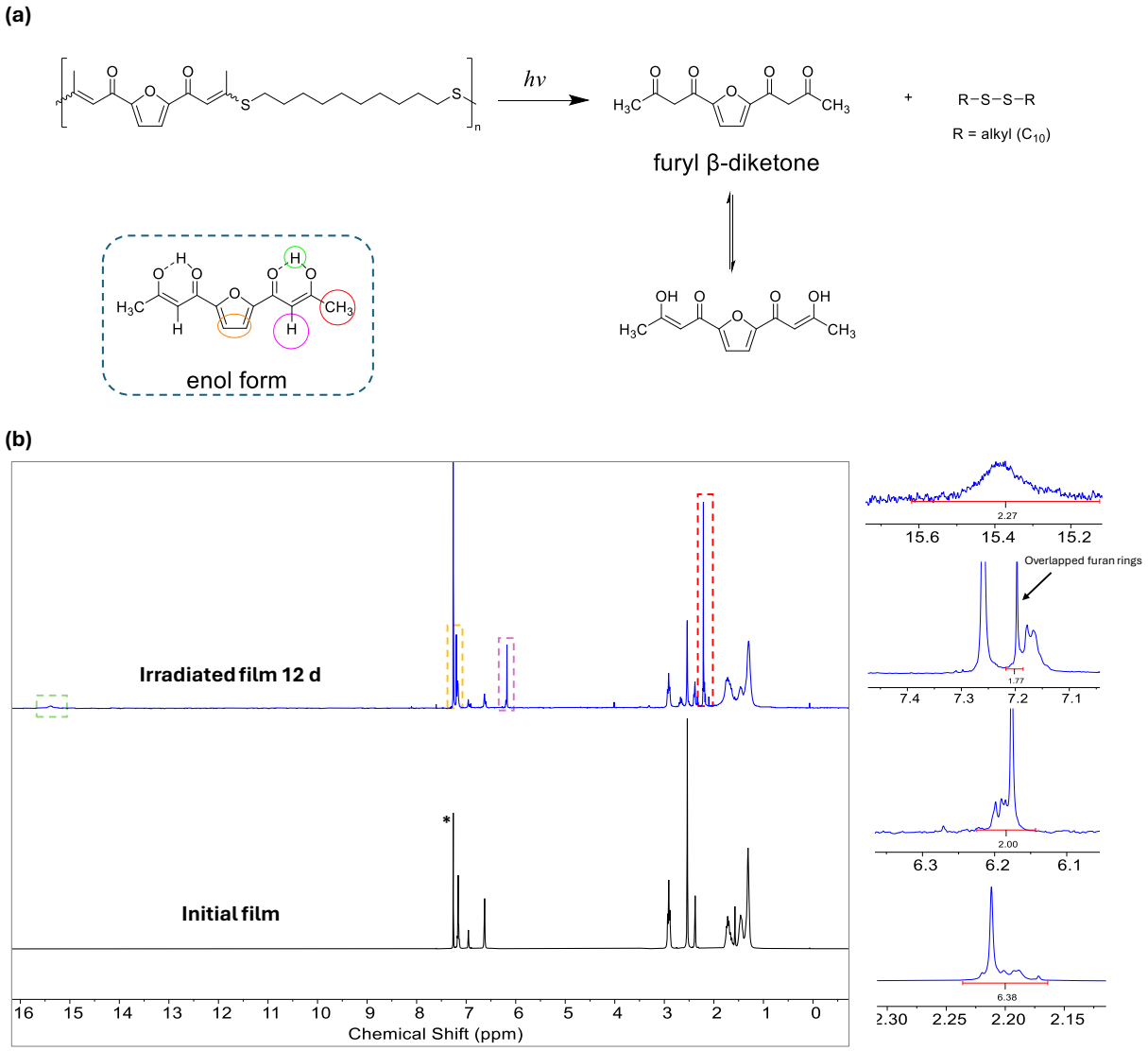

Figure 7. (a) Proposed photodegradation pathway of representative thiol-yne based PKs. (b) ^{1}H NMR spectra of the representative film polyketone F-C_{10}T without irradiation and after irradiation for 12 days. The solvent peak ($CDCl_3$) is marked with asterisks.

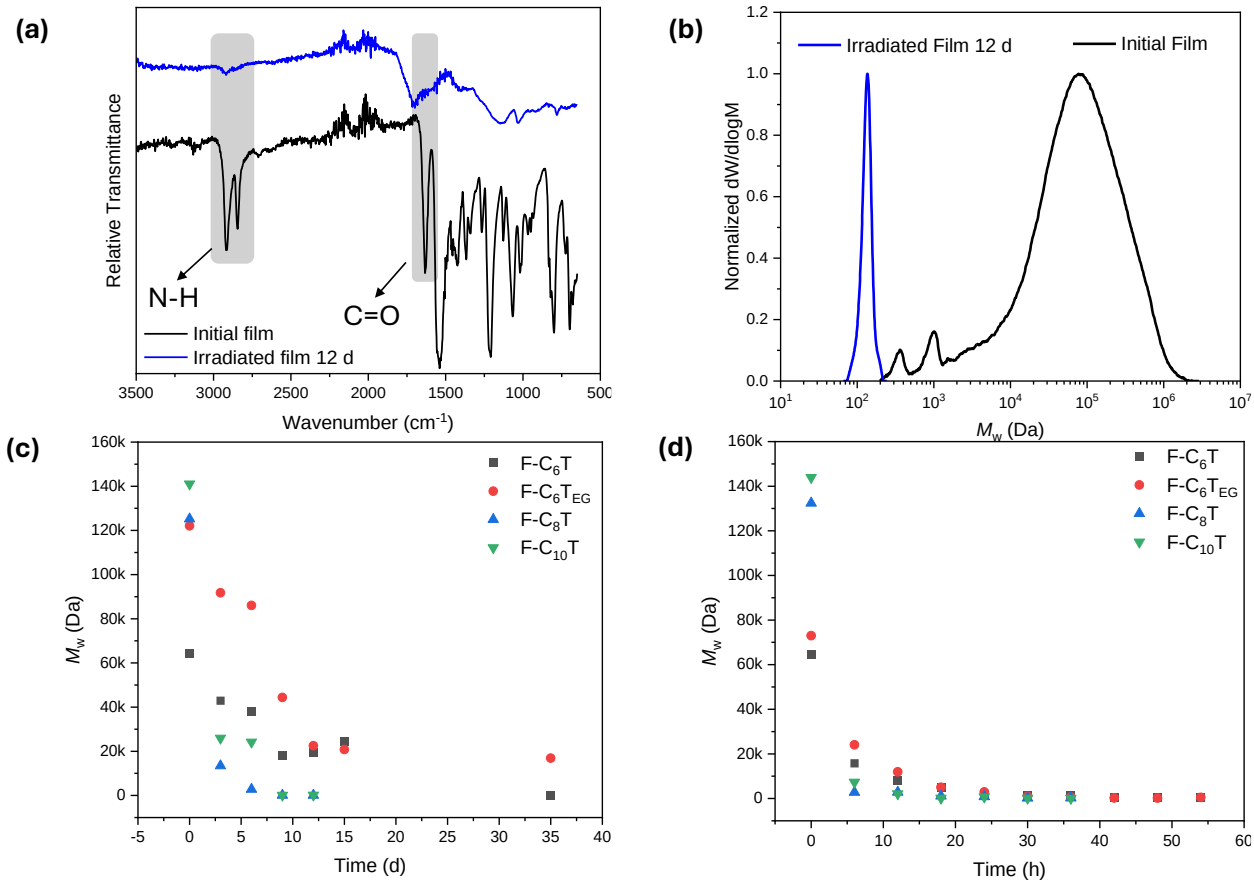

Figure 8. (a) FTIR spectra stacked of initial and irradiated film F-C_{10}T. (b) Normalized size exclusion chromatograms (SEC) of the irradiated polymer film ($CHCl_3$, 0.5% NEt_3, 40 °C) analysis against poly(styrene) (PS) standards. (c) SEC analysis of polyketones as irradiated film sample. (d) SEC analysis of polyketones as irradiated solution sample (20 mg/mL $CDCl_3$) (*Agilent PS standards cover a M_w range from 162 Da to 15 x 10^6 Da, therefore 162 Da is considered as zero* (*0*)).

After the photodegradation of the polymer films in an environmental weathering chamber (accelerated weathering test), SEC and ^{1}H NMR spectroscopic analysis of the degraded PKs was conducted. The result suggested that the repeat unit length of the aliphatic chains and/or the presence of ether bonds in the thiol comonomers also help to accelerate the degradation rate while maintaining the same degradation pathway and the major degradation product (**Supplementary Figures S23-S33**). The predominant degradation product has a hydroxyl group (low and broad signal, δ = 15.40 ppm), a methyl group (δ = 2.21 ppm), and a methine group (δ = 6.18 ppm). The proton resonance from the hydroxyl group leading the chemical shift downfield is due

to the internal hydrogen bond interaction between ketone and hydroxyl groups. The FTIR spectra analysis revealed a change in the peak intensities and shapes indicating that photodegradation occurred (**Figure 8a**). Also, the size exclusion chromatograms indicated a significant reduction in molecular weight after 12 days (**Figure 8b**).

In contrast to films, the solution-phase photodegradation experiments proceeded with faster kinetics and produced more degradation products as assessed by ^{1}H NMR spectroscopy (**Supplementary Figures S29-S32**) due to the lower band gap of HOMO and LUMO energy within the polymer system resulting in further degradation of the furan ring. Within 54 h under UV light irradiation, the polymers were fully degraded, and the appearance of some other peaks suggests the photodegradation products were potentially degraded as well under these conditions. Furthermore, the SEC analysis revealed a substantial decrease in the molecular weight of the polyketone films during the initial three days, followed by a gradual decline (**Figure 8c**). Compared to the film state, polyketones in solution state degraded faster and their molecular weight significantly decreased within hours. This difference in degradation rate can be simply understood by the availability of photolytic bonds in film and solution state. (**Figure 8d**). Polyketone film samples exhibited a uniform concentration of photolytic bonds, whereas in polymer solution, the bond concentration can be less or non-uniform as a result of the formation of random coils by dispersed individual polymer chains in solvents.[54]

To gain more insight into the reaction pathway, model polyketones were synthesized using a primary thiol and ynone photochemically degraded under identical conditions. A reaction between the ynone and 1-hexanethiol was then performed to obtain mono-functional thia-Michael adduct as a representative model of the previously synthesized polyketone (F-C_6T). The model polyketone NMR spectra indicate the presence of *cis*/*trans* isomers in which the *trans*-isomer is dominant (**Supplementary Figure S34-S37**). The ^{1}H NMR spectra of the degraded mono-functional thia-Michael adduct model in the environmental weathering chamber (accelerated weathering test) showed rapid

degradations in which the methyl group, methine group, and hydroxyl group from the β-diketone (enol form) unit appeared in 5 h with low intensities. However, the emergence of some new peaks after 2 h indicated the possibility of a further reaction of the initially formed photodegradation products (**Supplementary Figure S38**).

Furthermore, the model polyketone with phenyl ring (Ph-C_6T) was employed considering its better photostability (absence of furan group). The NMR spectra indicated the formation of β-diketone (enol form) with cleaner photodegradation products than with the furan ring (**Supplementary Figure S39**). In order to confirm the degradation products, Gas Chromatography-Mass Spectroscopy (GC-MS) analysis was used. The chromatograms of both model furan- and phenyl-based polyketones showed the formation of β-diketones as the major products (m/z: 150 and 162 respectively) (**Supplementary Figures S40-S43**). This result is also in accordance with the study mentioned earlier (unpublished work).

CONCLUSION

Thiol-yne 'click reaction proved as a facile click polymerization that enables to produce high molecular weight polyketones at room temperature. In this work, polyketones with a range of thermal and mechanical properties have been successfully synthesized and characterized. All polymers showed amorphous behaviour as indicated by the absence of melting peaks, with T_g in the range of 47 °C to 64 °C. A trend shows that increasing the repeat unit lengths and the molecular weights tend to enhance the tensile strength of the polymers. Moreover, a polyketone with outstanding mechanical properties (elongation at break, σ = 36 MPa) and excellent thermal stability ($T_{d,5\%}$ over 260 °C) has been successfully synthesized in mild reaction conditions. In addition, these polymers showed photodegradability which follows a more selective pathway than Norrish pathways. We believe that the outstanding tensile strength as well as the eco-friendly degradation products shown by these polyketones enable them potentially to be an alternative to the conventional plastic PET in scale and cost-effectiveness.

ASSOCIATED CONTENT

Complete descriptions of experimental procedures including monomers and polymers synthesis, NMR spectra, size exclusion chromatograms, DSC and TGA thermograms, and tensile testing.

AUTHOR INFORMATION

Corresponding Author

Andrew P. Dove − School of Chemistry, The University of Birmingham, Birmingham B15 2TT, U.K; orcid.org/ 0000-0001-8208-9309; Email: a.dove@bham.ac.uk

Authors

Lukmanul H. Samada − School of Chemistry, The University of Birmingham, Birmingham B15 2TT, U.K.

Maher A. Alraddadi − School of Chemistry, The University of Birmingham, Birmingham B15 2TT, U.K.; Chemical Skills Department, Royal Commission for Yanbu Colleges & Institutes, Yanbu Industrial City, Saudi Arabia.

Joshua C. Worch − School of Chemistry, The University of Birmingham, Birmingham B15 2TT, U.K.; Department of Chemistry, Virginia Tech, 24061, USA.; orcid.org/ 0000-0002-4354-8303

Arianna Brandolese − School of Chemistry, The University of Birmingham, Birmingham B15 2TT, U.K.

Author Contributions

The manuscript was written through the contributions of all authors. All authors have given approval to the final version of the manuscript.

Acknowledgements

A.P.D., A.B., and J.C.W. acknowledge funding from the European Research Council (ERC) under the European Union's Horizon 2020 research and innovation program under grant agreement no. 681559. M.A. acknowledges funding from The Royal Commission for Jubail and Yanbu (RCJY). L.H.S thanks Indonesian Endowment Fund for Education (LPDP) agency for funding support.

Notes

The authors declare no competing financial interest.

REFERENCES

1. Reddy, R. L., Reddy, V. S. & Gupta, G. A. Study of Bio-plastics As Green & Sustainable Alternative to Plastics. *Int. J. Emerg. Technol. Adv. Eng.* **3**, 82–89 (2013).
2. Klemeš, J. J., Fan, Y. Van & Jiang, P. Plastics: friends or foes? The circularity and plastic waste footprint. *Energy Sources, Part A Recover. Util. Environ. Eff.* **43**, 1549–1565 (2021).
3. Tessnow-von Wysocki, I. & Le Billon, P. Plastics at sea: Treaty design for a global solution to marine plastic pollution. *Environ. Sci. Policy* **100**, 94–104 (2019).
4. Rodgers, K., Mayes, W. M., Santoro, O., Redshaw, C., Mccumskay, R. & Parsons, D. R. Comparative assessment of marine weathering of ROP-derived biopolymers against conventional plastics. *Mar. Pollut. Bull.* **167**, 112272 (2021).
5. Spierling, S., Knüpffer, E., Behnsen, H., Mudersbach, M., Krieg, H., Springer, S., Albrecht, S., Herrmann, C., Endres, H. J. Bio-based plastics - A review of environmental, social and economic impact assessments. *J. Clean. Prod.* **185**, 476–491 (2018).
6. Iwata, T. Biodegradable and bio-based polymers: Future prospects of eco-friendly plastics. *Angew. Chemie - Int. Ed.* **54**, 3210–3215 (2015).
7. do Val Siqueira, L., Arias, C. I. L. F., Maniglia, B. C. & Tadini, C. C. Starch-based biodegradable plastics: methods of production, challenges and future perspectives. *Curr. Opin. Food Sci.* **38**, 122–130 (2021).
8. Mangaraj, S., Yadav, A., Bal, L. M., Dash, S. K. & Mahanti, N. K. Application of Biodegradable Polymers in Food Packaging Industry: A Comprehensive Review. *J. Packag. Technol. Res.* **3**, 77–96 (2019).
9. Poulopoulou, N., Kasmi, N., Bikiaris, D. N., Papageorgiou, D. G., Floudas, G. & Papageorgiou, G. Z. Sustainable Polymers from Renewable Resources: Polymer Blends of Furan-Based Polyesters. *Macromol. Mater. Eng.* **303**, 1–8

(2018).

10. Lopera-Valle, A., Caputo, J. V., Leão, R., Sauvageau, D., Luz, S. M. & Elias, A. Influence of epoxidized Canola Oil (eCO) and Cellulose Nanocrystals (CNCs) on the mechanical and thermal properties of polyhydroxybutyrate (PHB)-Poly(lactic acid) (PLA) blends. *Polymers (Basel).* **11**, (2019).
11. Zia, K. M., Noreen, A., Zuber, M., Tabasum, S. & Mujahid, M. Recent developments and future prospects on bio-based polyesters derived from renewable resources: A review. *Int. J. Biol. Macromol.* **82**, 1028–1040 (2016).
12. Sevim, K. & Pan, J. A model for hydrolytic degradation and erosion of biodegradable polymers. *Acta Biomater.* **66**, 192–199 (2018).
13. Frank, A., Rath, S. K., Boey, F. & Venkatraman, S. Study of the initial stages of drug release from a degradable matrix of poly(d,l-lactide-co-glycolide). *Biomaterials* **25**, 813–821 (2004).
14. Miao, S., Wang, P., Su, Z. & Zhang, S. Vegetable-oil-based polymers as future polymeric biomaterials. *Acta Biomater.* **10**, 1692–1704 (2014).
15. Woodard, L. N. & Grunlan, M. A. Hydrolytic Degradation and Erosion of Polyester Biomaterials. *ACS Macro Lett.* **7**, 976–982 (2018).
16. Haider, T. P., Völker, C., Kramm, J., Landfester, K. & Wurm, F. R. Plastics of the Future? The Impact of Biodegradable Polymers on the Environment and on Society. *Angew. Chemie - Int. Ed.* **58**, 50–62 (2019).
17. Yu, L., Dean, K. & Li, L. Polymer blends and composites from renewable resources. *Prog. Polym. Sci.* **31**, 576–602 (2006).
18. Cywar, R.M., Rorrer, N.A., Hoyt, C.B. *et al.* Bio-based polymers with performance-advantaged properties. *Nat. Rev. Mater* **7**, 83–103 (2022).
19. Shankar, S. & Shikha. *Renewable and Nonrenewable Energy Resources: Bioenergy and Biofuels*. *Principles and Applications of Environmental Biotechnology for a Sustainable Future.* Springer, Singapore (2017).
20. Amin, D. R., Begum, D. D. A. & Gafur, D. A. Study of Process Parameters for Making Biodegradable Linear Low Density Polyethylene in Natural Weathering Conditions. *IOSR J. Appl. Chem.* **10**, 79–90 (2017).

21. Lin, H., Pearson, A., Kazemi, Y., Kakroodi, A., Hammami, A., Heydrich, M., Xu, B. & Naguib, H. E. Influence of hygrothermal conditioning on the chemical structure and thermal mechanical properties of aliphatic polyketone. *Polym. Degrad. Stab.* **179**, 109260 (2020).
22. Seo, D. C., Jeon, I., Bae, S. & Jho, J. Y. Morphology and Mechanical Properties of the Polyketone/Polycarbonate Blends Compatibilized with Polyamides. *Macromol. Res.* **28**, 1142–1148 (2020).
23. Cho, J., Lee, S. K., Eem, S. H., Jang, J. G. & Yang, B. Enhanced mechanical and thermal properties of carbon fiber-reinforced thermoplastic polyketone composites. *Compos. Part A Appl. Sci. Manuf.* **126**, 105599 (2019).
24. Bianchini, C. & Meli, A. Alternating copolymerization of carbon monoxide and olefins by single-site metal catalysis. *Coord. Chem. Rev.* **225**, 35–66 (2002).
25. Belov, G. P. & Novikova, E. V. Polyketones - alternating copolymers of carbon monoxide. *Usp. Khim.* **73**, 292–320 (2004).
26. Hwang, S. Y., An, J. B., Park, B. C., Kim, T. & Hwang, T. S. Synthesis of sulfonated polyketone membranes by a direct sulfonation reaction and their properties. *J. Ind. Eng. Chem.* **81**, 464–474 (2020).
27. Vodyakov Vladimir, N., Kotin, A. V., Kuznetsov, V. V., Kulikovskaya, K. A., Radaykina, E. A. & Murneva, M. I. The effect of thermal degradation processes on the physical-mechanical and rheological properties of polyketone. *Key Eng. Mater.* **869**, 140–145 (2020).
28. Norrish, R., Bamford, C. Photo-decomposition of Aldehydes and Ketones. *Nature* **140**, 195–196 (1937).
29. Yang, Y. *et al.* Progress in polyketone materials: blends and composites. *Polym. Int.* **67**, 1478–1487 (2018).
30. ASH, Carlton, Edwin, Waters, Dixie, Green, Weinkauf, Donald, H. Polyketone polymer composition. *Eur. Pat. Off.* **99**, 1–10 (2001).
31. Samples, E. M., Schuck, J. M., Joshi, P. B., Willets, K. A. & Dobereiner, G. E. Synthesis and Properties of N-Arylpyrrole-Functionalized Poly(1-hexene- alt-CO). *Macromolecules* **51**, 9323–9332 (2018).

32. Vavasori, A. & Ronchin, L. *Polyketones: Synthesis and Applications*. *Ency of Polymer Sci and Tech,* **1**, 1-41 (2017).

33. Park, S. A., Jeon, H., Kim, H., Shin, S. H., Choy, S., Hwang, D. S., Koo, J. M., Jegal, J., Hwang, S. Y., Park, J. & Oh, D. X. Sustainable and recyclable super engineering thermoplastic from biorenewable monomer. *Nat. Commun.* **10**, 2601 (2019).

34. Yang, Z., Zhang, J., Qian, G., Duan, X. & Zhou, X. Production of biomass-derived monomers through catalytic conversion of furfural and hydroxymethylfurfural. *Green Chem. Eng.* **2**, 158–173 (2021).

35. Zeng, F. R., Xu, J., Xiong, Q., Qin, K. X., Xu, W. J., Wang, Y. X., Liu, Z. J., Li, Z. L., Li, Z. C. Aliphatic polyketones via cross-metathesis polymerization: Synthesis and post-polymerization modification. *Polymer.* **185**, 121936 (2019).

36. Isikgor, F. H. & Becer, C. R. Lignocellulosic biomass: a sustainable platform for the production of bio-based chemicals and polymers. *Polym. Chem.* **6**, 4497–4559 (2015).

37. Papageorgiou, G. Z., Tsanaktsis, V. & Bikiaris, D. N. Synthesis of poly(ethylene furandicarboxylate) polyester using monomers derived from renewable resources: Thermal behavior comparison with PET and PEN. *Phys. Chem. Chem. Phys.* **16**, 7946–7958 (2014).

38. Papageorgiou, G. Z., Tsanaktsis, V., Papageorgiou, D. G., Chrissafis, K., Exarhopoulos, S. & Bikiaris, D. N. Furan-based polyesters from renewable resources: Crystallization and thermal degradation behavior of poly(hexamethylene 2,5-furan-dicarboxylate). *Eur. Polym. J.* **67**, 383–396 (2015).

39. Ruhemann, S. LVII. The Combination of Mercaptans with Unsaturated Ketonic Compounds. *J. Chem. Soc., Trans*. **87**, 461−468 (1905).

40. Billiet, L., Fournier, D. & Du Prez, F. Step-growth polymerization and ‘click’ chemistry: The oldest polymers rejuvenated. *Polymer.* **50**, 3877–3886 (2009).

41. Mather, B. D., Viswanathan, K., Miller, K. M. & Long, T. E. Michael addition reactions in macromolecular design for emerging technologies. *Prog. Polym. Sci.*

31, 487–531 (2006).

42. Pirman, T., Ocepek, M. & Likozar, B. Radical Polymerization of Acrylates, Methacrylates, and Styrene: Biobased Approaches, Mechanism, Kinetics, Secondary Reactions, and Modeling. *Ind. Eng. Chem. Res.* **60**, 9347–9367 (2021).
43. Li, B., Huang, D., Qin, A. & Tang, B. Z. Progress on Catalytic Systems Used in Click Polymerization. *Macromol. Rapid Commun.* **39**, 1–15 (2018).
44. Michael A. On the addition of sodium acetacetic ether and analogous sodium compounds to unsaturated organic ethers. *Am Chem J.* **9**, 115 (1887).
45. Hu, Y., Daoud, W. A., Cheuk, K. K. L. & Lin, C. S. K. Newly developed techniques on polycondensation, ring-opening polymerization and polymer modification: Focus on poly(lactic acid). *Materials (Basel).* **9**, 1-15 (2016).
46. Gevrek, T. N. & Sanyal, A. Furan-containing polymeric Materials: Harnessing the Diels-Alder chemistry for biomedical applications. *Eur. Polym. J.* **153**, 110514 (2021).
47. Bell, C. A., Yu, J., Barker, I. A., Truong, V. X., Cao, Z., Dobrinyin, A. V., Becker, M. L. & Dove, A. P. Independent Control of Elastomer Properties through Stereocontrolled Synthesis. *Angew. Chem. Int. Ed.* **55**, 13076–13080 (2016).
48. Worch, J. C., Stubbs, C. J., Price, M. J. & Dove, A. P. Click Nucleophilic Conjugate Additions to Activated Alkynes: Exploring Thiol-yne, Amino-yne, and Hydroxyl-yne Reactions from (Bio)Organic to Polymer Chemistry. *Chem. Rev.* **121**, 6744–6776 (2021).
49. Nair, D. P., Podgórski, M., Chatani, S., Gong, T., Xi, W., Fenoli, C. R. & Bowman, C. N. The Thiol-Michael addition click reaction: A powerful and widely used tool in materials chemistry. *Chem. Mater.* **26**, 724–744 (2014).
50. Worch, J. C. & Dove, A. P. Click Step-Growth Polymerization and E/Z Stereochemistry Using Nucleophilic Thiol–yne/–ene Reactions: Applying Old Concepts for Practical Sustainable (Bio)Materials . *Acc. Chem. Res*. **55**, 2355–2369 (2022).
51. Qu, T., Nan, G., Ouyang, Y., Bieketuerxun, B., Yan, X., Qi, Y. & Zhang, Y.

Structure–Property Relationship, Glass Transition, and Crystallization Behaviors of Conjugated Polymers. *Polymers (Basel).* **15**, 4268 (2023).

52. Manicardi, A., Cadoni, E. & Madder, A. Visible-light triggered templated ligation on surface using furan-modified PNAs. *Chem. Sci.* **11**, 11729–11739 (2020).

53. Varni, A. J., Fortney, A., Baker, M. A., Worch, J. C., Qiu, Y., Yaron, D., Bernhard, S., Noonan, K. J. T. & Kowalewski, T. Photostable Helical Polyfurans. *J. Am. Chem. Soc.* **141**, 8858–8867 (2019).

54. Lyu, S. & Untereker, D. Degradability of Polymers for Implantable Biomedical Devices. *Int. J. Mol. Sci*. **10**, 4033-4065 (2009).

2.2 Supporting Information

Supplementary Information

Versatile Synthesis of Bio-based Photodegradable Polyketones with Controllable Thermomechanical Properties

Lukmanul H. Samada[†], Maher A. Alraddadi[†#], Joshua C. Worch [†§], Arianna Brandolese[†], Andrew P. Dove[†*]

[†]School of Chemistry, The University of Birmingham, Edgbaston, Birmingham, B15 2TT, UK.

[§]Department of Chemistry, Virginia Tech, Blacksburg, VA 24061, USA.

[#]Chemical Skills Department, Royal Commission for Yanbu Colleges & Institutes, Yanbu Industrial City, Saudi Arabia.

*Corresponding to: A.Dove@bham.ac.uk

Materials and methods

Unless otherwise specified, all chemicals and solvents were obtained from Sigma-Aldrich, VWR Chemicals, Apollo Scientific, or Fisher Scientific and utilized in their original form without additional purification. Directly from our solvent drying and degassing tower, dry THF was used.

Proton and Carbon Nuclear Magnetic Resonance (^{1}H NMR and ^{13}C NMR)

A Bruker DPX-300 and DPX-400 spectrometer was used to record ^{1}H NMR and ^{13}C NMR spectra. All chemical shifts were reported in ppm and were referenced to the solvent signal Chloroform-*d* ($CDCl_3$) = 7.26 ppm. The multiplicity of the peaks was denoted as s = singlet, d = doublet, t = triplet, q = quadruplet, m = multiplet, ddd = doublet of doublets of doublets, qt = quartet of triplets, pd = pentet of doublets.

High Resolution Mass spectrometry (HRMS) was carried out by the School of Chemistry, University of Birmingham utilizing electrospray ionization on a Waters GCT Premier instrument, as well as employing chemical H+ ionization on a Waters Xevo G2-XS instrument.

Size exclusion chromatography (SEC)

SEC measurements were conducted in $CHCl_3$ using an Agilent 1260 Infinity II Multi-Detector GPC/SEC System equipped with RI, ultraviolet (UV, = 309 nm), and viscometer detectors. The polymers were eluted using an Agilent guard column (PLGel 5 M, 50 7.5 mm) and two Agilent mixed-C columns (PLGel 5 μM, 300 × 7.5 mm) using $CHCl_3$ (buffer 0.5% NEt_3) as the mobile phase (flow rate = 1 mL min^{-1}, 40 °C). Number average molecular weights (M_n), weight average molecular weights (M_w), and dispersity ($Đ$ = M_w/M_n) were calculated using Agilent GPC/SEC software (vA.02.01) in comparison to a 15-point calibration curve (M_p = 162–3,187,000 g mol^{-1}) based on poly(styrene) standards (Easivial PS-M/H, Agilent). The weight average molecular weights (M_w) are expressed in g mol^{-1} or Da.

Differential Scanning Calorimetry (DSC)

Mettler-Toledo Stare system DSC3+ was used to detect thermal transitions including glass transition temperature (T_g), melting temperature (T_m), and crystallization temperature (T_c). Unless otherwise specified, all samples were evaluated at a heating rate of 10 °C min^{-1}.

As the thermal curve's inflection point, both the glass transition temperature and the topological freezing temperature were utilized.

Thermogravimetric analysis (TGA)

A Q50 - Thermogravimetric Analyzer was used to collect TGA data (TA instruments). Thermograms were recorded in an N_2 atmosphere at a heating rate of 10 K min^{-1}, from 25 ^oC to 800 ^oC, with an average sample weight of around 7 mg.

Tensile testing

All uniaxial tensile tests were conducted on a Testometric M350-5CT tensometer with a 5 kgF load cell for synthesized polymers and a 50 kgF load cell for commercial polymers. All measurements were conducted at room temperature and 10 mm min^{-1} strain rate. A bespoke ASTM Die D-638 Type V was utilized to manually cut polymer film samples into dumbbell shapes. The sample is approximately 1.8 mm wide and 1.0 mm thick. A minimum of three specimens were examined for each sample, and the mean average values of the strain at break, stress at break, strain at yield, stress at yield, toughness, and Young's modulus are presented.

Photodegradation Studies

All films and solutions of polyketones were irradiated in the environmental weathering chamber (accelerated weathering test) using Xenon lamp with wavelength 340 nm, BPT 50 °C, and irradiation intensity 50 W/m^2. The timer is set up in that instrument with various time frames. The instrument is calibrated using an irradiation calibrator prior to use and every 1,000 hours of running. The irradiated polymer was then monitored and analyzed by ^{1}H NMR, FTIR, SEC, and GC-MS for analysis of the photodegradation products of the model compounds (small molecules).

Gas Chromatography-Mass Spectroscopy (GC-MS)

GC-MS was performed on a Shimadzu GCMS QP2010 SE system with an HP-5 MS fused silica column (5% phenyl methyl siloxane 30.0m × 250 μm, film thickness 0.25 μm), interfaced with 5675C Inert MSD with Triple-Axis detector. The temperature programming for the separation of the sample was set to 40 °C for 2 min, ramped to 300 °C at 6 °C·min^{-1}, and held for 20 min and ramped to 300 °C at 6 °C·min^{-1}. The injection temperature was 300

°C, with a 1.0 µL injection volume. The helium carrier gas flow rate was set at 1 mL·min^{-1}.

Synthesis of *N*^{2},*N*^{5}-dimethoxy-*N*^{2},*N*^{5}-dimethylfuran-2,5-dicarboxamide

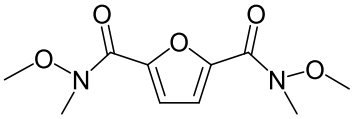

The procedure was derived from published sources and a previous protocol.[1] Furan dicarboxylic acid (FDCA) (10 g, 64 x 10^{-3} mol, 1.0 equiv.) and thionyl chloride ($SOCl_2$) (38 mL, 320 x 10^{-3} mol, 5.0 equiv.) were added to a 2-neck round-bottom flask with a magnetic stirrer, and 3 drops of DMF were then added. An exhaust tube was attached to NaOH bath, and the reaction mixture was then heated at 50 °C and stirred until soluble. The acid chloride solution was cooled down at room temperature and the excess of $SOCl_2$ was removed by high vacuum *N,O*-dimethylhydroxylamine hydrochloride (13.75 g, 141 x 10^{-3} mol, 2.2 equiv.) was added to the reaction mixture while cooling down to 0 °C (in an ice bath). The dropping funnel was used to progressively add trimethylamine (NEt_3) (26 mL, 2691 x 10^{-3} mol, 4.2 equiv.) to the reaction mixture (dropwise slowly, over 30 minutes). The reaction produces a white precipitate (ammonium salt by-product) and is exothermic. After adding trimethylamine, the reaction mixture was taken out from the cooling bath and left for one hour at room temperature. The reaction mixture was diluted with dichloromethane, and then transferred to a separatory funnel. The organic layer was washed with 1 M HCl (2x100 mL), followed by saturated $NaHCO_3$ solution (2x100 mL) and brine (2x100 mL). The organic layer was dried over magnesium sulphate and concentrated using a rotary evaporator. The reaction mixture was purified by recrystallisation with methanol to obtain a brown solid product (13.8 g, 89% yield). **^{1}H NMR** (400 MHz, Chloroform-*d*) δ 7.15 (s, 2H), 3.81 (s, 6H), 3.34 (s, 6H); **^{13}C NMR** (101 MHz, Chloroform-*d*) δ 158.76, 147.27, 118.03, 61.95, 33.49. **HRMS** (ESI-TOF) (*m*/*z*): $[M + H]^+$ calculated for $C_{10}H_{15}N_2O_5$, 243.0981; found, 243.0984. **EA (C,H,N)** %C 49.51, %H 5.88, %N 11.71.

Synthesis of 1,1'-(furan-2,5-diyl)bis(but-2-yn-1-one)

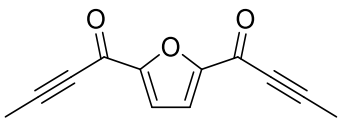

The procedure was derived from published sources and a previous protocol.[2] In dried glassware and under Schlenk condition, the furyl Weinreb amide (5 g, 21 x 10^{-3} mol, 1.0

equiv.) was introduced to a 2-neck round-bottom flask. It was then diluted through cannula transfer with 1 M dry THF. Then, 1-propynylmagnesium bromide solution 0.5 M in THF (99 mL, 50 x 10^{-3} mol, 2.4 equiv.) was introduced by cannula into the Weinreb amide solution, and the solution was cooled down to 5 °C (in an ice bath). Then, the 1-propynylmagnesium bromide solution was added slowly (over 45 minutes) to the reaction mixture while stirring in an ice bath. The mixture was then kept at room temperature overnight to react. The mixture was subsequently cooled down to 0 °C for approximately 30 minutes. After the reaction mixture had been cooled, it was rapidly quenched with 1 M HCl solution (100 mL). The crude mixture was then transferred to a separatory funnel and washed with ethyl acetate (2x100 mL) and brine (2x100 mL). The resulting "extracted" layer was then filtered and dried over magnesium sulphate. The organic solution was finally concentrated with a rotary evaporator. The reaction mixture was purified with ethanol recrystallization to get a brown solid monomer (3.30 g, 80% yield). **^{1}H NMR** (400 MHz, Chloroform-*d*) δ 7.33 (s, 2H), 2.15 (s, 6H); **^{13}C NMR** (101 MHz, Chloroform-*d*) δ 165.53, 154.56, 119.85, 94.02, 78.46, 4.64. **HRMS** (ESI-TOF) (*m*/*z*): $[M + H]^+$ calculated for $C_{12}H_9O_3$, 200.0479; found, 200.0475. **EA (C,H,N)** %C 72.03, %H 4.11.

General procedure for thiol-yne "click" polymerization

In a 20 ml scintillation vial, the furyl diynone monomer (0.5 g, 2.5 x 10^{-3} mol, 1.0 equiv.) was mixed with 1,6-hexanedithiol (0.375 g, 2.5 x 10^{-3} mol, 1.0 equiv.) (dithiol was fully washed with DCM (2 mL) during transferring to the diynone monomer). The reaction mixture was diluted with DCM (3 mL) cooled down to 0 °C in an ice bath. After that, 1,8-Diazabicyclo[5.4.0] undec-7-ene (DBU) (3.80 µl 24.98 µmol, 0.01 equiv.) was added and kept at room temperature for two hours. To inhibit crosslinking prior to precipitation, butylated hydroxytoluene (BHT) 20% w/w was added to the reaction mixture. The polymer solution was precipitated into diethyl ether (250 mL) and subsequently redissolved in DCM (10 mL) and reprecipitated in diethyl ether (250 mL) to eliminate any leftover BHT. Finally, the polymer was dried *in vacuo* at room temperature for 24 h, and then under high vacuum at 40 °C for 24 h to yield brown polymer. The *cis*/*trans* isomer was determined based on a previous published work.[3]

a) Polyketone F-C₆T

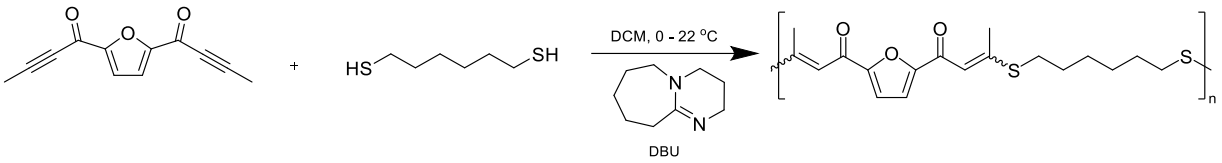

Scheme S1. Synthetic pathway of F-C_6T from furan-based diynone and 1,6-hexanedithiol.

The polymer was obtained as a brown solid (0.90 g, 95% yield). **^{1}H NMR** spectra (400 MHz, Chloroform-*d*) δ 7.15 (d, *J* = 4.2 Hz, 2H, *trans*/*cis* overlapped), 6.95 (s, 1H, *cis* overlapped), 6.64 (s, 1H, *trans* overlapped), 2.92 (t, 4H), 2.53 (s, 4H (*trans*), 2.38 (s, 2H, *cis*) 1.75 (s, 4H), 1.47 (d, *J* = 25.8 Hz, 7H, overlapped with H_2O), *cis*/*trans*: 38/62; **^{13}C NMR** (101 MHz, Chloroform-*d*) δ 175.77$_{trans}$, 175.35$_{cis}$, 164.28$_{trans}$, 164.25$_{cis}$, 154.87$_{trans}$, 154.40$_{cis}$, 116.61, 116.03, 111.89, 31.79, 30.87, 28.62, 27.43, 24.71, 22.42; SEC ($CHCl_3$ + 0.5% NEt_3): M_n = 10,135, M_w = 92,007, $Đ_M$ = 9.07.

b) Polyketone F-C₆T$_{EG}$

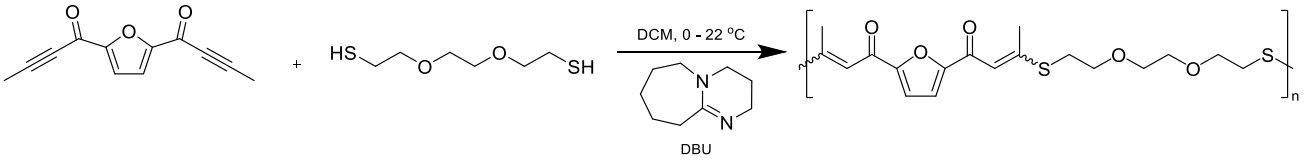

Scheme S2. Synthetic pathway of F-C_6T from furan based diynone and 2,2′-(Ethylenedioxy)diethanethiol

The polymer was obtained as a brown solid (0.98 g, 95% yield). **^{1}H NMR** spectra (400 MHz, Chloroform-*d*) δ 7.16 (d, *J* = 6.4 Hz, 2H, *trans*/*cis* overlapped), 6.94 (s, 1H, *cis* overlapped), 6.68 (s, 1H, *trans* overlapped), 3.80 – 3.70 (m, 3H overlapped), 3.69 (tdd, *J* = 13.0, 8.9, 3.3 Hz, 6H, overlapped), 3.15 (t, 4H), 2.53 (s, 4H, *trans*), 2.39 (s, 2H, *cis*), *cis*/*trans*: 38/62; **^{13}C NMR** (101 MHz, Chloroform-*d*) δ 175.77$_{trans}$, 175.68$_{cis}$, 163.58$_{trans}$, 163.43$_{cis}$, 154.86$_{trans}$, 154.45$_{cis}$, 116.73$_{cis}$, 116.45$_{trans}$, 112.13$_{cis}$, 111.95$_{trans}$, 70.65$_{trans}$, 69.89$_{cis}$, 68.48, 31.78, 30.74, 24.78, 22.36; SEC ($CHCl_3$ + 0.5% NEt_3): M_n = 11,187 , M_w =86,608, $Đ_M$ = 7.74.

c) Polyketone F-C$_8$T

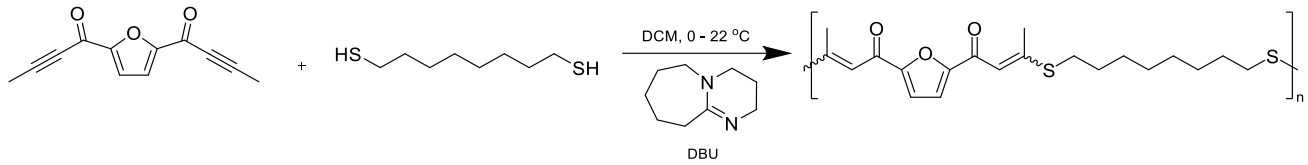

Scheme S3. Synthetic pathway of F-C$_6$T from furan based diynone and 1,8-octanedithiol

The polymer was obtained as a dark brown solid (0.99 g, 97% yield). **^{1}H NMR** spectra (400 MHz, Chloroform-*d*) δ 7.16 (d, *J* = 2.1 Hz, 2H, *trans*/*cis* overlapped), 6.95 (d, *J* = 4.9 Hz, 1H, *cis* overlapped), 6.62 (d, *J* = 5.2 Hz, 1H, *trans* overlapped), 2.89 (t, 4H), 2.53 (s, 5H), 2.37 (d, *J* = 5.9 Hz, 2H overlapped), 1.69 (ddd, *J* = 28.7, 14.2, 7.6 Hz, 5H), 1.42 (ddd, *J* = 46.9, 11.3, 5.6 Hz, 9H, overlapped with H_2O), *cis*/*trans*: 27/73; **^{13}C NMR** (101 MHz, Chloroform-*d*) δ 175.74$_{trans}$, 175.37$_{cis}$, 165.02$_{trans}$, 164.50$_{cis}$, 155.89$_{trans}$, 154.96$_{cis}$, 116.56, 115.96, 111.89, 31.95, 31.00, 29.06, 28.92, 27.46, 24.71, 22.46; SEC ($CHCl_3$ + 0.5% NEt_3): M_n = 24,556, M_w = 100,668, $Đ_M$ = 4.10.

d) Polyketone F-C$_{10}$T

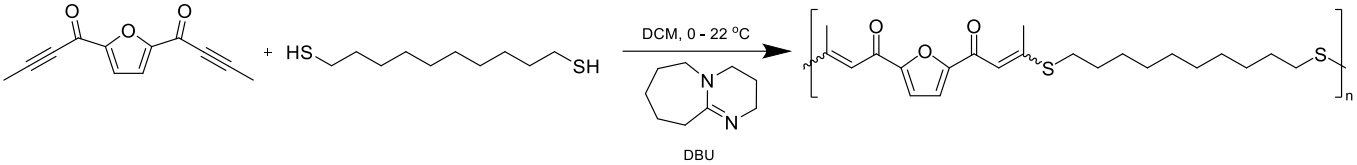

Scheme S4. Synthetic pathway of F-C$_6$T from furan based diynone and 1,10-decanedithiol

The polymer was obtained as a dark brown. **^{1}H NMR** spectra (400 MHz, Chloroform-*d*) δ 7.15 (d, *J* = 4.6 Hz, 2H, *trans*/*cis* overlapped), 6.95 (s, 0.5H, *cis*), 6.63 (s, 1.5H, *trans*), 2.91 (t, 4H), 2.54 (s, 4H, *trans*), 2.38 (s, 2H, *cis*), 1.78 – 1.48 (m, 6H), 1.48 – 1.24 (m, 12H), *cis*/*trans*: 26/74; **^{13}C NMR** (101 MHz, Chloroform-*d*) δ 177.38$_{trans}$, 175.79$_{cis}$, 164.57$_{trans}$, 163.36$_{cis}$, 155.40$_{trans}$, 154.98$_{cis}$, 116.55, 115.94, 111.87, 32.00, 31.05, 29.38, 29.21, 29.01, 27.48, 24.71, 22.46; SEC ($CHCl_3$ + 0.5% NEt_3): M_n = 44,014, M_w = 138,074, $Đ_M$ = 3.14. (1.05 g, 96% yield).

Model Compounds Synthesis

a) Model F-C₆T

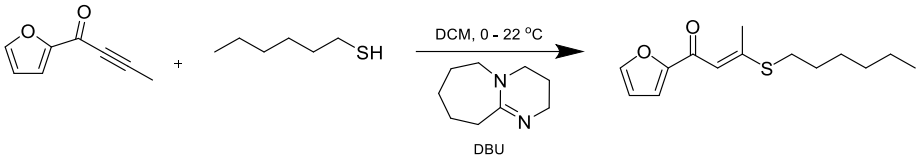

Scheme S5. Synthetic pathway of model F-C_6T from furan based ynone and hexanethiol.

In a 20 ml scintillation vial, furan ynone (0.3 g, 2.24 x 10^{-3} mol, 1.0 equiv.) was dissolved in DCM (2 mL) after 1-hexanethiol (0.264 g, 2.24 x 10^{-3} mol, 1.0 equiv.) was fully washed with DCM (3 mL) during transferring to the ynone solution. In an ice bath, the reaction mixture was cooled down to 0 °C. After that, 1,8-Diazabicyclo[5.4.0] undec-7-ene (DBU) (3.40 µl, 22.37 µmol, 0.01 equiv.) was added and kept at room temperature for two hours to yield viscous solution. Finally, it was dried *in vacuo* at room temperature for 24 h to yield dark brown oil (0.48 g, 85%). *1-(furan-2-yl)-3-(hexylthio)but-2-en-1-one* **^{1}H NMR** spectra (400 MHz, Chloroform-*d*) δ 7.52 (s, 0.5H, *trans*), 7.50 (s, 0.5H, *cis*) 7.12 (d, *J* = 2.8 Hz, 1H, *trans/cis* overlapped), 6.58 (s, 1H), 6.49 (d, *J* = 6.5 Hz, 1H, overlapped), 2.87 (t, 2H), 2.51 (s, 2H), 2.35 (s, 1H), 1.75 – 1.63 (m, 2H), 1.45 (qt, *J* = 10.2, 5.8 Hz, 2H), 1.31 (pd, *J* = 7.7, 3.0 Hz, 4H), 0.90 (s, 3H); **^{13}C NMR** (101 MHz, Chloroform-*d*) δ 177.12$_{cis}$, 176.02$_{trans}$, 162.45$_{trans}$, 162.19$_{cis}$, 154.58$_{trans}$, 154.10$_{cis}$, 145.24$_{trans}$, 145.07$_{cis}$, 116.15$_{cis}$, 115.52$_{trans}$, 112.25, 112.21, 31.85, 31.41, 31.32, 30.89, 29.09, 28.72, 28.69, 27.52, 24.53, 22.50, 22.16, 14.00. **HRMS** (ESI-TOF) (*m*/*z*): $[M + H]^+$ calculated for $C_{14}H_{20}O_2S$, 252.1180; found, 252.1179.

b) Model Ph-C₆T

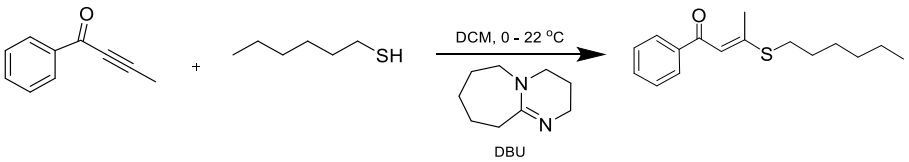

Scheme S6. Synthetic pathway of model Ph-C_6T from phenyl-based ynone and hexanethiol.

In a 20 ml scintillation vial, phenyl ynone (0.3 g, 2.08 x 10^{-3} mol, 1.0 equiv.) was dissolved in DCM (5 mL) after 1-hexanethiol (0.246 g, 2.08 x 10^{-3} mol, 1.0 equiv.) was added. In a bath of ice, the reaction mixture was cooled down to 0 °C. After that, 1,8-Diazabicyclo[5.4.0] undec-7-ene (DBU) (3.17 µl, 20.81 µmol, 0.01 equiv.) was added and

kept at room temperature for two hours to yield viscous solution. Finally, it was dried *in vacuo* at room temperature for 24 h to yield dark brown oil (0.45 g, 82%). *(E)-3-(hexylthio)-1-phenylbut-2-en-1-one* **^{1}H NMR** (400 MHz, Chloroform-*d*) δ 7.95 – 7.88 (m, 2H), 7.54 – 7.41 (m, 3H), 7.00 (s, 0.5H, *cis*), 6.63 (s, 0.5H, *trans*), 2.88 (s, 2H, *trans*), 2.51 (s, 1H, *cis*), 1.77 – 1.64 (m, 2H), 1.54 – 1.45 (m, 3H), 1.35 – 1.29 (m, 4H), 0.92 – 0.88 (m, 3H); **^{13}C NMR** (101 MHz, Chloroform-*d*) δ 188.21$_{cis}$, 187.77$_{trans}$, 162.38$_{cis}$, 161.81$_{trans}$, 140.01$_{trans}$, 138.86$_{cis}$, 133.93$_{cis}$, 131.97$_{trans}$, 129.59$_{cis}$, 128.47$_{trans}$, 127.93, 127.86, 116.61$_{cis}$, 113.32$_{trans}$, 31.86, 31.44, 31.36, 30.86, 29.03, 28.77, 27.60, 24.67, 22.51, 22.17, 14.04. **HRMS** (ESI-TOF) (*m*/*z*): $[M + H]^+$ calculated for $C_{16}H_{22}OS$, 262.1386; found, 262.1390.

NMR spectra of precursor and monomer

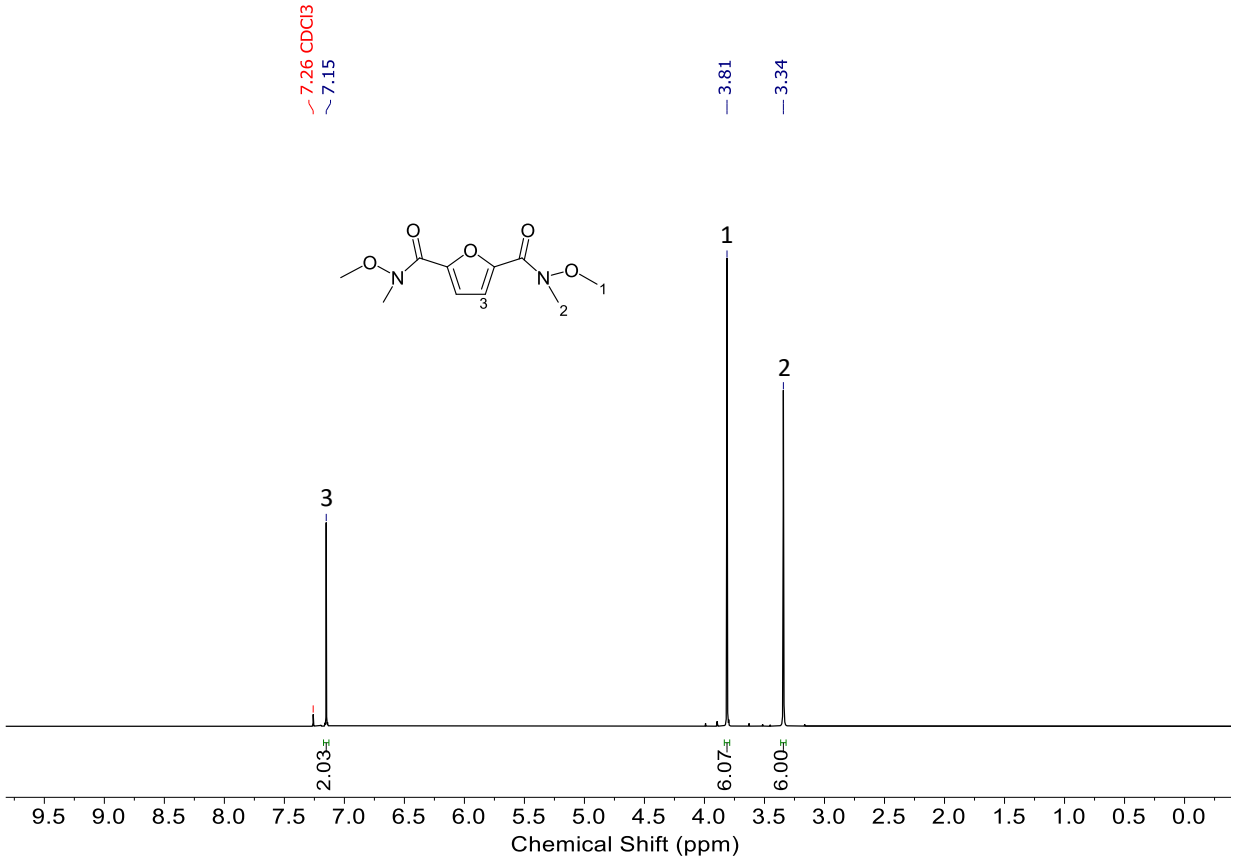

Figure S1. ^{1}H NMR spectrum (400 MHz, Chloroform-*d*) of furyl Weinreb amide

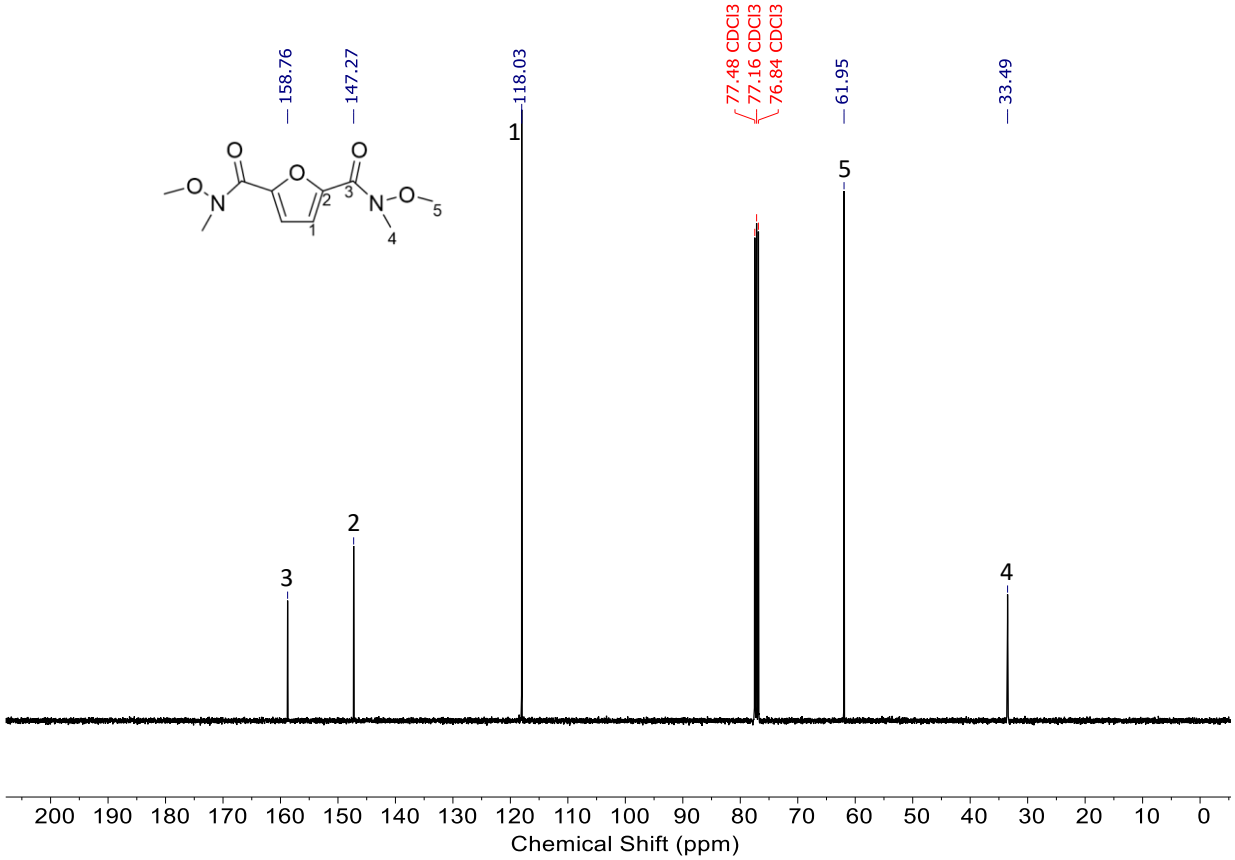

Figure S2. ^{13}C NMR spectrum (101 MHz, Chloroform-*d*) of furyl Weinreb amide

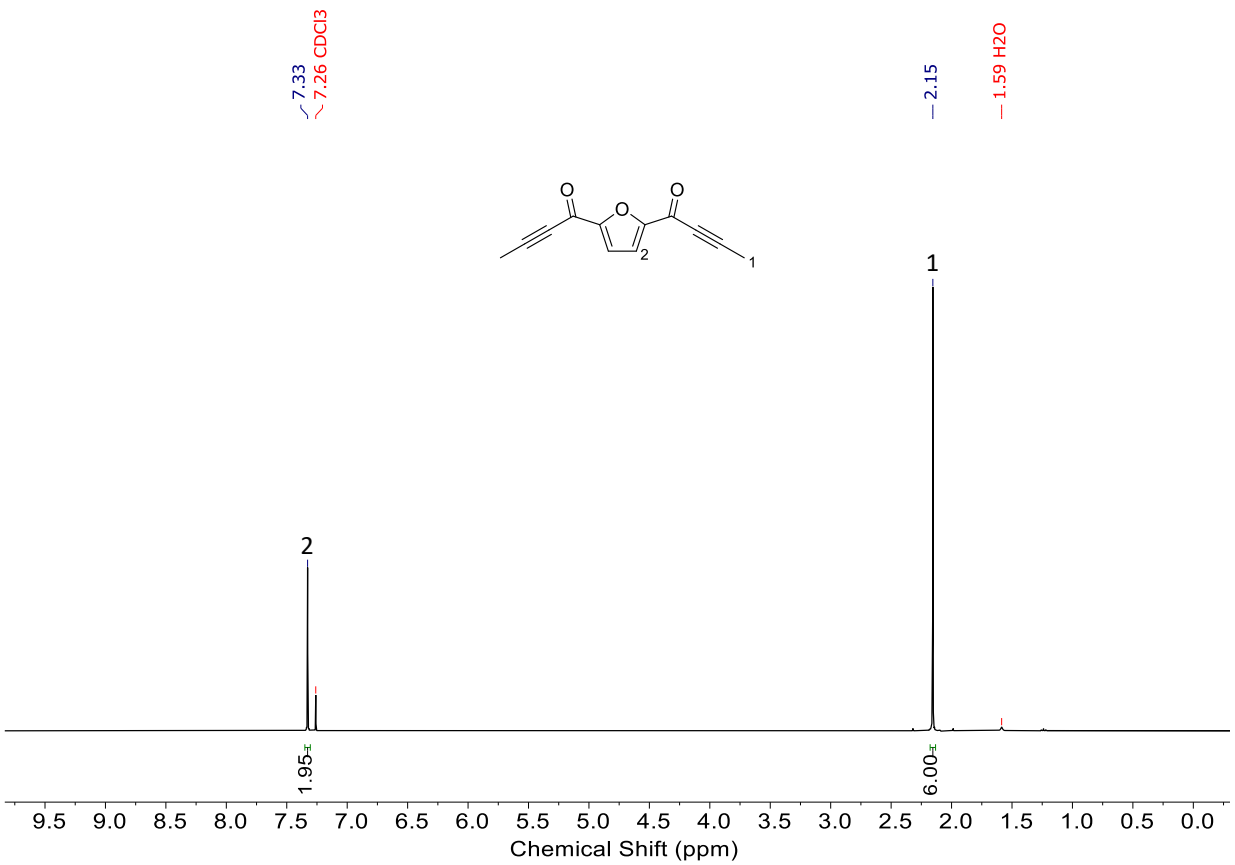

Figure S3. ^{1}H NMR spectrum (400 MHz, Chloroform-*d*) of diynone monomer

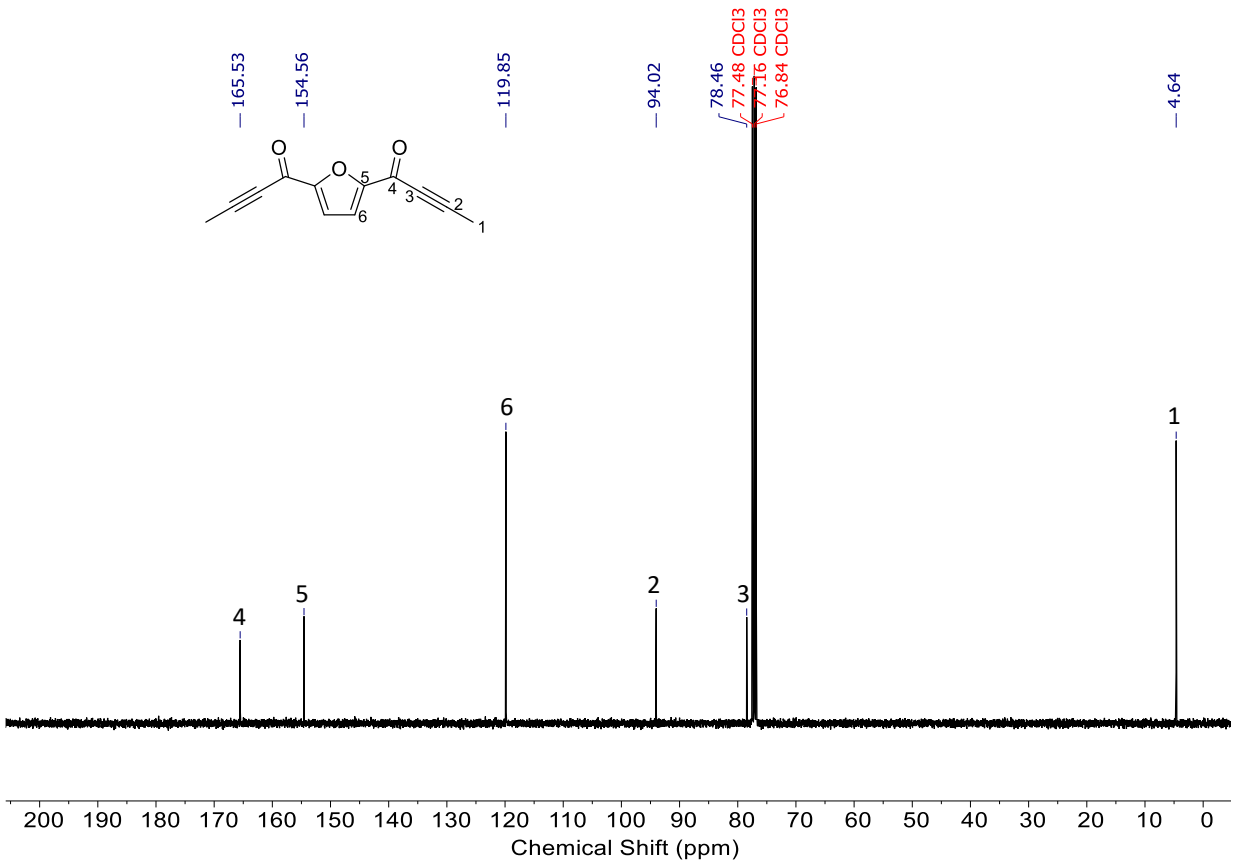

Figure S4. ^{13}C NMR spectrum (101 MHz, Chloroform-*d*) of diynone monomer

Infrared spectra of the precursor and monomer

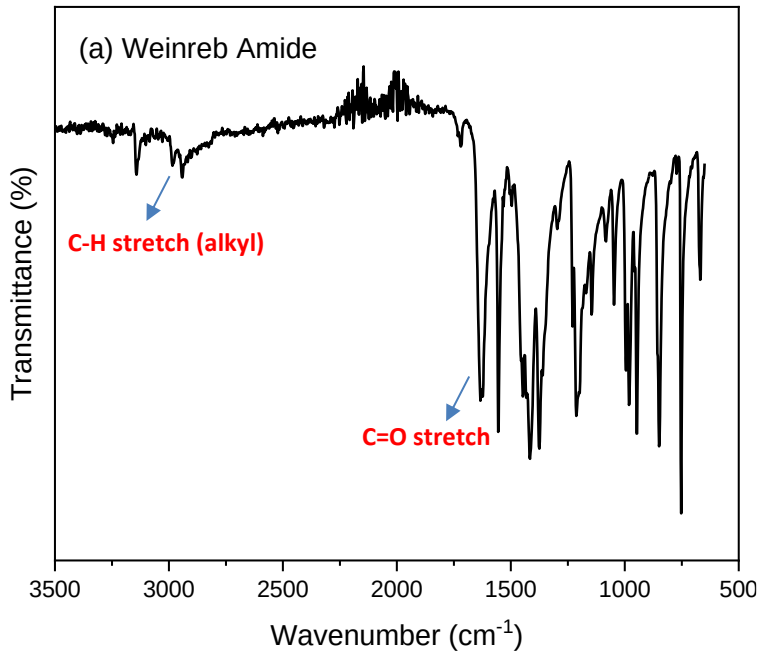

Figure S5. FTIR spectra of furyl Weinreb amide

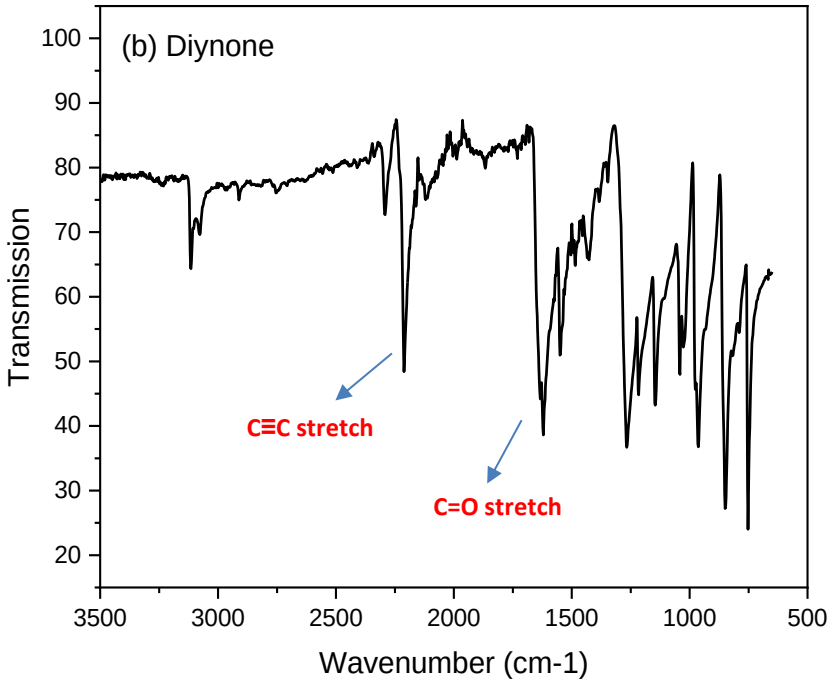

Figure S6. FTIR spectra of diynone monomer

Infrared spectra of polymers

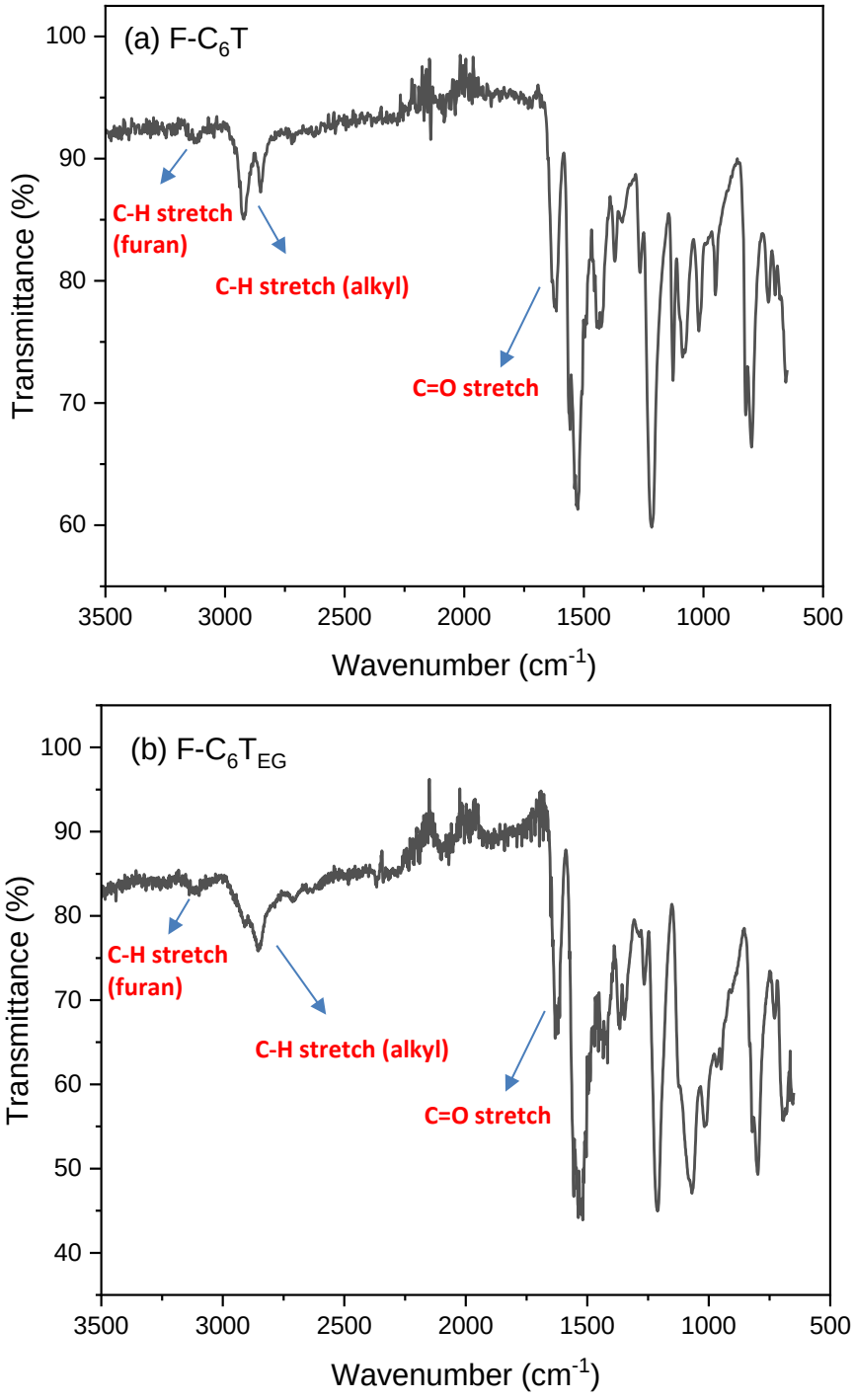

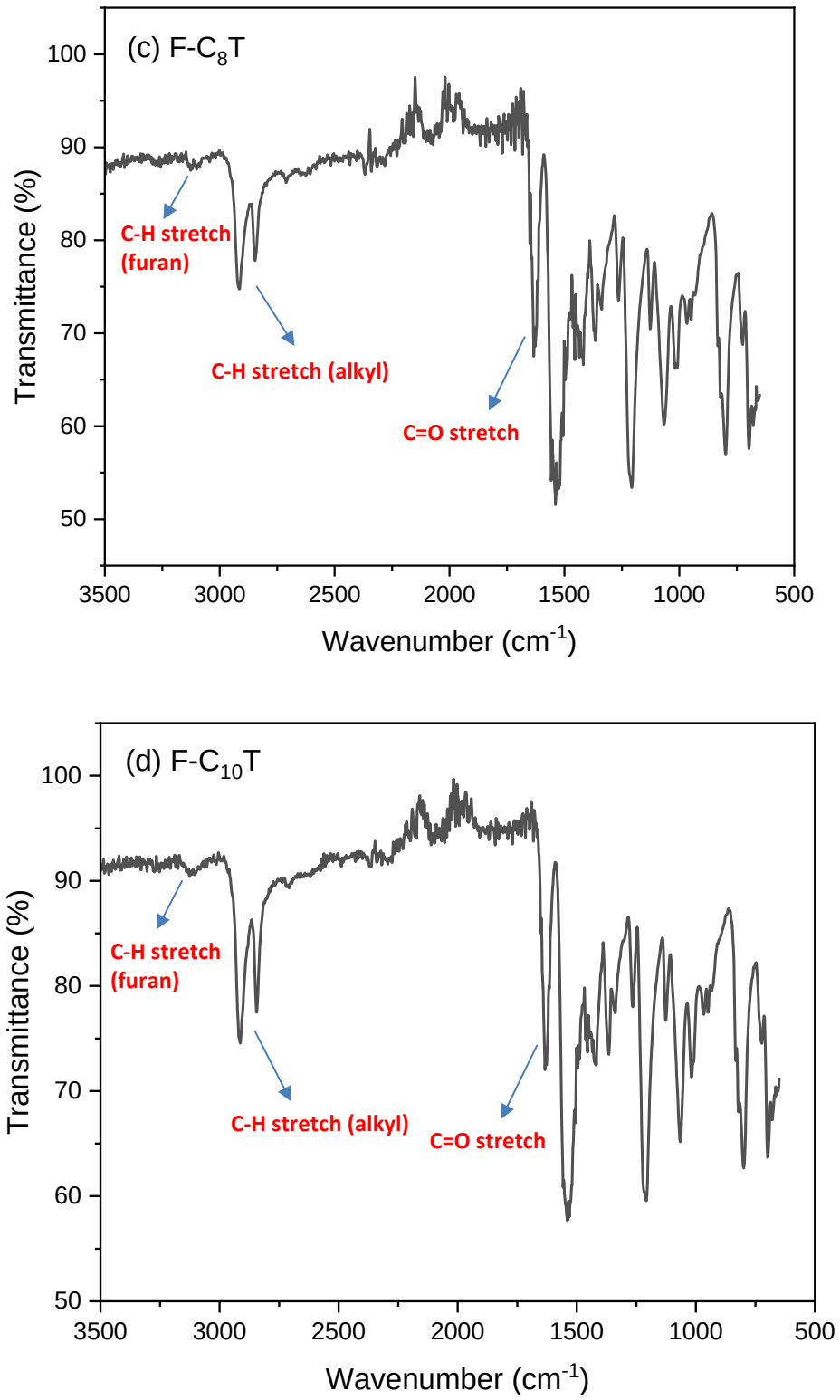

Figure S7. FTIR spectra of (a) F-C_6T, (b) F-C_6T_{EG}, (c) F-C_8T, (d) F-C_{10}T

Size exclusion chromatograms of polymers

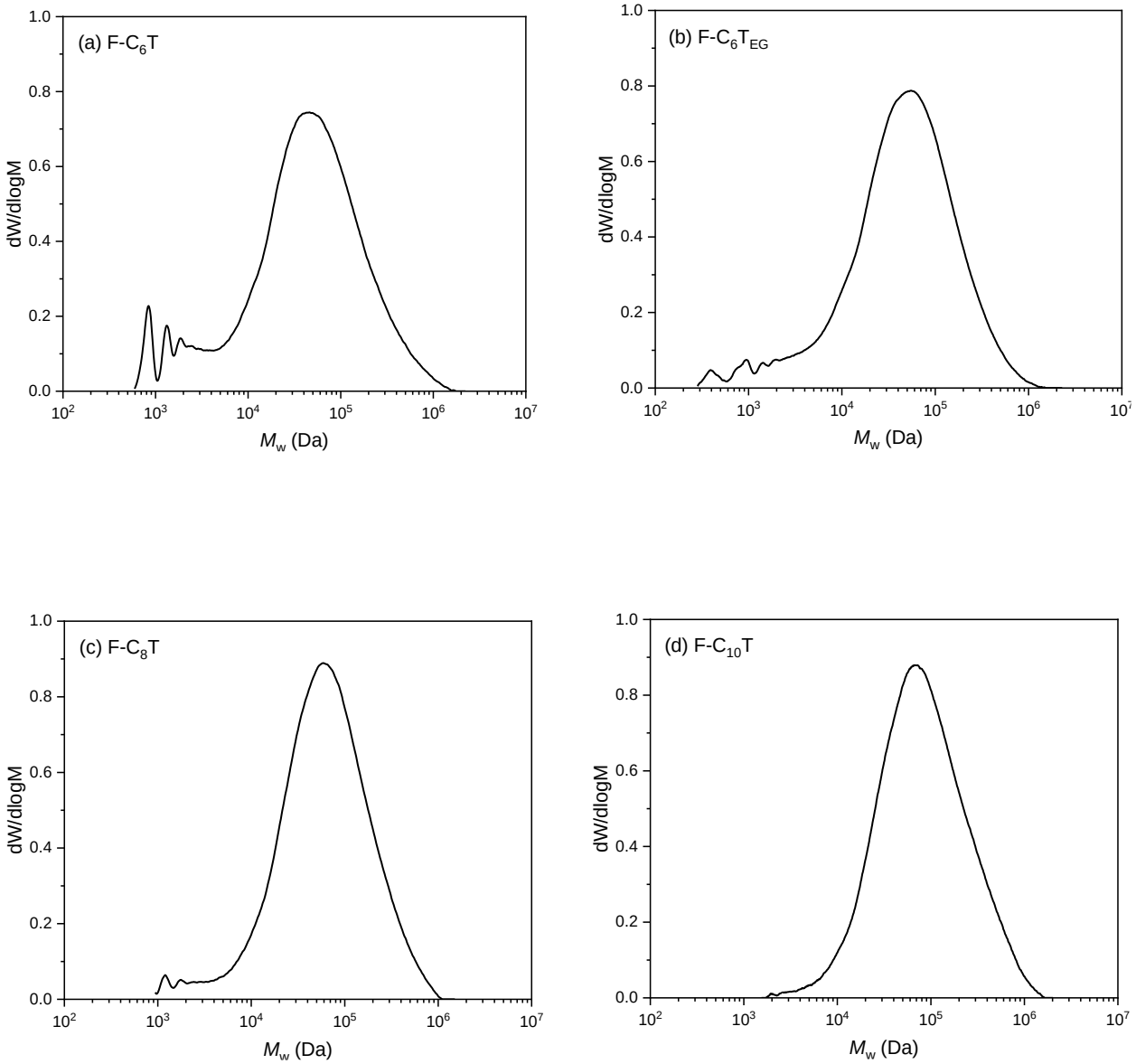

Figure S8. Size exclusion chromatograms of (a) F-C_6T, (b) F-C_6T_{EG}, (c) F-C_8T, (d) F-C_{10}T ($CHCl_3$, 0.5% NEt_3, 40 °C) analysis against poly(styrene) (PS) standards.

NMR spectra of polymers

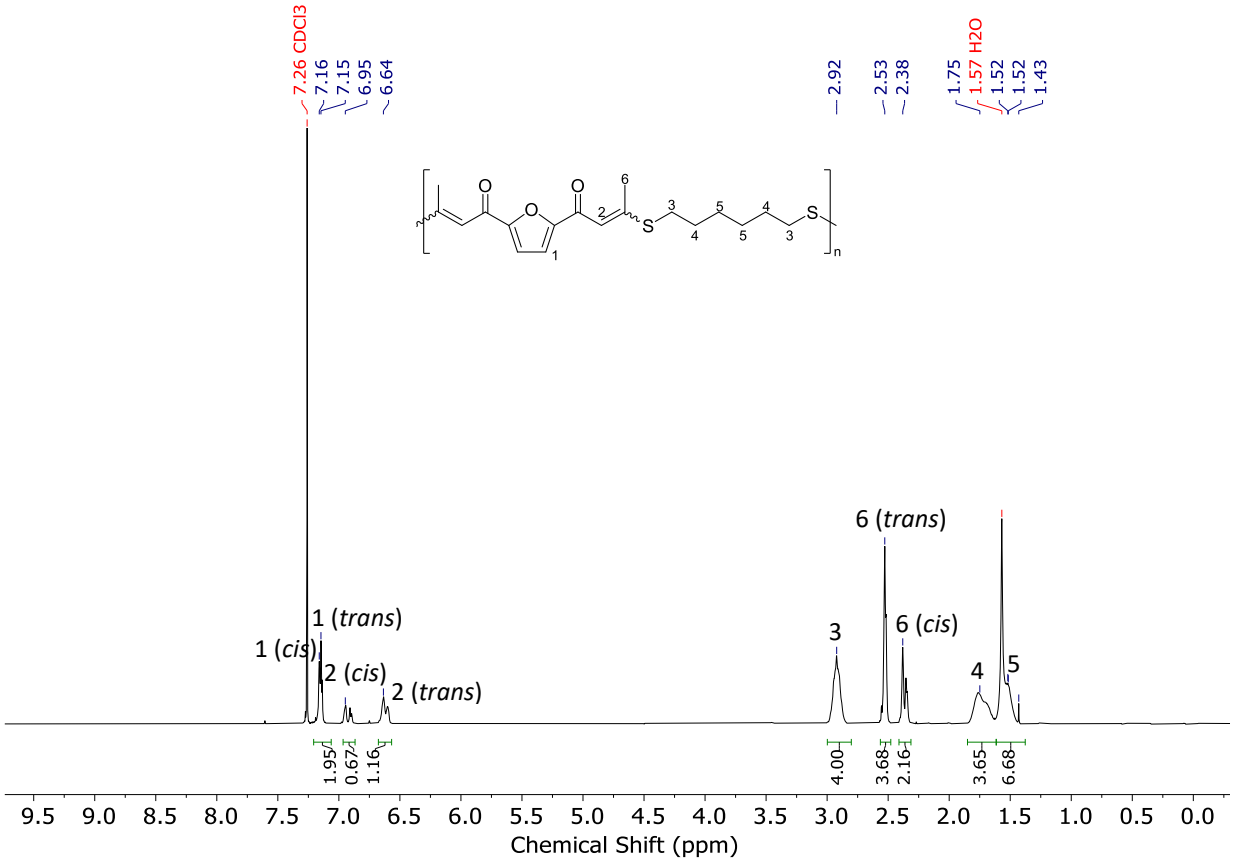

Figure S9. ^{1}H NMR spectrum (400 MHz, Chloroform-*d*) of polyketone F-C$_6$T

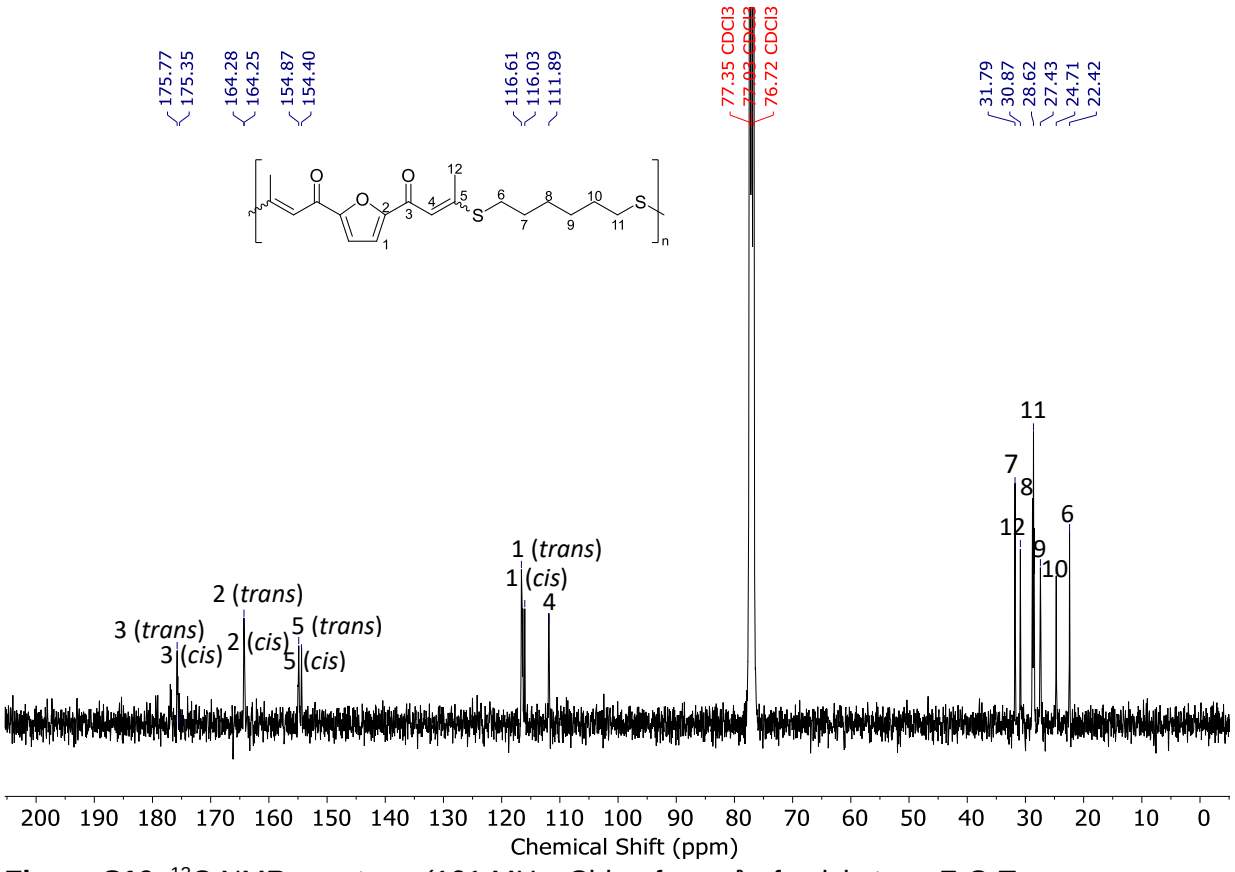

Figure S10. ^{13}C NMR spectrum (101 MHz, Chloroform-*d*) of polyketone F-C$_6$T

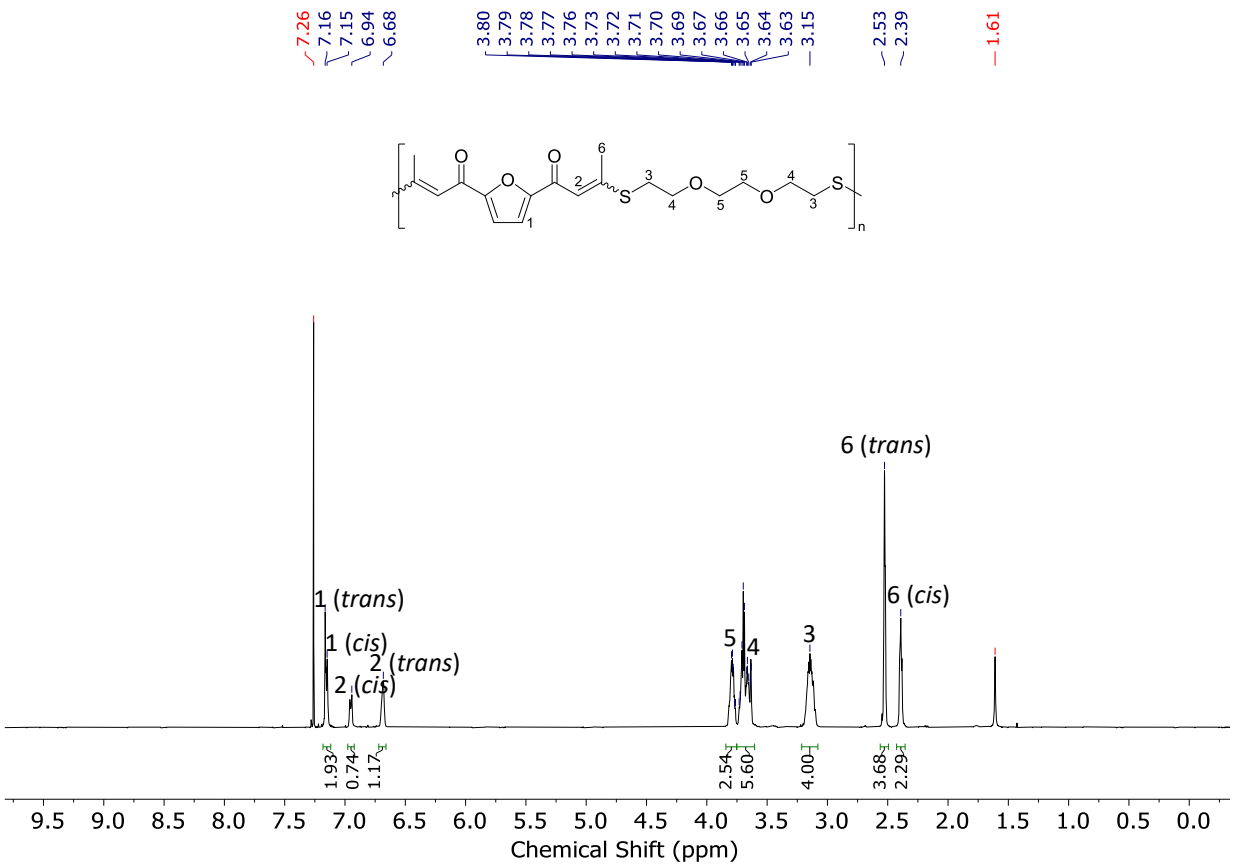

Figure S11. ^{1}H NMR spectrum (400 MHz, Chloroform-*d*) of polyketone F-C$_6$T$_{EG}$

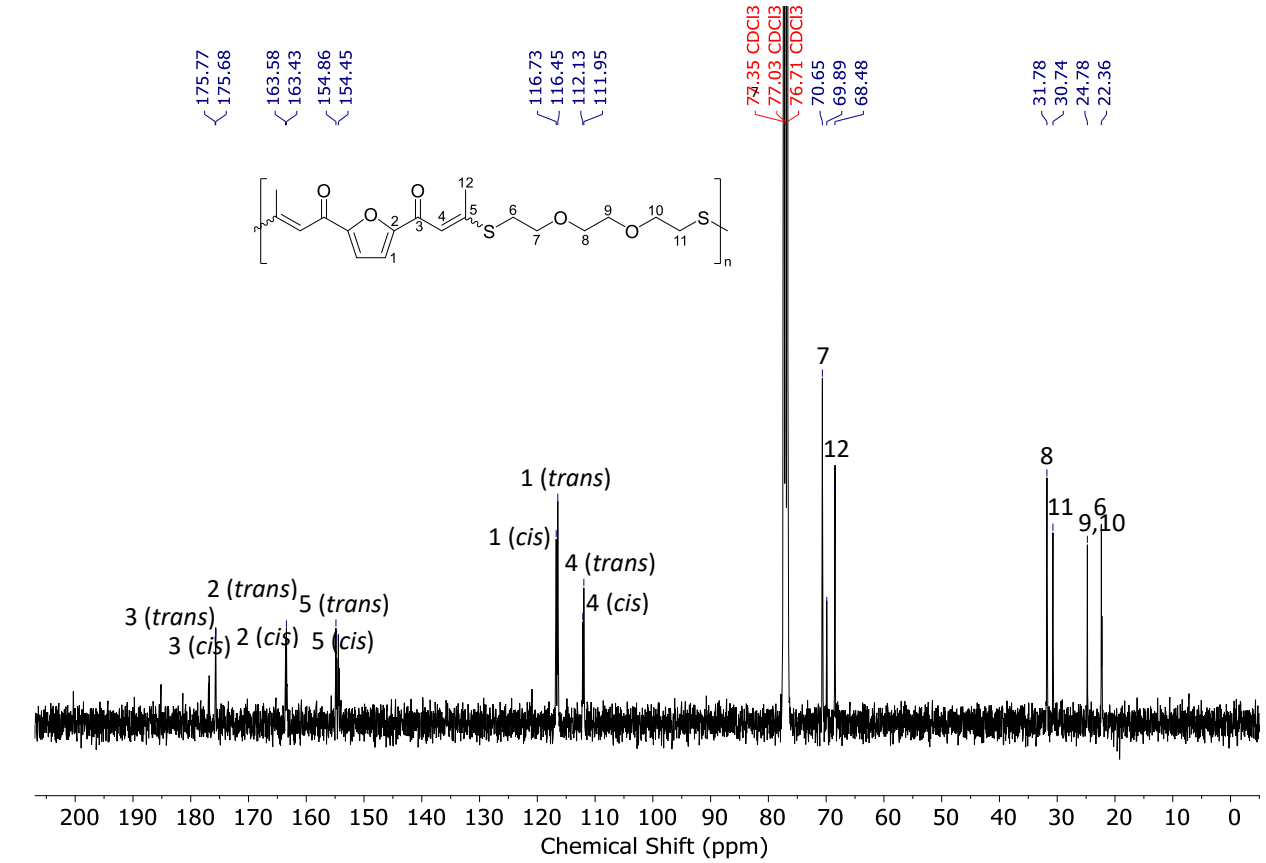

Figure S12. ^{13}C NMR spectrum (101 MHz, Chloroform-*d*) of polyketone F-C$_6$T$_{EG}$

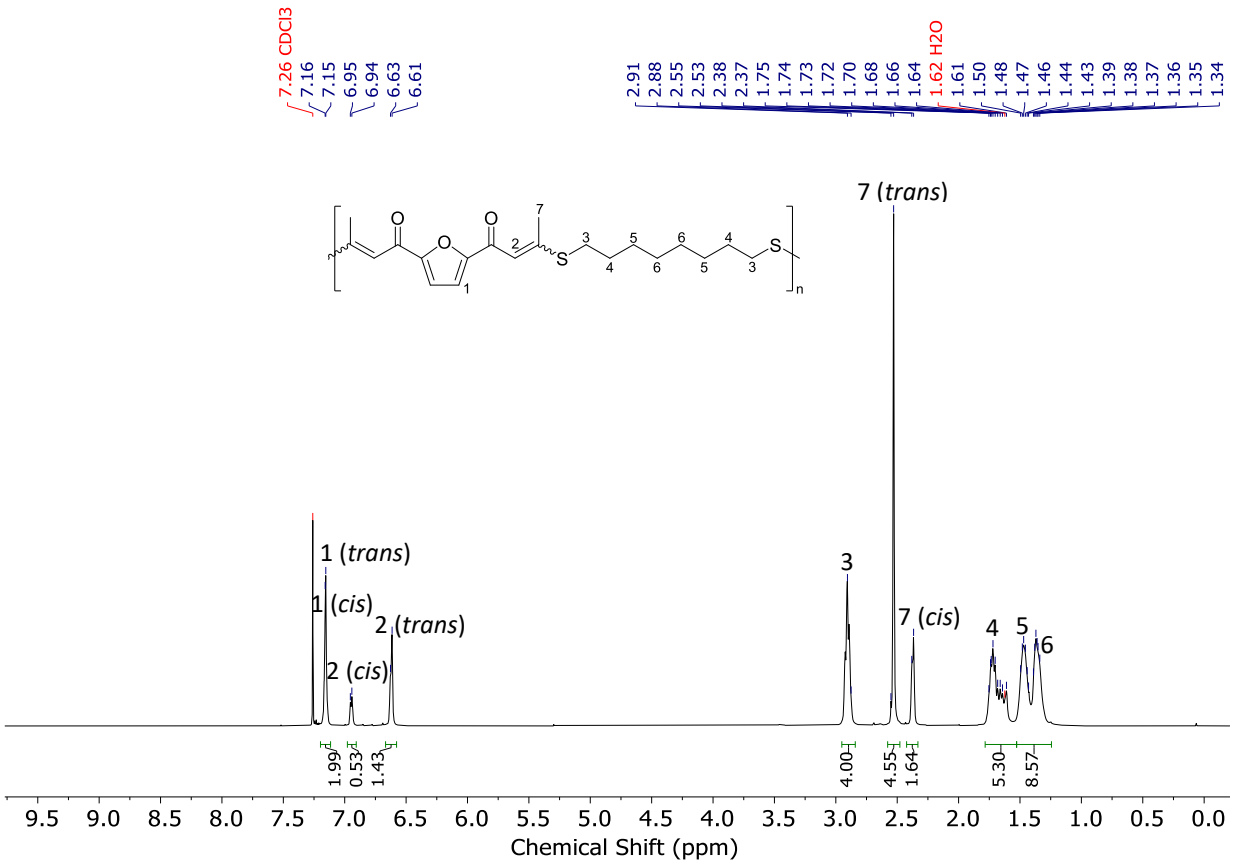

Figure S13. ^{1}H NMR spectrum (400 MHz, Chloroform-*d*) of polyketone F-C$_8$T

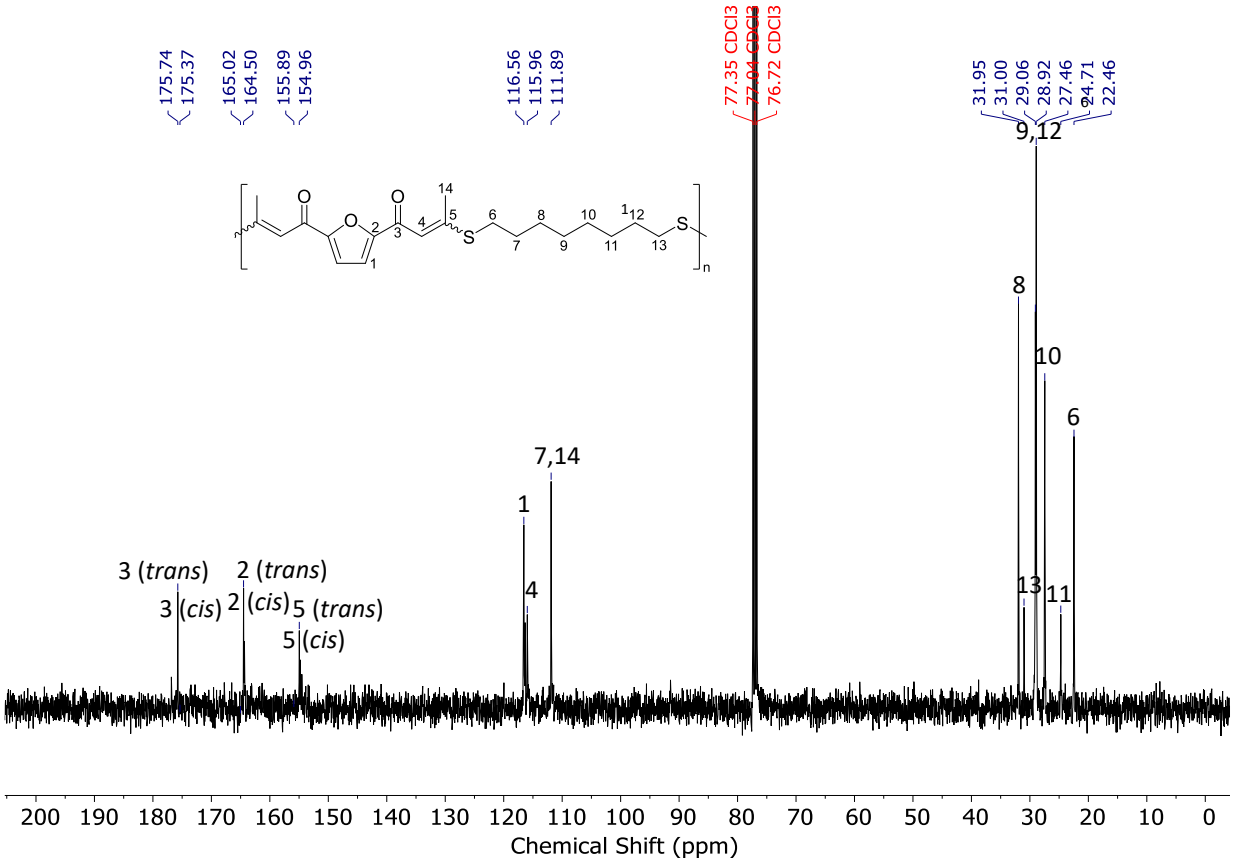

Figure S14. ^{13}C NMR spectrum (101 MHz, Chloroform-*d*) of polyketone F-C$_8$T

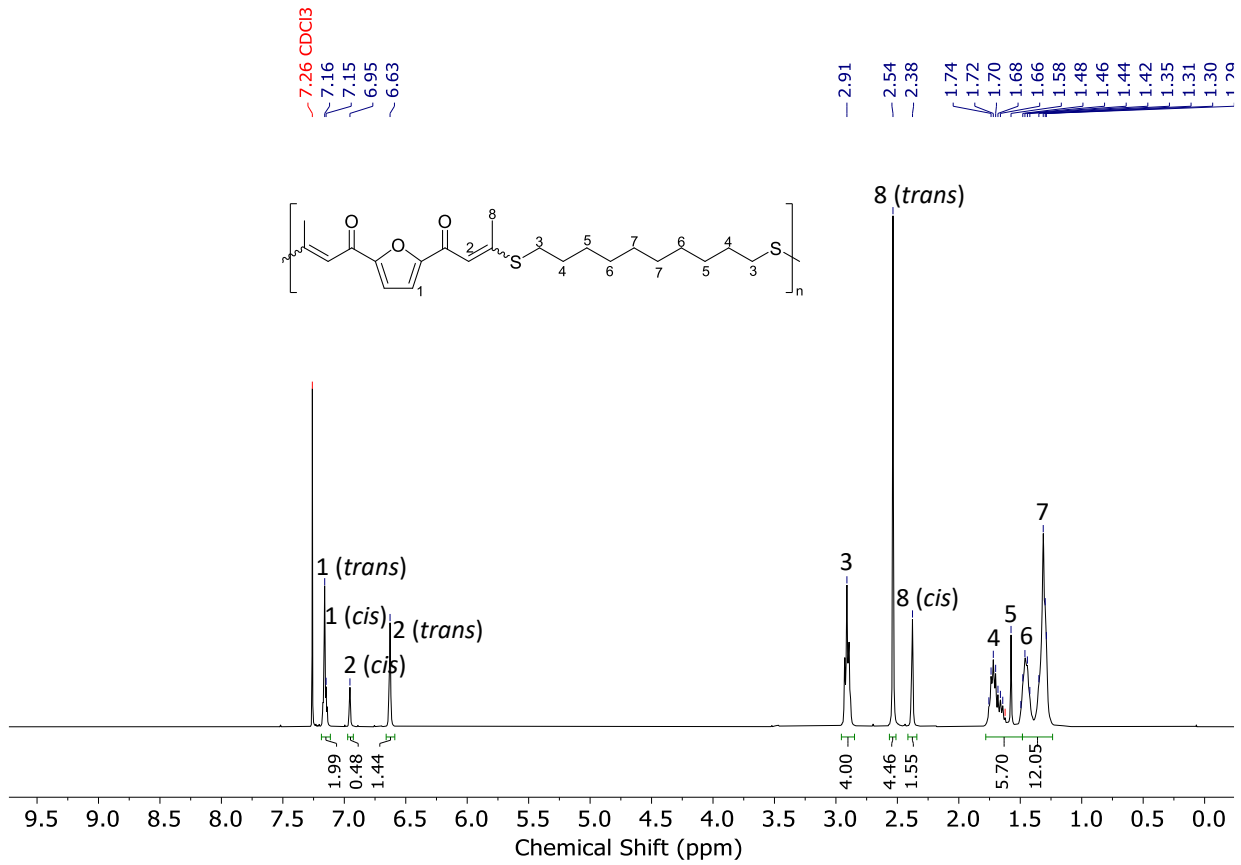

Figure S15. ^{1}H NMR spectrum (400 MHz, Chloroform-*d*) of polyketone F-C$_{10}$T

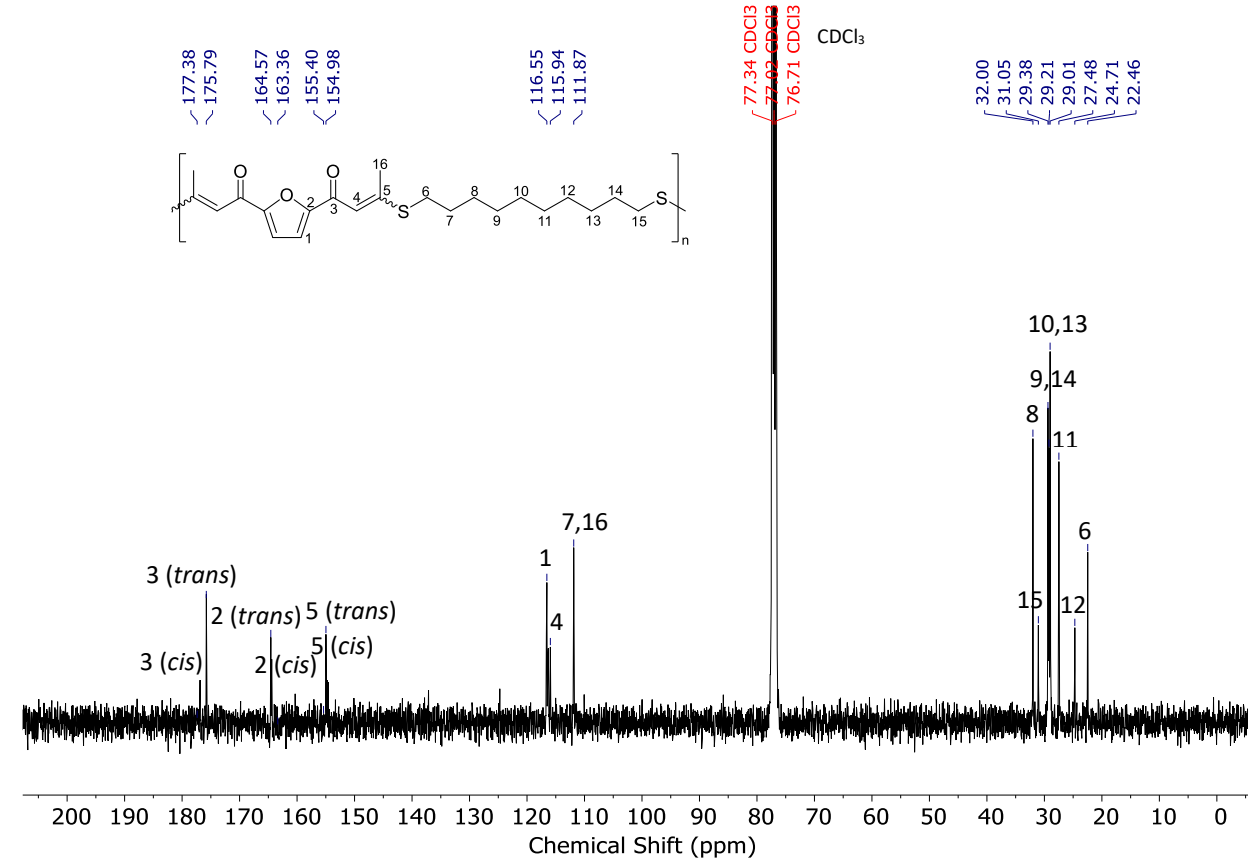

Figure S16. ^{13}C NMR spectrum (101 MHz, Chloroform-*d*) of polyketone F-C$_{10}$T

Film Preparation

To evaluate the thermomechanical properties of the polymers, the film was made by solvent cast method. The polymer sample (0.5 g) was first dissolved in dichloromethane (2.5 mL) until homogenous. The polymer solution was then filtered using a GPC filter to remove any particulates, transferred to a Teflon beaker and left the solvent evaporate for 24 hours. The resultant film was finally dried under a high vacuum at room temperature for 3 days to anneal.

Physical appearance of the polyketone films

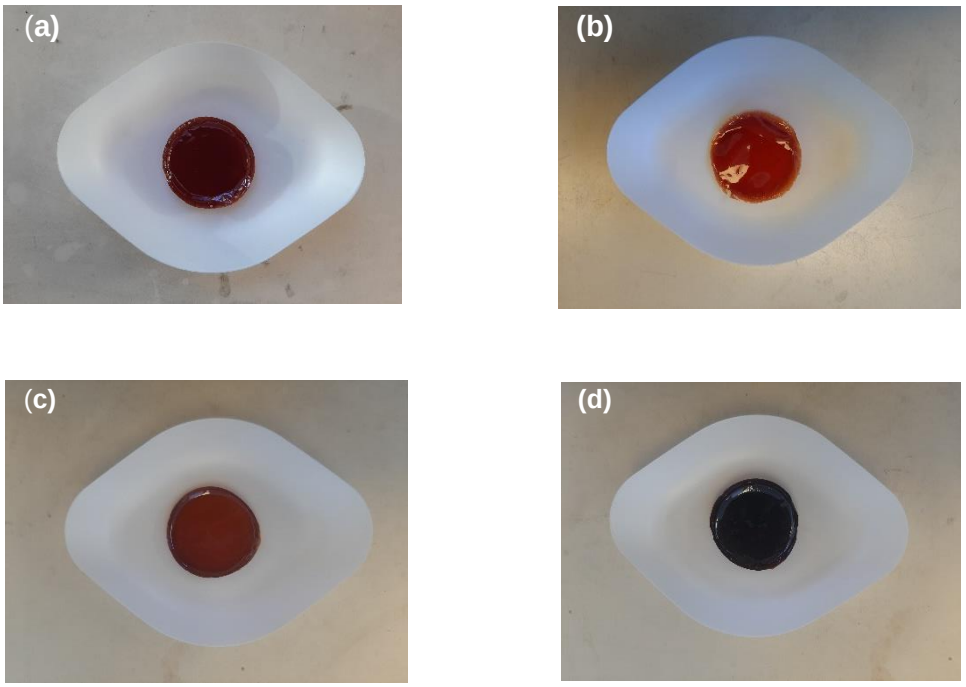

Figure S17. Physical appearance of polymer films (a) F-C_6T, (b) F-C_6T_{EG}, (c) F-C_8T, (d) F-C_{10}T

DSC thermograms of polymers

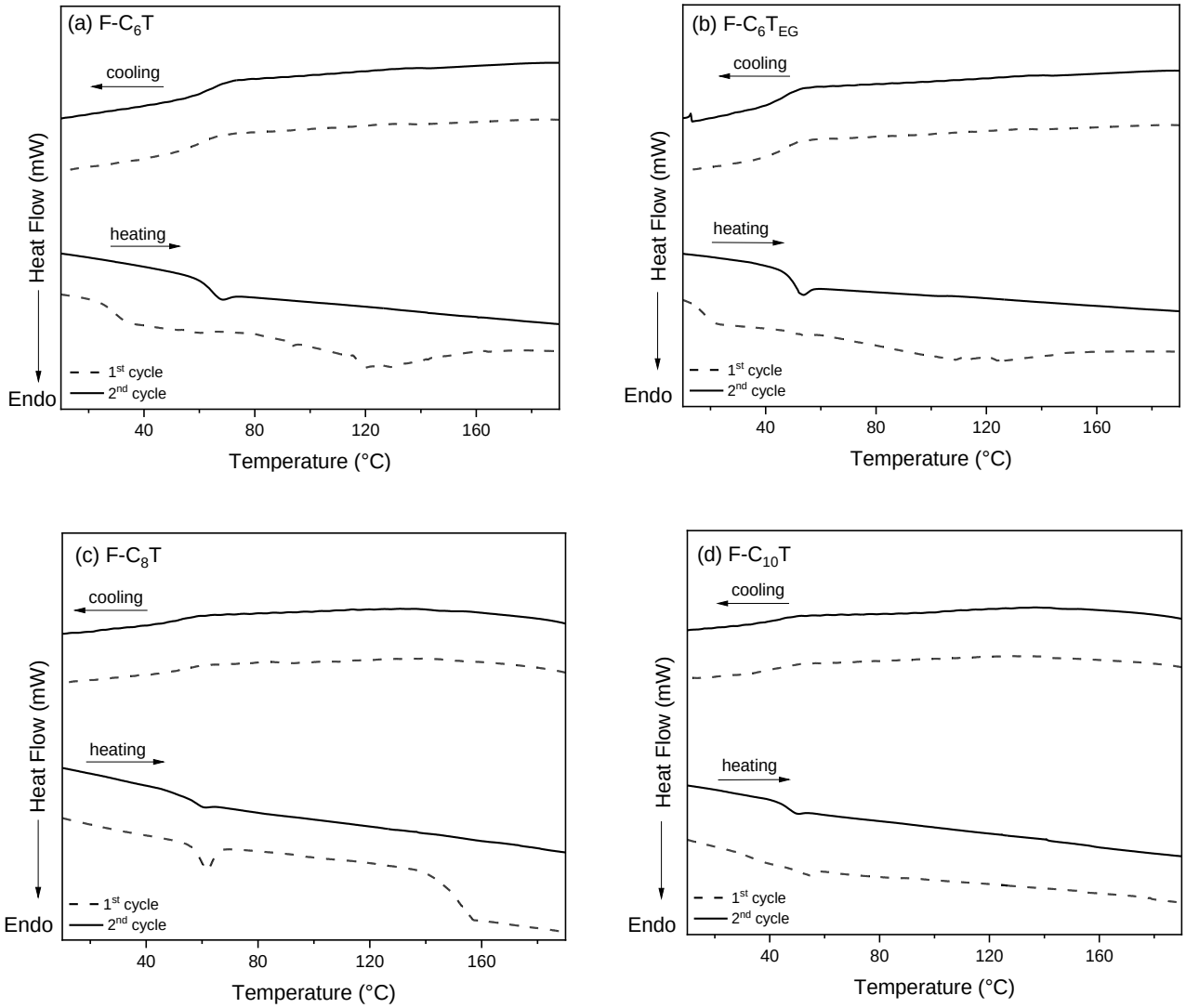

Figure S18. DSC thermograms showing heating and cooling cycles of polyketones (a) F-C_6T, (b) F-C_6T_{EG}, (c) F-C_8T, (d) F-C_{10}T

TGA thermograms of polymers

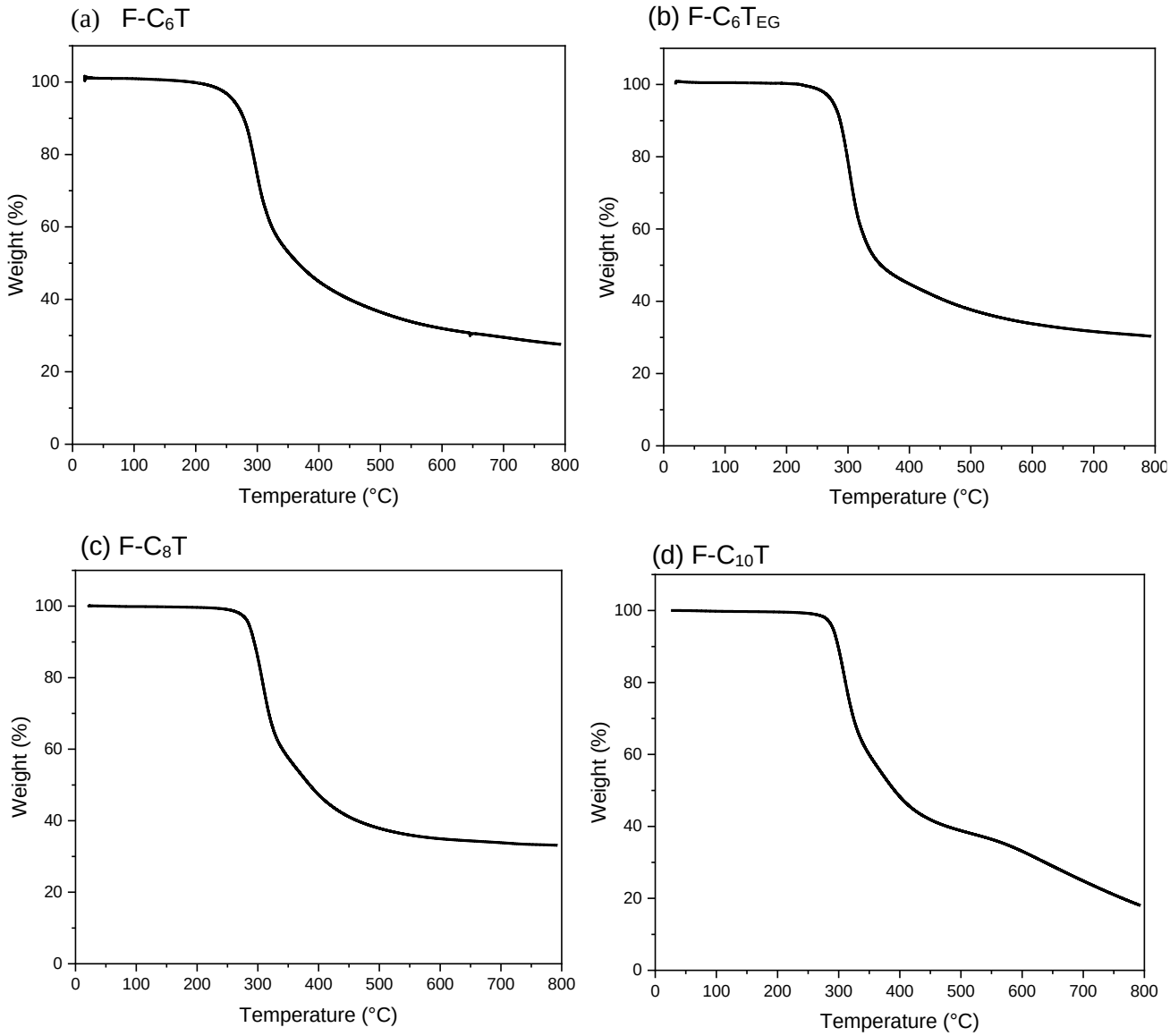

Figure S19. TGA thermograms of (a) F-C_6T, (b) F-C_6T_{EG}, (c) F-C_8T, (d) F-C_{10}T

DSC thermograms of commodity plastics

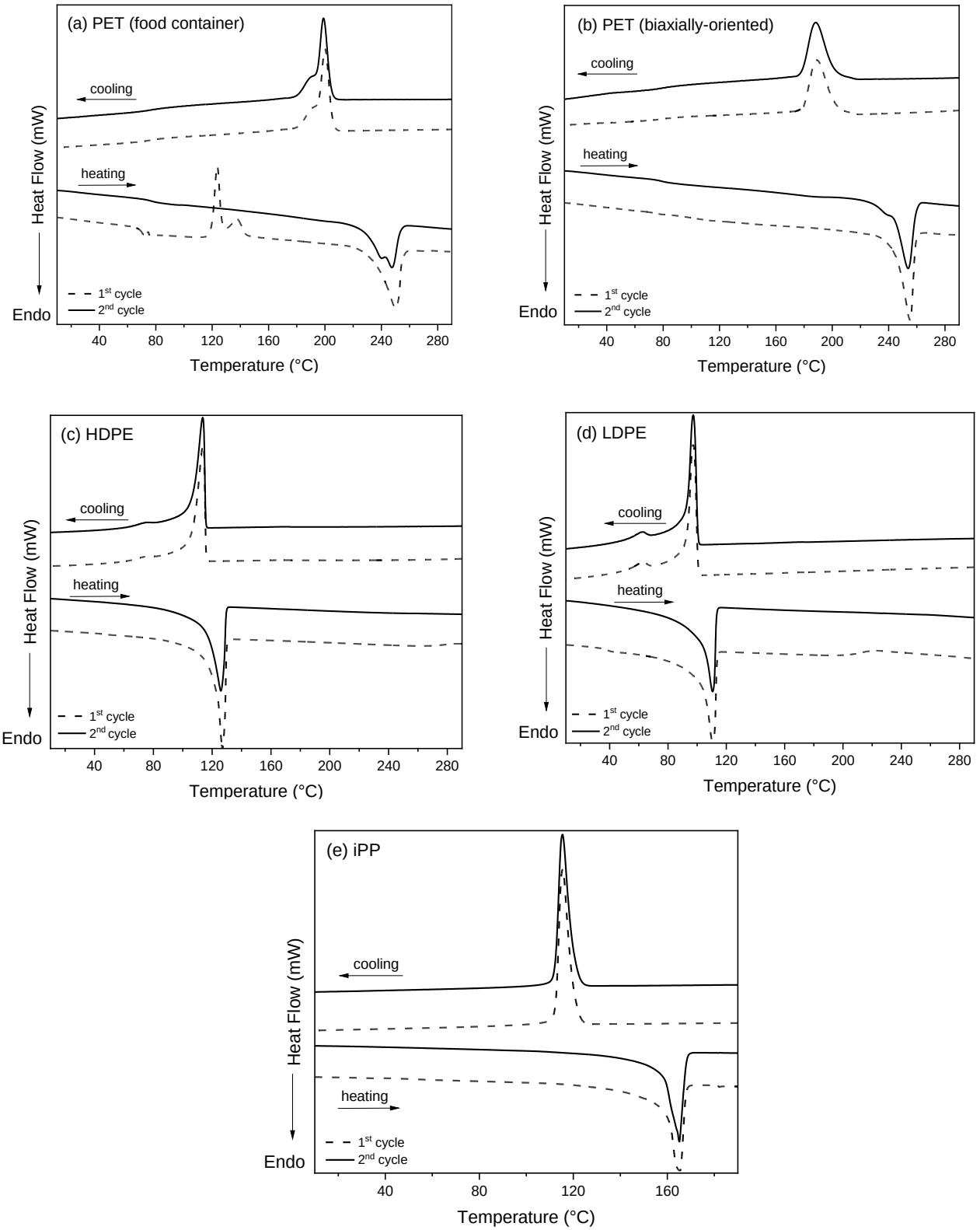

Figure S20. DSC thermograms showing heating and cooling cycles of (a) PET from food container, (b) Biaxially-Oriented PET, (c) HDPE, (d) LDPE, (e) iPP

Stress *vs* strain curves of polymers

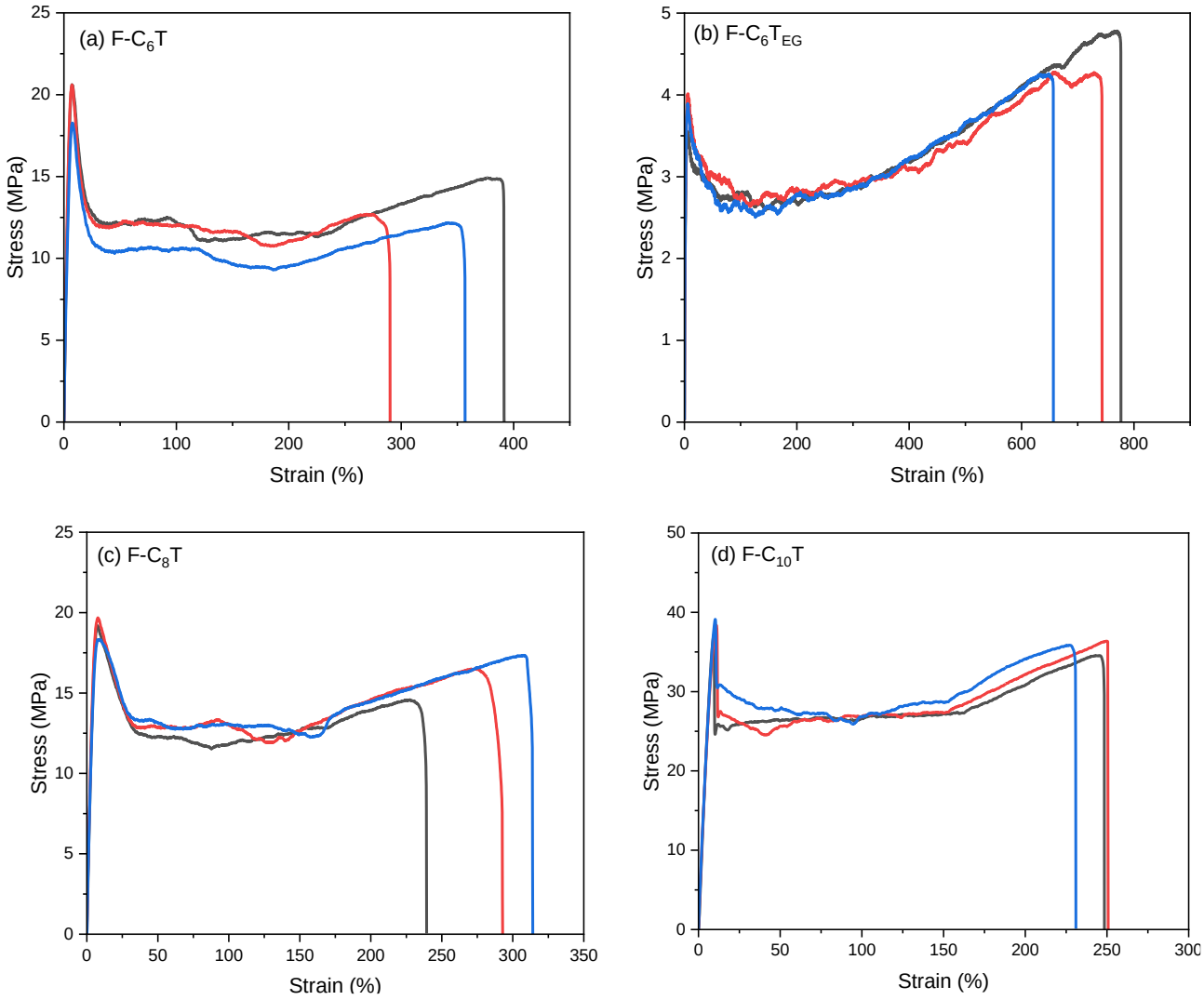

Figure S21. Stress *vs* strain curves for (a) F-C_6T, (b) F-C_6T_{EG}, (c) F-C_8T, (d) F-C_{10}T tested at 10 °C min^{-1}, 22 °C

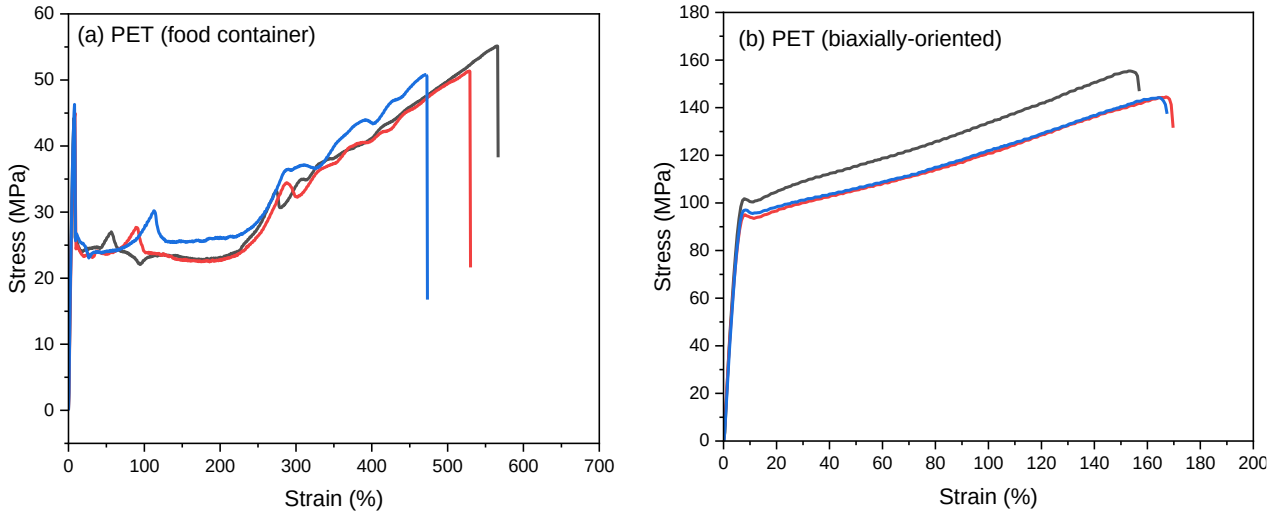

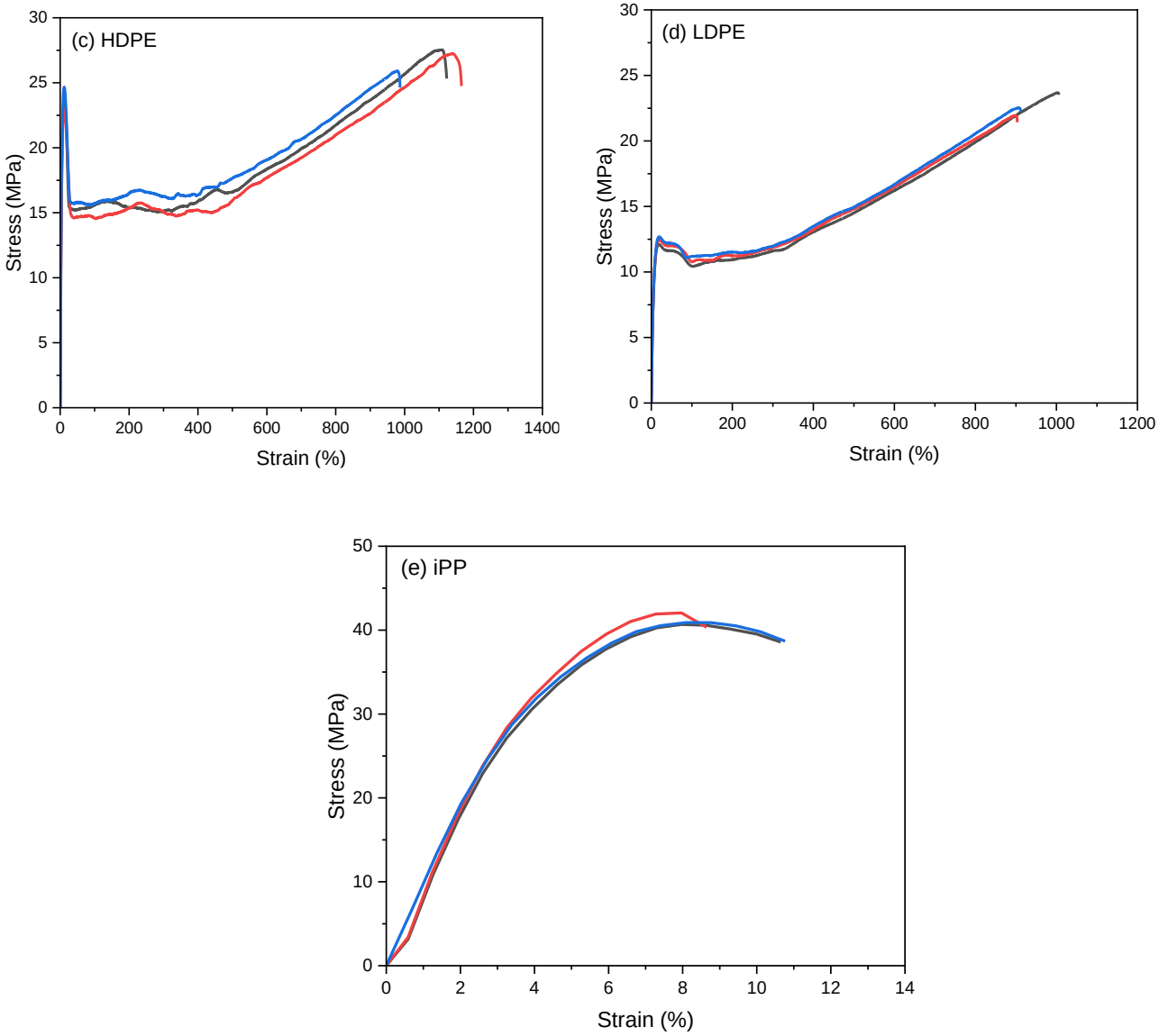

Figure S22. Stress *vs* strain curves for (a) PET (food container), (b) Biaxially-Oriented PET, (c) HDPE, (d) LDPE, (e) iPP tested at 10 °C min^{-1}, 22 °C

Table 1. Mechanical properties of polyketones tuned by controlling the chain flexibility

Polyketone (PK)	*Young's Modulus (MPa)*	*Strain @ Break (%)*	*Stress @ Break (MPa)*	*Strain @ Yield (%)*	*Stress @ Yield (MPa)*	*Toughness ($MJ.m^{-3}$)*
F-C_6T	466.1±39.8	357.0±57.1	13.3±1.4	7.2±0.2	19.8±1.3	40.9±7.6
F-C_6T_{EG}	191.0±8.6	749.0±44.1	4.6±0.3	6.1±0.5	4.0±0.6	25.1±1.2
F-C_8T	426.7±29.5	286.9±38.1	16.1±1.4	7.9±0.8	19.1±0.7	39.0±7.1
F-C_{10}T	516.7±10.7	256.8±20.5	35.6±0.9	10.1±0.7	38.2±0.9	69.7±1.9

*n =3

NMR spectra of irradiated polyketones in the film state

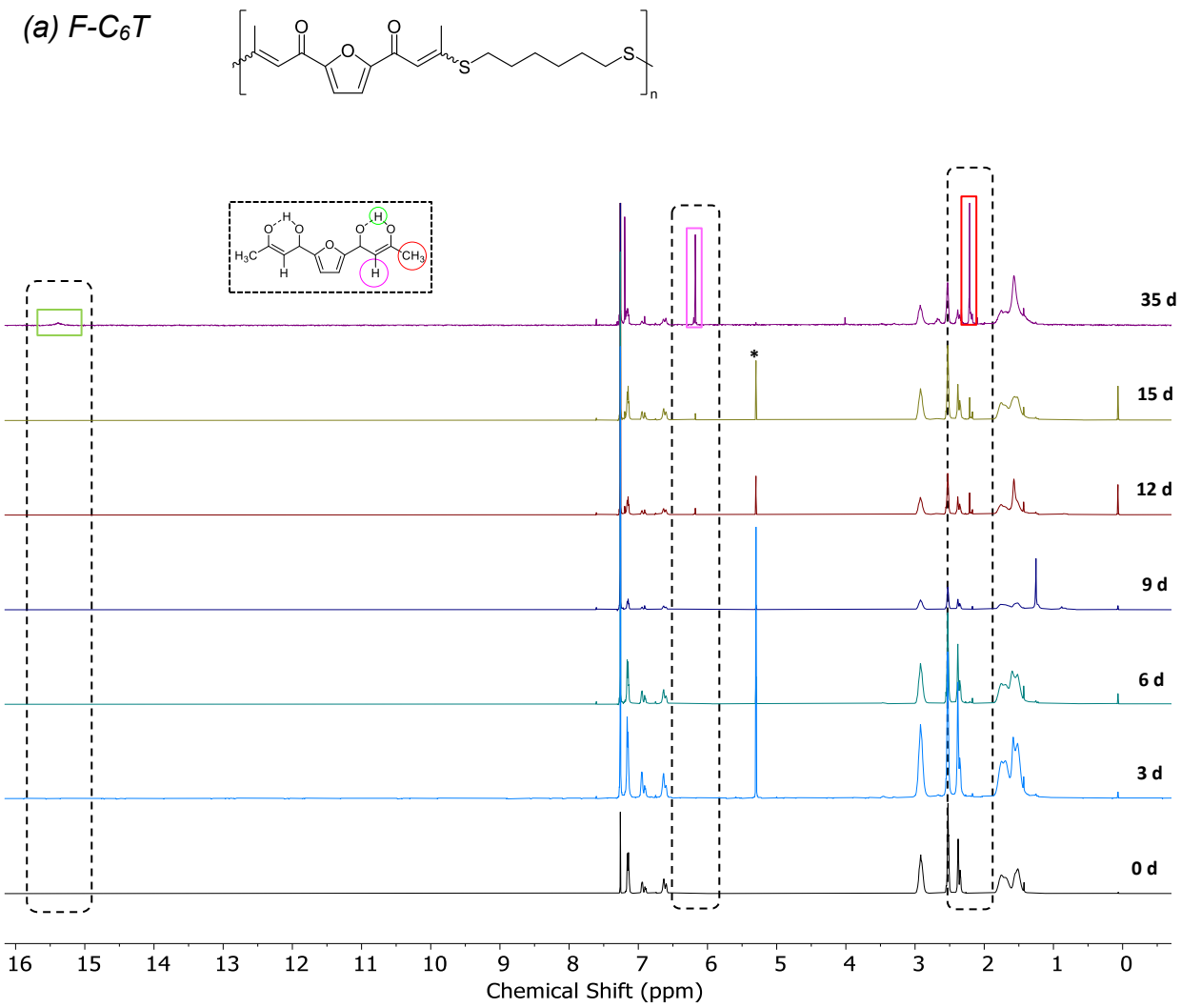

Figure S23. ^{1}H NMR spectra of polymer film F-C_6T stacked to illustrate the change of spectrum for 35 d. **residual DCM*

(b) F-C₆T_EG

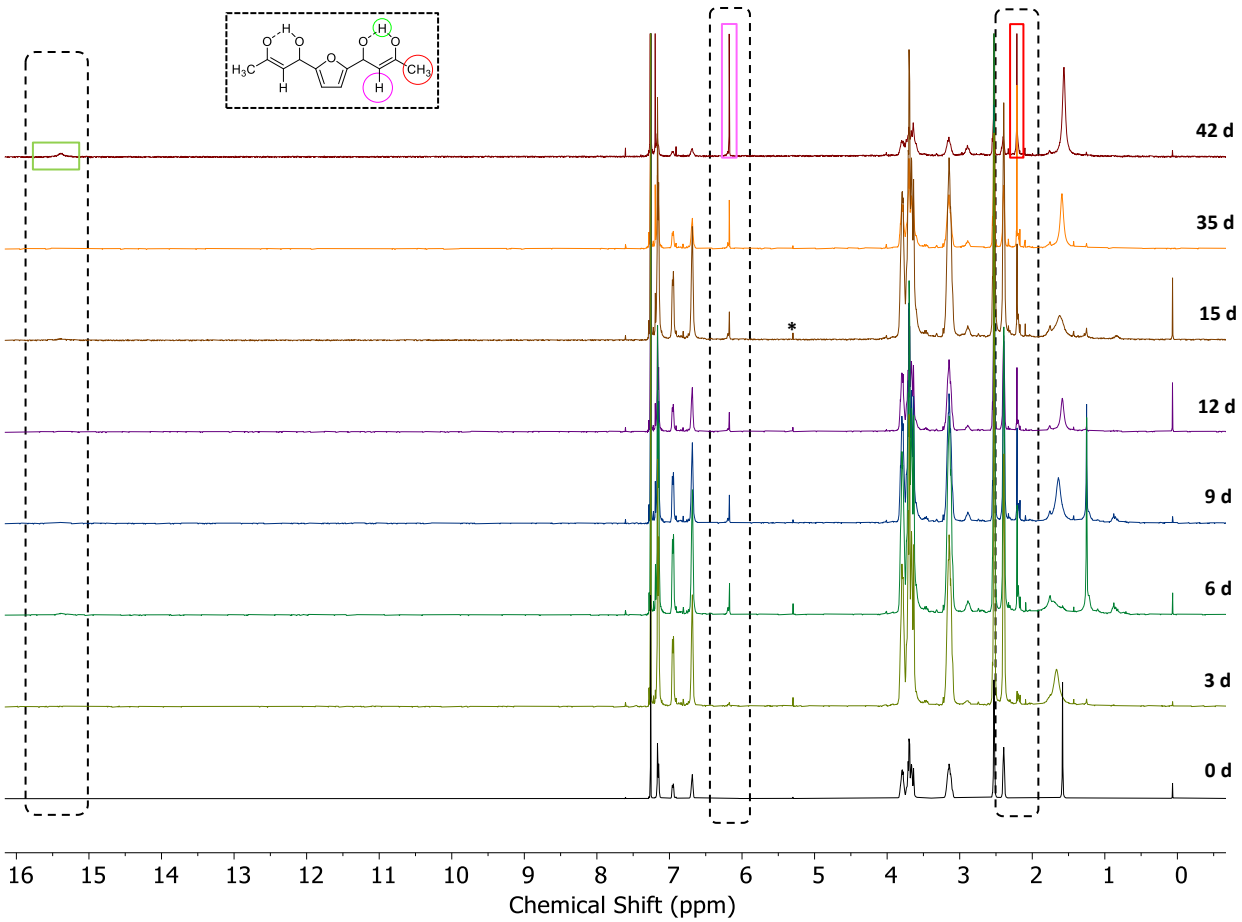

Figure S24. ^{1}H NMR spectra of polymer film F-C$_6$T$_{EG}$ stacked to illustrate the change of spectrum for 35 d.**residual DCM*

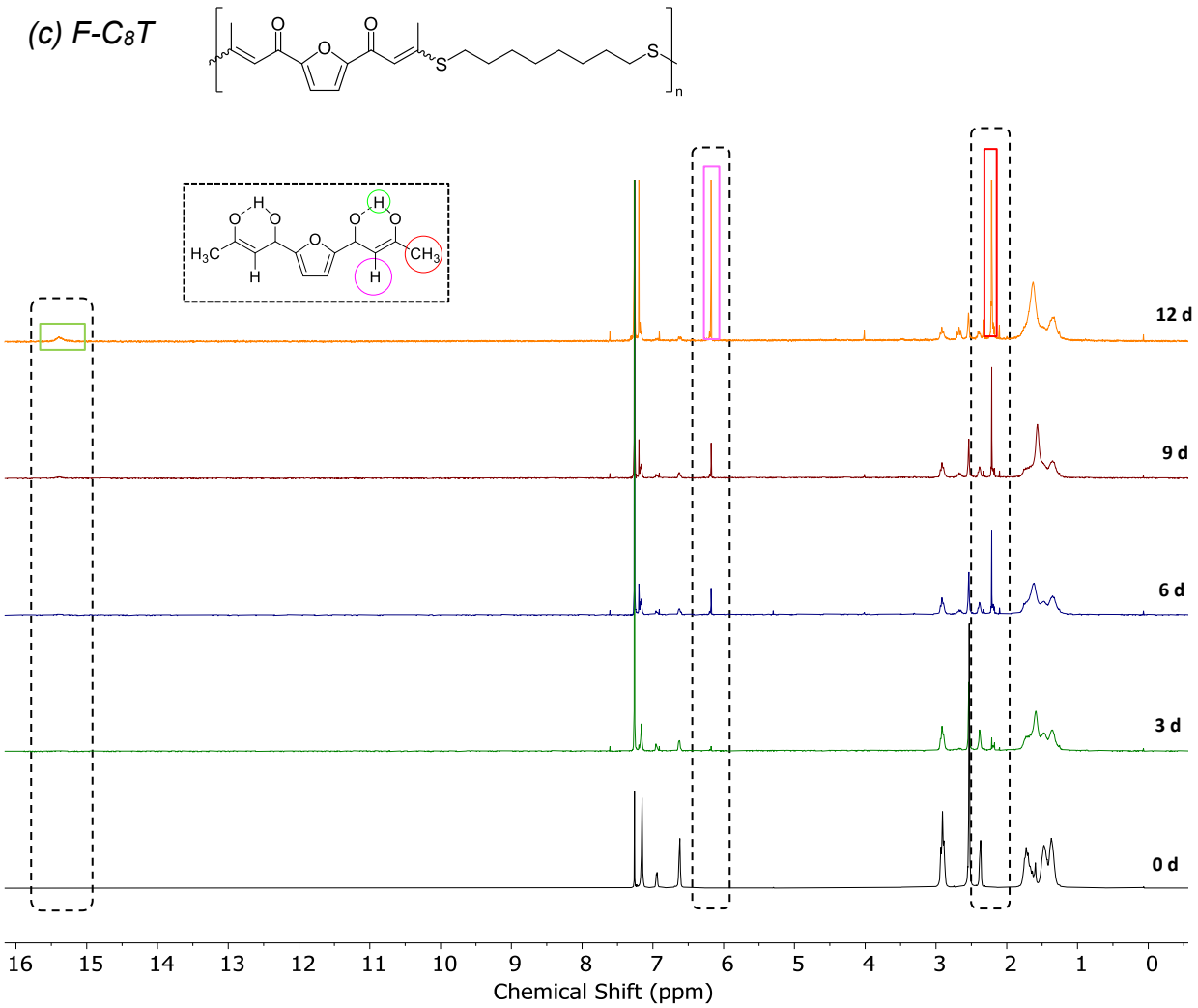

Figure S25. ^{1}H NMR spectra of polymer film F-C_8T stacked to illustrate the change of spectrum for 12 d

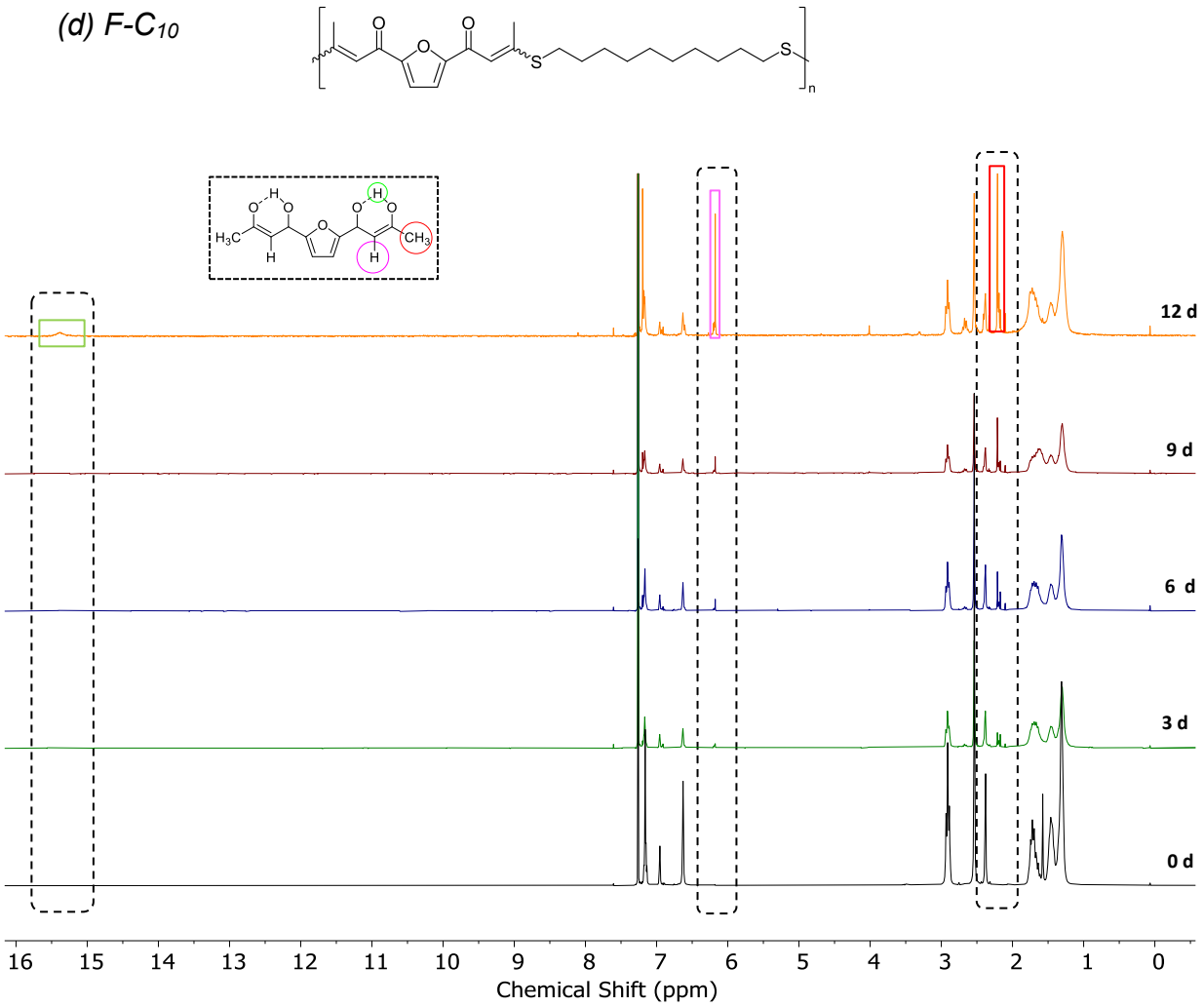

Figure S26. ^{1}H NMR spectra of polymer film F-C_{10}T stacked to illustrate the change of spectrum for 12 d

Size exclusion chromatograms of irradiated PK films

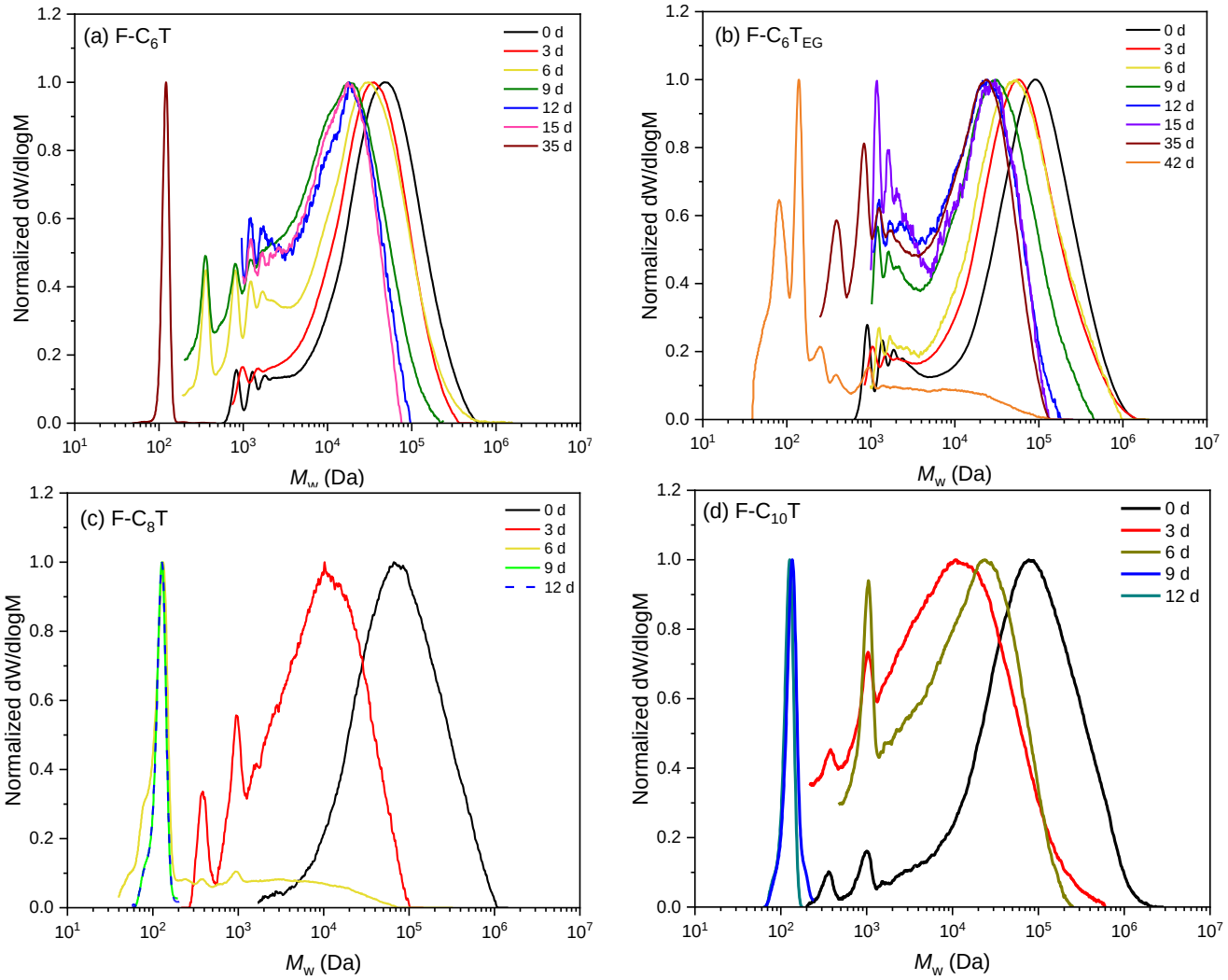

Figure S27. Size exclusion chromatograms of polymer PKs films of (a) F-C_6T, (b) F-C_6T_{EG}, (c) F-C_8T, (d) F-C_{10}T

Infrared spectra of the irradiated polymer films

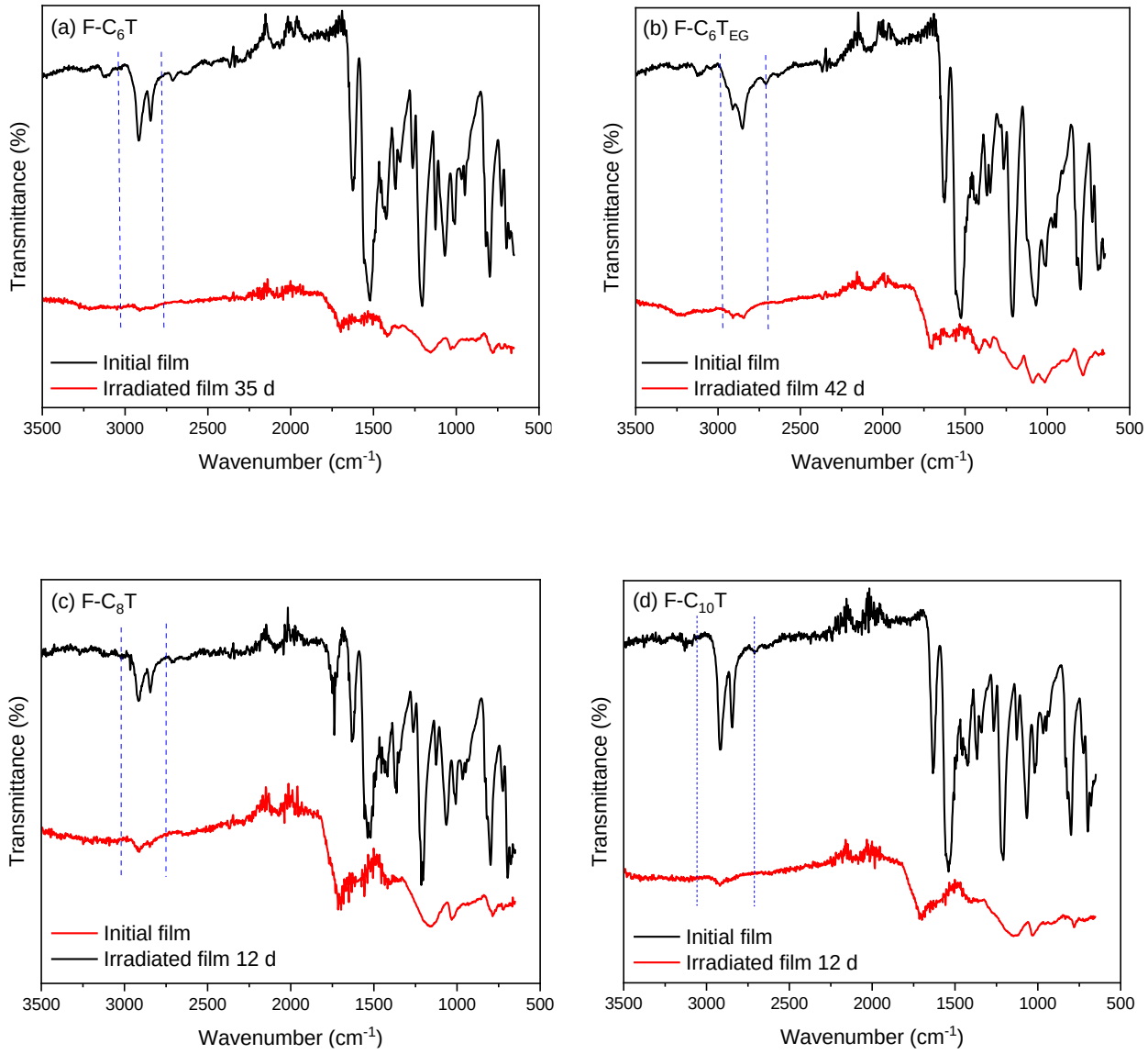

Figure S28. FTIR spectra of initial and irradiated (a) F-C_6T, (b) F-C_6T_{EG}, (c) F-C_8T, (d) F-C_{10}T

^{1}H NMR stack of irradiated polyketones solution (20 mg/mL $CDCl_3$)

(a) F-C_6T

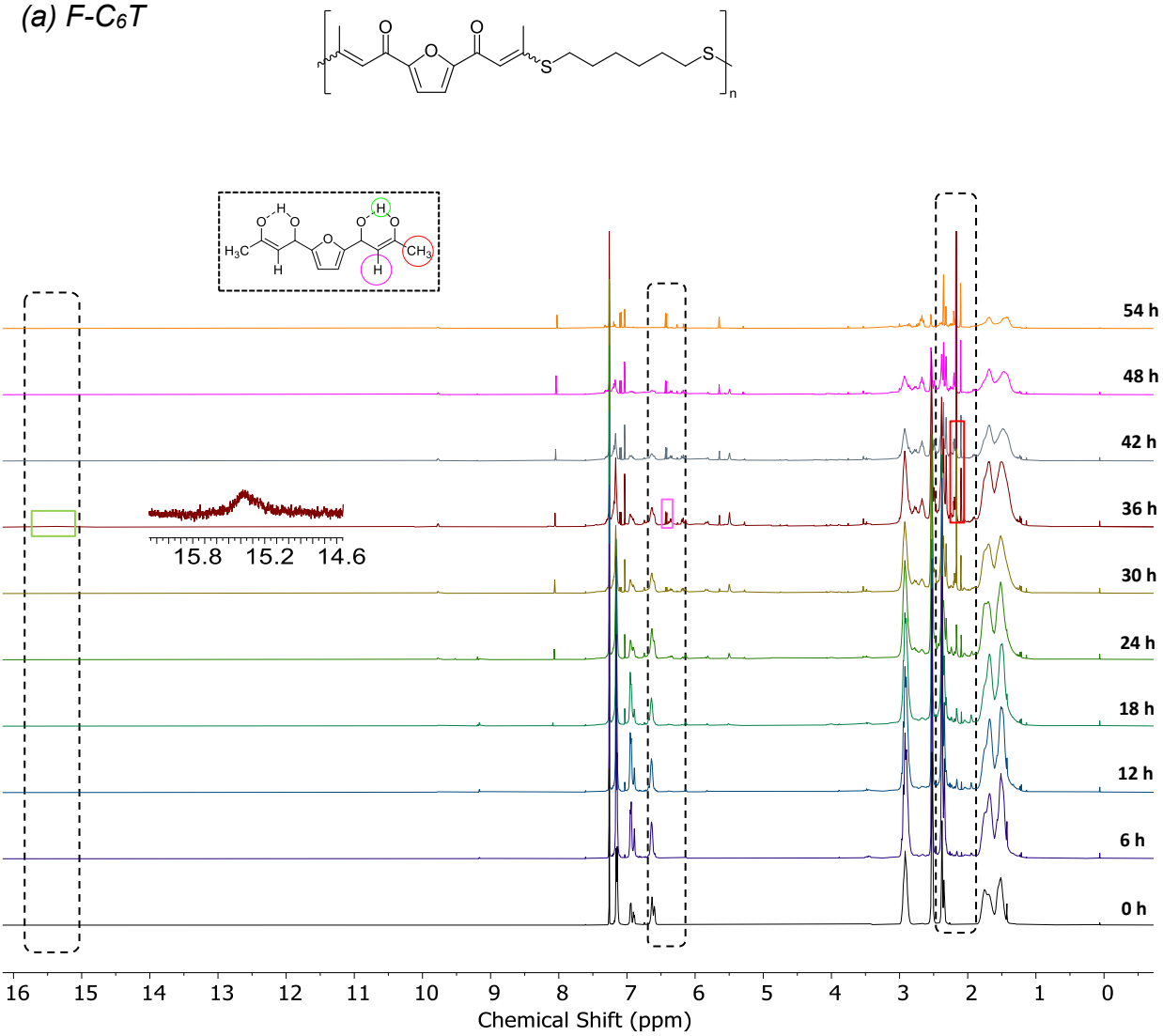

Figure S29. ^{1}H NMR spectra of polymer F-C_6T (yellow solution) stacked to illustrate the change of spectrum until fully degraded (colorless solution)

(b) F-C_6T_{EG}

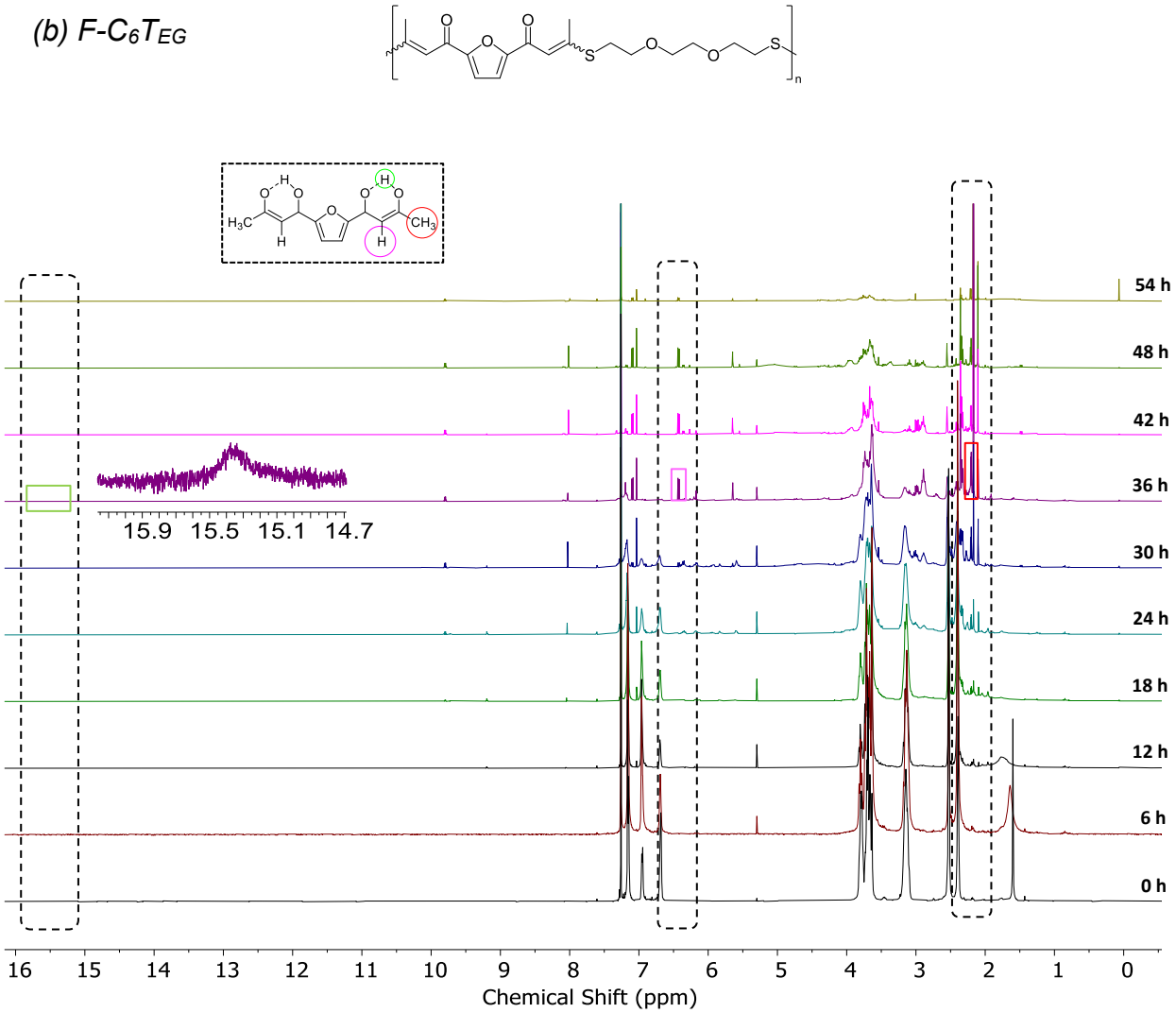

Figure S30. ^{1}H NMR spectra of polymer F-C_6T_{EG} (yellow solution) stacked to illustrate the change of spectrum until fully degraded (colorless solution)

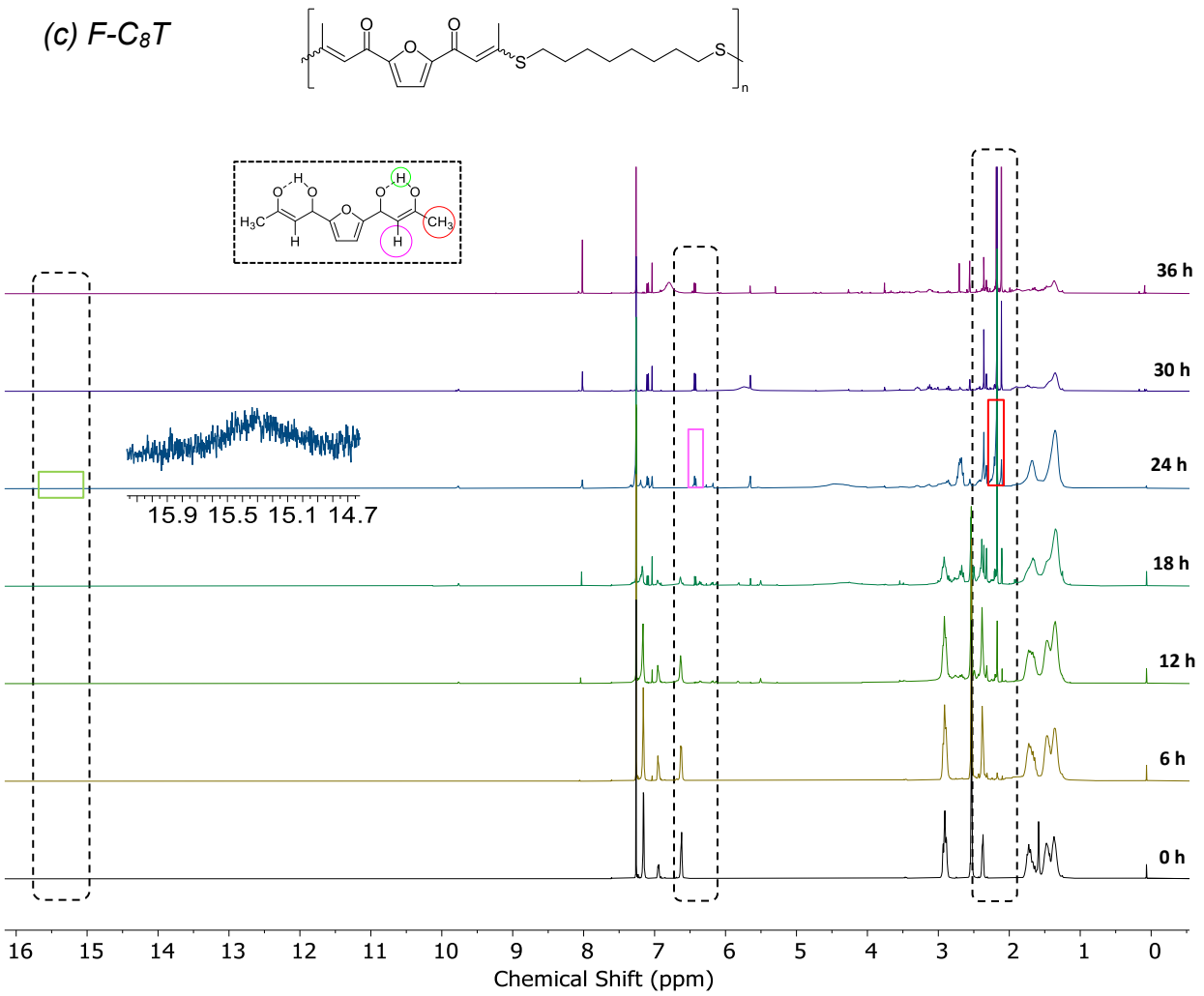

Figure S31. ^{1}H NMR spectra of polymer F-C_8T (yellow solution) stacked to illustrate the change of spectrum until fully degraded (colorless solution)

(d) F-C_{10}T

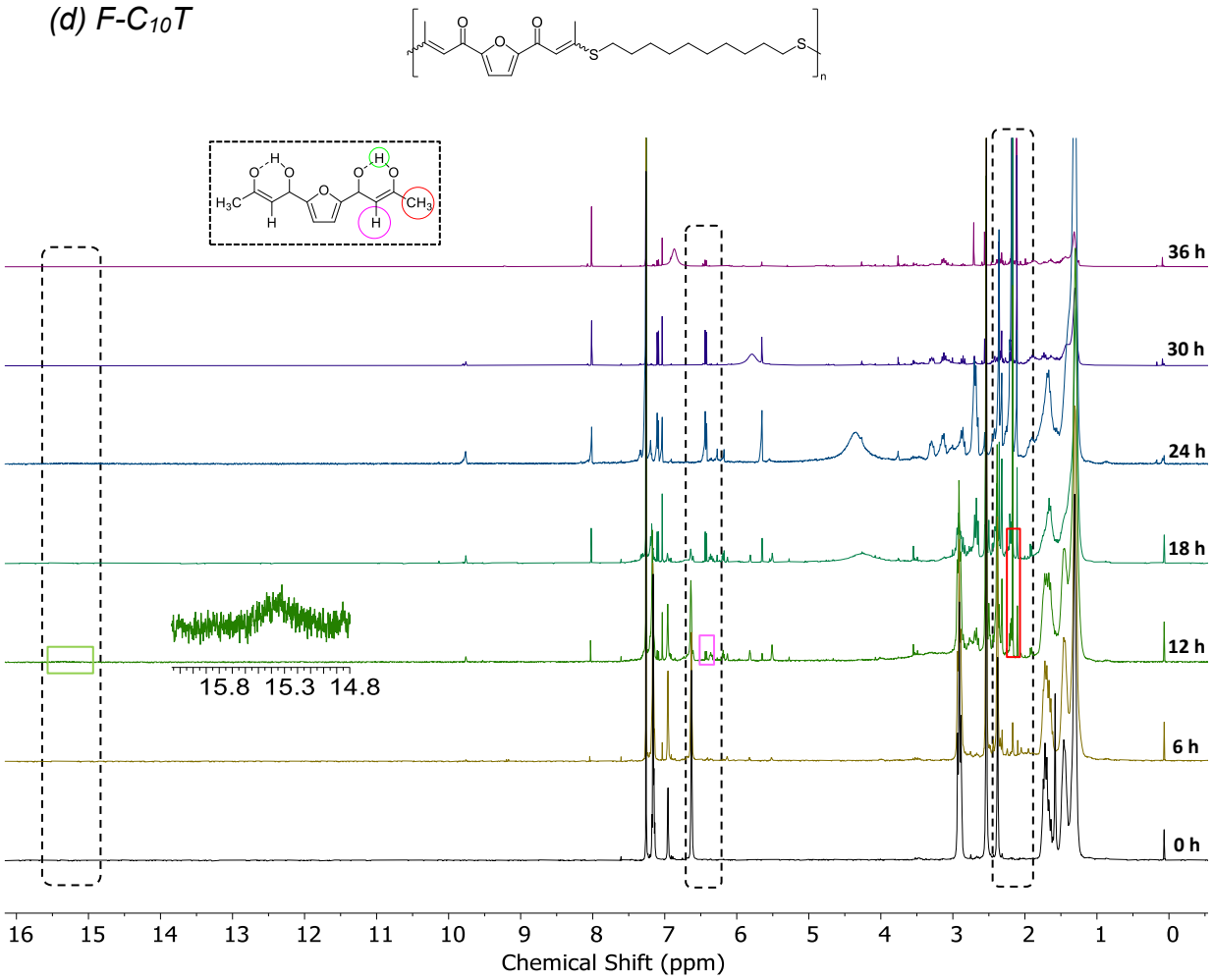

Figure S32. ^{1}H NMR spectra of polymer F-C_{10}T (yellow solution) stacked to illustrate the change of spectrum until fully degraded (colorless solution)

Size exclusion chromatograms of irradiated PK solutions

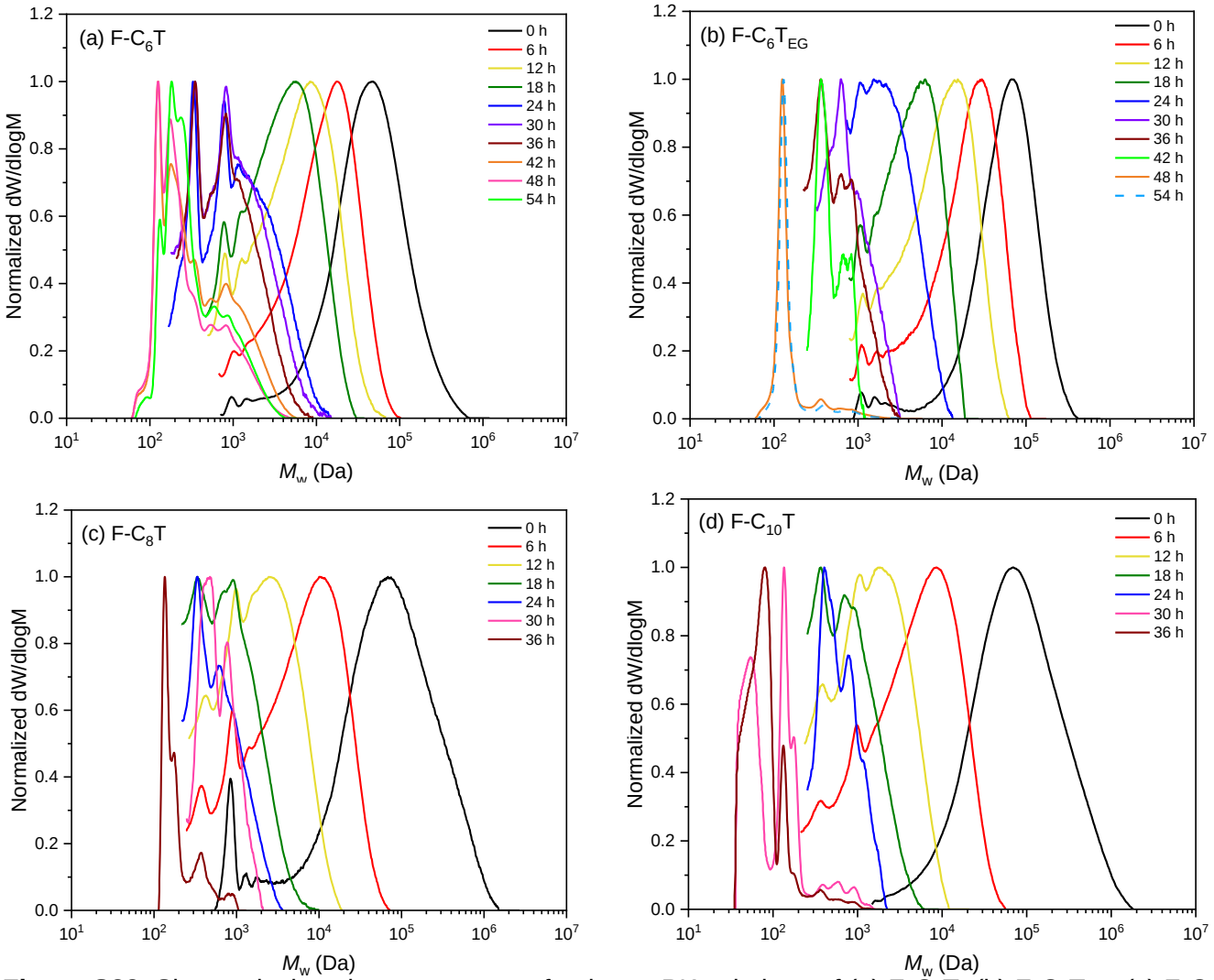

Figure S33. Size exclusion chromatograms of polymer PK solutions of (a) F-C_6T, (b) F-C_6T_{EG}, (c) F-C_8T, (d) F-C_{10}T

NMR spectra of the model compounds (small molecules)

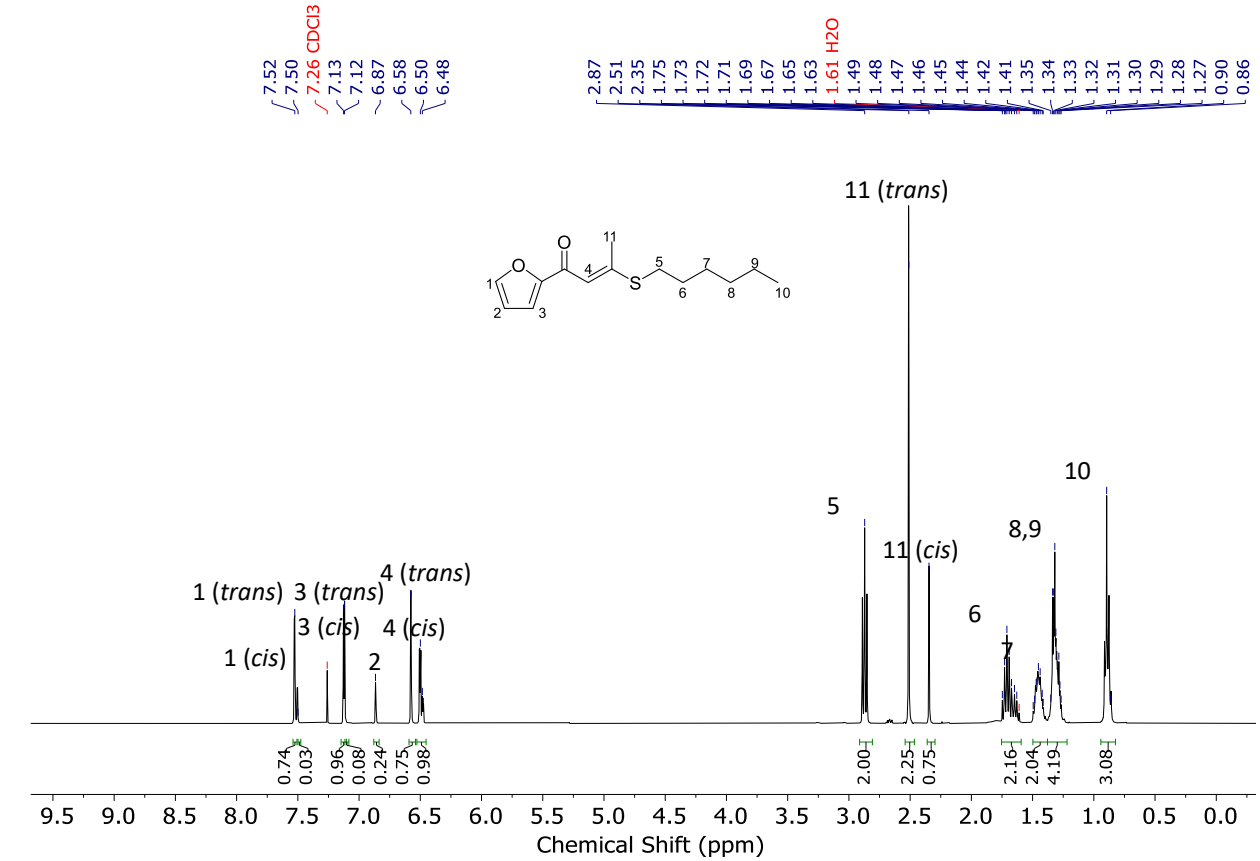

Figure S34. ^{1}H NMR spectrum (400 MHz, Chloroform-*d*) of model F-C_6T

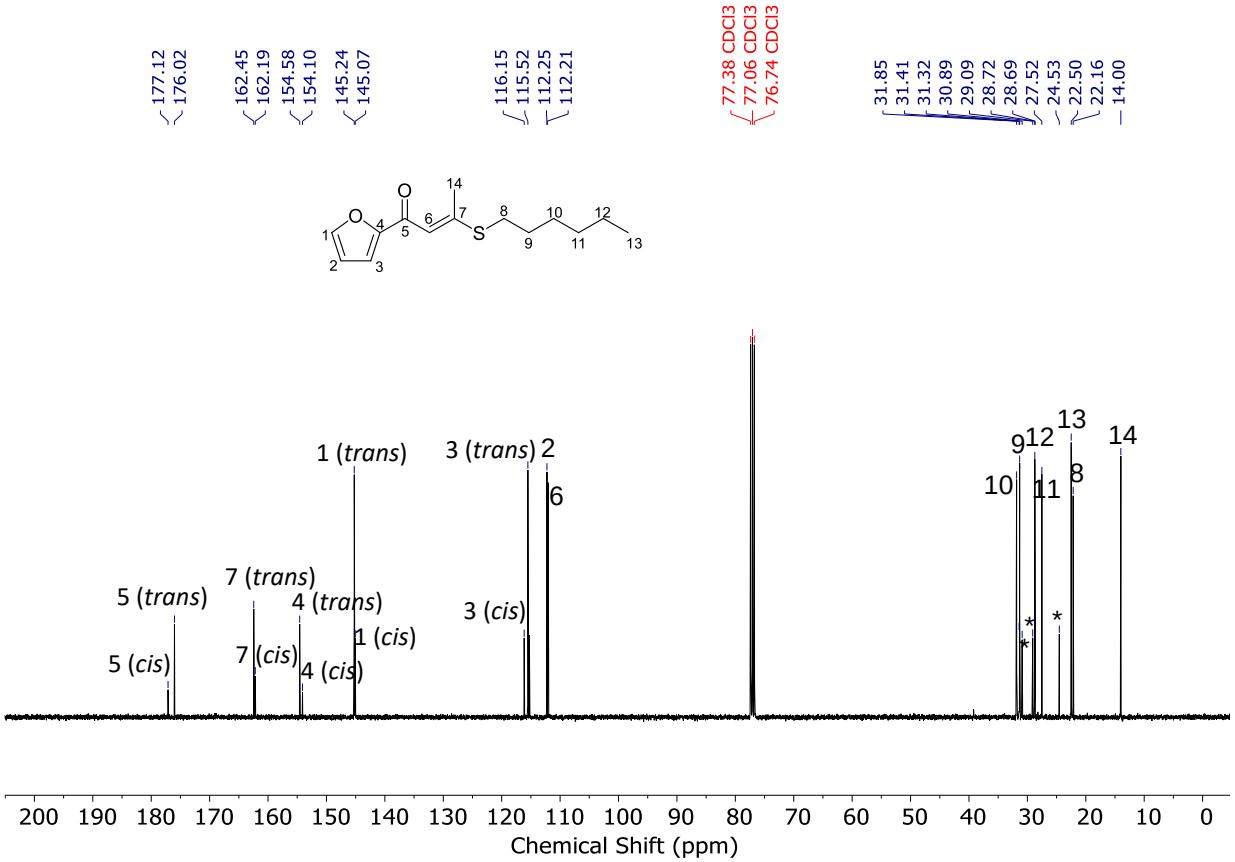

Figure S35. ^{13}C NMR spectrum (101 MHz, Chloroform-*d*) of model F-C_6T.**rotamers*

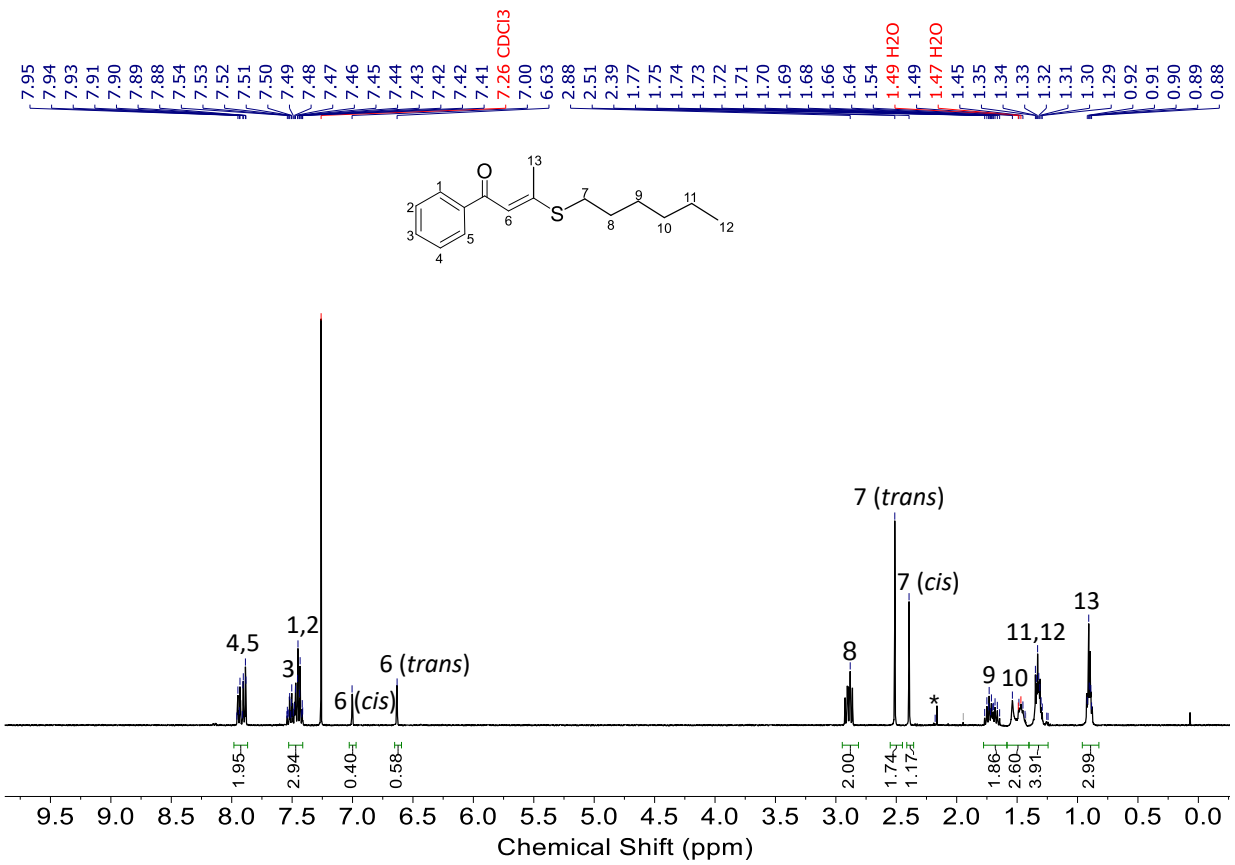

Figure S36. ^{1}H NMR spectrum (400 MHz, Chloroform-*d*) of model Ph-C_6T.**acetone*

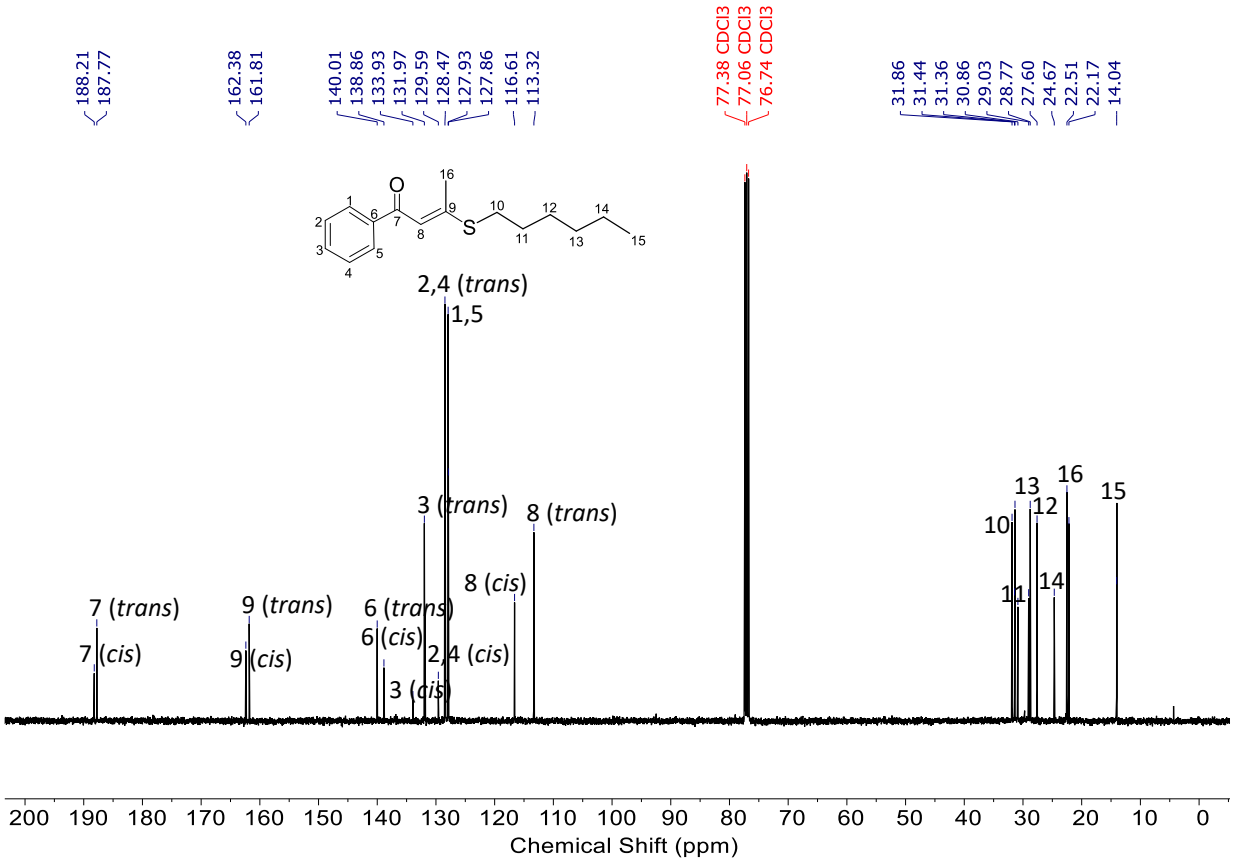

Figure S37. ^{13}C NMR spectrum (101 MHz, Chloroform-*d*) of model Ph-C_6T

NMR spectra of irradiated model polyketones (20 mg/mL $CDCl_3$)

a) Model F-C_6T

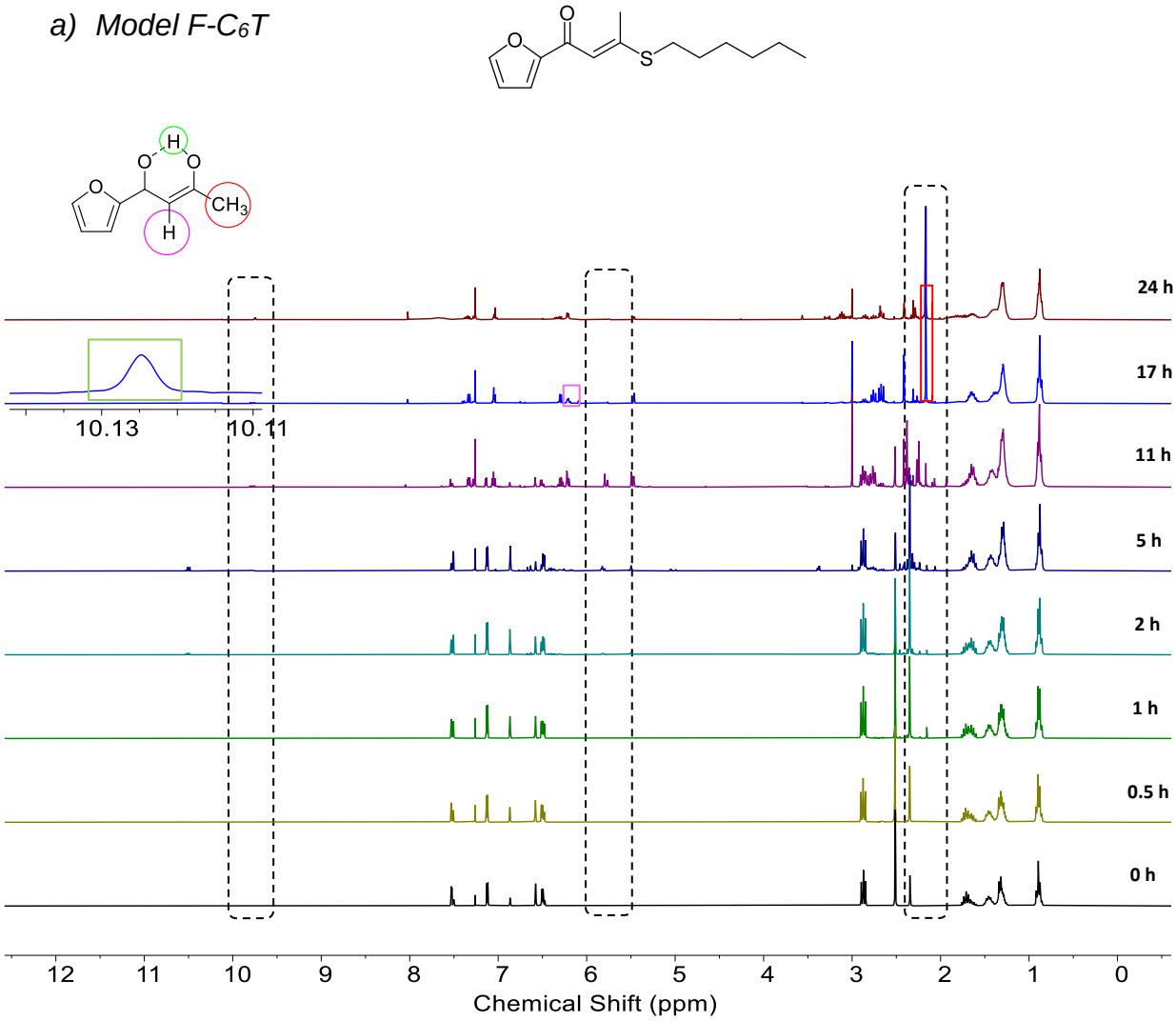

Figure S38. ^{1}H NMR spectra of model F-C_6A stacked to illustrate the change of spectrum for 24 h

b) Model Ph-C_6T

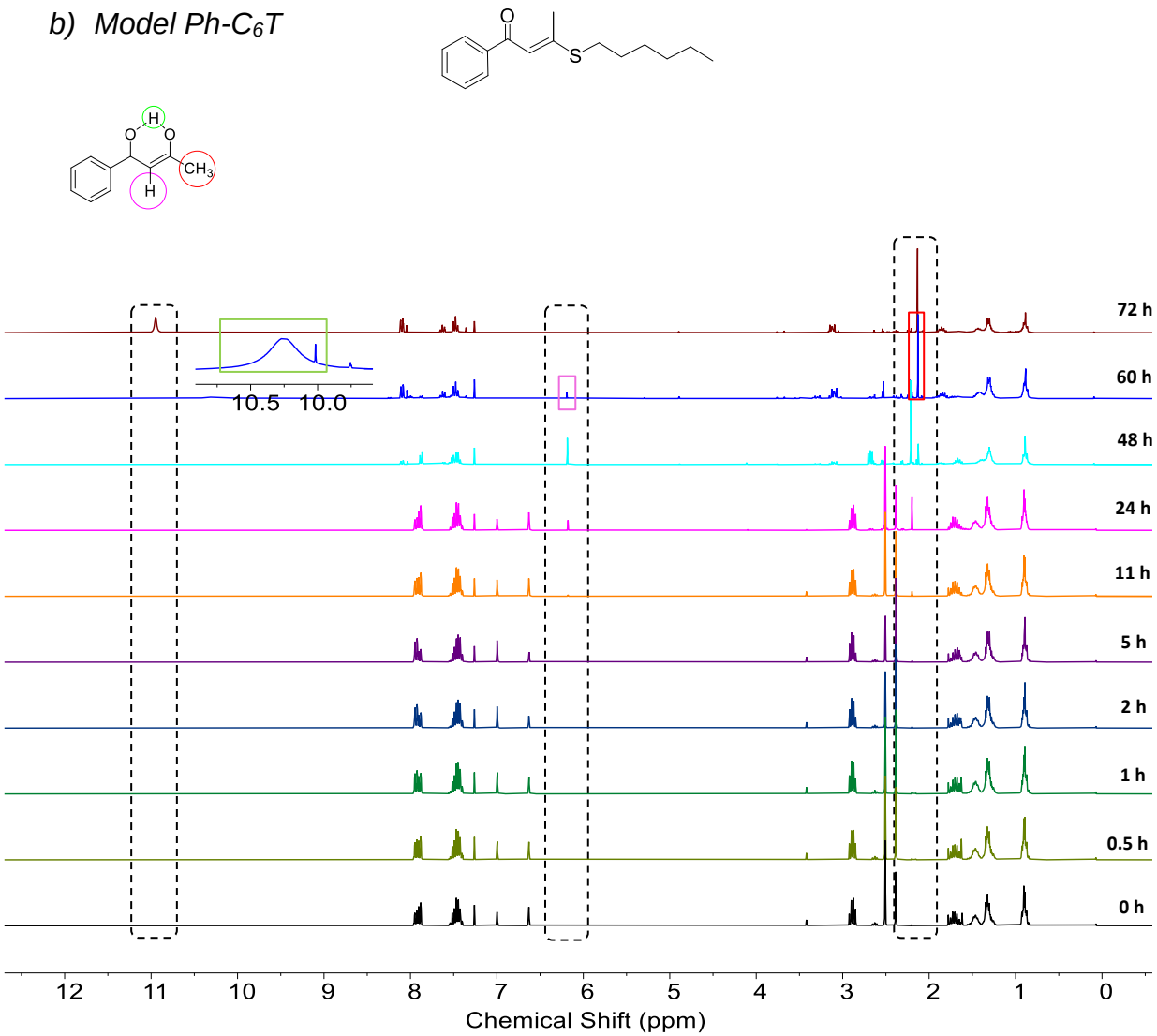

Figure S39. ^{1}H NMR spectra of model Ph-C_6T stacked to illustrate the change of spectrum for 72 h

GC-MS chromatograms of irradiated model compounds

a) Model F-C_6T

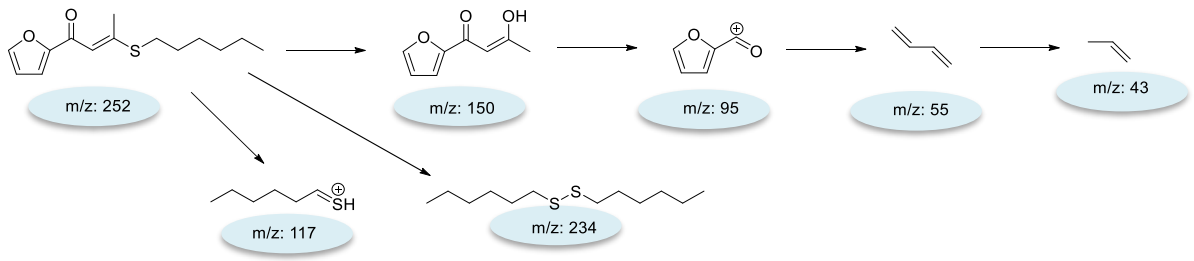

Scheme S7. Fragmentation of irradiated model F-C_6T

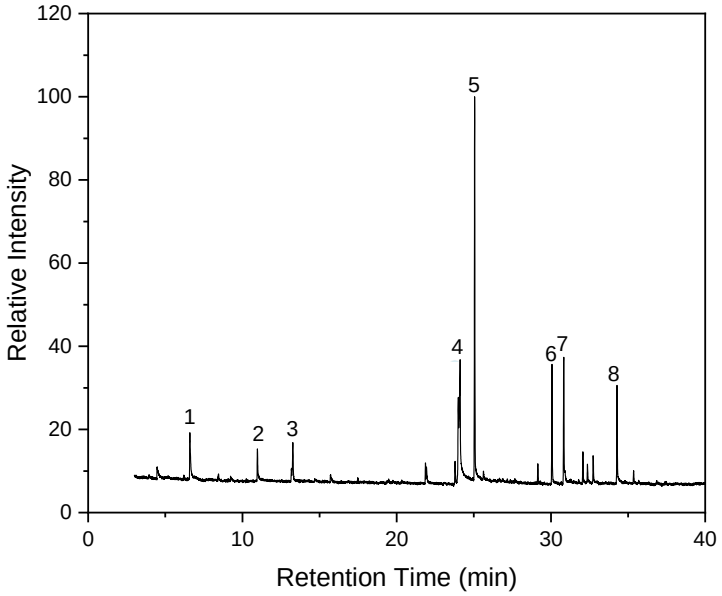

Figure S40. GC chromatogram of irradiated model F-C_6T

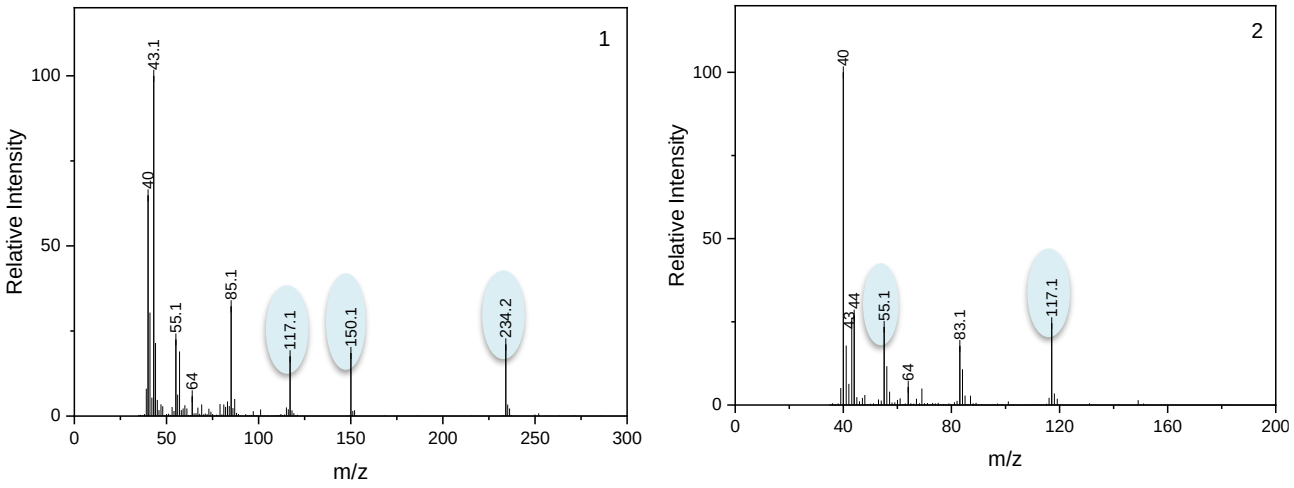

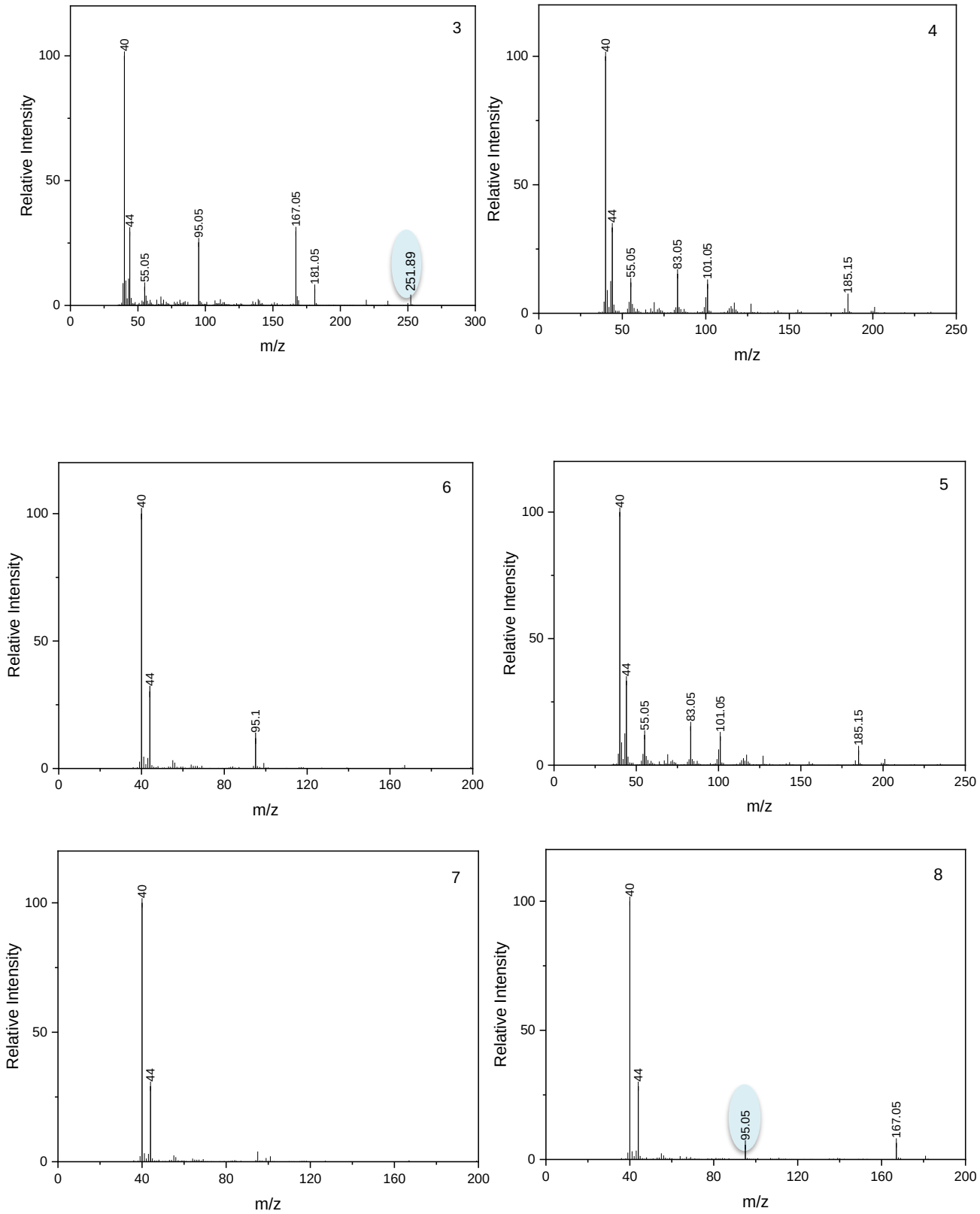

Figure S41. MS chromatogram of irradiated model F-C_6T

b) Model Ph-C_6T

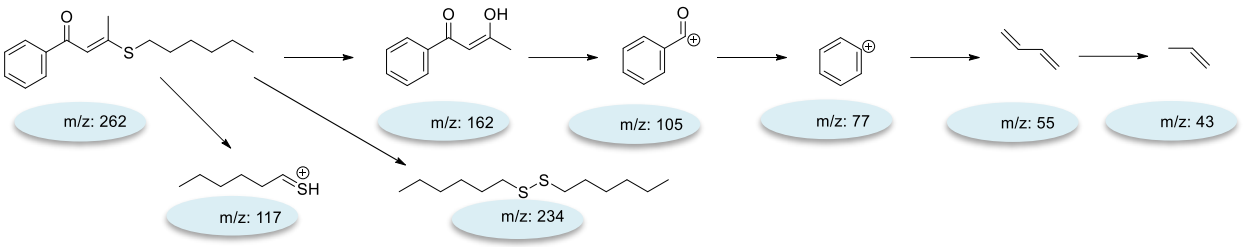

Scheme 8. Fragmentation of irradiated model Ph-C_6T

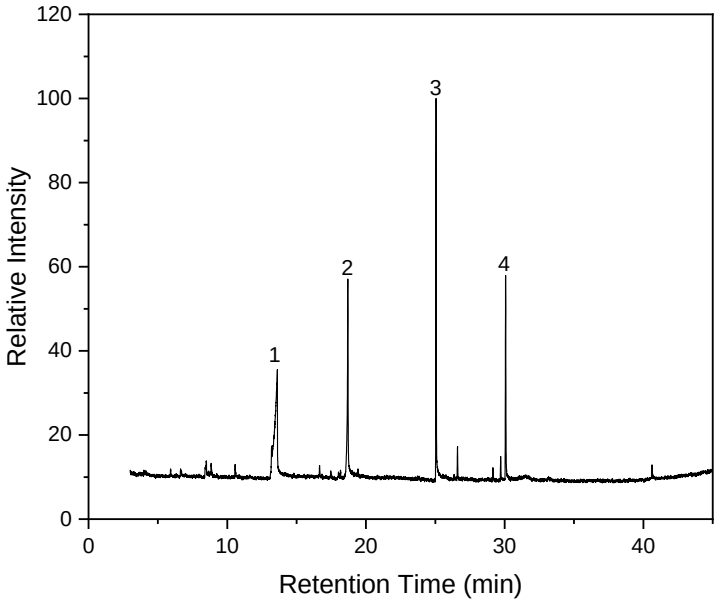

Figure S42. GC chromatogram of irradiated model Ph-C_6T

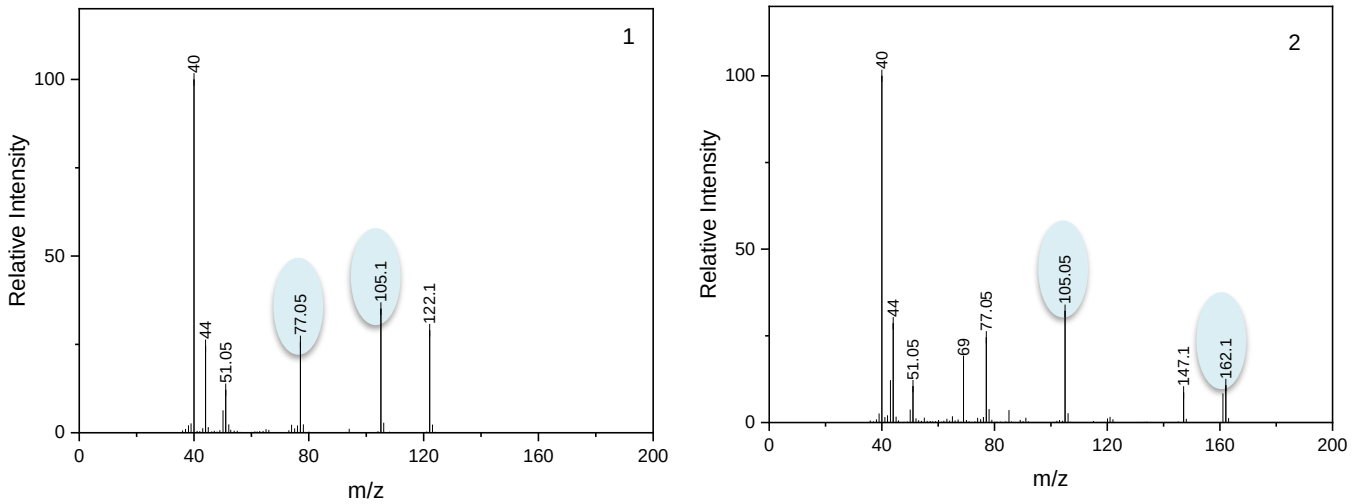

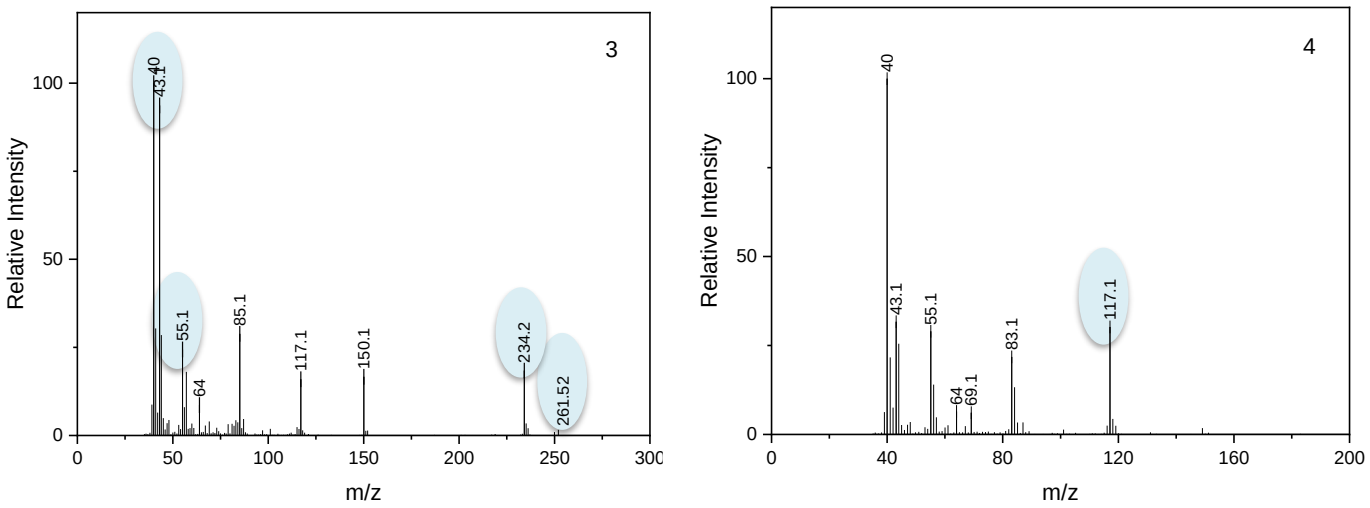

Figure S43. MS chromatogram of irradiated model Ph-C_6T

References

1. Nahm, S. & Weinreb, S. M. N-methoxy-n-methylamides as effective acylating agents. *Tetrahedron Lett.* **22**, 3815–3818 (1981).
2. Niu, T. *et al.* A powerful reagent for synthesis of Weinreb amides directly from carboxylic acids. *Org. Lett.* **11**, 4474–4477 (2009).
3. Worch, J. C., Stubbs, C. J., Price, M. J. & Dove, A. P. Click Nucleophilic Conjugate Additions to Activated Alkynes: Exploring Thiol-yne, Amino-yne, and Hydroxyl-yne Reactions from (Bio)Organic to Polymer Chemistry. *Chem. Rev.* **121**, 6744–6776 (2021).

CHAPTER 3: SPONTANEOUS AMINO-YNE CLICK POLYMERIZATION TO GENERATE PHOTODEGRADABLE BIO-DERIVED POLYKETONES WITH TUNABLE THERMOOMECHANICAL PROPERTIES

3.1 Manuscript and overview

Title: Spontaneous Amino-yne Click Polymerization to Generate Photodegradable Bio-Derived Polyketones with Tunable Thermomechanical Properties

Authors: **Lukmanul H. Samada**[1], Neha Yadav[1], Joshua C. Worch[1,2], Arianna Brandolese[1], Andrew P. Dove[1]*

Affiliations: [1] School of Chemistry, The University of Birmingham, Edgbaston, Birmingham, B15 2TT, UK.
[2]Department of Chemistry, Virginia Tech, 24061, USA

Manuscript Prepared

Co-author contributions: Dr. Neha Yadav (University of Birmingham) synthesized the precursor and imaged microcapsules using SEM. Dr. Joshua C. Worch (University of Birmingham; Virginia Tech) provided technical and synthetic guidance and editing of this manuscript. Dr. Arianna Brandolese (University of Birmingham) provided editing of the manuscript. Prof. Andrew P. Dove (University of Birmingham) supervised in addition to providing guidance and editing the manuscript.

Overview:

Following on from Chapter 2, we wanted to investigate the nitrogen-containing linear polyketones with a similar polymerization approach. Spontaneous amino-yne click reaction gained our attention as this type of reaction can take place in the absence of an external catalyst at mild reaction conditions.

We decided to replace the dithiol comonomer with a diamine comonomer to understand the effect of amine insertion on their thermomechanical properties and photodegradability. We found a range of mechanical performances (σ = 9-41 MPa), in which the polyketone containing 1,6-hexanediamine displays a comparable tensile strength to PET (but owing half of its elongation at break value). The thermal stability of the polymer was excellent as well. In addition, the photodegradation products indicated a secondary photolysis (further degradation) occurred towards the degradation products that we observed in Chapter 2. We hypothesized this typical degradation occured due to the presence of amine.

Considering the formation of hydrogen bonds within the polymer chains, we synthesized a range of homopolymers to show how significant this intermolecular force influences the mechanical performances. We evaluated the effect of chain length, ether bonds, and steric bulk in the polymeric fashion on their phyco-chemical properties. The hydrogen bonds play an important role in controlling their mechanical performance, thermal stability, and photodegradation pathway. Furthermore, this polymer can be employed as a microcapsule shell for photo-triggered release through interfacial click polymerization. It is essential for some applications, such as agriculture and the biomedical field.

Spontaneous Amino-yne Click Polymerization to Generate Photodegradable Bio-Derived Polyketones with Tunable Thermomechanical Properties

Lukmanul H. Samada[1], Neha Yadav[1], Joshua C. Worch[1,3], Arianna Brandolese[1], Andrew P. Dove[1,*]

[1]School of Chemistry, University of Birmingham, B15 2TT, UK. [2]Department of Chemistry, Virginia Tech, 24061, USA.

*E-mail: a.dove@bham.ac.uk

Abstract

Polyketones (PKs) are intrinsically photodegradable polymers, and they could possess thermomechanical performance similar to thermoplastics such as polyesters and polycarbonates. However, prior research on polyketones is centred on integrating non-renewably sourced ketones into polyolefin-like polymer backbones that undergo non-selective photodegradation. Herein, we prepared polyketones using 2,5-furandicarboxylic acid as a renewable bio-sourced monomer along with abundant and commercially available diamines through click polyaddition under mild reaction conditions. The thermomechanical properties and photodegradation behavior of the synthesized PKs are tuned through modifications in chain flexibility achieving high molecular weights (M_w up to 164 kDa). These PKs show a wide range of glass transition temperatures and mechanical performances. Furthermore, the irradiated PKs follow a selective photodegradation pathway with the formation of α-diketone and acetone as the major products. Click polymerization is here also explored as a new approach for surfactant-free dye encapsulation by an interfacial polyaddition method to generate photodegradable polyketone microcapsules that can be applicable for UV-triggered prolonged-release.

Introduction

Commodity plastics derived from petroleum resources have poor degradability and the significant decrease in the oil fuel reserve has led researchers to explore the use of alternative renewable feedstocks.[1–4] Biomass feedstocks can thus represent a valuable alternative to fossil-based compounds and they are easily converted into polymerizable monomers to produce synthetic bio-based plastics. Some building blocks can be used as bio-based monomers, such as carboxylic acids and alcohols, including 2,5-furandicarboxylic acid (FDCA).[5]

FDCA, starch derivative, has become an alternative building block to substitute terephthalic acid (TPA) and isophthalic acid (IPA) in the production of polyesters due to its structural similarity.[6-9] Besides polyesters, some polymers can be synthesized from FDCA, such as polyamides, polyurethanes, and epoxy resins.[10,11] While several techniques have been explored for polymerizing FDCA, the typical approach involves conventional direct polycondensation resulting in low molecular weight polymers, low yield, and restricted shape, which requires high-temperature reaction condition.[12] However, recently two-step melt polycondensation and ring opening polymerization of macrocycles have been exploited to achieve higher molecular weight and to reduce the by-products formed.[13,14]

Photodegradable plastics are manufactured primarily from oil-derived feedstocks that are transformed into polyolefin-like structures known as photodegradable polymers. These polymers tend to breakdown within a few months of exposure to sunlight, generating short chains by cleavage of the carbonyl group.[15] The incorporation of light-sensitive chemical compounds or copolymers “photosensitizers” including diketones, carbonyl-containing species, and ferrocene derivatives into polymer production proves to weaken polymer bonds and make them susceptible to ultraviolet light.[16] Among photodegradable plastics, polyketones (PKs) have gained increasing attention as they have the potential to enhance the sustainability of polymer synthesis.[17] However, their synthesis requires dangerous reagents (*e.g.*, carbon monoxide), harsh reaction conditions (high pressure polymerizations), and bespoke metal catalysts.[18-20] Despite being first reported in the 1950s by Hoehn and co-workers, in the early 1980s, a new category of polyketones was synthesized by Doyle and co-workers *via* metal-catalyzed copolymerization of CO/ethylene using efficient palladium catalysts.[21-23] Later, Mecking and co-workers exploited ADMET copolymerization to generate long-spaced polyketones to be an alternative method to ethylene/CO copolymerizations.[24]

Polyketones are used to toughen immiscible polymer blends with a crosslinked elastomeric shell and a hard glassy shell, in addition to their compatibilism function.[25] Earlier studies exhibited that the addition of stabilizer and carbon black enable to enhance the mechanical strength and improve their resistance to UV light.[26-28] These conventional polyketones commonly undergo Norrish-type photodegradation, which is uncontrolled and leads to multiple reaction products and/or microplastic formation from incomplete degradation.[29-33]

Thiol-ene, thiol-yne and thiol-epoxy click polymerizations have been reported as facile and efficient click polymerization and novel active free-radical polymerizations.[34-36] The metal-free click polymerization enables monomers to polymerize readily at ambient temperature in an open atmosphere.[37] In addition, the insertion of heteroatoms into the alkyne polymer backbones can yield new polymers with novel structures and properties.[38] Similarly, other native groups, such as amines and hydroxyl groups, can also be employed in the polymer chain of PKs.[39] Thiol-Michael addition has been massively used in producing polymers due to their beneficial features, such as regio-selectivity, high efficiency, and mild condition reaction.[40] While the use of thiols along with Michael acceptor for polymer preparation has been widely explored,[41-43] the use of diamines instead is still at its infancy. Amines are considered to be more sustainable, easily accessible and cheaper than thiol and have recently been used to fabricate nitrogen-containing functional polymers under mild conditions. They can also produce diverse product structures and high molecular weight polymers with easy isolation.[44] Moreover, amines are stronger nucleophiles that can act as both reactants as well as a catalyst, whereas the susceptibility of thiols towards oxidation requires the use of external catalysts due to their poor nucleophilicity.[45]

Recently, our group has been exploring thiol-yne click polymerizations with a more selective photodegradation pathway, resulting β-diketone (enol form) as a major product and disulfide as a minor product (unpublished work). As part of our group's interest in improving the sustainability of polymers, herein, we developed a series of novel polyketones from bio-derived feedstocks using a click chemistry approach at room temperature without the presence of any external catalysts. Here, we explore an *aza*-Michael addition reaction using FDCA as renewable feedstock, and commercially available diamines as an abundant and practical sustainable comonomer for amino-yne click polymerization which has been found to have an analogue photodegradable linkage as thiol-yne click reaction-based products. These polyketones display

comparable tensile strength properties to commodity plastics (but having half of their elongation at break value). Furthermore, we employed this technique to fabricate surfactant free dye-loaded microcapsules *via* interfacial polymerization, which is essential for many applications, such as crop protection in agriculture. Lastly, UV light exposure is carried out to rupture the microcapsule shell and release the encapsulated dye.

Results

Polymer Synthesis and Characterization. Spontaneous amino-yne click polymerization was first reported in 2017 by Tang and co-workers, and since then, it has become more interesting and attractive than thiol-yne click polymerizations considering their cost effectiveness and robustness.[46] Additionally, amino-yne-based polymers have become a topic of interest due to the presence of dynamic bonds in their backbone.[47] Moreover, their stereoselectivity was investigated by density functional theory (DFT) calculation which discovered that in polymers derived from secondary amines, the *E*-configuration is the dominant isomeric unit.[46] Stereo- and regioselective polymers with high yields at room temperature without the presence of any external catalyst were obtained using amino-yne click reaction.[48] Sustainability of these polyketones can be improved by employing biobased building blocks, such as carbohydrates and vegetable oils, to be the first step towards circularity and reduce fossil fuel dependence.[49-51]

To employ amino-yne click reaction, an activated alkyne is required. Here, monomers were prepared using 2,5-furandicarboxylic acid (FDCA) as a renewable feedstock which can be extracted from plant starches *via* saccharification, dehydration, and oxidation.[52] Diynone monomers (F) were thus obtained with a good yield (>80%). The ^{1}H NMR spectrum demonstrated the key peaks at δ = 2.15 ppm and 7.33 ppm (Fig. S3). Furthermore, FTIR spectra shows the triple bonds of alkynes (-C≡C-) which are detected at 2200 cm^{-1} (Supplementary Fig. S31). Those analysis indicate the formation of diynone. These monomers underwent amino-yne click polymerization along with linear primary and secondary diamines.

Diamines were expected to provide superior mechanical properties due to their ability to generate more hydrogen bonds in the polymer backbone. Different diamines such as 1,6-hexanediamine, *N,N'*-dimethyl-1,6-hexanediamine, 2,2' (ethylenedioxy)bis(ethylamine), 1,8-octanediamine, 1,10-decanediamine, and 1,12-dodecanediamine (Fig. 1) were employed to produce a variety of PKs. The effect of chain flexibility on the thermomechanical performances

of the resultant polymers was further investigated (Table 1).

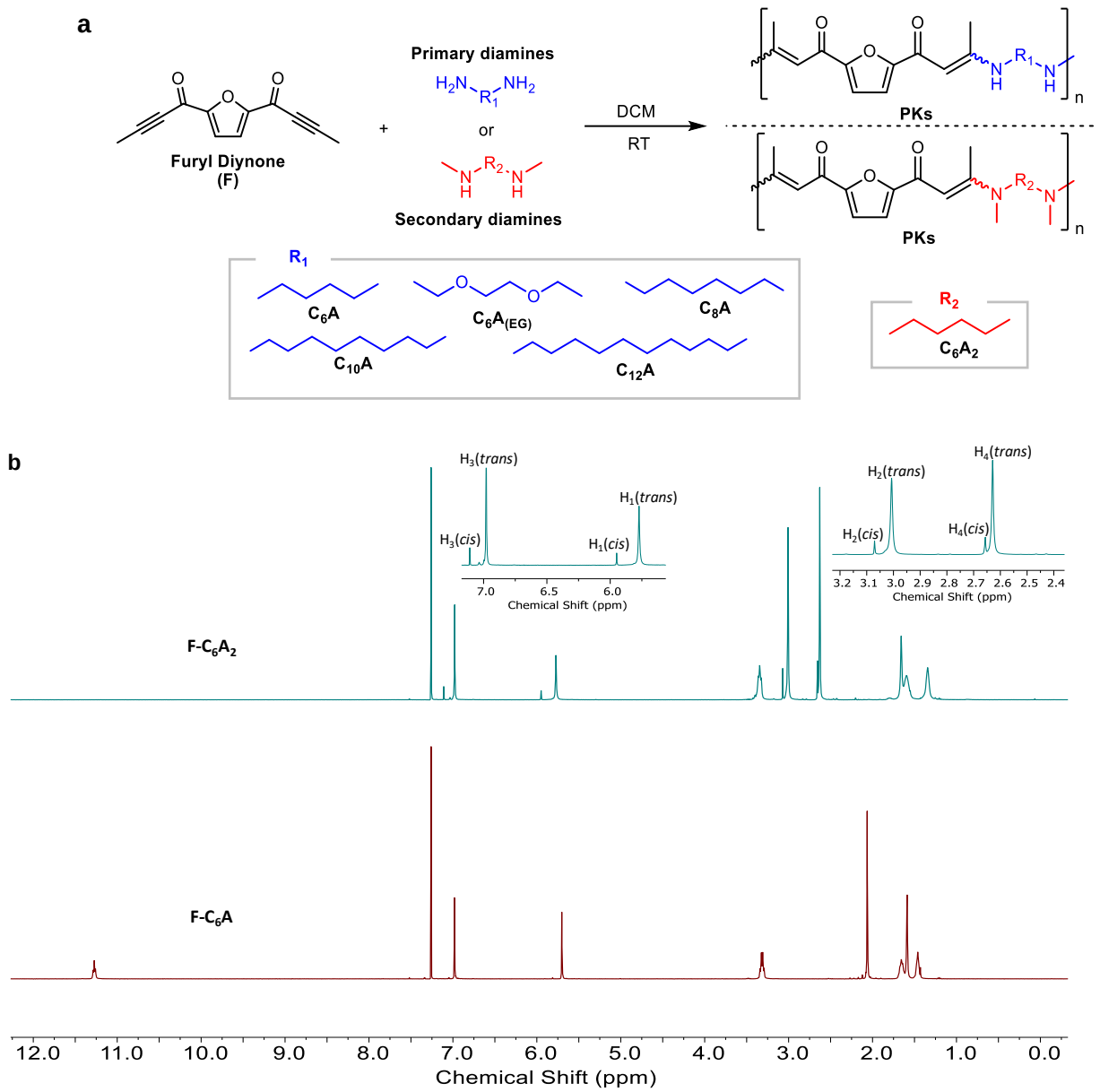

Fig. 1 Synthesis and characterization of polyketones. a Synthesis of furan-based linear polyketones by spontaneous amino-yne click polymerization. **b** Representative ^{1}H NMR spectrum ($CDCl_3$, 25 ºC, 400 MHz) of F-C_6A_2 and F-C_6A. *Cis* and *trans* proton resonances were assigned according to previous published work.[46,54,55]

Table 1 Characterization of material properties for annealed polyketones.

PKs	M_w[a] (kDa)	$Đ_M$[a] (M_w/M_n)	%*cis*[b]	T_g[c] (°C)	$T_{d,5\%}$[d] (°C)	E[e] (Mpa)	σ_b[f] (Mpa)	ε_b[g] (%)	U_T[h] (MJ·m^{-3})
F-C$_6$A	129	6.92	100	117	294	669 ± 33	41.1 ± 3.26	165 ± 11.38	57.9 ± 7.08
F-C$_6$A$_2$	43	3.72	5	104	242	319 ± 45	8.8 ± 0.23	161 ± 12.92	14.5 ± 1.19
F-C$_6$A$_{EG}$	89	5.34	75	84	297	444 ± 41	21.3 ± 2.95	39 ± 8.88	5.5 ± 1.66
F-C$_8$A	83	6.18	100	90	294	332 ± 2	31.2 ± 2.76	182 ± 18.68	42 ± 6.69
F-C$_{10}$A	78	5.07	100	82	323	312 ± 9	37.4 ± 1.24	294 ± 14.19	70.9 ± 5.17
F-C$_{12}$A	164	8.97	100	69	326	286 ± 14	36.3 ± 1.23	305 ± 5.69	68.5 ± 2.17

[a]M_w and $Đ_M$ were determined by size exclusion chromatography ($CHCl_3$, 0.5% NEt_3, 40 °C) analysis against poly(styrene) (PS) standards. [b]%*cis* content determined by ^{1}H NMR spectroscopic analysis. [c]T_g was obtained from the

2nd heating cycle. [d]$T_{d,5\%}$ was determined from the material loses 5% of mass weight. [e]Young's modulus. [f]Stress at break. [g]Strain at break (n = 3). [h]Tensile toughness (n = 3). Uncertainty is presented as the standard deviation of samples.

Polymerizations were conducted at room temperature in an open environment with a monomer concentration of 0.5 M and a reaction time of 3 h using dichloromethane (DCM) as an aprotic solvent, to enhance the nucleophilicity of diamine monomers. Overall, relatively high yields were achieved, with molecular weight (M_w) up to 168 kDa when primary diamines were used. Differently, secondary diamine led to lower M_w (43 kDa) mainly due to the steric hindrance effect, which affects the chain extension and inhibits the chain propagation.[53] A broad dispersity ($Đ_M$) in the range of 3−9 was obtained for all polymers as a consequence of the step-growth polymerization approach (Supplementary Fig. S33).

Analysis by ^{1}H NMR spectroscopy showed that amino-yne polymerization with primary diamines stereo-selectively lead to the formation of *cis* (*Z*) isomer whereas secondary diamines favorably lead to the *trans* (*E*) isomer according to DFT calculation. Similar to other primary diamines, F-C_6A_{EG} also exhibited dominant *cis* (*Z*) isomer (Supplementary Fig. S17-S23). These phenomena can be attributed to the conjugate additions of primary amines to acetylenic Michael acceptors that typically favor the *Z*-configuration due to intramolecular hydrogen bonding with the adjacent carbonyl moiety, primarily when propiolates, propiolamides, and ynones are employed.[54] He *et al*. performed a theoretical simulation using methyl propiolate and diethylamine (secondary amine) as a model reaction, indicating that the *E*-configuration is a dominant isomeric unit in the polymers.[46,54,55] Moreover, the addition of D_2O into the polymer solution (dissolved in $CDCl_3$) was carried out to confirm the formation of N-H bonds from the resulting PKs (Supplementary Fig. S19).

Thermal and mechanical properties. The flexibility of polymeric chains can affect thermal stability and mechanical performance, such as ductility, stiffness, flexibility, and toughness of the PKs. The thermal properties of the materials were initially probed using thermogravimetric analysis (TGA) and the degradation temperature ($T_{d,5\%}$) was ≥ 285 °C indicating excellent thermal stability (Fig. 2a).

The secondary diamine led to the formation of the least thermally stable homopolymer owing to lower molecular weight as a consequence of steric hindrance. However, polymers derived from primary diamines showed no significant difference in weight loss. The considerable weight loss was demonstrated in the 300−500 °C range, indicating these polymers' remarkably high thermal

stability. In addition, the resultant polyketones are amorphous, as noted in the differential scanning calorimetry (DSC) with various glass transition temperature (T_g) values. Relatively high T_gs were detected, and they gradually decreased with extension in the repeat unit lengths (Table 1, Fig. 2b). This difference can be attributed to the longer chains of polyketones that enable the chain mobility to decrease as more entangled, which will provide enhanced free volume and thus lower the T_g value.

Interestingly, F-C_6A_{EG} had a lower T_g than F-C_6A due to ether bonds (C-O) that increase the flexibility of the polymer chains. Insertion of the polar group enables the restriction of the backbone rotation and reduces the conformational changes of the backbone. F-C_6A_2 containing a secondary diamine with methyl substituent also had a lower T_g than the one with primary diamine F-C_6A, due to the steric effect that increases the free volume amongst the polymer chains and therefore minimizes intermolecular interactions between the main chains. Chain flexibility also significantly affected the mechanical performance of the polyketones therefore additional investigations of the mechanical properties for the polymers with different composition were conducted.

The Ultimate Tensile Strength (UTS) of PKs was measured by tensometer with values between 10 and 45 MPa, with the strain at the break between 40% and 300%. The polyketone F-C_6A_2 with secondary amine showed lower tensile strength due to lower molecular weight ascribed to the presence of bulkier groups (CH_3 *vs* H). However, enhancing the intermolecular force interactions between polymer chains by inserting etheric bonds between the amide bonds lowers the strain in F-C_6A_{EG}. The combination of hydrogen bonds and etheric bonds presence leads to high stiffness but low toughness due to the lack of energy dissipation mechanisms, which restricts the working strain range of such polymers (Fig. 2c). The polyketone with the most extended chain length (F-C_{12}A) has the highest strain value but lowest stress value compared to other primary amine-based polyketones (Fig. 2d).

An increase in the chain length of the polymer also improved the ductility and flexibility with reduced stiffness. Amongst all polyketones, F-C_6A (UTS = ~ 40 MPa) showed the closer tensile strength to PET compared to other synthesized polyketones (Fig. 2e). Most resultant polyketones indicate that they are strong materials (tough and ductile). This mechanical performance superiority enables polyketones to be potentially better photodegradable plastics

and an alternative to conventional polyketones.

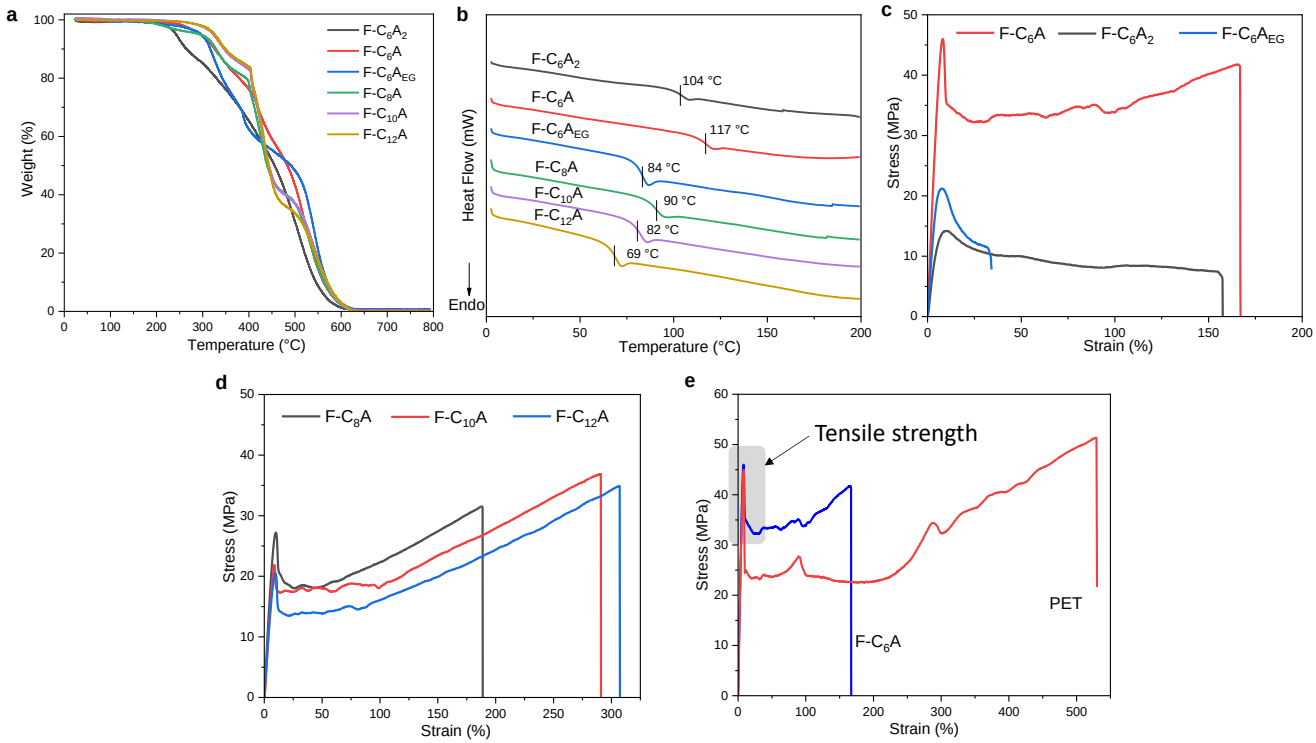

Fig. 2 Thermomechanical characterization of polyketones. a Thermogravimetric analysis of homopolymers at 10 K·min^{-1}. **b** DSC thermograms of 2nd heating cycle tested at 10 °C min^{-1}. Position of T_g for each homopolymer sample is indicated with a vertical hash mark. **c** Homopolymers of differently structured diamines. Exemplary stress *vs* strain curves were tested at 10 mm min^{-1}, 22 °C. **d** Homopolymers of homologous of primary diamines. Exemplary stress *vs* strain curves were tested at 10 mm min^{-1}, 22 °C. **e** Mechanical properties comparison between PK F-C$_6$A and PET.

Photodegradation Study. The photodegradation could be an advantage when applied in the environment. The photodegradability of synthesized polyketones was therefore investigated by irradiating them either in film or solution states. A controlled xenon light (wavelength 340 nm; with irradiation intensity 50 W/m^2), (environmental weathering chamber test method) was used for the studies, which provides a light source that is the closest to that of the solar spectrum (. Here, PKs in a film state showed higher stability than in the solution state when subjected to photodegradation and thus, their degradability resulted to be much slower than when are in solution state. Amino-yne based polyketone F-C$_6$A showed a photodegradation pathway different to our previous studies with thiol-yne based polyketones (unpublished work). In the irradiation of the amino-yne based polyketones, the α-diketone and acetone were detected as the major degradation products and amine as minor products (Fig. 3). In solution state, the furyl β-diketone was further degrading into β-diketone and furyl radical. The β-diketone then degraded to α-diketone and acetone. Furthermore, as previously observed the furyl radical could

further decompose to highly volatile acetylene and ketene[56] (Fig. 3c, Supplementary Fig. S45-S51). Finally, the ketene then was able to decompose to carbon monoxide and methylene as previously reported by Burton and co-worker (Fig. 3c).[57] This proposed pathway seemed to be more selective than Norrish-type photodegradation pathways that are typical for conventional polyketones.[25]

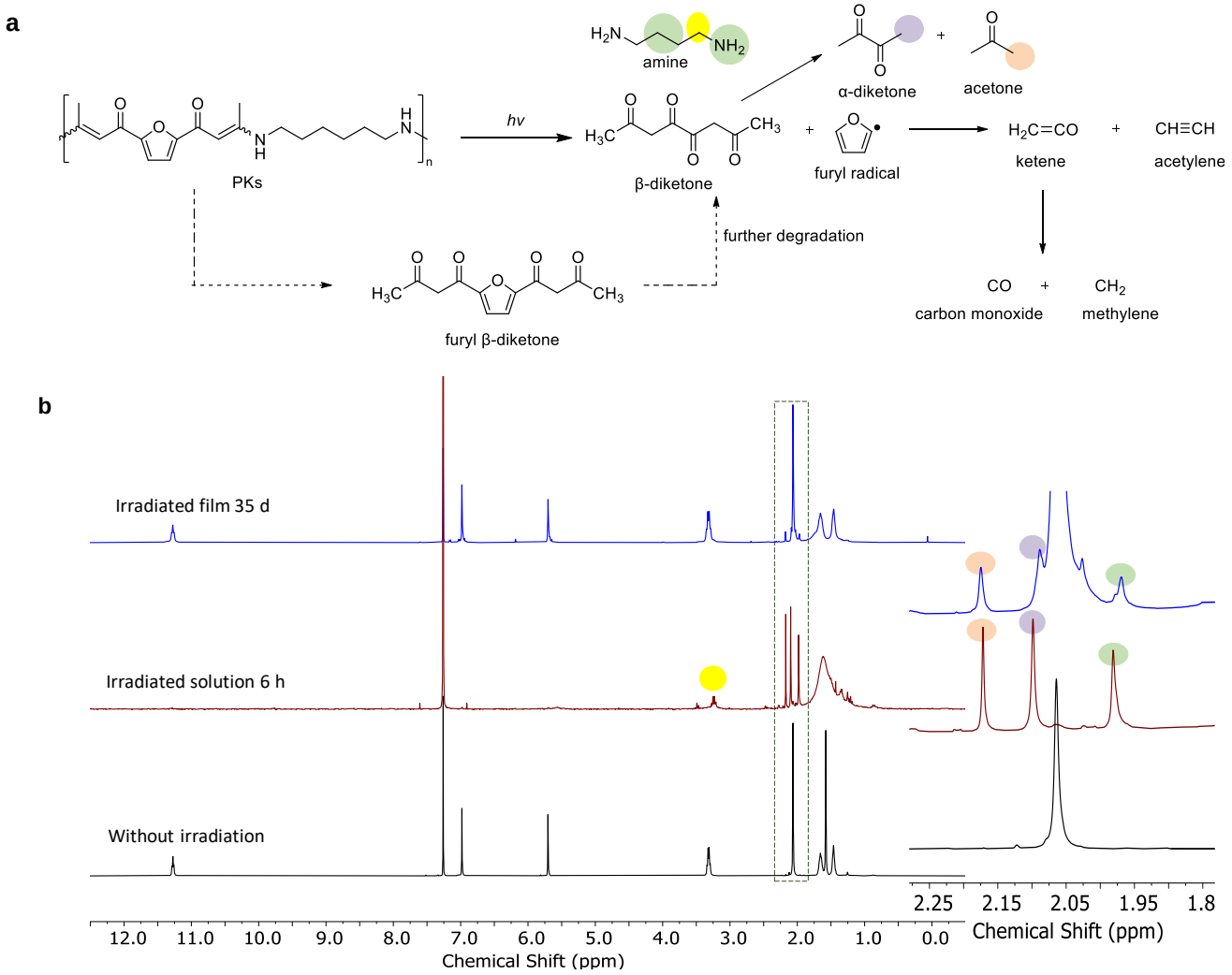

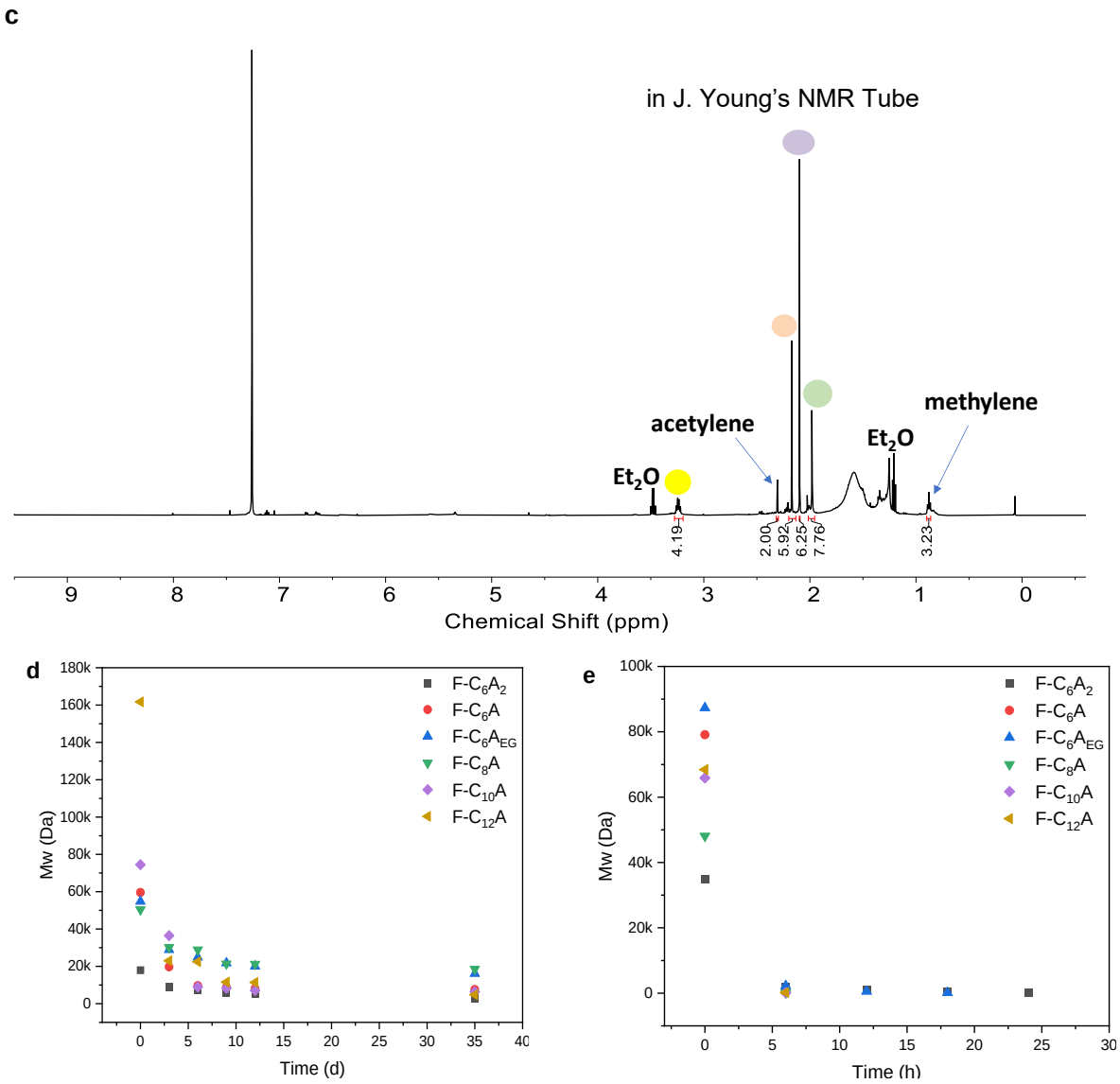

Fig 3. Polyketones photodegradation. **a** the formation of α-diketone and acetone as the major photodegradation products and its derivatives. **b** ^{1}H NMR spectra stacked of representative film polyketone F-C_6A and its solution after irradiation in $CDCl_3$. The solvent peak is marked with an asterisk. **c** ^{1}H NMR spectra of representative polyketone F-C_6A solution in $CDCl_3$ using a J Young NMR tube (close system). **d** SEC analysis of polyketones as irradiated film sample. **e** GPC analysis of polyketones as irradiated solution sample (20 mg/mL $CDCl_3$) (*Agilent PS standards cover a M_w range from 162 Da to 15 x 10^6 Da, therefore 162 Da is considered as zero* (*0*)).

Similarly, the ^{1}H NMR spectra of all the PKs presented analogous peaks at 2.09 ppm and 2.17 ppm corresponding to the formation of α-diketone and acetone, respectively (Supplementary Fig. S39-S50). In addition, in the film state, the molecular weight detected through SEC analysis was significantly reduced during the first three days, then decreased very slowly. Differently, in the solution state, the molecular weight rapidly declined within hours (Fig. 3d). The photolytic bond concentration was homogenous throughout a solid polymer sample. However, it can be

uniform or less uniform in highly concentrated solutions where polymer chains overlap. In polymer solutions at low concentrations, individual polymer chains form coils that are disseminated in the solvent; consequently, dilute systems are no longer homogeneous.[58]

The above results confirmed that synthesized PKs have a different C-C bonds cleavage compared to the thiol-yne-based polymers (unpublished work). Here, furan containing polymers results in a faster photodegradation likely because furan is more electron-rich, therefore it has a higher frontier MOs (high HOMO energy level), which makes it susceptible to reaction with singlet O_2.[59] Also, it was anticipated that the furan's susceptibility to photooxidation contributed to a faster degradation rate, meanwhile furan can act as a photosensitizer itself to generate the singlet O_2 after irradiation. Indeed, the furan ring is not as stable as the phenyl ring, therefore, in the solution state, the β-diketone degraded after prolonged irradiation due to the free radical reaction. This degradation phenomenon was also previously investigated by Varni *et al*.[60] To gain better understanding on the PKs degradation mechanism, small molecules containing furan and phenyl aromatic rings were prepared and subjected to the same photodegradation conditions.

After irradiation, the model ketones were analyzed by ^{1}H NMR spectroscopy to confirm the formation of α-diketone and acetone, and by gas chromatography-mass spectroscopy (GC-MS) through the analysis of each single fragment. The model compound containing the phenyl ring was more stable, therefore the analysis of its degradation products was simpler than in the case when a furyl ring is present (Supplementary Fig. S51 & S52). The new ^{1}H NMR spectroscopy peaks that appeared throughout the irradiation process are analogous to the ones obtained through the degradation of PKs, thus confirming the chemical structure of the degradation products previously hypothesized. Overall, α-diketone, acetone and amine are the final products, and they are safer than Norrish photodegradation products for the environment based on their material safety data sheet (MSDS). These degradation products are also confirmed by the full NMR characterization (including 2D NMR) as well as electron ionization-mass spectrometry (EI-MS) (Supplementary Fig. S56-S71). Furthermore, photodegradation is not really dependent on environmental conditions such as temperature, moisture, pH, *etc*., and only requires sunlight exposure, a major advantage for waterways and litter.

Polyketone microcapsules with a photocleavable shell UV-triggered release. Interfacial polyaddition technique is carried out to form microcapsules due to its novelty, simplicity, and allows microparticle formation in an aqueous environment at room temperature. In addition, this method was used to minimize the need to use surfactants and generates unique microparticle architectures that adapted from Strobel and co-workers' work who used spray drying method.[61] Here, the monodisperse polyketone microcapsules were prepared *via* interfacial click polymerization following a polyaddition reaction. This simple approach does not generate any by-product and permits controllable shell thickness. Thus, an aqueous solution of diamine comonomer was prepared by dissolving it with 5-carboxytetramethylrhodamine (5-TAMRA) dye in deionized water (DI). With the aim to achieve the preparation of strong microcapsules shells that allows a prolonged release, 1,6-hexanediamine was selected as an aqueous monomer, considering its role in providing good mechanical strength in the isolated polymers reported above. Similarly, the diynone monomer was solubilized in DCM and used as an organic phase (so called continuous phase). The aqueous solution was thus added to the continuous phase and then stirred using Silverson mixer at 3000 rpm for 3 hours to generate microcapsules after drying.

In order to remove the remaining unencapsulated dye from the microcapsules' surface, the resultant microcapsules were dialyzed in DI water for 7 days. The particle size and size distribution of the microcapsules were analyzed by dynamic light scattering (DLS). In addition, TGA analysis was employed to determine the thermal stability of the microcapsules (Fig. 4a), and their morphology was observed by scanning electron microscopy (SEM). The release study was conducted by irradiating 15 mg of microcapsules dispersed in DI water for 6 hours and the concentration of the released dye was measured and monitored for 4 weeks (Fig. 4b). However, the major limitation on the use of organic fluorescent dyes is their photostability,[62-64] indeed, 5-TAMRA was chosen because it showed good photostability under 6 hours UV irradiation (Supplementary Fig. S76). The significant weight loss (measured through TGA analysis) was detected in the range of 300−500 ^{o}C, demonstrating these microcapsules have excellent thermal stability, whereas, after photodegradation, the thermal stability is remarkably decreased due to reduced molecular weight.

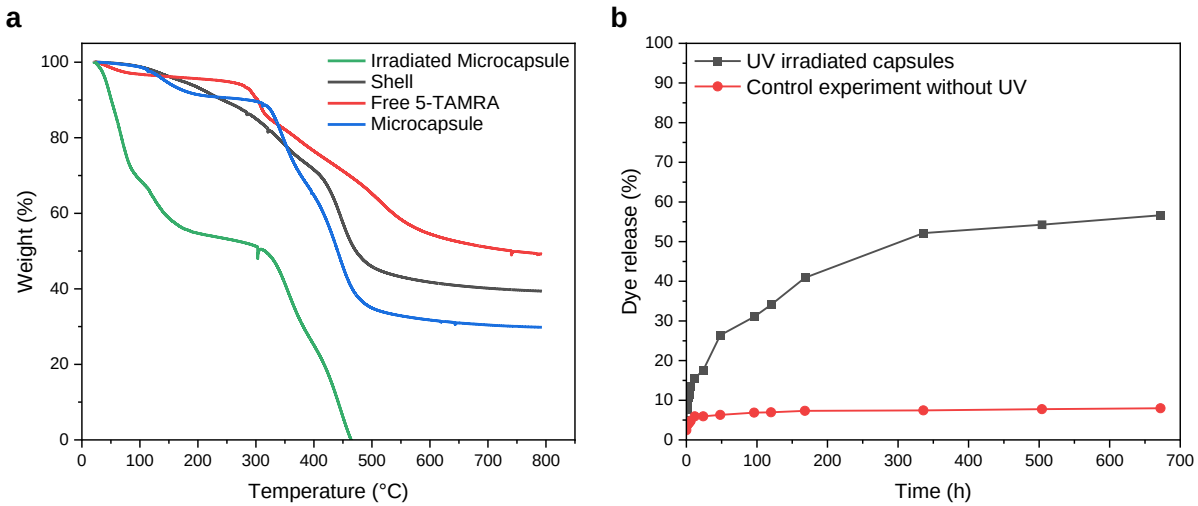

Fig. 4. Thermal and spectroscopic analysis of microcapsule. **a** Thermogravimetric analysis of homopolymers at 10 K·min^{-1}. **b** Measurement of released 5-TAMRA after photodegradation (λ_{max} 550 nm).

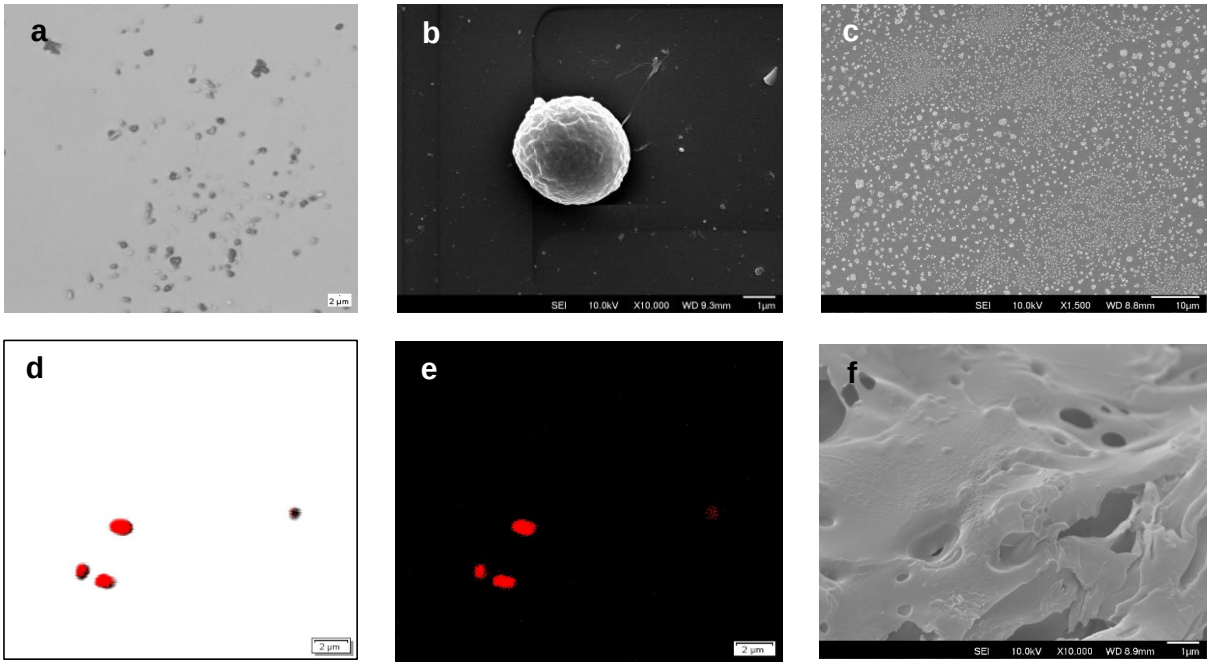

Fig. 5 Morphology characteristics of the microcapsules. a Optical microscopy image. **b** SEM image of single microcapsule before UV irradiation. **c** SEM image of multiple microcapsules before UV irradiation. **d** Confocal fluorescence microscopy bright-field image. **e** Confocal fluorescence microscopy. **f** SEM image after UV irradiation (collapsed state).

Using DLS the microcapsules obtained demonstrate *Z*-average 1.11 µm (1,118 d.nm) and polydispersity index 0.883 (Supplementary Fig. S81). The microencapsulation methodology here used allowed the preparation of microcapsules with defined particle size, dispersity, and morphology.[65] Furthermore, the enhanced shell thickness (microcapsule wall), affected by the mechanical strength of the polymer matrix formed, permitted a prolonged dye release during

and after irradiation.

The concentration of 5-TAMRA released after photolysis was accurately determined and monitored by UV-Vis spectroscopy (Supplementary Fig. S79). The optical microscopy and SEM images indicate that we successfully generate microcapsules with spherical shapes (Fig. 5a-5c), while the dye encapsulation is also confirmed by confocal microscopy images (Fig. 5d & 5e). Based on the photo-release curve supported by SEM images (Fig. 5f), the microcapsules exhibit the collapse of the polymer matrix as a result of rupturing triggered by controlled UV light. Then, the dye was released slowly for 4 weeks. To easily determine the concentration of encapsulated dye, after 4 weeks, the microcapsules were ruptured manually using an ultrasonicator and measured its concentration using UV-Vis spectroscopy.

Discussion. The facile click polymerization *via* spontaneous step-growth polyaddition of diynones and diamines was carried out in the open environment under mild reaction conditions without the presence of external catalysts. Monomers were obtained from renewable feedstocks to generate high molecular weight polyketones with high T_g. The obtained PKs provide a wide range of structure-property-variations and comparable tensile strength to commercial plastics. The chain length, intermolecular forces, and steric bulk relatively affect the thermomechanical properties of the polyketones despite the absence of polyolefin backbone. Synthesized novel polyketones could be alternatives to conventional polyketones and potentially better plastics than polyesters and polycarbonates. Furthermore, these polyketones present a novel degradation pathway that is more selective and does not follow the common Norrish pathway, whereas degrade into small molecules. Spontaneous amino-yne click polymerization also provides a novel strategy to generate photodegradable microcapsules by interfacial click polyaddition. The photo-triggered release exhibited prolonged release of the dye which is beneficial for crop protection in the agriculture sector.

Methods

General. All air sensitive compounds were employed under a dry nitrogen atmosphere using standard Schlenk techniques. All compounds, unless otherwise indicated, were purchased from commercial sources, and used as received. The following chemicals were vacuum distilled prior to use and stored in Young's tapped ampoules under N_2 atmosphere: *N,N'*-dimethyl-1,6-hexanediamine and 2,2' (Ethylenedioxy)bis(ethylamine) (Sigma-Aldrich, ≥ 98%).

All solvents and chemicals used for recrystallisation were used as received. Unless otherwise specified, all chemicals and solvents were obtained from Sigma-Aldrich, VWR Chemicals, Apollo Scientific, or Fisher Scientific and utilized in their original form without additional purification. THF was used directly from a solvent drying and degassing tower. All polymer reactions were precipitated into diethyl ether and dried in vacuo at ambient temperature for 24 h and then at 40 °C overnight (c. a. 16 h). After processing, all samples were annealed for 3 days at room temperature in the vacuum oven before analysis.

Characterization techniques

NMR spectroscopy. NMR spectroscopy experiments were performed at 298 K on a Bruker DPX-400 NMR spectrometer equipped operating at 400 MHz for ^{1}H (100.57 MHz for ^{13}C). All chemical shifts were reported in ppm and were referenced to residual proton solvent (δ = 7.26 for $CDCl_3$), and ^{13}C NMR spectra are referenced to the solvent signal (δ = 77.16 for $CDCl_3$). The multiplicity of the peaks was denoted as s = singlet, d = doublet, t = triplet, q = quadruplet, and m = multiplet.

High Resolution Mass spectrometry (HRMS). HRMS was carried out by the School of Chemistry, University of Birmingham utilizing electrospray ionization on a Waters GCT Premier instrument, as well as employing chemical H^+ ionization on a Waters Xevo G2-XS instrument.

Infrared spectroscopy (FT-IR). FT-IR analysis was conducted using an Agilent Technologies Cary 630 FTIR spectrometer. A total of 16 scans were conducted in the range of 600 to 4000 cm^{-1} with a resolution of 4 cm^{-1}. The obtained spectra were adjusted to account for background absorbance.

Size exclusion chromatography (SEC). SEC measurements were conducted in $CHCl_3$ using an Agilent 1260 Infinity II Multi-Detector GPC/SEC System equipped with RI, ultraviolet (UV = 309 nm), and viscometer detectors. The polymers were eluted using an Agilent guard column (PLGel 5 M, 50 7.5 mm) and two Agilent mixed-C columns (PLGel 5 μM, 300 × 7.5 mm) using $CHCl_3$ (buffer 0.5% NEt_3) as the mobile phase (flow rate = 1 mL min^{-1}, 40 °C). Number average molecular weights (M_n), weight average molecular weights (M_w), and dispersities ($Đ_M = M_w/M_n$) were calculated using Agilent GPC/SEC software (vA.02.01) in comparison to a 15-point calibration curve (M_p = 162–3,187,000 g mol^{-1}) based on poly(styrene) standards (Easivial PS-M/H, Agilent). The weight average molecular weights (M_w) are expressed in Da.

Gas Chromatography-Mass Spectroscopy (GC-MS). GC-MS was performed on a Shimadzu GCMS QP2010 SE system with an HP-5 MS fused silica column (5% phenyl methyl siloxane

30.0m × 250 μm, film thickness 0.25 μm), interfaced with 5675C Inert MSD with Triple-Axis detector. The temperature programming for the separation of the sample was set to 40 °C for 2 min, ramped to 300 °C at 6 °C·min^{-1}, and held for 20 min and ramped to 300 °C at 6 °C·min^{-1}. The injection temperature was 300 °C, with a 1.0 μL injection volume. The helium carrier gas flow rate was set at 1 mL·min^{-1}.

Thermal characterization. Determination of the thermal properties of the polymer were carried out using a STARe system DSC3 with an auto-sampler (Mettler Toledo, Switzerland). Disc shapes measuring 5 mm in diameter and 0.4 − 0.6 mm in thickness and weighing between 9 − 14 mg were cut from annealed polymer films. Thermograms were obtained in 40 μL aluminum pans from 0 to 200 °C at a heating rate of 10 K·min^{-1} for two heating/cooling cycles. The glass transition temperature (T_g) was determined by the minimum of the first derivative in the second heating cycle of DSC. Thermal degradation was quantified using a Q550 Thermogravimetric analyzer (TA instruments). Thermograms were recorded under an N_2 atmosphere at a heating rate of 10 K·min^{-1} from 25 to 800 °C with an average sample weight of around 7 mg. Decomposition temperatures were reported at the 5% weight loss temperature ($T_{d,5\%}$).

Mechanical Testing. All uniaxial tensile tests were conducted on a Testometric M350-5CT tensometer with a 5 kgF load cell for synthesized polymer films and a 50 kgF load cell for commercial polymers. All measurements were conducted at room temperature and 10 mm min^{-1} strain rate. A bespoke ASTM Die D-638 Type V was utilized to manually cut polymer film samples into dumbbell shapes. The sample is approximately 1.8 mm wide and 1.0 mm thick. Three specimens were examined for each sample, and the mean average values of the strain at break, stress at break, strain at yield, stress at yield, toughness, and Young's modulus are presented. The solvent cast method is employed to afford smooth and thin films and annealed for 3 days in the vacuum oven at room temperature.

Bifunctional furyl Weinreb amide synthesis. The procedure was adapted from published sources.[63-64] 2,5-furandicarboxylic acid (FDCA) (10 g, 64 mmol, 1.0 equiv.) were dissolved in dichloromethane (to prepare a 1 M solution), and thionyl chloride (38 mL, 320 mmol, 5 equiv. for bifunctional compound) were added to a 2-neck round-bottom flask equipped with magnetic stirrer and dropping funnel. Then, three drops of dimethylformamide (DMF), were added and the

reaction mixture was cooled down to 0 °C (with an ice bath). *N,O*-dimethylhydroxylamine hydrochloride (13.75 g, 141 mmol, 2.2 equiv.) was added to the reaction mixture while trimethylamine (NEt_3) (26 mL, 2691 mmol, 4.2 equiv.) was progressively added to the reaction mixture (dropwise slowly, over 30 minutes). The reaction produced a white precipitate (ammonium salt by-product). After completed addition of trimethylamine, the reaction mixture was taken from the cooling bath and stirred for one hour at room temperature. The dichloromethane-diluted reaction mixture was then transferred to a separatory funnel and the organic layer was washed with 1 M HCl, followed by saturated $NaHCO_3$ solution and brine. The organic layer was dried ($MgSO_4$), filtered and concentrated under reduced pressure. The crude product was purified by recrystallisation with methanol to give the title compound as a brown solid (13.5 g, 87% yield).

N^2,N^5-dimethoxy-N^2,N^5-dimethylfuran-2,5-dicarboxamide **^{1}H NMR** spectra (400 MHz, $CDCl_3$) δ 7.17 (s, 2H), 3.83 (s, 6H), 3.36 (s, 6H); **^{13}C NMR** (101 MHz, $CDCl_3$) δ 158.49, 146.99, 117.75, 61.67, 33.22. **HRMS** (ESI-TOF) (m/z): $[M + H]^+$ calculated for $C_{10}H_{15}N_2O_5$, 243.0981; found, 243.0987.

Monofunctional Furyl Weinreb Amide Synthesis. The procedure was adapted from published sources.[63-64] 2-furoic acid or benzoic acid (89 mmol, 1.0 equiv.) were dissolved in dichloromethane (to prepare a 1 M solution), and thionyl chloride (27 mL, 223 mmol, 2 equiv.) were added to a 2-neck round-bottom flask equipped with magnetic stirrer and dropping funnel. Then, three drops of dimethylformamide (DMF), were added and the reaction mixture was cooled down to 0 °C (with an ice bath). *N,O*-dimethylhydroxylamine hydrochloride (9.9 g, 98 mmol, 2.2 equiv.) was added to the reaction mixture while trimethylamine (NEt_3) (18 mL, 187 mmol, 4.2 equiv.) was progressively added to the reaction mixture (dropwise slowly, over 30 minutes). The reaction produced a white precipitate (ammonium salt by-product). After completed addition of trimethylamine, the reaction mixture was taken from the cooling bath and stirred for one hour at room temperature. The dichloromethane-diluted reaction mixture was then transferred to a separatory funnel and the organic layer was washed with 1 M HCl (2x100 Ml), followed by saturated $NaHCO_3$ solution (2x100 mL) and brine (2x100 Ml). The organic layer was dried ($MgSO_4$), filtered and concentrated under reduced pressure.

N-methoxy-N-methylfuran-2-carboxamide After drying, the product was obtained as a translucent light-yellow oil (12.2 g, 88% yield) and used in the following reaction step without

further purification. **^{1}H NMR** spectra (400 MHz, $CDCl_3$) δ 7.56 (s, 1H), 7.11 (s, 1H), 6.51 – 6.44 (m, 1H), 3.74 (s, 3H), 3.32 (s, 3H); **^{13}C NMR** (101 MHz, $CDCl_3$) δ=159.12, 145.67, 145.22, 117.36, 111.58, 61.35, 33.15. **HRMS** (ESI-TOF) (m/z): $[M + H]^+$ calculated for $C_7H_9NO_3$, 155.0576; found, 155.0578.

N-methoxy-N-methylbenzamide After drying, the product was obtained as a translucent light-yellow oil (12.7 g, 94% yield) and used in the following reaction step without further purification.**^{1}H NMR** spectra (400 MHz, $CDCl_3$) δ 7.63 – 7.56 (m, 1H), 7.44 – 7.27 (m, 1H), 3.48 (s, 1H), 3.28 (s, 1H); **^{13}C NMR** (101 MHz, CDCl3) δ= 169.97, 134.15, 130.56, 128.14, 128.02, 61.03, 33.80. **HRMS** (ESI-TOF) (m/z): $[M + H]^+$ calculated for $C_8H_6O_2$, 165.0784; found, 165.0786.

Synthesis of diynone monomers. In dried glassware and under Schlenk conditions, 1.0 equiv. of the Weinreb amide was introduced to a 2-neck round-bottom flask and then diluted through cannula transfer with 1 M dry THF. Then, 1-propynylmagnesium bromide solution 0.5 M in THF (2.4 equiv. for bifunctional compound or 1.2 equiv. for monofunctional compounds) was slowly added (over 45 minutes) through cannula to the reaction mixture cooled to 5 °C (with an ice bath). The mixture was kept at room temperature overnight to react. The mixture was subsequently cooled down to 0 °C for approximately 30 minutes and rapidly quenched with 1 M HCl to prevent double addition between amines and ynone. The crude mixture was transferred to a separatory funnel and washed with ethyl acetate and brine. The resulting extracted layer was then dried ($MgSO_4$), filtered and concentrated under reduced pressure.

1,1'-(furan-2,5-diyl)bis(but-2-yn-1-one) The product was purified through recrystallisation in ethanol, affording a brown solid l (3.36 g, 81% yield).**^{1}H NMR** spectra (400 MHz, $CDCl_3$) δ 7.33 (s, 2H), 2.15 (s, 6H); **^{13}C NMR** (101 MHz, $CDCl_3$) δ 165.22, 154.24, 119.54, 93.71, 78.14, 4.32. **HRMS** (ESI-TOF) (*m*/*z*): $[M + H]^+$ calculated for $C_{12}H_9O_3$, 201.0552; found, 201.0560.

1-(furan-2-yl)but-2-yn-1-one The product was purified through column chromatography (2:1 Hex/EtOAc) to afford translucent a light-yellow oil (3.61 g, 84% yield). **^{1}H NMR** spectra (400 MHz, $CDCl_3$) δ 7.61 (dd, *J* = 1.7, 0.8 Hz, 1H), 7.29 (dd, *J* = 3.6, 0.8 Hz, 1H), 6.52 (dd, *J* = 3.6, 1.7 Hz, 1H), 2.08 (s, 3H); **^{13}C NMR** (101 MHz, $CDCl_3$) δ 164.96, 153.15, 147.81, 120.76, 112.54, 91.29, 78.25, 4.25. **HRMS** (ESI-TOF) (*m*/*z*): $[M + H]^+$ calculated for $C_8H_6O_2$, 134.0362; found, 134.0362.

1-phenylbut-2-yn-1-one The product was purified through column chromatography (2:1

Hex/EtOAc) to afford translucent a light-yellow oil (3.78 g, 87% yield). **^{1}H NMR** spectra (400 MHz, $CDCl_3$) δ 8.19 – 8.10 (m, 2H), 7.64 – 7.56 (m, 1H), 7.56 – 7.40 (m, 2H), 2.16 (s, 3H); **^{13}C NMR** (101 MHz, $CDCl_3$) δ 178.25, 136.83, 133.94, 129.60, 128.63, 128.50, 127.01, 92.49, 79.01, 4.36. **HRMS** (ESI-TOF) (*m*/*z*): $[M + H]^+$ calculated for C_8H_6O, 144.0570; found, 144.0572.

Representative polymerization of click polyketones F-C_6A. In a 20 ml glass vial, 1 equiv. of furan-based ynone was dissolved in DCM and stirred for about 1 h in ice bath. Later, diamine (1.0 equiv.) was added and then stirred for 3 h at room temperature. To inhibit crosslinking prior to precipitation, 10% w/w butylated hydroxytoluene (BHT) was added to the reaction mixture. The polymer solution was precipitated into diethyl ether and subsequently reprecipitated to eliminate any traces of BHT. Finally, it was dried in a vacuum oven at 40 °C for 24 h to afford F-C_6A polyketons as a pale-yellow polymer (1.10 g, 96% yield). **^{1}H NMR** spectra (400 MHz, $CDCl_3$) δ 11.27 (s, 2H), 6.98 (s, 2H), 5.70 (s, 2H), 3.32 (q, J = 6.6 Hz, 4H), 2.06 (s, 6H), 1.74 – 1.37 (m, 14H); **^{13}C NMR** (101 MHz, $CDCl_3$) δ 176.60, 165.65, 154.71, 113.49, 91.92, 43.25, 29.71, 26.52, 19.26; **SEC analysis** ($CHCl_3$ + 0.5% NEt_3) M_n = 18,693, M_w = 129,402, $Đ_M$ = 6.92.

Film Preparation. To evaluate the thermomechanical properties of the polymers, the film was made by solvent cast method. The polymer sample (0.5 g) was first dissolved in dichloromethane (2.5 mL) until homogenous. The polymer solution was then filtered using a GPC filter to remove any particulates and transferred to a Teflon beaker. Then, it was left to evaporate for 24 hours. The resultant film was finally dried under a high vacuum at room temperature for 3 days to anneal.

Microcapsule Preparation. In a 20 ml scintillation vial, diynone monomer (0.4 g, 2 mmol, 1 equiv.) was solubilized in 10 mL DCM that would act as an organic phase or continuous phase. 1,6-hexanediamine (0.23 g, 2 mmol, 1 equiv.) and 5-TAMRA dye (0.1 g) were solubilized in 5 mL DI water, this aqueous solution was then mixed with the continuous phase and stirred using Silverson mixer at 3000 rpm for 3 hours. The reaction mixture was also kept for 3 days at room temperature in the closed vial to ensure the dye was maximally encapsulated. Then, the microcapsules were decanted and washed with DI water three times. In order to completely remove the any remaining unencapsulated dye on the microcapsules' surface, the resultant capsules were dialyzed in DI water for 7 days.

Photodegradation Studies. All films and solutions of polyketones were irradiated in the environmental weathering chamber (accelerated weathering test) using Xenon lamp with wavelength 340 nm, BPT 50 °C, and irradiation intensity 50 W/m^2. The timer is set up in that instrument with various time frames. The instrument is calibrated using an irradiation calibrator prior to use and every 1,000 hours of running. The irradiated polymer was then monitored and analyzed by ^{1}H NMR, FTIR, SEC, and GC-MS for analysis of the photodegradation products of the model compounds.

References

1. Park, S. A., Jeon, H., Kim, H., Shin, S. H., Choy, S., Hwang, D. S., Koo, J. M., Jegal, J., Hwang, S. Y., Park, J. & Oh, D. X. Sustainable and recyclable super engineering thermoplastic from biorenewable monomer. *Nat. Commun.* **10**, 2601 (2019).
2. Fenouillot, F., Rousseau, A., Colomines, G., Saint-Loup, R. & Pascault, J. P. Polymers from renewable 1,4:3,6-dianhydrohexitols (isosorbide, isomannide and isoidide): A review. *Prog. Polym. Sci.* **35**, 578–622 (2010).
3. Tsujimoto, T. & Uyama, H. Full biobased polymeric material from plant oil and poly(lactic acid) with a shape memory property. *ACS Sustain. Chem. Eng.* **2**, 2057–2062 (2014).
4. Galbis, J. A., García-Martín, M. D. G., De Paz, M. V. & Galbis, E. Synthetic Polymers from Sugar-Based Monomers. *Chem. Rev.* **116**, 1600–1636 (2016).
5. Isikgor, F. H. & Becer, C. R. Lignocellulosic biomass: a sustainable platform for the production of bio-based chemicals and polymers. *Polym. Chem.* **6**, 4497–4559 (2015).
6. Kamran, M., Davidson, M. G., de Vos, S., Tsanaktsis, V. & Yeniad, B. Synthesis and characterization of polyamides based on 2,5-furandicarboxylic acid as a sustainable building block for engineering plastics. *Polym. Chem.* **13**, 3433–3443 (2022).
7. Li, J., Tu, Y., Lu, H., Li, X., Yang, X. & Tu, Y. Rapid synthesis of sustainable poly(ethylene 2,5-furandicarboxylate)-block-poly(tetramethylene oxide) multiblock copolymers with tailor-made properties via a cascade polymerization route. *Polymer.* **237**, 124313 (2021).
8. Drault, F., Snoussi, Y., Paul, S., Itabaiana, I. & Wojcieszak, R. Recent Advances in Carboxylation of Furoic Acid into 2,5-Furandicarboxylic Acid: Pathways towards Bio-Based Polymers. *ChemSusChem* **13**, 5164–5172 (2020).

9. Sun, L., Zhang, Y., Wang, J., Liu, F., Jia, Z., Liu, X. & Zhu, J. 2,5-Furandicarboxylic acid as a sustainable alternative to isophthalic acid for synthesis of amorphous poly(ethylene terephthalate) copolyester with enhanced performance. *J. Appl. Polym. Sci.* **136**, 1–12 (2019).
10. Terzopoulou, Z., Papadopoulos, L., Zamboulis, A., Papageorgiou, D. G., Papageorgiou, G. Z. & Bikiaris, D. N. Tuning the properties of furandicarboxylic acid-based polyesters with copolymerization: A review. *Polymers.* **12**, 1209 (2020).
11. Bao, F., Song, Y., Liu, Q., Song, C. & Liu, C. Partial bio-based poly (aryl ether ketone) derived from 2 , 5-furandicarboxylic acid with enhanced processability. *Polym. Degrad. Stab.* **161**, 309–318 (2019).
12. Ruhemann, S. The Combination of Mercaptans with Unsaturated Ketonic Compounds. J. Chem. Soc., Trans. **87**, 461−468 (1905).
13. Rosenboom, J. G., Hohl, D. K., Fleckenstein, P., Storti, G. & Morbidelli, M. Bottle-grade polyethylene furanoate from ring-opening polymerisation of cyclic oligomers. *Nat. Commun.* **9**, 1–7 (2018).
14. Hong, S., Min, K. D., Nam, B. U. & Park, O. O. High molecular weight bio furan-based co-polyesters for food packaging applications: Synthesis, characterization and solid-state polymerization. *Green Chem.* **18**, 5142–5150 (2016).
15. Shankar, S. & Shikha. *Renewable and Nonrenewable Energy Resources: Bioenergy and Biofuels*. *Principles and Applications of Environmental Biotechnology for a Sustainable Future* (2017).
16. Amin, D. R., Begum, D. D. A. & Gafur, D. A. Study of Process Parameters for Making Biodegradable Linear Low Density Polyethylene in Natural Weathering Conditions. *IOSR J. Appl. Chem.* **10**, 79–90 (2017).
17. Dodge, H. M., Natinsky, B. S., Jolly, B. J., Zhang, H., Mu, Y., Chapp, S. M., Tran, T. V., Diaconescu, P. L., Do, L. H., Wang, D., Liu, C. & Miller, A. J. M. Polyketones from Carbon Dioxide and Ethylene by Integrating Electrochemical and Organometallic Catalysis. *ACS Catal.* **13**, 4053-4059 (2023).
18. Lommerts, B. J. The influence of catalyst remnants on thermal degradation during melt processing of high melting ethylene-carbon monoxide copolymers. *Polymer.* **42**, 6283–6287 (2001).
19. Chen, S. Y., Pan, R. C., Chen, M., Liu, Y., Chen, C. & Lu, X. B. Synthesis of Nonalternating

Polyketones Using Cationic Diphosphazane Monoxide-Palladium Complexes. *J. Am. Chem. Soc.* **143**, 10743–10750 (2021).

20. Bie, Z., Yao, Z., Jie, S., Hu, J., Pei, L., Li, B. G., Wang, P. & Wang, Z. Activation of a Palladium-Based Catalyst by Hexafluoroisopropanol for Polyketone Synthesis via Homogeneous Solution Polymerization. *Ind. Eng. Chem. Res.* **62**, 867–873 (2023).
21. You, A., Be, M. A. Y. & In, I. Dynamic mechanical profile of polyketone compared to conventional technical plastics Dynamic Mechanical Profile of Polyketone Compared to Conventional Technical Plastics. *AIP Conf. Proc***. 1779**, 070008-1 - 070008-5 (2016).
22. Brubaker, M. M., Coffman, D. D., Hoehn, H. H. Polyketones Synthesis and Characterization of Ethylene/Carbon Monoxide Copolymers, A New Class of Polyketones. **74**, 1509-1515 (1952).
23. Drent, E., Broekhoven, J. A. M. Van & Doyle, M. J. Efficient palladium catalysts for the copolymerization of carbon monoxide with olefins to produce perfectly alternating polyketones. J*ournal of Organomet. Chem.* **417**, 235–251 (1991).
24. Ortmann, P., Wimmer, F. P. & Mecking, S. Long-Spaced Polyketones from ADMET Copolymerizations as Ideal Models for Ethylene/CO Copolymers. *ACS Macro Lett.* **4**, 704–707 (2015).
25. Yang, Y., Li, S. Y., Bao, R. Y., Liu, Z. Y., Yang, M. B., Tan, C. B., Yang, W. Progress in polyketone materials: blends and composites. *Polym. Int.* **67**, 1478–1487 (2018).
26. ASH, Carlton, Edwin, Waters, Dixie, Green, Weinkauf, Donald, H. Polyketone polymer composition. *Eur. Pat. Off.* **99**, 1–10 (2001).
27. Samples, E. M., Schuck, J. M., Joshi, P. B., Willets, K. A. & Dobereiner, G. E. Synthesis and Properties of N-Arylpyrrole-Functionalized Poly(1-hexene- alt-CO). *Macromolecules* **51**, 9323–9332 (2018).
28. Vavasori, A. & Ronchin, L. *Polyketones: Synthesis and Applications*. *Ency of Polymer Sci and Tech,* **1**, 1-41 (2017).
29. Norrish, R., Bamford, C. Photo-decomposition of Aldehydes and Ketones. *Nature* **140**, 195–196 (1937).
30. Kolb, H. C., Finn, M. G. & Sharpless, K. B. Click Chemistry: Diverse Chemical Function from a Few Good Reactions. *Angew. Chemie - Int. Ed.* **40**, 2004–2021 (2001).
31. Qin, A., Lam, J. W. Y. & Tang, B. Z. Click polymerization: Progresses, challenges, and opportunities. *Macromolecules* **43**, 8693–8702 (2010).

32. Qin, A., Jim, C. K. W., Lu, W., Lam, J. W. Y., Häussler, M., Dong, Y., Sung, H. H. Y., Williams, I. D., Wong, G. K. L. & Tang, B. Z. Click polymerization: Facile synthesis of functional poly(aroyltriazole)s by metal-free, regioselective 1,3-dipolar polycycloaddition. *Macromolecules* **40**, 2308–2317 (2007).
33. Qin, A., Lam, J. W. Y. & Tang, B. Z. Click polymerization. *Chem. Soc. Rev.* **39**, 2522–2544 (2010).
34. Shi, Y., Sun, J. Z. & Qin, A. Click polymerization: The aurora of polymer synthetic methodology. *J. Polym. Sci. Part A Polym. Chem.* **55**, 616–621 (2017).
35. Hu, X., Zhao, X., He, B., Zhao, Z., Zheng, Z., Zhang, P., Shi, X., Kwok, R. T. K., Lam, J. W. Y., Qin, A. & Tang, B. Z. A simple approach to bioconjugation at diverse levels: Metal-free click reactions of activated alkynes with native groups of biotargets without prefunctionalization. *Research* **2018**, 3152870 (2018).
36. Yao, B., Hu, T., Zhang, H., Li, J., Sun, J. Z., Qin, A. & Tang, B. Z. Multi-functional hyperbranched poly(vinylene sulfide)s constructed via spontaneous thiol-yne click polymerization. *Macromolecules* **48**, 7782–7791 (2015).
37. Macdougall, L. J., Pérez-Madrigal, M. M., Shaw, J. E., Worch, J. C., Sammon, C., Richardson, S. M. & Dove, A. P. Using Stereochemistry to Control Mechanical Properties in Thiol–Yne Click-Hydrogels. *Angew. Chemie - Int. Ed.* **60**, 25856–25864 (2021).
38. Stubbs, C. J., Khalfa, A. L., Chiaradia, V., Worch, J. C. & Dove, A. P. Intrinsically Re-curable Photopolymers Containing Dynamic Thiol-Michael Bonds. *J. Am. Chem. Soc.* **144**, 11729–11735 (2022).
39. Stubbs, C. J., Worch, J. C., Prydderch, H., Wang, Z., Mathers, R. T., Dobrynin, A. V., Becker, M. L. & Dove, A. P. Sugar-Based Polymers with Stereochemistry-Dependent Degradability and Mechanical Properties. *J. Am. Chem. Soc.* **144**, 1243–1250 (2022).
40. Yao, B., Hu, T., Zhang, H., Li, J., Sun, J. Z., Qin, A. & Tang, B. Z. Multi-functional hyperbranched poly(vinylene sulfide)s constructed via spontaneous thiol-yne click polymerization. *Macromolecules* **48**, 7782–7791 (2015).
41. Chen, X., Bai, T., Hu, R., Song, B., Lu, L., Ling, J., Qin, A. & Tang, B. Z. Aroylacetylene-Based Amino-Yne Click Polymerization toward Nitrogen-Containing Polymers. *Macromolecules* **53**, 2516–2525 (2020).
42. Sheldon, R. A. Metrics of Green Chemistry and Sustainability: Past, Present, and Future. *ACS Sustainable Chem. Eng.* **6**, 32-48 (2018)

43. Kandemir, D., Luleburgaz, S., Gunay, U. S., Kumbaraci, V. & Durmaz, H. Ultrafast Poly(disulfide) Synthesis in the Presence of Organocatalysts. *Macromolecules* **55**, 7806-7816 (2022)
44. Hartley, G. H. & Guillet, J. E. Photochemistry of ketone polymers. I. Studies of ethylene-carbon monoxide copolymers. *Macromolecules* **1**, 165–170 (1968).
45. Norrish, R. & Bamford, C. Photo-decomposition of Aldehydes and Ketones. *Nature*, **140**, 195–196 (1937).
46. He, B., Su, H., Bai, T., Wu, Y., Li, S., Gao, M., Hu, R., Zhao, Z., Qin, A., Ling, J. & Tang, B. Z. Spontaneous Amino-yne Click Polymerization: A Powerful Tool toward Regio- and Stereospecific Poly(β-aminoacrylate)s. *J. Am. Chem. Soc.* **139**, 5437–5443 (2017).
47. Chen, X., Hu, R., Qi, C., Fu, X., Wang, J., He, B., Huang, D., Qin, A. & Tang, B. Z. Ethynylsulfone-based spontaneous amino-yne click polymerization: A facile tool toward regio- and stereoregular dynamic polymers. *Macromolecules* **52**, 4526–4533 (2019).
48. He, B., Zhang, J., Zhang, H., Liu, Z., Zou, H., Hu, R., Qin, A., Kwok, R. T. K., Lam, J. W. Y. & Tang, B. Z. Catalyst-Free Multicomponent Tandem Polymerizations of Alkyne and Amines toward Nontraditional Intrinsic Luminescent Poly(aminomaleimide)s. *Macromolecules* **53**, 3756–3764 (2020).
49. Geng, Z., Shin, J. J., Xi, Y. & Hawker, C. J. Click chemistry strategies for the accelerated synthesis of functional macromolecules. *J. Polym. Sci.* **59**, 963–1042 (2021).
50. Scoponi, M., Pradella, F. & Carassiti, V. Photodegradable polyolefins. Photo-oxidation mechanisms of innovative polyolefin copolymers containing double bonds. *Coord. Chem. Rev.* **125**, 219–230 (1993).
51. Hartley, G. H. & Guillet, J. E. Photochemistry of ketone polymers. II. Studies of model compounds. *Macromolecules* **1**, 413–417 (1968).
52. Milić, M., de María, P. D. & Kara, S. A patent survey on the biotechnological production of 2,5-furandicarboxylic acid (FDCA): Current trends and challenges. *EFB Bioeconomy J.* **3**, 100050 (2023).
53. Wang, X. & Hadjichristidis, N. Steric Hindrance Drives the Boron-Initiated Polymerization of Dienyltriphenylarsonium Ylides to Photoluminescent C5-Polymers. *Angew. Chemie - Int. Ed.* **60**, 22469–22477 (2021).
54. Worch, J. C., Stubbs, C. J., Price, M. J. & Dove, A. P. Click Nucleophilic Conjugate Additions to Activated Alkynes: Exploring Thiol-yne, Amino-yne, and Hydroxyl-yne

Reactions from (Bio)Organic to Polymer Chemistry. *Chem. Rev.* **121**, 6744–6776 (2021).

55. Zhang, J., Zhang, Z. & Wang, J. Zang, G., Sun, J.Z., Tang, B.Z. Polymer Chemistry Recent progress in the applications of amino – yne click chemistry. **1**, 2978–2986 (2021).
56. Bosire, J. O., Kibet, J. K., Cheplogoi, P. K., Rono, N. K., Limo, S. C. & Okumu, T. Molecular Modeling of Furan From the Thermal Degradation of Scrap Tyres. *Int. J. of Bas and App Chem Sci*. **5**, 17–23 (2015).
57. Burton, M. and Chanmugam, J. Reaction of Free Methylene: Photolysis of Ketene in Presence of Other Gases. *J. Chem. Soc.* **78**, 1-11 (1970).
58. Lyu, S. & Untereker, D. Degradability of Polymers for Implantable Biomedical Devices. *Int. J. Mol. Sci*. **10**, 4033-4065 (2009).
59. Montagnon, T., Kalaitzakis, D., Triantafyllakis, M., Stratakis, M. & Vassilikogiannakis, G. Furans and singlet oxygen – why there is more to come from this powerful partnership. *Chem. Commun.* **50**, 15480–15498 (2014).
60. Varni, A. J., Fortney, A., Baker, M. A., Worch, J. C., Qiu, Y., Yaron, D., Bernhard, S., Noonan, K. J. T. & Kowalewski, T. Photostable Helical Polyfurans. *J. Am. Chem. Soc.* **141**, 8858–8867 (2019).
61. Strobel, S. A., Scher, H. B. & Jeoh, T. Surfactant-Free d-Limonene Encapsulation in Spray-Dried Alginate Microcapsules Cross-Linked by In Situ Internal Gelation. *ACS Food Sci. Technol.* **3**, 909-918 (2023).
62. Helmerich, D. A., Beliu, G., Matikonda, S. S., Schnermann, M. J. & Sauer, M. Photoblueing of organic dyes can cause artifacts in super-resolution microscopy. *Nat. Methods* **18**, 253–257 (2021).
63. Dubey, R., Shami, T. C. & Bhasker Rao, K. U. Microencapsulation technology andapplications. *Def. Sci. J.* **59**, 82–95 (2009).
64. Rosenboom, J. G., Hohl, D. K., Fleckenstein, P., Storti, G. & Morbidelli, M. Bottle-grade polyethylene furanoate from ring-opening polymerisation of cyclic oligomers. *Nat. Commun.* **9**, 1–7 (2018).
65. Demchenko, A. P. Photobleaching of organic fluorophores: Quantitative characterization, mechanisms, protection. *Methods Appl. Fluoresc.* **8**, 022001 (2020).

Acknowledgments

A.P.D., A.B., and J.C.W. acknowledge funding from the European Research Council (ERC) under the European Union's Horizon 2020 research and innovation programme under grant agreement no. 681559. N.Y. acknowledges funding from Unilever. L.H.S thanks Indonesian Endowment Fund for Education (LPDP) agency for funding support.

Author contributions

The manuscript was written through the contributions of all authors. All authors have given approval to the final version of the manuscript. L.H.S. performed all monomers and polymers synthesis, microencapsulation, thermomechanical testing, and photodegradation. The SEM imaging and precursor synthesis were conducted by N.Y. Synthetic and mechanical testing guidance were provided by J.C.W. Data analysis was aided by A.B. The project was conceived and led by A.P.D.

Competing interest

The authors declare no conflict of interests.

Correspondence and requests for materials should be addressed to Andrew P. Dove.

3.2 Supporting Information

Supplementary Information

Spontaneous Amino-yne "Click" Polymerization to Generate Photodegradable Bioderived Polyketones with Tunable Thermomechanical Properties

Lukmanul H. Samada,[1] Neha Yadav,[1] Joshua C. Worch,[1,2] Arianna Brandolese,[1] Andrew P. Dove[1]*

[1]School of Chemistry, The University of Birmingham, Edgbaston, Birmingham, B15 2TT, UK.

[2]Department of Chemistry, Virginia Tech, Blacksburg, VA 24061, USA.

*Corresponding to: A.Dove@bham.ac.uk

Synthetic procedures

Overview for the 2-step synthesis of ynone from FDCA

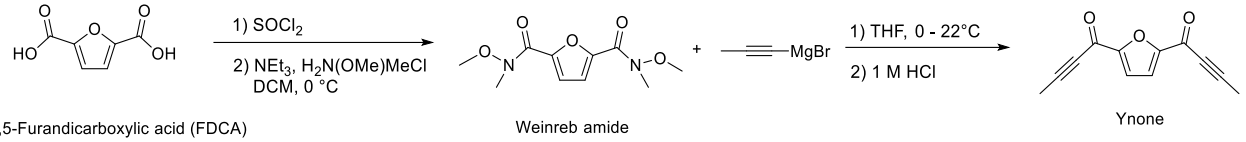

2,5-Furandicarboxylic acid (FDCA) Weinreb amide Ynone

Scheme S1. Synthetic pathway from FDCA to ynone. Adapted from the previous protocol.[1]

Weinreb Amide Synthesis

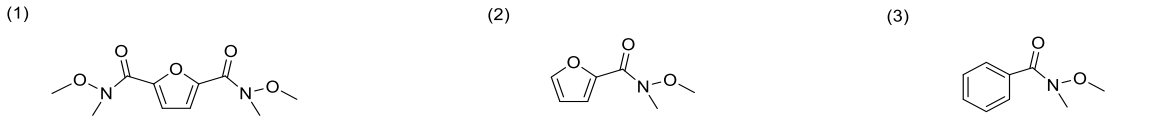

N^2,*N*^{5}-dimethoxy-*N*^{2},*N*^{5}-dimethylfuran-2,5-dicarboxamide *N*-methoxy-*N*-methylfuran-2-carboxamide *N*-methoxy-*N*-methylbenzamide

Synthesis of *N*^{2},*N*^{5}-dimethoxy-*N*^{2},*N*^{5}-dimethylfuran-2,5-dicarboxamide

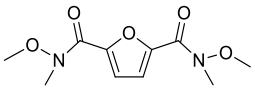

The procedure was adapted from a published source.[2] 2,5-furandicarboxylic acid (FDCA) (10 g, 64 x 10^{-3} mol, 1.0 equiv.) was placed into a 2-neck round bottom flask with a magnetic bar. Thionyl chloride ($SOCl_2$) (38 mL, 320 x 10^{-3} mol, 5.0 equiv.) was added slowly and then 3 drops of dimethylformamide (DMF) were added. An exhaust tube was attached to NaOH bath, and the reaction mixture was then heated at 50 °C and stirred until soluble. The acid chloride solution was cooled down at room temperature and the excess $SOCl_2$ was removed by high vacuum. *N,O*-dimethylhydroxylamine hydrochloride (13.75 g, 141 x 10^{-3} mol, 2.2 equiv.) was added to the reaction mixture while cooling down to 0 °C (in an ice bath). The dropping funnel was used to progressively add trimethylamine (NEt_3) (26 mL, 2691 x 10^{-3} mol, 4.2 equiv.) to the reaction mixture (dropwise slowly, over 30 minutes). The reaction produces a white precipitate (ammonium salt by-product) and is exothermic. After adding NEt_3, the reaction mixture was taken out from the cooling bath and left for one hour at room temperature. The reaction mixture was diluted with DCM, and then transferred to a separatory funnel. The organic layer was washed with 1 M HCl (2x100 mL), followed by saturated $NaHCO_3$ solution (2x100 mL) and brine (2x100 mL). The organic layer was concentrated using a rotary evaporator after being dried with $MgSO_4$. The reaction mixture was further purified by recrystallization with methanol to

afford brown solid **1** (13.5 g, 87% yield). *N^2,N^5-dimethoxy-N^2,N^5-dimethylfuran-2,5-dicarboxamide* **^{1}H NMR** (400 MHz, Chloroform-*d*) δ 7.17 (s, 2H), 3.83 (s, 6H), 3.36 (s, 6H); **^{13}C NMR** (101 MHz, Chloroform-*d*) δ 158.49, 146.99, 117.75, 61.67, 33.22. **HRMS** (ESI-TOF) (*m*/*z*): $[M + H]^+$ calculated for $C_{10}H_{15}N_2O_5$, 243.0981; found, 243.0987.

Synthesis of *N*-methoxy-*N*-methylfuran-2-carboxamide

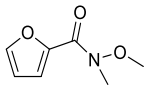

1.0 equiv. of 2-furoic acid (10 g, 89 x 10^{-3} mol) was placed into a 2-neck round bottom flask with a magnetic bar. Thionyl chloride (27 mL, 223 x 10^{-3} mol, 2.5 equiv.) was added slowly and then 3 drops of dimethylformamide (DMF) were added. An exhaust tube was attached to the NaOH bath, and the reaction mixture was then heated at 50 °C and stirred until soluble. The acid chloride solution was cold down at room temperature and the excess $SOCl_2$ was removed by vacuum. *N,O*-dimethylhydroxylamine hydrochloride (9.9 g, 98 x 10^{-3} mol, 1.1 equiv.) added to the reaction mixture while cooled down to 0 °C (in an ice bath). The dropping funnel was used to progressively add trimethylamine (NEt_3) (18 mL, 187 x 10^{-3} mol, 2.1 equiv.) to the reaction mixture (dropwise slowly, over 30 minutes). The reaction produces a white precipitate (ammonium salt by-product) and is exothermic. After adding NEt_3, the reaction mixture was taken from the cooling bath and left for one hour at room temperature. The reaction mixture was diluted with DCM (100 mL), then transferred to a separatory funnel. The organic layer was washed with 1 M HCl (2x100 mL), followed by saturated $NaHCO_3$ solution (2x100 mL) and brine (2x100 mL). The organic layer was concentrated using a rotary evaporator after being dried with $MgSO_4$. The reaction mixture was further dried *in vacuo* at room temperature for 24 h to afford translucent light-yellow oil **2** (12.2 g, 88% yield). *N-methoxy-N-methylfuran-2-carboxamide* **^{1}H NMR** (400 MHz, Chloroform-*d*) δ 7.56 (s, 1H), 7.12 (s, 1H), 6.48 (s, 1H), 3.74 (s, 3H), 3.32 (s, 3H); **^{13}C NMR** (101 MHz, Chloroform-*d*) δ 159.12, 145.67, 145.22, 117.36, 111.58, 61.35, 33.15. **HRMS** (ESI-TOF) (*m*/*z*): $[M + H]^+$ calculated for $C_7H_9NO_3$, 155.0576; found, 155.0578.

Synthesis of *N*-methoxy-*N*-methylbenzamide

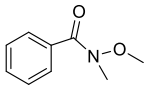

Benzoic acid (10 g, 82 x 10^{-3} mol, 1.0 equiv.) was placed into a 2-neck round bottom flask with a magnetic bar. Thionyl chloride (24 mL, 205 x 10^{-3} mol, 2.5 equiv.) was added slowly and then 3 drops of dimethylformamide (DMF) were added. An exhaust tube was attached to NaOH bath, and the reaction mixture was then heated at 50 °C and stirred until soluble. The acid chloride solution was cold down at room temperature and the excess $SOCl_2$ was removed by vacuum. *N,O*-dimethylhydroxylamine hydrochloride (9.1 g, 90 x 10^{-3} mol, 1.1 equiv.) added to the reaction mixture while cooled down to 0 °C (in an ice bath). The dropping funnel was used to progressively add trimethylamine (NEt_3) (17 mL, 172 x 10^{-3} mol, 2.1 equiv.) to the reaction mixture (dropwise slowly, over 30 minutes). The reaction produces a white precipitate (ammonium salt by-product) and is exothermic. After adding NEt_3, the reaction mixture was taken from the cooling bath and left for one hour at room temperature. The reaction mixture was diluted with DCM (300 mL), then transferred to a separatory funnel. The organic layer was washed with 1 M HCl (2x100 mL), followed by saturated $NaHCO_3$ solution (2x100 mL) and brine (2x100 mL). The organic layer was concentrated using a rotary evaporator after being dried with $MgSO_4$. The reaction mixture was further dried *in vacuo* at room temperature for 24 h to afford translucent light-yellow oil **3** (12.7 g, 94% yield). *N-methoxy-N-methylbenzamide* **^{1}H NMR** (400 MHz, Chloroform-*d*) δ 7.61 – 7.58 (m, 2H), 7.40 – 7.30 (m, 3H), 3.48 (s, 3H), 3.28 (s, 3H); **^{13}C NMR** (101 MHz, Chloroform-*d*) δ 169.97, 134.15, 130.56, 128.14, 128.02, 61.03, 33.80. **HRMS** (ESI-TOF) (*m*/*z*): $[M + H]^+$ calculated for $C_8H_6O_2$, 165.0784; found, 165.0786.

Ynone Synthesis

(4)

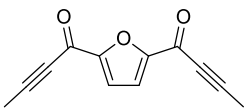

1,1'-(furan-2,5-diyl)bis(but-2-yn-1-one)

(5)

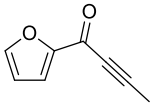

1-(furan-2-yl)but-2-yn-1-one

(6)

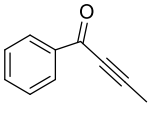

1-phenylbut-2-yn-1-one

Synthesis of 1,1'-(furan-2,5-diyl)bis(but-2-yn-1-one)

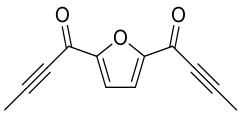

In dried glassware and under Schlenk condition, the furyl Weinreb amide (5 g, 21 x 10^{-3} mol, 1.0 equiv.) was introduced to a 2-neck round-bottom flask. It was then diluted through cannula transfer with 250 mL dry THF. Then, 1-propynylmagnesium bromide solution 0.5 M in THF (99 mL, 50 x 10^{-3} mol, 2.4 equiv.) was introduced by cannula into the Weinreb amide solution, and the solution was cooled down to 0 °C (in an ice bath). After that, the 1-propynylmagnesium bromide solution was added slowly (over 45 minutes) to the reaction mixture while stirring in the ice bath. The mixture was then kept at room temperature overnight to react. The mixture was subsequently cooled down to 0 °C again for approximately 30 minutes. After the reaction mixture has been cooled down, it was rapidly quenched with 1 M HCl solution (100 mL). The crude mixture is transferred to a separatory funnel and washed with ethyl acetate (2x100 mL) and brine (2x100 mL). The resulting extracted layer was then filtered and dried with magnesium sulphate. The organic solution was finally concentrated with a rotary evaporator. To purify the reaction mixture, ethanol recrystallisation was further used to afford brown solid **4** (3.36 g, 81%). *1,1'-(furan-2,5-diyl)bis(but-2-yn-1-one)* **^{1}H NMR** (400 MHz, Chloroform-*d*) δ 7.33 (s, 2H), 2.15 (s, 6H); **^{13}C NMR** (101 MHz, Chloroform-*d*) δ 165.22, 154.24, 119.54, 93.71, 78.14, 4.32. **HRMS** (ESI-TOF) (*m*/*z*): $[M + H]^+$ calculated for $C_{12}H_9O_3$, 200.0479; found, 200.0476.

Synthesis of 1-(furan-2-yl)but-2-yn-1-one

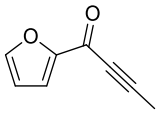

In dried glassware and under Schlenk conditions, the monofunctional furyl Weinreb amide **2** (5 g, 32 x 10^{-3} mol, 1.0 equiv.) is introduced to a 2-neck round-bottom flask. It was then diluted through cannula transfer with 250 mL dry THF. Then, 1-propynylmagnesium bromide solution 0.5 M in THF (77 mL, 39 x 10^{-3} mol, 1.2 equiv.) was introduced by cannula into the Weinreb solution, and the solution was cooled to 0 °C (in an ice bath). After that, the 1-propynylmagnesium bromide solution was added slowly (over 45 minutes) to the reaction mixture while stirring in the ice bath. The mixture was then kept at room temperature overnight to react. The mixture was subsequently cooled down to 0 °C again

for approximately 30 minutes. After the reaction mixture had been cooled down, it was rapidly quenched with 1 M HCl (100 mL). The crude mixture was transferred to a separatory funnel and washed with ethyl acetate (2x100 mL) and brine (2x100 mL). The resulting extracted layer was then filtered and dried with magnesium sulphate. The organic solution was finally concentrated with a rotary evaporator. The resultant reaction mixture was further purified using column chromatography to afford translucent light-yellow oil **5** (3.61 g, 84% yield)**.** R_f (2:1 Hex/EtOAc). *1-(furan-2-yl)but-2-yn-1-one* **^{1}H NMR** (400 MHz, Chloroform-*d*) δ 7.61 (s, 1H), 7.29 (s, 1H), 6.53 (s, 1H), 2.08 (s, 3H); **^{13}C NMR** (101 MHz, Chloroform-*d*) δ 164.96, 153.15, 147.81, 120.76, 112.54, 91.29, 78.25, 4.25. **HRMS** (ESI-TOF) (*m*/*z*): $[M + H]^+$ calculated for $C_8H_6O_2$, 134.0362; found, 134.0362.

Synthesis of 1-phenylbut-2-yn-1-one

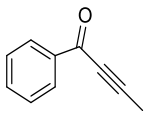

In dried glassware and under Schlenk conditions, the monofunctional furyl Weinreb amide **3** (5 g, 30 x 10^{-3} mol, 1.0 equiv.) was introduced to a 2-neck round-bottom flask. It was then diluted through cannula transfer with 250 mL dry THF. Then, 1-propynylmagnesium bromide solution 0.5 M in THF (73 mL, 36 x 10^{-3} mol, 2.4 equiv.) was introduced by cannula into the Weinreb solution, and the solution was cooled to 0 °C (in an ice bath). After that, the 1-propynylmagnesium bromide solution was added slowly (over 45 minutes) to the reaction mixture while stirring in the ice bath. The mixture was then kept at room temperature overnight to react. The mixture was subsequently cooled down to 0 °C again for approximately 30 minutes. After the reaction mixture has been cooled down, it was rapidly quenched with 1 M HCl (100 mL). The crude mixture was transferred to a separatory funnel and washed with ethyl acetate (2x100 mL) and brine (2x100 mL). The resulting extracted layer was then filtered and dried with magnesium sulphate. The organic solution was finally concentrated with a rotary evaporator. The resultant reaction mixture was further purified using column chromatography to afford translucent light-yellow oil **6** (3.78 g, 87% yield)**.** R_f (2:1 Hex/EtOAc). *1-phenylbut-2-yn-1-one* **^{1}H NMR** (400 MHz, Chloroform-*d*) δ 8.16 – 8.13 (m, 2H), 7.62 – 7.58 (m, 1H), 7.52 – 7.43 (m, 2H), 2.16 (s, 3H); **^{13}C NMR** (101 MHz, Chloroform-*d*) δ 178.25, 136.83, 133.94, 129.60, 128.63, 128.50, 92.49, 79.01, 4.36. **HRMS** (ESI-TOF) (*m*/*z*): $[M + H]^+$ calculated for C_8H_6O, 144.0570; found, 144.0572.

General Procedure for Amino-yne "Click" Polymerization

An example of amino-yne step-growth "click" polymerization is as follows: In a 20 ml scintillation vial, furyl diynone monomer **4** (0.5 g, 2.5 x 10^{-3} mol, 1.0 equiv.) was dissolved in DCM (2 mL), then stirred for about 1 h to homogenize it. During the diynone solution was cooled down to 0 °C in the ice bath, 1,6-hexanediamine (0.29 g, 2.5 x 10^{-3} mol, 1.0 equiv.) was dissolved and fully washed with DCM (3 mL), then transferred to the diynone solution. Then, it was stirred for 3 h at room temperature resulting in a viscous solution. To inhibit crosslinking prior to precipitation, butylated hydroxytoluene (BHT) 10% w/w was added to the reaction mixture. The polymer solution was precipitated into diethyl ether (250 mL) and collected by decanting the supernatant. The resultant polymer was then subsequently redissolved in DCM (10 mL) and reprecipitated in diethyl ether (250 mL) to eliminate any leftover BHT, collected by decanting the supernatant. Finally, the polymer was dried *in vacuo* at room temperature for 24 h, and then under high vacuum at 40 °C for 24 h to yield pale yellow polymer.

1) Polymer F-C_6A_2

Scheme S2. Synthetic pathway of F-C_6A_2 from furyl diynone and *N,N'*-dimethyl-1,6-hexanediamine

The polymer was obtained as a pale yellow solid. **^{1}H NMR** (400 MHz, Chloroform-*d*) δ 7.11 (s, 0H, *cis*), 6.98 (s, 2H, *trans*), 5.95 (s, 0H, *cis*), 5.77 (s, 2H, *trans*), 3.34 (dt, *J* = 13.4, 10.1 Hz, 4H), 3.07 (s, 0H, *cis*), 3.01 (s, 6H, *trans*), 2.66 (s, 0H, *cis*), 2.63 (s, 6H, *trans*), 1.55 (d, *J* = 25.9 Hz, 4H), 1.34 (s, 4H); **^{13}C NMR** (101 MHz, Chloroform-*d*) δ 176.60, 164.39$_{cis}$, 163.54$_{trans}$, 156.10, 114.51$_{cis}$, 113.99$_{trans}$, 91.28$_{cis}$, 90.18$_{trans}$, 53.73, 51.95, 38.52, 37.83, 26.62, 26.12, 24.07, 16.82$_{cis}$, 16.38$_{trans}$; **SEC analysis** ($CHCl_3$ + 0.5% NEt_3) M_n = 11,522, M_w = 42,877 Da, $Đ_M$ = 3.72. (1.25 g, 97% yield).

2) Polymer F-C$_6$A

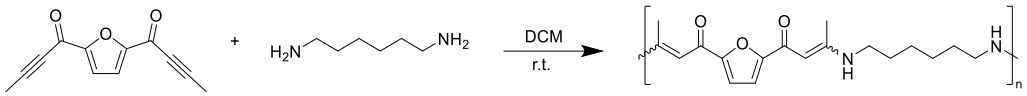

Scheme S3. Synthetic pathway of F-C$_6$A from furyl diynone and 1,6-hexanediamine

The polymer was obtained as a pale yellow solid. **^{1}H NMR** (400 MHz, Chloroform-*d*) δ 11.27 (s, 2H), 6.98 (s, 2H), 5.70 (s, 2H), 3.32 (q, *J* = 6.5 Hz, 4H), 2.06 (s, 6H), 1.67 – 1.64 (m, 4H, overlaps with H_2O), 1.46 (td, *J* = 8.4, 8.0, 4.2 Hz, 4H); **^{13}C NMR** (101 MHz, Chloroform-*d*) δ 176.60, 165.65, 154.71, 113.49, 91.92, 43.25, 29.71, 26.52, 19.26; **SEC analysis** ($CHCl_3$ + 0.5% NEt_3) M_n = 18,693, M_w = 129,402 Da, $Đ_M$ = 6.92. (1.10 g, 96% yield).

3) Polymer F-C$_6$A$_{EG}$

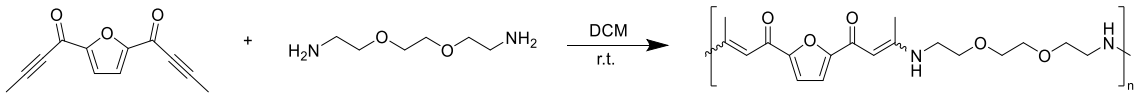

Scheme S4. Synthetic pathway of F-C$_6$A$_{EG}$ from furyl diynone and 2,2'(ethylenedioxy)bis(ethylamine)

The polymer was obtained as a light yellow solid. **^{1}H NMR** (400 MHz, Chloroform-*d*) δ 11.26 (s, 2H), 6.99 (s, 0.5H, *trans*), 6.98 (s, 1.5H, *cis*), 5.74 (s, 0.5H, *trans*), 5.70 (s, 1.5H, *cis*), 3.67 – 3.63 (m, 8H), 3.49 (q, *J* = 5.6 Hz, 4H), 2.05 (s, 4.5H, *cis*), 2.02 (s, 1.5H, *trans*); **^{13}C NMR** (101 MHz, Chloroform-*d*) δ 176.66, 165.76, 154.73, 113.54, 92.15, 70.87, 70.18, 65.88, 43.42, 19.45, 15.29; **SEC analysis** ($CHCl_3$ + 0.5% NEt_3) M_n = 16,582, M_w = 88,549 Da, $Đ_M$ = 5.34. (1.27 g, 97% yield).

4) Polymer F-C$_8$A

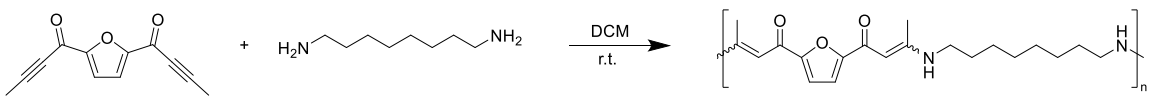

Scheme S5. Synthetic pathway of F-C$_8$A from furyl diynone and 1,8-octanediamine

The polymer was obtained as a brown solid. ^{1}H NMR (400 MHz, Chloroform-*d*) δ 11.26 (s, 2H), 6.98 (s, 2H), 5.70 (s, 2H), 3.31 (q, *J* = 6.7 Hz, 4H), 2.06 (s, 6H), 1.65 – 1.61 (m, 4H, overlaps with H_2O), 1.35 (q, *J* = 13.8, 10.6 Hz, 8H); **^{13}C NMR** (101 MHz,

Chloroform-*d*) δ 176.54, 165.63, 154.72, 113.45, 91.82, 43.41, 29.85, 29.09, 26.78, 19.28; **SEC analysis** ($CHCl_3$ + 0.5% NEt_3) M_n = 13,441, M_w =83,124 Da, $Đ_M$= 6.18. (1.24 g, 96% yield).

5) Polymer F-C_{10}A

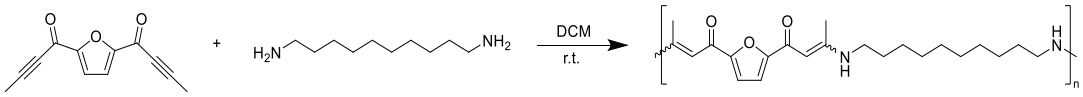

Scheme S6. Synthetic pathway of F-C_{10}A from furyl diynone and 1,10-decanediamine

The polymer was obtained as a pale yellow solid. **^{1}H NMR** (400 MHz, Chloroform-*d*) δ 11.26 (s, 2H), 6.98 (s, 2H), 5.70 (s, 1H), 3.31 (q, *J* = 6.7 Hz, 4H), 2.06 (s, 7H), 1.61 (d, *J* = 15.0 Hz, 4H, overlaps with H_2O), 1.42 – 1.29 (m, 12H, overlaps with H_2O); **^{13}C NMR** (101 MHz, Chloroform-*d*) δ 176.53, 165.60, 154.73, 113.44, 91.78, 43.47, 29.91, 29.35, 29.24, 26.85, 19.28; **SEC analysis** ($CHCl_3$ + 0.5% NEt_3) M_n = 15,009, M_w =76,095 Da $Đ_M$= 5.07. (1.38 g, 96% yield).

6) Polymer F-C_{12}A

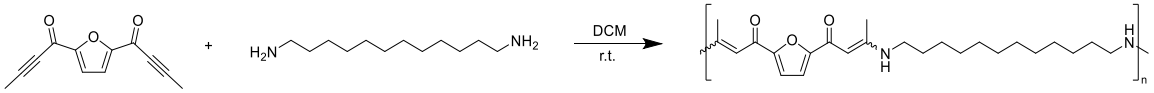

Scheme S7. Synthetic pathway of F-C_{12}A from furyl diynone and 1,12-dodecanediamine

The polymer was obtained as a pale yellow solid. **^{1}H NMR** (400 MHz, Chloroform-*d*) δ 11.26 (s, 2H), 6.98 (s, 2H), 5.70 (s, 2H), 3.31 (q, *J* = 6.7 Hz, 4H), 2.06 (s, 6H), 1.57 (t, *J* = 7.5 Hz, 4H, overlaps with H_2O), 1.40 – 1.27 (m, 16H, overlaps with H_2O); **^{13}C NMR** (101 MHz, Chloroform-*d*) δ 176.53, 165.59, 154.73, 113.43, 91.77, 43.48, 29.94, 29.53, 29.43, 29.29, 26.88, 19.28; **SEC analysis** ($CHCl_3$ + 0.5% NEt_3) M_n = 18,245 Da, M_w =163,684 Da, $Đ_M$= 8.97. (1.50 g, 95% yield).

Model Compounds Synthesis

1) Model F-C_6A

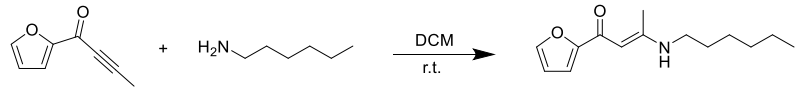

Scheme S8. Synthetic pathway of model F-C_6A from furan ynone and hexylamine

In a 20 ml scintillation vial, 1 equiv. of furan ynone 5 (0.3 g, 2.24 x 10^{-3} mol) was dissolved in DCM (5 mL), and then stirred for about 1 h to homogenize it. While the ynone solution was cooled to 0 °C in the ice bath, the 1 equiv. of hexylamine (0.226 g, 2.24 x 10^{-3} mol) was added and then stirred for 3 h at room temperature resulting in a viscous solution. The reaction mixture was dried *in vacuo* at room temperature for 24 h to yield yellow oil (0.47 g, 89%). *(E)-1-(furan-2-yl)-3-(hexylamino)but-2-en-1-one* **^{1}H NMR** (400 MHz, Chloroform-*d*) δ 11.15 (s, 1H), 7.62 (dd, J = 1.7, 0.8 Hz, 0.5H, *trans*), 7.42 (dd, J = 1.8, 0.8 Hz, 0.5H, *cis*), 7.30 (dd, J = 3.6, 0.8 Hz, 0.5H, *trans*), 6.94 (dd, J = 3.4, 0.9 Hz, 0.5H, *cis*), 6.54 (dd, J = 3.6, 1.7 Hz, 0.5H, *trans*), 6.43 (dd, J = 3.5, 1.8 Hz, 0.5H, *cis*), 5.58 (s, 1H), 3.27 (t, 2H), 2.10 (s, 0.5H, *trans*), 2.03 (s, 2.5H, *cis*), 1.61 (tt, J = 7.6, 6.5 Hz, 2H), 1.42 – 1.27 (m, 6H), 0.88 (t, 3H); **^{13}C NMR** (101 MHz, Chloroform-*d*) δ 177.01, 165.15, 154.57, 147.77, 143.66, 111.79, 91.21, 43.38, 31.48, 29.95, 26.54, 22.51, 19.29, 14.02. HRMS (ESI-TOF) (m/z): $[M + H]^+$ calculated for $C_8H_6O_2$, 235.1567; found, 235.1570.

2) Model Phenyl-C_6A

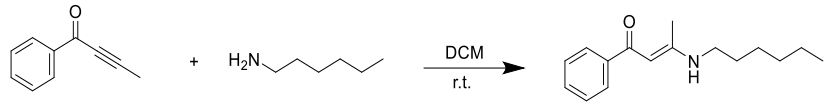

Scheme S9. Synthetic pathway of model Ph-C_6A from phenyl ynone and hexylamine

In a 20 ml scintillation vial, 1 equiv. of furyl ynone **6** (0.3 g, 2.08 x 10^{-3} mol) was dissolved in DCM (5 mL), then stirred for 1 h to homogenize. During the ynone solution was cooled down to 0 °C, the 1 equiv. of hexylamine (0.21 g, 2.08 x 10^{-3} mol) is added and then stirred for 3 h at room temperature resulting in a viscous solution. The reaction mixture was dried *in vacuo* at room temperature for 24 h to yield yellow oil (0.34 g, 96%). *(E)-3-(hexylamino)-*

1-phenylbut-2-en-1-one **^{1}H NMR** (400 MHz, Chloroform-*d*) δ 11.45 (s, 1H), 7.89 – 7.84 (m, 2H overlapping), 7.42 – 7.36 (m, 3H overlapping), 5.66 (s, 1H), 3.31 (t, 2H), 2.07 (s, 3H), 1.65 (tt, *J* = 7.7, 6.5 Hz, 2H), 1.46 – 1.29 (m, 6H, overlaps with H_2O), 0.90 (t, 3H); **^{13}C NMR** (101 MHz, Chloroform-*d*) δ 187.52, 164.90, 140.54, 128.13, 126.85, 91.88, 43.39, 31.50, 30.06, 26.62, 22.53, 19.43, 14.04. **HRMS** (ESI-TOF) (*m*/*z*): $[M + H]^+$ calculated for $C_{16}H_{23}NO$, 245.1774; found, 245.1775.

NMR Spectra

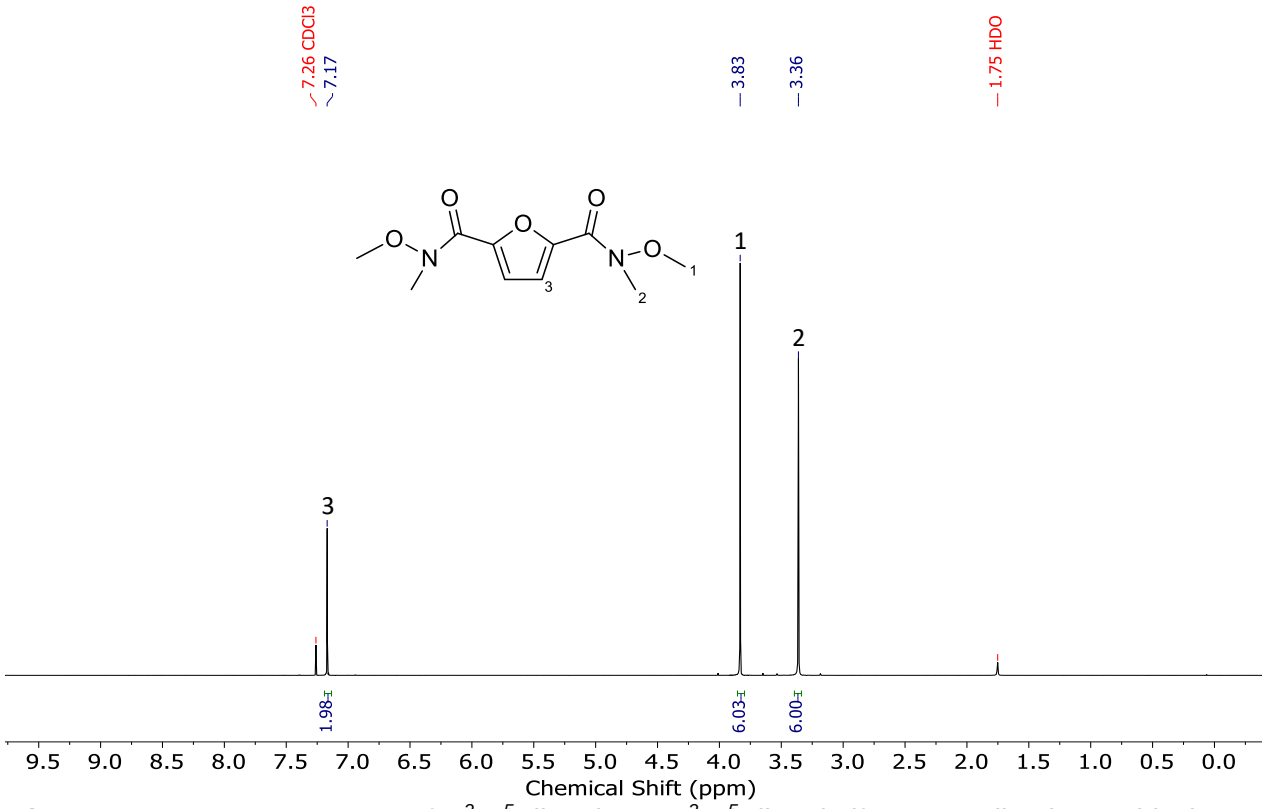

Figure S1. 1H NMR spectrum of N^2,N^5-dimethoxy-N^2,N^5-dimethylfuran-2,5-dicarboxamide (400 MHz, Chloroform-*d*)

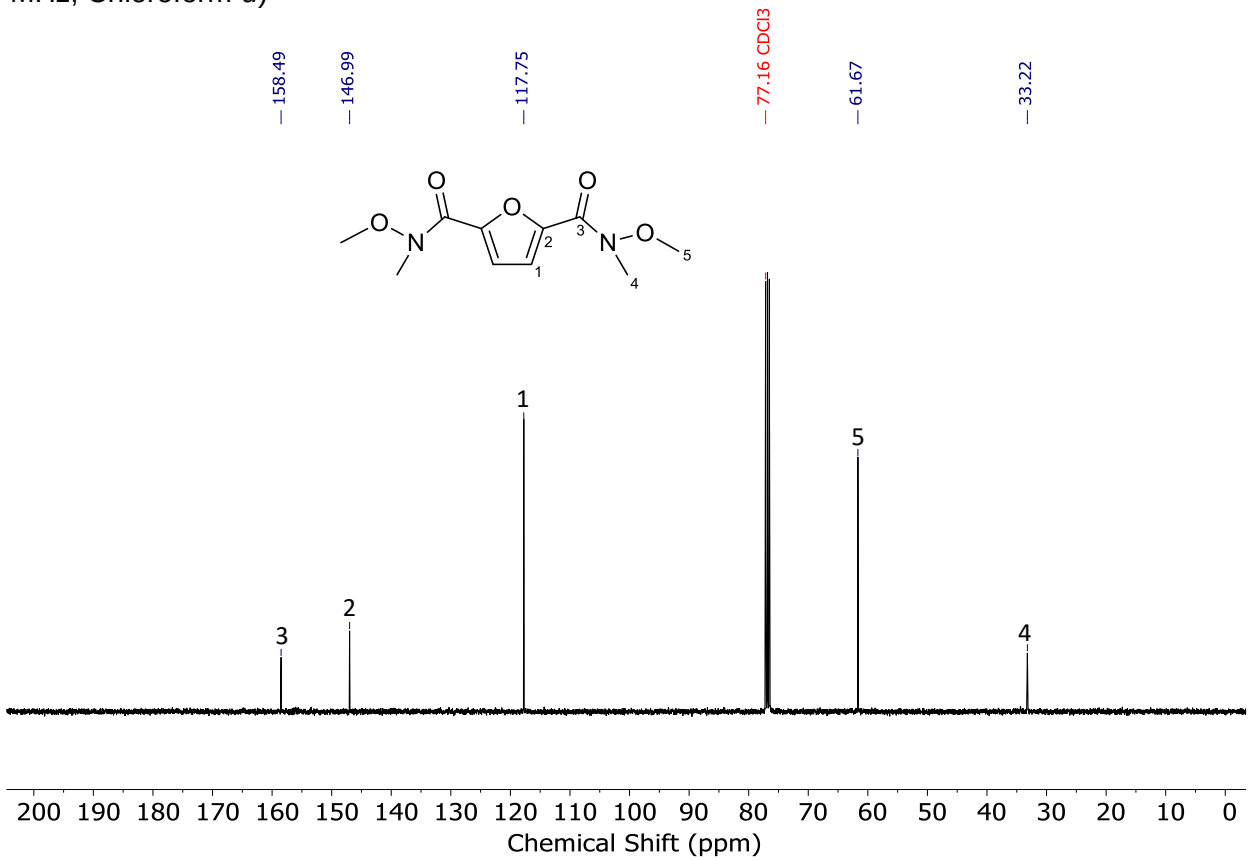

Figure S2. ^{13}C NMR spectrum of N^2,N^5-dimethoxy-N^2,N^5-dimethylfuran-2,5-dicarboxamide (101 MHz, Chloroform-*d*)

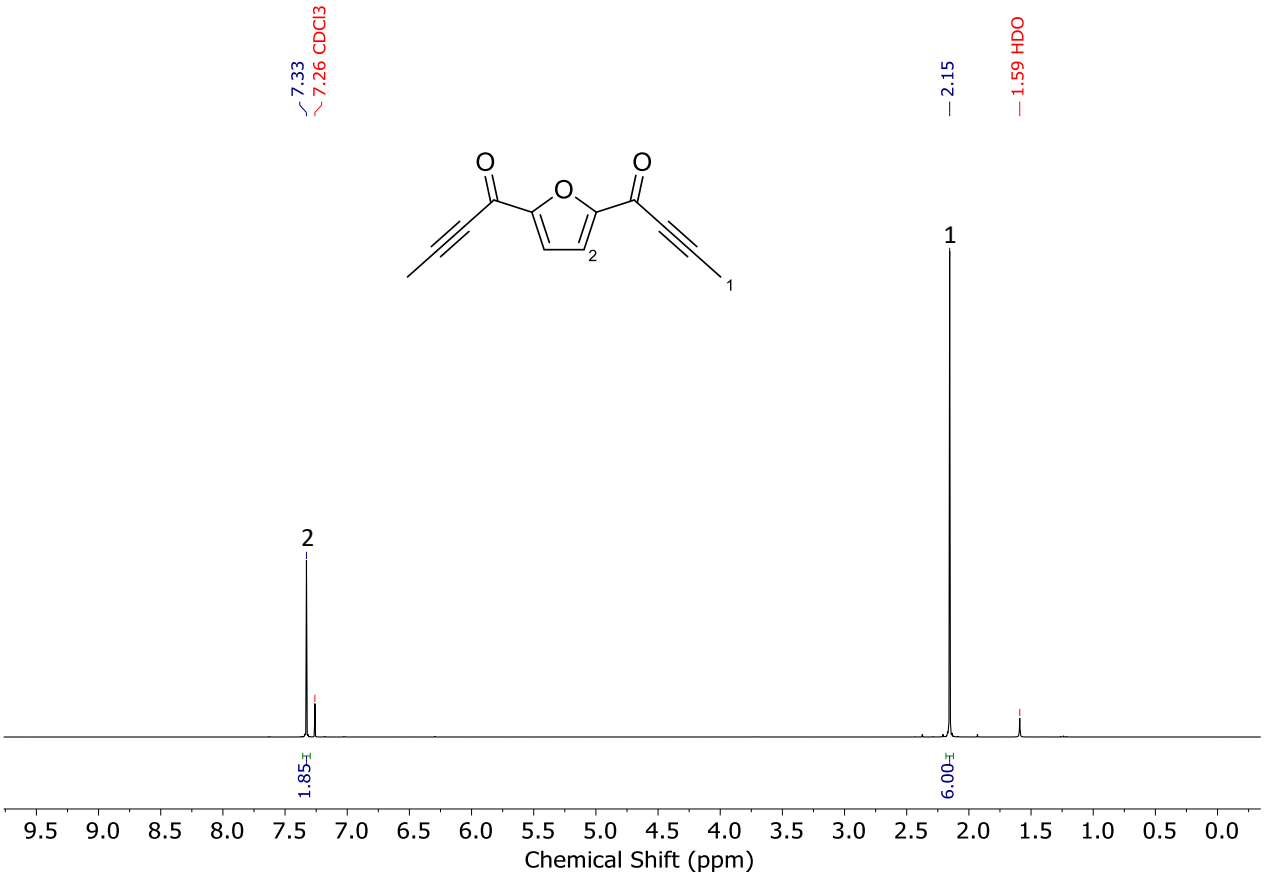

Figure S3. ^{1}H NMR spectrum of 1,1'-(furan-2,5-diyl)bis(but-2-yn-1-one) (400 MHz, Chloroform-*d*)

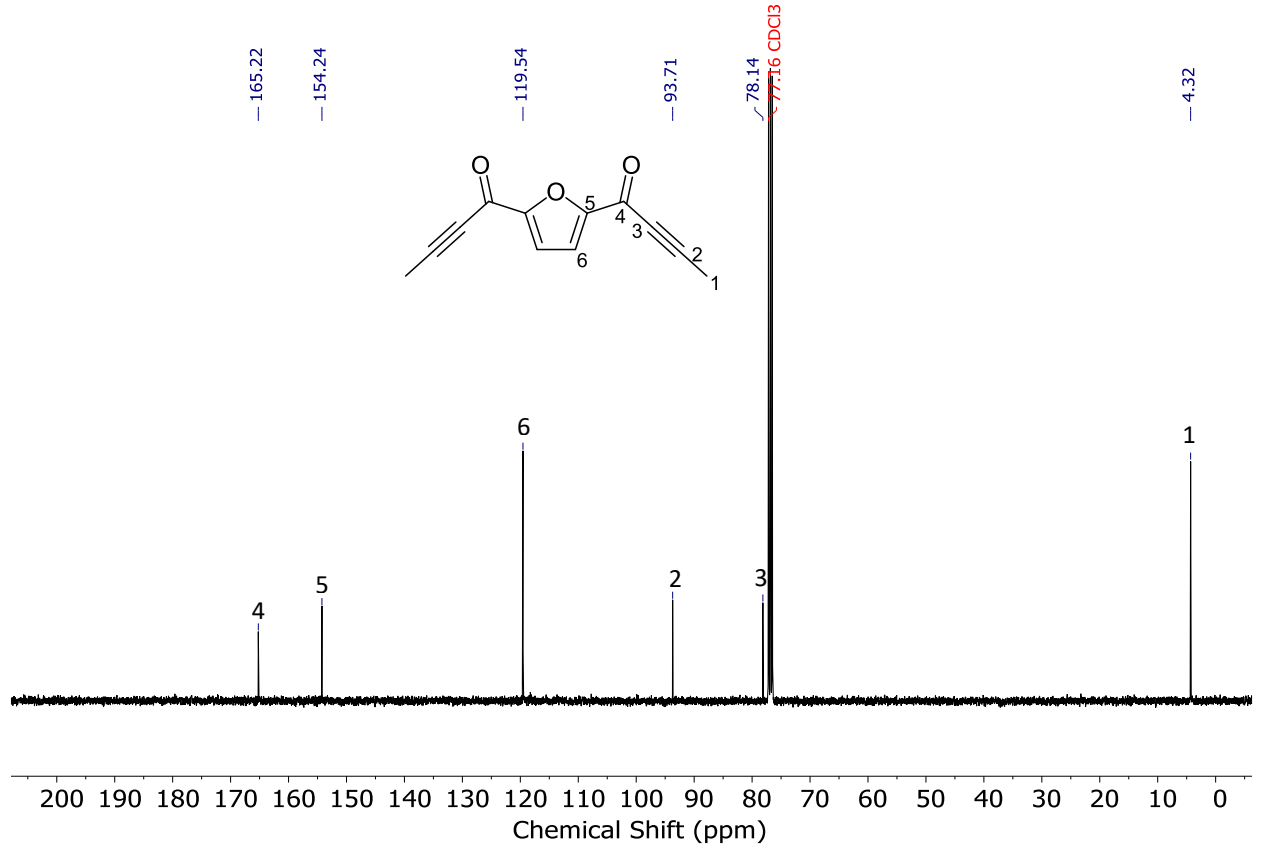

Figure S4. ^{13}C NMR spectrum of 1,1'-(furan-2,5-diyl)bis(but-2-yn-1-one) (101 MHz, Chloroform-*d*)

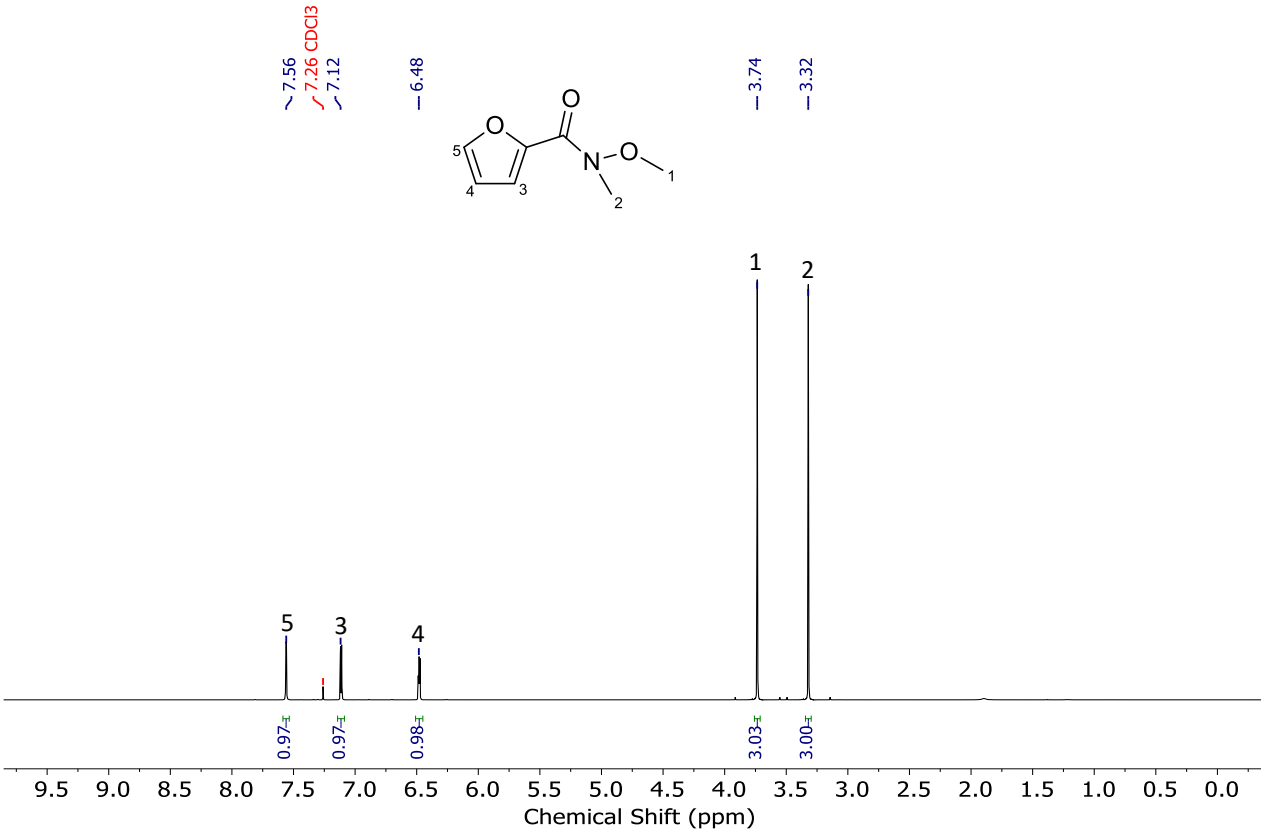

Figure S5. ^{1}H NMR spectrum of *N*-methoxy-*N*-methylfuran-2-carboxamide (400 MHz, Chloroform-*d*)

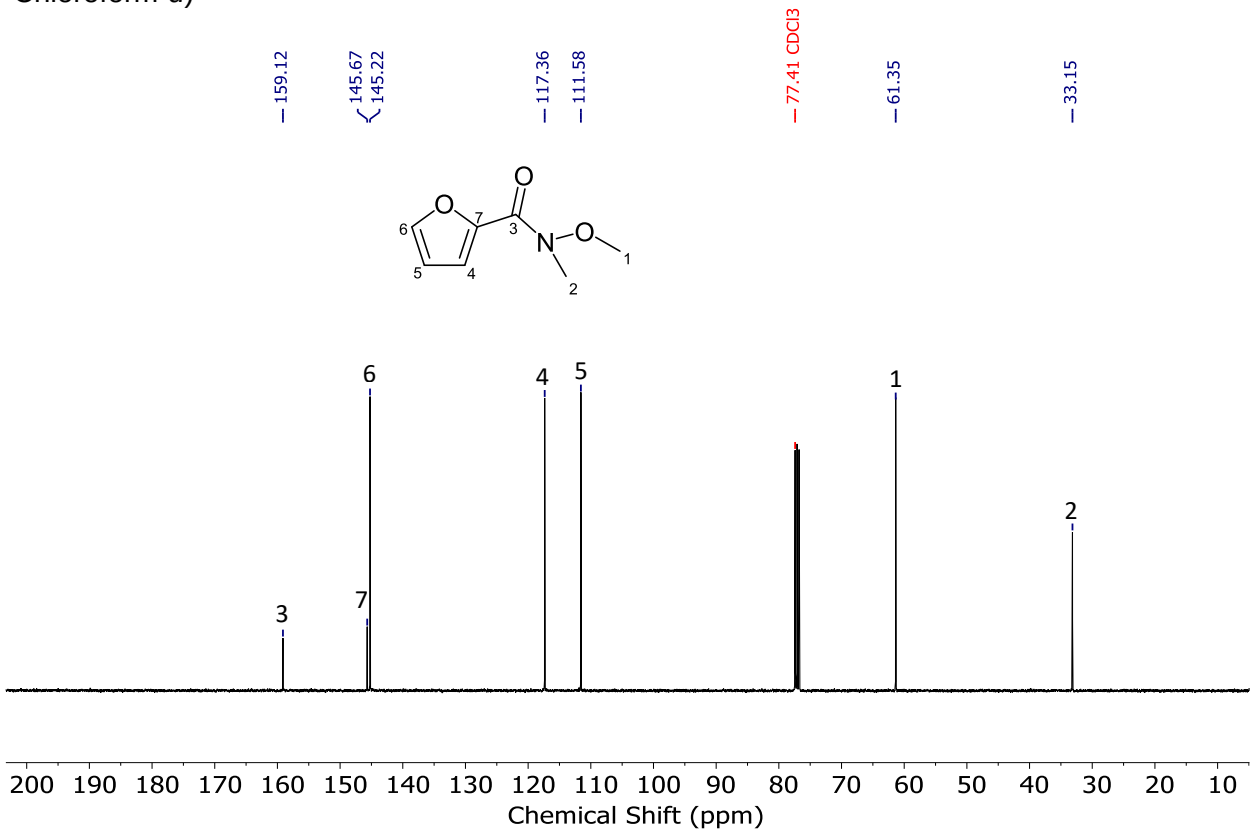

Figure S6. ^{13}C NMR spectrum of *N*-methoxy-*N*-methylfuran-2-carboxamide (101 MHz, Chloroform-*d*)

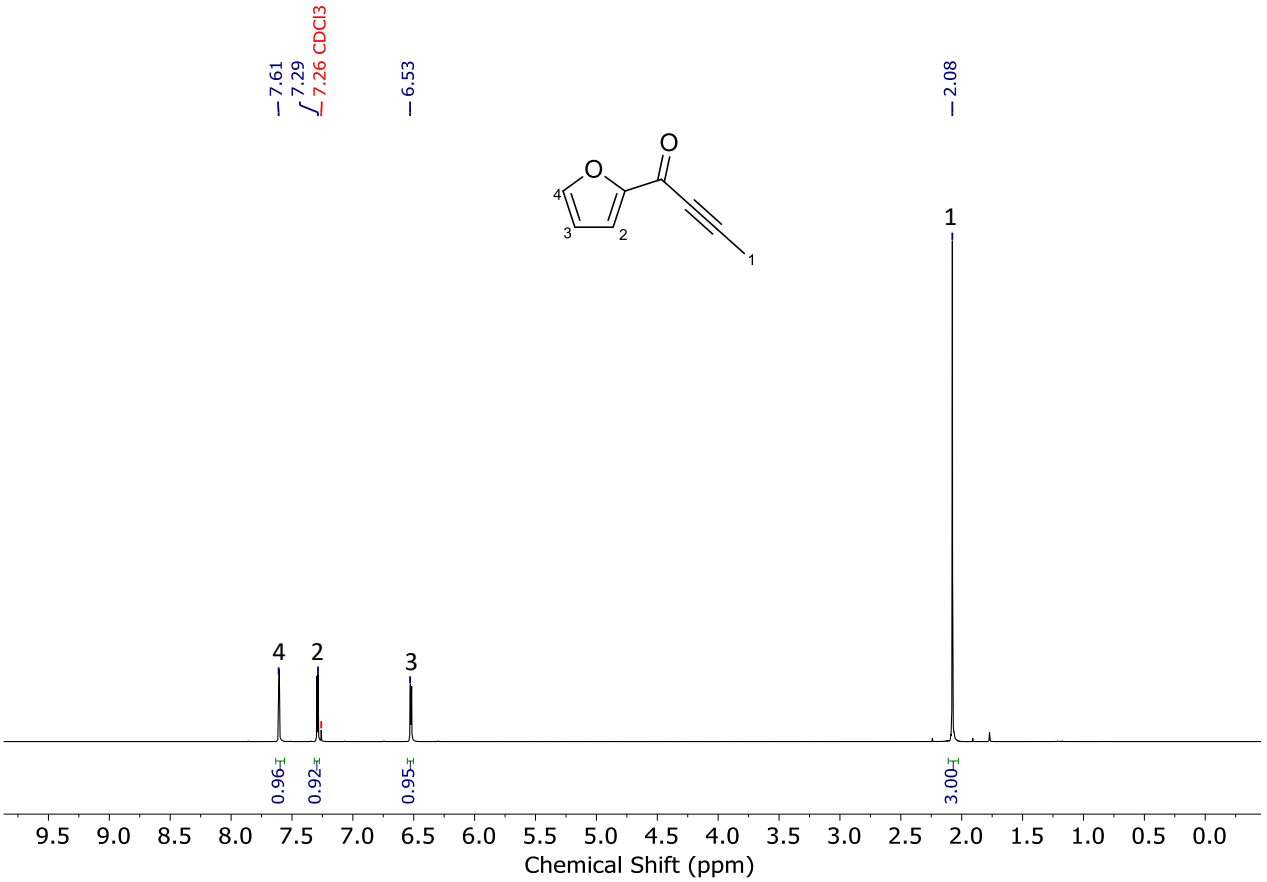

Figure S7. ^{1}H NMR spectrum of 1-(furan-2-yl)but-2-yn-1-one (400 MHz, Chloroform-*d*)

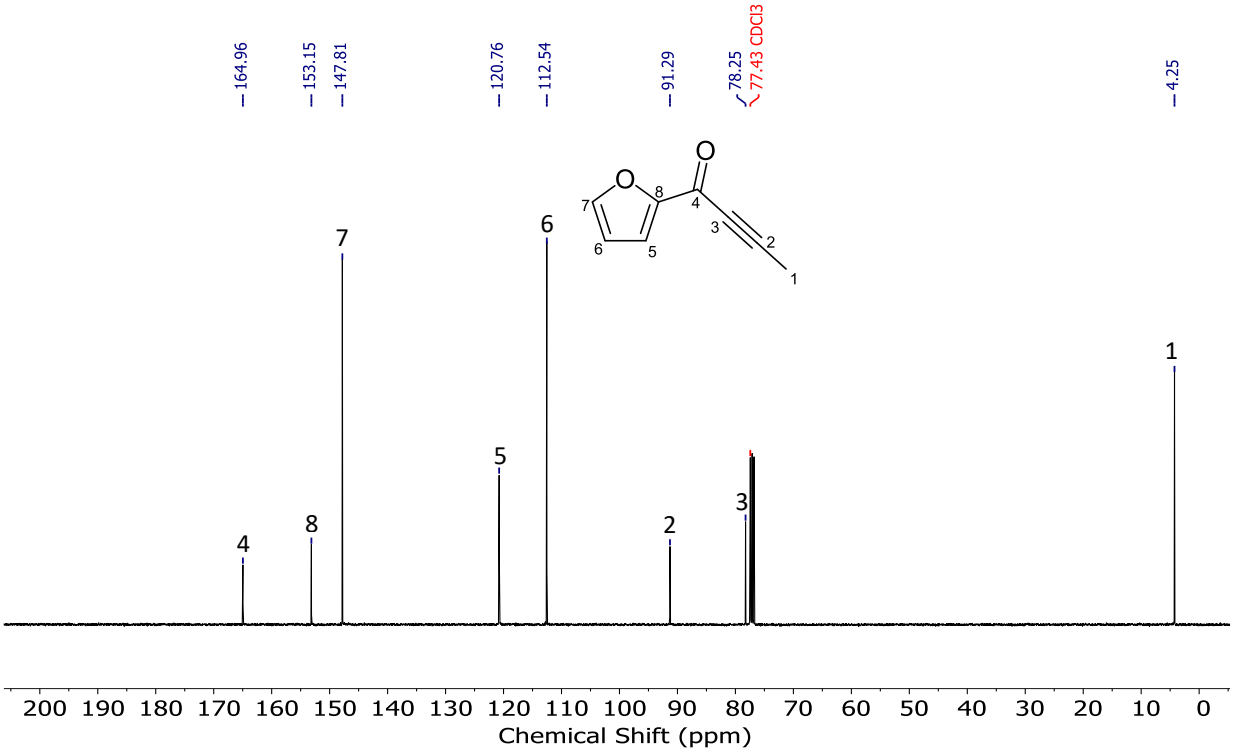

Figure S8. ^{13}C NMR spectrum of 1-(furan-2-yl)but-2-yn-1-one (101 MHz, Chloroform-*d*)

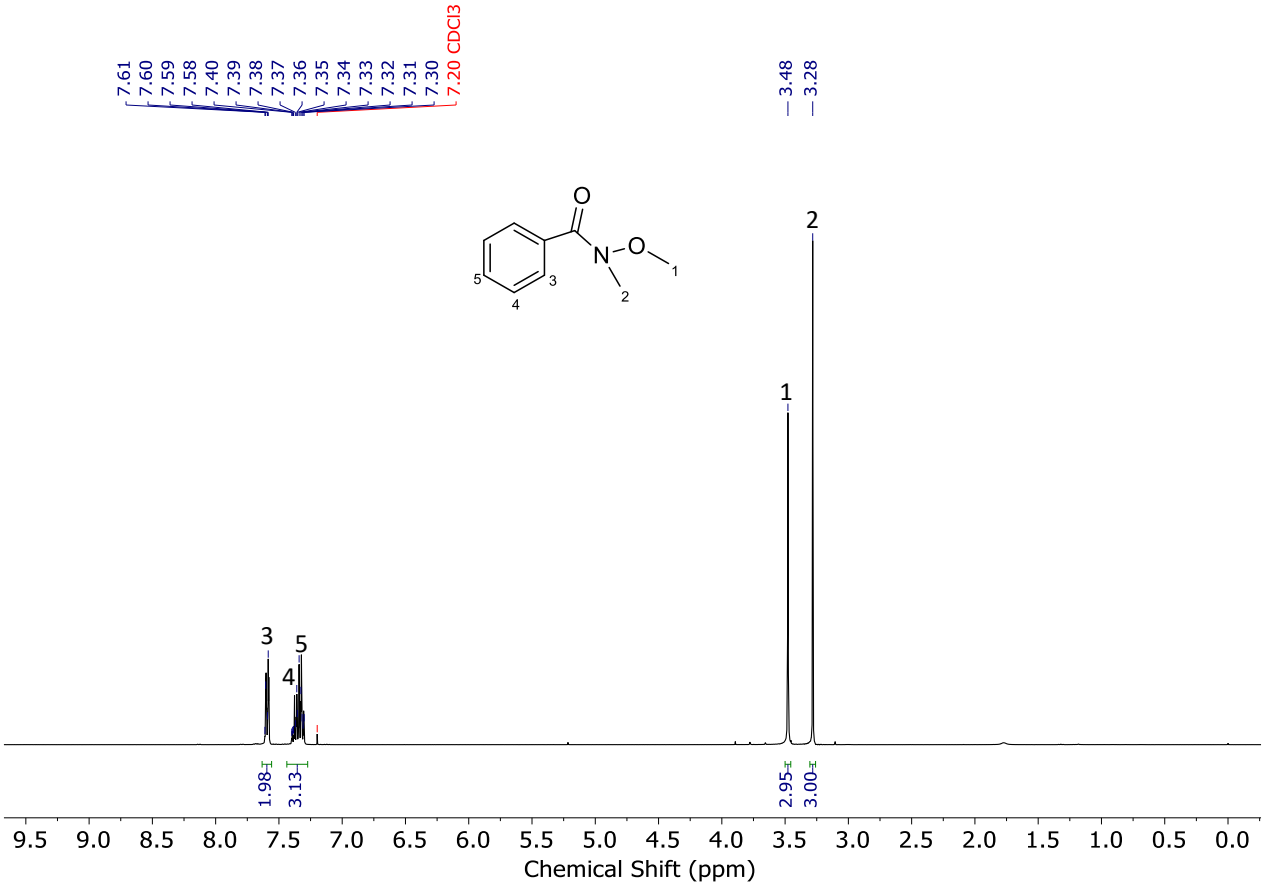

Figure S9. ^{1}H NMR spectrum of *N*-methoxy-*N*-methylbenzamide (400 MHz, Chloroform-*d*)

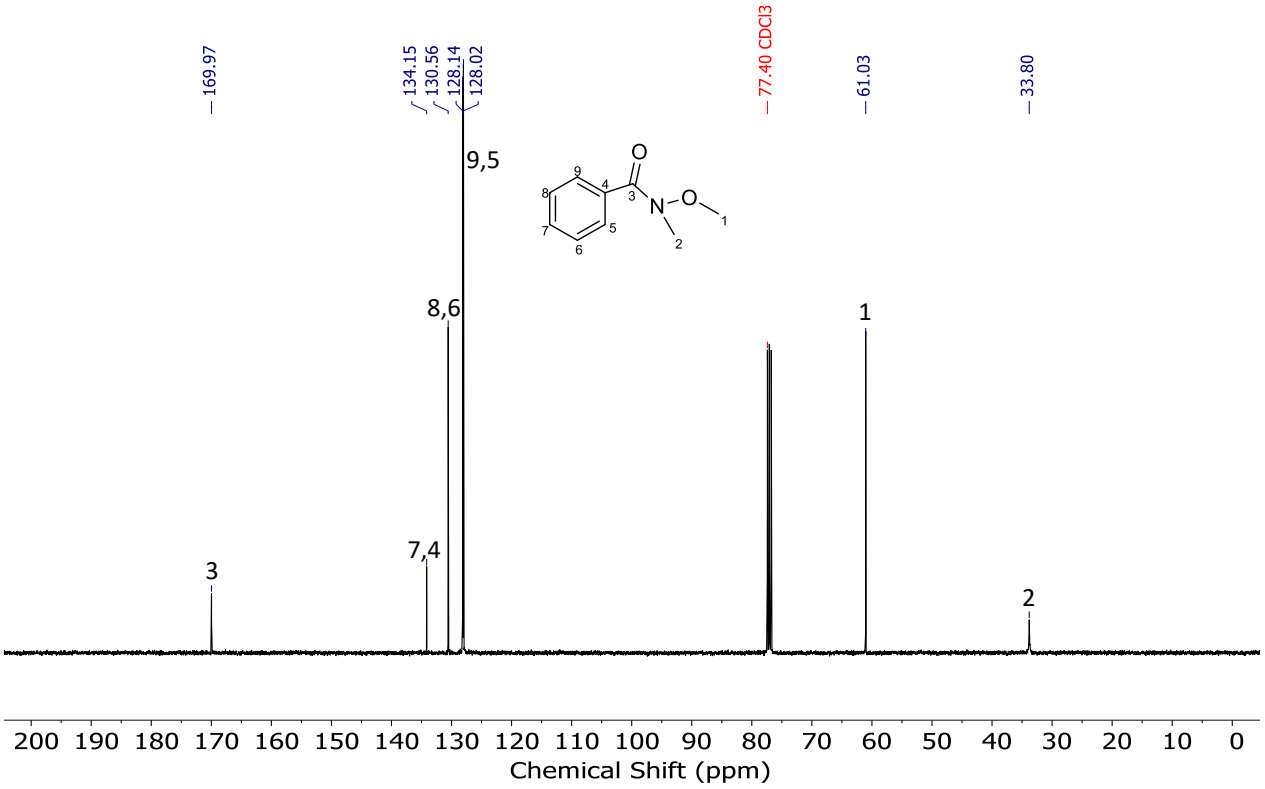

Figure S10. ^{13}C NMR spectrum of *N*-methoxy-*N*-methylbenzamide (101 MHz, Chloroform-*d*)

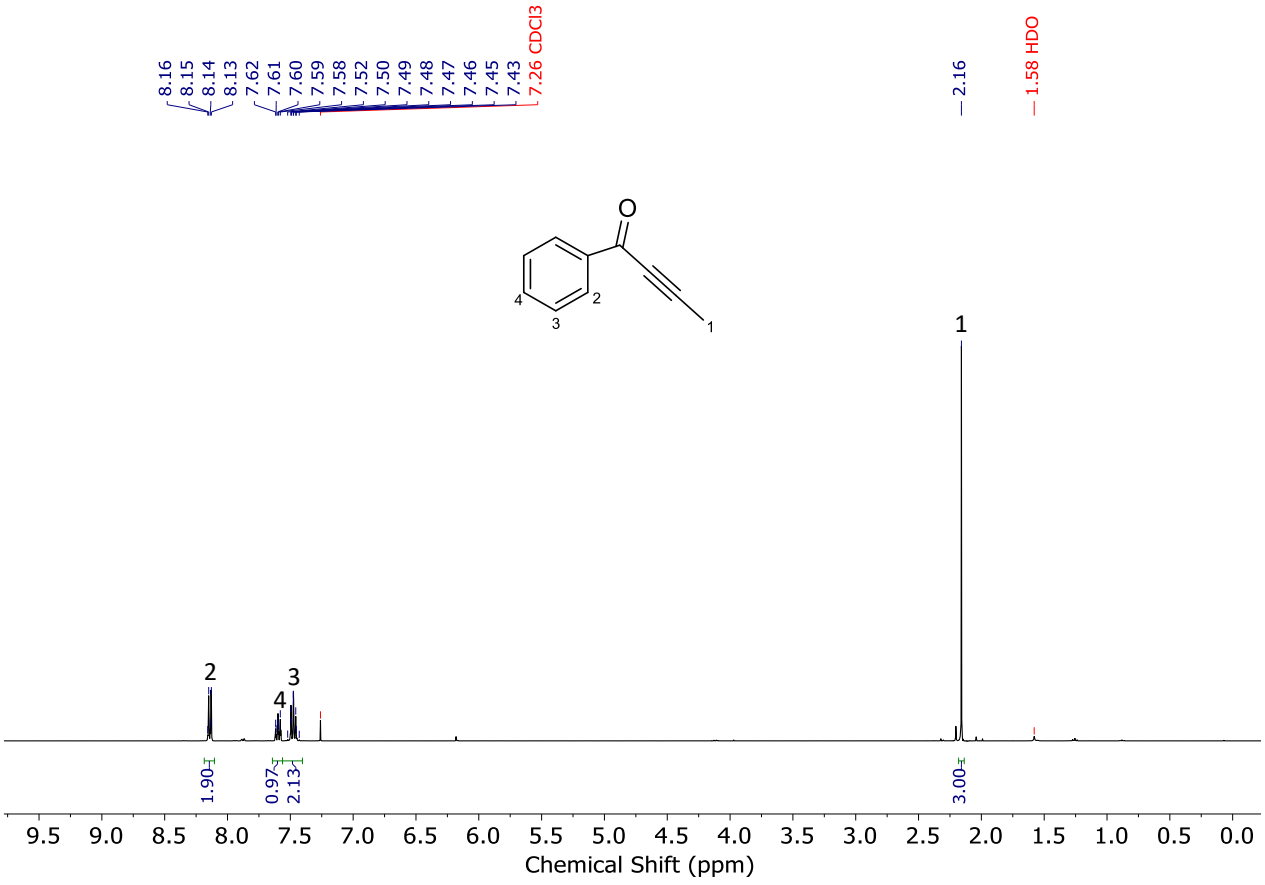

Figure S11. ^{1}H NMR spectrum of 1-phenylbut-2-yn-1-one (400 MHz, Chloroform-*d*)

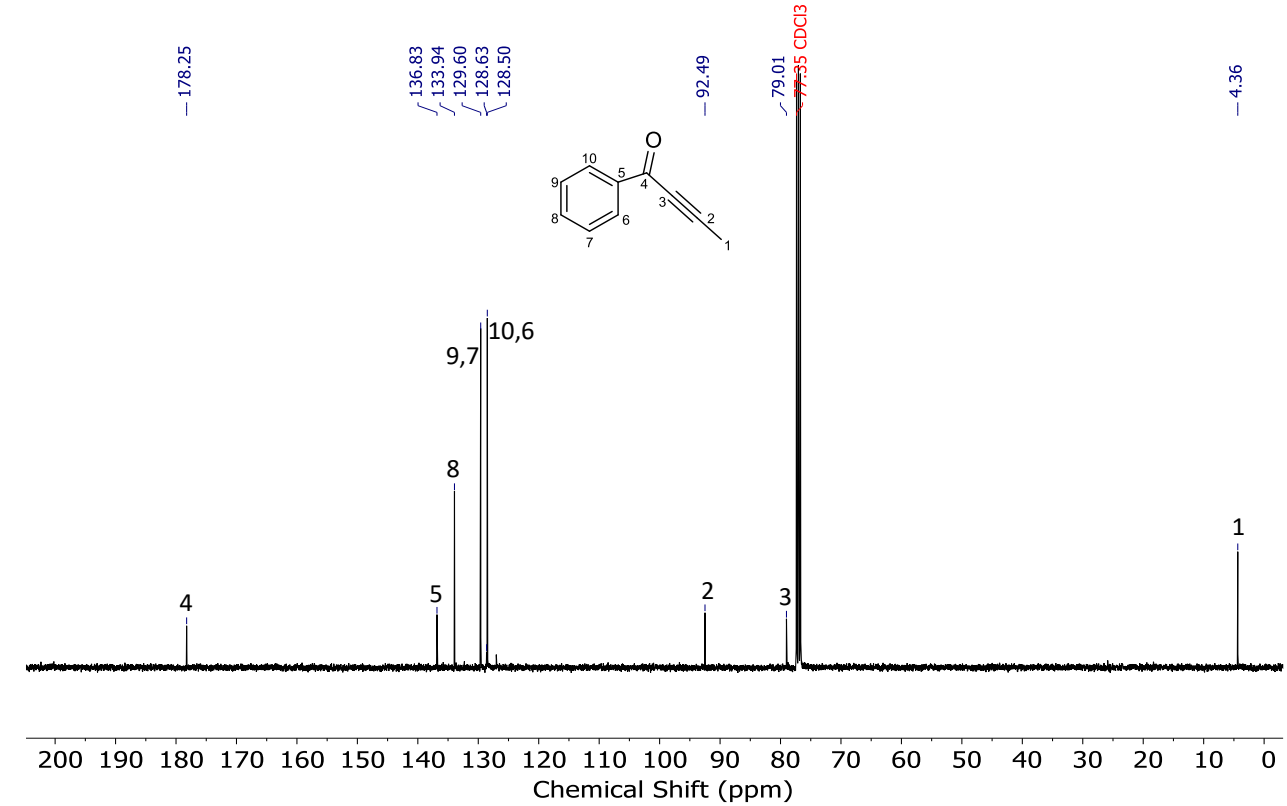

Figure S12. ^{13}C NMR spectrum of 1-phenylbut-2-yn-1-one (101 MHz, Chloroform-*d*)

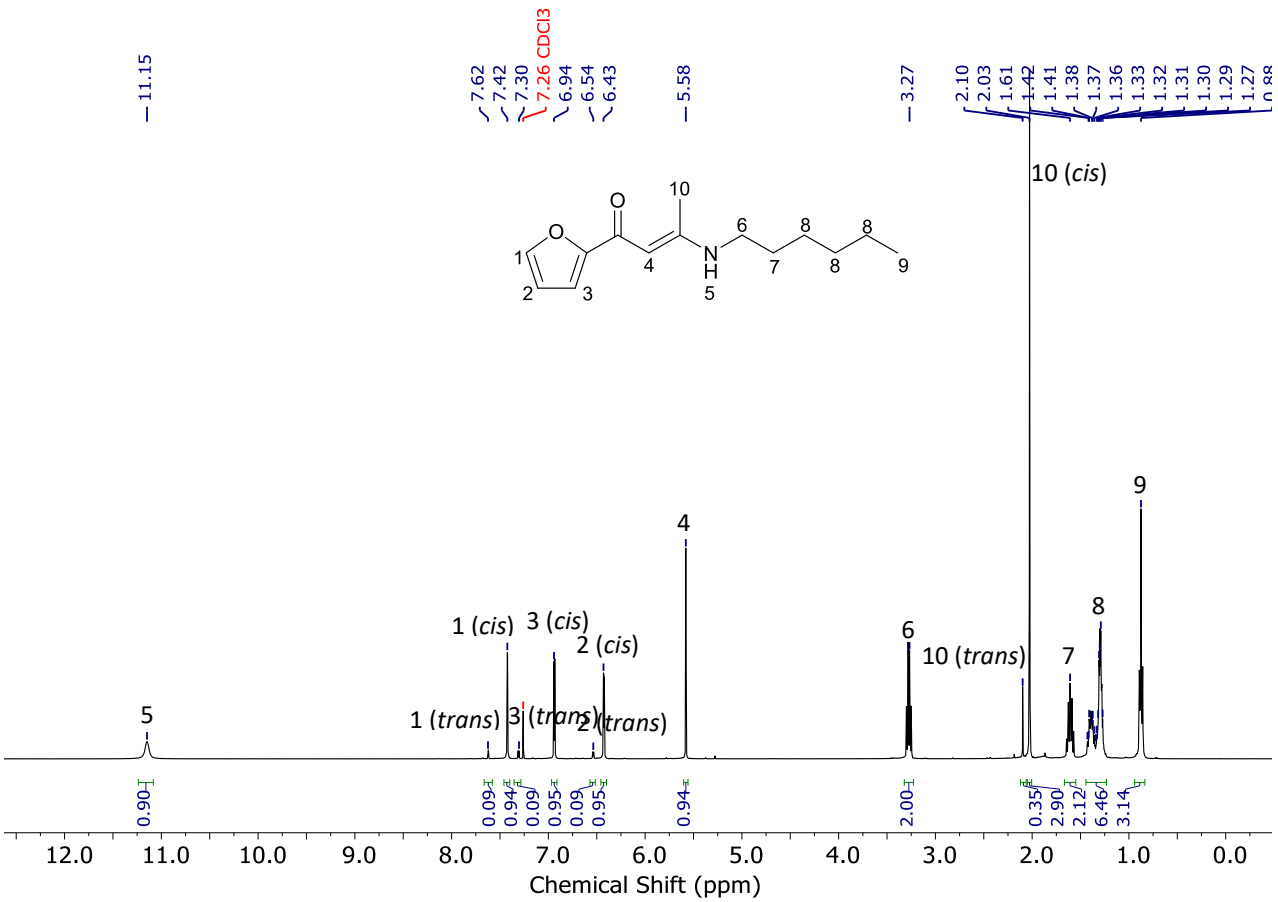

Figure S13. ^{1}H NMR spectrum of model compound F-C$_6$A (400 MHz, Chloroform-*d*)

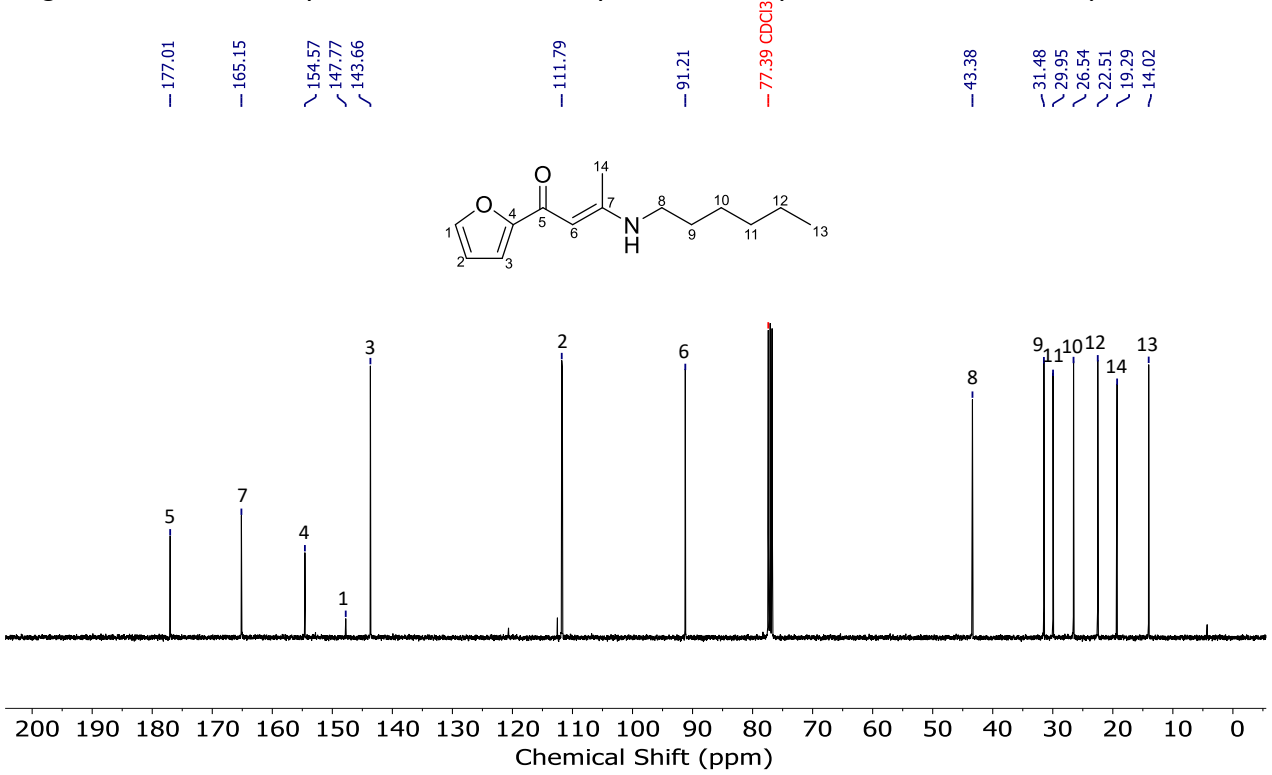

Figure S14. ^{13}C NMR spectrum of model compound F-C$_6$A (400 MHz, Chloroform-*d*)

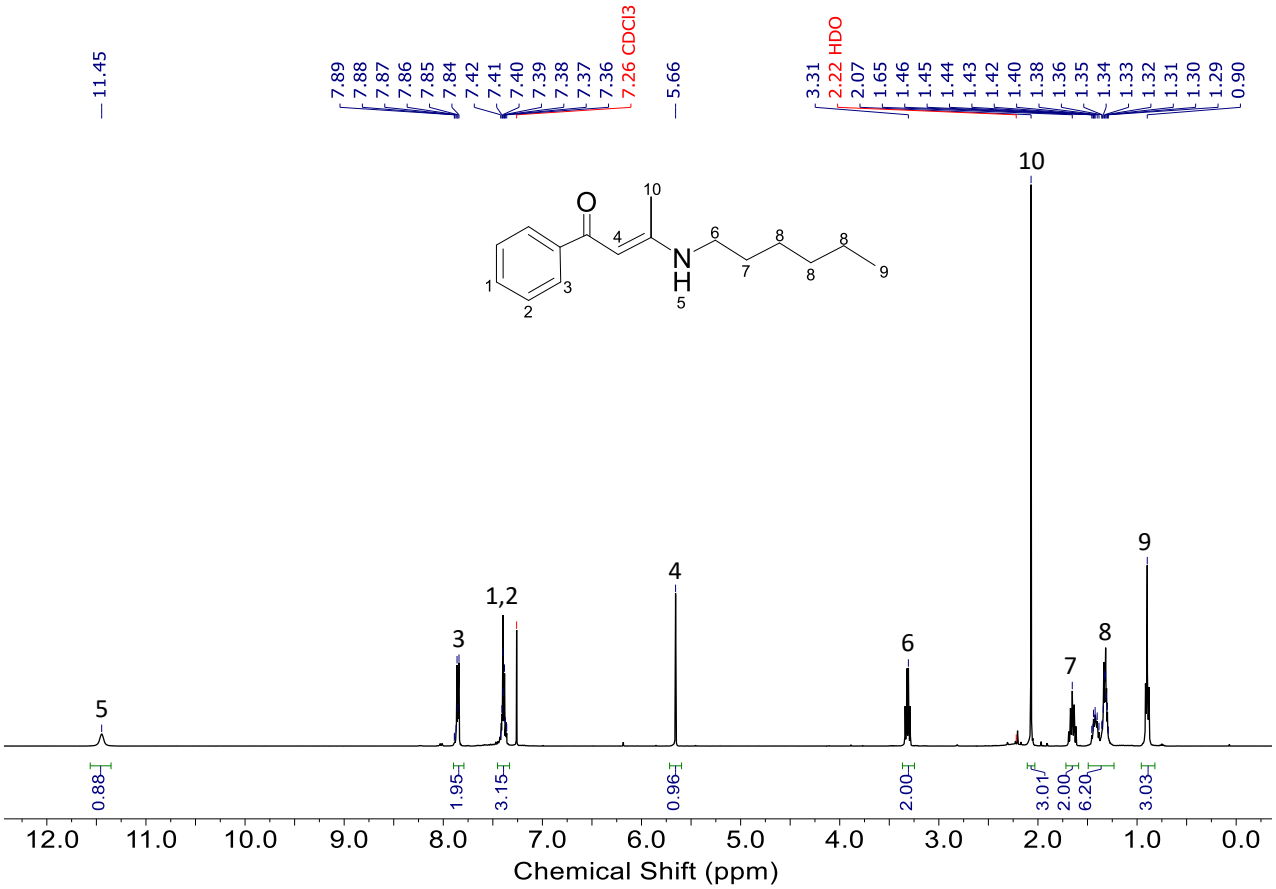

Figure S15. ^{1}H NMR spectrum of model compound Ph-C_6A (400 MHz, Chloroform-*d*)

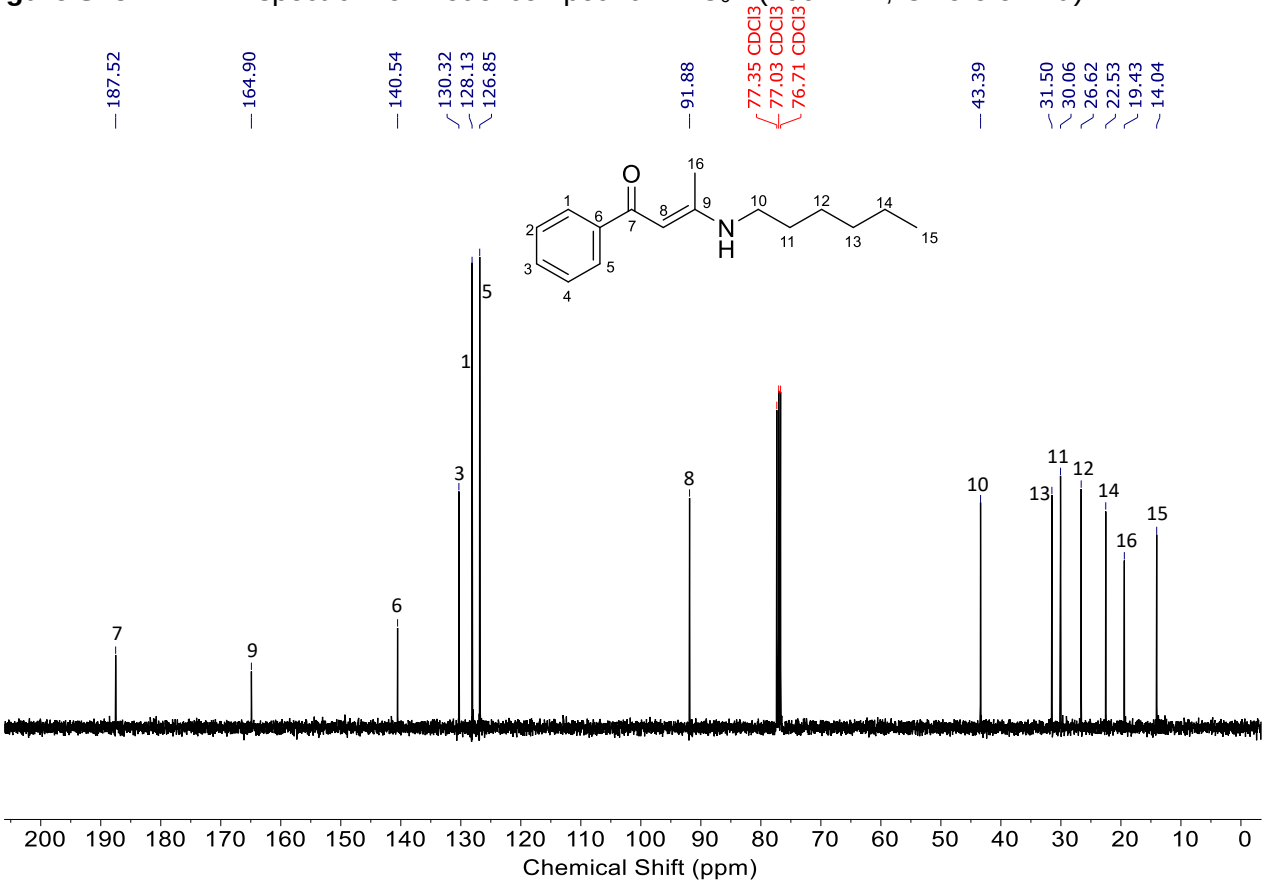

Figure S16. ^{13}C NMR spectrum of model compound Ph-C_6A (400 MHz, Chloroform-*d*)

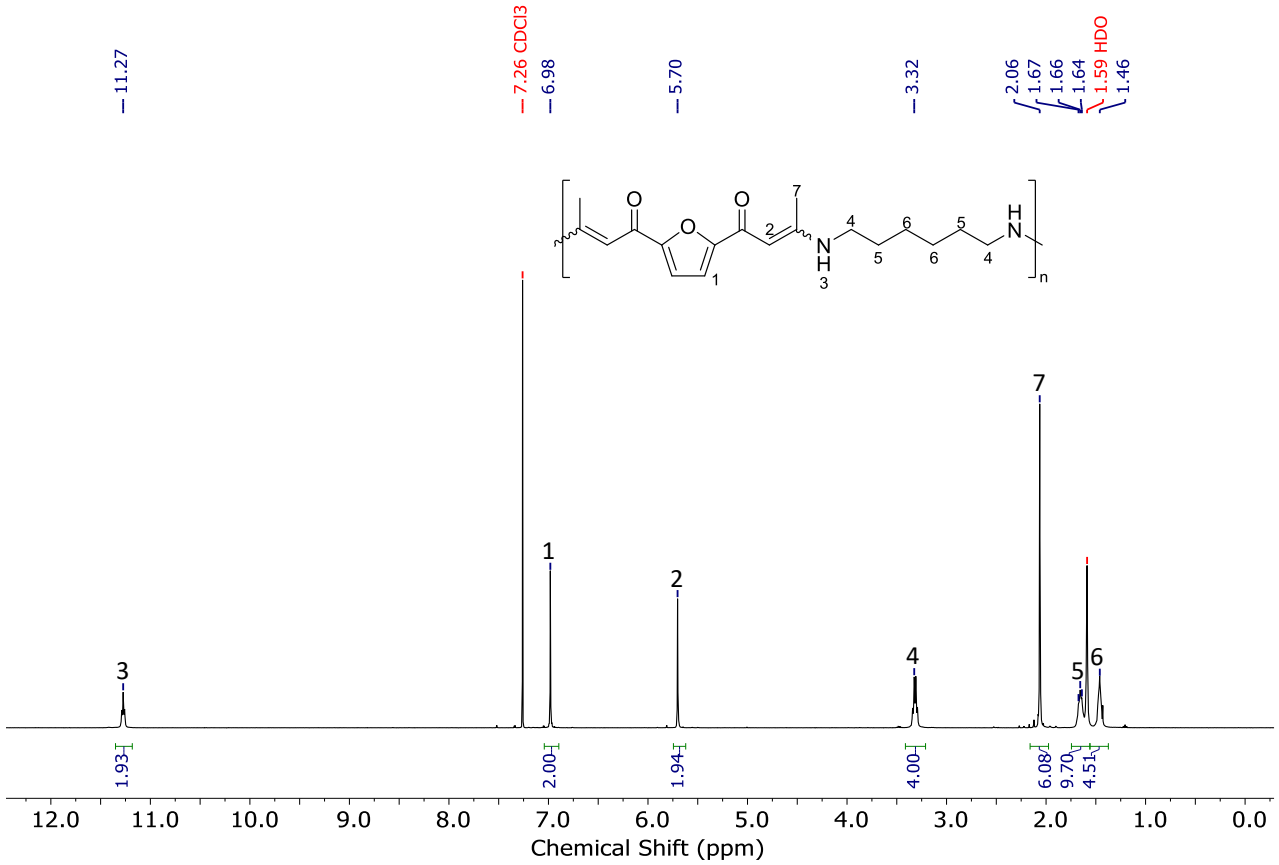

Figure S17. ^{1}H NMR spectrum of F-C$_6$A (400 MHz, Chloroform-*d*)

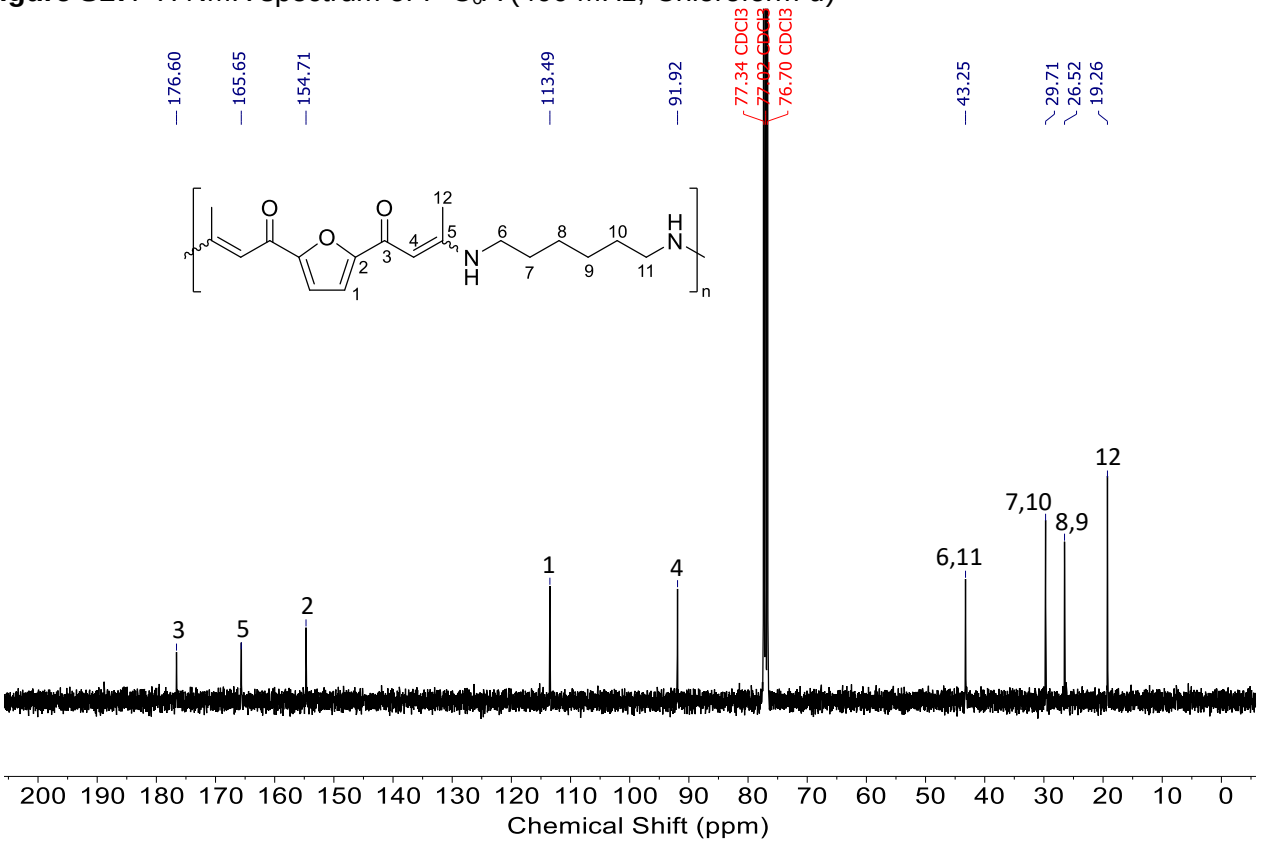

Figure S18. ^{13}C NMR spectrum of F-C$_6$A (101 MHz, Chloroform-*d*)

NMR spectra stacked to show the presence of N-H bond in representative polymer

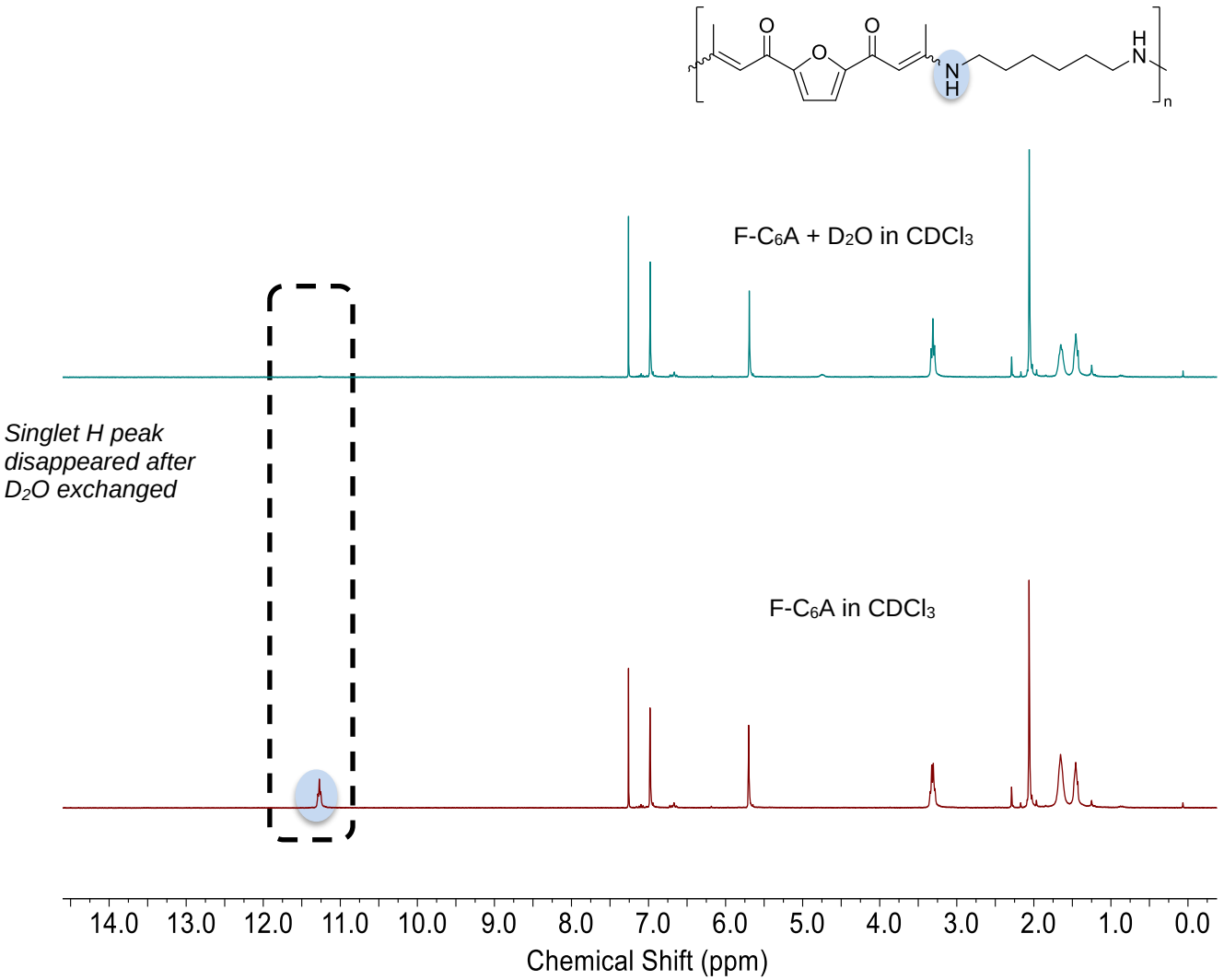

Figure S19. ^{1}H NMR spectra stacked of F-C_6A and F-C_6A + D_2O (400 MHz, Chloroform-*d*)

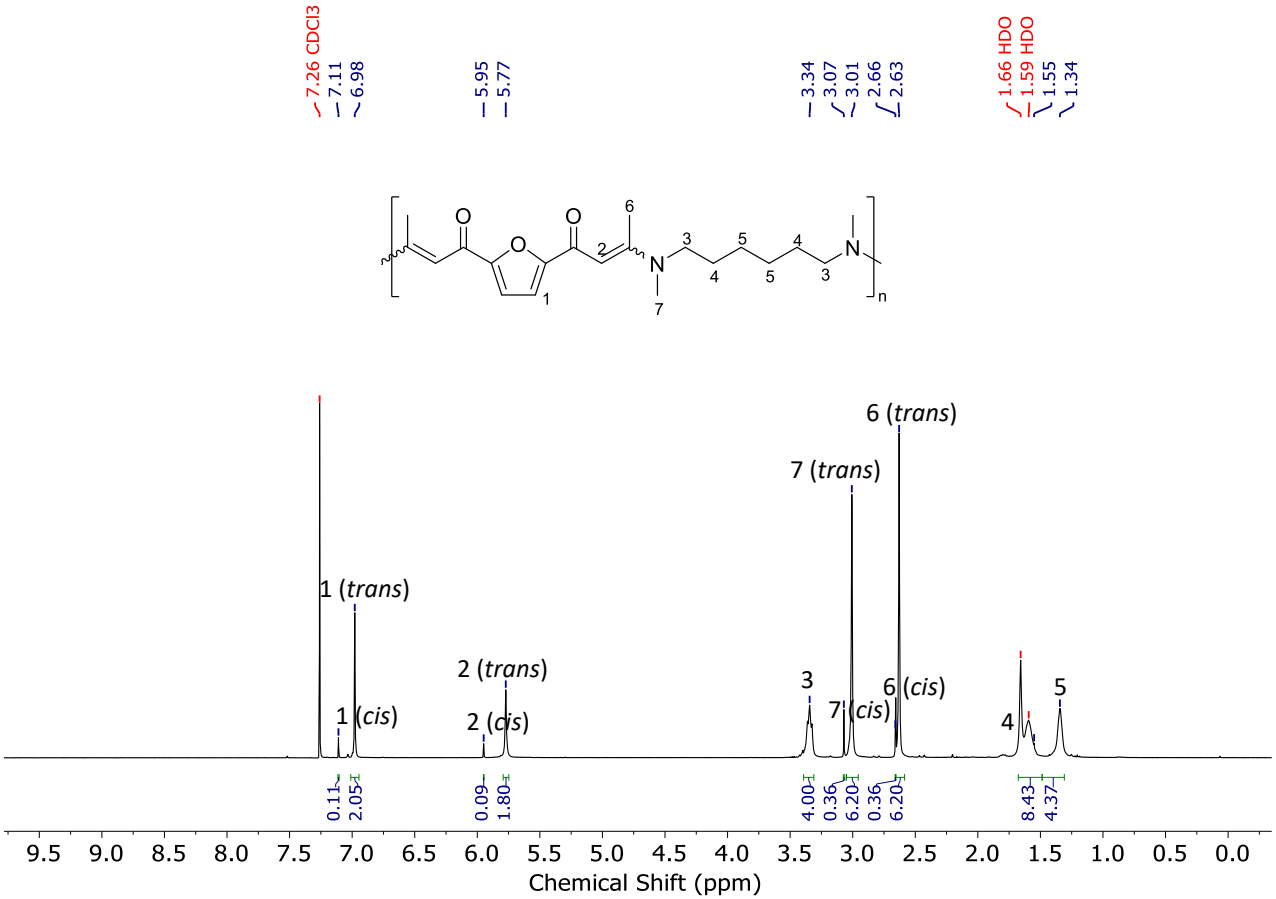

Figure S20. ^{1}H NMR spectrum of F-C$_6$A$_2$ (400 MHz, Chloroform-*d*)

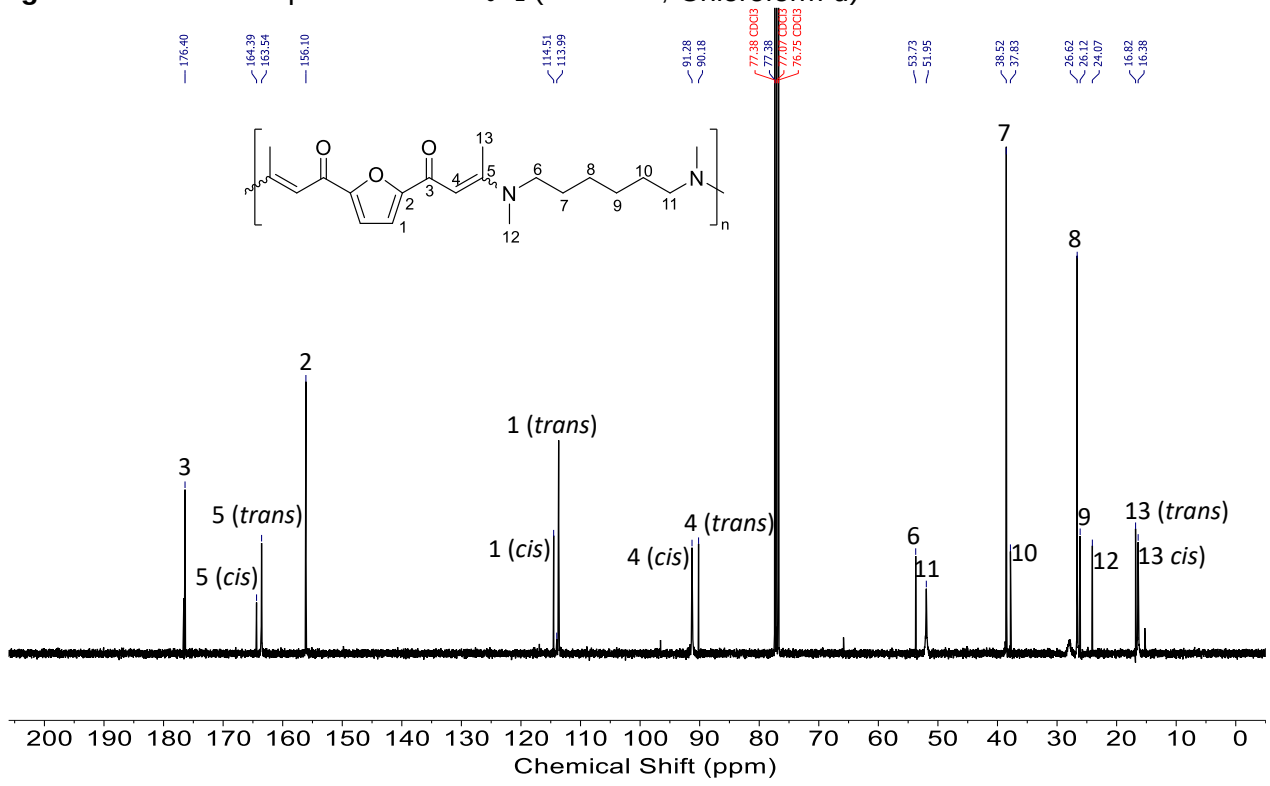

Figure S21. ^{13}C NMR spectrum of F-C$_6$A$_2$ (101 MHz, Chloroform-*d*)

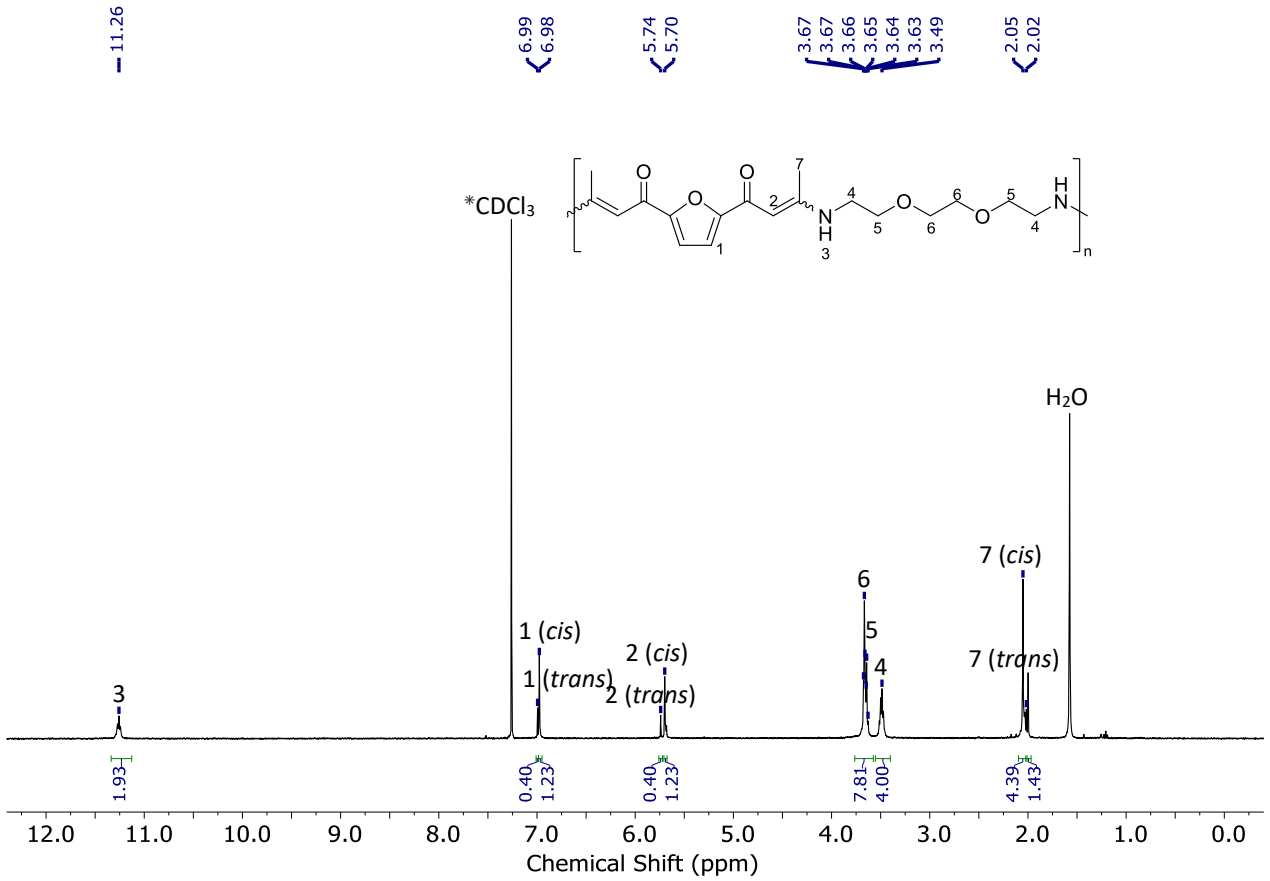

Figure S22. ^{1}H NMR spectrum of F-C$_6$A$_{EG}$ (400 MHz, Chloroform-*d*)

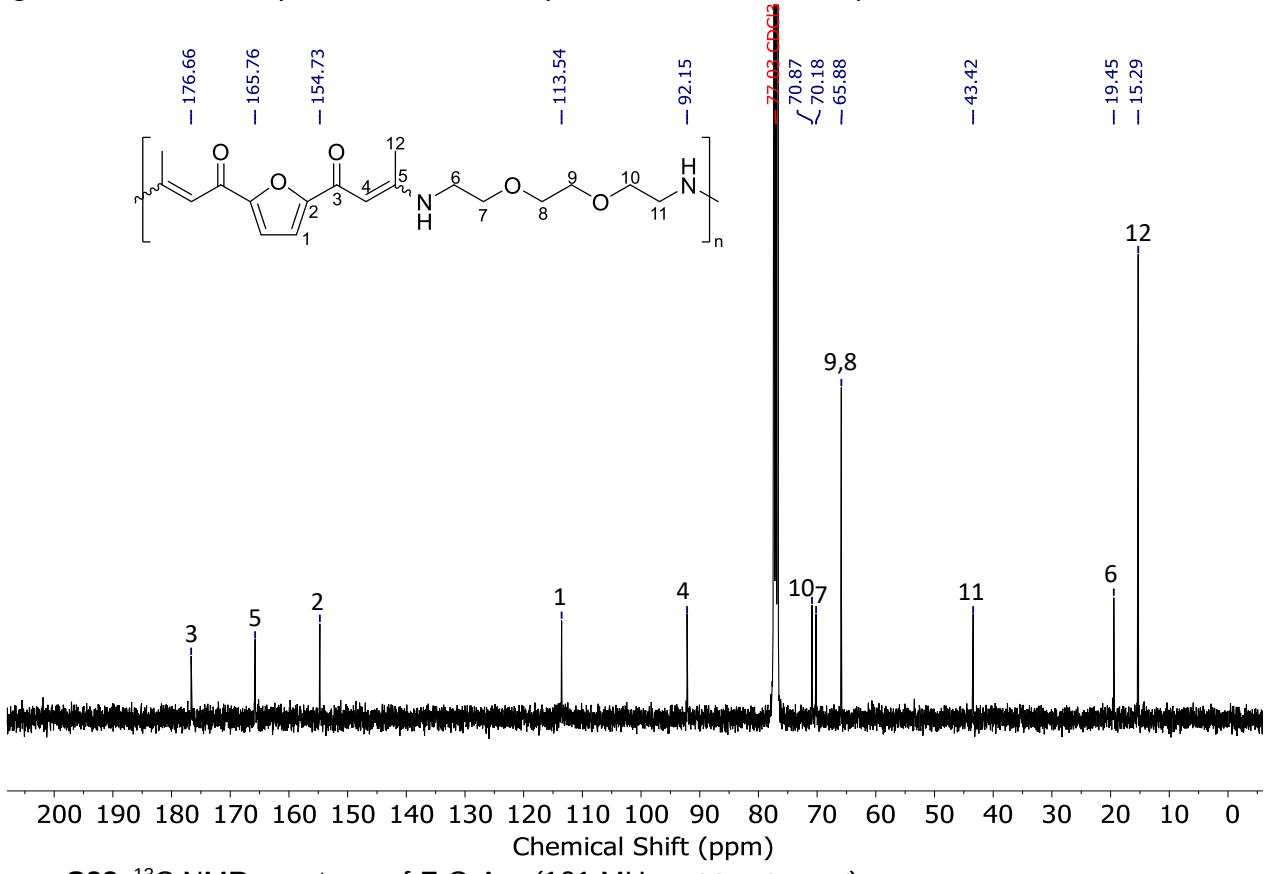

Figure S23. ^{13}C NMR spectrum of F-C$_6$A$_{EG}$ (101 MHz, Chloroform-*d*)

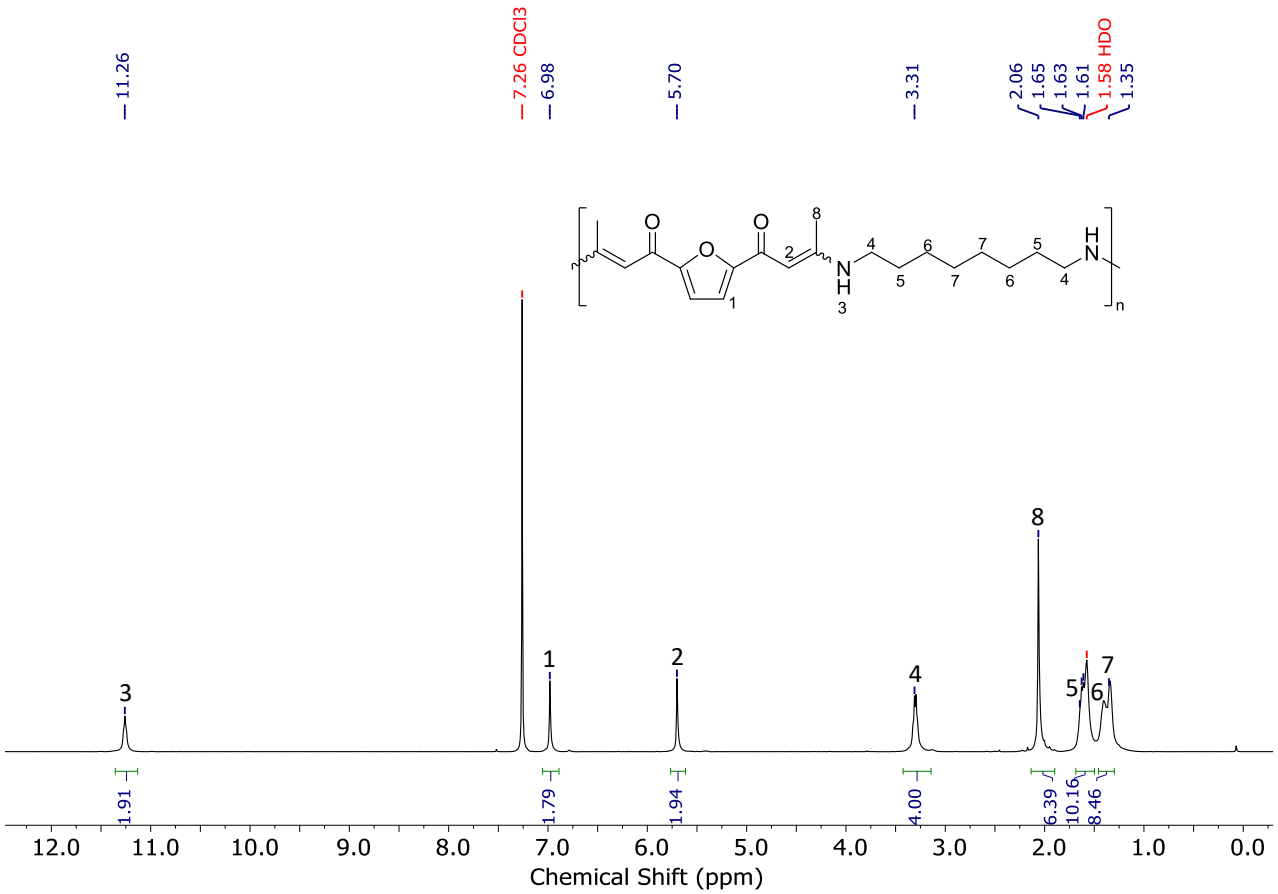

Figure S24. ^{1}H NMR spectrum of F-C$_8$A (400 MHz, Chloroform-*d*)

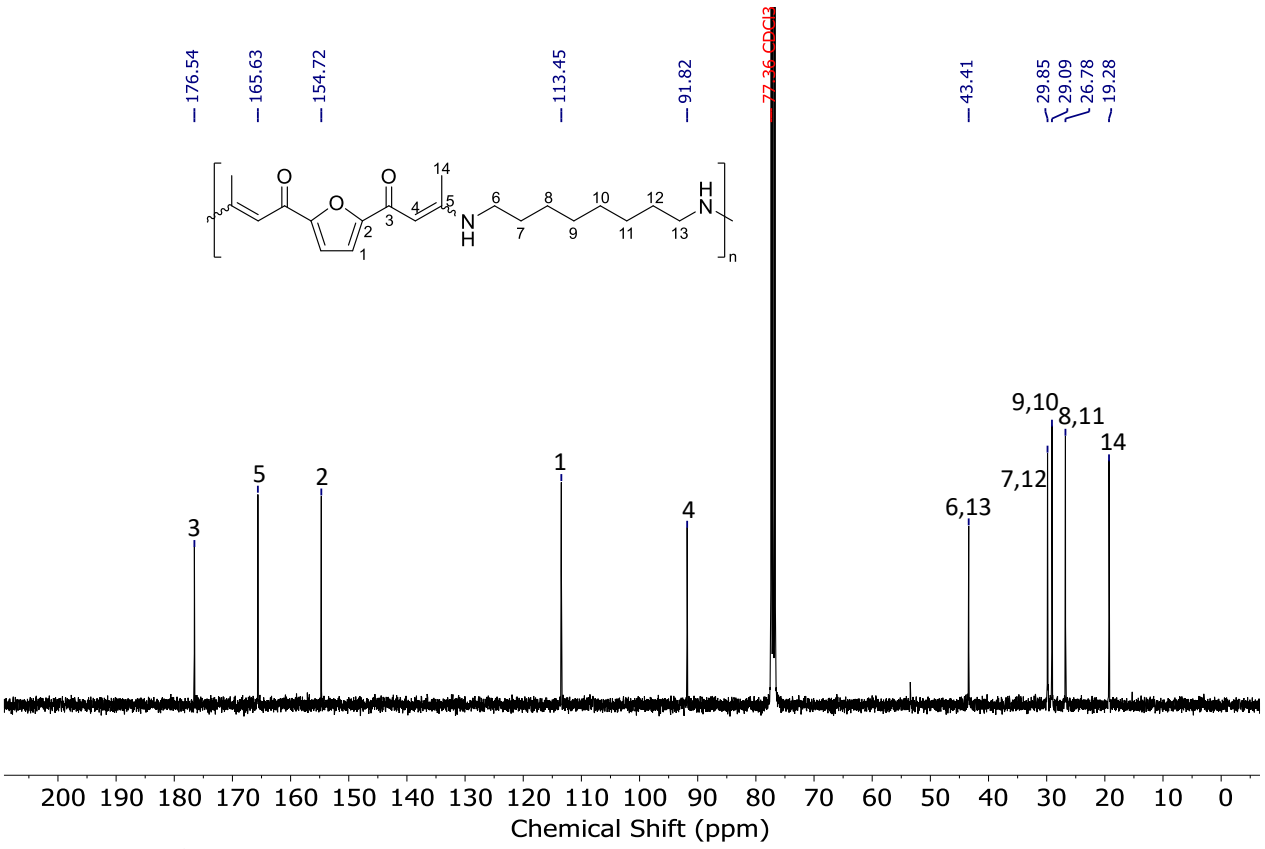

Figure S25. ^{13}C NMR spectrum of F-C$_8$A (101 MHz, Chloroform-*d*)

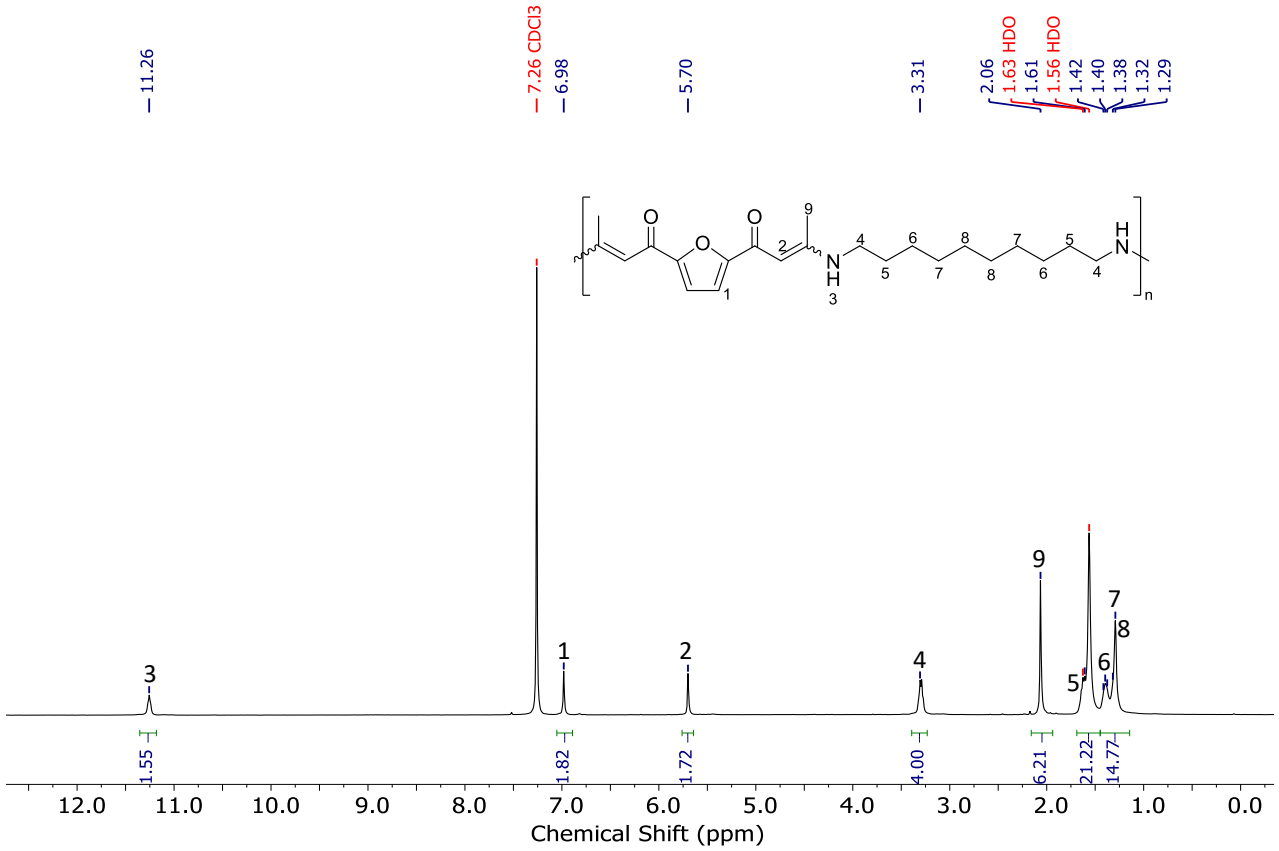

Figure S26. ^{1}H NMR spectrum of F-C_{10}A (400 MHz, Chloroform-*d*)

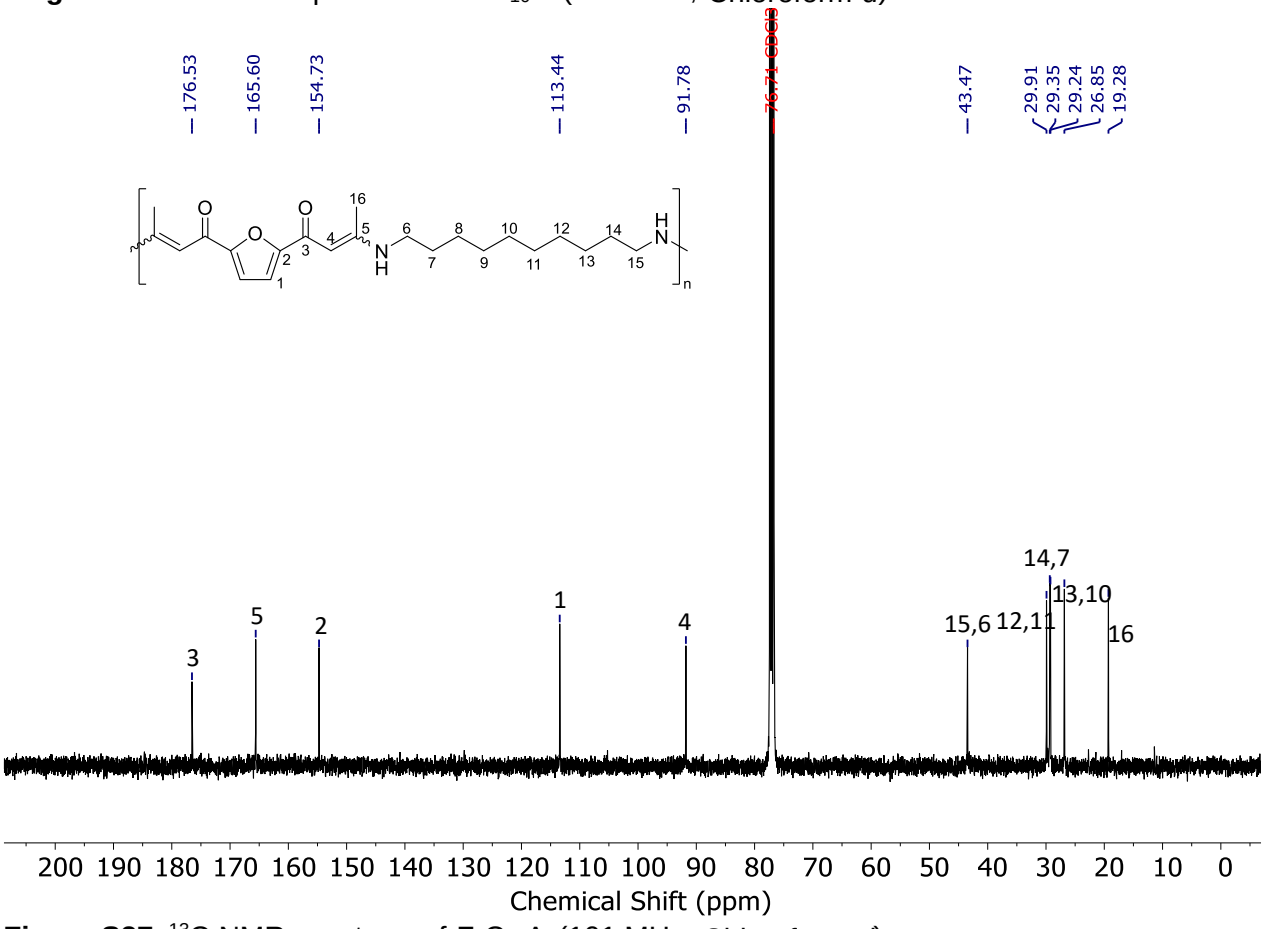

Figure S27. ^{13}C NMR spectrum of F-C_{10}A (101 MHz, Chloroform-*d*)

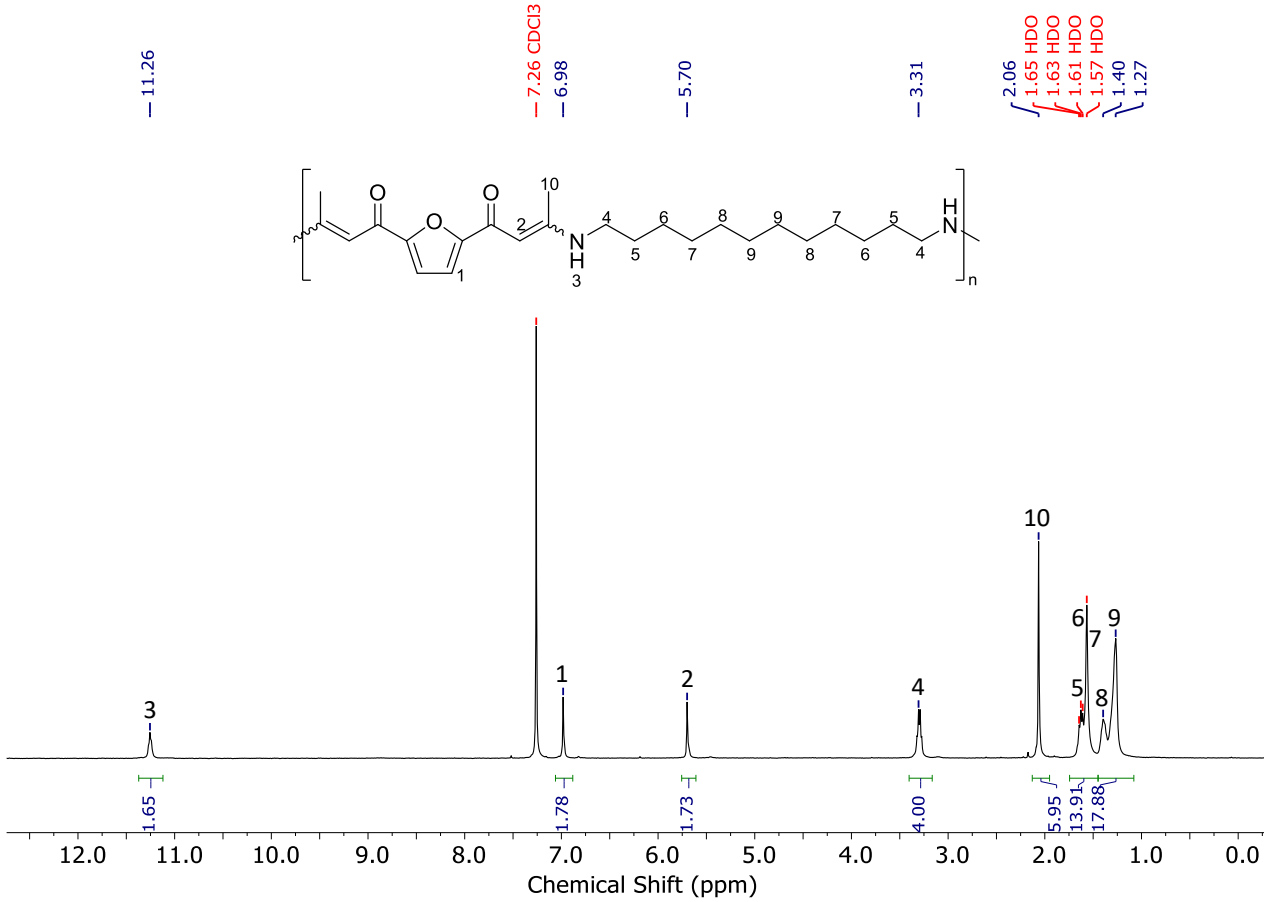

Figure S28. ^{1}H NMR spectrum of F-C_{12}A (400 MHz, Chloroform-*d*)

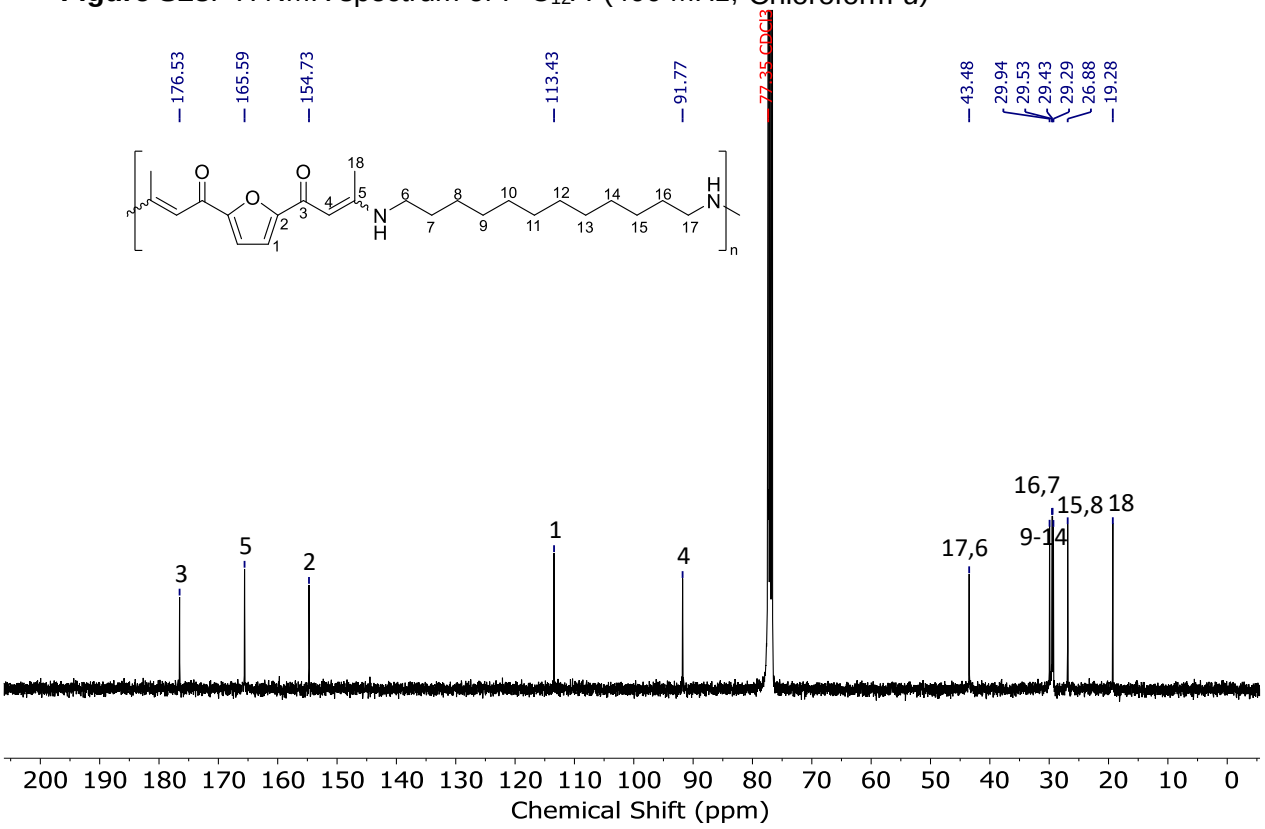

Figure S29. ^{13}C NMR spectrum of F-C_{12}A (101 MHz, Chloroform-*d*)

Infrared spectra of precursors and monomer

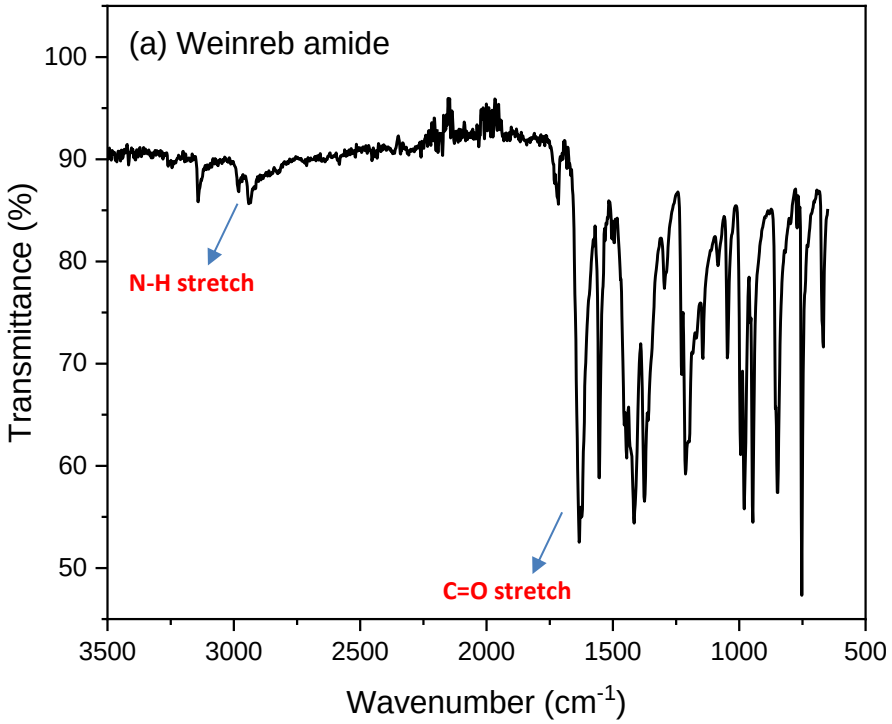

Figure S30. FTIR spectra of bifunctional Weinreb amide and 2,5-Furandicarboxylic acid

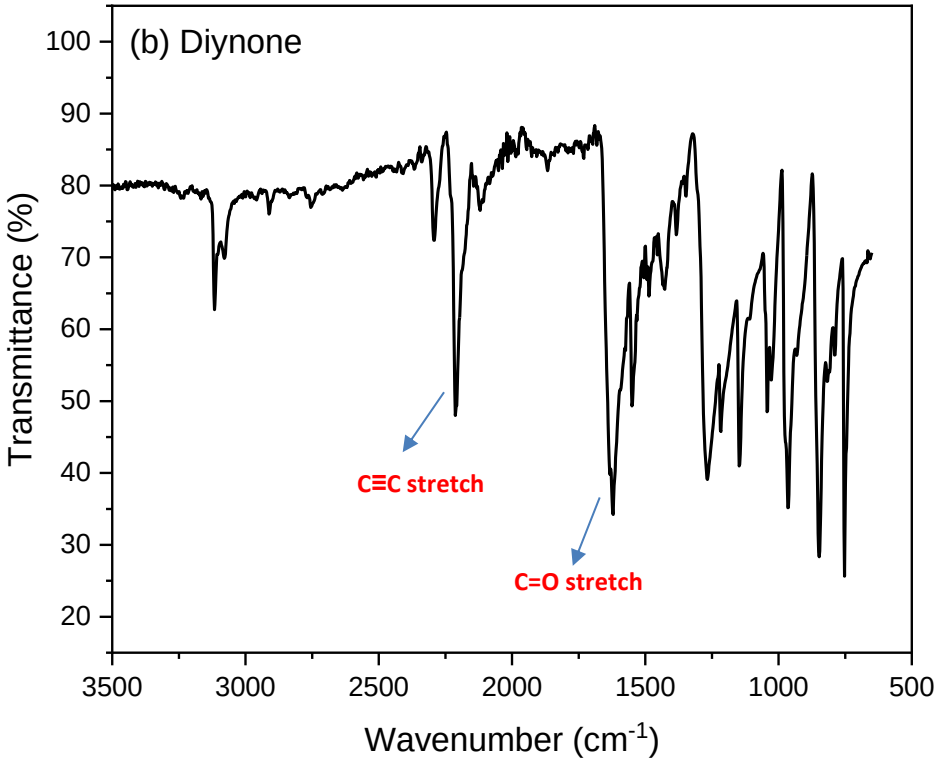

Figure S31. FTIR spectra of diynone and bifunctional Weinreb amide

Infrared spectra of representative polymer

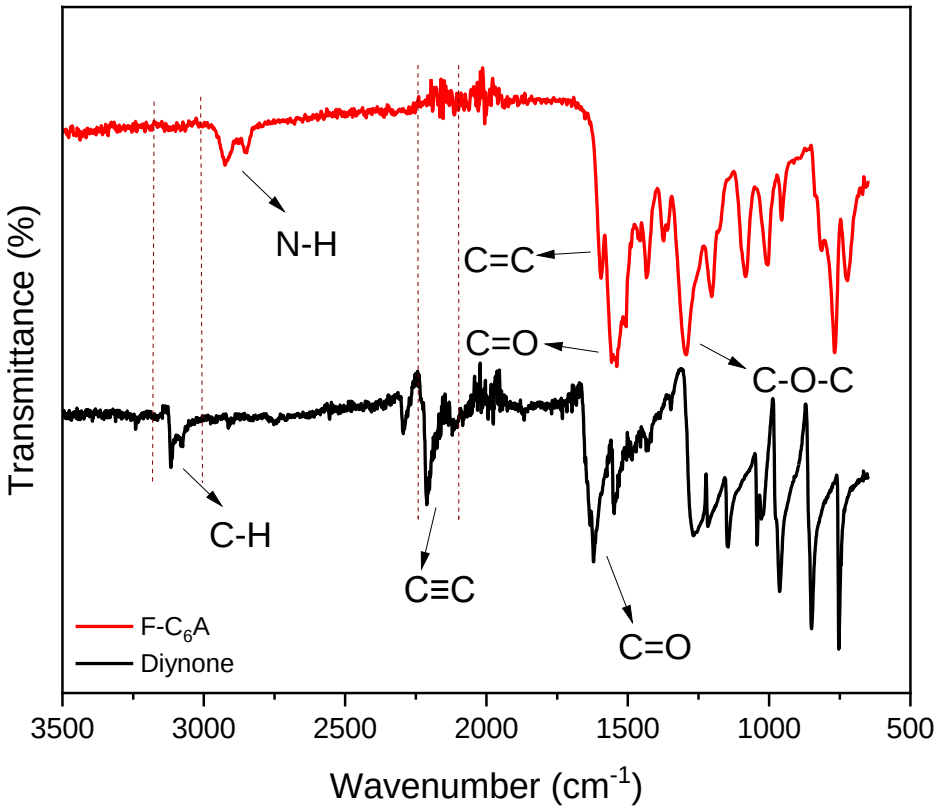

Figure S32. FTIR spectra of F-C_6A and diynone

Size exclusion chromatograms of all polymers

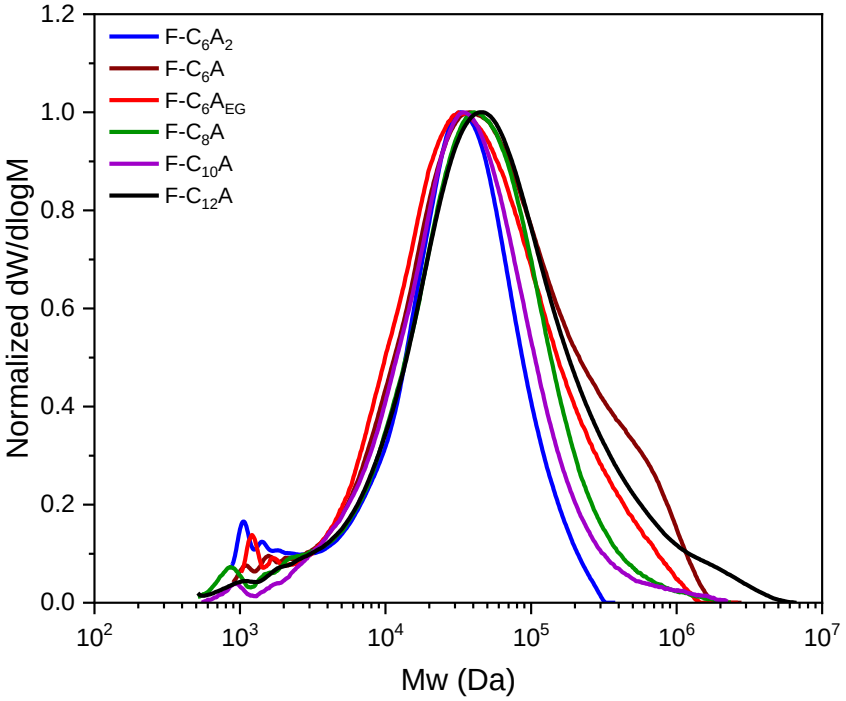

Figure S33. Normalized size exclusion chromatograms of all polymers ($CHCl_3$, 0.5% NEt_3, 40 °C) analysis against poly(styrene) (PS) standards

Thermogravimetric analysis of polymers

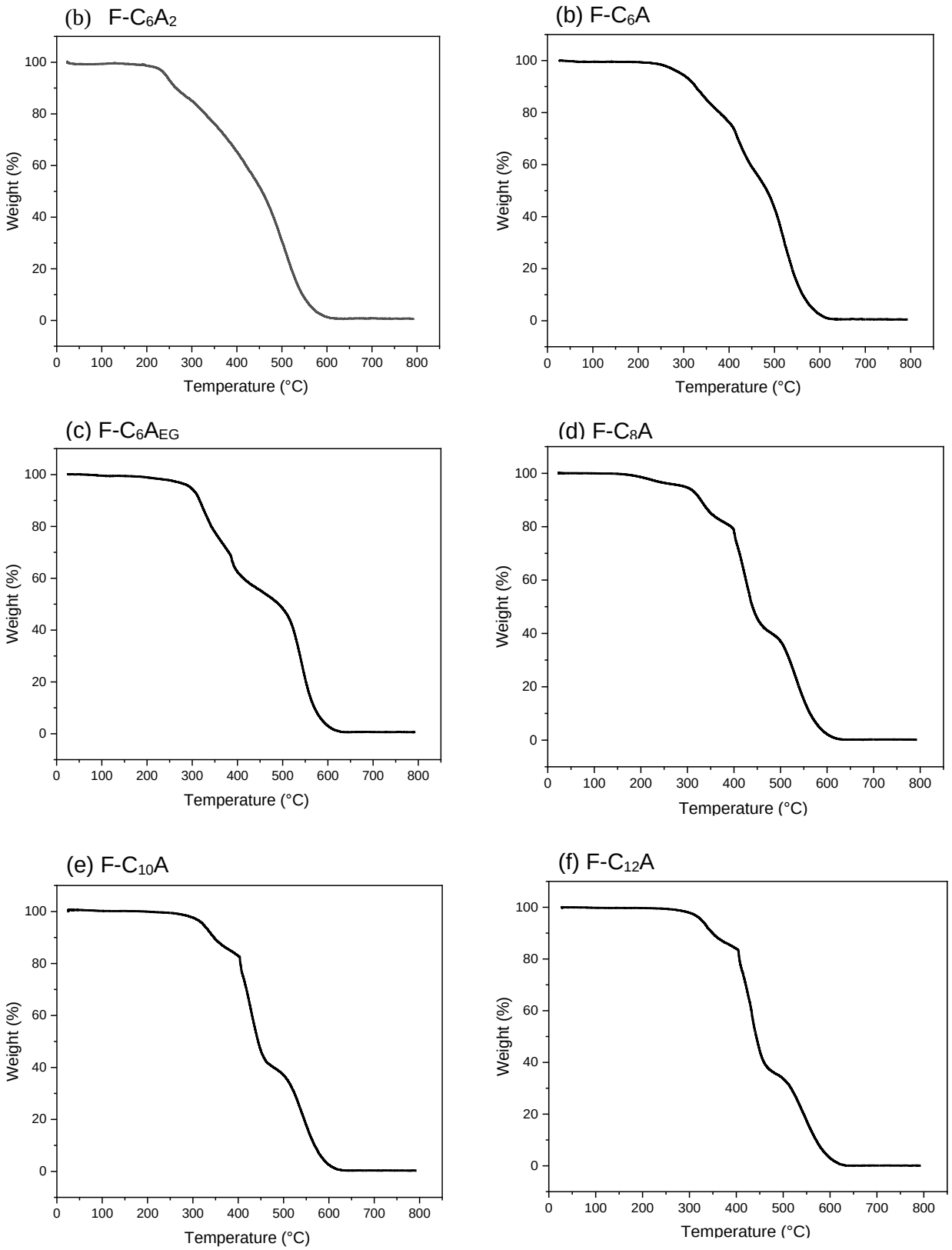

Figure S34. Thermogravimetric analysis of polymers at a heating rate of 10 K·min^{-1} (a) F-C_6A_2; (b) F-C_6A; (c) F-C_6A_{EG}; (d) F-C_8A; (e) F-$C_{10}A$; (f) F-$C_{12}A$

Differential Scanning Calorimetry analysis of polymers

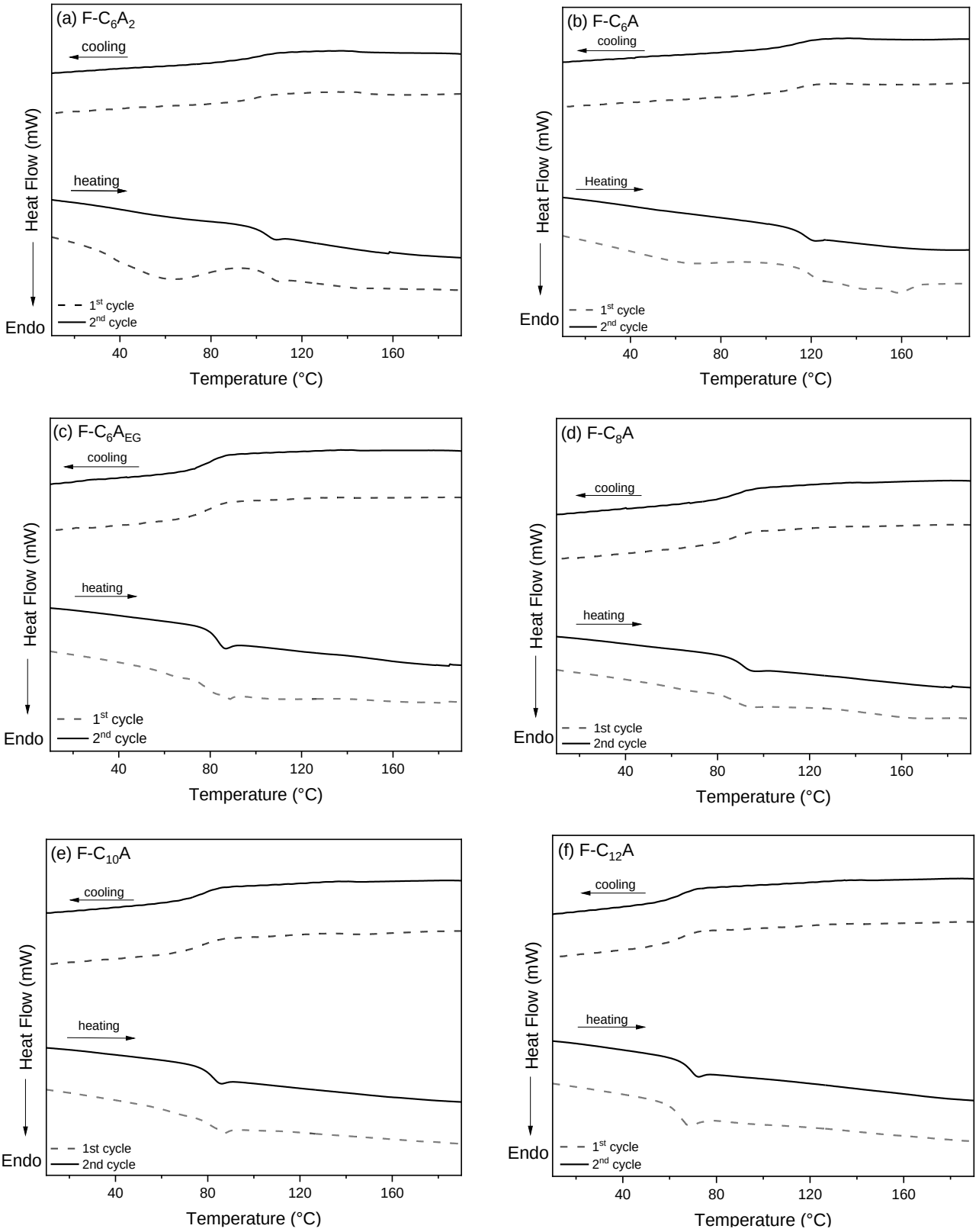

Figure S35. DSC thermograms showing heating and cooling cycles of 3-days annealed polymers at a rate of 10 K·min^{-1} (a) F-C_6A_2; (b) F-C_6A; (c) F-C_6A_{EG}; (d) F-C_8A; (e) F-C_{10}A; (f) F-C_{12}A

Tensile curve of polymers

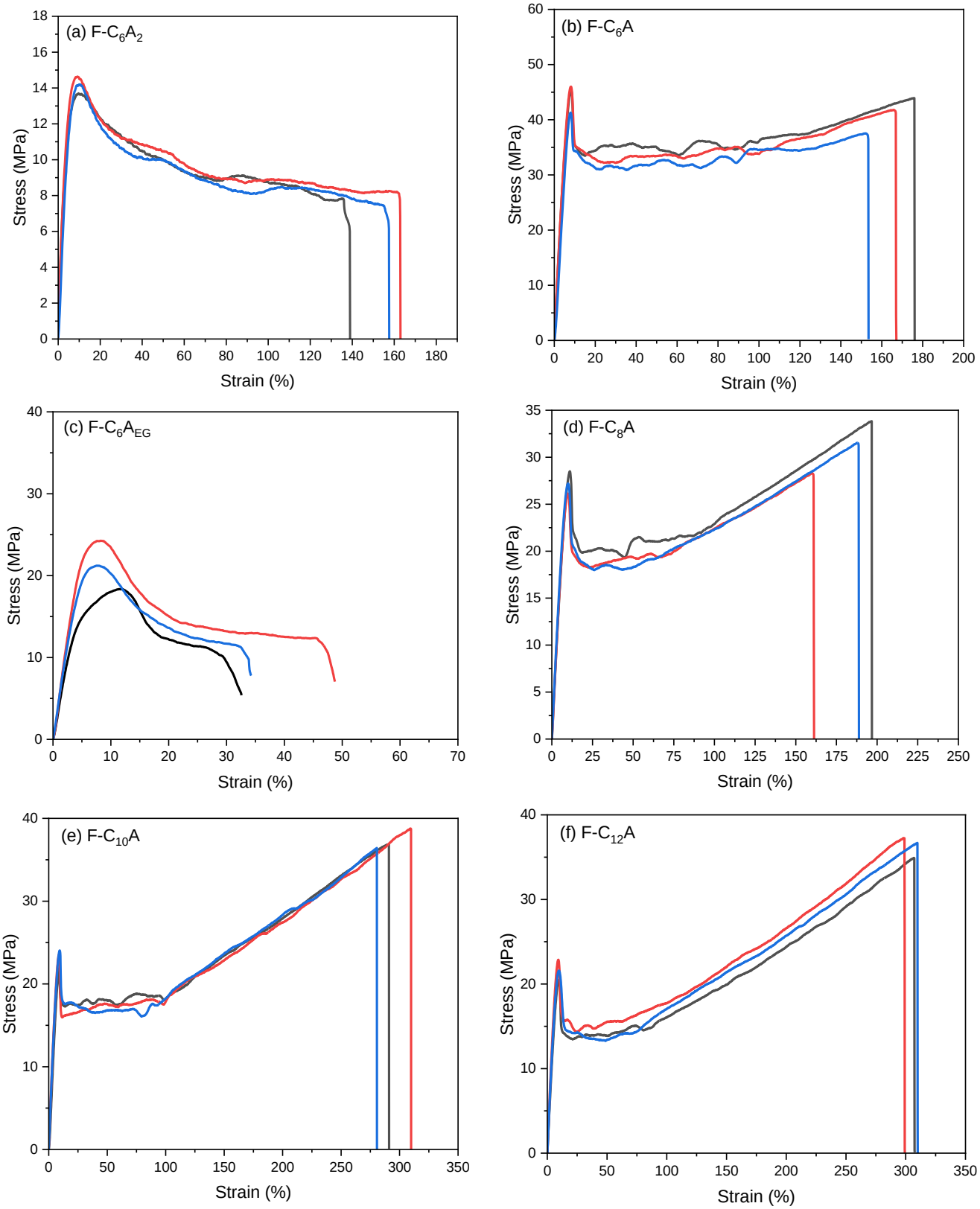

Figure S36. Stress *vs* strain curve for 3-day annealed polymer samples (a) F-C_6A_2; (b) F-C_6A; (c) F-C_6A_{EG}; (d) F-C_8A; (e) F-$C_{10}A$; (f) F-$C_{12}A$. *n = 3*

Tensile curve of commodity plastics

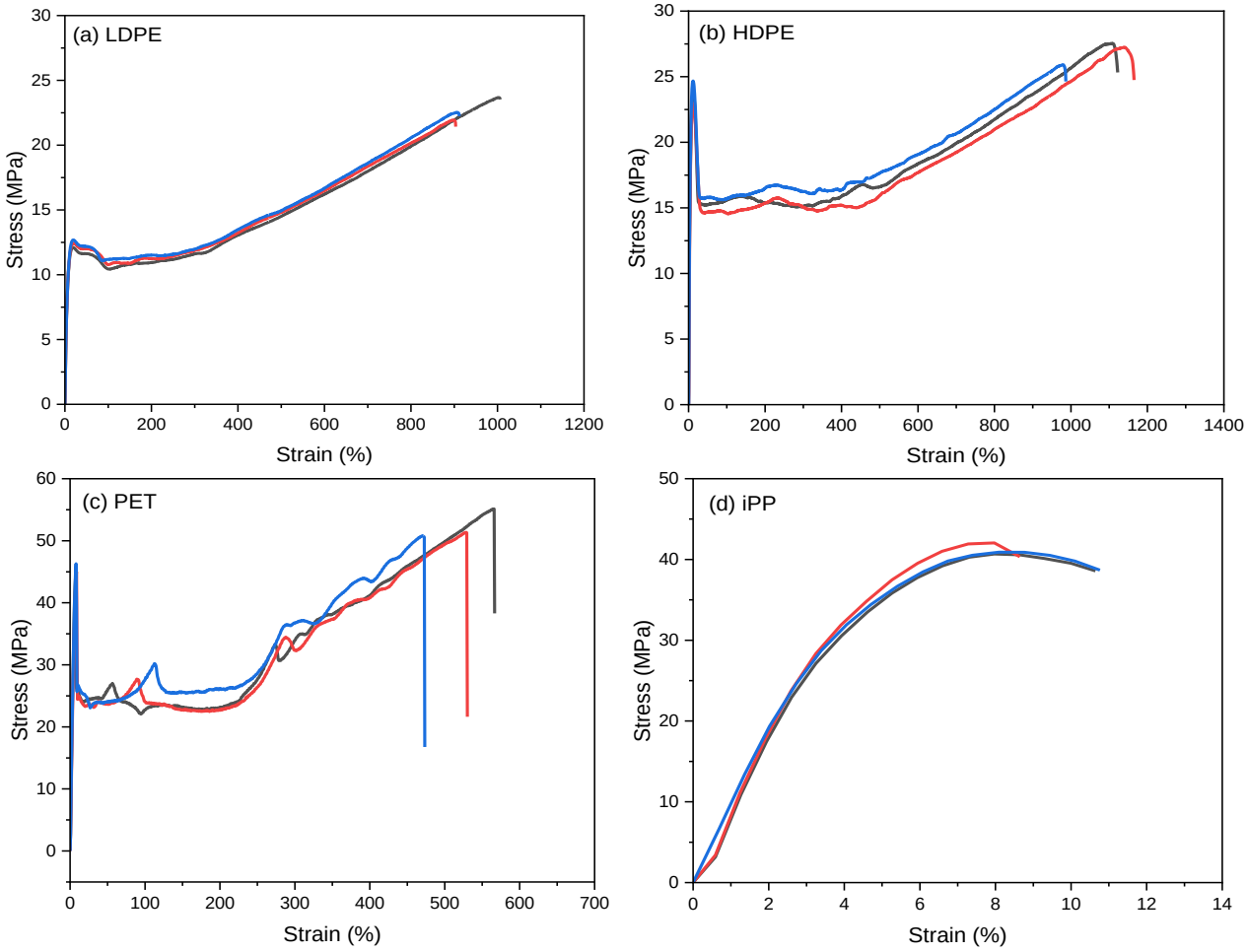

Figure S37. Stress *vs* strain curve for commodity plastic samples (a) LDPE; (b) HDPE; (c) PET; (d) *i*PP. *n = 3*

Impact of molecular weight upon tensile properties

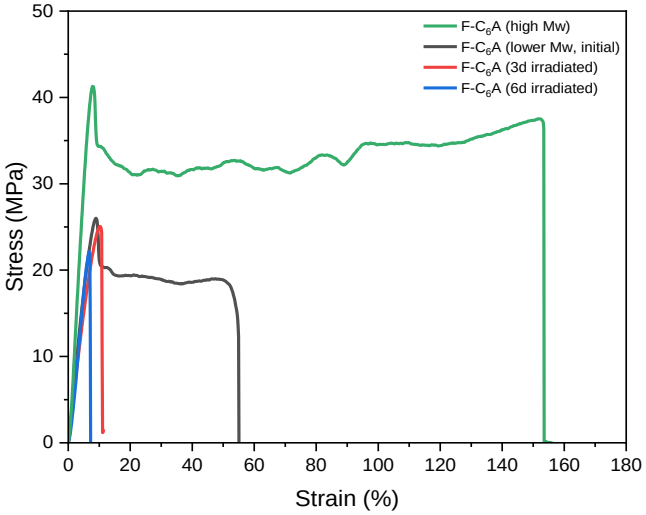

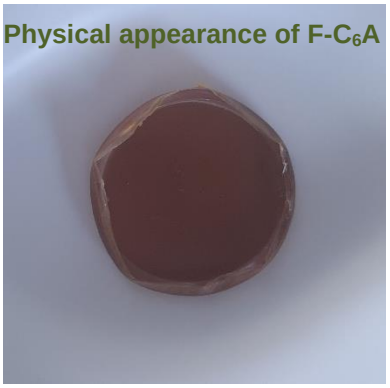

Figure S38. Representative stress *vs* strain curve of F-C_6A (a) High Mw (129 kDa); (b) Low Mw (74 kDa; control); (c) Irradiated for 3d (18 kDa); (d) Irradiated for 6d (16 kDa) tested at 10 mm·min^{-1} and 22 °C. **Irradiation intensity (50 W/m^2)*

Photodegradation studies

a) Polymer F-C$_6$A$_2$

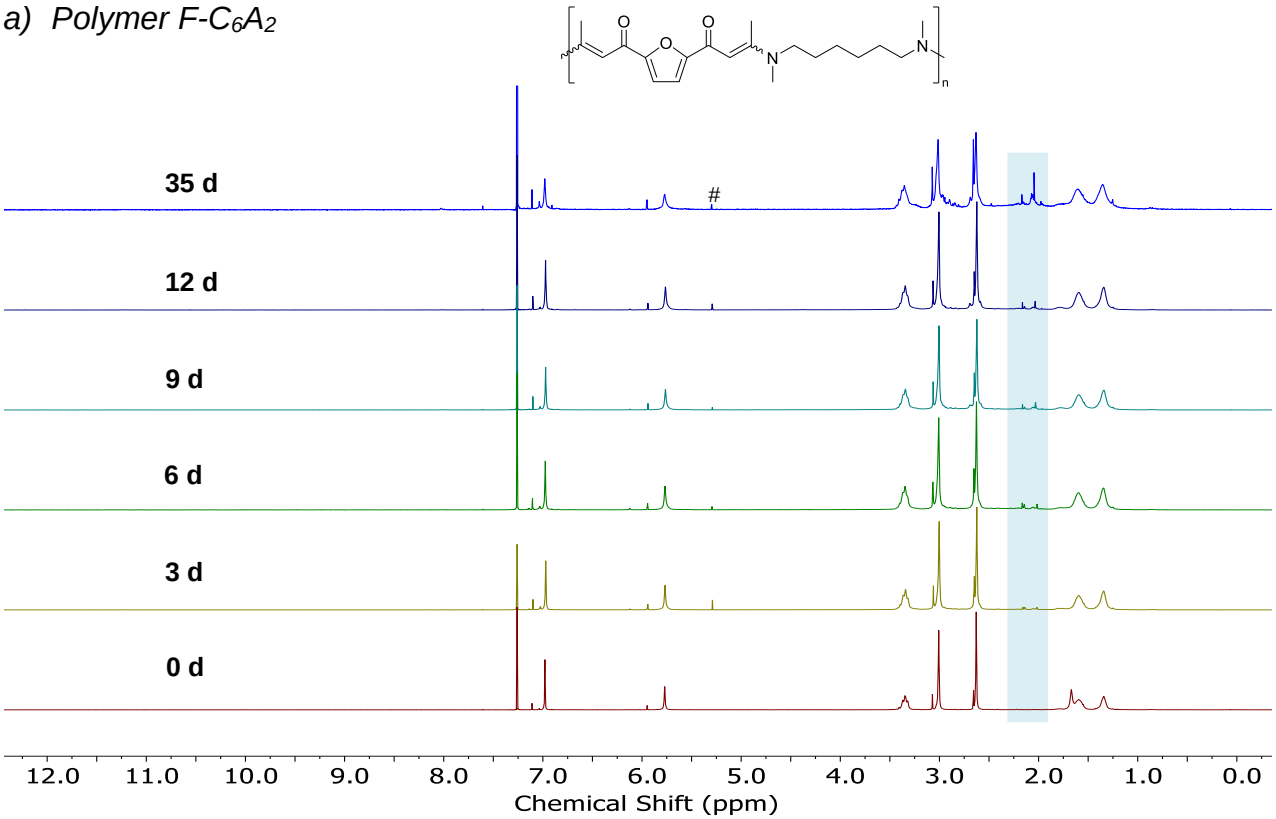

Figure S39. ^{1}H NMR spectra of polymer film F-C$_6$A$_2$ stacked to illustrate the change of spectrum for 35 days. *#residual DCM*

b) Polymer F-C$_6$A

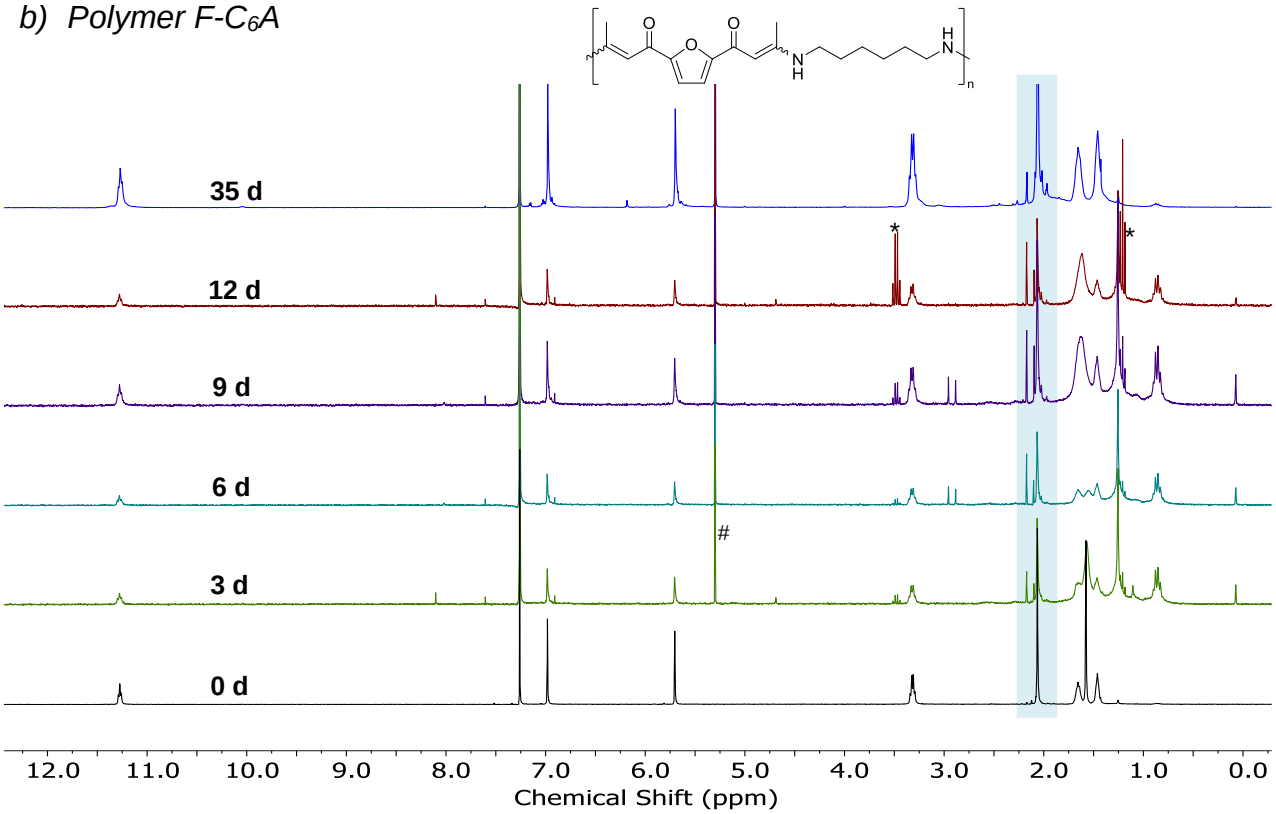

Figure S40. ^{1}H NMR spectra of polymer film F-C$_6$A stacked to illustrate the change of spectrum for 35 days. **Residual ether, #residual DCM*

c) Polymer F-C$_6$A$_{EG}$

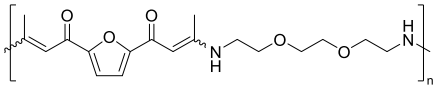

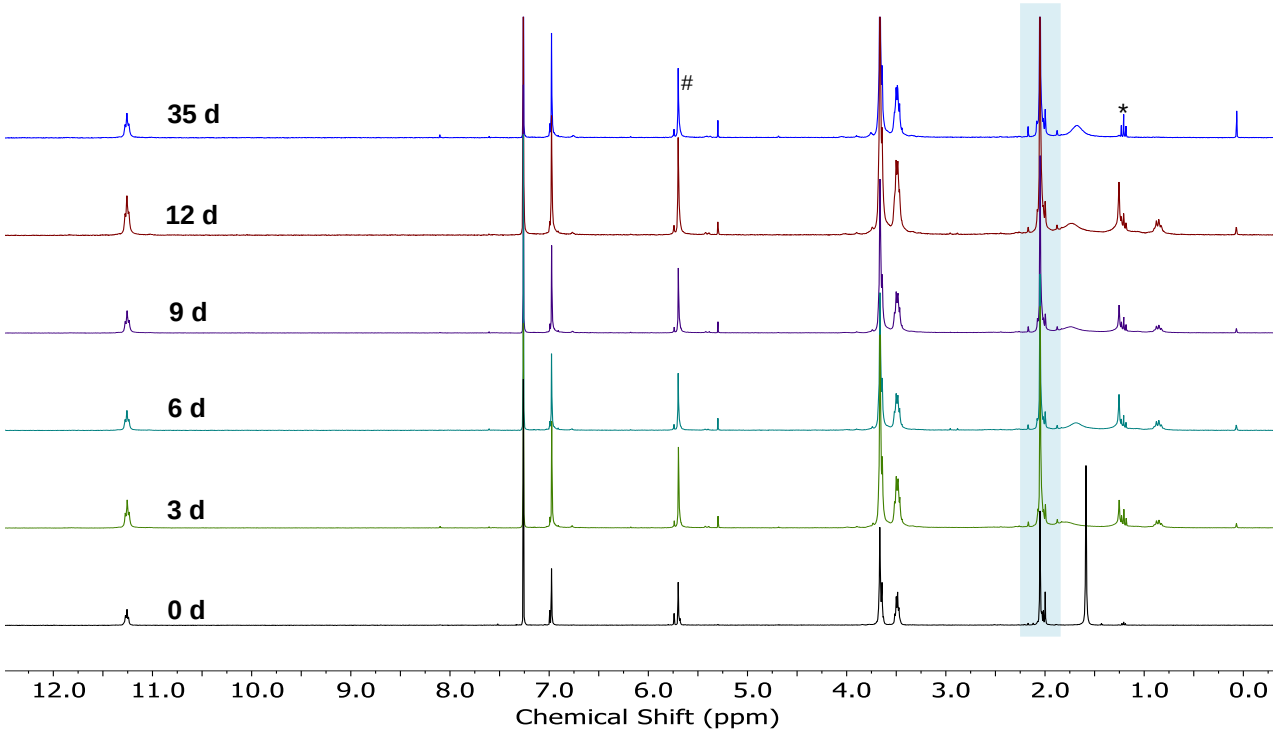

Figure S41. ^{1}H NMR spectra of polymer film F-C_6A_{EG} stacked to illustrate the change of spectrum for 35 days. **Residual ether, #residual DCM*

d) Polymer F-C_8A

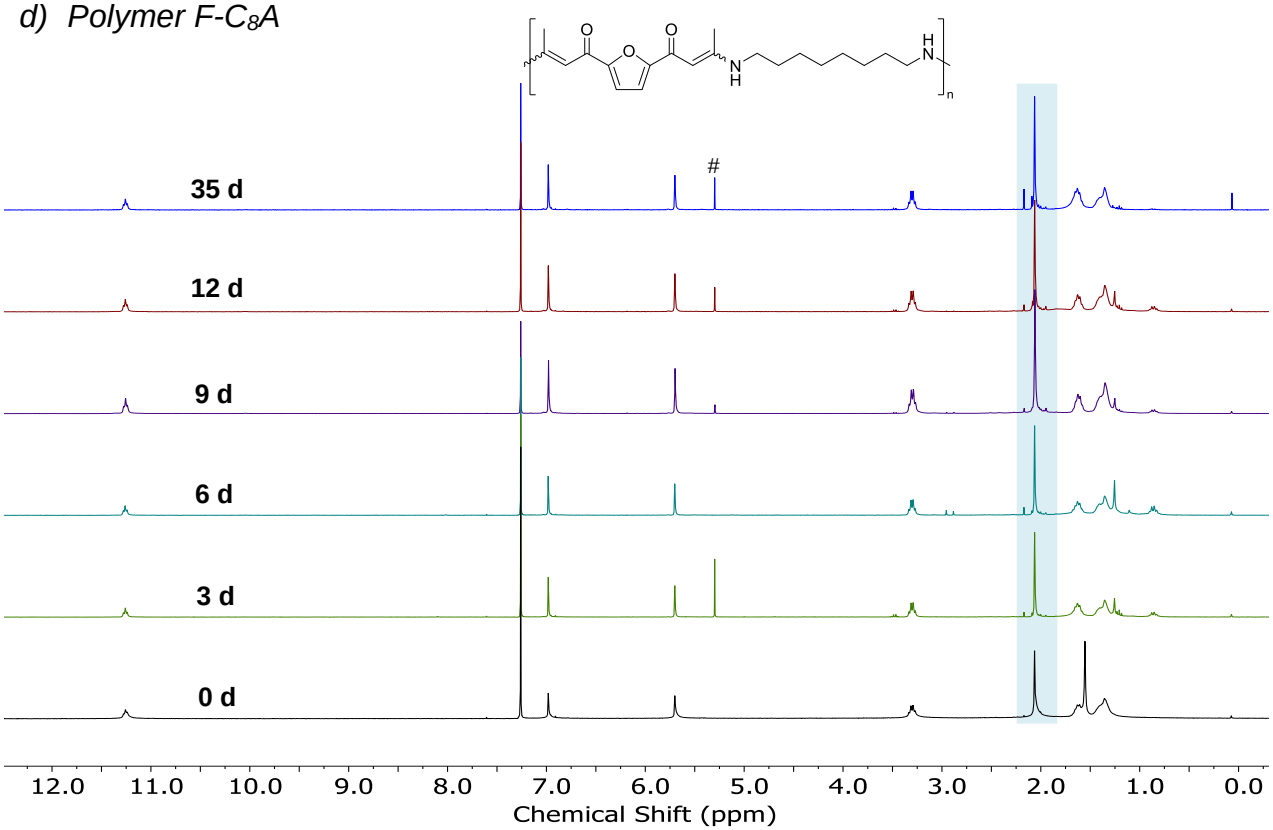

Figure S42. ^{1}H NMR spectra of polymer film F-C_8A stacked to illustrate the change of spectrum for 35 days. *#residual DCM*

e) Polymer F-$C_{10}A$

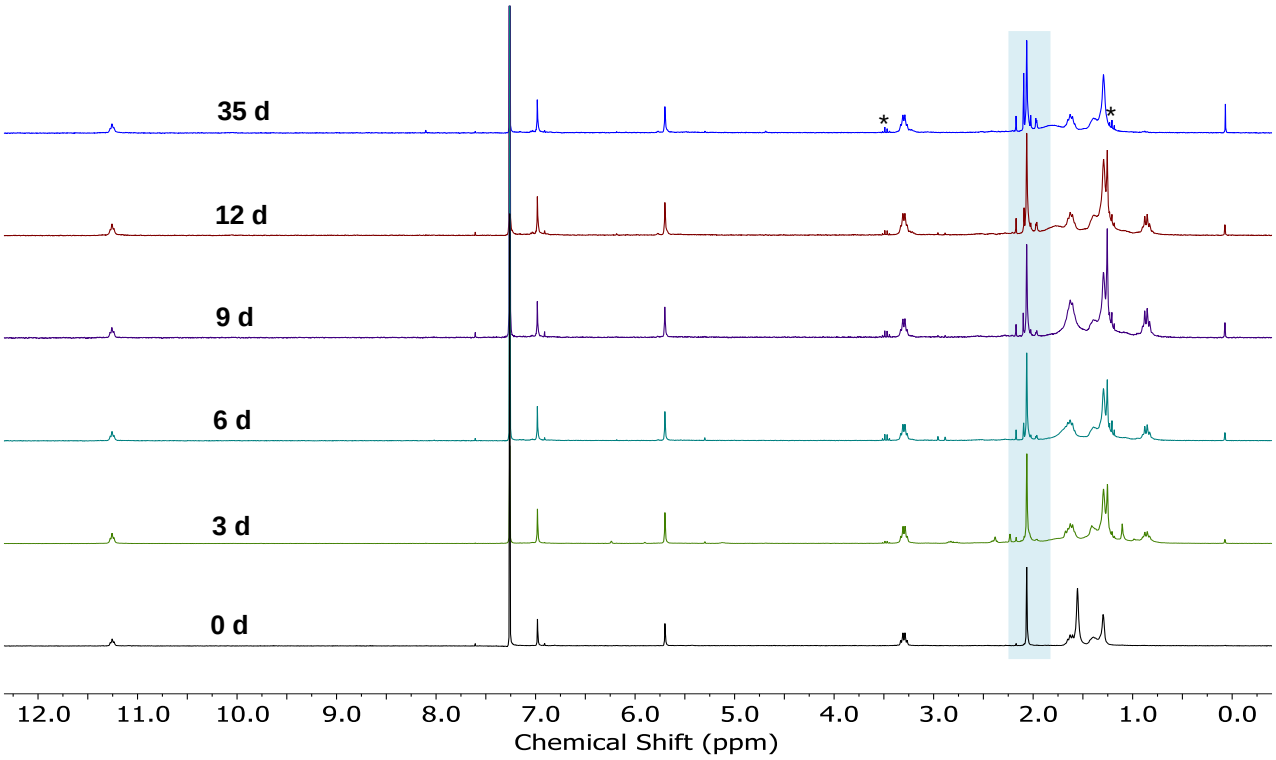

Figure S43. ^{1}H NMR spectra of polymer film F-C_{10}A stacked to illustrate the change of spectrum for 35 days. **Residual ether*

f) Polymer F-C_{12}A

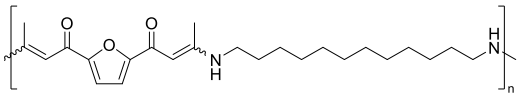

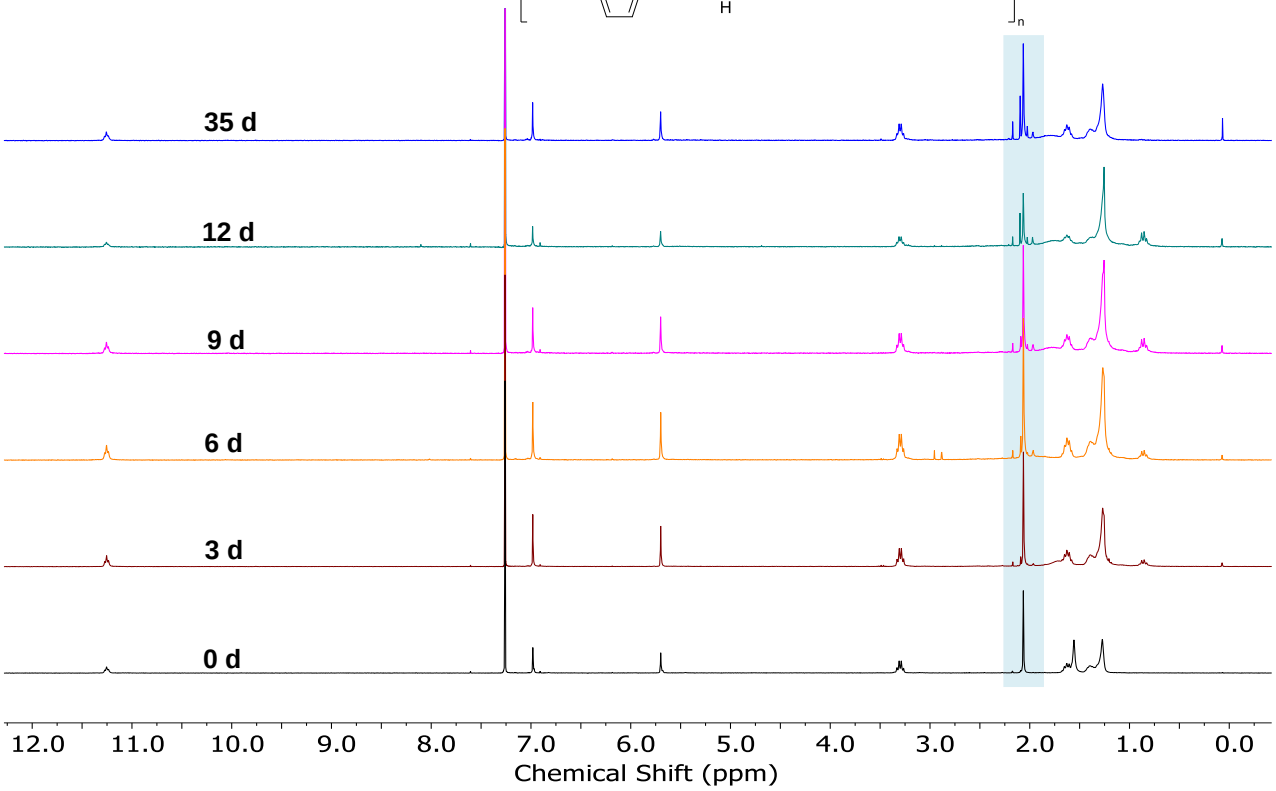

Figure S44. ^{1}H NMR spectra of polymer film F-C_{12}A stacked to illustrate the change of spectrum for 35 days

^{1}H NMR stack of irradiated polymers solution (20 mg/mL $CDCl_3$)

a) Polymer F-C_6A_2 in $CDCl_3$

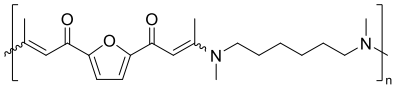

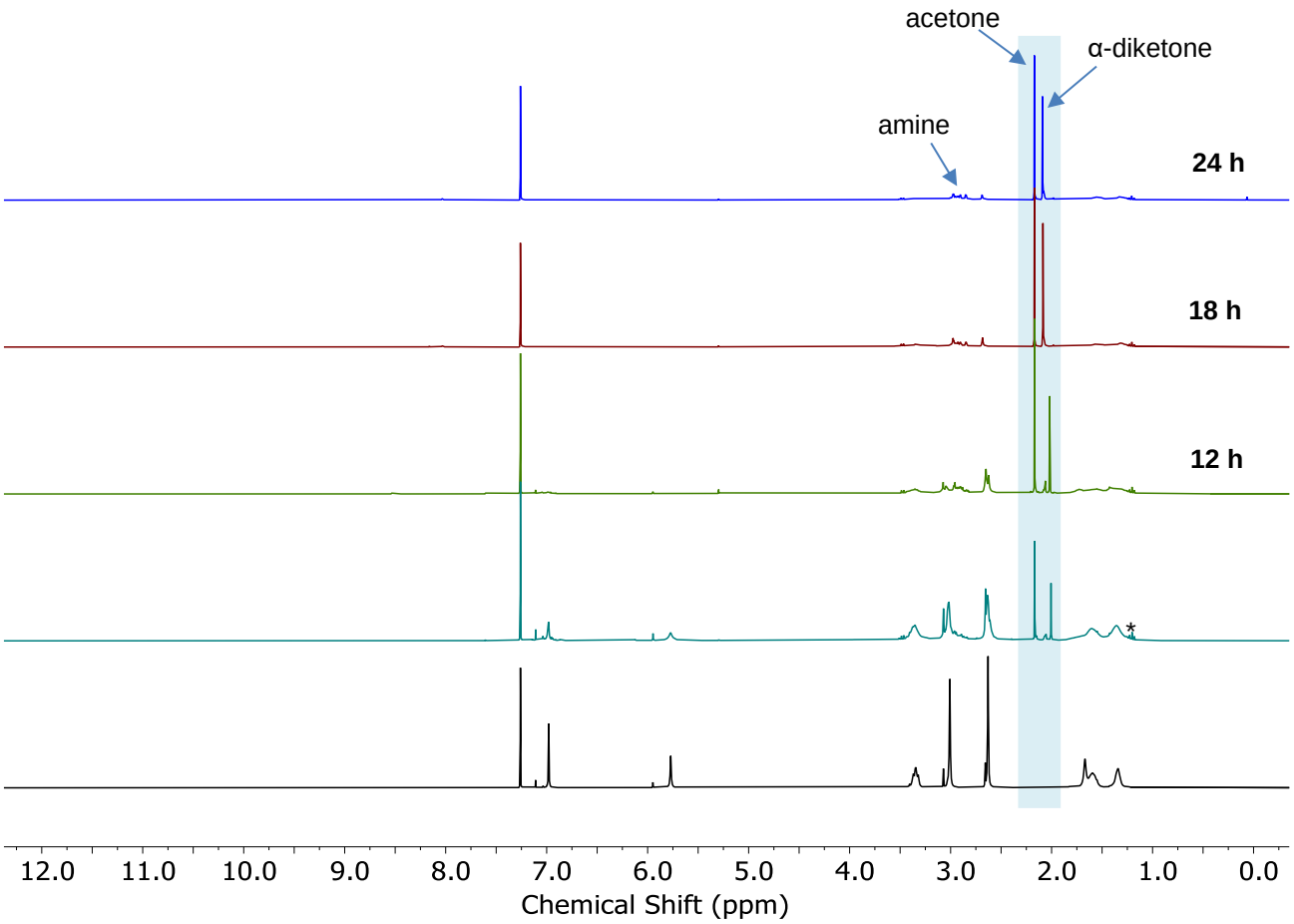

Figure S45. ^{1}H NMR spectra of polymer F-C_6A_2 (yellow) stacked to illustrate the change of spectrum until fully degraded (colorless). *Residual ether

b) Polymer F-C_6A in $CDCl_3$

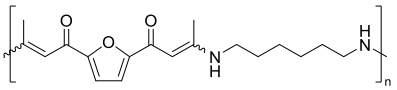

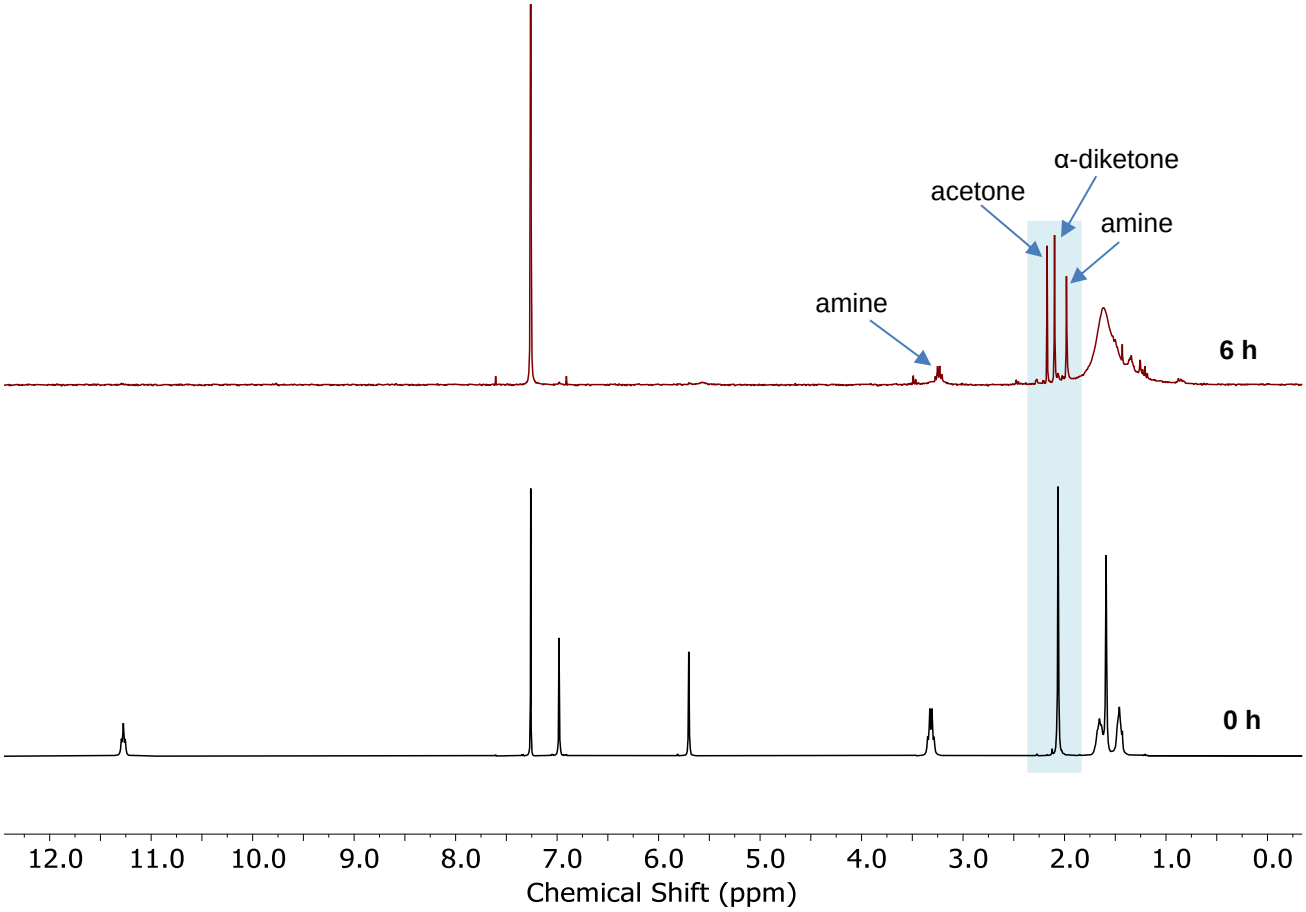

Figure S46. ^{1}H NMR spectra of polymer F-C_6A (yellow) stacked to illustrate the change of spectrum until fully degraded (colorless)

c) Polymer F-C_6A_{EG} in $CDCl_3$

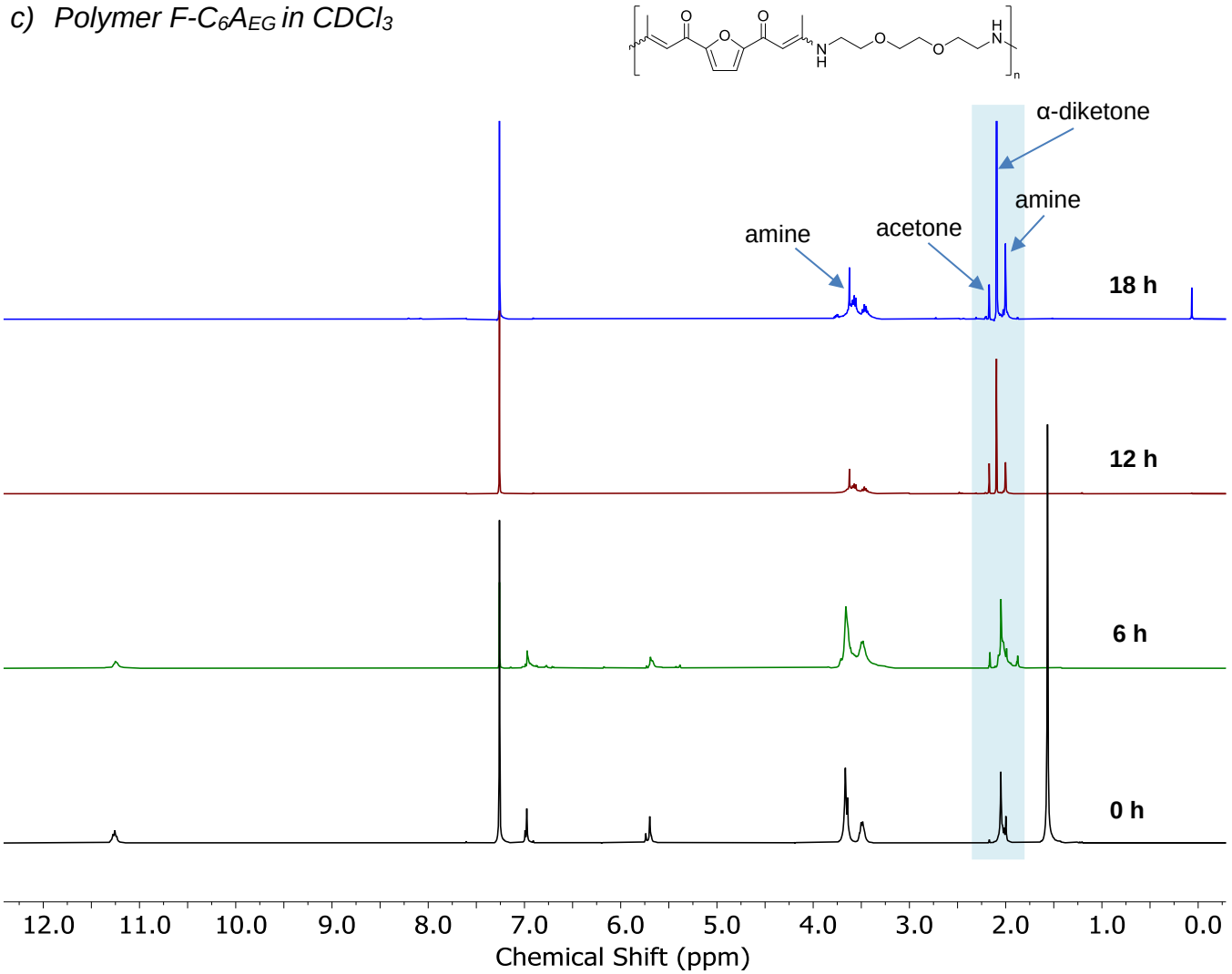

Figure S47. ^{1}H NMR spectra stacked of polymer F-C_6A_{EG} (yellow solution) stacked to illustrate the change of spectrum until fully degraded (colorless solution)

d) Polymer F-C_8A in $CDCl_3$

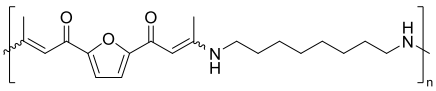

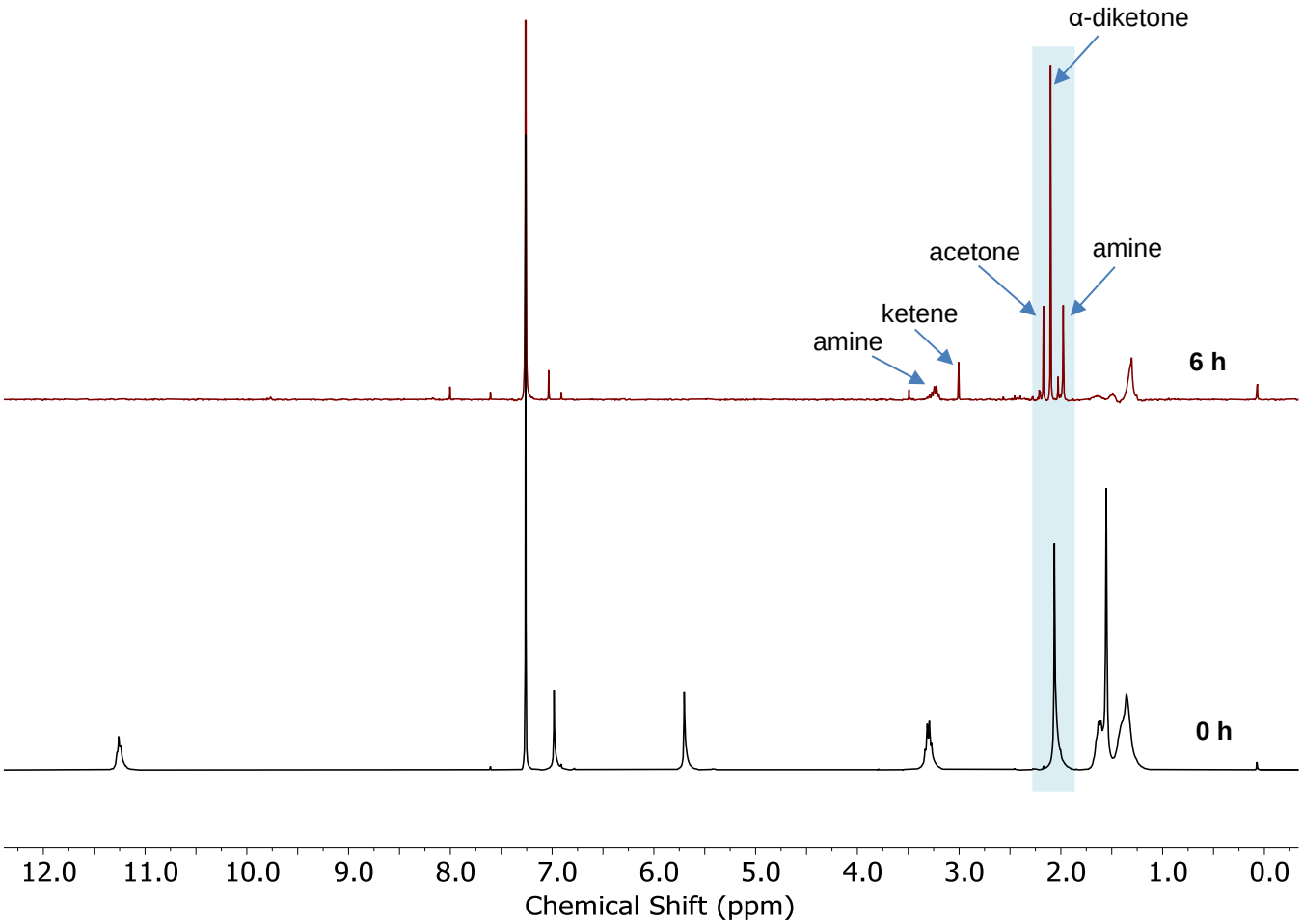

Figure S48. ^{1}H NMR spectra of polymer F-C_8A (yellow solution) stacked to illustrate the change of spectrum until fully degraded (colorless solution)

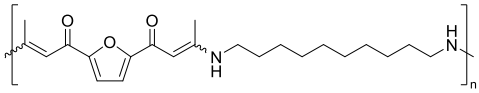

e) Polymer F-C_{10}A in $CDCl_3$

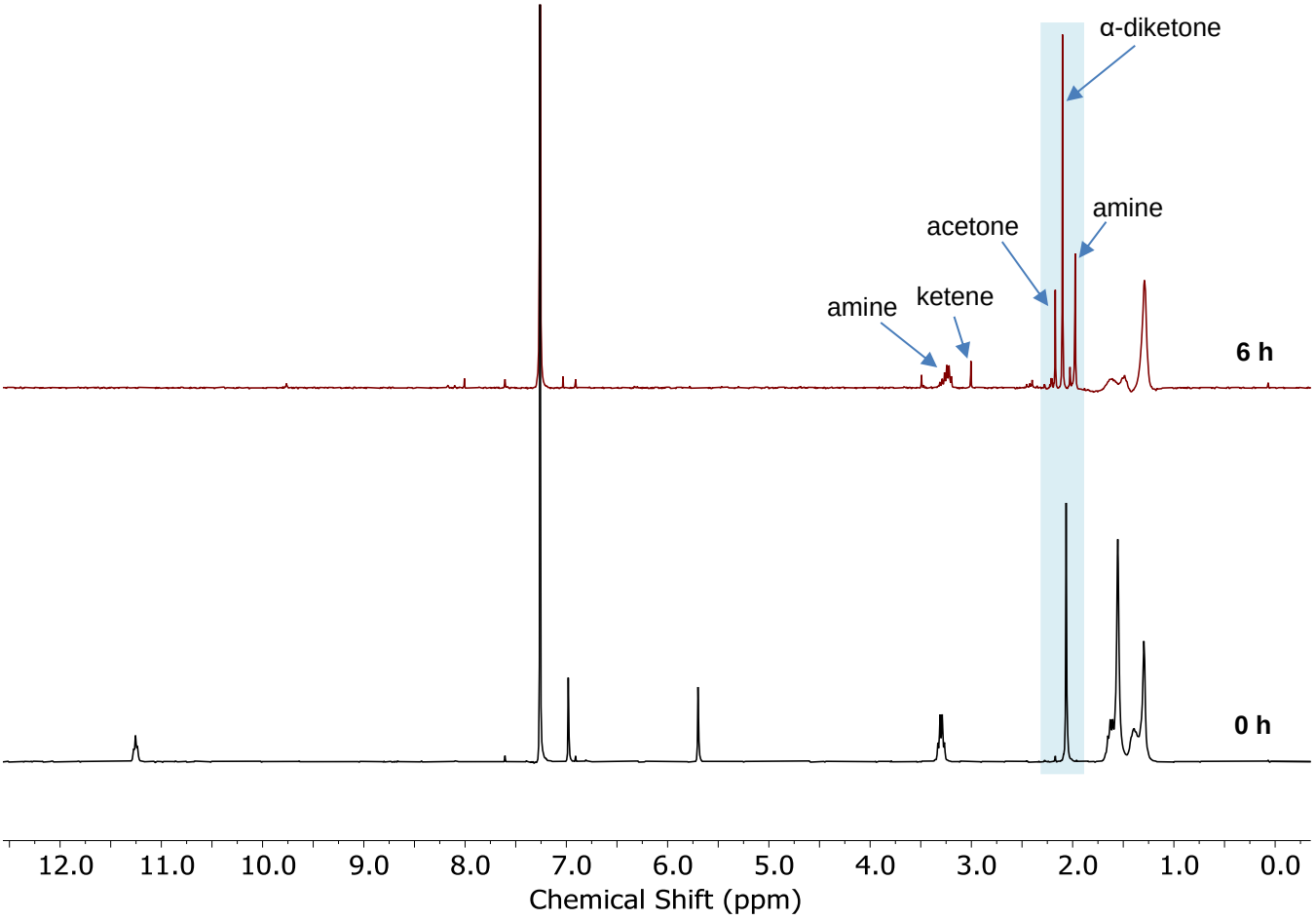

Figure S49. ^{1}H NMR spectra of polymer F-C_{10}A (yellow solution) stacked to illustrate the change of spectrum until fully degraded (colorless solution)

f) Polymer F-C_{12}A in $CDCl_3$

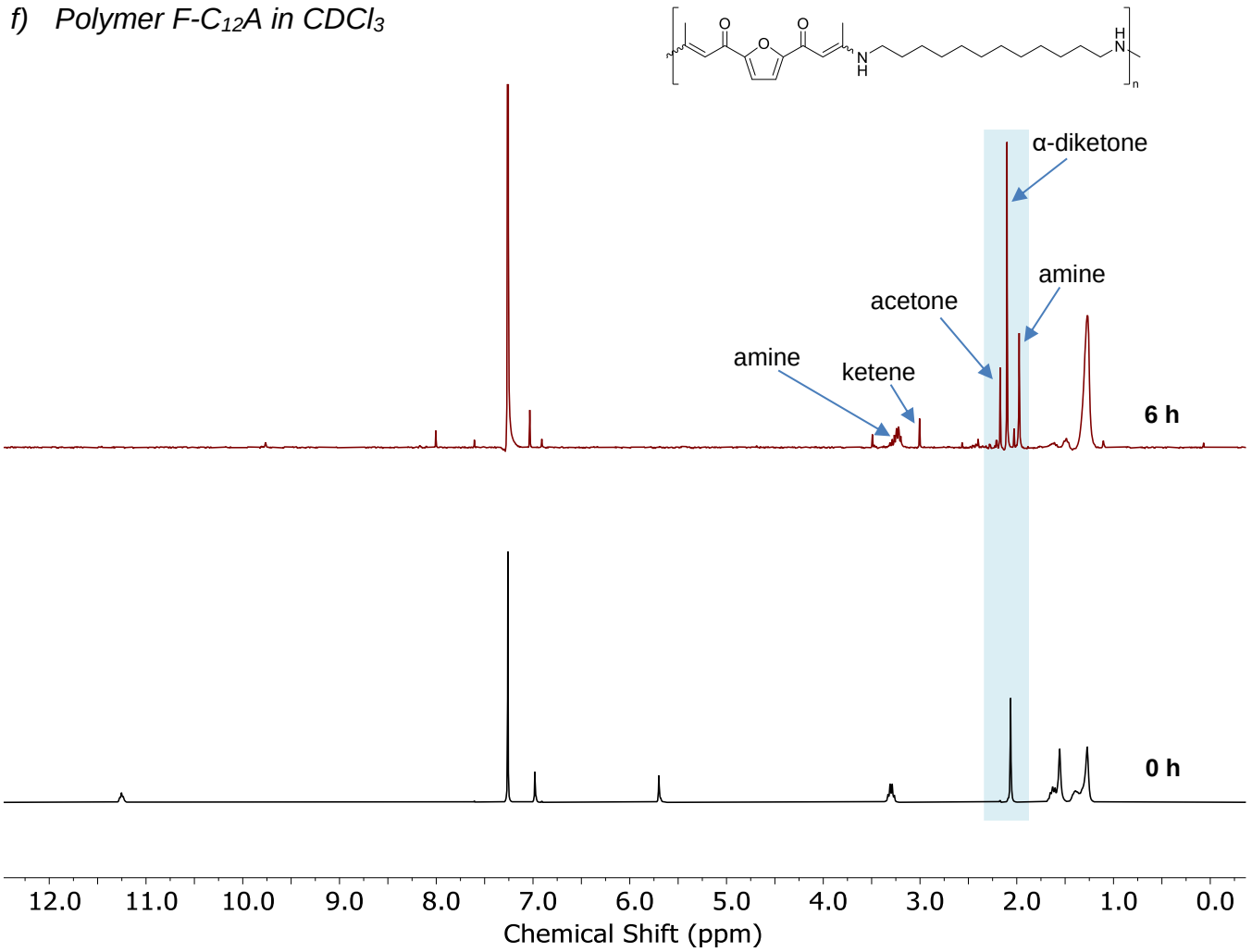

Figure S50. ^{1}H NMR spectra of polymer F-C_{12}A (yellow solution) stacked to illustrate the change of spectrum until fully degraded (colorless solution)

^{1}H NMR stack of irradiated model compounds

a) Model F-C_6A

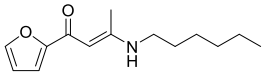

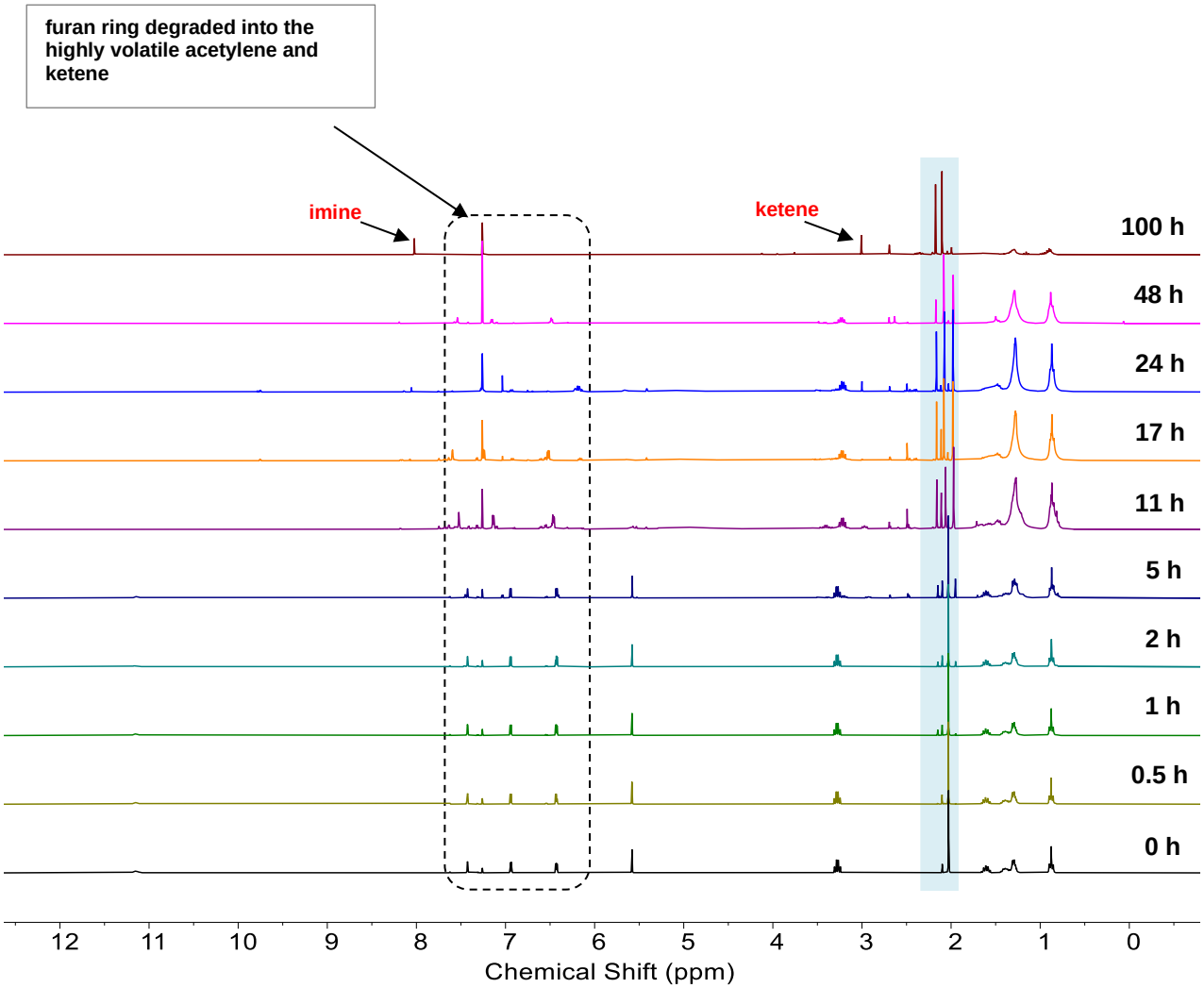

Figure S51. ^{1}H NMR spectra of model F-C_6A stacked to illustrate the change of spectrum for 100 h

b) Model Ph-C_6A

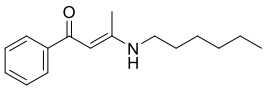

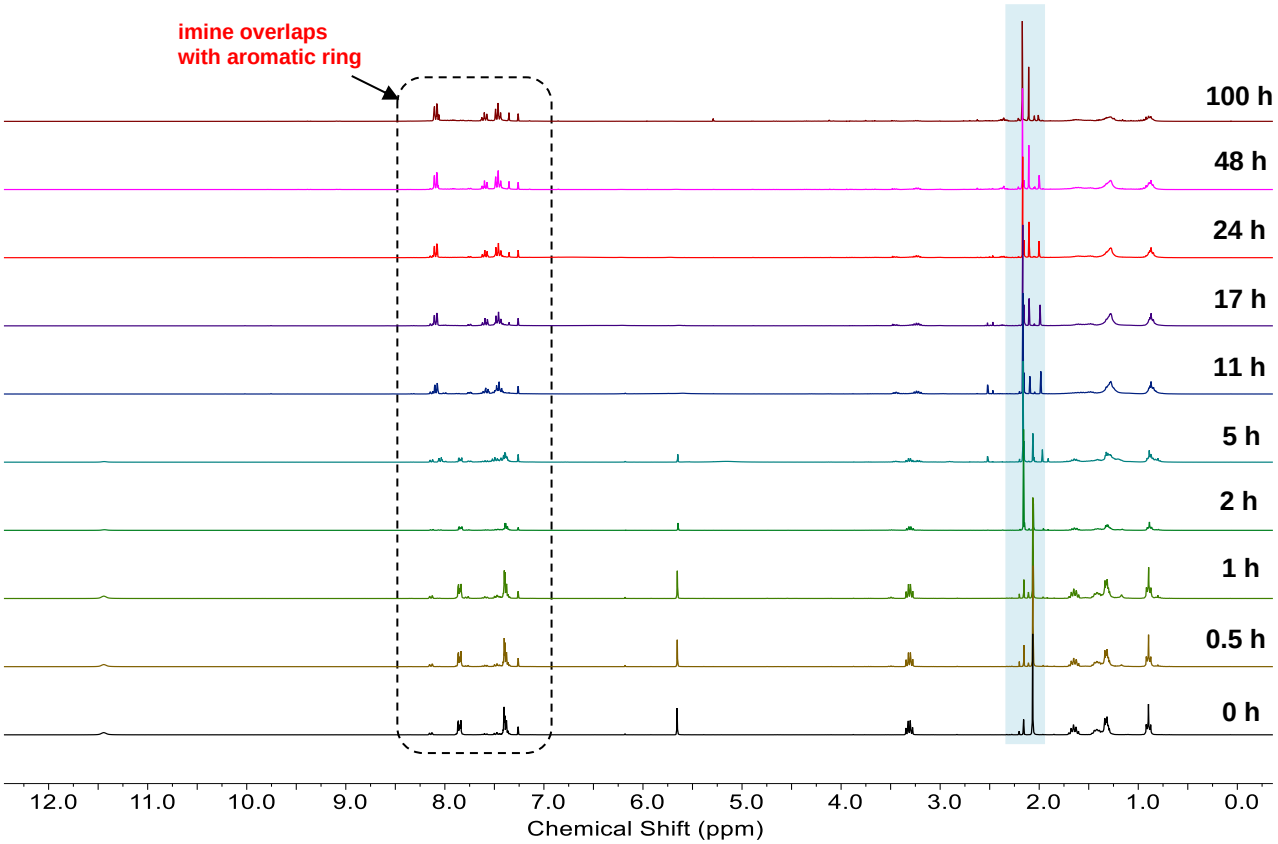

Figure S52. ^{1}H NMR spectra of model Ph-C_6A stacked to illustrate the change of spectrum for 100 h

Infrared spectra of representative irradiated polyketone film

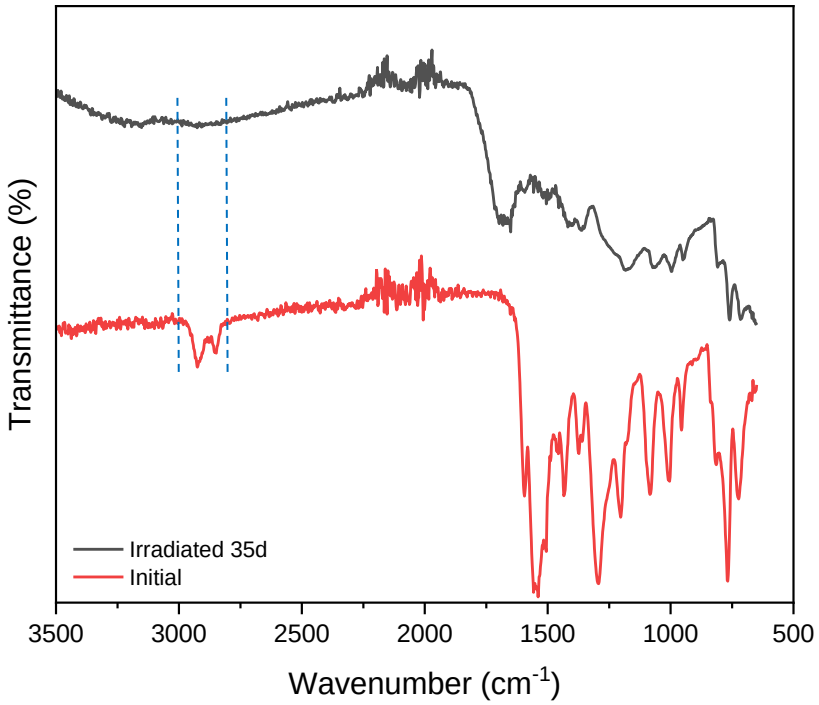

Figure S53. FTIR spectra of F-C_6A before and after irradiation

Size exclusion chromatograms of all irradiated films

a) Irradiated polymer films

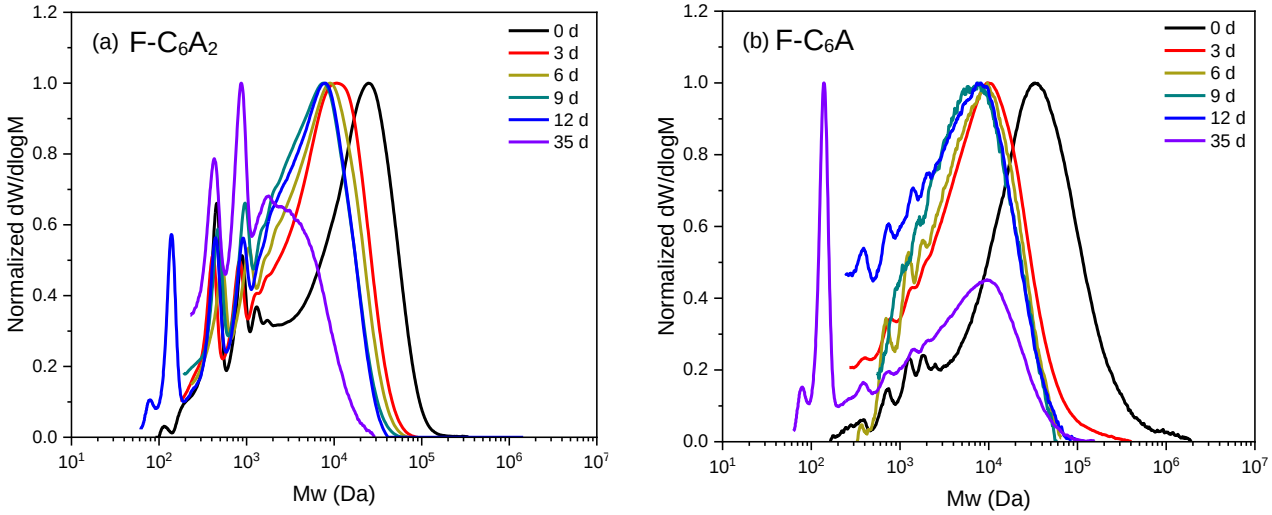

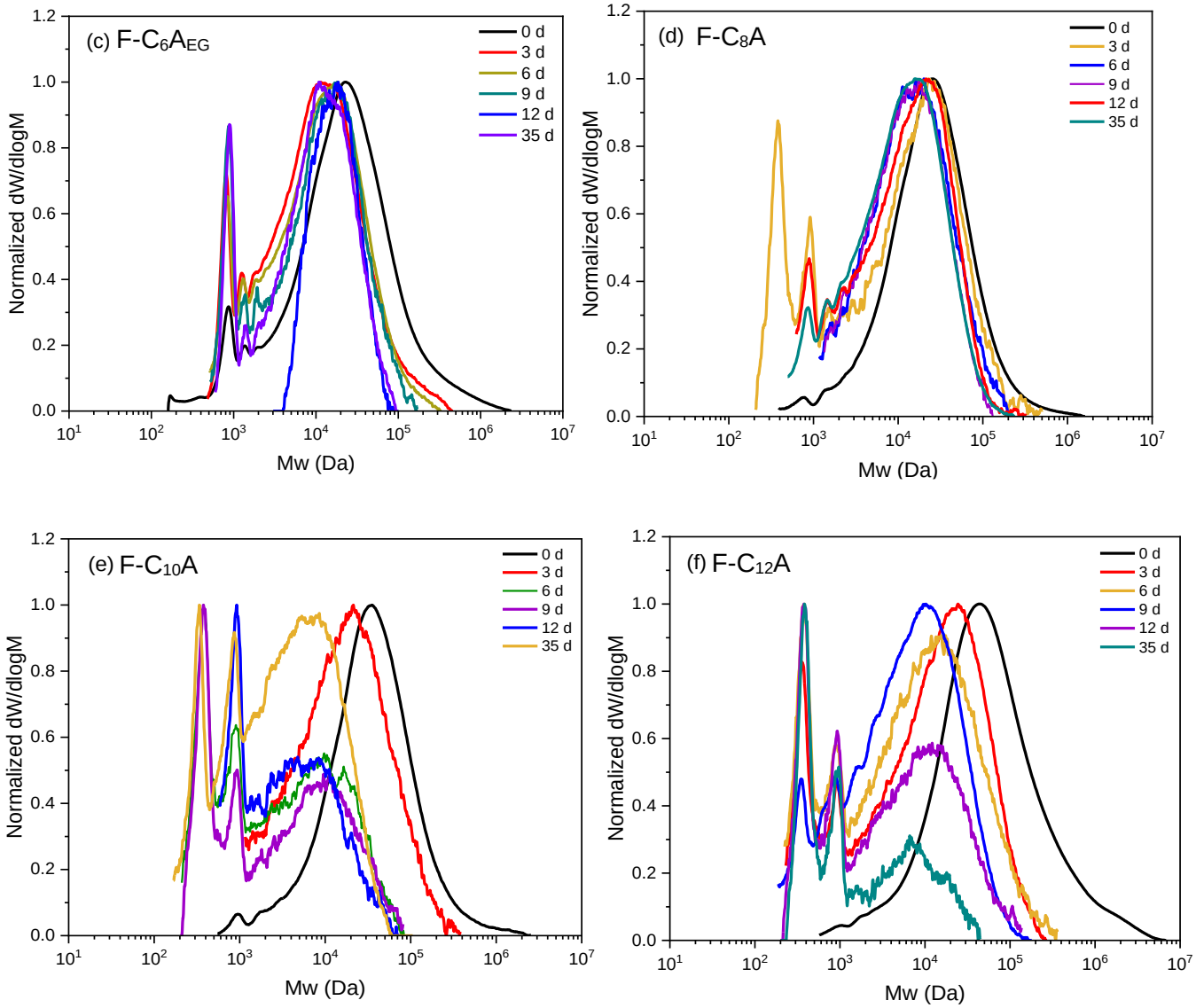

Figure S54. Normalized size exclusion chromatograms of irradiated polymer films ($CHCl_3$, 0.5% NEt_3, 40 °C) analysis against poly(styrene) (PS) standards. (a) F-C_6A_2; (b) F-C_6A; (c) F-C_6A_{EG}; (d) F-C_8A; (e) F-$C_{10}A$; (f) F-$C_{12}A$

Size exclusion chromatograms of all irradiated polymers (20 mg/mL $CDCl_3$)

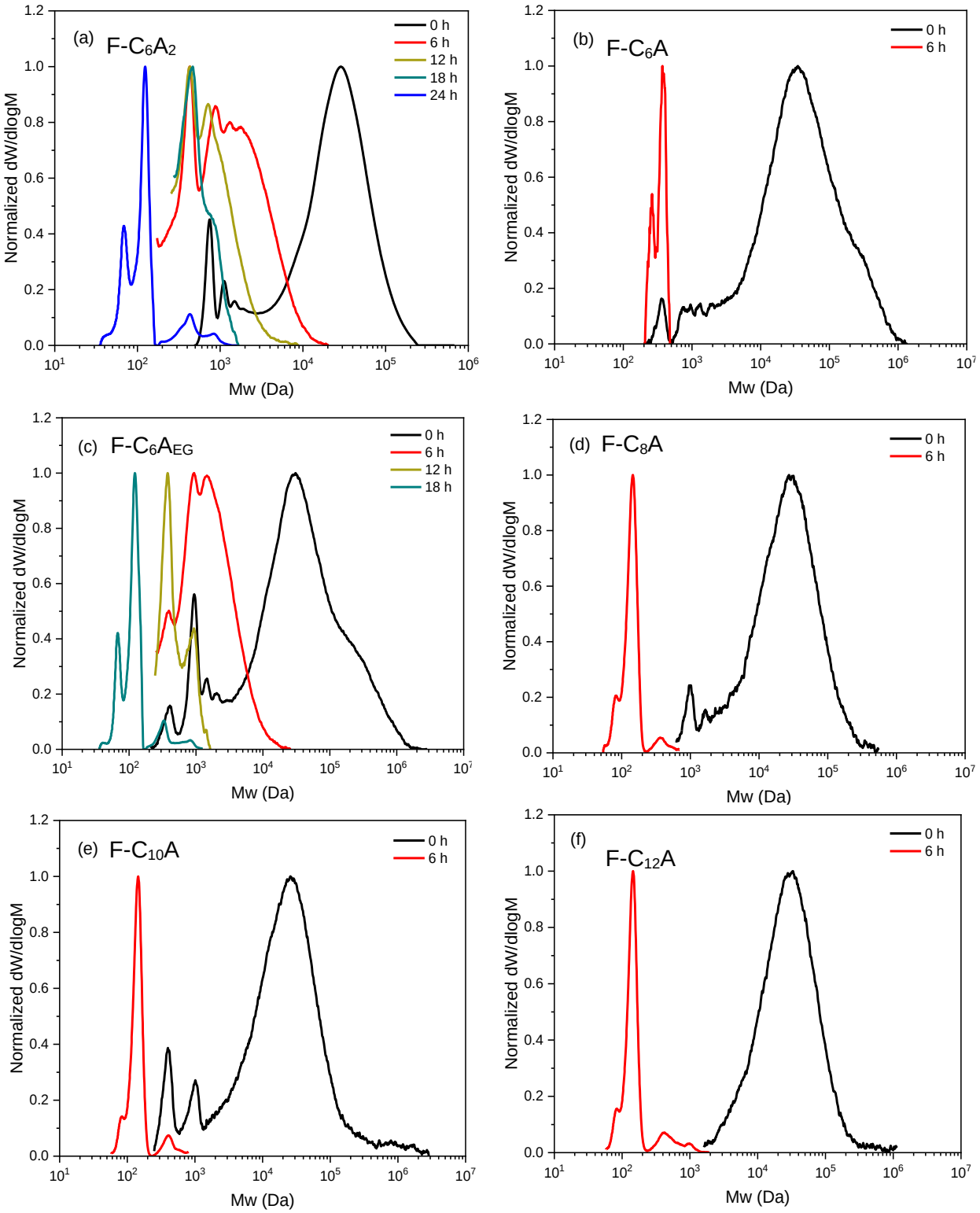

Figure S55. Normalized size exclusion chromatograms of irradiated polymer solutions ($CHCl_3$, 0.5% NEt_3, 40 °C) analysis against poly(styrene) (PS) standards. (a) F-C_6A_2; (b) F-C_6A; (c) F-C_6A_{EG}; (d) F-C_8A; (e) F-$C_{10}A$; (f) F-$C_{12}A$

Photodegradation products of F-C_6A

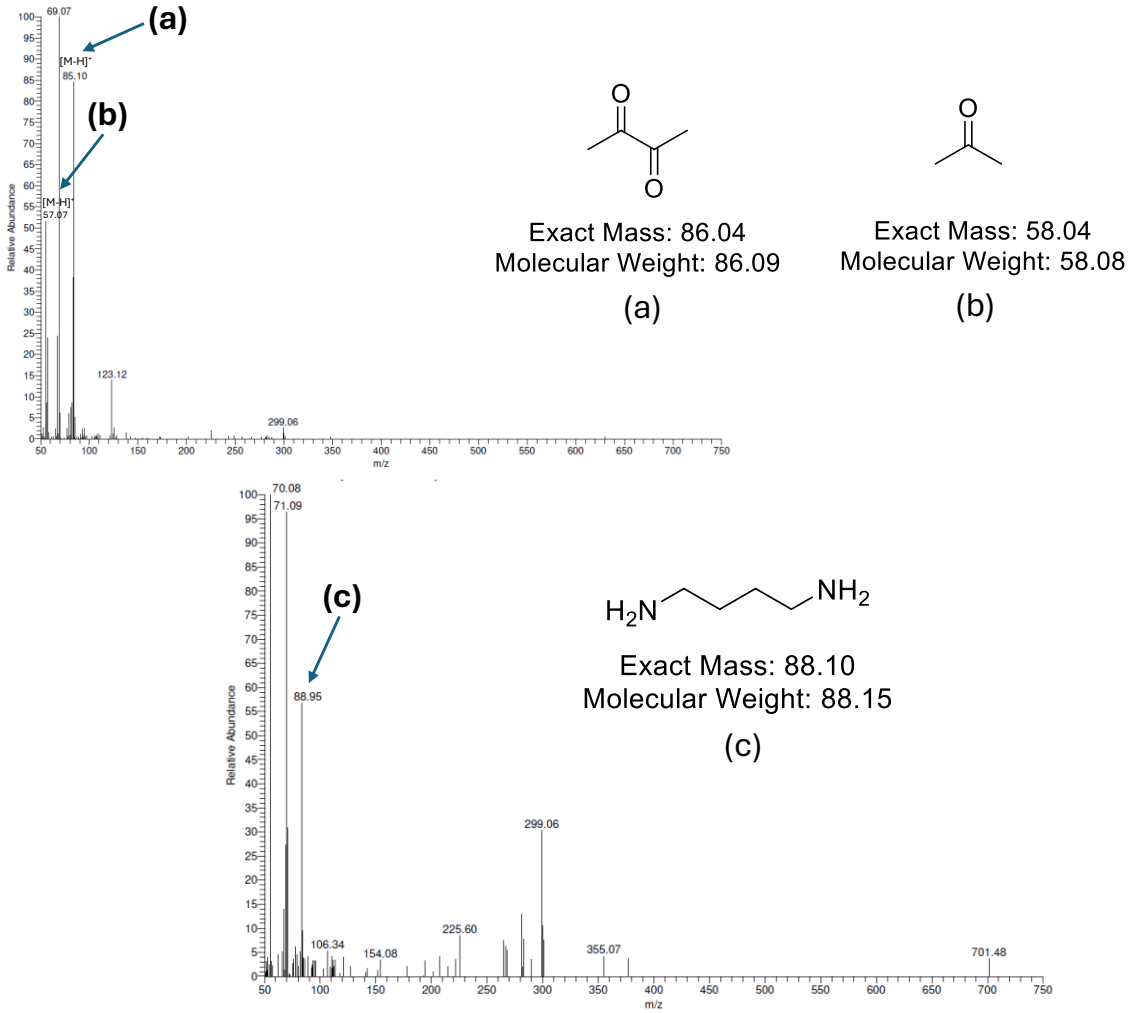

Figure S56. Mass spectra (EI-H+) of photodegradation ($CDCl_3$, 340 nm) for F-C_6A solution

Photodegradation products of F-C_6A_{EG}

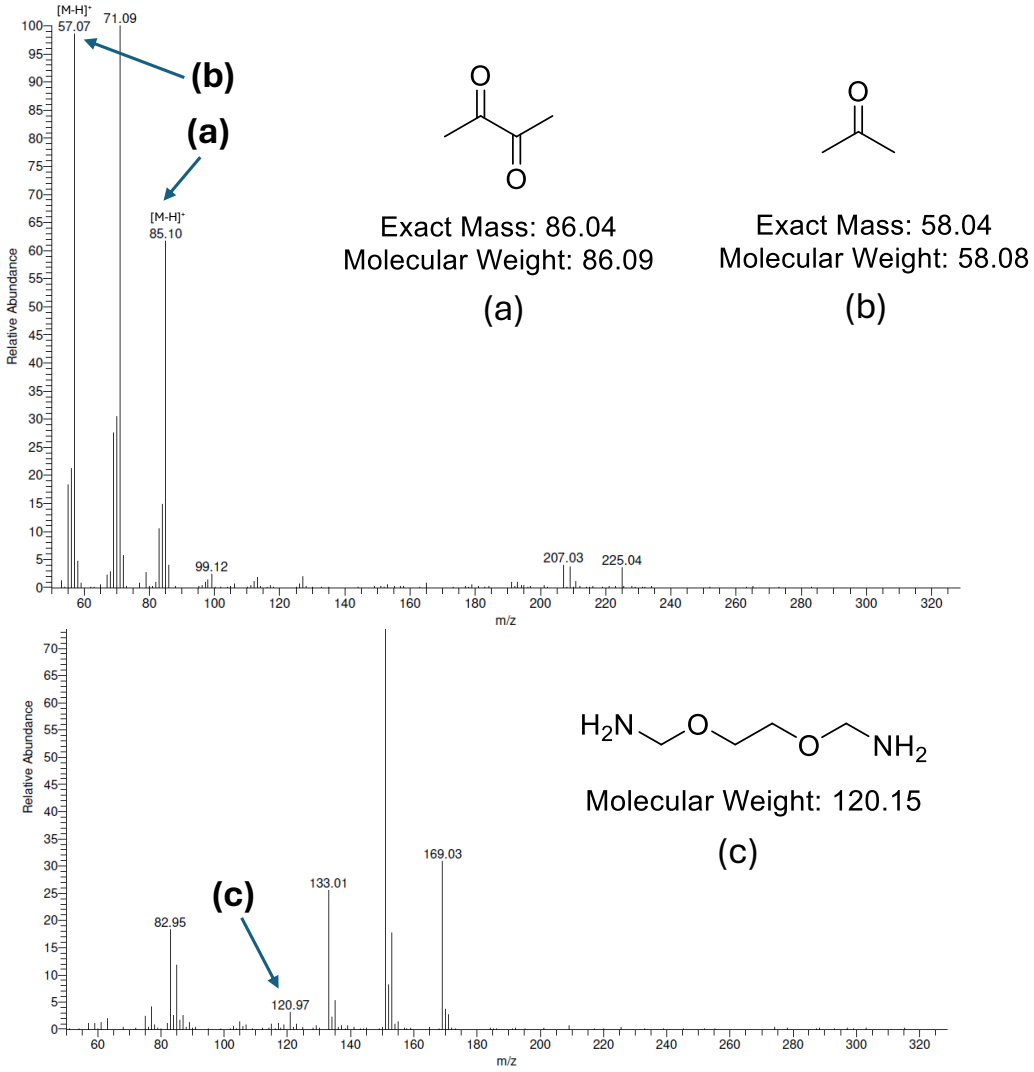

Figure S57. Mass spectra (EI-H+) of photodegradation ($CDCl_3$, 340 nm) for F-C_6A_{EG} solution

Photodegradation products of F-C_6A_2

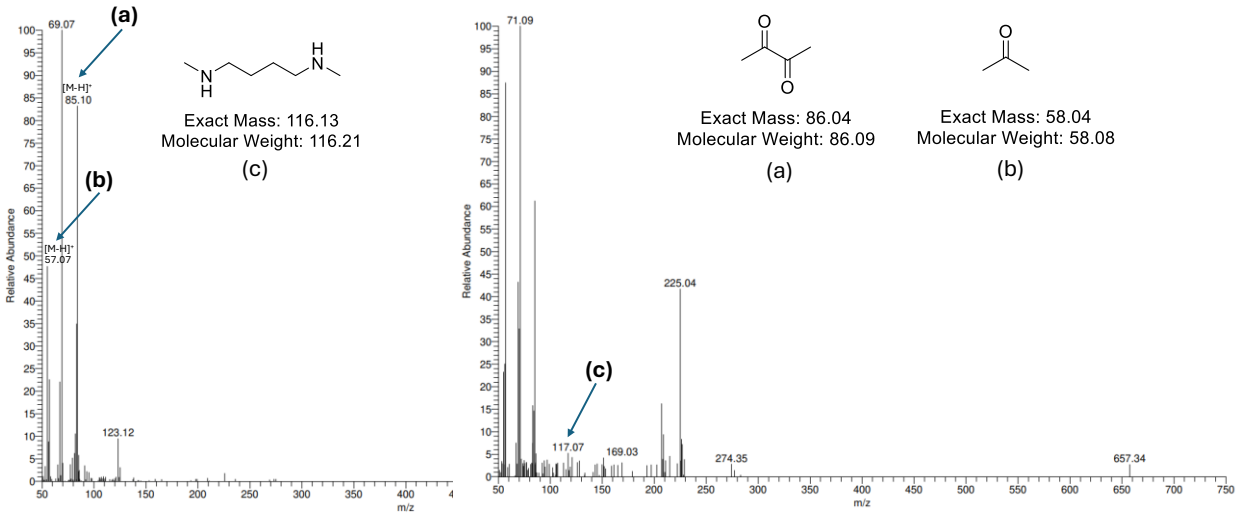

Figure S58. Mass spectra (EI-H+) of photodegradation ($CDCl_3$, 340 nm) for F-C_6A_2 solution

NMR spectra of photodegradation of concentrated representative sample F-C_6A_2 (PK based secondary amine, 50 mg/2 mL in $CDCl_3$)

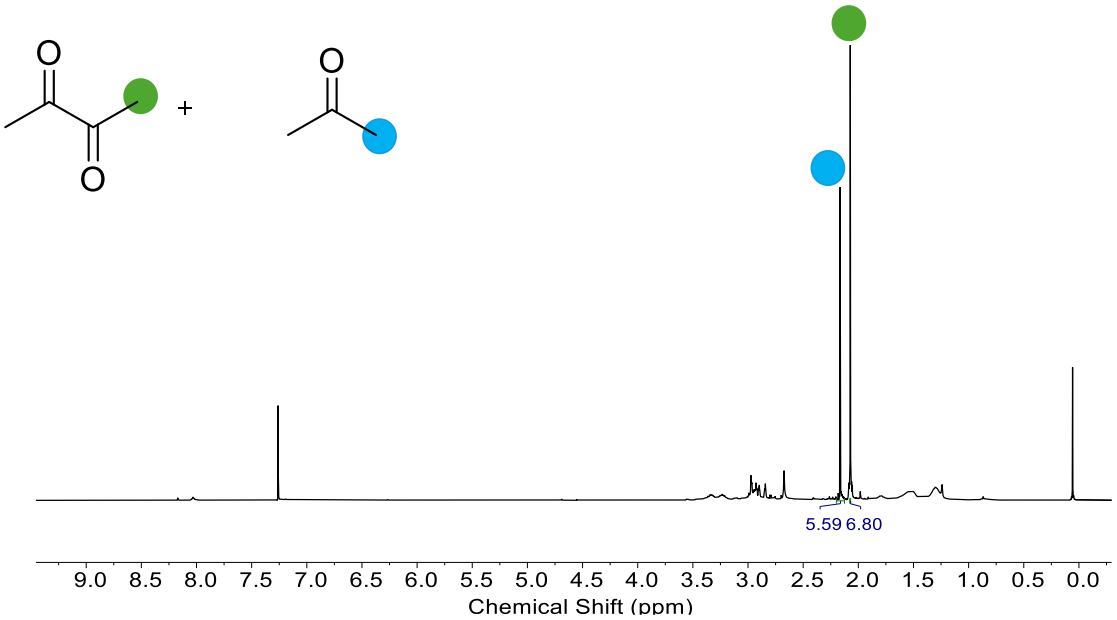

Figure S59. ^{1}H NMR spectrum of photodegraded F-C_6A_2 (284 h) (400 MHz, Chloroform-*d*)

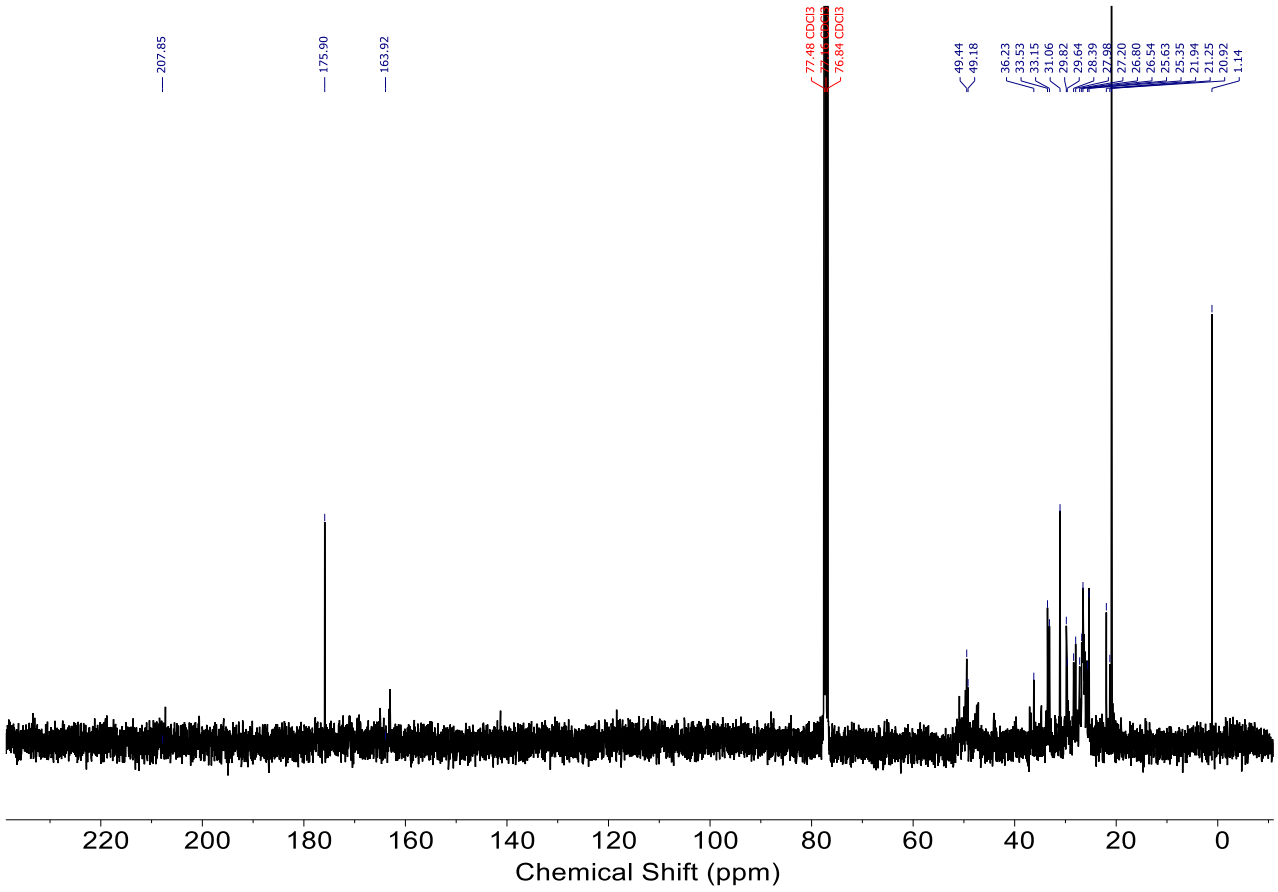

Figure S60. ^{13}C NMR spectrum of photodegraded F-C_6A_2 (284 h) (400 MHz, Chloroform-*d*)

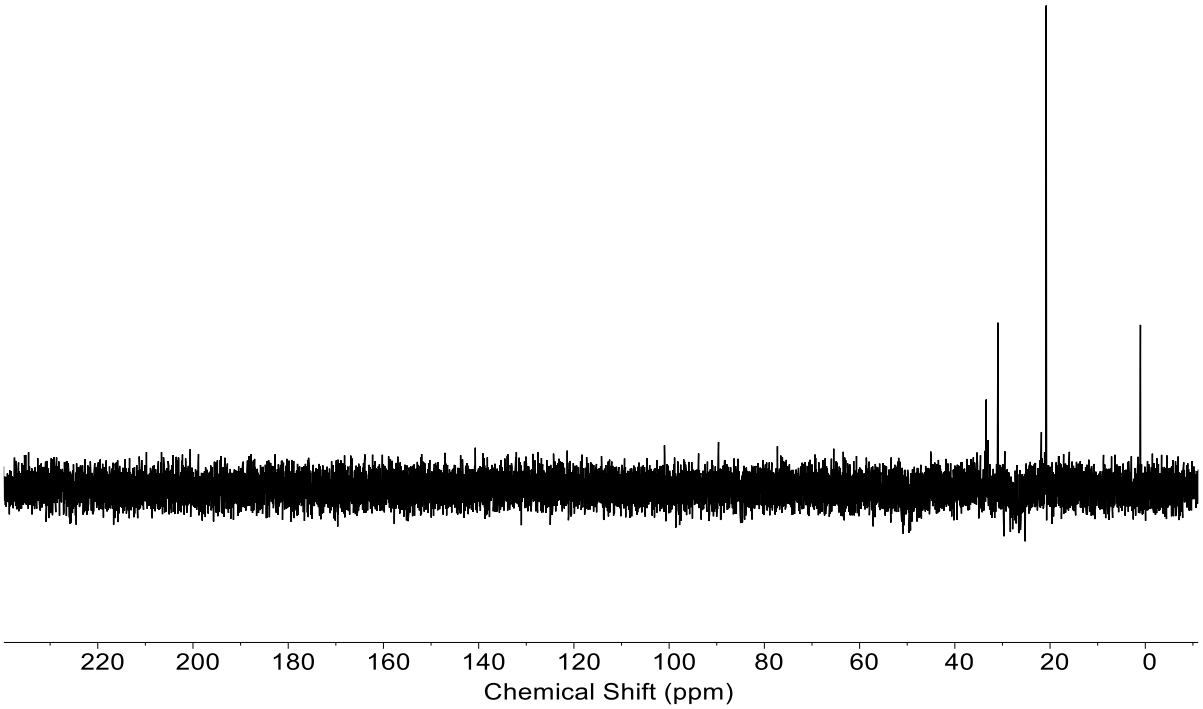

Figure S61. ^{13}C DEPT 135 NMR spectrum of photodegraded F-C_6A_2 (284 h) (400 MHz, Chloroform-*d*)

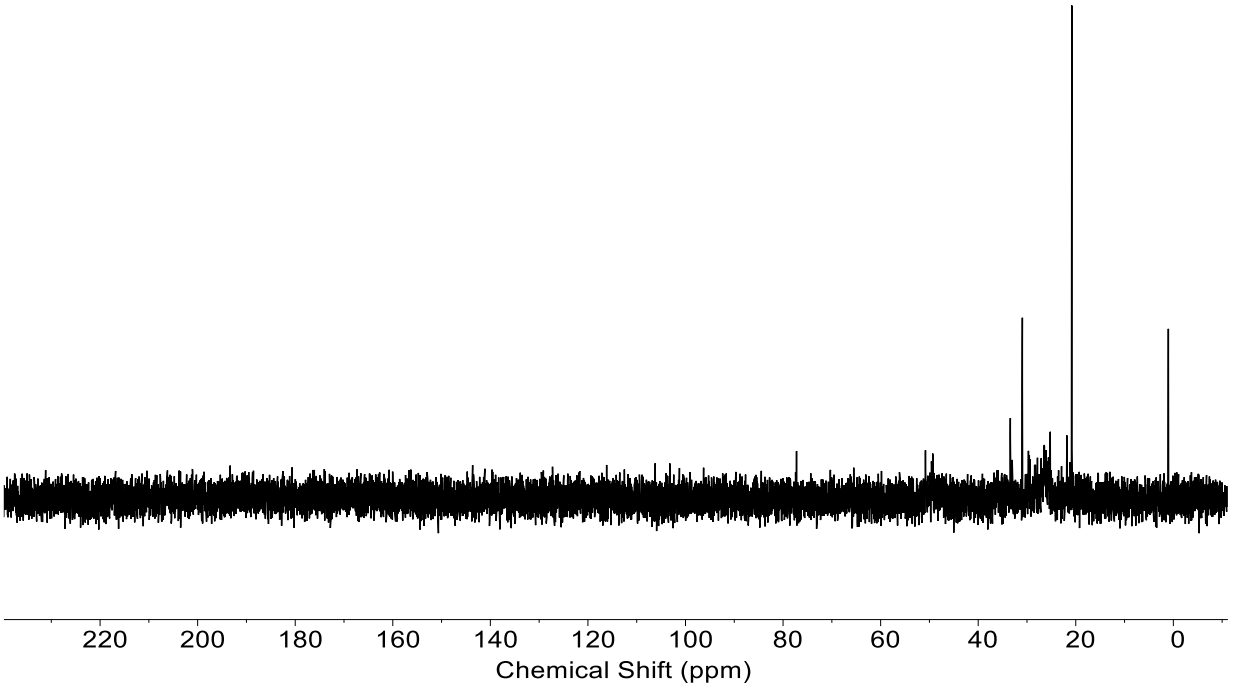

Figure S62. ^{13}C DEPT 45 NMR spectrum of photodegraded F-C_6A_2 (284 h) (400 MHz, Chloroform-*d*)

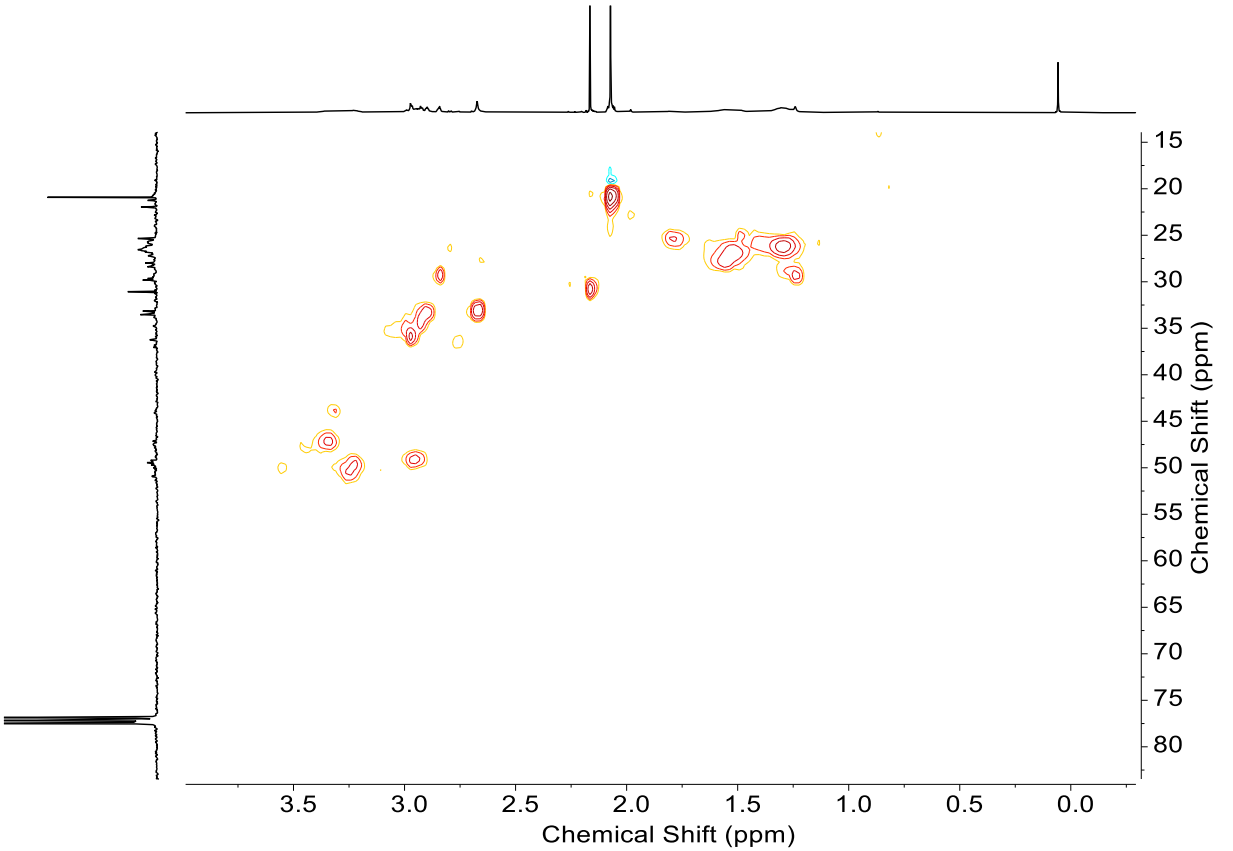

Figure S63. ^{1}H-^{13}C HSQC NMR spectrum of photodegraded F-C_6A_2 (284 h) (400 MHz, Chloroform-*d*)

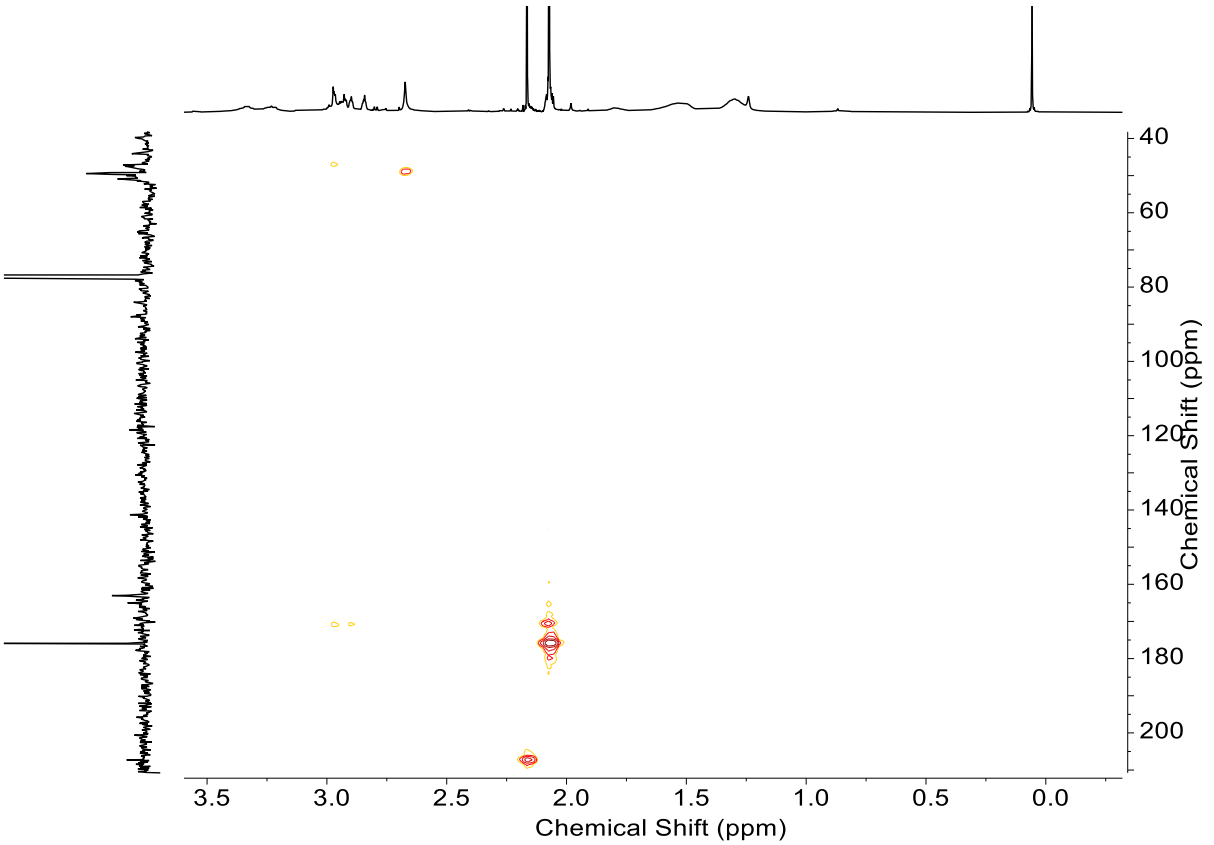

Figure S64. ^{1}H-^{13}C HMBC NMR spectrum of photodegraded F-C_6A_2 (284 h) (400 MHz, Chloroform-*d*)

Photodegradation products of model Ph-C$_6$A

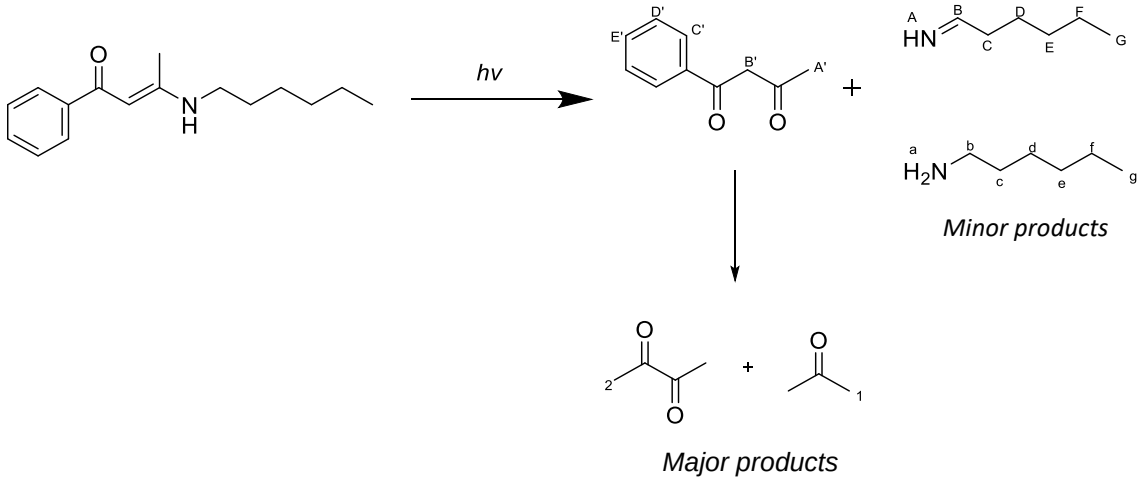

Scheme S10. The formation of α-diketone and acetone as major photodegradation products (proposed photodegradation pathway for amino-yne-based polyketone).

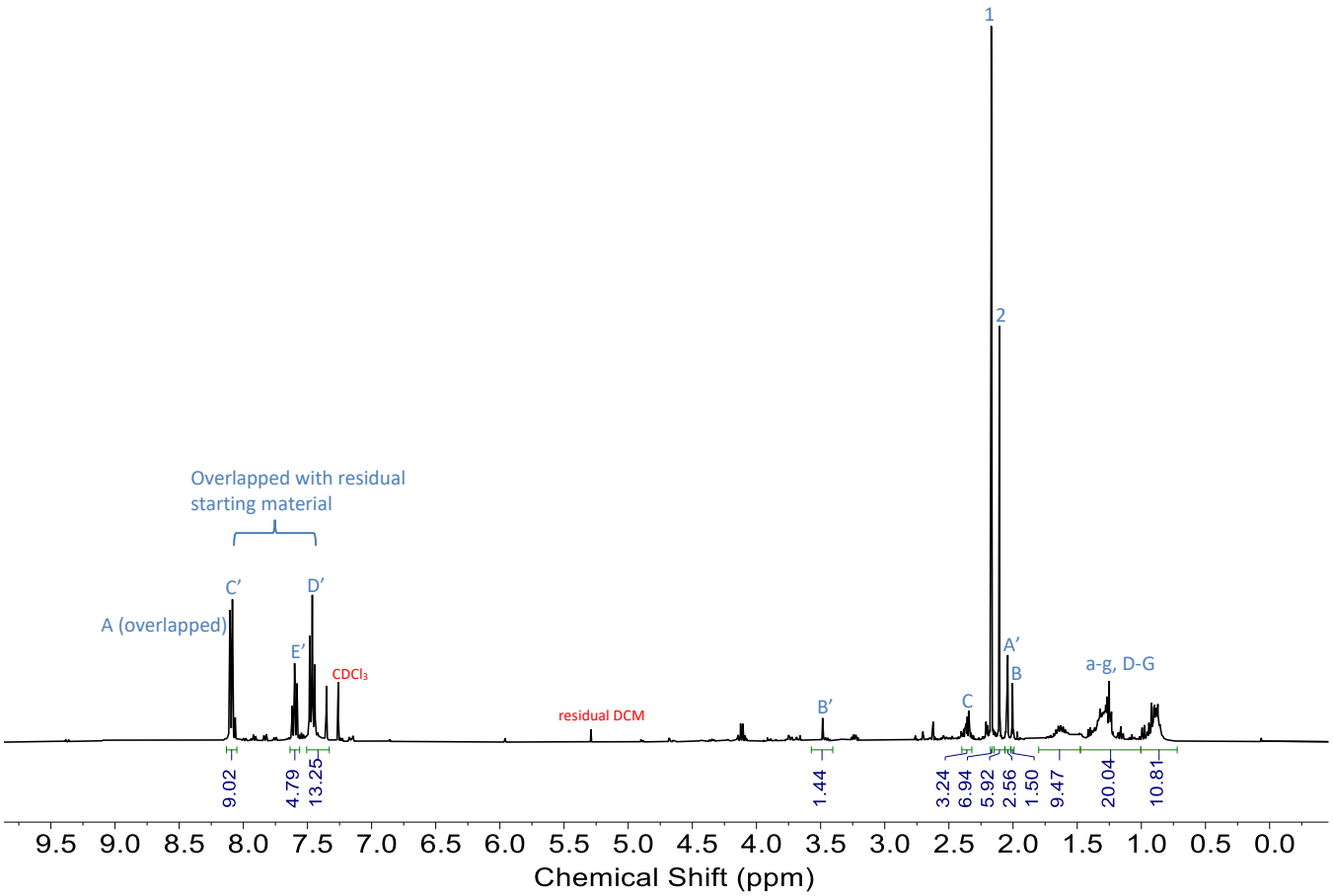

Figure S65. ^{1}H NMR spectrum of fully photodegraded model Ph-C$_6$A (150 h) (400 MHz, Chloroform-d)

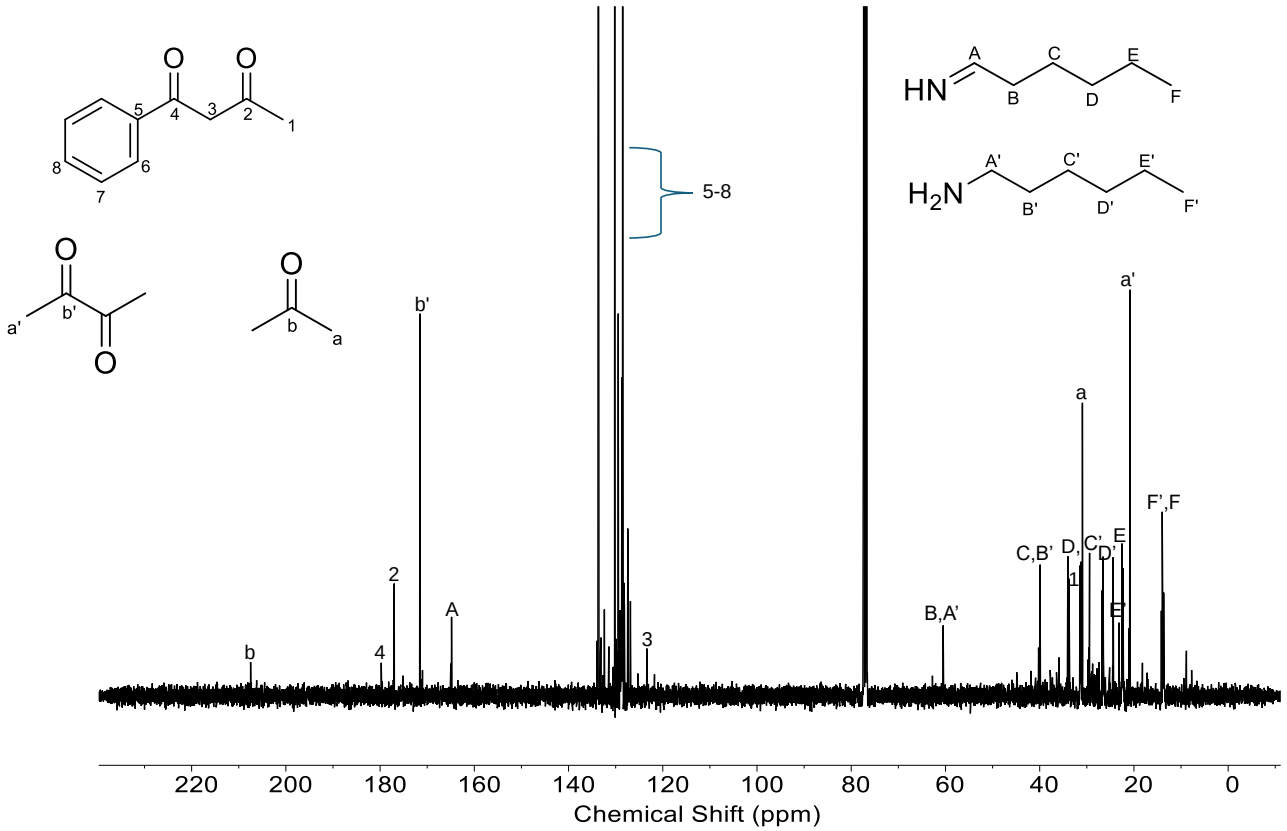

Figure S66. ^{13}C NMR spectrum of fully photodegraded model Phenyl-C_6A (150 h) (400 MHz, Chloroform-d)

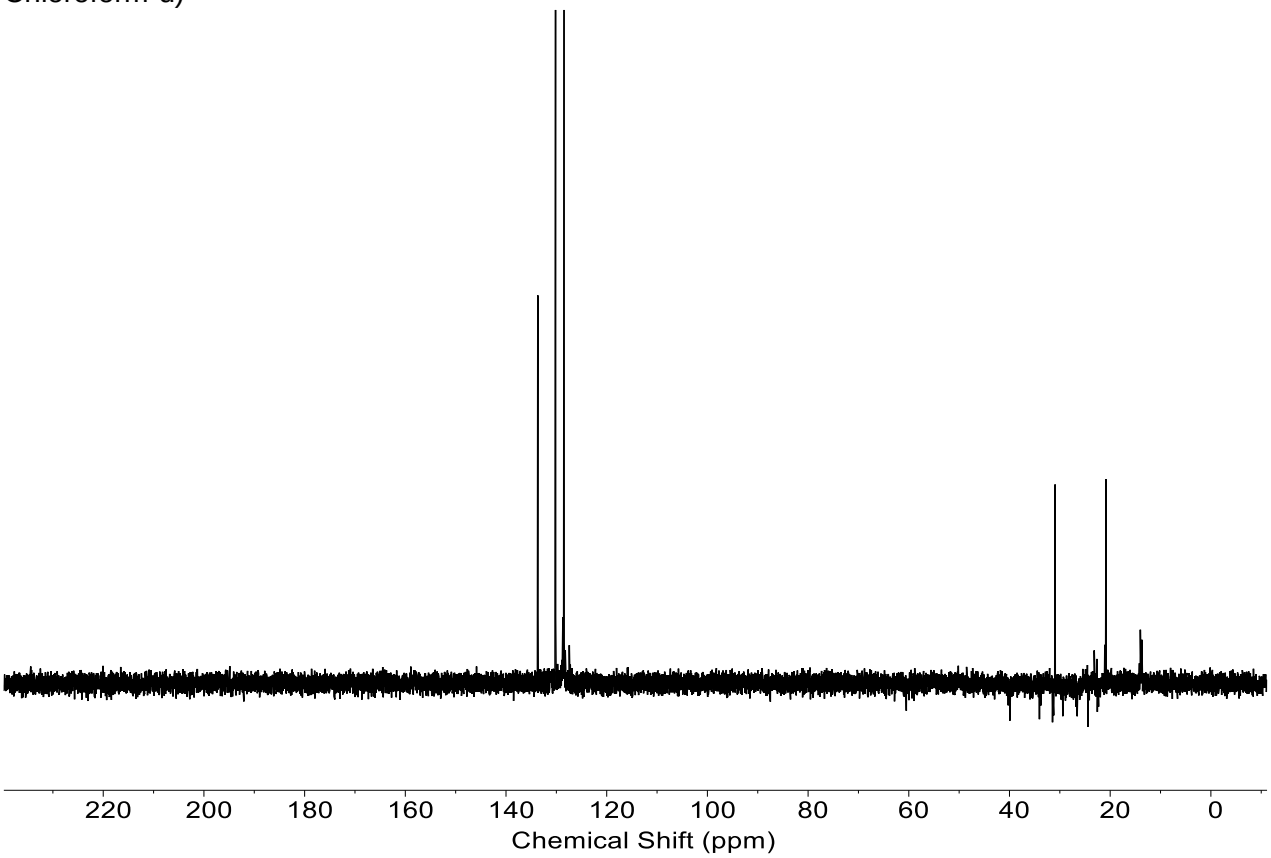

Figure S67. ^{13}C DEPT 135 NMR spectrum of fully photodegraded model Phenyl-C_6A (150 h) (400

MHz, Chloroform-d)

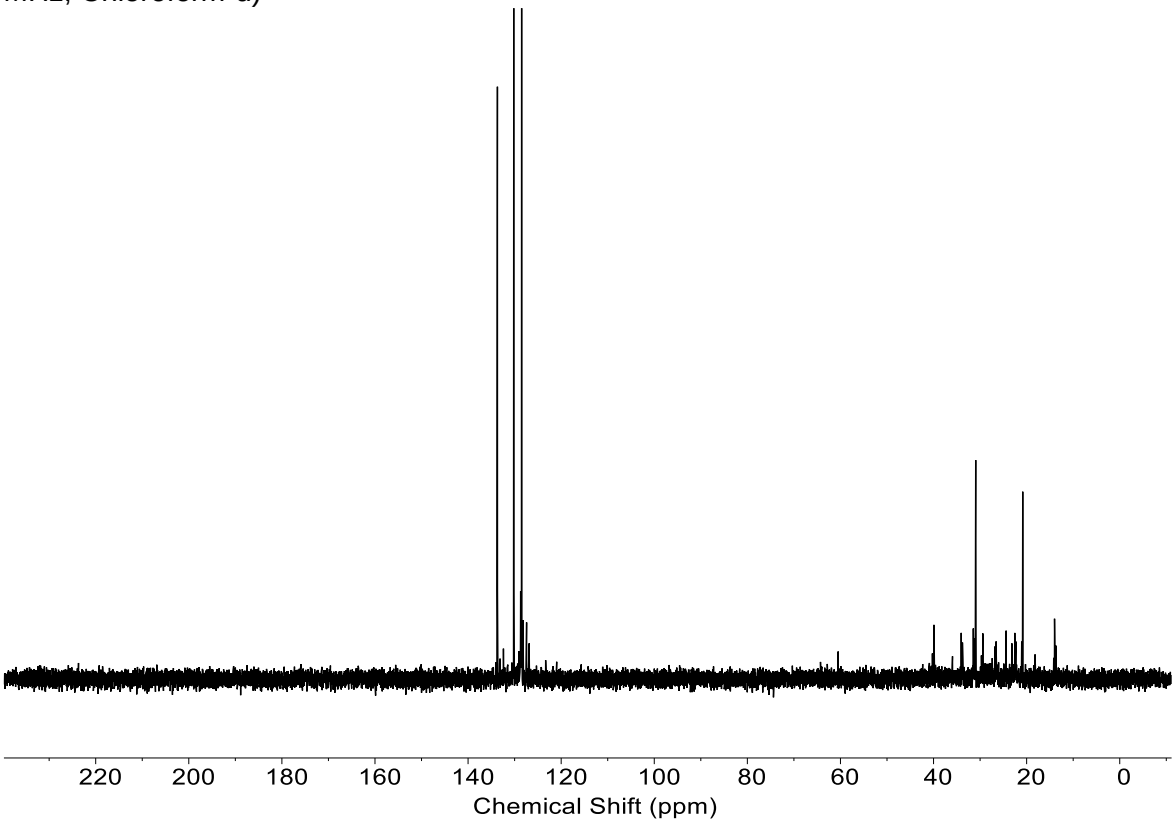

Figure S68. ^{13}C DEPT 45 NMR spectrum of fully photodegraded model Phenyl-C_6A (150 h) (400 MHz, Chloroform-d)

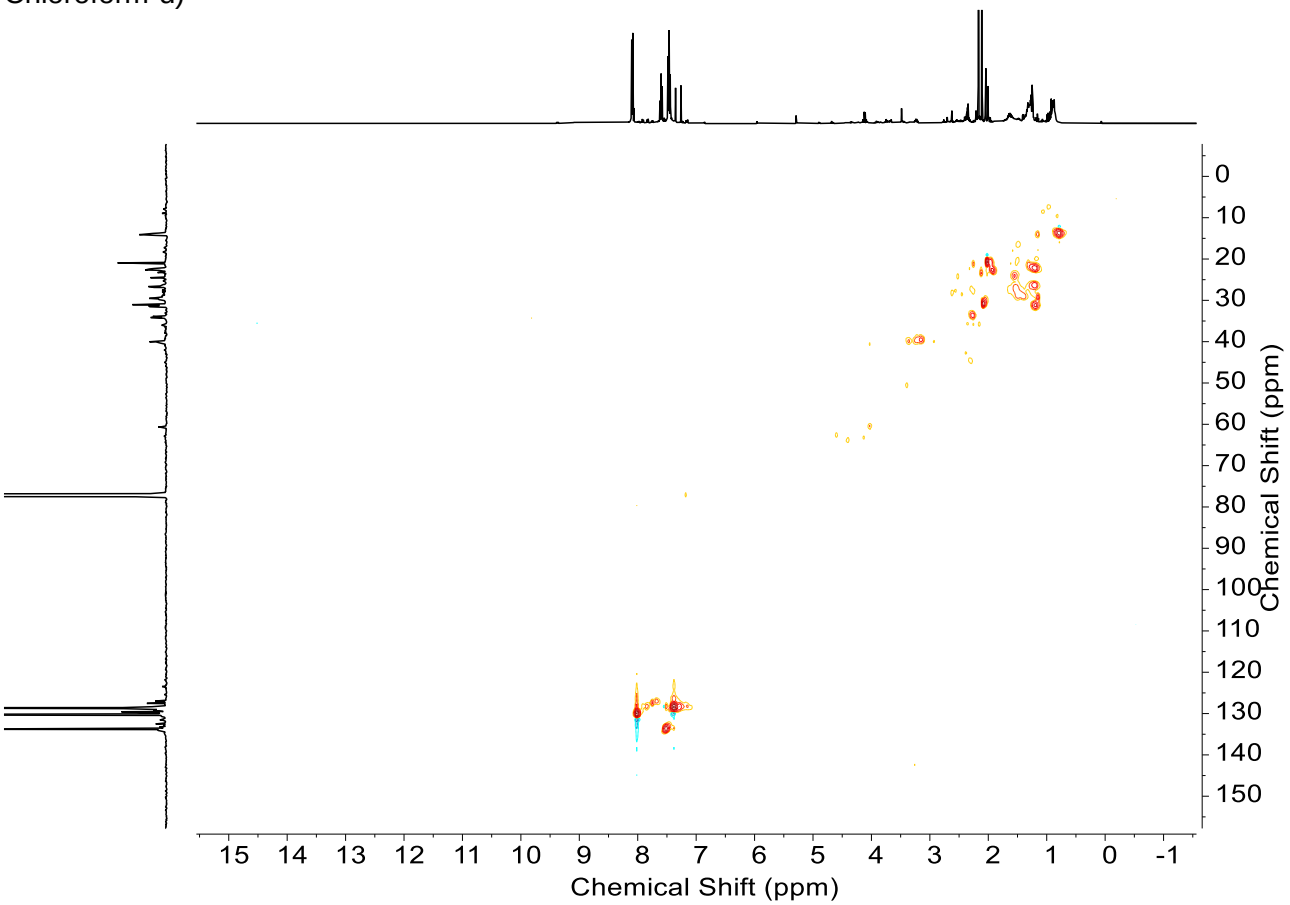

Figure S69. ^{1}H-^{13}C HSQC NMR spectrum of fully photodegraded model Phenyl-C_6A (150 h) (400

MHz, Chloroform-*d*)

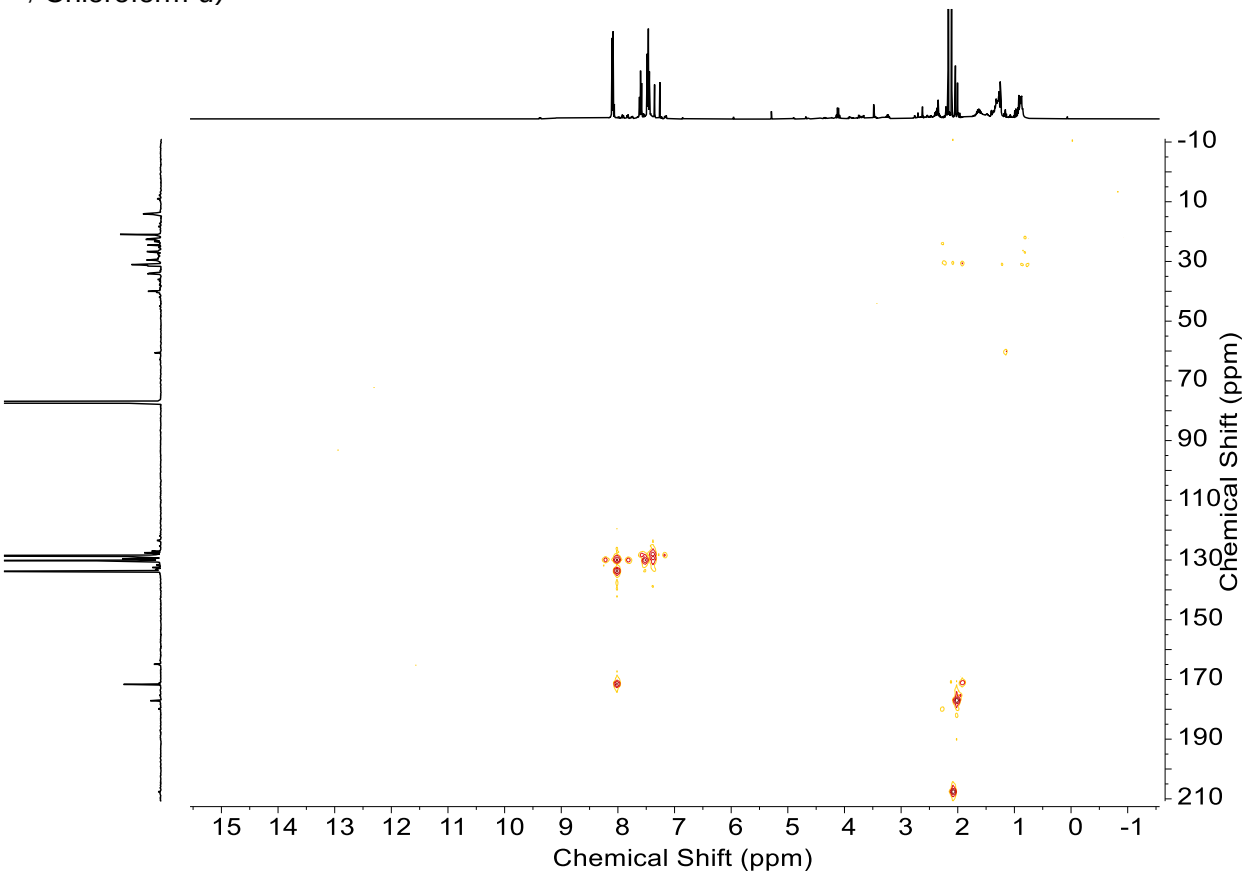

Figure 70. ^{1}H-^{13}C HMBC NMR spectrum of fully photodegraded model Phenyl-C_6A (150 h) (400 MHz, Chloroform-*d*)

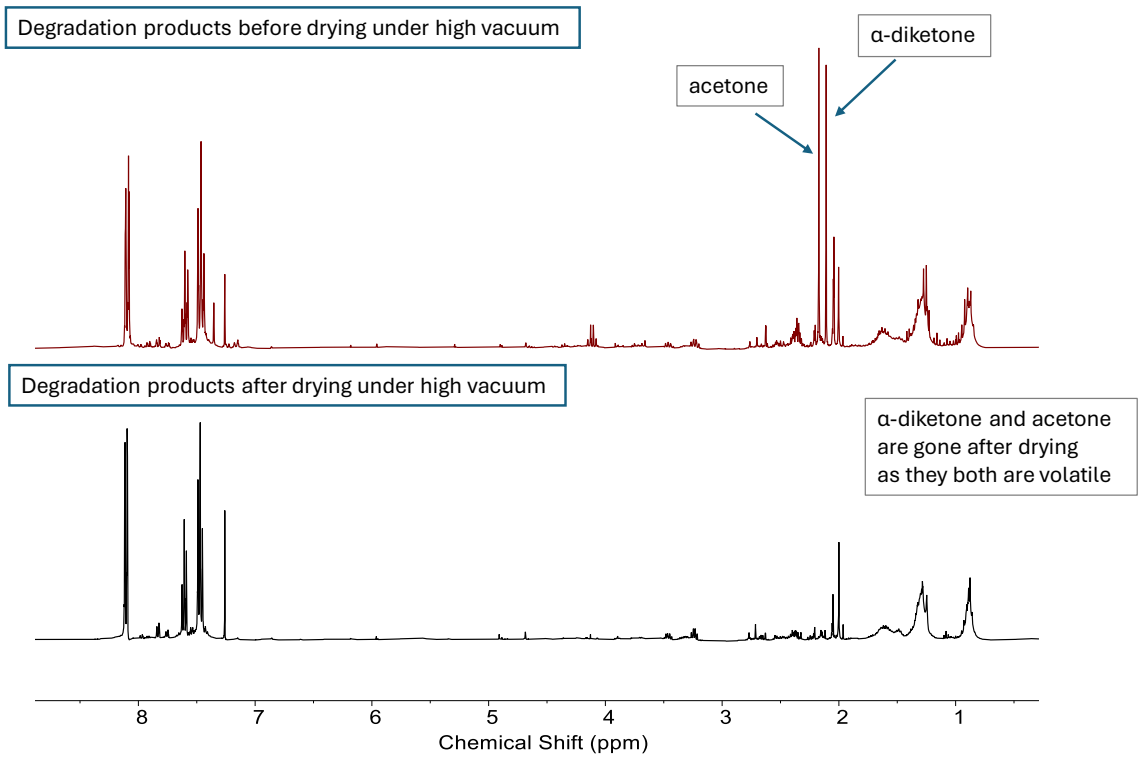

Figure S71. ^{1}H NMR spectrum of fully photodegraded model Phenyl-C_6A (150 h) before and after drying under high vacuum (400 MHz, Chloroform-*d*)

GC-MS chromatograms of irradiated model compounds

a) Model F-C_6A

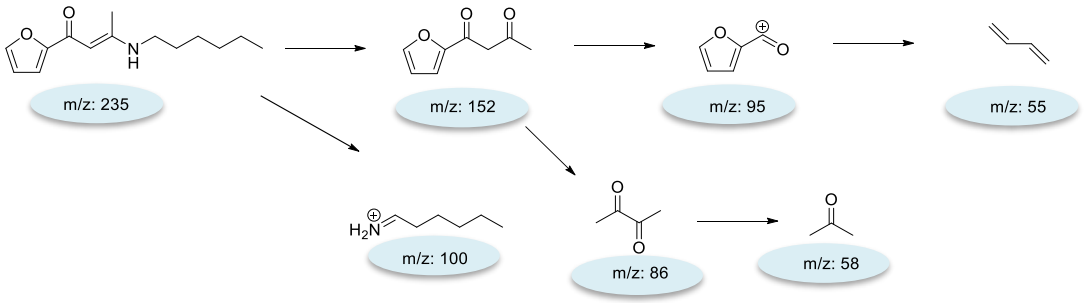

Scheme S11. Fragmentation of 24 h irradiated model F-C_6A

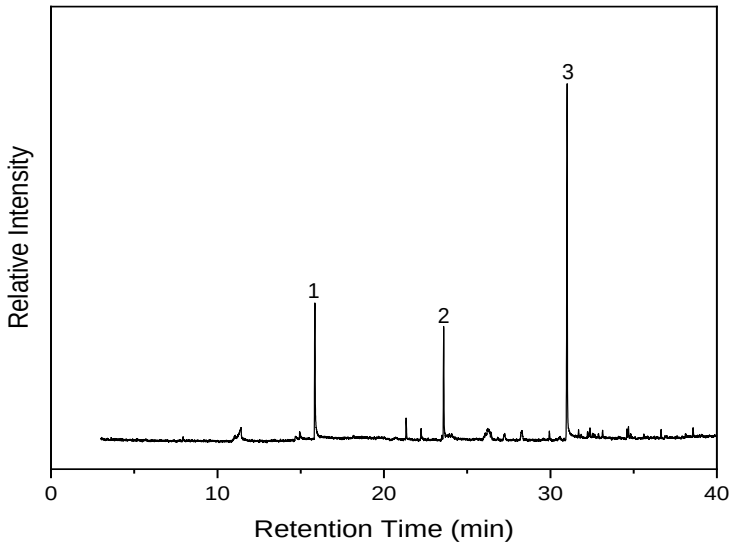

Figure S72. GC chromatogram of irradiated model F-C_6A for 24 h

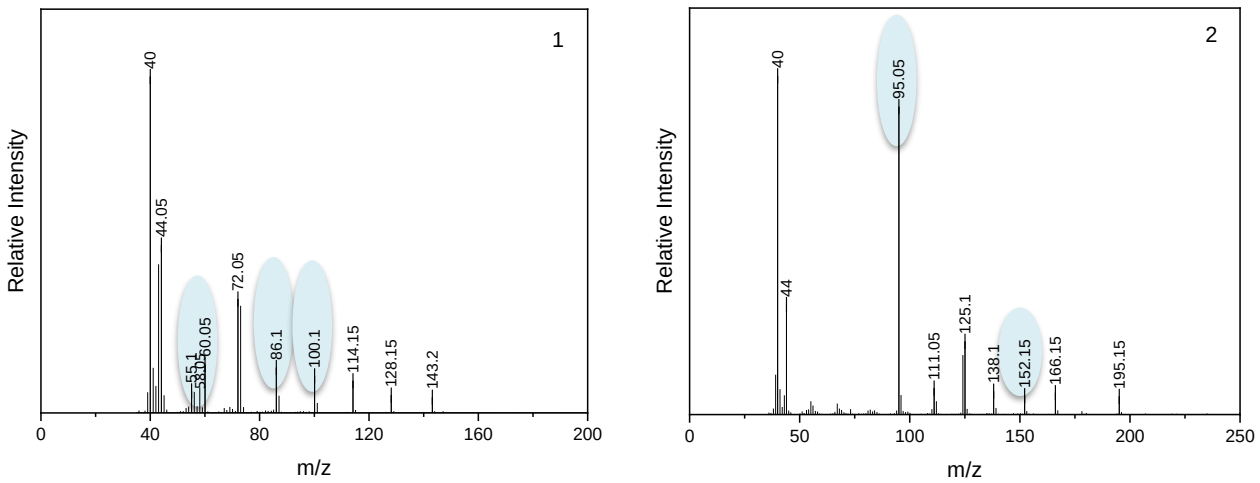

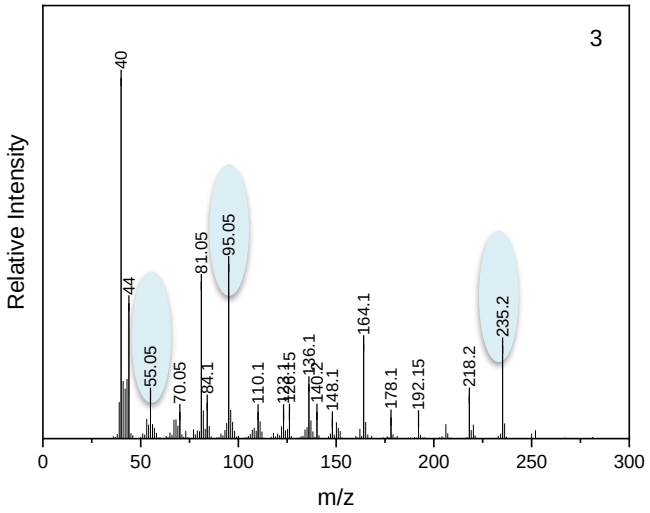

Figure S73. MS chromatogram of 24 h irradiated model F-C_6A

b) Model Phenyl-C_6A

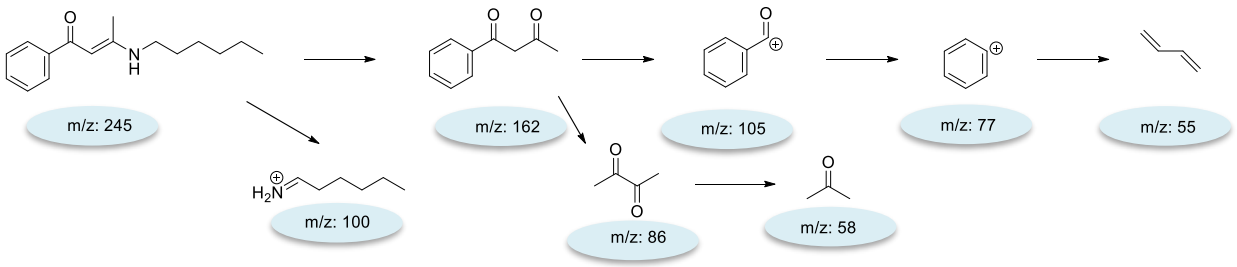

Scheme S12. Fragmentation of 24 h irradiated model Ph-C_6A

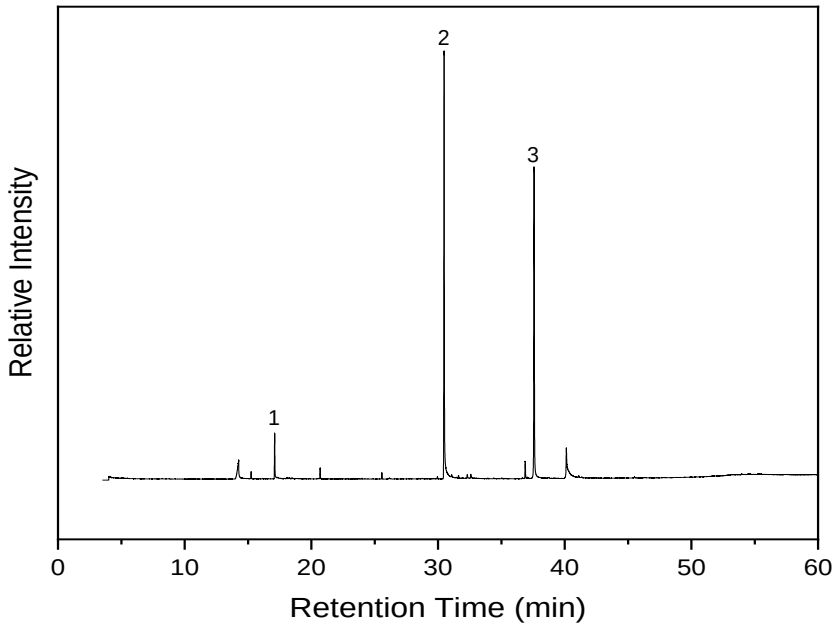

Figure S74. GC chromatogram of 24 h irradiated model Ph-C_6A

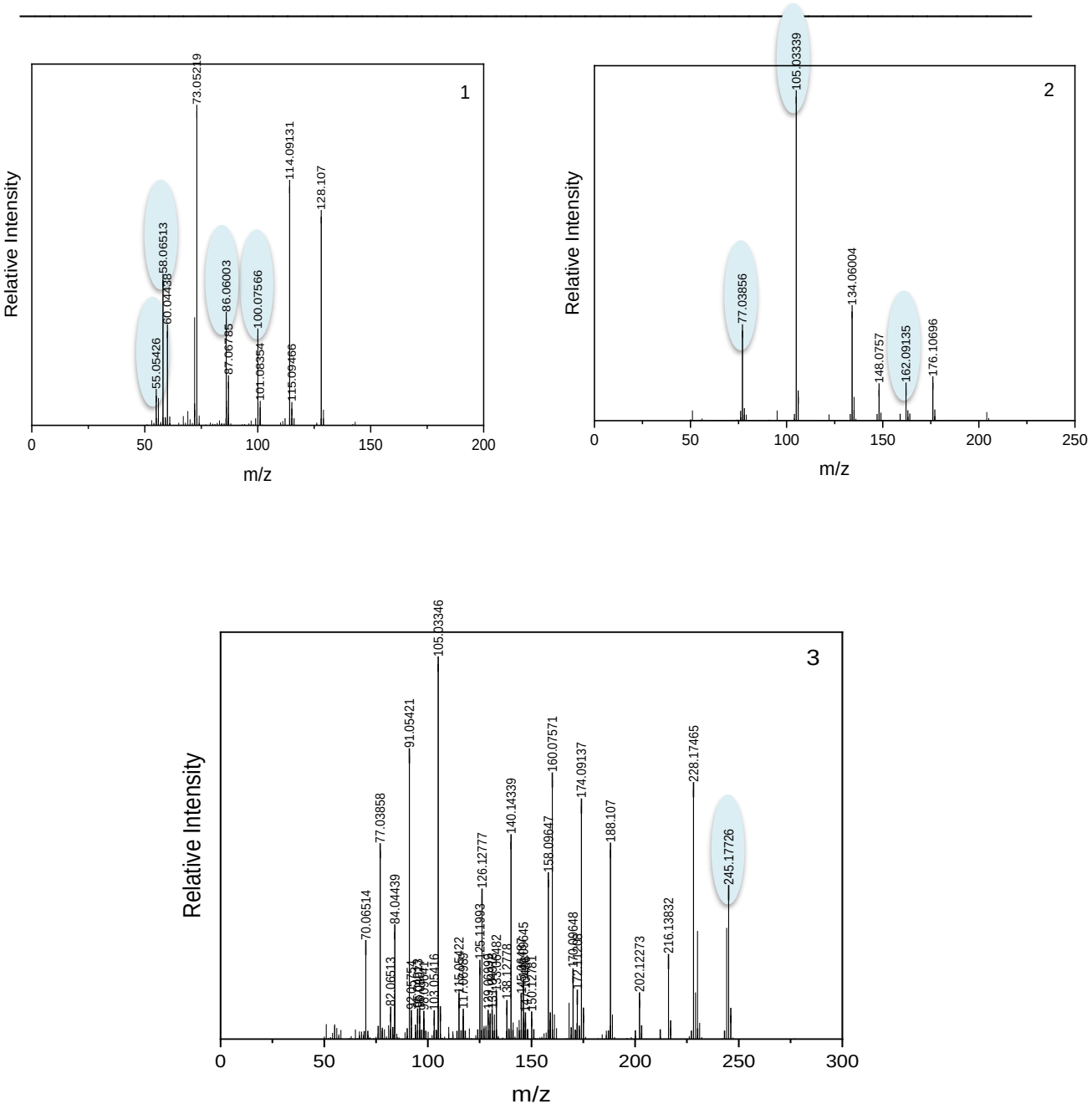

Figure S75. MS chromatogram of 24 h irradiated model Ph-C_6A

Encapsulation of 5-TAMRA dye

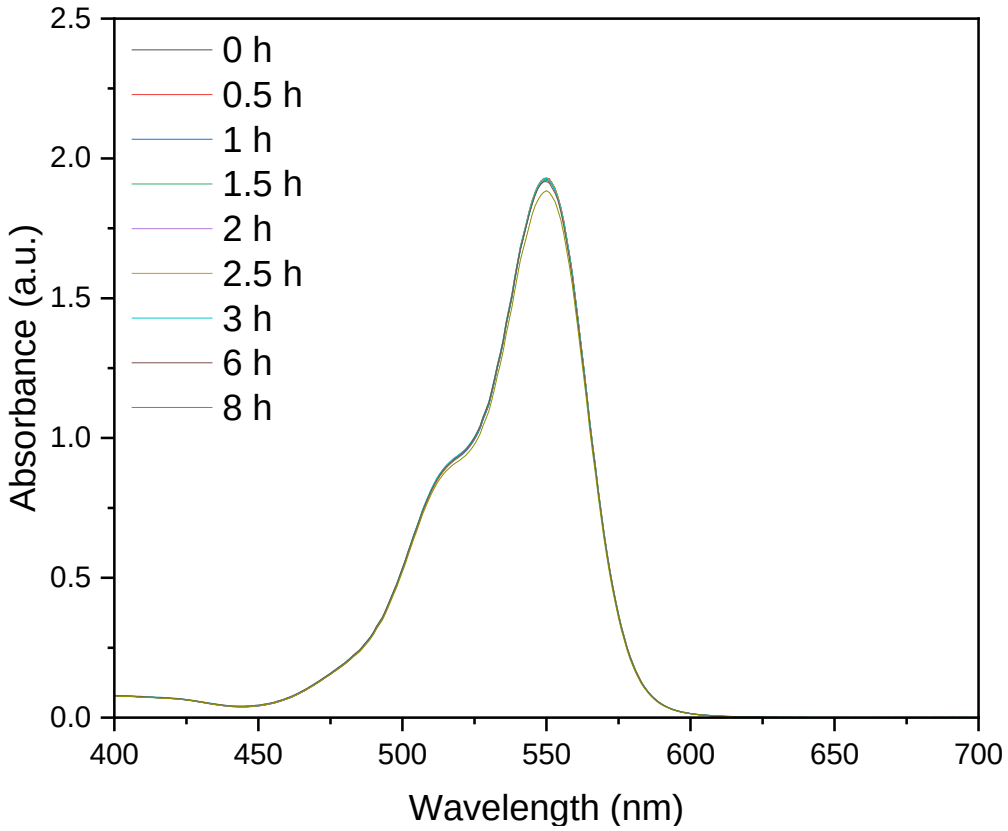

Figure S76. UV-Vis curve of irradiated free 5-TAMRA (λ_{max} 550 nm)

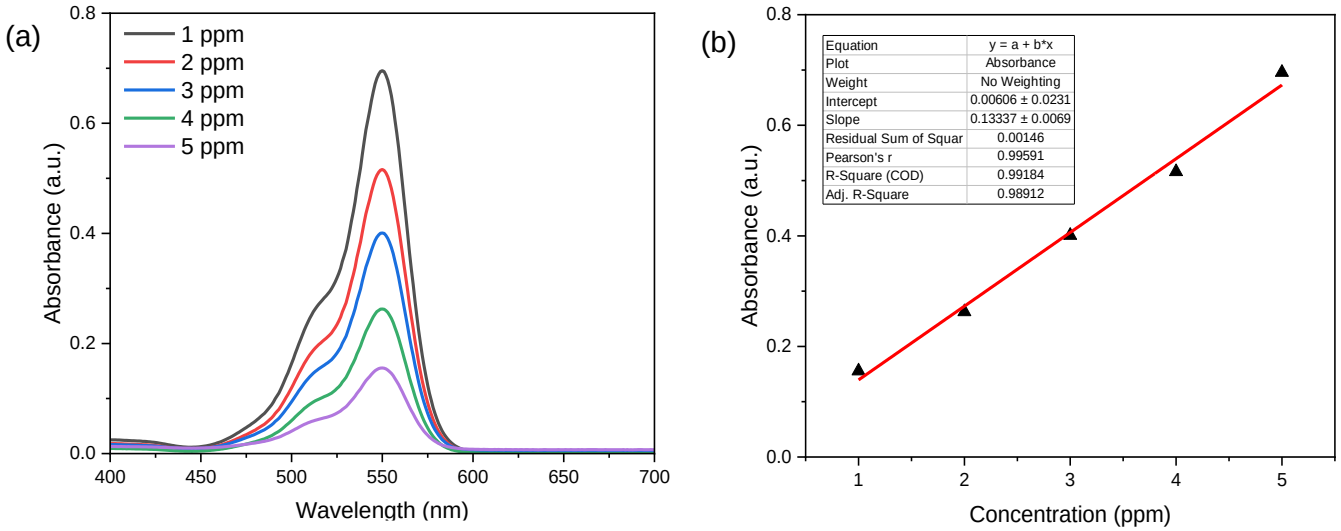

Figure S77. (a) UV-Vis curve of free 5-TAMRA; (b) 5-TAMRA standard curve

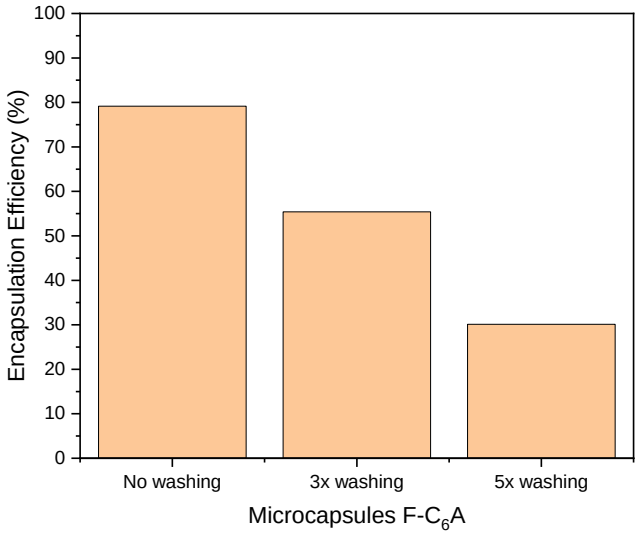

Figure S78. Encapsulation efficiency of 5-TAMRA loaded microcapsule (λ_{max} 550 nm)

Photo-triggered release of 5-TAMRA loaded microcapsules

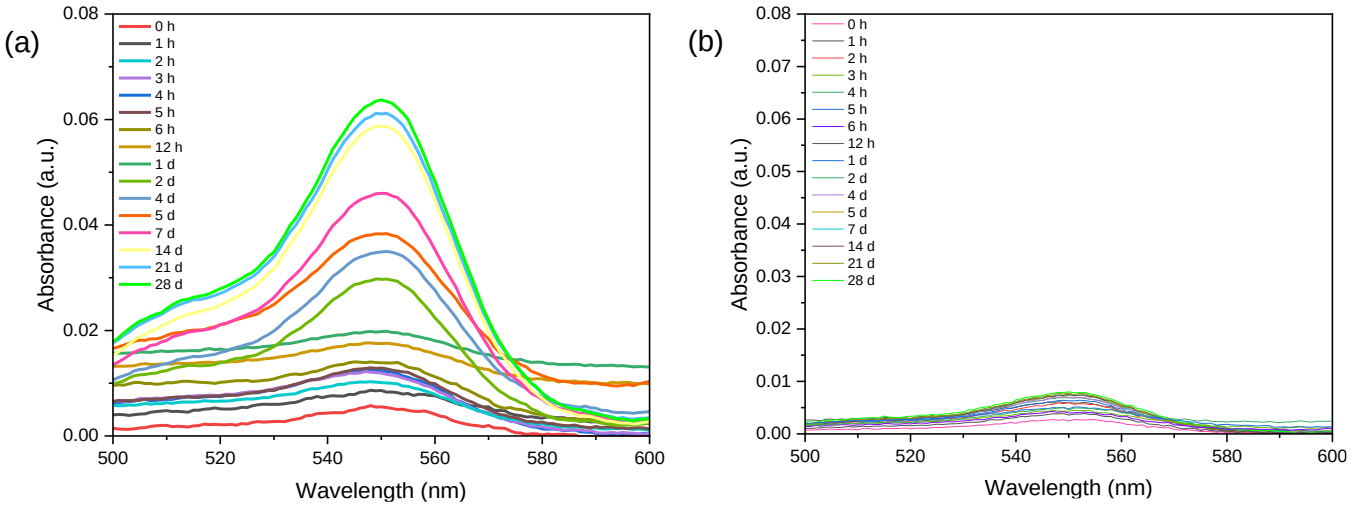

Figure S79. (a) UV-Vis curve of 5-TAMRA released during and after 6h light exposure; (b) 5-TAMRA released with no light exposure (control experiment) (λ_{max} 550 nm).

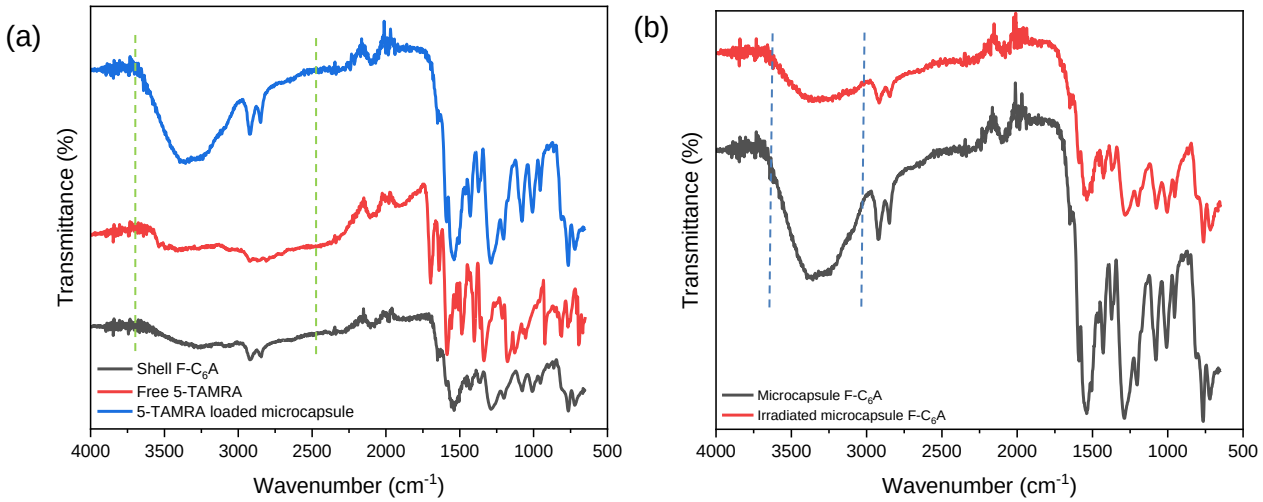

Figure S80. FTIR spectra of (a) microcapsule, free 5-TAMRA, and its shell; (b) initial and irradiated microcapsules

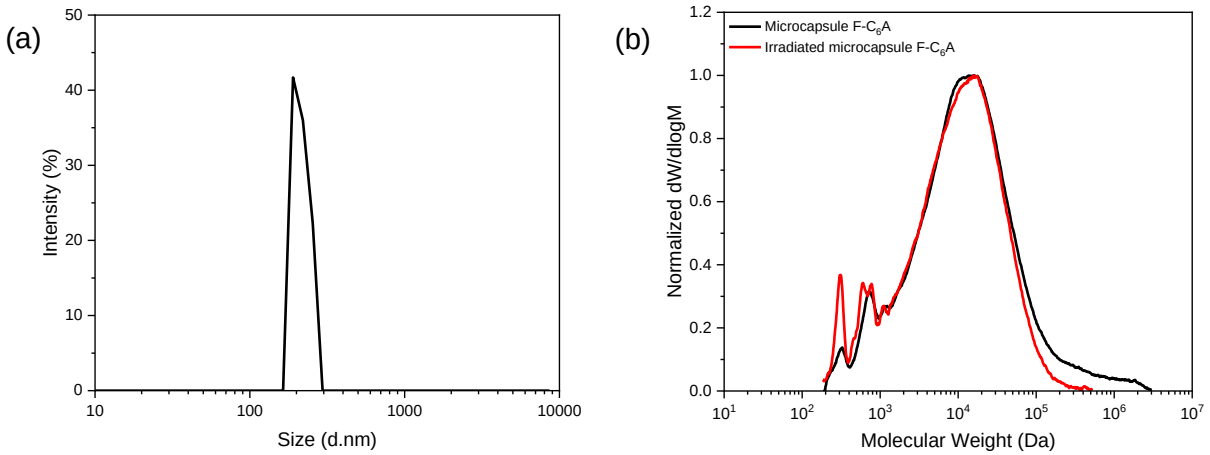

Figure S81. (a) Particle size analysis of dispersed microcapsules by DLS; (b) Normalized size exclusion chromatograms of initial and irradiated microcapsules ($CHCl_3$, 0.5% NEt_3, 40 °C) analysis against poly(styrene) (PS) standards

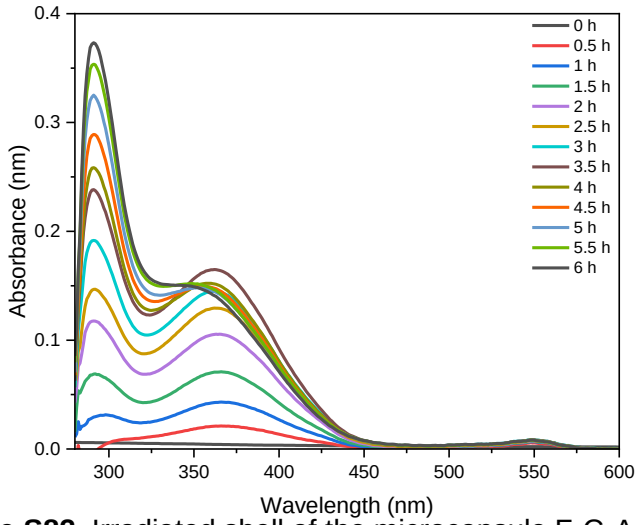

Figure S82. Irradiated shell of the microcapsule F-C_6A in medium DI water

SEM images of 5-TAMRA loaded microcapsules

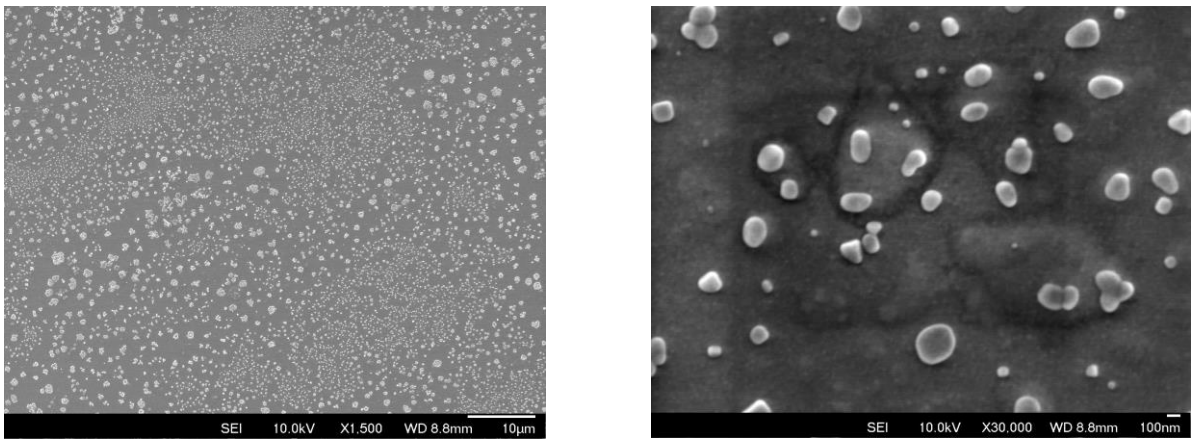

Figure S83. SEM images of multiple microcapsules with different magnifications

Confocal microscopy images of single 5-TAMRA loaded microcapsule

(a) 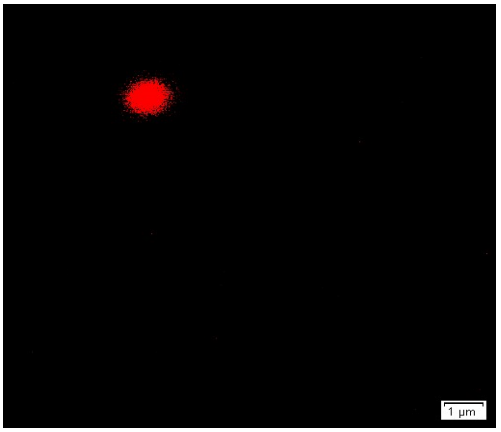

(b) 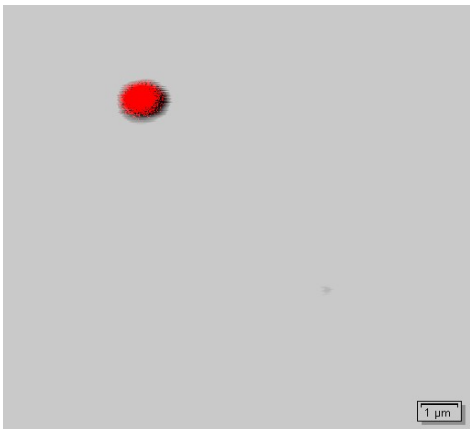

Figure S84. (a) Confocal fluorescence microscopy image of single microcapsule; (b) Confocal fluorescence microscopy bright-field image of single microcapsule

References

1. Nahm, S. & Weinreb, S. M. N-methoxy-n-methylamides as effective acylating agents. *Tetrahedron Lett.* **22**, 3815–3818 (1981).
2. Niu, T. *et al.* A powerful reagent for synthesis of Weinreb amides directly from carboxylic acids. *Org. Lett.* **11**, 4474–4477 (2009).

CHAPTER 4: TUNING THERMOMECHANICAL PROPERTIES OF PHOTODEGRADABLE COPOLYKETONES VIA SPONTANEOUS AMINO-YNE "CLICK" COPOLYMERIZATION

4.1 Manuscript and overview

Title: Spontaneous Amino-yne Click Polymerization to Generate Photodegradable Bio-Derived Polyketones with Tunable Thermomechanical Properties

Authors: **Lukmanul H. Samada**[1], Joshua C. Worch[1,2], Arianna Brandolese[1], Andrew P. Dove[1]*

Affiliations: [1]School of Chemistry, The University of Birmingham, Edgbaston, Birmingham, B15 2TT, UK.
[2]Department of Chemistry, Virginia Tech, 24061, USA

Manuscript Prepared

Co-author contributions: Dr. Josh Worch (University of Birmingham) provided technical and synthetic guidance. Dr. Arianna Brandolese (University of Birmingham) analyzed the data and edited the manuscript. Prof. Andrew P. Dove (University of Birmingham) supervised in addition to providing guidance and editing the manuscript.

Overview:

This chapter aims to improve the mechanical performance of the resulting homopolymer which has a low tensile strength and strain at break. We incorporated different comonomers via click copolymerization to obtain optimal mechanical properties. The optimization was conducted by varying the comonomer feeding molar ratio.

The composition comonomers generally would lead to the different chain flexibility and interactions among the polymer chains. As a result, the thermal and mechanical properties will be different. In our study, we incorporated 1,6-hexanediamine (HMDA) and 2,2'-(ethylenedioxy)bis(ethylamine) (EDEA) to attain a diverse thermomechanical performance. Homopolymer with comonomer HMDA exhibited a remarkable tensile strength and elongation, whilst the homopolymer with comonomer EDEA illustrated a low tensile strength and elongation. Therefore, we expect to enhance the mechanical performance of the polymer containing EDEA and have a variety of thermomechanical features.

We attempted to vary the molar ratio of the comonomers inserted. We found a range of glass transition temperatures, thermal decomposition, and mechanical performances. Surprisingly, the molar ratio of HMDA and EDEA peaking at 10/90 displays a comparable tensile strength to HDPE (but owing half of their elongation at break value). Furthermore, the glass transition temperature was aligned with the comonomer composition within the polymeric system. Additionally, the irradiated polymers exhibit similar degradation products and pathways as we obtained in Chapter 3.

Tuning Thermomechanical Properties of Photodegradable Copolyketones *via* Spontaneous Amino-yne "Click" Copolymerization

Lukmanul H. Samada[†], Joshua C. Worch[§,†], Arianna Brandolese[†], Andrew P. Dove[*,†]

[*,†]School of Chemistry, University of Birmingham, B15 2TT, UK. [§]Department of Chemistry, Virginia Tech, 24061, USA.
E-mail: a.dove@bham.ac.uk

ABSTRACT: Furan-containing photodegradable polymers (polyketones) gained interest in the fabrication of thermoplastics due to their renewability and sustainability. However, conventional polyketones have a lack of structure diversity that limit their range of thermomechanical properties. Herein, we report on polyketones preparation *via* amino-yne "click" copolymerization between various feeding molar ratios of different aliphatic diamines and ketone alkyne monomer without the presence of external catalysts. The resulting copolymers exhibited amorphous behaviour with high glass transition temperature values (T_g = 80 – 116 °C) and excellent thermal stability ($T_{d,5\%}$ ≥ 268 °C). In addition, the mechanical performances can also be tuned through chain flexibility and intermolecular forces setting according to the composition of comonomers inserted. We found that poly(HMDA$_{10}$-*co*-EDEA$_{90}$) showed a comparable tensile strength to the commodity plastic HDPE (but owing half of their elongation at break value). Furthermore, the irradiated representative copolymer demonstrated a novel photodegradation pathway. This pathway differs from the Norrish pathway that is commonly observed in conventional polyketones.

Introduction

Over the past few years, bio-based plastics derived from biomasses have been intensively developed to replace commodity plastics (petroleum-based plastics) thanks to their compatibility with the environment.[1–3] Consequently, the demand towards degradable bio-based plastics, such as poly(lactic acid) (PLA), polyhydroxyalkonates (PHAs), poly(butylene succinate) (PBS), has significantly increased which mainly utilized in the plastic manufacturing.[4–6] These plastics are frequently embedded with plasticizer, photosensitizer, or other additives due to their poor thermomechanical properties and uncontrolled/incomplete degradation.[7,8] However, they fragmented into microplastics or

toxic by-products contaminating water and soil that affect adversely to the human and animal health.[9–11]

The lack of degradability of these petro-based plastics is due to strong C-C bonds in their backbone. To overcome this limitation, researchers attempted to incorporate either photodegradable or biodegradable functionalities into the polymeric chains to increase their degradation rate.[12] In this regard, polyketones have recently been considered as a valuable option in polymer material synthesis. In fact, they contain a ketone moiety that is inherently photodegradable in which light enables to trigger the C-C bond cleavage through the radical auto-oxidation process in the presence of oxygen within the polymers (no need for photosensitizers).[13] The chain scissions of the conventional polyketones typically undergo *via* Norrish pathways either mechanism type I or II.[14] These pathways promoted uncontrolled free-radical reaction under UV light radiation resulting in reduced molecular weight.[15–17] Polyketones are potential high-performance thermoplastic polymers due to their excellent tensile strength, chemical and abrasion resistance.[18–20] Matsutani and co-workers previously synthesized semi-aromatic polyketones with 1,3-adamantanedimethylene moiety which exhibited remarkable thermal stability and flexibility.[21] Meanwhile, Jho and co-workers prepared aliphatic polyketones by polycarbonate blending *via* melt mixing to enhance the impact strength of the resulting polymers.[22] In addition, in order to produce great thermomechanical properties, the polyketones were also fabricated by incorporating carbon fibers into the polymeric system.[23] These synthesis techniques were employed by polycondensation reactions that limit the variety of the polymeric structure-property and are typically inefficient polymerization.

A facile strategy to construct polyketones efficiently with controlled and diverse architectures, functionality, and high yield leads to the "click" chemistry approach.[24] For example, amino-yne click reaction (*aza*-Michael addition) was first introduced by Tang and co-workers as a powerful strategy to yield multifunctional polymers between amines and

propiolates.[24,25] Step-growth click fashion enables to prepare polymers using more than two monomers rapidly and efficiently.[25] This reaction occurs at ambient reaction conditions and without the addition of external catalysts, resulting in high molecular weight polymers.[26,27] Furthermore, there are some factors that affect the efficiency of the reaction, such as amine basicity, solvents, Michael acceptor electrophilicity, and temperature.[28]

In our previous studies, we successfully synthesized a series of furan-based polyketones with a wide range of thermomechanical performances. We found that polyketones containing comonomer 1,6-hexanediamine (HMDA) exhibited an excellent tensile strength, however when we employed comonomer 2,2'-(ethylenedioxy)bis(ethylamine) (EDEA), the resulting polyketones indicated a low tensile strength. In this study, we attempted to improve the tensile strength of the polyketones containing EDEA by incorporating HMDA into the polymeric structure (Fig. 1). We applied a series of different feeding molar ratios of the comonomers to achieve better mechanical properties of the polymers, and they potentially enable to replace the commodity plastics. In addition, we also irradiated the representative resulting copolymer to UV light to demonstrate the similarity in the photodegradation pathway, as we did against their homopolymer counterparts from our past studies. They indicated the formation of α-diketone and acetone as the major products (unpublished work).

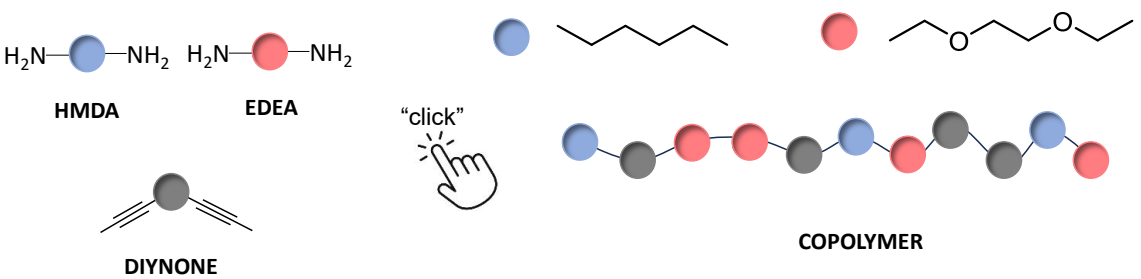

Fig. 1. General illustration of the fabrication of copolyketones *via* amino-yne click copolymerization

Results and discussion

We initially synthesized the Weinreb amide as a precursor to prepare ketone alkyne monomer (diynone). 2,5-Furandicarboxylic acid (FDCA) was used as a building block of Weinreb amide synthesis due to its bio-renewability and other considerable properties which enable it to act as a photosensitizer. Through one-pot reaction, the furyl Weinreb amide was successfully synthesized as clearly confirmed by nuclear magnetic resonance (NMR) spectroscopy, fourier-transform infrared (FTIR) spectroscopy, and other characterizations. The characteristic NMR peaks can be seen in the region of 3.36 ppm and 3.83 ppm indicating the formation of *N*-Alkoxy Amide group (Fig. S1 & S2). Furthermore, the very broad O-H bond absorption over the range 2500-3300 cm^{-1} from FDCA disappeared, indicating that the carboxylic acid group was completely converted into *N*-Alkoxy Amide. The activated alkyne (diynone) was then prepared by reacting the resulting Weinreb amide with Grignard reagent under a nitrogen flow, confirmed by the appearance of the methyl peak at δ = 2.16 (Fig. S3). The stretch alkyne (-C≡C-) bond can also be found at 2200 cm^{-1} as shown in the FTIR spectrum. The purity of the resultant diynone monomer plays a crucial role in yielding high molecular weight polymers as the reactions undergo *via* step-growth click polymerization.

In order to understand how the comonomer compositions affected the mechanical performance of the resulting polymers, both comonomer HMDA and EDEA were used. Previously, we reported that the polyketones using comonomer EDEA (F-C_6A_{EG}) exhibited poor tensile strength. Meanwhile, the polyketones using comonomer HMDA (F-C_6A) demonstrated an outstanding tensile strength (Fig. S29), upon this evidence we sought to enhance the tensile strength of the previously synthesized polyketones containing EDEA by its copolymerization with HMDA.

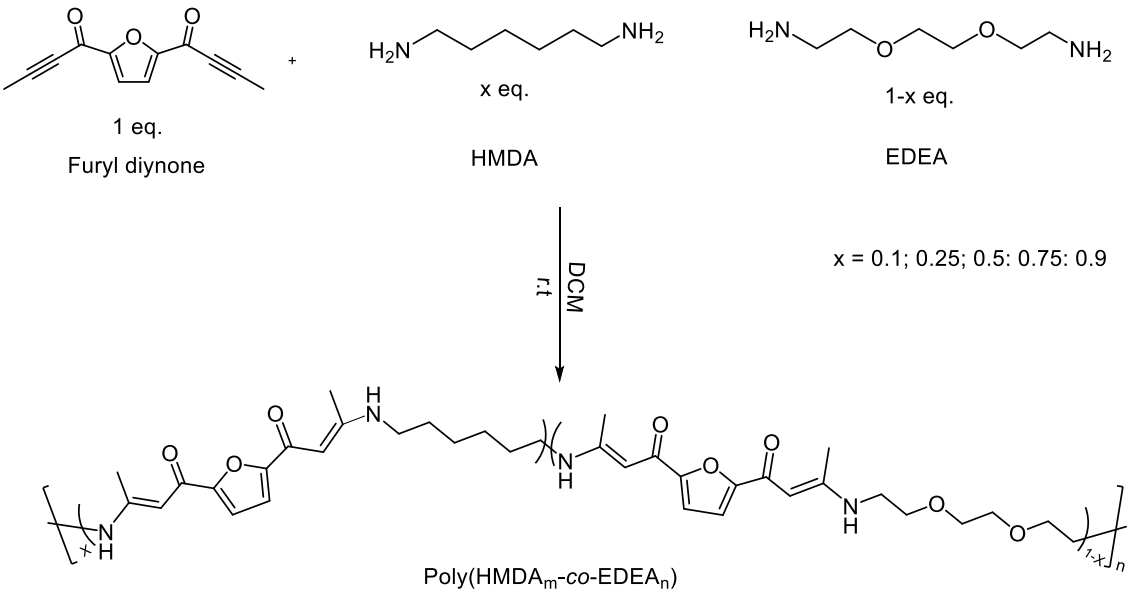

Scheme 1. Copolymerization of diynone with HMDA and EDEA comonomers using various feeding molar ratios to generate copolyketones.

The NMR spectra of synthesized PKs show clear peak intensity changes in the region of δ = 3-4 ppm which are attributed to the different terminal methylene moieties from distinct comonomers (For proton and carbon NMR spectra, please see Fig. S5-S18). These NMR spectra of copolymers also demonstrate the incorporation of comonomer HMDA and EDEA structures that indicated the formation of copolymers. Additionally, the different intensities of those characteristic peaks revealed the proportion of each altered comonomers used.

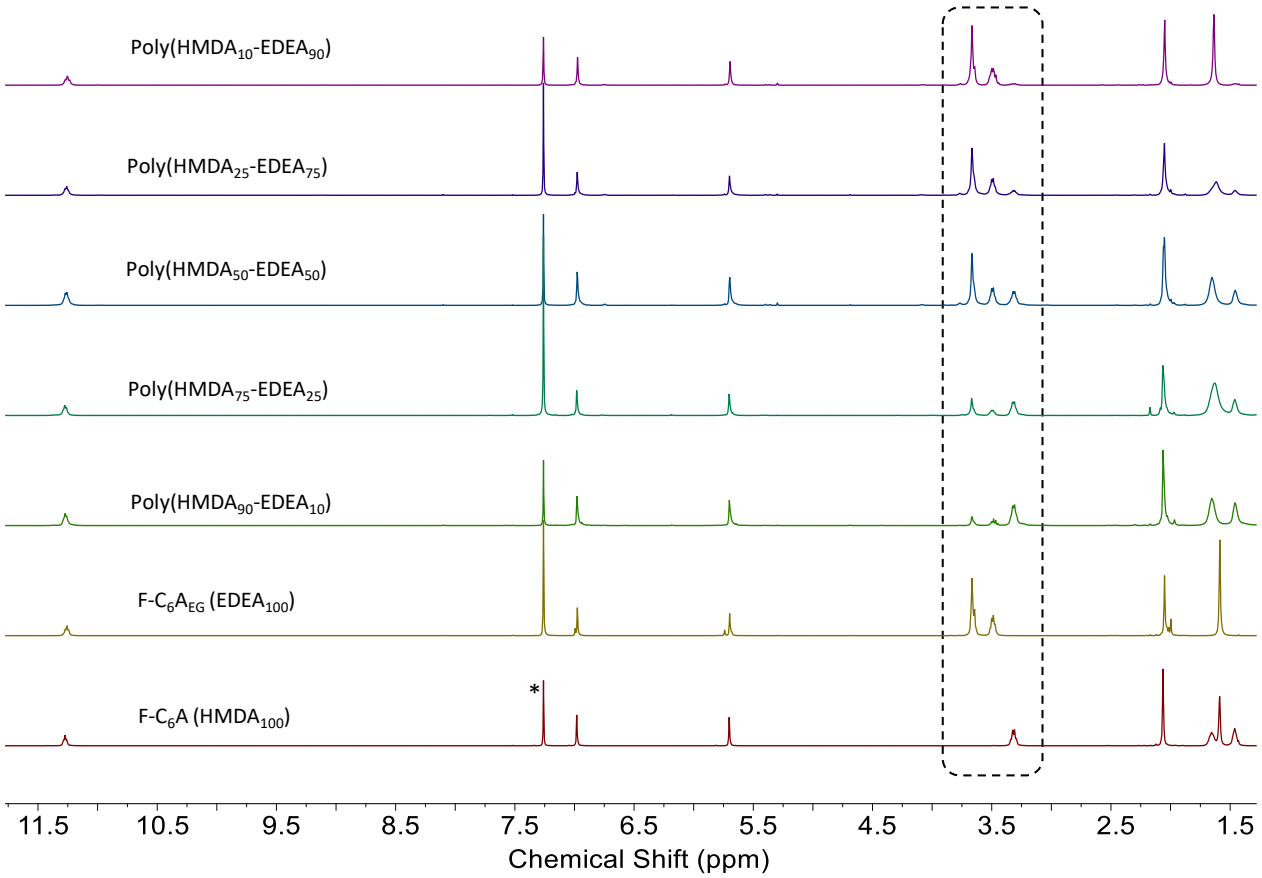

Fig. 2 ^{1}H NMR spectra stacked of copolyketones with various feeding molar ratios of HMDA and EDEA in $CDCl_3$. The solvent peaks are marked with asterisks.

The step-growth "click" copolymerization of HMDA and EDEA with alkyne monomers successfully generated high molecular weight copolymers (M_w up to 132 kDa) with broad dispersity ($Đ_M$) in the range of 4-13 (Fig. 3a). The products are very easily isolated through precipitation into the diethyl ether without formation of by-products or further purification.[29,30] A range of copolyketones was produced from diynone monomers with 2,5-furandicarboxylic acid (FDCA) as a building block *via aza*-Michael addition (amino-yne "click" reaction) with commercial diamines. FTIR spectra display a change of the peak intensity corresponding to the stretch N-H bond in the range of 2500-3000 cm^{-1}, indicating the formation of a copolymer (Fig. 3b).

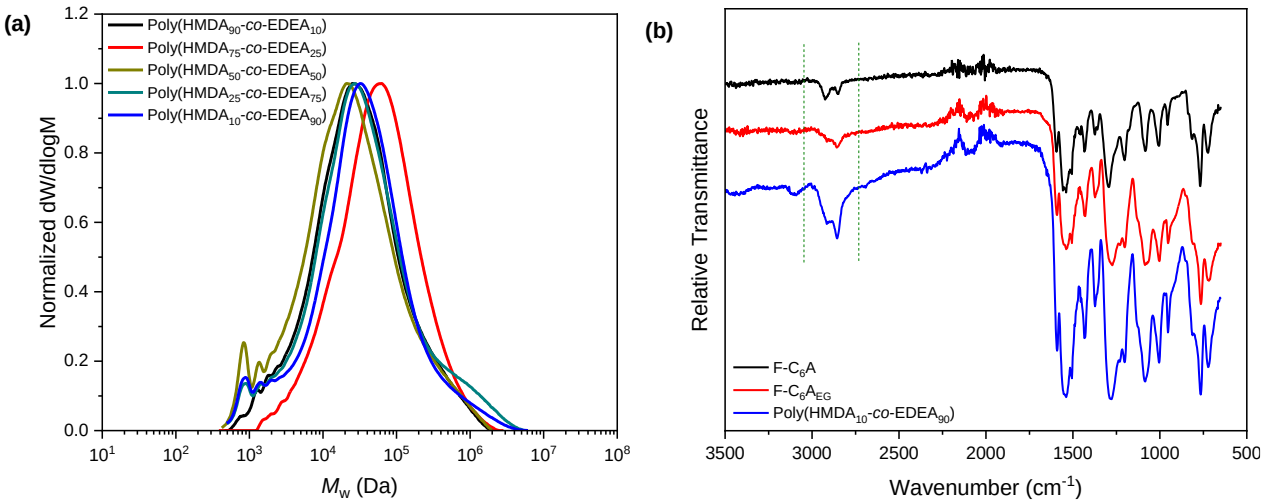

Fig. 3 (a) Normalized size exclusion chromatogram of thiol-yne based PKs ($CHCl_3$, 0.5% NEt_3, 40 °C) analysis against poly(styrene) (PS) standards. (b) FTIR spectra stacked of F-C_6A, F-C_6A_{EG}, and Poly($HMDA_{10}$-*co*-$EDEA_{90}$).

We initially used HMDA 90% and EDEA 10% as comonomers to generate desired copolyketones with particular properties, subsequently followed by HMDA 75%: EDEA 25%, HMDA 50%: EDEA 50%, HMDA 25%: EDEA 75%, and HMDA 10%: EDEA 90% (Table 1). The feeding molar ratio significantly influences the physicochemical properties in general, such as molecular weights, mechanical and thermal properties.[31,32] Copolymerizations of furyl diynone with comonomers HMDA and EDEA were conducted aiming to a series of polyketones with a range of thermomechanical properties. Molar ratios of comonomers were varied to figure out the best composition to obtain the desired properties (Fig. 1). The copolymerization reaction was conducted under mild reaction conditions for 3 hours at room temperature with no use of catalyst in dichloromethane (DCM) solvent to afford a free standing-film after solvent cast. The films were then annealed for 3 days under a high vacuum at room temperature to remove the remaining traces of solvent.

Differential Scanning Calorimetry (DSC) was employed to obtain the glass transition temperature (T_g) value of each copolymer and thermogravimetric analysis (TGA) was used to investigate the thermal stability of the polymers. The trend of T_g values exhibits the T_g

decreased with higher EDEA content. These results indicated that EDEA content increases the free volume in the polymer system due to enhanced chain flexibility and ether bonds (C-O-C) that lead to the lower T_g values (Fig. 4a). T_g values trend was affected by the composition of both comonomers as a consequence of the change of polymer backbone interactions. All copolyketones showed amorphous behavior with high T_g. They also demonstrated remarkable thermal stability with a significant weight loss in the range of 300-500 ºC (Fig. 4b). Overall, the polymer chain architectures enable them to control their physicochemical behaviors and thermomechanical performances.

Table 1. Thermomechanical properties of copolyketones are tuned by controlling the comonomers' composition.

Entry	M_w[a] (kDa)	$Đ_M$[a] (M_w/M_n)	%*cis*[b]	T_g[c] (°C)	$T_{d,5\%}$[d] (°C)	E[e] (MPa)	σ_b[f] (MPa)	ε_b[g] (%)	U_T[h] ($MJ \cdot m^{-3}$)
F-C_6A ($HMDA_{100}$)*	129	6.92	100	117	294	669 ± 33	41.1 ± 3.26	165 ± 11.38	57.9 ± 7.08
F-C_6A_{EG} ($EDEA_{100}$) *	89	5.34	75	84	297	444 ± 41	21.3 ± 2.95	39 ± 8.88	5.5 ± 1.66
Poly($HMDA_{90}$-*co*-$EDEA_{10}$)	78	6.79	100	116	303	465 ± 50	26.0 ± 3.22	126 ± 22.11	29.1 ± 5.94
Poly($HMDA_{75}$-*co*-$EDEA_{25}$)	115	4.69	100	109	296	442 ± 45	21.6 ± 2.56	6.4 ± 0.50	0.9 ± 0.16
Poly($HMDA_{50}$-*co*-$EDEA_{50}$)	81	10.78	100	100	293	741 ± 48	27.6 ± 5.79	23.2 ± 2.65	6.7 ± 0.23
Poly($HMDA_{25}$-*co*-$EDEA_{75}$)	132	13.06	100	86	285	308 ± 20	15.6 ± 1.90	306 ± 19.91	38.0 ± 6.00
Poly($HMDA_{10}$-*co*-$EDEA_{90}$)	105	10.59	100	80	268	468 ± 14	20.7 ± 3.04	482 ± 55.73	72.4 ± 13.80

[a]M_w and $Đ_M$ were determined by size exclusion chromatography ($CHCl_3$, 0.5% NEt_3, 40 °C) analysis against poly(styrene) (PS) standards. [b]%*cis* content determined by ^{1}H NMR spectroscopic analysis. [c]T_g was obtained from the 2nd heating cycle. [d]$T_{d,5\%}$ was determined from the material loses 5% of mass weight. [e]Young's modulus. [f]Stress at break. [g]Strain at break (n = 3). [h]Tensile toughness (n = 3). Uncertainty is presented as the standard deviation of samples. **see Fig. S28*

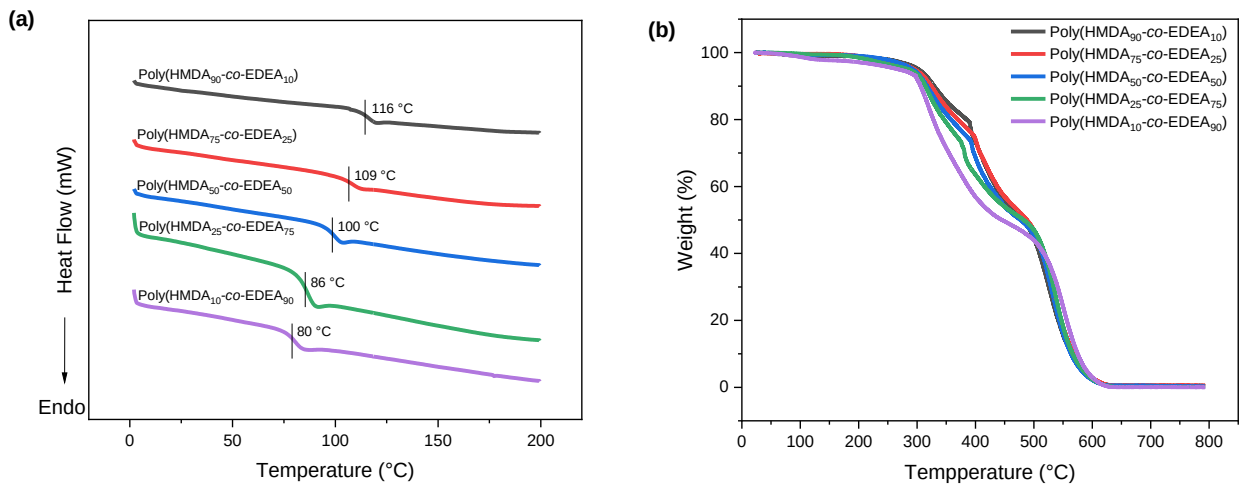

Fig. 4 (a) DSC thermograms of 2nd heating cycle tested at 10 °C min^{-1}. The position of T_g for each copolymer sample is indicated with a vertical hash mark. (b) Thermogravimetric analysis of copolymers at 10 $K \cdot min^{-1}$

Chain flexibility and intermolecular forces have generally exhibited a significant effect on the mechanical performance of the resultant polyketones. They could be enhanced by inserting more content of comonomer EDEA with ether bonds (C-O-C). It was required to investigate the best composition of EDEA to generate a desired tensile strength which is comparable to the commodity plastics. This copolymerization offers a diversity of polyketones with a wide range of strain and stress values when varying the molar ratios of comonomer compositions (Fig. 5a).

Poly (HMDA$_{90}$-*co*-EDEA$_{10}$) exhibits high stress at break value (σ_b = 26 MPa), but lower strain at break (ε_b = 126%). Poly(HMDA$_{75}$-*co*-EDEA$_{25}$) and poly(HMDA$_{50}$-*co*-EDEA$_{50}$) demonstrate poor mechanical performances (brittle). However, when we significantly increased more content of comonomer EDEA, the strain at break rose (more flexibel) as shown by poly(HMDA$_{25}$-*co*-EDEA$_{75}$) and poly(HMDA$_{10}$-*co*-EDEA$_{90}$) (Tabel 1). Among all synthesized copolyketones, poly(HMDA$_{10}$-*co*-EDEA$_{90}$) shows a comparable tensile strength to the commercial HDPE (but owing half of their elongation at break value) (Fig. 5b). This copolyketone exhibits a tough and ductile polymer material. In general, insertion of the comonomer EDEA could mostly improve the ductility, meanwhile, the comonomer HMDA content could increase the tensile toughness of the materials.

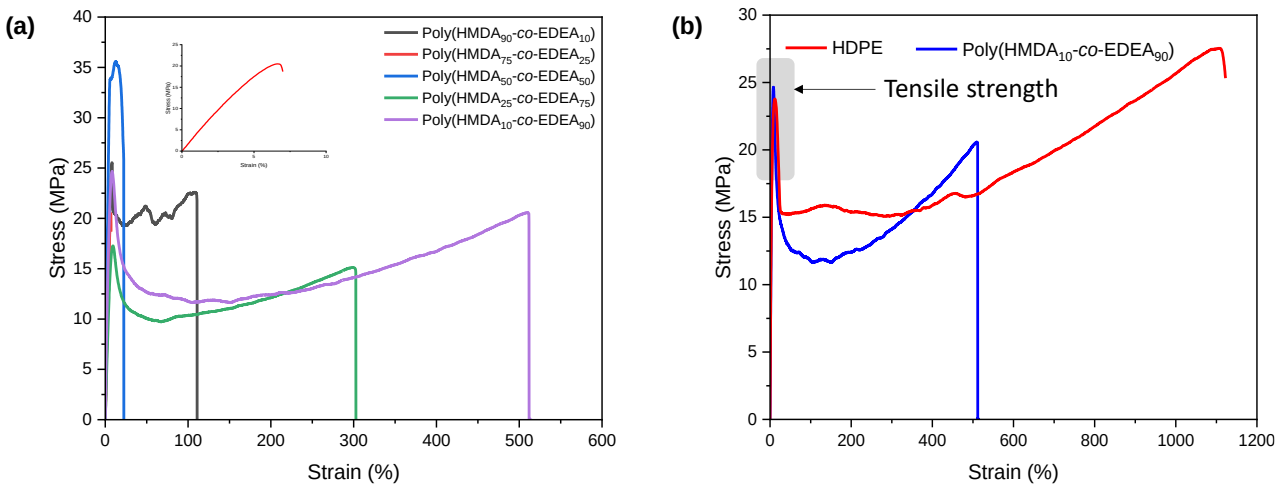

Fig. 5 Exemplary stress *vs* strain curves tested at 10 mm min^{-1}, 22 °C (a) Copolyketones from C_6A and C_6A_{EG} with various feeding molar ratios (b) HDPE and poly(HMDA$_{10}$-*co*-EDEA$_{90}$)

The exposure to ultraviolet (UV) light can lead to the substantial deterioration of several materials. The photodegradation study was conducted by irradiating the representative copolymer both in solution and film state with controlled UV light (wavelength 340 nm, irradiance 50 W/m^2). UV radiation induces photooxidative degradation, leading to the fragmentation of polymer chains, generation of free radicals, reduction in molecular weight, deterioration of mechanical properties, and ultimately rendering the materials worthless, with an uncertain timeframe.[33] In addition, the degradation products also display a similar photodegradation pathway as observed in our previous studies (a more selective pathway than the Norrish pathways). In the film and solution state, the major products are α-diketone and acetone which showed singlet peaks at δ = 2.09 ppm and δ = 2.17 ppm respectively (Fig. S32). After they were fully degraded in the solution state, the singlet peak at δ = 11.4 ppm disappeared (Fig. S33). This indicates the complete cleavage of N-H bonds in the polymer backbones. In addition, the FTIR spectra also confirmed the formation of degradation products in which the N-H bonds absorption is in the range of 2500-3000 cm^{-1} clearly disappeared after irradiation (Fig. 6b). Furthermore, the furan moiety at δ = 7 ppm disappeared due to the further degradation to the highly volatile acetylene and ketene as we found in our previous studies (unpublished work).

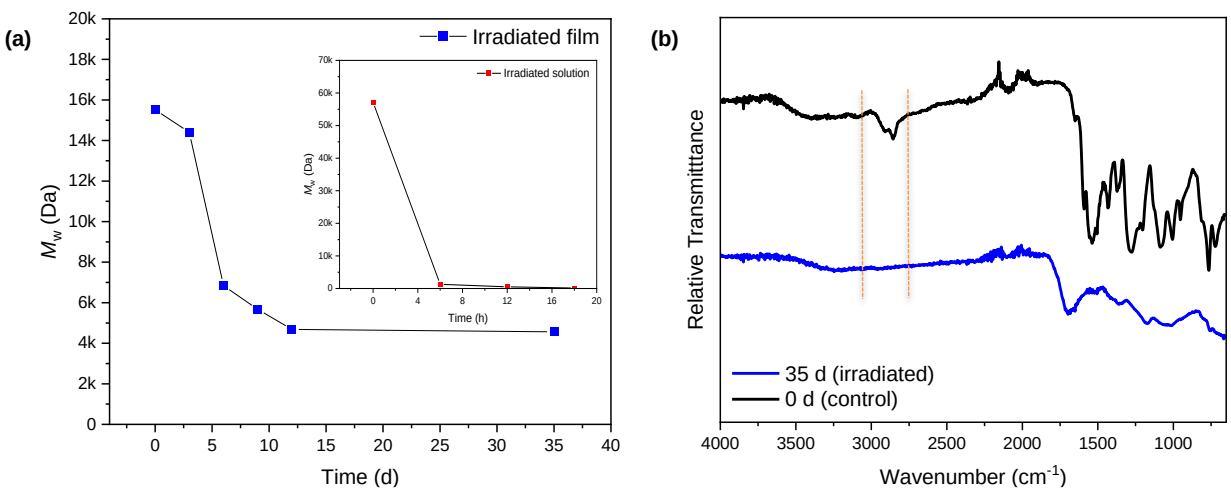

Fig. 6 (a) SEC analysis of poly(HMDA$_{10}$-*co*-EDEA$_{90}$) as an irradiated film and irradiated solution sample (*Agilent PS standards cover a M_w range from 162 Da to 15 x 10^6 Da, therefore 162 Da is considered as zero* (*0*)). (b) FTIR spectroscopy of freshly processed film and irradiated film.

The molecular weight exhibited a much more significant drop in the solution state compared to the film state (Fig. 6a). The polymer film exhibits uniform distribution of photolytic bond concentrations within its polymer chains (in contrast to the dilute polymer solution system). The dilute polymer solution, which was disseminated in the solvent and produced random coils, exhibits non-uniform concentrations of photolytic bonds in the polymer chains.[34] This polymer system enables to accelerate the free radical reaction (*via* chain scission) and resulting in a rapid fall in molecular weight.

Conclusion

The copolyketones system was formulated to integrate 1,6-hexanediamine and 2,2'-(ethylenedioxy)bis(ethylamine) into furan-based ketone alkyne monomer through an *aza*-Michael addition reaction. This process allows to produce a diverse array of thermomechanical features with the absence of external catalysts. The synthesized copolyketones were discovered to behave as amorphous polymers, exhibiting a high glass transition temperature. The molar ratio of these comonomers could efficiently change the thermomechanical performances of the polymers by altering the chain flexibility in their polymer backbones. Poly(HMDA$_{10}$-*co*-EDEA$_{90}$) demonstrates a comparable tensile strength to HDPE (but owing half of their elongation at break value), a commonly used commercial plastic. In addition, the irradiated representative copolymer exhibited a novel photodegradation pathway, with the α-diketone and acetone becoming the major products. These polymer materials potentially serve as alternative photodegradable thermoplastics to commercially available thermoplastics.

Experimental

Materials

1,6-hexanediamine 98% was purchased from Fischer Scientific and 2,2'(Ethylenedioxy)bis(ethylamine) 98% was purchased from Sigma Aldrich. 2,2'(Ethylenedioxy)bis(ethylamine) was distilled under vacuum before use and stored under

N_2 in a Schlenk-flash. Anhydrous THF was used directly from our solvent drying and degassing tower. All other chemicals were used as they were received.

Measurements

A Bruker DPX-300 and DPX-400 spectrometer was used to record ^{1}H NMR (300 MHz and 400 MHz) and ^{13}C NMR (100.57 MHz) spectra at 298 K for all NMR experiments. ^{1}H NMR spectra are referenced to residual proton solvent (δ 7.26 for $CDCl_3$) and ^{13}C NMR spectra are referenced to the solvent signal (δ 77.2 for $CDCl_3$). The resonance multiplicities are described as s (singlet), d (doublet), t (triplet), q (quartet), m (multiplet), dt (doublet of triplets), tt (triplet of triplets), qt (quartet of triplets).

Size Exclusion Chromatography (SEC) measurements in $CHCl_3$ were performed using an Agilent 1260 Infinity II Multi-Detector GPC/SEC System equipped with RI, ultraviolet (UV, = 309 nm), and viscometer detectors. The polymers were eluted through an Agilent guard column (PLGel 5 μM, 50 × 7.5 mm) and two Agilent mixed-C columns (PLGel 5 μM, 300 × 7.5 mm) using $CHCl_3$ (buffered with 0.5% NEt_3) as the mobile phase (flow rate = 1 mL·min-1, 40 °C). The weight average molecular weights (M_w) are expressed in Dalton (Da). Number average molecular weight (M_n), weight average molecular weight (M_w) and dispersity ($Đ_M = M_w/M_n$) were determined using Agilent GPC software against a 15-point calibration curve (M_p = 162 – 3,187,000 g·mol^{-1}) based on polystyrene standards (Easivial PS-M/H, Agilent).

Mettler-Toledo Stare system DSC3+ (Mettler Toledo, Switzerland) was used to detect thermal transitions, including glass transition temperature (T_g), melting temperature (T_m), and crystallization temperature (T_c). Samples were added to 40 μL aluminum pans with a heating rate of 10 K min^{-1} and were recorded from 0−200 °C with two heating and cooling rate cycles. 10 − 15 mg were cut from annealed polymer films. The glass transition temperature (T_g) was determined by the minimum of the first derivative in the second heating cycle.

A Q550 Thermogravimetric Analyzer (TA instruments) was used to collect TGA data. Thermograms were recorded under N_2 atmosphere at a heating rate of 10 K min^{-1} from 25

^{o}C to 800 ^{o}C, with an average sample weight of around 7 mg. Decomposition temperatures were reported at the 5% weight loss temperature ($T_{d,\,5\%}$).

All uniaxial tensile tests were performed on a Testometric M350-5CT tensometer with a 5 kgF load cell for synthesized polymers and a 50 kgF load cell for commercial polymers. All measurements were performed at room temperature and 10 mm min^{-1} strain rate. A bespoke ASTM Die D-638 Type V was utilized to cut polymer film samples into dumbbell shapes manually. The sample is approximately 1.8 mm wide and 1.0 mm thick. Each specimen was clamped into the tensile holders and subjected to a strain rate of 10 mm·min^{-1} until failure. A minimum of three tensile tests were repeated for each sample, and the mean average values of the strain at break, stress at break, toughness, and Young's modulus are presented.

Synthesis of N^2,N^5-dimethoxy-N^2,N^5-dimethylfuran-2,5-dicarboxamide

N^2,N^5-dimethoxy-N^2,N^5-dimethylfuran-2,5-dicarboxamide was prepared following previously published work.[35] 2,5-furandicarboxylic acid (FDCA) (10 g, 64 x 10^{-3} mol, 1.0 equiv.) and thionyl chloride ($SOCl_2$) (38 mL, 320 x 10^{-3} mol, 5 equiv.) were added to a 2-neck round-bottom flask with a magnetic stirrer, and 3 drops of DMF were then added. An exhaust tube was attached to a NaOH bath, and the reaction mixture was then heated at 50 °C and stirred until soluble. The acid chloride solution was cooled down at room temperature and the excess of $SOCl_2$ was removed by high vacuum. *N,O*-dimethylhydroxylamine hydrochloride (13.75 g, 141 x 10^{-3} mol, 2.2 equiv.) was added to the reaction mixture after it was cooled down to 0 °C (in an ice bath). The dropping funnel was used to progressively add trimethylamine (NEt_3) (26 mL, 2691 mmol, 4.2 equiv.) to the reaction mixture (dropwise slowly, over 30 minutes). The reaction produces an exothermic white precipitate (ammonium salt by-product). After adding trimethylamine, the reaction mixture was taken from the ice bath and left for one hour at room temperature. The reaction mixture was diluted with dichloromethane, and then transferred to a separatory funnel. The organic layer was washed with 1 M HCl (2x100 mL), followed by saturated $NaHCO_3$ solution (2x100 mL) and brine (2x100 mL). After

being dried over magnesium sulphate, the organic layer was concentrated using a rotary evaporator. The reaction mixture was purified by recrystallization with methanol to afford a brown solid product (14.1 g, 91% yield). *N^2,N^5-dimethoxy-N^2,N^5-dimethylfuran-2,5-dicarboxamide* **^{1}H NMR** spectra (400 MHz, $CDCl_3$) δ 7.17 (s, 2H), 3.83 (s, 6H), 3.36 (s, 6H); **^{13}C NMR** (101 MHz, $CDCl_3$) δ 158.82, 147.33, 118.07, 62.00, 33.55.

Synthesis of 1,1'-(furan-2,5-diyl)bis(but-2-yn-1-one)

1,1'-(furan-2,5-diyl)bis(but-2-yn-1-one) was prepared following previously published work.[36] In dried glassware and under Schlenk conditions, furyl Weinreb amide (5 g, 21 x 10^{-3} mol, 1.0 equiv.) was introduced to a 2-neck round-bottom flask. It was then diluted through cannula transfer with 1 M anhydrous THF. Then, 1-propynylmagnesium bromide solution 0.5 M in THF (99 mL, 50 x 10^{-3} mol, 2.4 equiv.) was introduced by cannula into the Weinreb solution, and the solution was cooled to 5 °C in an ice bath. After cooling down the solution, the 1-propynylmagnesium bromide solution 0.5 M in THF was added slowly (over 45 minutes) to the reaction mixture while stirring in an ice bath. The mixture was then left at room temperature overnight to react. The mixture was subsequently cooled down to 0 °C for approximately 30 minutes. After the reaction mixture has been cooled down, it was rapidly quenched with 1 M HCl (100 mL). The crude mixture was transferred to a separatory funnel and washed with ethyl acetate (2x100 mL) and brine (2x100 mL). The resulting "extracted" layer was filtered and dried over magnesium sulphate. The organic solution was finally concentrated with a rotary evaporator. The reaction mixture was recrystallized with ethanol to obtain a brown solid monomer (3.40 g, 82% yield). *1,1'-(furan-2,5-diyl)bis(but-2-yn-1-one)* **^{1}H NMR** spectra (400 MHz, $CDCl_3$) δ 7.33 (s, 2H), 2.16 (s, 6H); **^{13}C NMR** (101 MHz, $CDCl_3$) δ 165.55, 154.57, 119.84, 94.02, 78.48, 4.65.

Synthesis of copolyketones from comonomer HMDA and EDEA

In a 20 ml glass vial, furyl ynone (0.5 g, 2.5 x 10^{-3} mol, 1.0 equiv.) was dissolved in DCM (2 mL), then stirred for about 1 h in the ice bath due to exothermic reaction prevention. During the ynone solution was cooled down to 0 °C, both HMDA (x equiv.) and EDEA (1-x equiv.) were diluted and washed with DCM (3 mL). They were mixed and added to the ynone solution, then stirred for 3 h at room temperature. To inhibit a crosslinking prior to precipitation, the butylated hydroxytoluene (BHT) about 20% w/w was added to the reaction mixture. The polymer solution was precipitated into diethyl ether and subsequently reprecipitated to eliminate any remaining BHT. Finally, it was further dried in a vacuum oven at 40 °C for 24 h to yield a solid polymer.

F-C$_6$A The polymer was obtained as a pale yellow solid. **^{1}H NMR** spectra (400 MHz, $CDCl_3$) δ 11.27 (s, 2H), 6.98 (s, 2H), 5.70 (s, 2H), 3.32 (q, *J* = 6.6 Hz, 4H), 2.06 (s, 6H), 1.74 – 1.37 (m, 14H); **^{13}C NMR** (101 MHz, $CDCl_3$) δ 176.60, 165.65, 154.71, 113.49, 91.92, 43.25, 29.71, 26.52, 19.26; **SEC analysis** ($CHCl_3$ + 0.5% NEt_3) M_n = 18,693, M_w = 129,402 Da, $Đ_M$ = 6.92.

F-C$_6$A$_{EG}$ The polymer was obtained as a light yellow solid. **^{1}H NMR** spectra (400 MHz, $CDCl_3$) δ 11.26 (s, 2H), 6.98 (s, 1H), 5.70 (s, 1H), 3.76 – 3.57 (m, 8H), 3.49 (q, *J* = 5.6 Hz, 4H), 2.03 (d, *J* = 13.8 Hz, 5H); **^{13}C NMR** (101 MHz, $CDCl_3$) δ 176.79, 165.89, 154.86, 113.67, 92.28, 71.00, 70.31, 66.01, 43.55, 19.58, 15.42; **SEC analysis** ($CHCl_3$ + 0.5% NEt_3) M_n = 16,582, M_w = 88,549 Da, $Đ_M$ = 5.34.

Poly(HMDA$_{90}$-co-EDEA$_{10}$) The polymer was obtained as a dark brown solid (1.70 g, 96% yield). **^{1}H NMR** spectra (400 MHz, $CDCl_3$, 298K,): δ 11.27 (s, 2H), 7.00 – 6.94 (m, 2H), 5.72 – 5.65 (m, 2H), 3.65 (s, 1H), 3.48 (q, *J* = 7.0 Hz, 1H), 3.32 (q, *J* = 6.6 Hz, 4H), 2.11 – 1.99 (m, 8H), 1.66 (t, *J* = 6.8 Hz, 6H), 1.49 – 1.42 (m, 4H); **^{13}C NMR** (101 MHz, 298K, $CDCl_3$) δ 177.04, 166.11, 155.16, 113.94, 92.37, 43.70, 30.16, 26.97, 19.72; **SEC analysis** ($CHCl_3$ + 0.5% NEt_3) M_n = 11,548, M_w = 78,450 Da, $Đ_M$ = 6.79.

Poly(HMDA$_{75}$-co-EDEA$_{25}$) The polymer was obtained as a brown solid (1.68 g, 95% yield). **^{1}H NMR** spectra (400 MHz, $CDCl_3$, 298K,): δ 11.28 (s, 2H), 7.01 – 6.94 (m, 2H), 5.73 – 5.65 (m, 2H), 3.66 (d, *J* = 6.6 Hz, 3H), 3.49 (d, *J* = 4.6 Hz, 1H), 3.32 (d, *J* = 6.5 Hz, 3H), 2.11 – 2.01 (m, 8H), 1.46 (s, 3H); **^{13}C NMR** (101 MHz, 298K, $CDCl_3$) δ 176.71, 165.79, 154.83, 113.63, 92.04, 43.55, 43.38, 29.84, 26.65, 19.40; **SEC analysis** ($CHCl_3$ + 0.5% NEt_3) M_n = 27,706, M_w = 106,578 Da, $Đ_M$ = 3.84.

Poly(HMDA$_{50}$-co-EDEA$_{50}$) The polymer was obtained as a dark brown solid (1.69 g, 95% yield). **^{1}H NMR** spectra (400 MHz, $CDCl_3$, 298K,): δ 11.27 (s, 2H), 6.98 (t, *J* = 1.2 Hz, 2H), 5.70 (t, *J* = 2.2 Hz, 2H), 3.66 (q, *J* = 5.1, 4.3 Hz, 5H), 3.48 (qt, *J* = 7.0, 3.8 Hz, 3H), 3.31 (q, *J* = 6.6 Hz, 2H), 2.05 (dt, *J* = 7.9, 4.2 Hz, 7H), 1.46 (s, 2H); **^{13}C NMR** (101 MHz, 298K, $CDCl_3$) δ 176.80, 165.89, 154.85, 113.64, 92.30, 92.04, 71.01, 70.32, 43.56, 43.39, 29.85, 26.66, 19.58, 19.41; **SEC analysis** ($CHCl_3$ + 0.5% NEt_3) M_n = 7,503, M_w = 80,917 Da, $Đ_M$ = 10.78.

Poly(HMDA$_{25}$-co-EDEA$_{75}$) The polymer was obtained as a dark brown solid (1.70 g, 96% yield). **^{1}H NMR** spectra (400 MHz, $CDCl_3$, 298K,): δ 11.26 (s, 2H), 6.98 (d, *J* = 1.1 Hz, 2H), 5.70 (d, *J* = 1.4 Hz, 2H), 3.70 – 3.62 (m, 8H), 3.49 (tt, *J* = 7.1, 3.1 Hz, 4H), 3.36 – 3.28 (m, 1H), 2.06 (d, *J* = 1.6 Hz, 2H), 2.06 – 2.01 (m, 5H), 1.46 (s, 1H); **^{13}C NMR** (101 MHz, 298K, $CDCl_3$) δ 176.81, 165.89, 154.88, 113.65, 92.30, 71.01, 70.33, 43.56, 29.85, 19.59; **SEC analysis** ($CHCl_3$ + 0.5% NEt_3) M_n = 10,137, M_w = 132,380 Da, $Đ_M$ = 13.06.

Poly(HMDA$_{10}$-co-EDEA$_{90}$) The polymer was obtained as a dark brown solid (1.68 g, 95% yield). **^{1}H NMR** spectra (400 MHz, $CDCl_3$, 298K,): δ 11.25 (s, 2H), 6.97 (s, 2H), 5.69 (s, 2H), 3.65 (d, *J* = 6.7 Hz, 8H), 3.55 – 3.41 (m, 4H), 2.05 (d, *J* = 2.8 Hz, 7H); **^{13}C NMR** (101 MHz, 298K, $CDCl_3$) δ 176.81, 165.89, 154.88, 113.65, 92.29, 71.02, 70.32, 66.01, 43.56, 19.58, 15.42; **SEC analysis** ($CHCl_3$ + 0.5% NEt_3) M_n = 9,911, M_w = 104,996 Da, $Đ_M$ = 10.59.

Author Contributions

L.H.S. synthesized the monomers and polymers, and performed thermomechanical testing as well as photodegradation. J.C.W. provided technical and synthetic guidance. A.B. analyzed the data and edited the manuscript. A.P.D conceived and supervised the project. The paper was written through the contributions of all authors. All authors have approved the final version of the paper.

Conflicts of Interest

There are no conflicts to declare.

Acknowledgements

A.P.D., A.B., and J.C.W. acknowledge funding from the European Research Council (ERC) under the European Union's Horizon 2020 research and innovation programme under grant agreement no. 681559. L.H.S thanks Indonesian Endowment Fund for Education (LPDP) agency for support funding.

Notes and references

1. Madhavan Nampoothiri, K., Nair, N. R. & John, R. P. An overview of the recent developments in polylactide (PLA) research. *Bioresour. Technol.* **101**, 8493–8501 (2010).
2. Zhao, X., Wang, Y., Chen, X., Yu, X., Li, W., Zhang, S., Meng, X., Zhao,Z. M., Dong, T., Anderson, A., Aiyedun, A., Li, Y., Webb, E., Wu, Z., Kunc, V., Ragauskas, A., Ozcan, S. & Zhu, H. Sustainable bioplastics derived from renewable natural resources for food packaging. *Matter* **6**, 97–127 (2023).
3. Mohee, R., Unmar, G. D., Mudhoo, A. & Khadoo, P. Biodegradability of biodegradable/degradable plastic materials under aerobic and anaerobic conditions. *Waste Manag.* **28**, 1624–1629 (2008).
4. Demirbas, A. Biodegradable plastics from renewable resources. *Energy Sources, Part A Recover. Util. Environ. Eff.* **29**, 419–424 (2007).

5. Haider, T. P., Völker, C., Kramm, J., Landfester, K. & Wurm, F. R. Plastics of the Future? The Impact of Biodegradable Polymers on the Environment and on Society. *Angew. Chemie - Int. Ed.* **58**, 50–62 (2019).

6. Naser, A. Z., Deiab, I. & Darras, B. M. Poly(lactic acid) (PLA) and polyhydroxyalkanoates (PHAs), green alternatives to petroleum-based plastics: a review. *RSC Adv.* **11**, 17151–17196 (2021).

7. Abdelmoez, W., Dahab, I., Ragab, E. M., Abdelsalam, O. A. & Mustafa, A. Bio- and oxo-degradable plastics: Insights on facts and challenges. *Polym. Adv. Technol.* **32**, 1981–1996 (2021).

8. Oliaei, E., Olsén, P., Lindström, T. & Berglund, L. A. Highly reinforced and degradable lignocellulose biocomposites by polymerization of new polyester oligomers. *Nat. Commun.* **13**, 1–12 (2022).

9. Chamas, A., Moon, H., Zheng, J., Qiu, Y., Tabassum, T., Jang, J. H., Abu-Omar, M., Scott, S. L. & Suh, S. Degradation Rates of Plastics in the Environment. *ACS Sustain. Chem. Eng.* **8**, 3494–3511 (2020).

10. Kim, M. S., Chang, H., Zheng, L., Yan, Q., Pfleger, B. F., Klier, J., Nelson, K., Majumder, E. L. W. & Huber, G. W. A Review of Biodegradable Plastics: Chemistry, Applications, Properties, and Future Research Needs. *Chem. Rev.* **123**, 9915–9939 (2023).

11. Filiciotto, L. & Rothenberg, G. Biodegradable Plastics: Standards, Policies, and Impacts. *ChemSusChem* **14**, 56–72 (2021).

12. Pal, D., Konar, D. & Sumerlin, B. S. Poly(Vinyl Ketones): New Directions in Photodegradable Polymers. *Macromol. Rapid Commun.* **44**, 1–12 (2023).

13. Daglen, B. C. & Tyler, D. R. Photodegradable plastics: End-of-life design principles. *Green Chem. Lett. Rev.* **3**, 69–82 (2010).

14. Guillet, J. Fundamental Processes in the Photodegradation of Polyolefins. *Adv. in Chem.* **169**, 1–10 (1978)

15. Reeves, J. A., De Alwis Watuthanthrige, N., Boyer, C. & Konkolewicz, D. Intrinsic and Catalyzed Photochemistry of Phenylvinylketone for Wavelength-Sensitive Controlled Polymerization. *ChemPhotoChem* **3**, 1171–1179 (2019).

16. Morgen, T. O., Baur, M., Göttker-Schnetmann, I. & Mecking, S. Photodegradable branched polyethylenes from carbon monoxide copolymerization under benign conditions. *Nat. Commun.* **11**, 1–7 (2020).

17. Norrish. Photo-Decomposition of Aldehydes and Ketones. 195–196 (1937).

18. Cho, S., Lee, J. S., Jang, H., ,Seorin Park, S.,Ji Hyun An, J. H. & Jang, J. Comparative studies on crystallinity, thermal and mechanical properties of

polyketone grown on plasma treated cvd graphene. *Polymers.* **13**, 1–15 (2021).

19. Yıldız, C., Seki, Y., Ekti, M., Aker, S., Leskeri, B. M., Sarikanat, M. & Altay, L. Improving Flame Retardant Properties of Aliphatic Polyketone (POK)-Based Composites. *ACS Omega* **8**, 9415–9422 (2023).

20. Cho, J., Jeon, I., Kim, S. Y., Lim, S. & Jho, J. Y. Improving Dispersion and Barrier Properties of Polyketone/Graphene Nanoplatelet Composites via Noncovalent Functionalization Using Aminopyrene. *ACS Appl. Mater. Interfaces* **9**, 27984–27994 (2017).

21. Matsutani, H., Arima, N., Ishikawa, Y., Matsunaga, M. & Okada, Y. Thermally Stable and Transparent Polyketone Resin. *2019 IEEE CPMT Symp. Japan, ICSJ 2019* **32**, 1–3 (2019).

22. Seo, D. C., Jeon, I., Bae, S. & Jho, J. Y. Morphology and Mechanical Properties of the Polyketone/Polycarbonate Blends Compatibilized with Polyamides. *Macromol. Res.* **28**, 1142–1148 (2020).

23. Cho, J., Lee, S. K., Eem, S. H., Jang, J. G. & Yang, B. Enhanced mechanical and thermal properties of carbon fiber-reinforced thermoplastic polyketone composites. *Compos. Part A Appl. Sci. Manuf.* **126**, 105599 (2019).

24. Geng, Z., Shin, J. J., Xi, Y. & Hawker, C. J. Click chemistry strategies for the accelerated synthesis of functional macromolecules. *J. Polym. Sci.* **59**, 963–1042 (2021).

25. Xia, L., Zhang, Z. & You, Y. Z. Synthesis of sequence-controlled polymers via sequential multicomponent reactions and interconvertible hybrid copolymerizations. *Polym. J.* **52**, 33–43 (2020).

26. Zhang, Z., You, Y. Z., Wu, D. C. & Hong, C. Y. A novel multicomponent reaction and its application in sequence-ordered functional polymer synthesis. *Polymer (Guildf).* **64**, 221–226 (2015).

27. Zhang, Y., Shen, J., Hu, R., Shi, X., Hu, X., He. B., Qin, & Tang, B. Z. Fast surface immobilization of native proteins through catalyst-free amino-yne click bioconjugation. Ch*em. Sci.* **11**, 3931–3935 (2020).

28. Lu, G., Godfrey, S., Herrlein, M. & Brook, M. A. Aza-Michael silicone cure is accelerated by β -hydroxyalkyl esters. 1935–1941 (2021) doi:10.1002/pol.20210390.

29. Khodadadi Yazdi, M. *et al.* Clickable polysaccharides for biomedical applications: A comprehensive review. *Prog. Polym. Sci.* **133**, 101590 (2022).

30. Zhang, J.. Zhang, Z., Jia Wang, Zang, Q., Sun, J. Z. & Tang, B. Z. Recent progress in the applications of amino-yne click chemistry. *Polym. Chem.* **12**, 2978–2986 (2021).

31. Zhansitov, A., Kurdanova. Z., Shakhmurzova, K., Slonov, A. Borisov, I. & Khashirova, K. Effect of Solvent and Monomer Ratio on the Properties of Polyphenylene Sulphone. *Polymers (Basel).* **15**, (2023).

32. Nigmatullin, R., Bencsik, M. & Gao, F. Influence of polymerisation conditions on the properties of polymer/clay nanocomposite hydrogels. *Soft Matter* **10**, 2035–2046 (2014).

33. Yousif, E. & Haddad, R. Photodegradation and photostabilization of polymers, especially polystyrene: Review. *Springerplus* **2**, 1–32 (2013).

34. Lyu, S. & Untereker, D. Degradability of Polymers for Implantable Biomedical Devices. *Int. J. Mol. Sci*. **10**, 4033-4065 (2009).

35. Nahm, S. & Weinreb, S. M. N-methoxy-n-methylamides as effective acylating agents. *Tetrahedron Lett.* **22**, 3815–3818 (1981).

36. Weiming Zhang, W., Huang, D., Xu, C., Haifeng Wang, H., Hu, Y. A powerful reagent for synthesis of weinreb amides directly from carboxylic acids. *Org. Lett.* **11**, 4474–4477 (2009).

4.1 Supporting Information

Supplementary Information

Tuning Thermomechanical Properties of Photodegradable Copolyketones via Spontaneous Amino-yne "Click" Copolymerization

Lukmanul H. Samada[†], Joshua C. Worch [†§], Arianna Brandolese[†], Andrew P. Dove[†]*

[†]School of Chemistry, The University of Birmingham, Edgbaston, Birmingham, B15 2TT, UK.

[§]Department of Chemistry, Virginia Tech, Blacksburg, VA 24061, USA.

*Corresponding to: A.Dove@bham.ac.uk

Synthetic scheme for monomer and precursor preparation

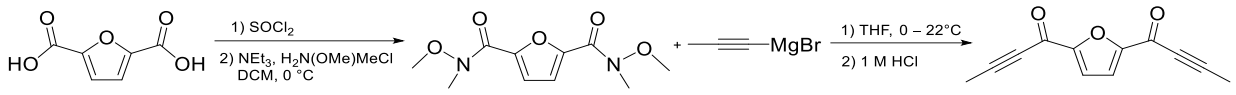

Scheme S1. (A) 2-Step synthesis of furan based diynone monomer using the Weinreb ketone synthesis.

Synthetic scheme for homopolymers and copolymers preparation

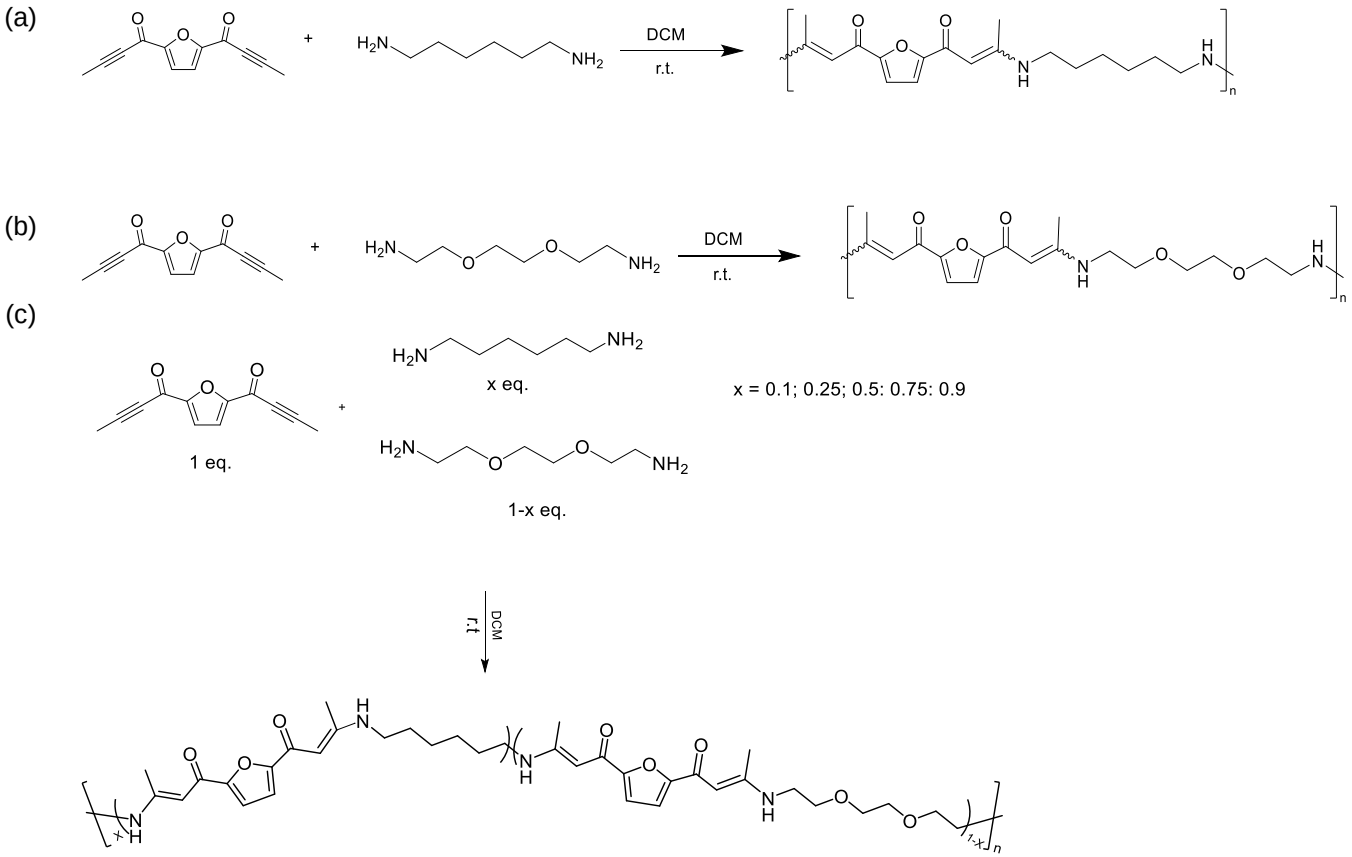

Scheme S2. (a) Spontaneous amino-yne "click" polyaddition between furyl diynone and 1,6-hexanediamine (HMDA) to yield polyketone F-C_6A. (b) Spontaneous amino-yne "click" polyaddition between furyl diynone and 2,2' (Ethylenedioxy)bis(ethylamine) (EDEA) to yield polyketone F-C_6A_{EG} (c) Copolymerization of furyl diynone with comonomer HMDA and EDEA

NMR spectra of monomer and precursor

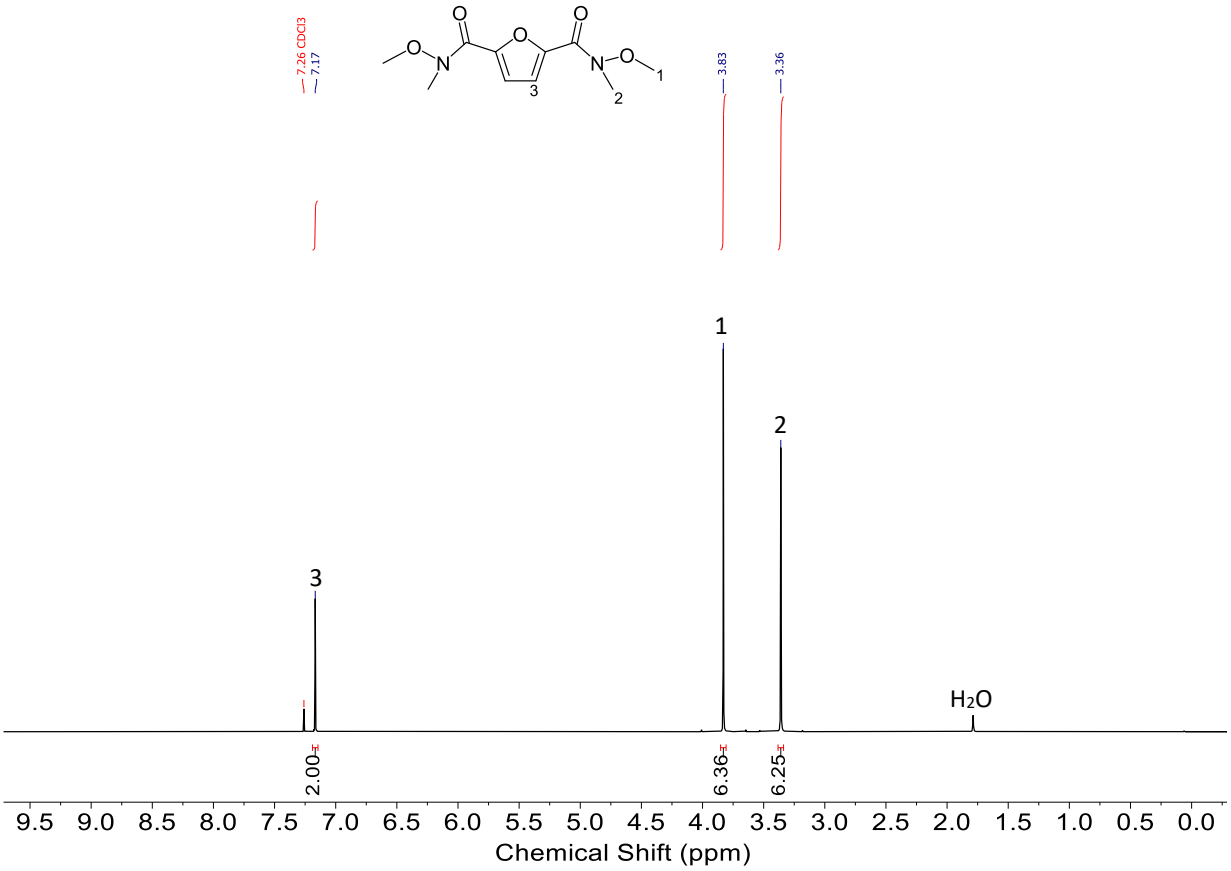

Figure S1. ^{1}H NMR spectrum (400 MHz, Chloroform-*d*) of furyl Weinreb amide

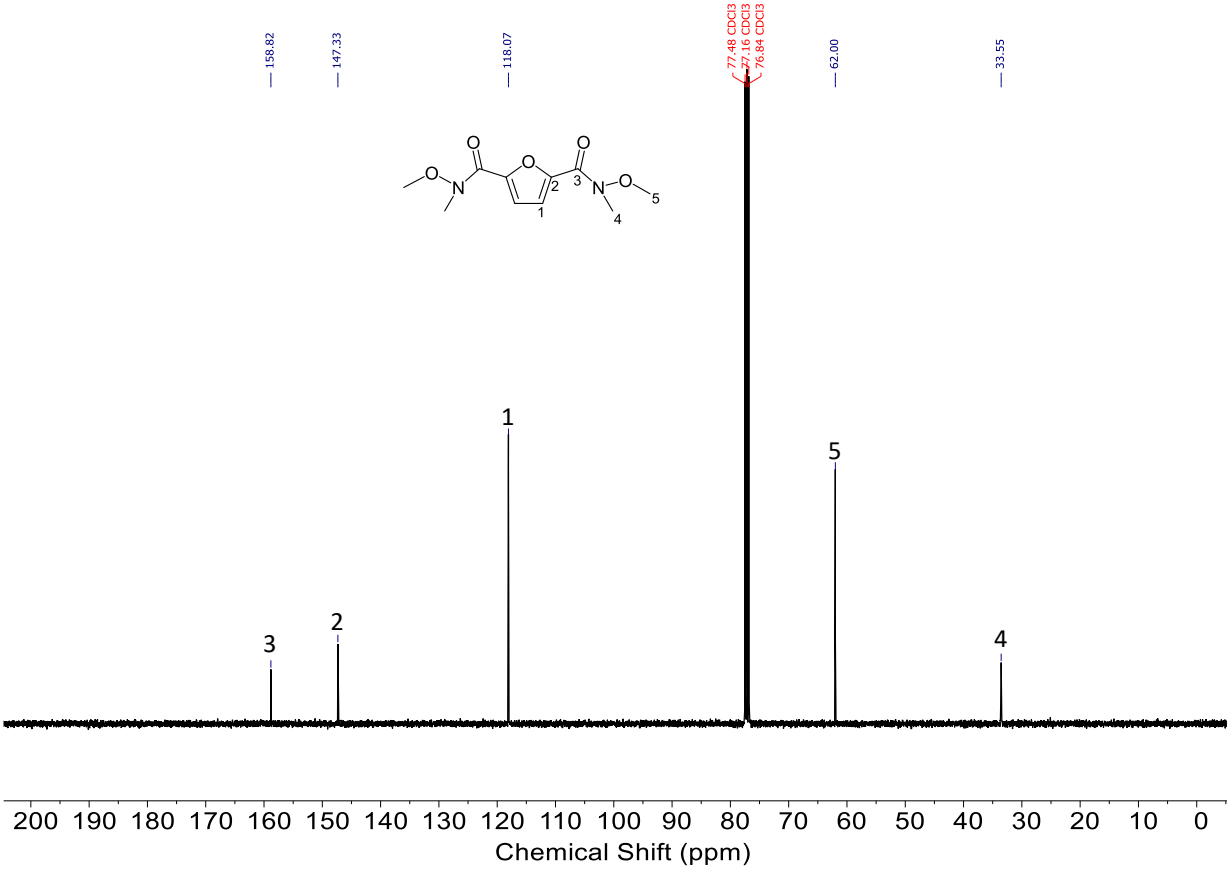

Figure S2. ^{13}C NMR spectrum (101 MHz, Chloroform-*d*) of furyl Weinreb amide

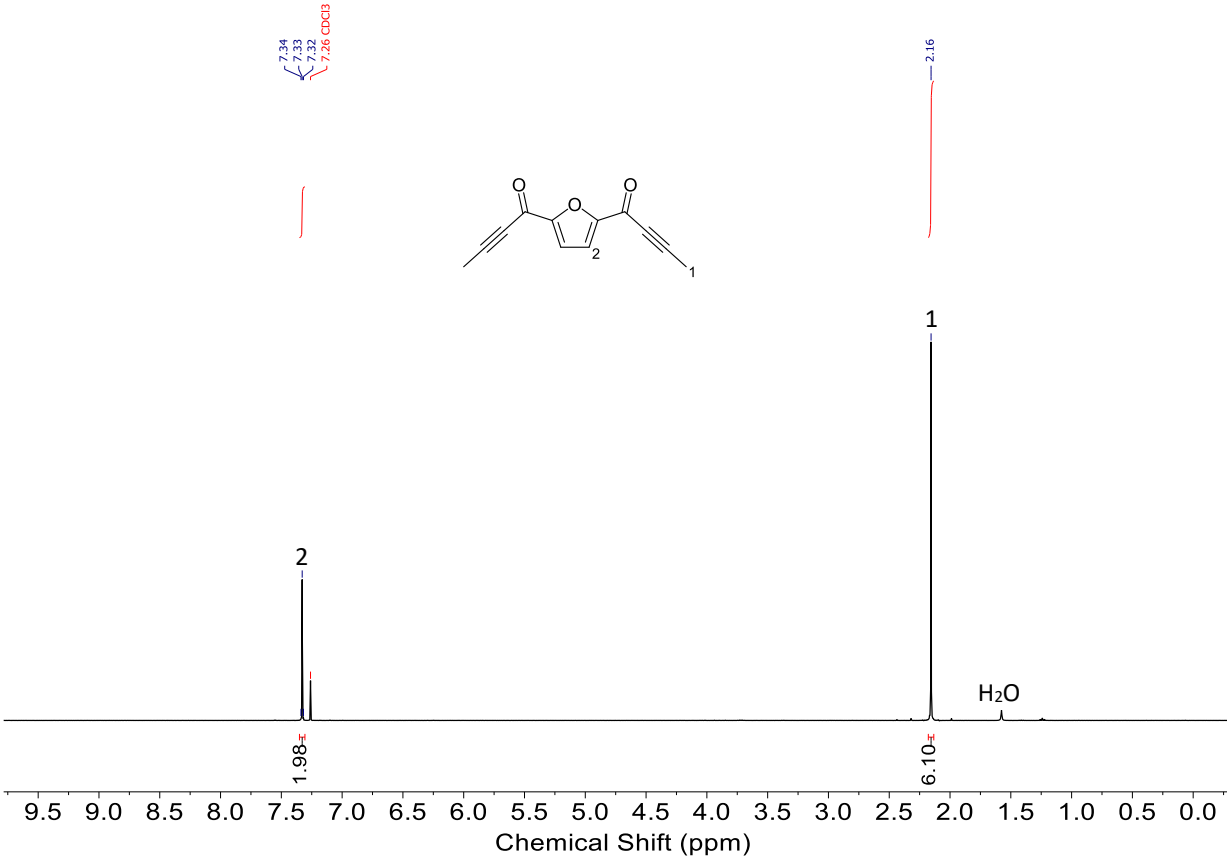

Figure S3. ^{1}H NMR spectrum (400 MHz, Chloroform-*d*) of furyl diynone

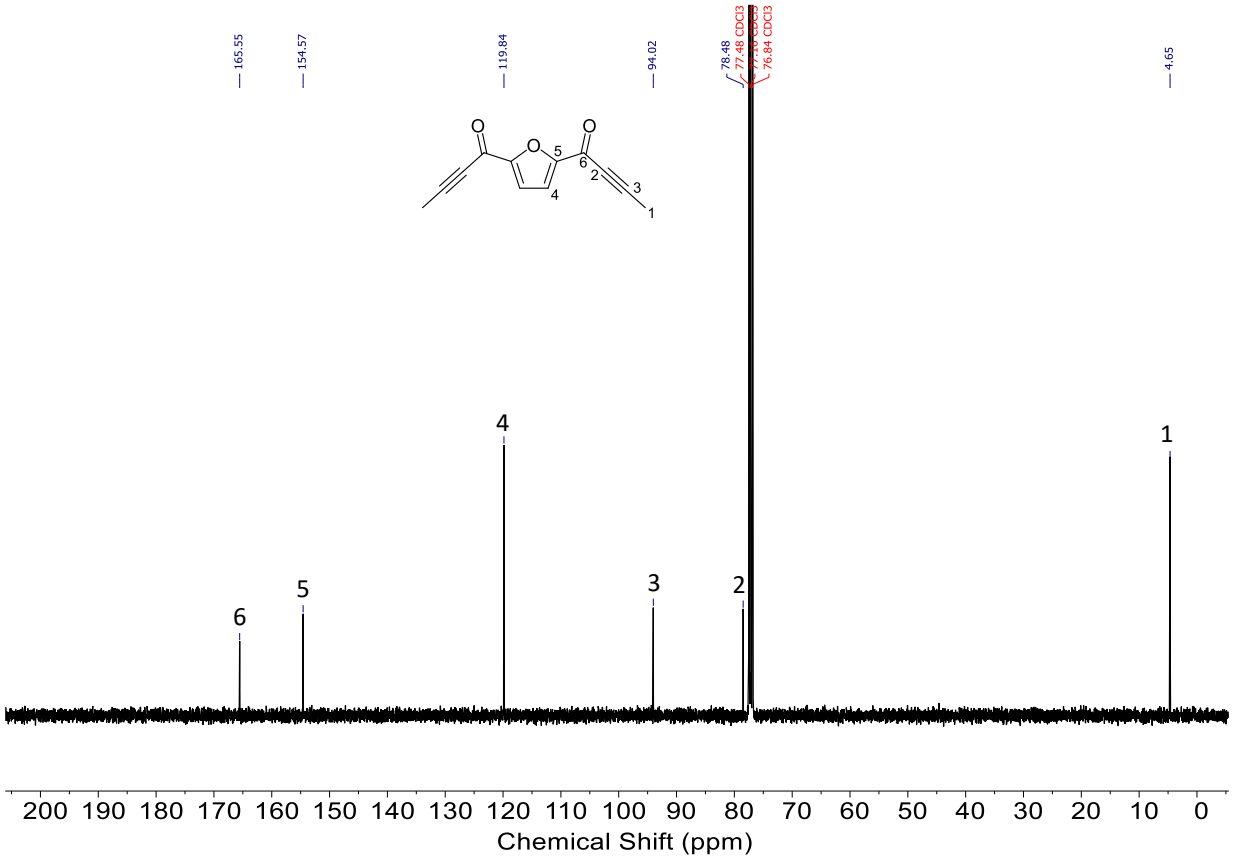

Figure S4. ^{13}C NMR spectrum (101 MHz, Chloroform-*d*) of diynone (ketone alkyne monomer)

NMR spectra of homopolymers

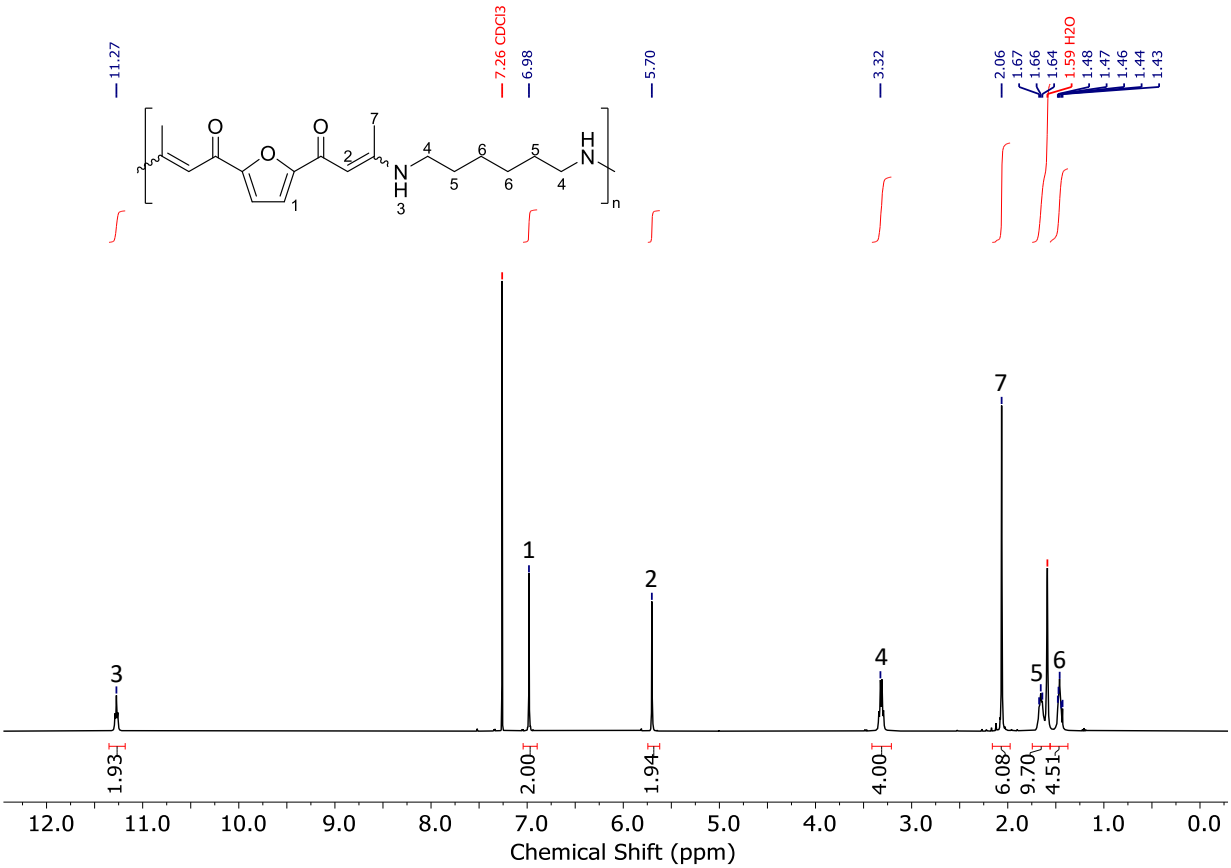

Figure S5. ^{1}H NMR spectrum (400 MHz, Chloroform-*d*) of polyketone F-C_6A. Reproduced from previous work (manuscript in preparation).

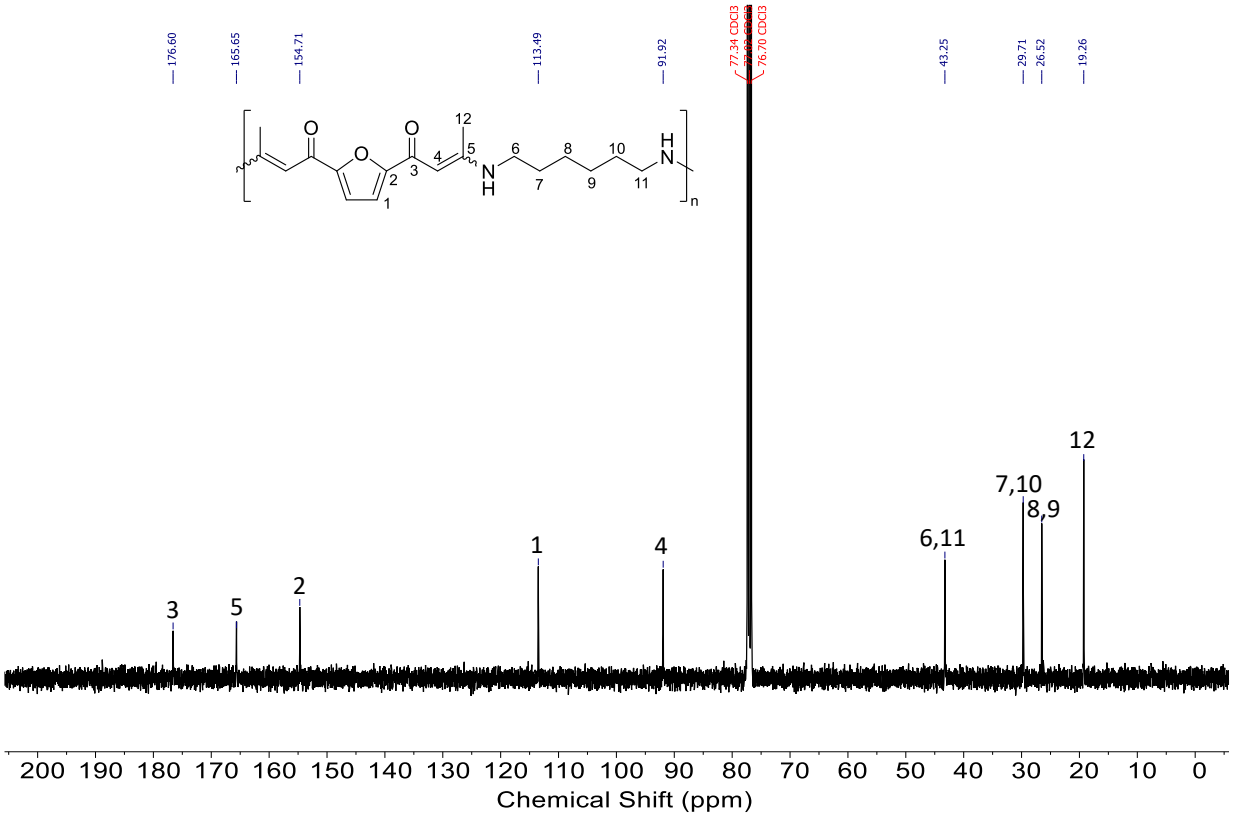

Figure S6. ^{13}C NMR spectrum (101 MHz, Chloroform-*d*) of polyketone F-C_6A. Reproduced from previous work (manuscript in preparation).

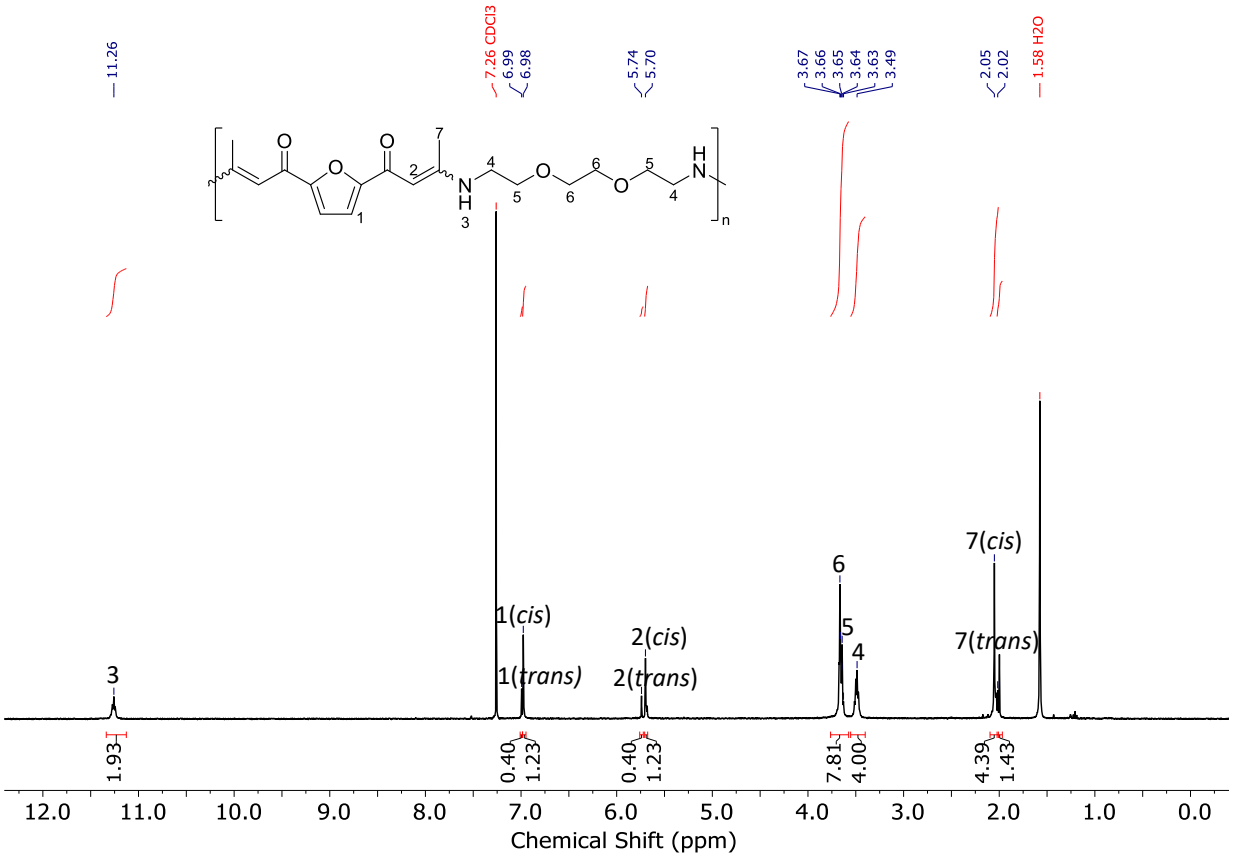

Figure S7. ^{1}H NMR spectrum (400 MHz, Chloroform-*d*) of polyketone F-C_6A_{EG}. Reproduced from previous work (manuscript in preparation).

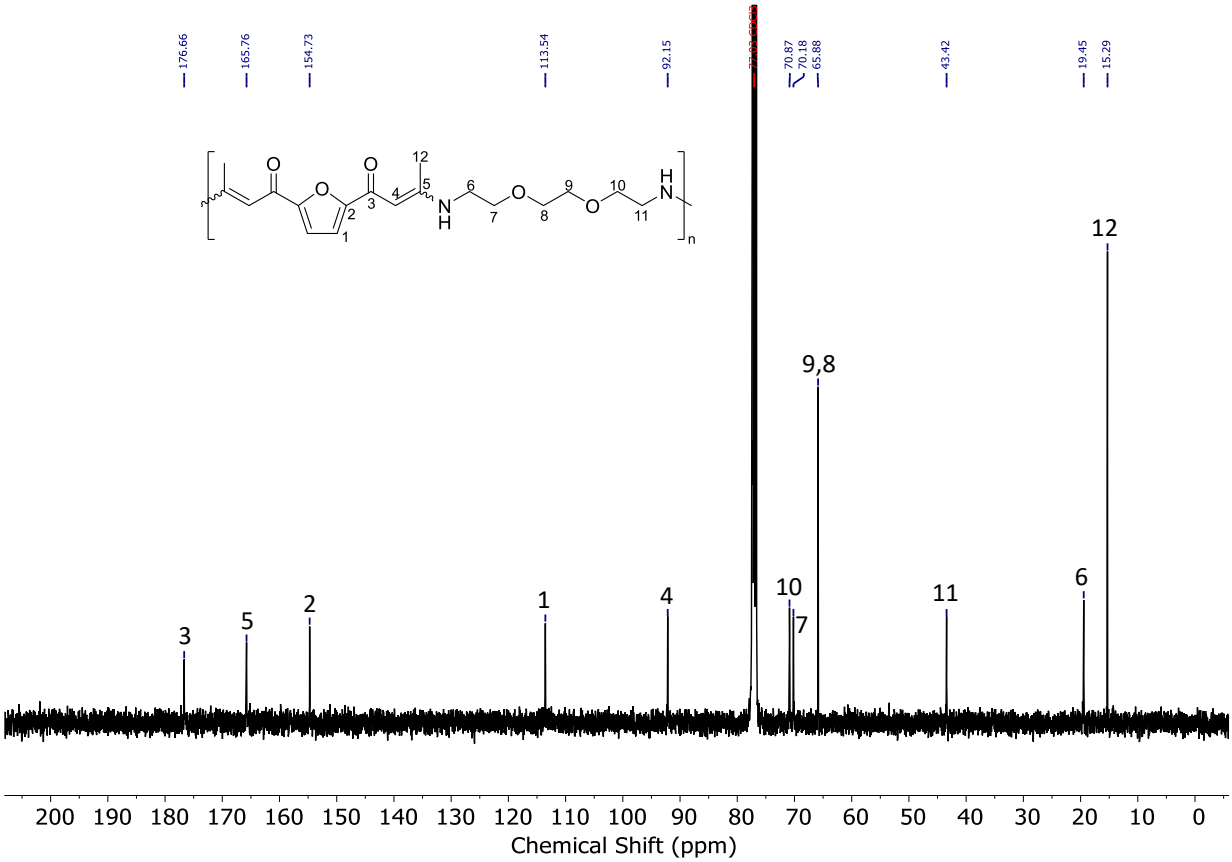

Figure S8. ^{13}C NMR spectrum (101 MHz, Chloroform-*d*) of polyketone F-C_6A_{EG}. Reproduced from previous work (manuscript in preparation).

NMR spectra of copolymers

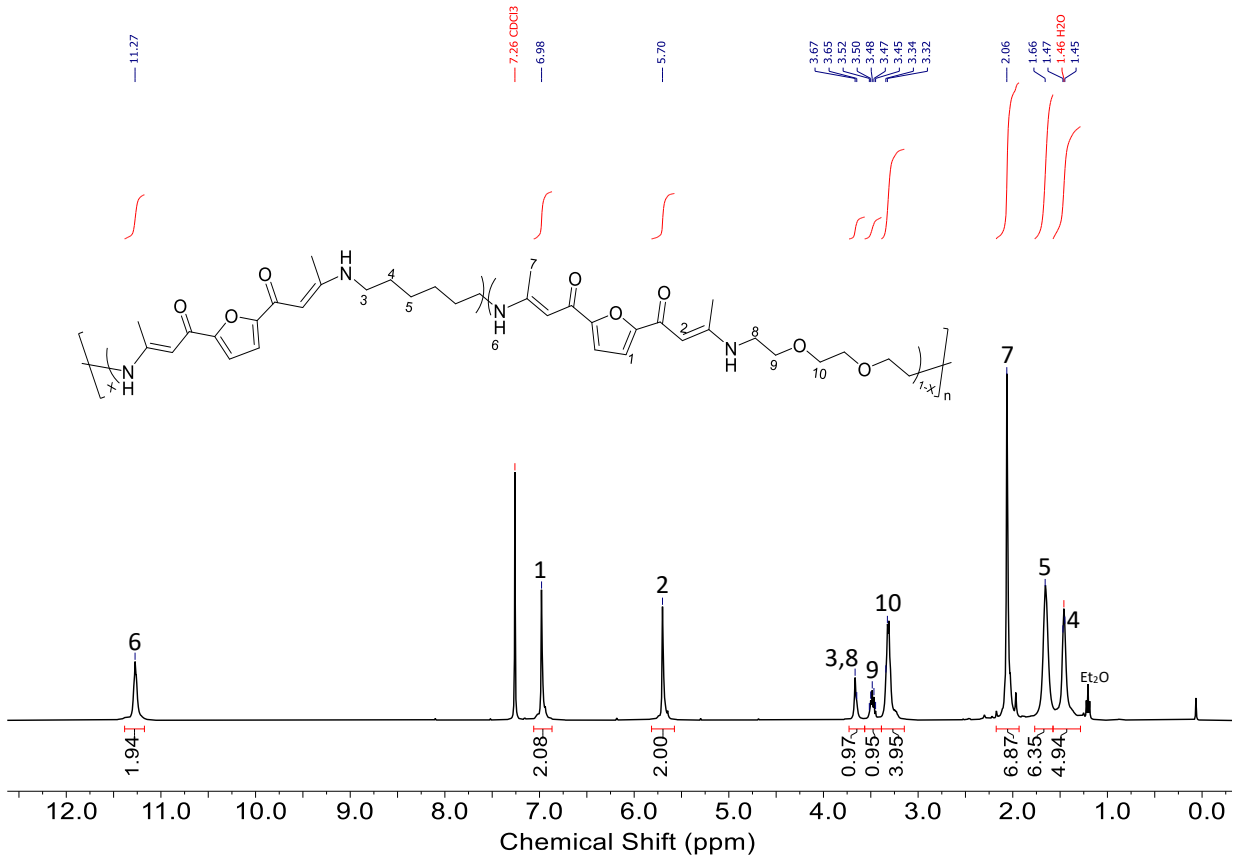

Figure S9. ^{1}H NMR spectrum of *poly(HMDA$_{90}$-co-EDEA$_{10}$)* (400 MHz, Chloroform-*d*)

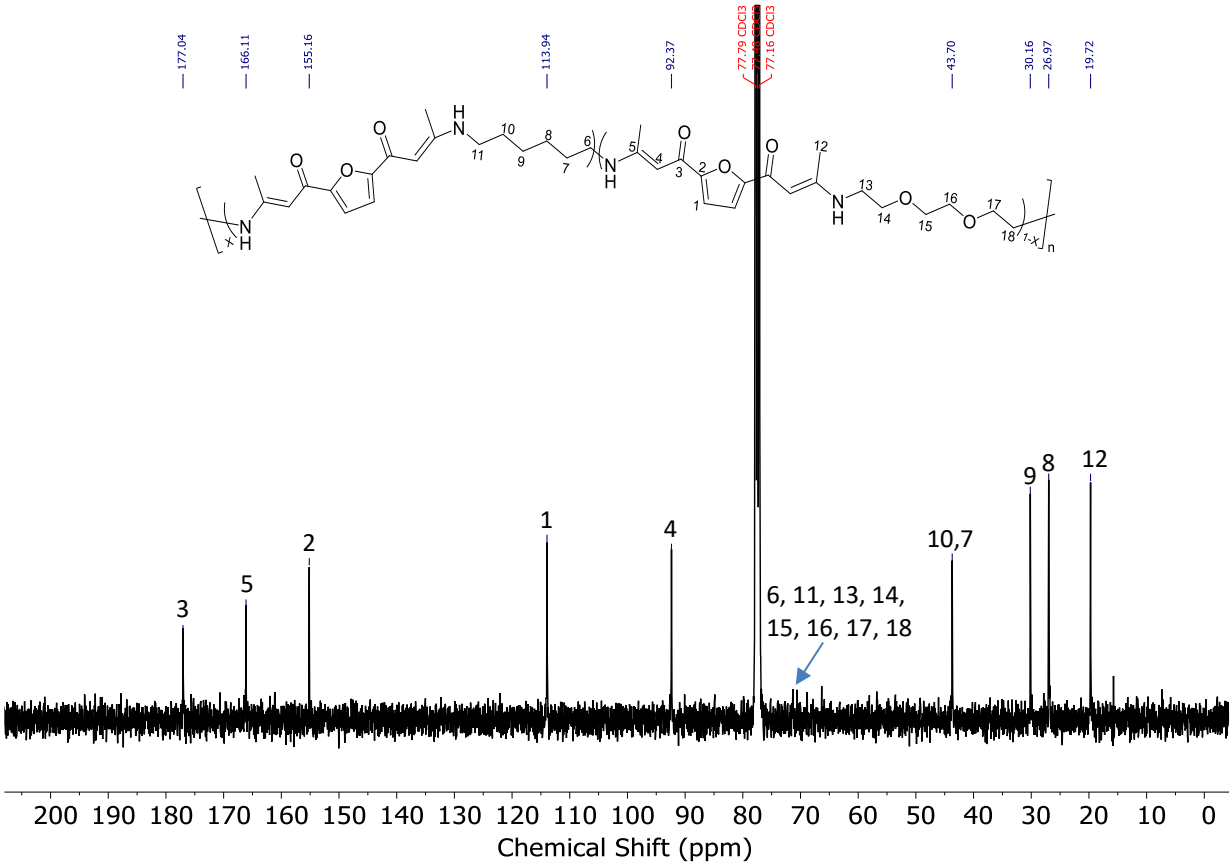

Figure S10. ^{13}C NMR spectrum (101 MHz, Chloroform-*d*) of *poly(HMDA$_{90}$-co-EDEA$_{10}$)*

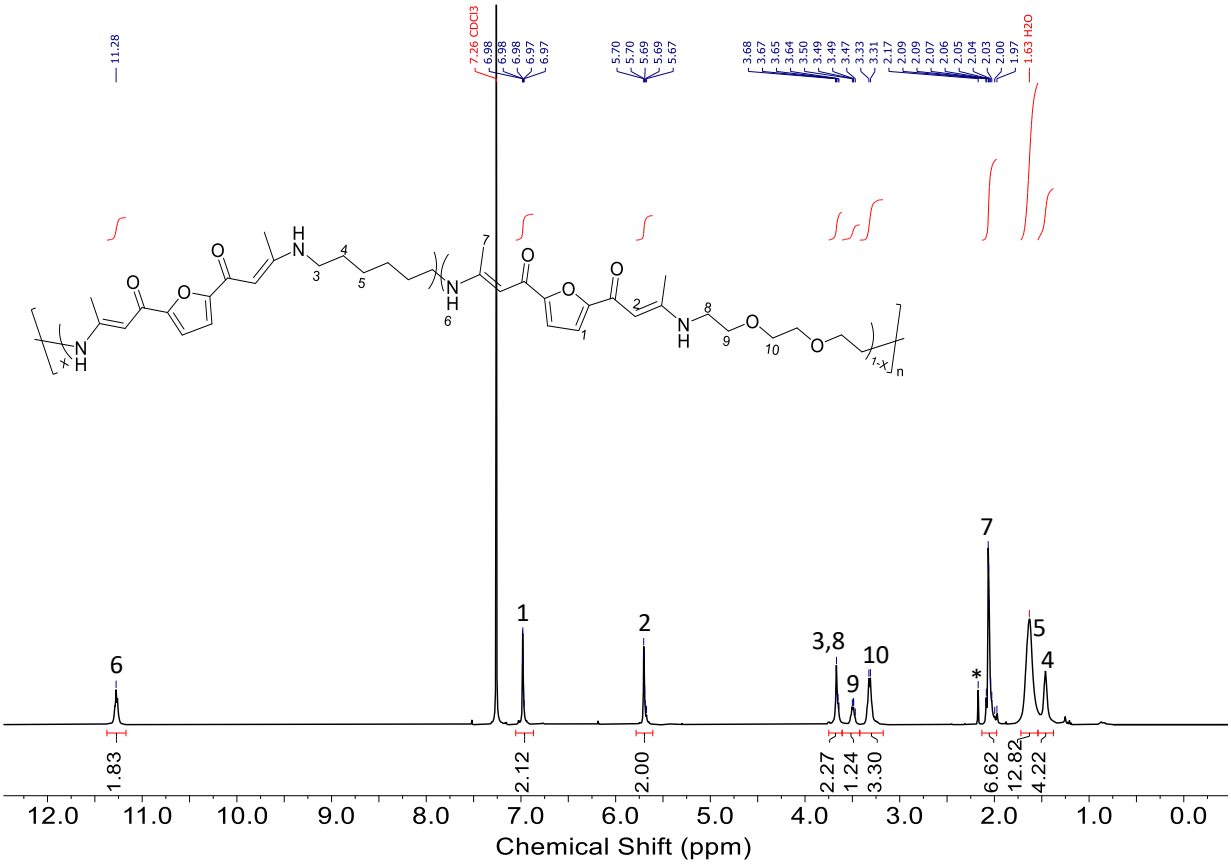

Figure S11. ^{1}H NMR spectrum (400 MHz, Chloroform-*d*) of *poly(HMDA$_{75}$-co-EDEA$_{25}$)*.*acetone

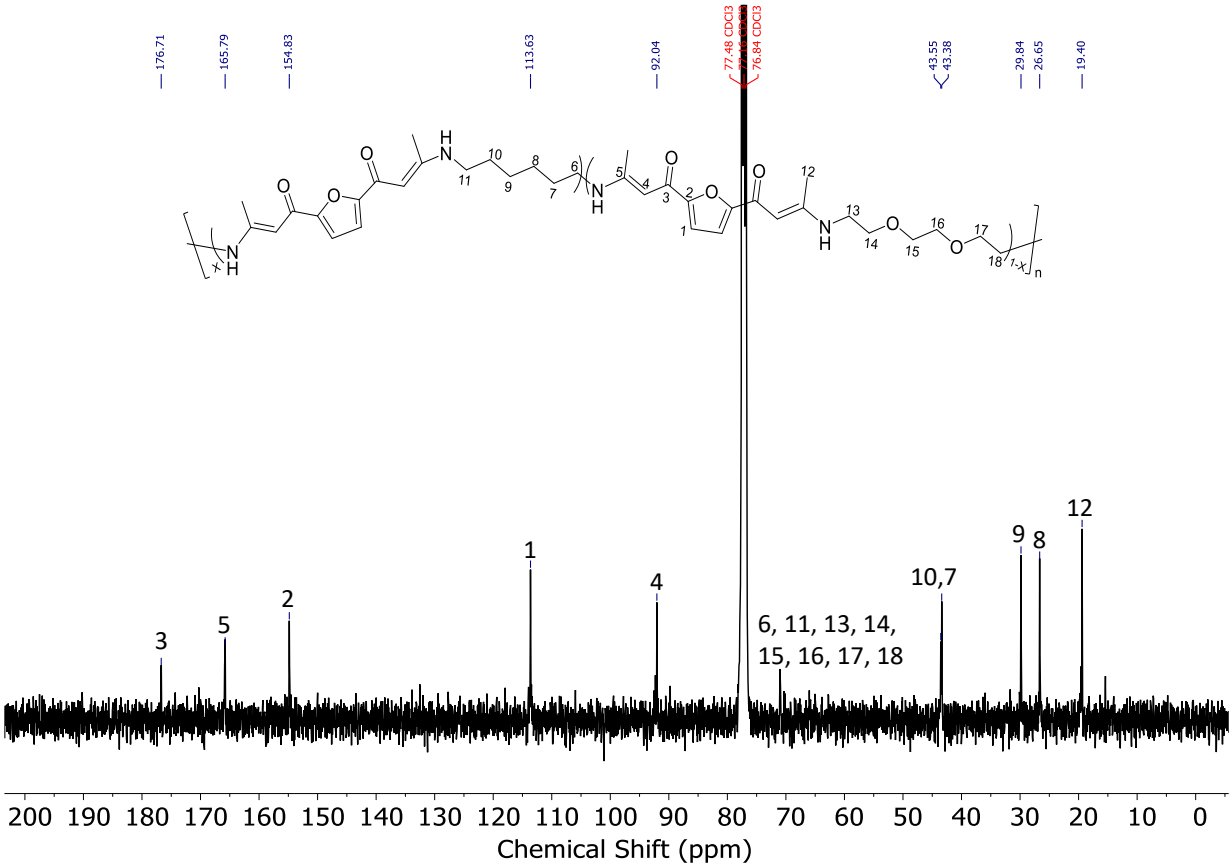

Figure S12. ^{13}C NMR spectrum (101 MHz, Chloroform-*d*) of *poly(HMDA$_{75}$-co-EDEA$_{25}$)*

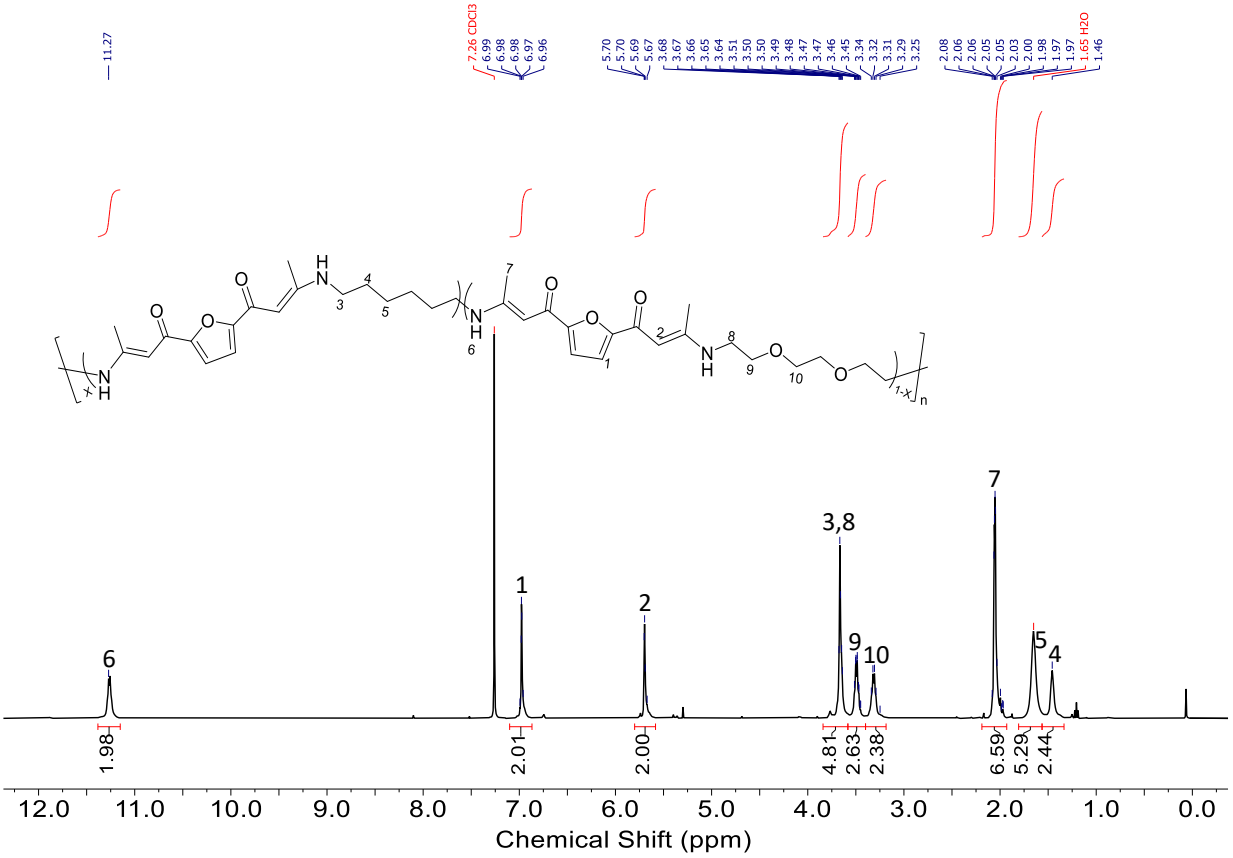

Figure S13. ^{1}H NMR spectrum (400 MHz, Chloroform-*d*) of *poly(HMDA$_{50}$-co-EDEA$_{50}$)*

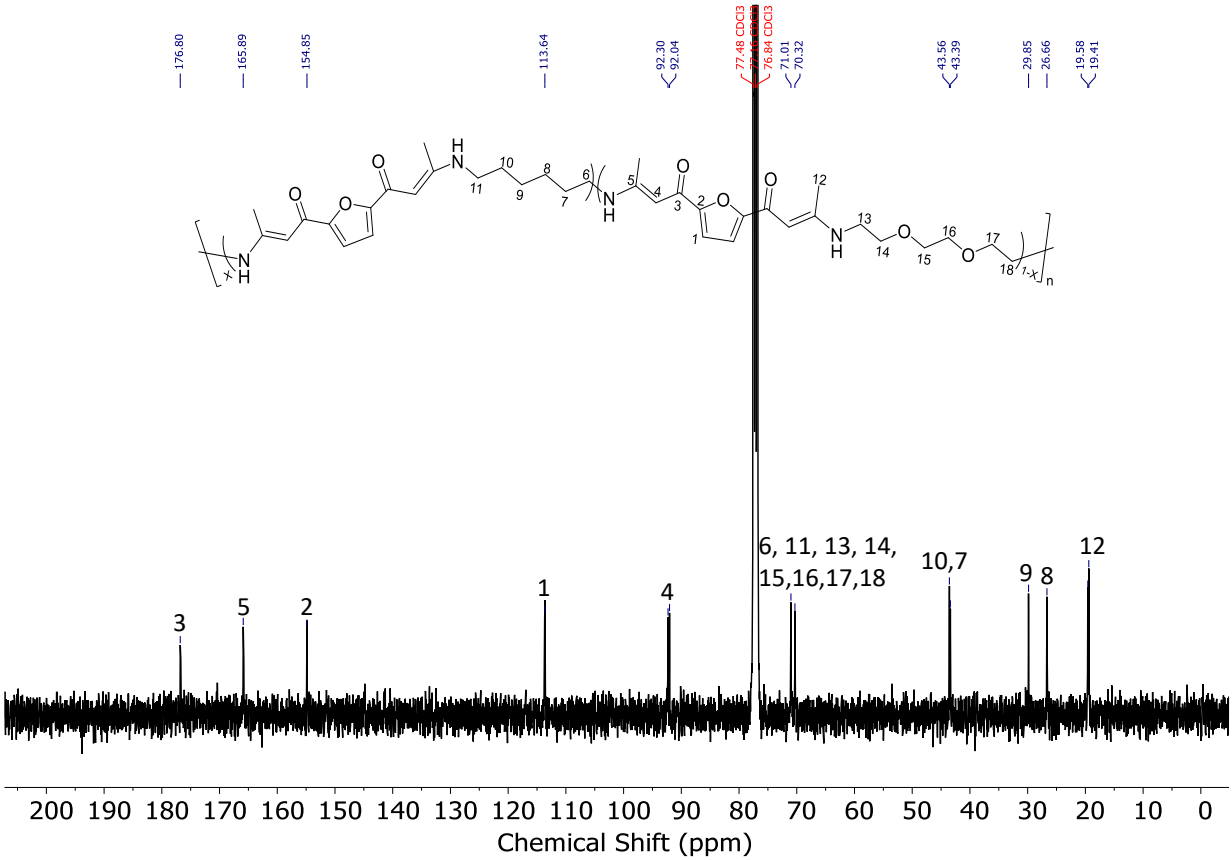

Figure S14. ^{13}C NMR spectrum (101 MHz, Chloroform-*d*) of *poly(HMDA$_{50}$-co-EDEA$_{50}$)*

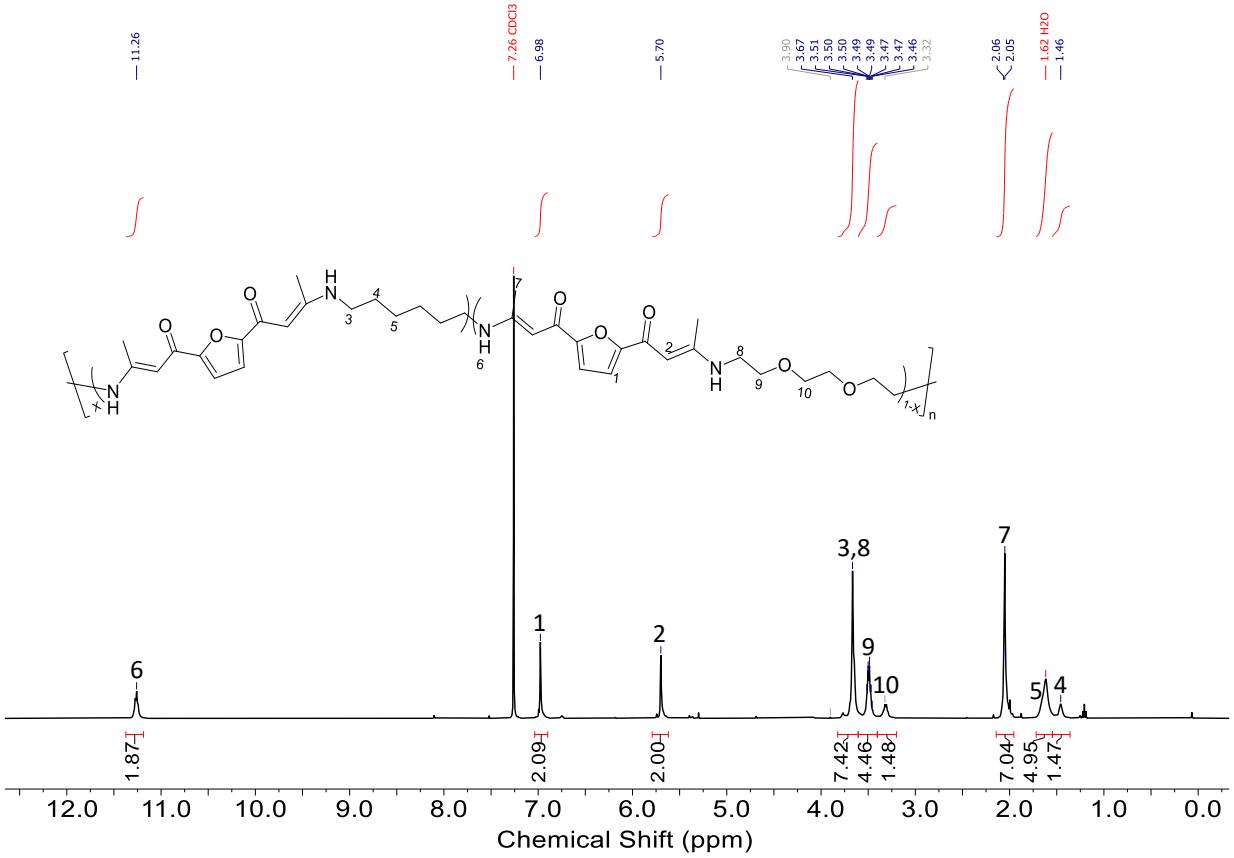

Figure S15. ^{1}H NMR spectrum (400 MHz, Chloroform-*d*) of *poly(HMDA$_{25}$-co-EDEA$_{75}$)*

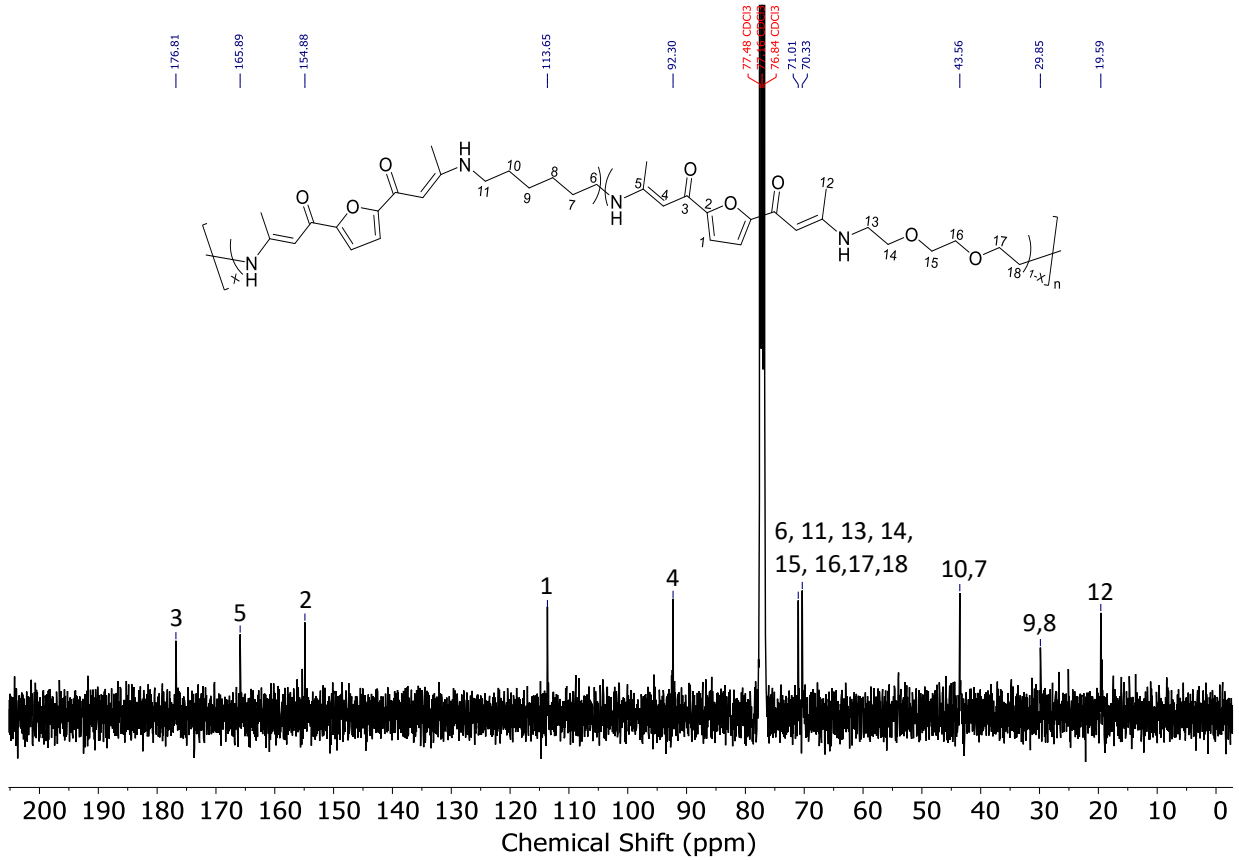

Figure S16. ^{13}C NMR spectrum (101 MHz, Chloroform-*d*) of *poly(HMDA$_{25}$-co-EDEA$_{75}$)*

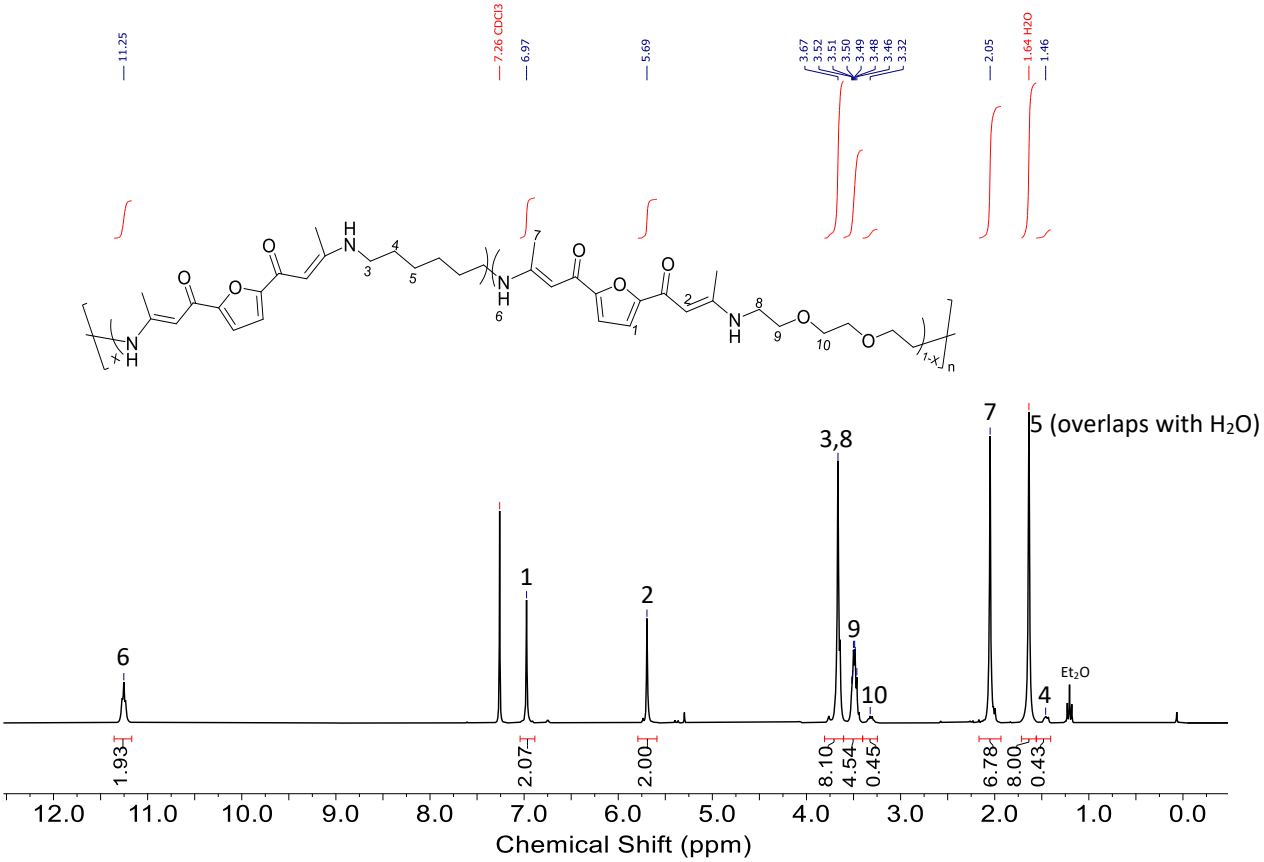

Figure S17. ^{1}H NMR spectrum (400 MHz, Chloroform-*d*) of *poly(HMDA$_{10}$-co-EDEA$_{90}$)*

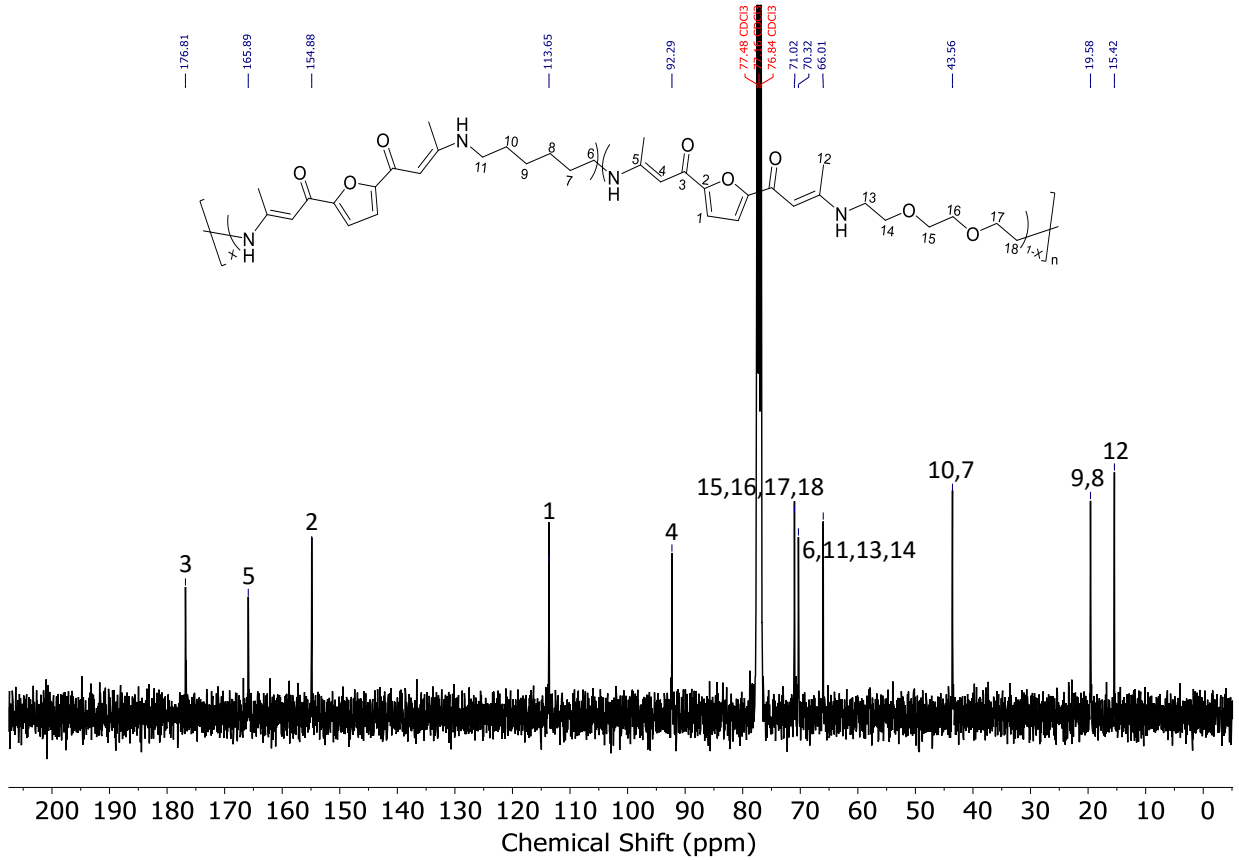

Figure S18. ^{13}C NMR spectrum (101 MHz, Chloroform-*d*) of *poly(HMDA$_{90}$-co-EDEA$_{10}$)*

Size exclusion chromatograms of homopolymers

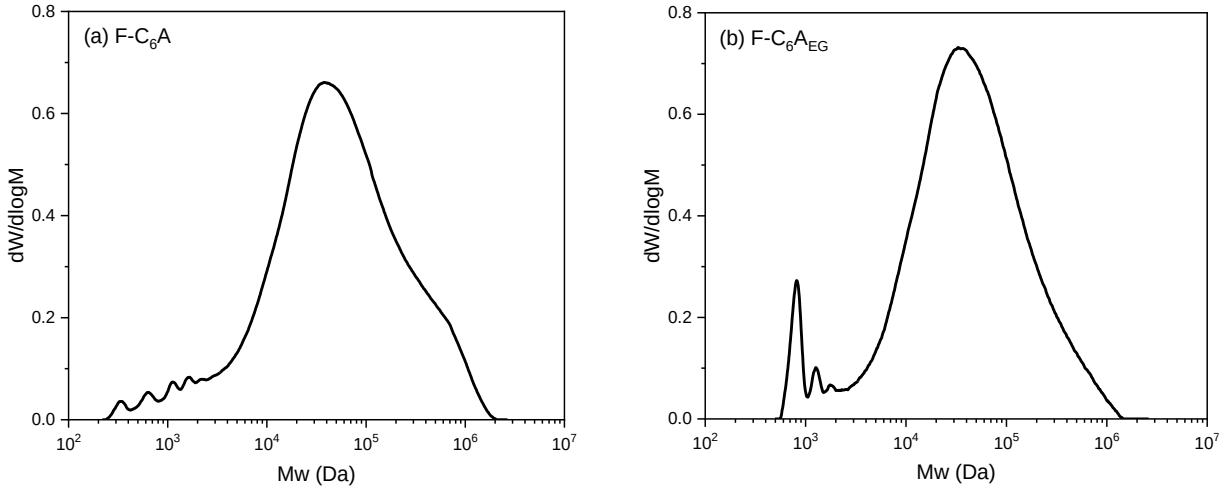

Figure S19. Size exclusion chromatograms of homopolymers (a) F-C_6A. (b) F-C_6A_{EG} ($CHCl_3$, 0.5% NEt_3, 40 °C) analysis against poly(styrene) (PS) standards.

Size exclusion chromatograms of copolymers

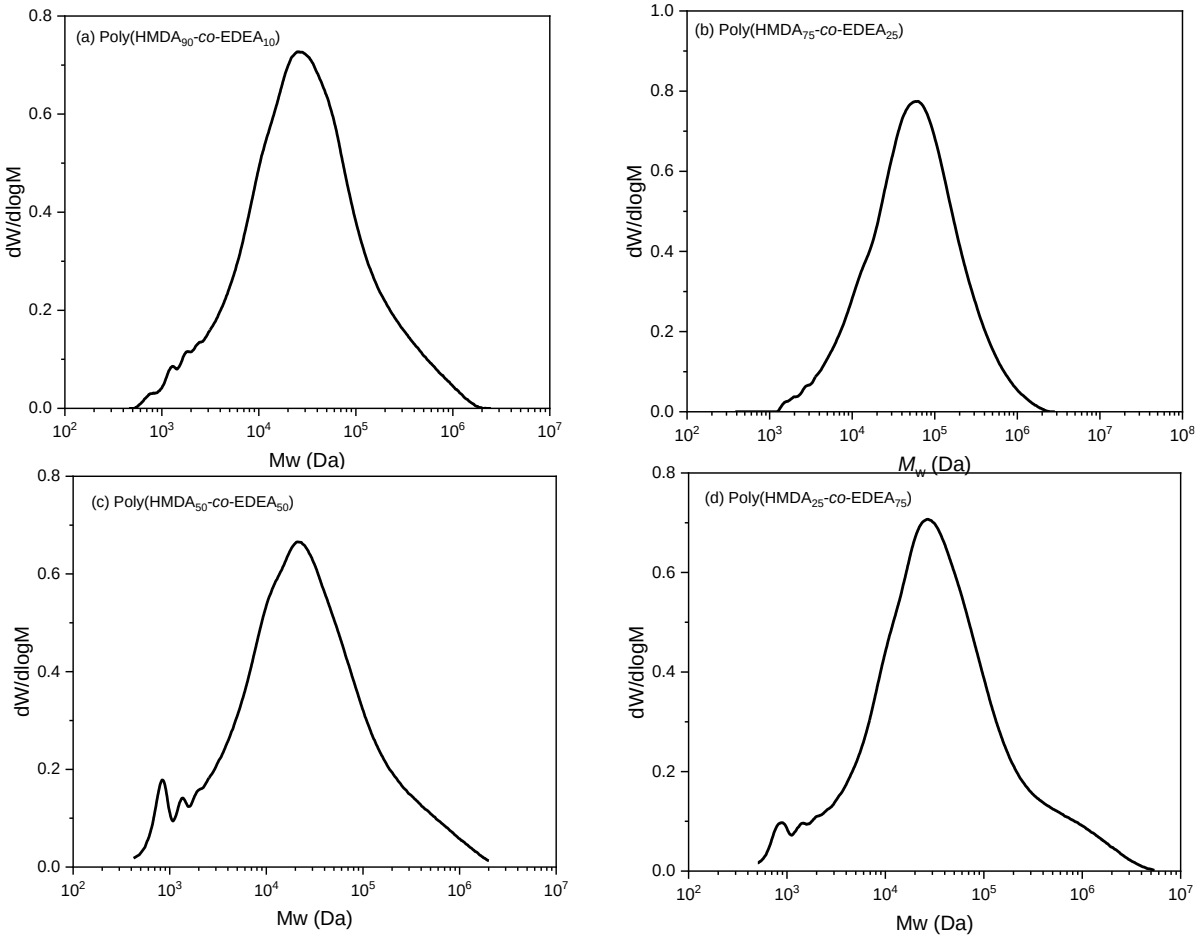

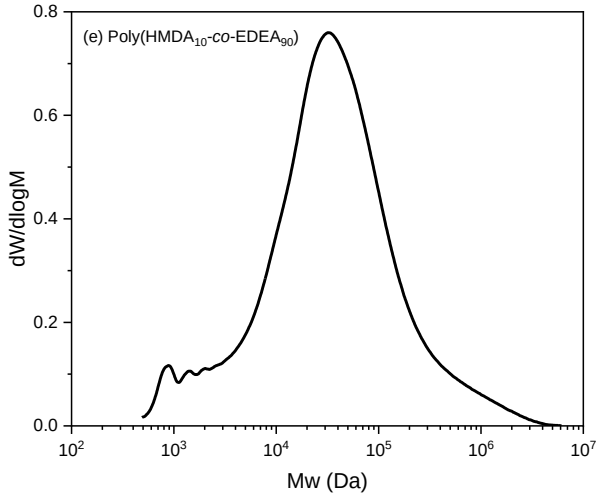

Figure S20. Size exclusion chromatograms of copolymers (a) poly(HMDA$_{90}$-*co*-EDEA$_{10}$). (b) poly(HMDA$_{75}$-*co*-EDEA$_{25}$). (c) poly(HMDA$_{50}$-*co*-EDEA$_{50}$). (d) poly(HMDA$_{25}$-*co*-EDEA$_{75}$). (e) poly(HMDA$_{10}$-*co*-EDEA$_{90}$) ($CHCl_3$, 0.5% NEt_3, 40 °C) analysis against poly(styrene) (PS) standards.

Infrared spectra of precursor and monomer

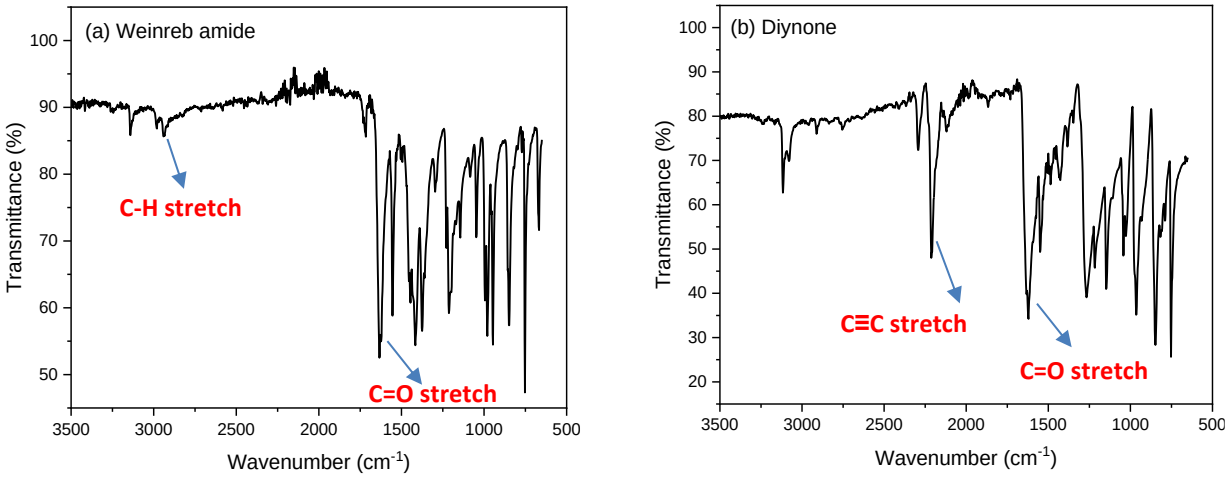

Figure S21. Infrared spectrum (a) Weinreb amide. (b) Diynone monomer

Infrared spectra of homopolymers

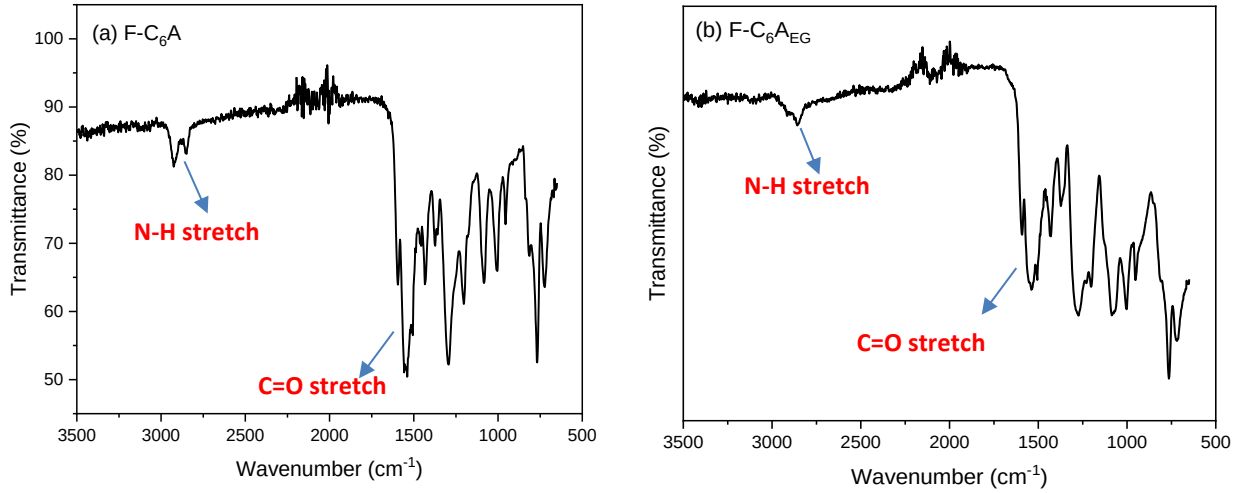

Figure S22. Infrared spectrum of homopolymers (a) F-C_6A. (b) F-C_6A_{EG}

Infrared spectra of copolymers

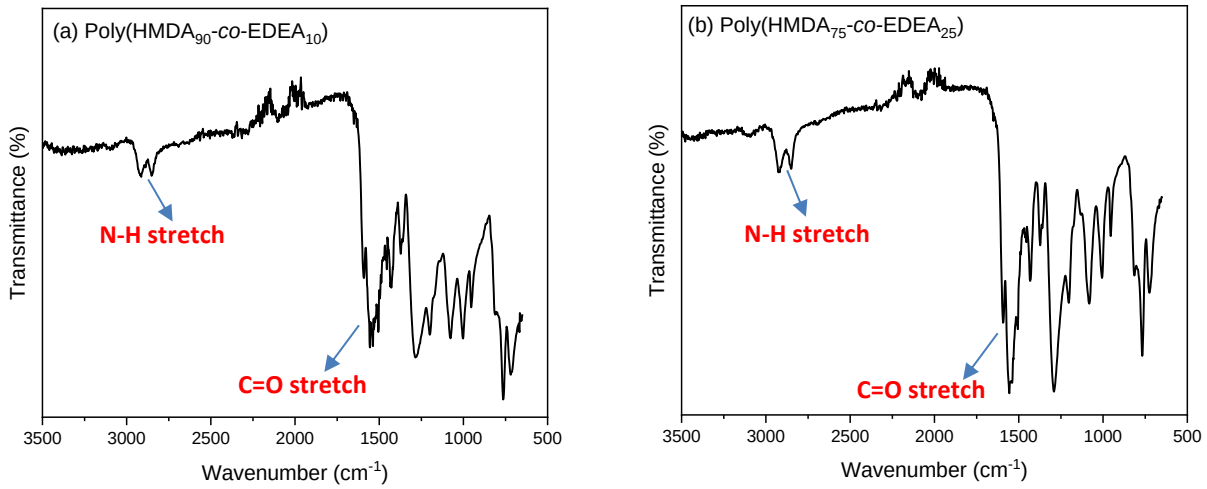

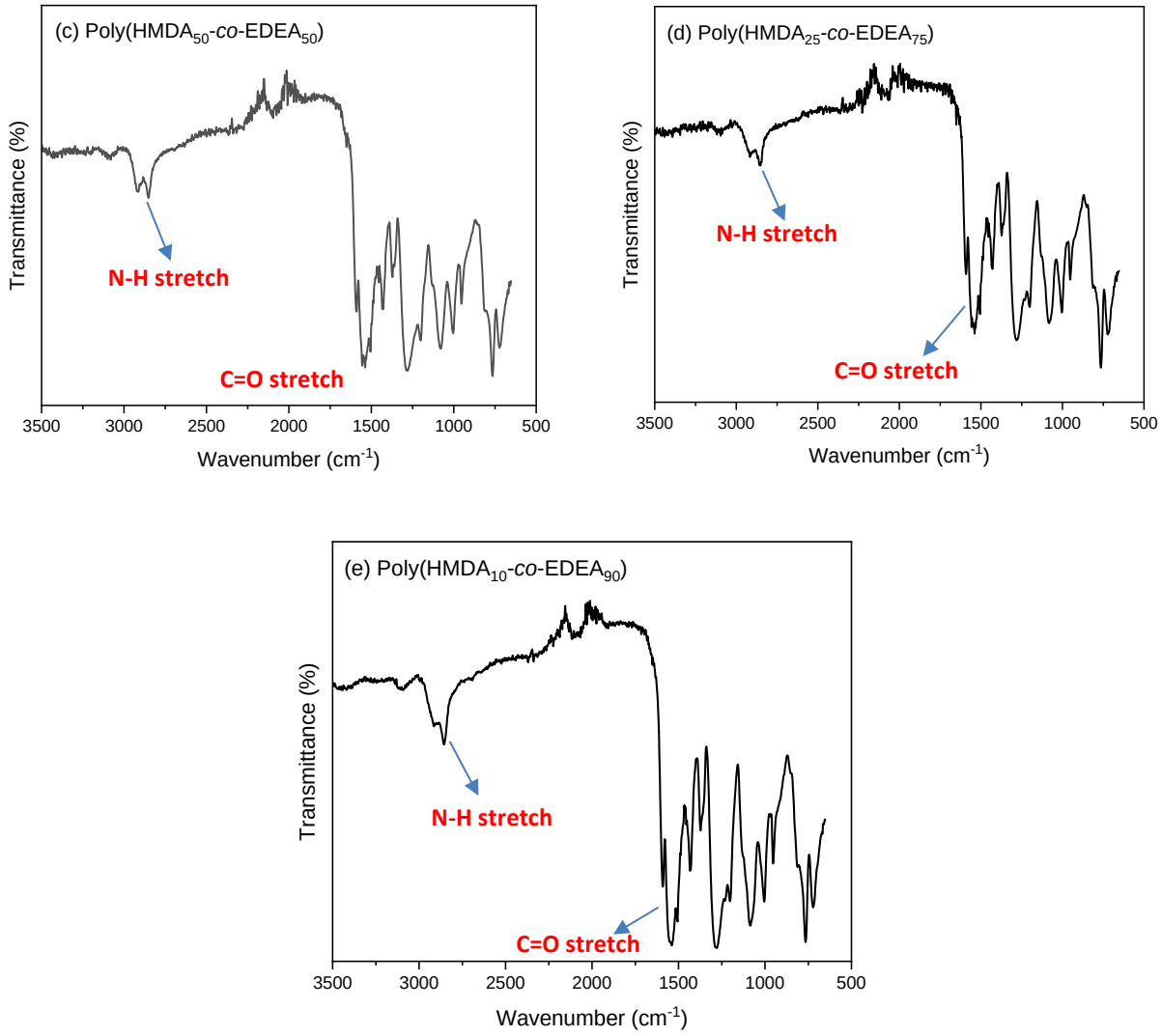

Figure S23. Infrared spectrum of copolymers (a) poly(HMDA$_{90}$-*co*-EDEA$_{10}$). (b) poly(HMDA$_{75}$-*co*-EDEA$_{25}$). (c) poly(HMDA$_{50}$-*co*-EDEA$_{50}$). (d) poly(HMDA$_{25}$-*co*-EDEA$_{75}$). (e) poly(HMDA$_{10}$-*co*-EDEA$_{90}$)

Film Preparation

To evaluate the thermomechanical properties of the polymers, the film was made by solvent cast method. The polymer sample (0.5 g) was first dissolved in dichloromethane (2.5 mL) until homogenous. The polymer solution was then filtered using a GPC filter to remove any particulates and transferred to a Teflon beaker. Then, it was left evaporate for 24 hours. The resultant film finally was dried under a high vacuum at room temperature for 3 days to anneal.

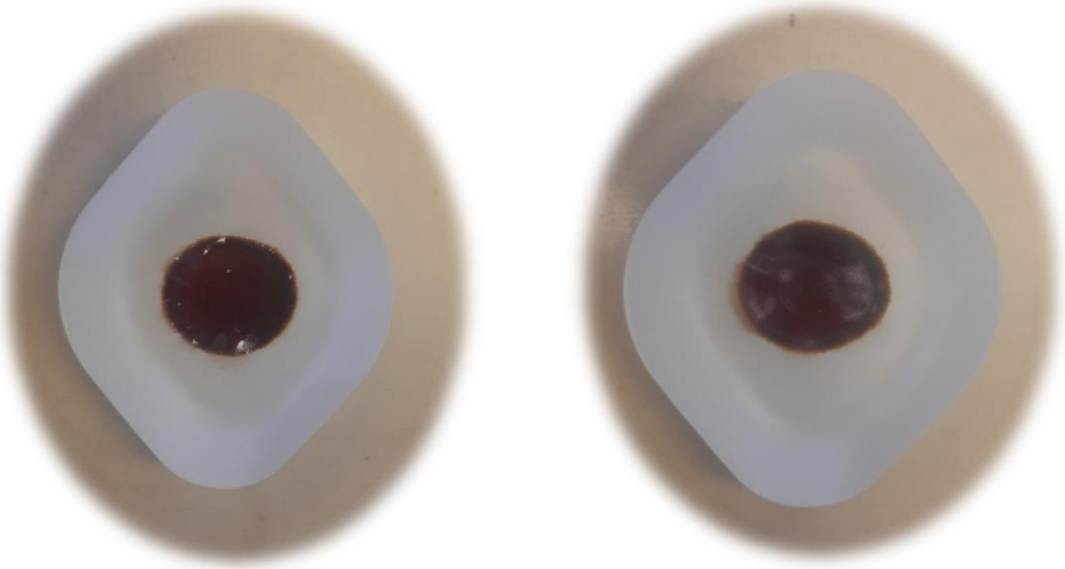

Figure S24. Physical appearance of representative copolymer film

DSC thermograms of homopolymers

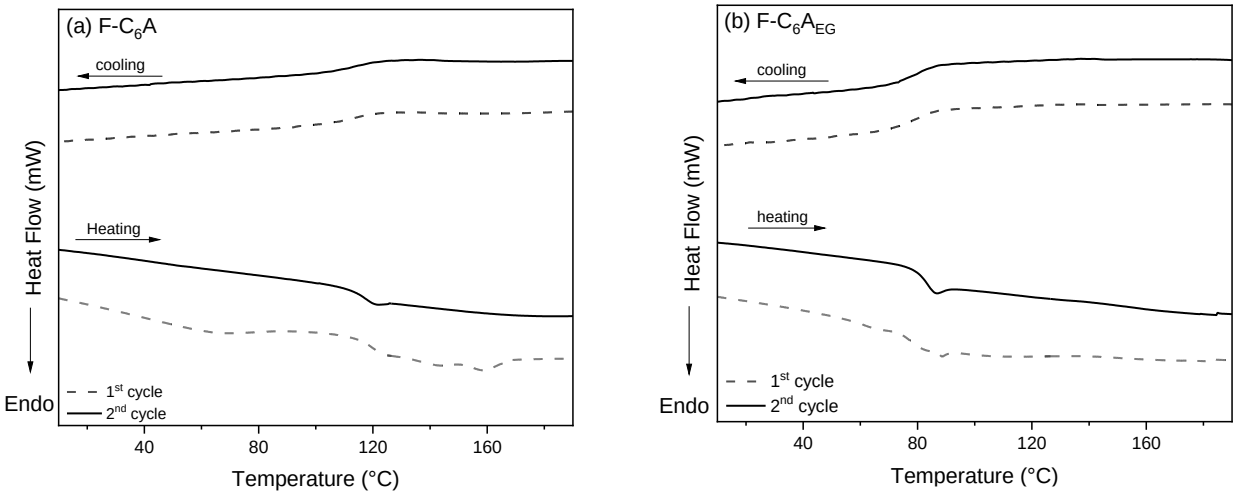

Figure S25. DSC thermograms of homopolymers (a) F-C_6A. (b) F-C_6A_{EG} 10 K·min^{-1} heating and cooling rate. Reproduced from previous work (manuscript in preparation).

DSC thermograms of copolymers

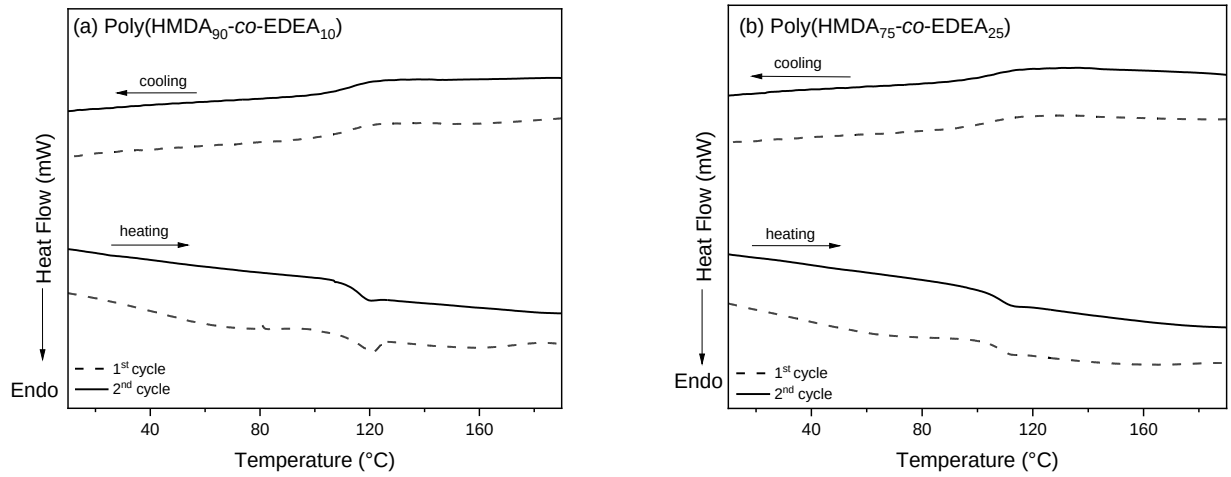

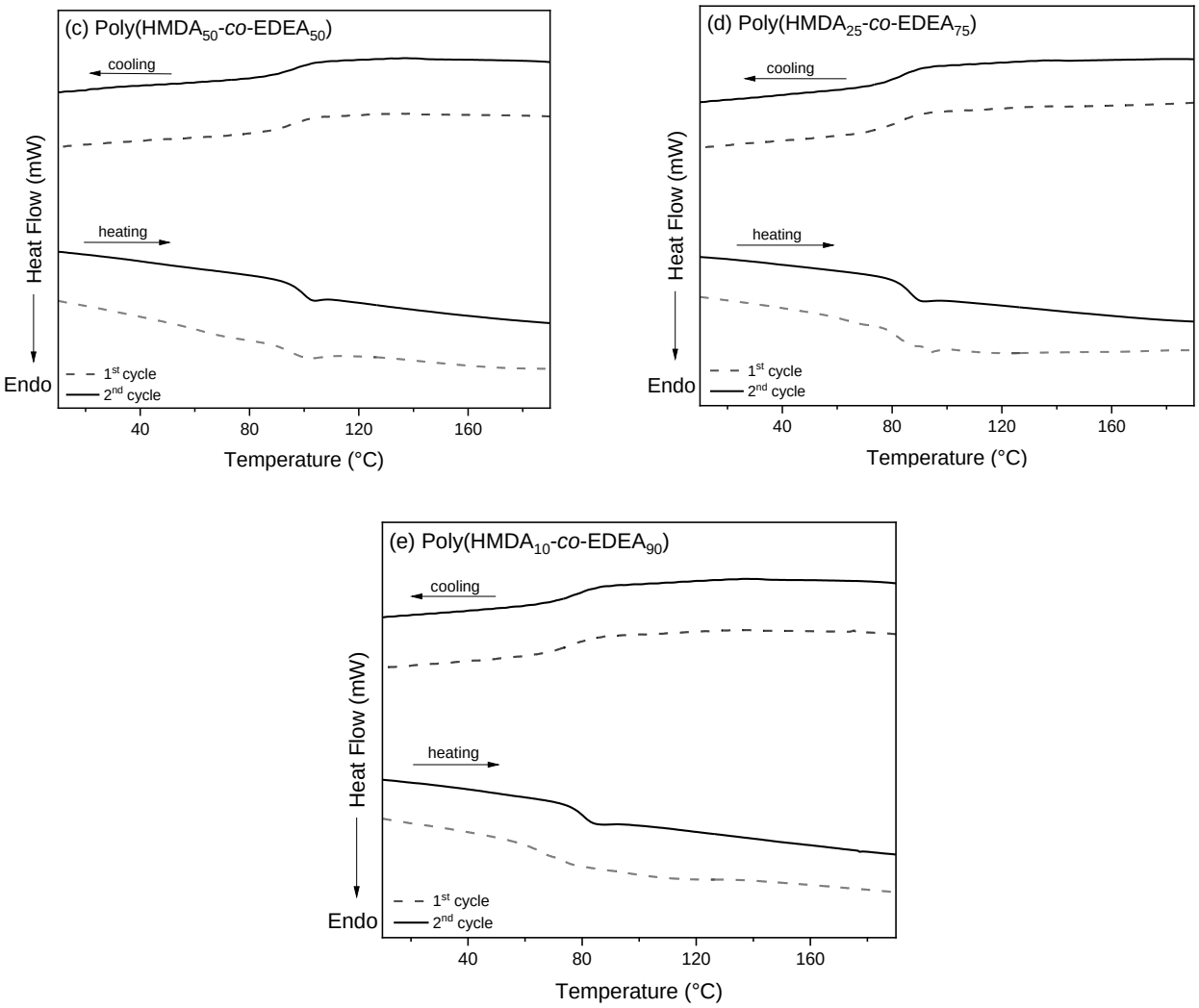

Figure S26. DSC thermograms of copolymers (a) Poly($HMDA_{90}$-*co*-$EDEA_{10}$). (b) Poly($HMDA_{75}$-*co*-$EDEA_{25}$). (c) Poly($HMDA_{50}$-*co*-$EDEA_{50}$). (d) Poly($HMDA_{25}$-*co*-$EDEA_{75}$). (e) Poly($HMDA_{10}$-*co*-$EDEA_{90}$). 10 K·min^{-1} heating and cooling rate

TGA thermograms of homopolymers

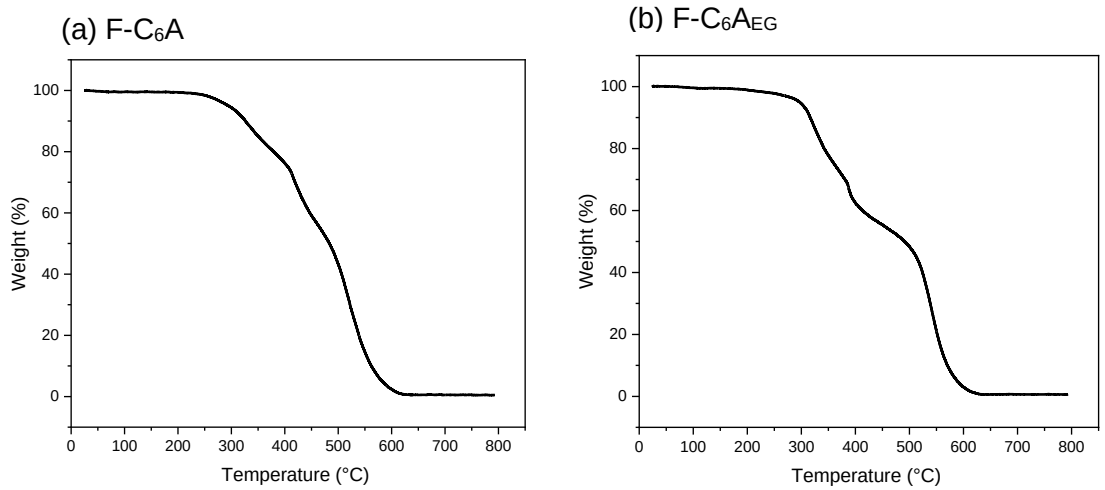

Figure S27. TGA thermograms of homopolymers (a) F-C_6A and(b) F-C_6A_{EG}. Reproduced from previous work (manuscript in preparation).

TGA thermograms of copolymer

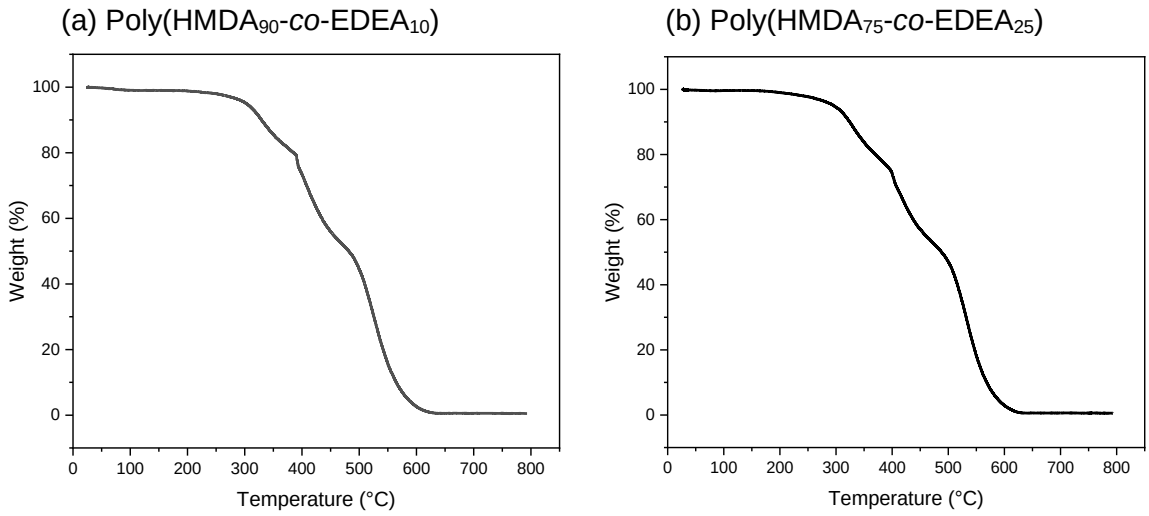

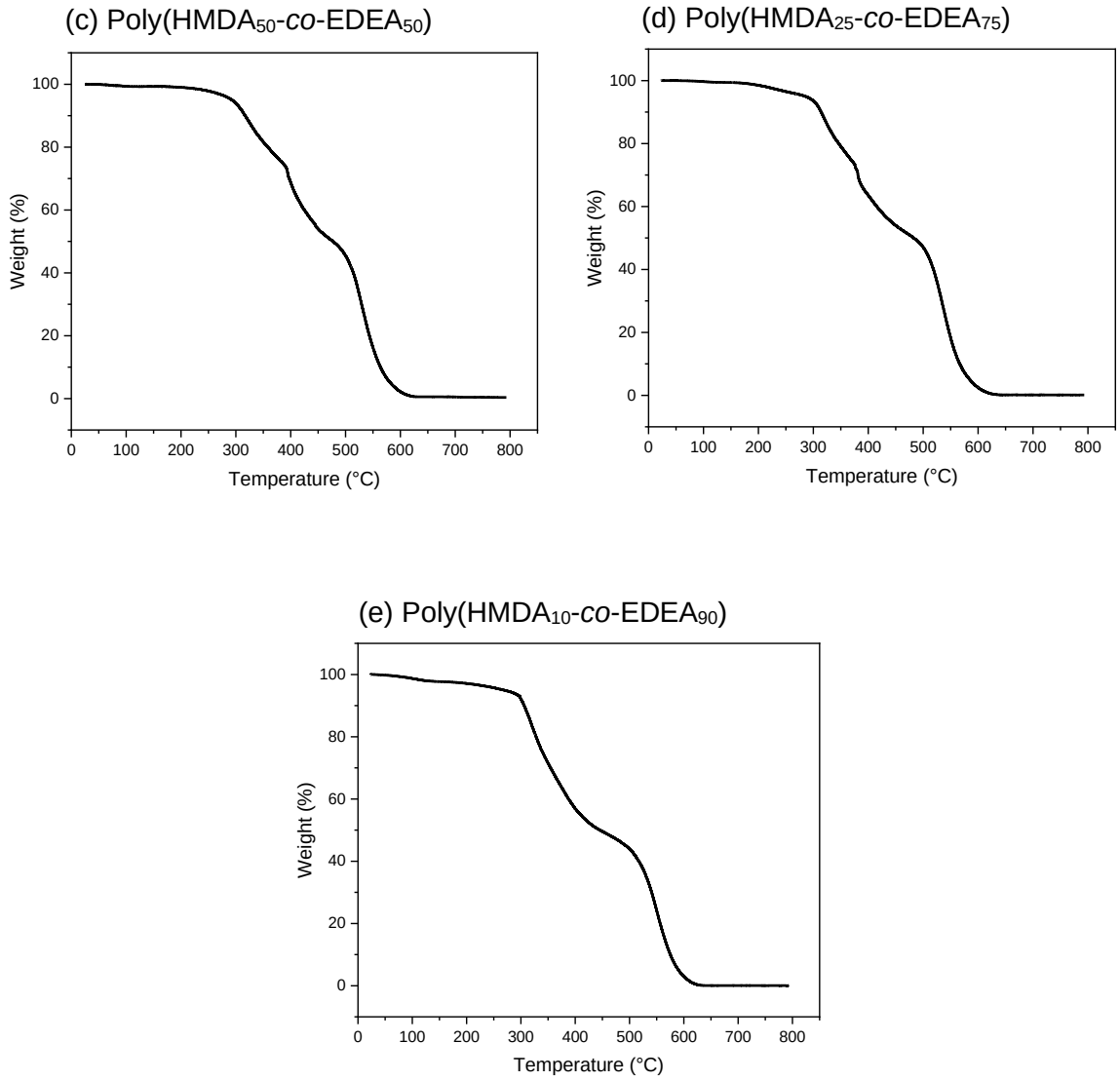

Figure S28. TGA thermograms of homopolymers (a) poly($HMDA_{90}$-*co*-$EDEA_{10}$). (b) poly($HMDA_{75}$-*co*-$EDEA_{25}$). (c) poly($HMDA_{50}$-*co*-$EDEA_{50}$). (d) poly($HMDA_{25}$-*co*-$EDEA_{75}$). (e) poly($HMDA_{10}$-*co*-$EDEA_{90}$)

Stress *vs* strain curves of homopolymers

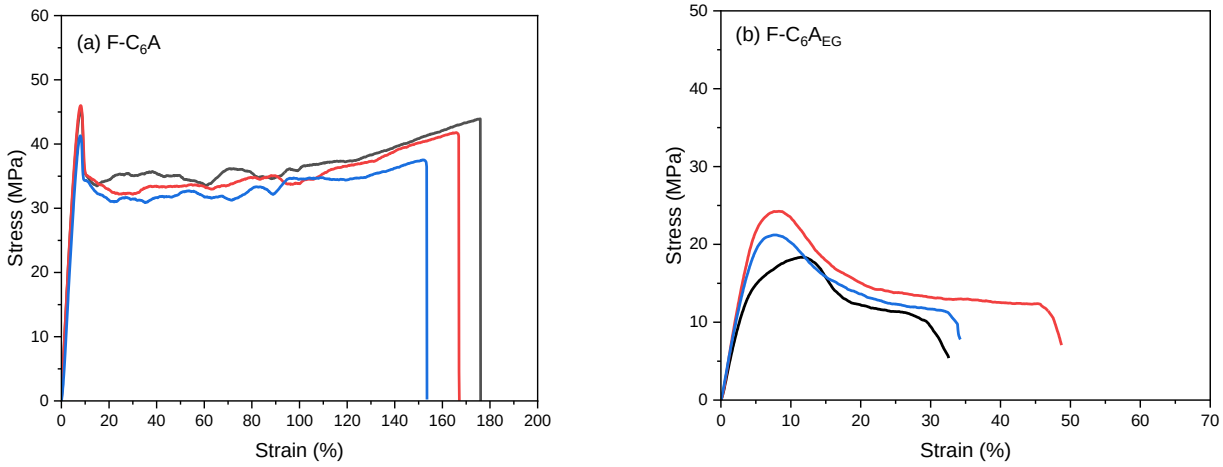

Figure S29. Tensile test curves for (a) F-C_6A. (b) F-C_6A_{EG} tested at 10 °C min^{-1}, 22 °C. Reproduced from previous work (manuscript in preparation).

Stress *vs* strain curves of copolymers

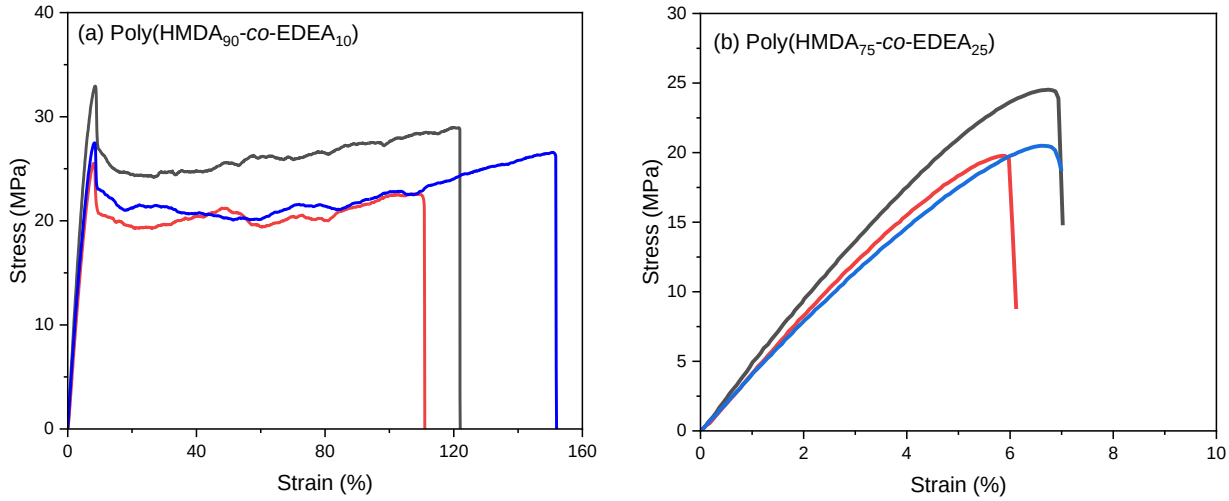

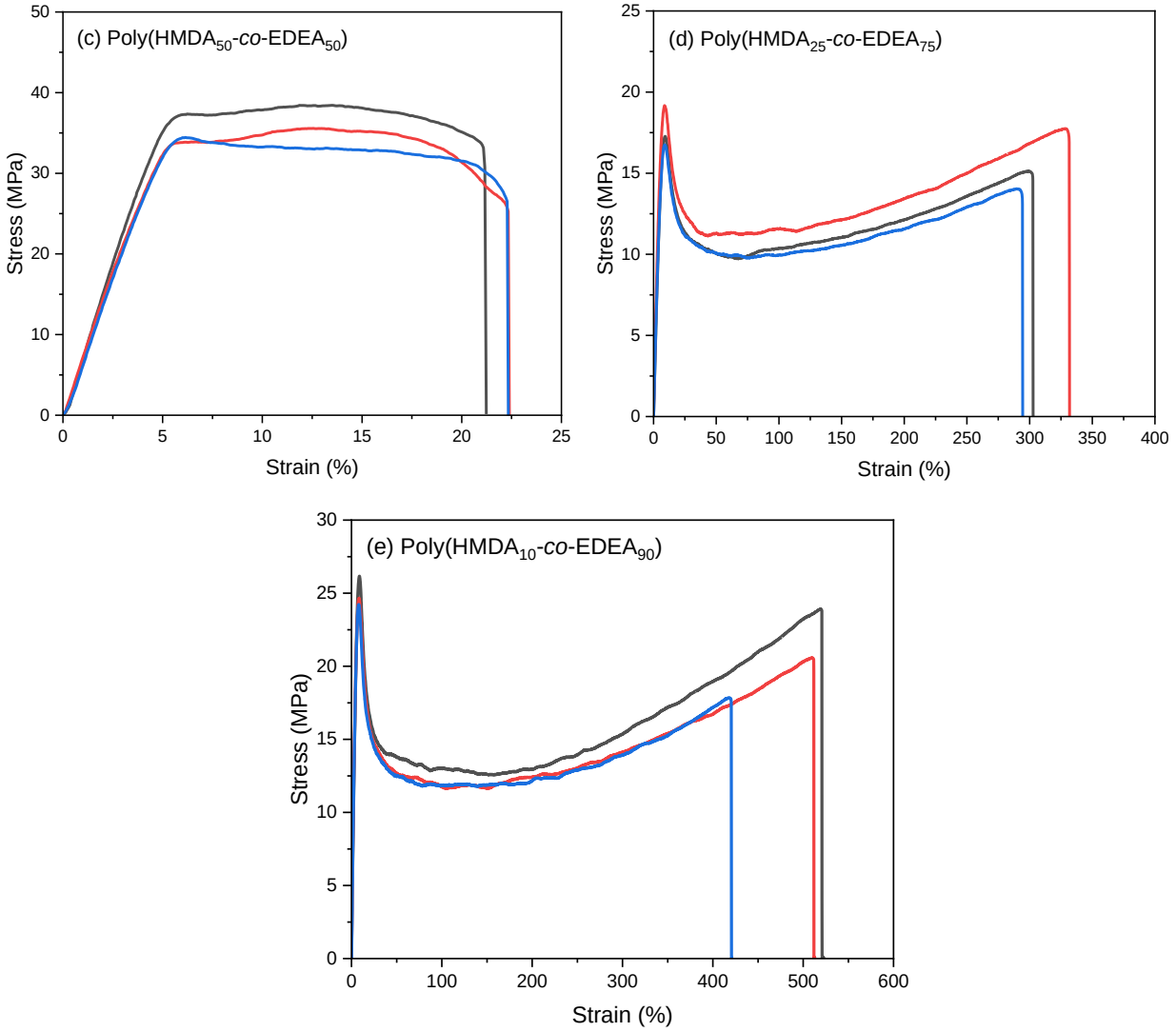

Figure S30. Tensile test curves for (a) Poly($HMDA_{90}$-*co*-$EDEA_{10}$). (b) Poly($HMDA_{75}$-*co*-$EDEA_{25}$). (c) Poly($HMDA_{50}$-*co*-$EDEA_{50}$). (d) Poly($HMDA_{25}$-*co*-$EDEA_{75}$). (e) Poly($HMDA_{10}$-*co*-$EDEA_{90}$) tested at 10 °C min^{-1}, 22 °C

Stress *vs* strain curves of commodity plastics

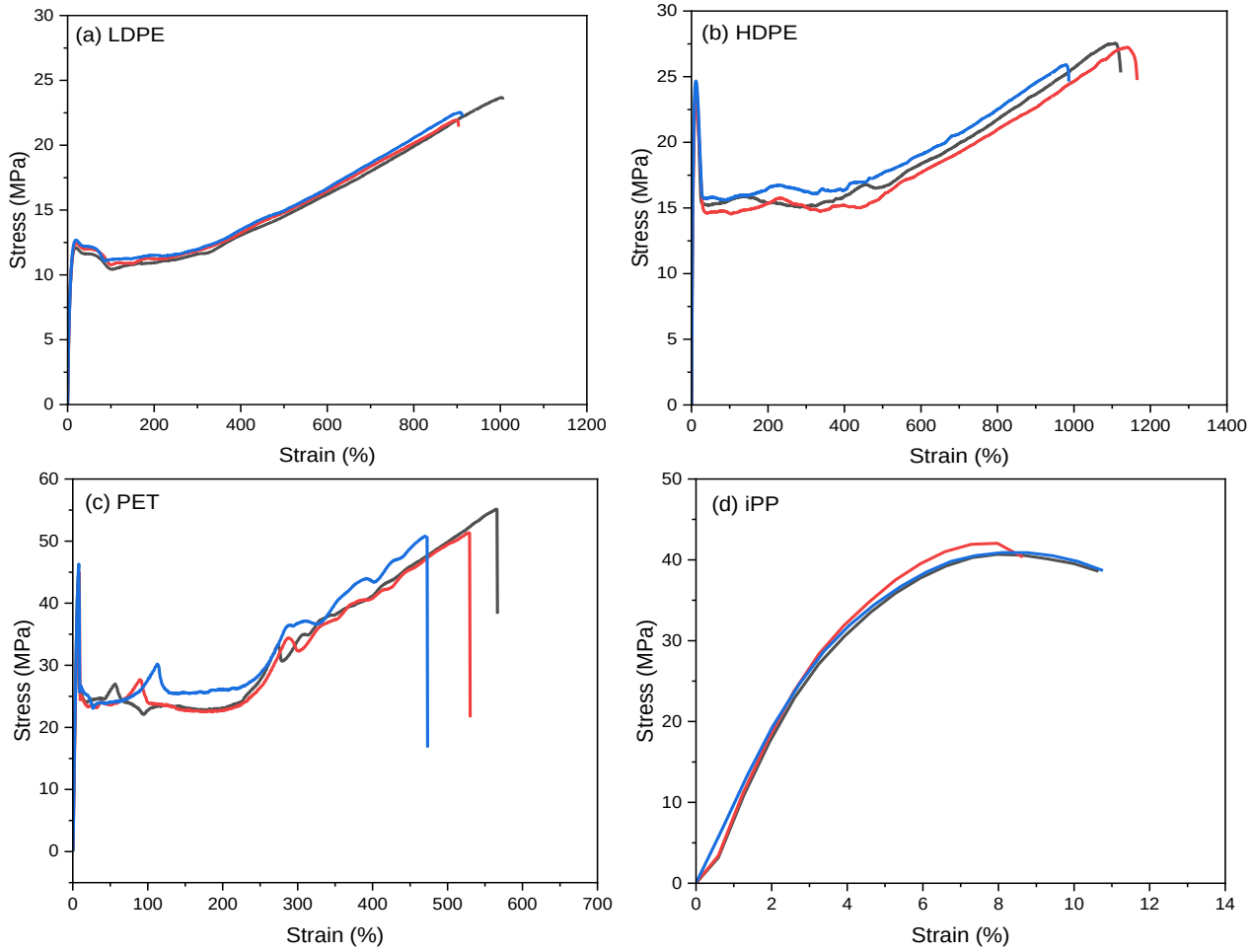

Figure S31. Stress *vs* strain curve for commodity plastic samples (a) LDPE; (b) HDPE; (c) PET; (d) *i*PP. *n = 3*. Reproduced from previous work (manuscript in preparation).

Table S1. Mechanical properties of polyketones and copolyketones tuned by controlling the chain flexibility

Polyketone /Copolyketone	*Young's Modulus (MPa)*	*Strain @ Break (%)*	*Stress @ Break (MPa)*	*Strain @ Yield (%)*	*Stress @ Yield (MPa)*	*Toughness ($MJ.m^{-3}$)*
F-C_6A	669 ± 33	165 ± 11.4	41.1±3.3	8.0±0.2	44.2±2.5	57.9±7.1
F-C_6A_{EG}	444 ± 41	39±8.9	21.3±2.9	9.1±2.0	21.3.0±2.9	5.5±1.2
Poly(HMDA$_{90}$-*co*-EDEA$_{10}$)	465±50	126±22.1	26.0±3.2	8.1±0.3	29.7±3.8	29.1±5.9
Poly(HMDA$_{75}$-*co*-EDEA$_{25}$)	442±45	6.4±0.5	21.6±2.6	6.3±0.5	21.6±2.6	0.9±0.2
Poly(HMDA$_{50}$-*co*-EDEA$_{50}$)	741±48	23.2±2.7	27.6±5.8	10.6±4.0	36.1±2.1	6.7±0.2
Poly(HMDA$_{25}$-*co*-EDEA$_{75}$)	308±20	306±19.9	15.6±1.9	8.9±0.2	17.7±1.3	38.1±6.0
Poly(HMDA$_{10}$-*co*-EDEA$_{90}$)	468±14	482±55.7	20.8±3.0	8.3±0.3	25.0±1.0	72.4±13.8

∗n = 3

Photodegradation studies

^{1}H-NMR stack of representative irradiated copolymer films

Poly(HMDA$_{10}$-co-EDEA$_{90}$)

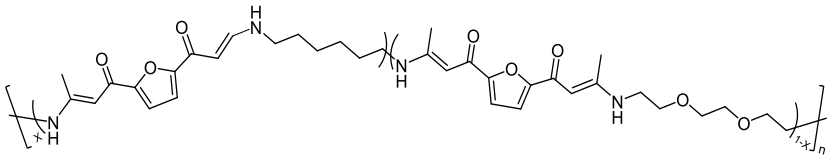

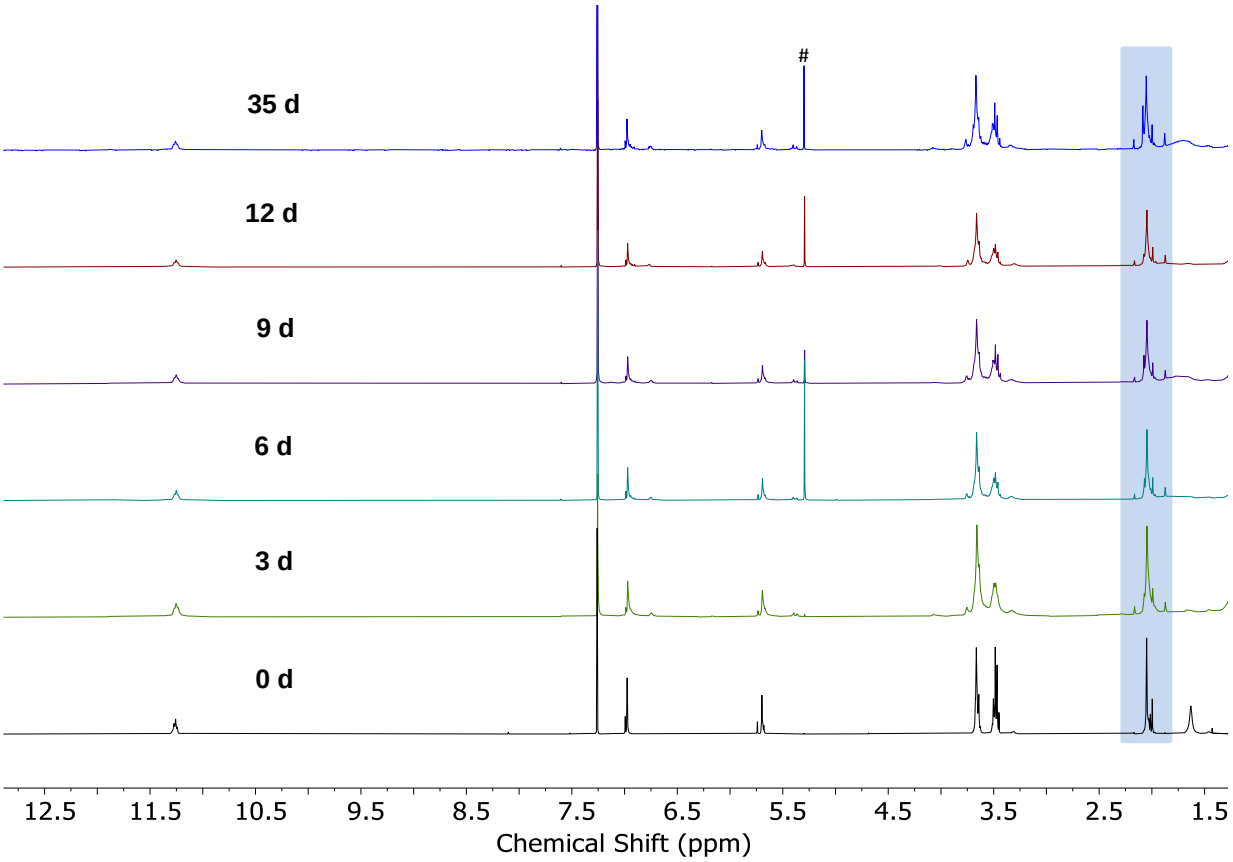

Figure S32. ^{1}H NMR spectra of copolymer poly(HMDA$_{10}$-*co*-EDEA$_{90}$) film stacked to illustrate the change of spectrum for 35 days. *#DCM residue*

^{1}H NMR stack of representative irradiated copolyketones solution (20 mg/mL $CDCl_3$)

Poly(HMDA$_{10}$-co-EDEA$_{90}$)

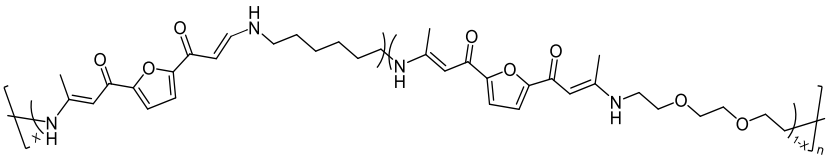

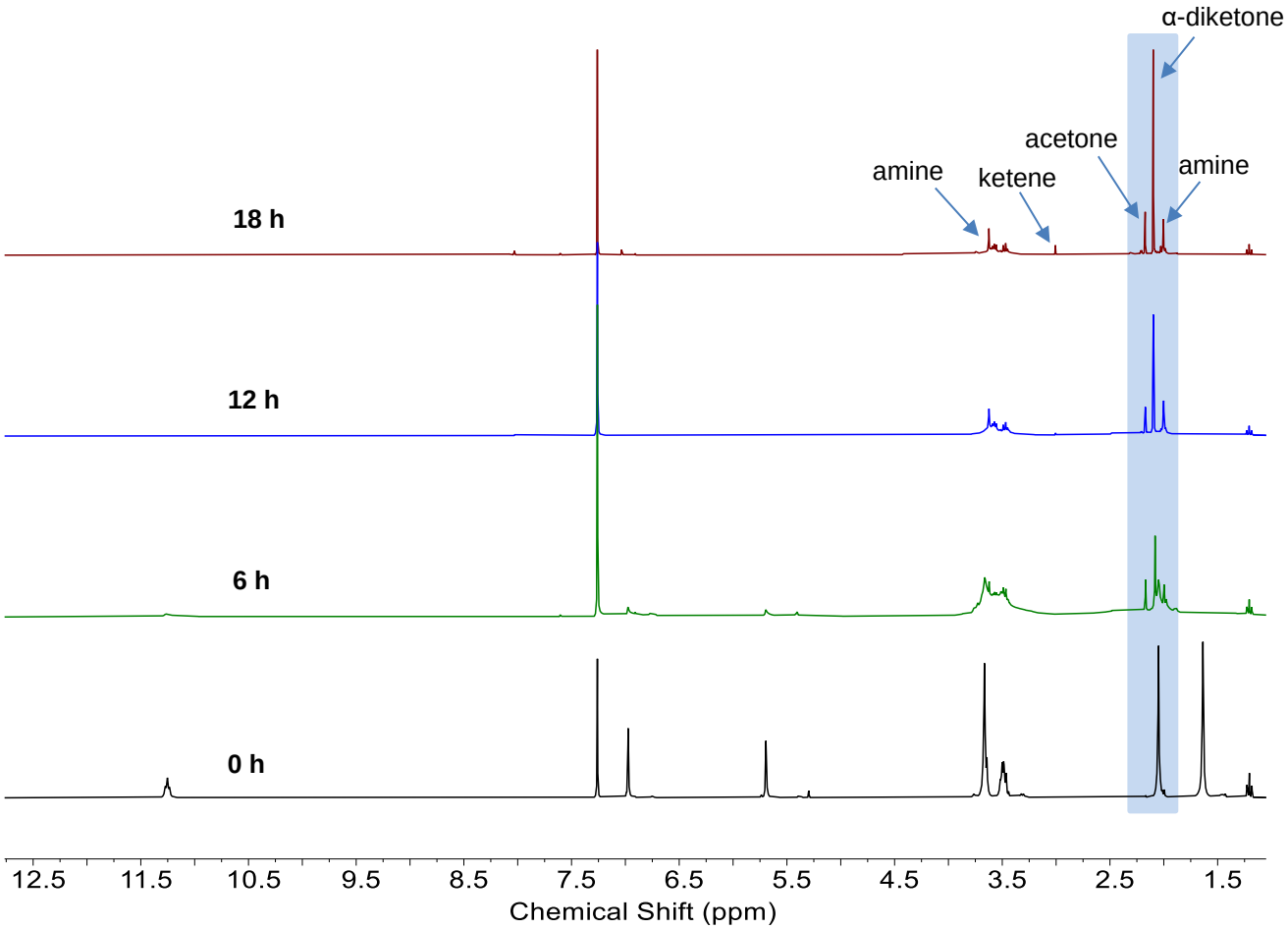

Figure S33. ^{1}H NMR spectra of polymer poly(HMDA$_{10}$-*co*-EDEA$_{90}$) (yellow solution) stacked to illustrate the change of spectrum until fully degraded (colorless solution)

Size exclusion chromatograms of representative irradiated copolymer films

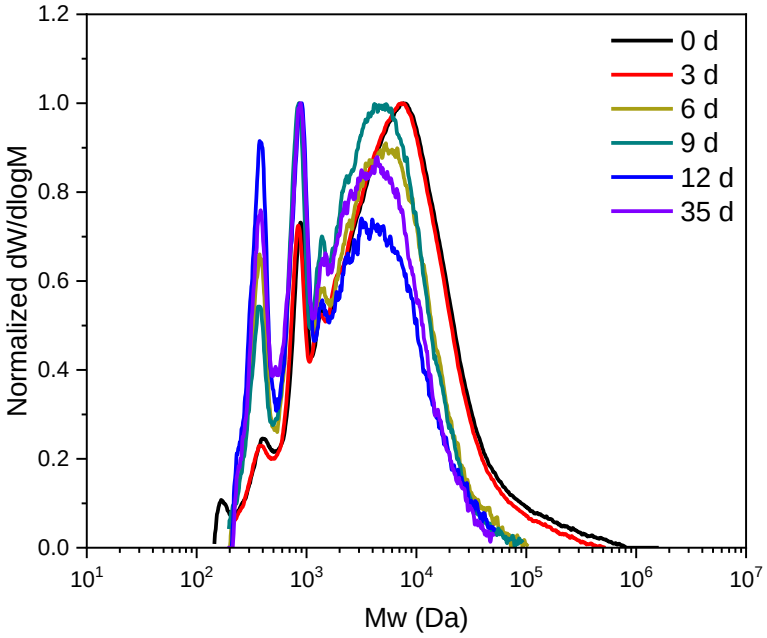

Figure S34. Normalized size exclusion chromatograms of representative irradiated copolymer films ($CHCl_3$, 0.5% NEt_3, 40 **°C**) analysis against poly(styrene) (PS) standards.

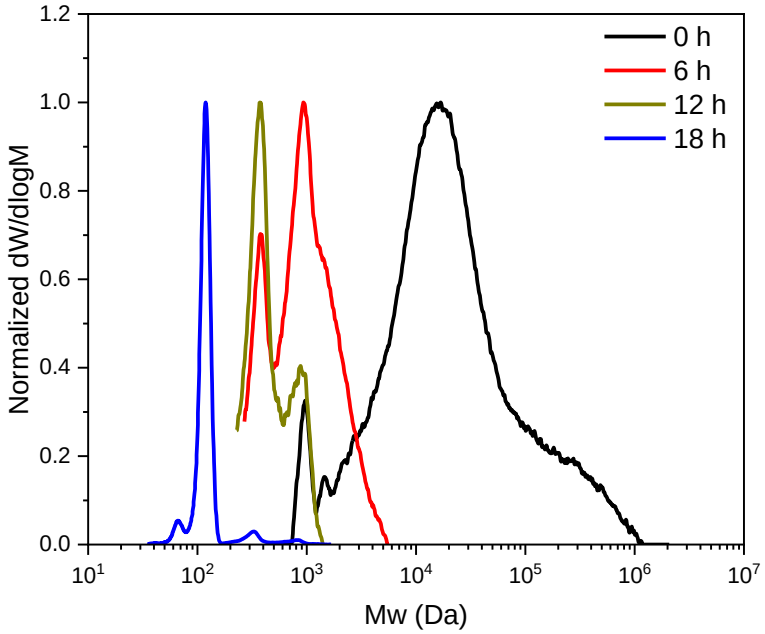

Figure S35. Normalized size exclusion chromatograms of representative irradiated copolymer solutions ($CHCl_3$, 0.5% NEt_3, 40 °C) analysis against poly(styrene) (PS) standards.

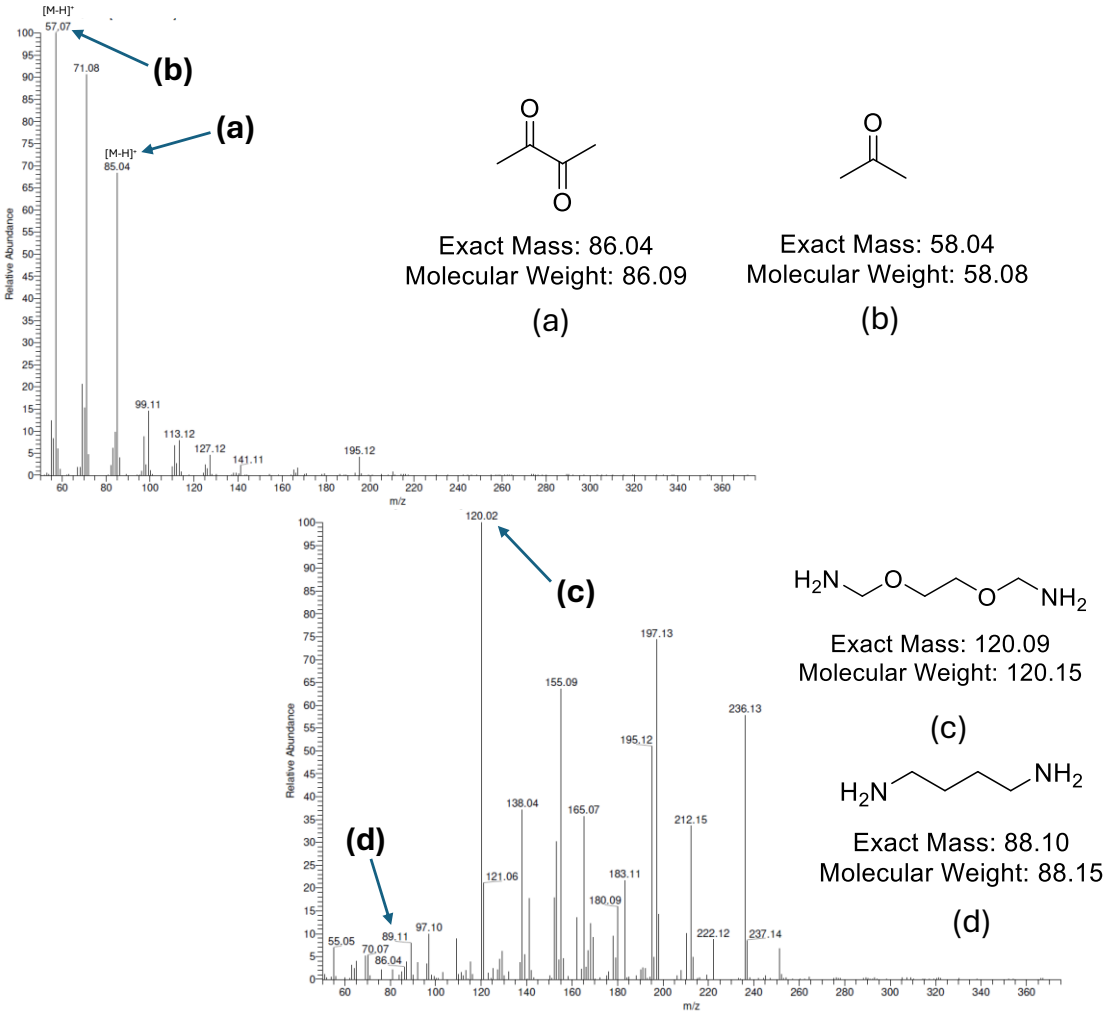

Figure 36. Mass spectra (EI-H+) of photodegradation ($CDCl_3$, 340 nm) for poly($HMDA_{10}$-*co*-$EDEA_{90}$) solution

CHAPTER 5: CONCLUSION AND OUTLOOK

CHAPTER 5

Conclusion and Outlook

This thesis has reported the development of a novel polyketone biomaterials platform from renewable resources with a wide range of thermomechanical properties. Additionally, the molecular structures of the polyketones were efficiently designed to target their photodegradability through photocleavable linkages in the ketone moiety. Click reaction approaches were chosen as straightforward methods for polymer synthesis owing to their high orthogonality, mild reaction conditions, and no side product formation. Thiol-yne and amino-yne click polymerization were conducted to prepare diverse homopolymers and copolymers with photodegradability behavior under UV light resulting in a more selective degradation pathway compared to the Norrish pathway.

In Chapter 2, the effect of chain flexibility and repeat unit length on the thermomechanical performance of the polyketones (PKs) was investigated. 2,5-furandicarboxylic acid (FDCA) was employed as a building block considering its renewability and ability to act as a photosensitizer. The FDCA was initially converted into a Weinreb amide by a one-pot reaction. Subsequently, the Weinreb amide was reacted with a Grignard reagent to afford an activated ketone alkyne monomer (diynone). Then, a range of PKs was synthesized *via* the thiol-yne step-growth polymerization of the diynone monomer with various commercially available dithiols. The resulting PKs possess diverse molecular structures aiming to obtain PKs with comparable mechanical performances to the commodity plastics. The PKs containing comonomer 1,10-decanedithiol exhibited outstanding tensile strength with high T_g and remarkable thermal stability, as well as comparable tensile strength towards PET

(but having half of its elongation at break value). Finally, the photodegradation of the resultant PKs was assessed by controlled UV light irradiation. The degradation products were characterized revealing that β-diketone in enol form was the major degradation product. Furthermore, model compound studies were conducted to define small molecules photodegradation products and to suggest a possible degradation pathway. The key findings of this chapter are that the thermomechanical properties of thiol-yne based polymers can be controlled through manipulation of the polymer backbones. Also, the degradation products of the synthesized polyketones follow a more selective pathway than Norrish pathways which are typically observed in the conventional polyketones.

In Chapter 3, the study was extended to generate polyketones by using diamines as comonomers owing to their abundance and cost-effectiveness. Additionally, diamines can be renewably sourced whereas dithiols are not. The spontaneous amino-yne click polymerization (*aza*-Michael addition) was conducted in mild reaction conditions to fabricate numerous PKs with diverse thermomechanical properties without using any external catalyst as diamines can act both as reactant and catalyst. Similarly observed for thiol-yne based PKs, the thermomechanical properties of amino-yne based PKs were also impacted by the repeat unit length, chain flexibility, and steric hindrance. PKs with comonomer 1,6-hexandedimine (F-C_6A) demonstrated excellent tensile strength with high T_g and outstanding thermal stability. Moreover, they exhibited higher tensile strength than thiol-yne based PKs (F-C_{10}T) owing to the hydrogen bond formation. These resulting PKs (F-C_6A) have a comparable tensile strength to PET compared to other synthesized amino-yne based PKs. (but having half of its elongation at break value) Photodegradation was assessed by examining the degradation products after UV light irradiation, in which α-diketone and acetone

were detected as the major products. Furthermore, the spontaneous amino-yne click polymerization method was applied to fabricate microcapsules *via* interfacial click polymerization which was considered a novel approach in the microencapsulation techniques. This technique involved a polyaddition reaction instead of polycondensation, which was also typically used in the interfacial polymerization between isocyanate and amine. The spherical dye-loaded microcapsules were successfully generated with excellent thermal stability and the absence of surfactant. Moreover, they showed a prolonged release upon UV light exposure. This study offers an alternative option of click polymerization by spontaneous amino-yne click reaction. This reaction involves amine comonomers which are more abundant and can be renewably sourced to generate polyketones (*e*.*g*. to fabricate degradable plastics and microcapsules) with a range of thermomechanical properties in the absence of external catalysts. Additionally, photodegradation follows a selective pathway as found in Chapter 2.

In Chapter 4, modifications in the polymer chain architecture of linear amino-yne based PKs were carried out to deliver improved mechanical performance. The addition of comonomers 1,6-hexanediamine (HMDA) and 2,2′-(ethylenedioxy)bis(ethylamine) (EDEA) across the activated alkyne is expected to enhance the toughness and ductility of the resulting PKs (F-C_6A_{EG}). A range of HMDA/EDEA molar ratios was investigated. The synthesized PKs demonstrated an improvement in toughness and ductility with the increments in the HMDA content, peaking at a molar ratio 90/10. They showed a comparable tensile strength to HDPE (but owing half of its elongation at break value). This approach showed an alternative copolymerization technique to conventional metal-catalyzed PKs copolymerization due to its versatility, sustainability, safety, efficiency, and cost-effectiveness.

Furthermore, when irradiated with UV light, amino-yne based PKs photodegraded into degradation products analogous to those obtained in Chapter 3. This chapter paves the way to improve the mechanical performance of the particular homopolymer through a copolymerization technique while maintaining the same photodegradation pathway.

These novel polyketones enable them to degrade into non-toxic small molecules and do not fragment into microplastics. Therefore, these photodegradable plastics are expected to contribute to reducing the microplastic accumulation that contaminates marine and landfills. In addition, both chain flexibility and Michael addition reactions have shown a great impact on the physicochemical properties of the polymer materials. Moreover, this approach could also be implemented in cross-linked polymer synthesis to manufacture different types of materials, such as thermosets and elastomers. These materials have significant potential as they offer improved performance similar to petroleum-based materials, while also addressing the unresolved issue of end-of-life disposal.

A more sustainable way to synthesize Weinreb amide still needs to be figured out in the future. Furthermore, in order to improve the tensile elongation of the synthesized polyketones, we are considering copolymerizing 1,6-hexanediamine with 2,2'-(ethylenedioxy)diethanethiol. Thus, we might enhance the tensile elongation while maintaining the tensile strength. Otherwise, post-polymerization modification would be also promising to conduct in the future. In terms of the safe photodegradation products towards the environments, humans, and animals, therefore the cell cytotoxicity assay would be carried out. This assay will be beneficial to evaluate acute systemic toxicity and cytotoxic effects to guarantee safety and efficacy prior to clinical

application.